Entwicklung neuartiger *Targeted Therapy*-Strategien zur Behandlung des chemotherapieresistenten Ovarialkarzinoms unter besonderer Berücksichtigung von Histondeacetylase-Inhibitoren

Inaugural-Dissertation

zur Erlangung des Doktorgrades
der Mathematisch-Naturwissenschaftlichen Fakultät
der Heinrich-Heine-Universität Düsseldorf

vorgelegt von

Jan Josef Bandolik
aus Viersen

Düsseldorf, März 2021

aus dem Institut für Pharmazeutische und Medizinische Chemie
der Heinrich-Heine-Universität Düsseldorf

Gedruckt mit der Genehmigung der
Mathematisch-Naturwissenschaftlichen Fakultät der
Heinrich-Heine-Universität Düsseldorf

Berichterstatter:

1. Prof. Dr. rer. nat. Matthias U. Kassack

2. Prof. Dr. med. Tanja Fehm

Tag der mündlichen Prüfung: 06.07.2021

Für meine Eltern Sigrid und Detlef, meine Schwester Lisa und meine Großmutter Margarete († 2019).

„Fragen wir […] nicht zuerst, was nicht geht oder was schon immer so war. Fragen wir zuerst, was geht, und suchen wir nach dem, was noch nie so gemacht wurde."

- Dr. Angela Merkel, 2019

Inhaltsverzeichnis

Abkürzungsverzeichnis

(q)PCR	(Quantitative) Polymerasekettenreaktion
17-AAG	17-N-allylamino-17-demethoxygeldanamycin; Tanespimycin
17-DMAG	17-Demethylaminoethylamino-17-demethoxygeldanamycin; Alvespimycin
2-HG	2-Hydroxyglutarat
ADP/ATP	Adenosindiphosphat/Adenosintriphosphat
Akt/AKT	Proteinkinase B (auch PKB)
APAF1	*Apoptotic protease activating factor 1*
ARID	*AT-rich interactive domain-containing protein*
ATP7B	Wilson-Protein (*Copper-transporting P-type adenosine triphosphate*)
BAK	*Bcl-2 homologous antagonist killer*
BRCA1/2	Brustkrebsgen 1/2 (*breast cancer 1/2, early onset*)
BTZ	Bortezomib
c-ABL	Tyrosinkinase ABL1
CCC	Klarzellkarzinom des Ovars (*clear cell carcinoma*)
cDDP	*cis*-Diammindichloridoplatin-II (Cisplatin)
CDKN2A/B	*Cyclin-dependent kinase inhibitor 2A/B*
CHDI	CHDI-00390576 (HDACi der CHDI [*Cure Huntingtons´s Disease Initiative*] Foundation)
CR	Geladene Linker-Region [HSP90]
CTCL	Cutanes T-Zelllymphom
CTD	C-terminale Domäne [HSP90]
CTR1	Kupfertransporter 1
DDR	DNA-Schädigung *(DNA damage response)*
DGGG	Deutsche Gesellschaft für Gynäkologie und Geburtshilfe
DNA	Desoxyribonucleinsäure (*desoxyribonucleic acid*)
DNMT	DNA-Methyltransferasen
EC	Endometrioides Karzinom des Ovars (*endometrioid carcinoma*)

EGFR/ErbB	Epidermaler Wachstumsfaktorrezeptor (*epidermal growth factor receptor)*
EGFRi	Inhibitor des EGF-Rezeptors
EMA	Europäische Arzneimittelagentur (*European Medicines Agency*)
ERCC1	DNA-Exzisionsreparaturprotein 1
ERK	Extrazellulär-Signal regulierte Kinasen
ESR1	Estrogenrezeptor 1
EZH2	*Enhancer of zeste homolog 2*
FACS	Fluoreszenzbasierte Durchflusszytometrie (*fluorescent activated cell sorter*)
FDA	Amerikanische Arzneimittelagentur (*Food and Drug Administration*)
FIGO	franz. Internationale Vereinigung für Gynäkologie und Geburtshilfe
FOXO1/3a	*Forkhead box protein O1/O3a*
GCL	Glutamatcysteinligase
GOG	Gynäkologische Onkologische Gruppe
GPCR	G-Protein gekoppelter Rezeptor
GSH	Glutathion
GST	Glutathion-S-Transferase
HAT	Histonacetyltransferasen
HDAC	Histondeacetylase
HDACi	Histondeacetylase-Inhibitor
HDM	Histondemethylasen
HGS(O)C	High-grade seröses Ovarialkarzinom
HMT	Histonmethyltransferasen
HR	Homologe Rekombination
IDH1/2	Isocitratdehydrogenase 1/2
JNK	c-Jun N-terminale Kinasen
LGS(O)C	Low-grade seröses Ovarialkarzinom
MAPK	MAP (*mitogen-activated protein*)-Kinase
MC	Muzinöses Karzinom des Ovars
MD	Mittlere Domäne [HSP90]

MMR	Fehlpaarungsreparatur (*DNA mismatch repair*)
MRP2	*Multidrug resistance protein 2*
mTOR	Ziel des Rapamycins im Säugetier (engl. *mammalian/mechanistic target of rapamycin)*
mTORC1/2	mTOR-Komplex 1 bzw. 2
MTT	3-(4,5-Dimethylthiazol-2-yl)-2,5-diphenyltetrazoliumbromid
NAD^+	Nicotinamidadenindinukleotid$^+$
NER	Nukleotid-Exzisionsreparatur (*nucleotide excision repair*)
NTD	N-terminale Domäne [HSP90]
PARP(i)	(Inhibitoren von) Poly-ADP-Ribose-Polymerase
PI3(K)	Phosphoinositid-3(-Kinasen)
PI3Ki	Inhibitor der Phosphoinositid-3-Kinase
PIP_2	Phosphatidylinositol-4,5-bisphosphat
PIP_3	Phosphatidylinositol-3,4,5-trisphosphat
PKB	Proteinkinase B (auch Akt/AKT)
PTEN	Phosphatase und Tensin Homolog
PUMA	*p53 upregulated modulator of apoptosis*
ROS	Reaktive Sauerstoffspezies
SAMRCB1	*SWI/SNF-related matrix-associated actin-dependent regulator of chromatin subfamily B member 1*
SF	Shift-Faktor einer Kombinationsbehandlung (Quotient aus IC_{50}-Werten des Bezugs-Wirkstoffs ohne und mit Kombinationsbehandlung)
SIRT	Sirtuin
SMARCA2	*Propable global transcription activator SNF2L2*
SMARCA4	*ATP-dependent chromatin remodeler SMARCA4*
STAT3	*Signal transducer and activator of transcription 3*
STIC	Seröse tubare intraepitheliale Karzinome
TET2	Tet-Methylcytosindioxygenase 2
TNM	Klassifikation eines Tumors nach Tumor, Nodus und Metastasen
UPS	Ubiquitin-Proteasom-System

VEGF(R)	(Rezeptor für den) Vaskulären endothelialen Wachstumsfaktor
WHO	Weltgesundheitsorganisation (*world health organization*)
WT1	Wilms-Tumor-Protein
ZBG	Zinkbindende Gruppe [HDACi-Pharmakophor]

Abbildungsverzeichnis

Anmerkungen zum Abbildungsverzeichnis:

Abbildung 4 und Abbildung 5 wurden aus Rocha et al., 2018, Clinics (*DNA repair pathways and cisplatin resistance: an intimate relationship*) entnommen, übersetzt und modifiziert. Der Artikel (und alle darin enthaltenen Abbildungen) wurden vom Verlag unter CC BY Lizenz veröffentlicht.

Abbildung 7 wurde aus Bates, 2020, NEJM (*Epigenetic Therapies for Cancer*) entnommen und übersetzt. Anmerkung zur Lizenz des Verlags: *Reproduced with permission from (Bates, 2020, NEJM), Copyright Massachusetts Medical Society.*

Abbildung 10 wurde aus Hoter et al., 2018, IJMS (*The HSP90 Family: Structure, Regulation, Function, and Implications in Health and Disease*) entnommen und übersetzt. Der Artikel (und alle darin enthaltenen Abbildungen) wurden vom Verlag MDPI unter CC BY Lizenz veröffentlicht.

Abstract

Ovarian carcinomas show by far the lowest survival rates among gynecological cancers, as they are usually diagnosed late and have already become more aggressive during their progression. Although many ovarian cancers are chemosensitive at diagnosis and respond well to platinum-containing chemotherapy, for example, there is the problem of cytostatic resistance. Resistance can develop during the course of treatment and causes a problem for the treatment of relapses. Therefore, the need arises to develop treatment strategies for platinum-resistant tumors, to slow down or prevent the development of such resistance.

The aim of the studies in this thesis was to develop synergistic drug combinations using cellular models. The cellular systems used were mainly, but not exclusively, cell lines serving as models for high-grade serous ovarian cancers (HGSOC). HGSOC are characterized by increased aggressiveness. Epigenetic dysregulations, particularly increased expression and activity of histone deacetylases (HDACs) promote initial tumorigenesis and resistance development. Therefore, histone deacetylase inhibitors (HDACi) served as promising combination partners to modulate the expression of apoptosis-related genes. We aimed to investigate whether combination with HDACi would result in enhancing effects of treatment with cisplatin or the proteasome inhibitor bortezomib. Bortezomib is well-known from the therapy of hematological tumors, where it is clinically used with success. Bortezomib also supports the induction of apoptosis by reducing the degradation of proapoptotic proteins. In addition, we aimed to investigate whether HDACi with specific class selectivity are beneficial. Combinations were characterized regarding their cytotoxicity (MTT assay) and apoptosis induction (subG1- and caspase-3/7 activation assays) and investigated for their mechanism by analysis of gene expression (qPCR, Western blot) and DNA damage (γH2AX assay). Functional effects were analyzed for synergism.

The first study demonstrated that HSP90 inhibitors and panobinostat (pan-HDACi) are generally able to sensitize ovarian cancer cells towards cisplatin. The follow-up study was performed with five cell lines modeling HGSOCs. It was shown that selective inhibition of class I HDACs by entinostat enhanced the cytotoxicity of cisplatin in a highly synergistic manner. The effect was more pronounced compared to panobinostat. Mechanistically, entinostat led to a superadditive increase in the rate of apoptotic cells, which was based on a shift in gene expression towards proapoptotic

genes. An extension of the dual combination of entinostat and cisplatin with kinase inhibitors (epidermal growth factor receptor inhibitors [lapatinib and afatinib] and phosphoinositide 3-kinase [buparlisib, dactolisib, and BGT-226]) showed an even greater increase in cytotoxicity and apoptosis induction of cisplatin even under reduced concentrations of entinostat. In the next study, the synergistic effect (cytotoxicity, apoptosis, caspase-3/7 activation, and formation of γH2AX) of bortezomib and the class IIa specific HDACi CHDI-00390576 was demonstrated on (cisplatin-resistant) non-HGSOC cell lines.

All in all, the combined use of (selective) HDACi with cisplatin or bortezomib offer the possibility to improve the therapy of aggressive and platinum-resistant ovarian cancer. Furthermore, promising impulses for the inclusion of kinase inhibitors in this combination therapy could be obtained.

Zusammenfassung

Ovarialkarzinome haben innerhalb der gynäkologischen Krebsarten bei weitem die geringsten Überlebensraten, da sie in der Regel spät diagnostiziert werden und im Laufe ihrer Progression bereits an Aggressivität zugenommen haben. Obwohl viele Ovarialtumore bei Diagnosestellung chemosensitiv sind und beispielsweise auf eine platinhaltige Chemotherapie gut ansprechen, besteht das Problem einer Zytostatikaresistenz. Diese kann sich im Laufe der Behandlung entwickeln und stellt ein Problem für die Behandlung von Rezidiven dar. Daher ergibt sich die Notwendigkeit, Behandlungsstrategien für platinresistente Tumore zu entwickeln, die Ausbildung einer entsprechenden Resistenz zu verlangsamen oder zu verhindern.

Das Ziel der Studien dieser Arbeit war die Entwicklung von synergistischen Wirkstoffkombinationen am zellulären Modell. Als zelluläre Systeme wurden vor allem, aber nicht nur, Zelllinien eingesetzt, die als Modelle für hochgradig seröse Ovarialkarzinome (HGSOC) dienen. HGSOC zeichnen sich durch eine erhöhte Aggressivität aus. Epigenetische Dysregulationen, insbesondere eine verstärkte Expression und Aktivität von Histondeacetylasen (HDACs), fördern die initiale Tumorentstehung und Resistenzentwicklung. Daher dienten Histondeacetylase-Inhibitoren (HDACi) als vielversprechende Kombinationspartner, um die Expression Apoptose-relevanter Gene zu modulieren. Es sollte überprüft werden, ob sich durch die Kombination mit HDACi verstärkende Effekte einer Behandlung mit Cisplatin oder dem Proteasom-Inhibitor Bortezomib ergeben. Bortezomib ist vor allem aus der Therapie von hämatologischen Tumoren bekannt und wird dort klinisch erfolgreich eingesetzt. Auch Bortezomib unterstützt die Einleitung der Apoptose, da die Degradierung proapoptotischer Proteine gesenkt wird. Zusätzlich sollte untersucht werden, ob HDACi mit einer bestimmten Klassen-Selektivität vorteilhaft sind. Die Kombinationen wurden hinsichtlich ihrer Zytotoxizität (MTT-Assay) und Apoptose-Auslösung (subG1- und Caspase-3/7-Aktivierungsassay) charakterisiert und teilweise mechanistisch aufgeklärt (Analysen der Genexpression per qPCR, Western Blot und γH2AX-Assay). Die Effekte wurden auf Synergismus untersucht.

In der ersten Studie konnte gezeigt werden, dass HSP90-Inhibitoren und Panobinostat (pan-HDACi) grundsätzlich in der Lage sind, Ovarialkarzinom-Zellen gegenüber Cisplatin zu sensitivieren. Die Folgestudie wurde an fünf Zelllinien durchgeführt, die modellhaft für HGSOCs stehen. Es konnte gezeigt werden, dass

durch die selektive Inhibierung von Klasse I HDACs durch Entinostat die Zytotoxizität von Cisplatin hochsynergistisch gesteigert werden konnten. Der Effekt war stärker ausgeprägt als unter Verwendung von Panobinostat. Als Basis des Effektes konnte eine superadditive Erhöhung der Rate apoptotischer Zellen bewiesen werden, was in einer Verschiebung der Genexpression hin zu proapoptotischen Genen begründet ist. Eine Erweiterung der dualen Kombination aus Entinostat und Cisplatin um Kinaseinhibitoren (Inhibitoren des epidermalen Wachstumsfaktorrezeptors [Lapatinib und Afatinib] und der Phosphoinositid-3-Kinase [Buparlisib, Dactolisib und BGT-226]) zeigte selbst unter verringerten Konzentrationen von Entinostat eine noch stärkere Erhöhung der Zytotoxizität und Apoptose-Auslösung von Cisplatin. In der nächsten Studie konnte die synergistische Wirkung (Zytotoxizität, Apoptose, Caspase-3/7-Aktivierung und Bildung von γH2AX) von Bortezomib und dem Klasse IIa spezifischen HDACi CHDI-00390576 an (Cisplatin-resistenten) nicht-HGSOC Zelllinien gezeigt werden.

Alles in allem bieten die kombinierte Anwendung von (selektiven) HDACi mit Cisplatin oder Bortezomib die Möglichkeit, die Therapie von aggressiven und platinresistenten Ovarialkarzinomen weiterzuentwickeln. Weiterhin konnten vielversprechende Impulse für die Einbeziehung von Kinaseinhibitoren in diese Kombinationstherapie generiert werden.

1 Einleitung

1.1 Tumorerkrankungen

Tumorerkrankungen können aus einer einzigen Zelle entstehen, die eine genetische Abweichung aufweist, sofern diese nicht durch körpereigene Reparaturmechanismen frühzeitig erkannt und eliminiert wird. Da prinzipiell jede Zelle des Körpers der Startpunkt einer Krebserkrankung sein kann, gibt es mehr als einhundert verschiedene denkbare Krebsarten, welche sich in ihrem spezifischen Verhalten und ihrer Reaktion auf eine etwaige Behandlung unterscheiden. Grundsätzlich muss zwischen benignen (gutartigen) und malignen (bösartigen) Tumoren unterschieden werden. Ein benigner Tumor zeichnet sich dadurch aus, dass er an seiner ursprünglichen Lokalisierung verbleibt, umliegendes Gewebe nicht invadiert und vor allem keine Metastasierung aufweist. Ein maligner Tumor weist dagegen invasives Verhalten und eine Neigung zur Metastasierung auf. Primäre Mechanismen für die Metastasierung stellen die Verbreitung von Tumorzellen des Primärtumors über die Blutbahn (hämatogene Metastasen) und die Lymphbahnen (lymphogene Metastasen) dar. Allerdings besteht auch die Möglichkeit der Penetration einzelner Tumorzellen durch verschiedene Barrieren im menschlichen Körper um beispielsweise auf die Oberfläche des Peritoneums, der Pleurahöhle oder des Perikards zu gelangen (1,2). Die Krankheitsbezeichnung „Krebs“ ist für maligne Tumore reserviert, da es sich auch bei einigen eher trivialen Erkrankungen (wie zum Beispiel einer Hautwarze oder einer gutartigen Fettgeschwulst [Lipom]) im definitorischen Sinne um einen benignen Tumor handelt. Nichtsdestotrotz muss stets bedacht werden, dass einige benigne Tumore zur malignen Transformation fähig sind und ihr Verhalten maligne Charakteristika entwickeln kann. Benigne Tumore weisen in der Regel eine deutlich leichtere Behandlungsstrategie auf und können zumeist durch chirurgische Eingriffe vollständig entfernt werden, während maligne Tumore aufgrund ihres Metastasierungspotentials besonders problematisch bezüglich ihrer Behandlung sind.

Tumore lassen sich im Hinblick auf ihre Entstehung in Karzinome, Sarkome oder Leukämien/Lymphome unterteilen. Rund 90 % der menschlichen Tumore sind Karzinome und stellen maligne Neubildungen epithelialer Zellen dar. Weitere etwa 8 % entfallen auf Leukämien bzw. Lymphome, welche aus blutbildenden Zellen oder

Zellen des Immunsystems entstehen. Die relativ selten auftretenden Sarkome sind solide Tumore, welche sich aus Muskel-, Knochen- oder Knorpelgewebe entwickeln. Eine weitere Klassifizierung von Tumorerkrankungen wird aufgrund des Ursprungsgewebes vorgenommen: so werden Karzinome des Eierstockgewebes beispielsweise als Ovarialkarzinome bezeichnet (3).

1.1.1 Entstehung einer Tumorerkrankung

Die Karzinogenese stellt einen mehrstufigen Prozess auf zellulärer Ebene dar, der im Wesentlichen auf Mutationen und der Selektion von Zellen beruht, welche ein verändertes Verhalten bezüglich ihrer Proliferations- und Überlebenseigenschaften aufweisen. Darüber hinaus zeigt eine Tumorzelle zunehmend invasives und metastasierendes Verhalten. Zusätzlich sind Tumore angiogenetisch aktiv. Sie bilden Blutgefäße aus, um die einzelnen Tumorzellen mit Sauerstoff und Nährstoffen zu versorgen. Im ersten Schritt, der Tumorinitiation, führen genetische Veränderungen zu ungehinderter Zellproliferation. Bei normaler Funktion der entsprechenden körpereigenen Reparaturprozesse kann eine gewisse Zahl an genetischen Mutationen toleriert werden. Theoretisch genügt jedoch eine einzige genetische Abnormität an der falschen Stelle, die nicht durch körpereigene Prozesse repariert wird. Im Zuge des unkontrollierten Wachstums entsteht durch Zellteilung eine erste Tumorzellpopulation. Innerhalb dieser Population kommt es aufgrund der regelhaft erhöhten chromosomalen Instabilität zu weiteren Mutationen, welche die Eigenschaften der jeweiligen Zelle verändern und beispielsweise zu einem noch stärker erhöhten Zellwachstum führt. Im Zuge der Tumorprogression werden genetisch veränderte Zellen innerhalb der Zellpopulation immer dominanter. Durch Zellteilung entstehen somit immer mehr Zellen, welche per Mutation potenziell invasive oder metastasierende Eigenschaften gepaart mit erhöhter Proliferationsrate aufweisen. Dieser Vorgang wird als klonale Selektion bezeichnet (3).

1.2 Ovarialkarzinome

Die häufigsten Ovarialkarzinome werden gemäß der Weltgesundheitsorganisation (WHO) und der aktuellen Leitlinie der Deutschen Gesellschaft für Gynäkologie und Geburtshilfe (DGGG; Stand März 2020, Version 4.0) in fünf histologische Typen unterteilt: high-grade serös (HGSC), klarzellig (CCC), endometrioid (EC), low-grade serös (LGSC) und muzinös (MC). Diese Unterteilung erfolgt auf Basis „ihrer Vorläuferläsionen, Ausbreitungsmuster und Überleben sowie ihrer Assoziation mit hereditären Tumorsyndromen und molekularer Pathogenese“ (4). Für diese Promotionsarbeit sind vor allem HGSC-, CCC- und EC-Typen von Relevanz, welche nun kurz auf Basis der Leitlinie charakterisiert werden.

HGSC liegen in mehr als 50 % der diagnostizierten Fälle vor und werden oft sehr spät, in einem fortgeschrittenen Stadium, entdeckt. Sie zeichnen sich durch eine erhöhte Proliferationsrate, hohe chromosomale Instabilität (damit erhöhtes Aufkommen von bzw. ein erhöhter Hang zu spontanen Mutationen) und durch eine regelhafte Mutation des Tumorsuppressors p53 aus. Bei jüngeren Patientinnen treten vermehrt LGSC auf, welche schrittweise über die Entwicklung von nicht-invasiven zu invasiven Tumoren entstehen. Die klinischen Verläufe sind in der Regel deutlich langsamer im Vergleich zu HGSC-Typen.

Ebenfalls eher in früheren Tumorstadien treten EC- und CCC-Typen auf, welche sich durch Assoziation mit einer atypischen Endometriose oder eines endometrioiden Karzinoms der Gebärmutter kennzeichnen lassen. Zur Differentialdiagnose des Typs der vorliegenden Krebserkrankung des Ovars wird in der Leitlinie ein Algorithmus basierend auf der Expression von vier Antigenen (WT1, p53, Napsin A und Progesteronrezeptor) angegeben, welcher auf einer großen kanadischen Studie (5) beruht (Abbildung 1).

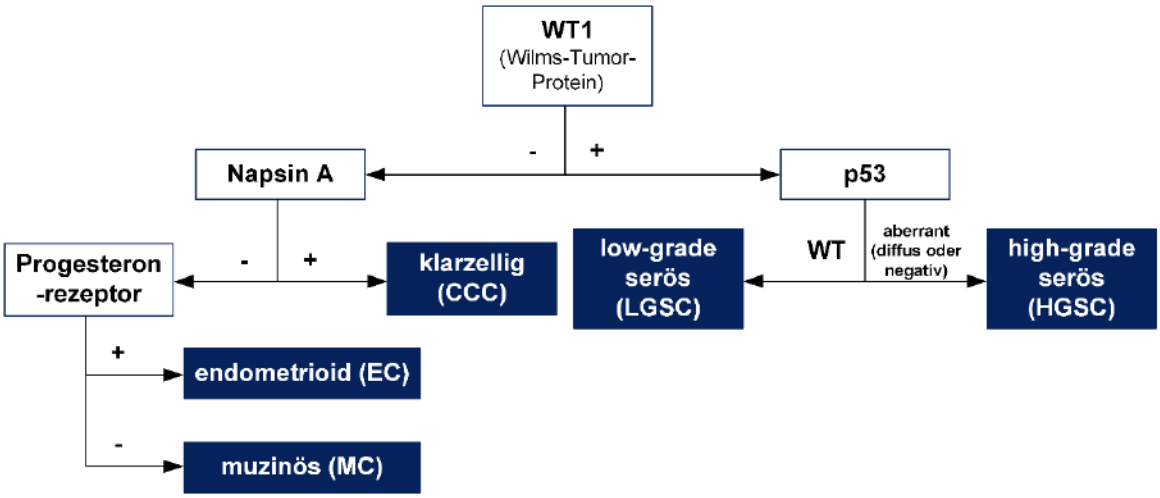

Abbildung 1: Algorithmus zur differentialdiagnostischen Klärung des Histotyps von Ovarialkarzinomen.

Die Abbildung wurde abgewandelt aus (4,5) übernommen.

WT1 (Wilms-Tumor-Protein) ist ein Transkriptionsfaktor und tritt gehäuft bei serösen Ovarialkarzinomen auf (WT1+). Liegt ein WT1-positiver Typ vor, wird auf Basis der Expression des Tumorsuppressors p53 die Unterscheidung in LGSC bzw. HGSC getroffen: Bei LGSC-Typen liegt p53 als unmutierter Wildtyp (WT) vor, während es in knapp 94 % der HGSC-Fälle als mutierte Form (nicht vorhanden oder verändert) vorliegt. Ist der untersuchte Tumor WT1-negativ (WT1-), wird der Status der Expression der Aspartat-Proteinase Napsin A bestimmt. In 92 % der Napsin A-positiven Tumoren, liegt ein CCC-Typ vor. Sollte der untersuchte Tumor ebenfalls Napsin A-negativ sein, wird untersucht, ob das Tumorgewebe Progesteronrezeptoren exprimiert. Knapp 85 % der EC-Typen weisen die Expression dieses Rezeptors auf. Ist die Tumorart WT1-negativ, Napsin A-negativ und weist keine Expression des Progesteronrezeptors auf, handelt es sich um ein muzinöses Ovarialkarzinom.

Unabhängig von der Einteilung in histologische Typen, können Ovarialkarzinome (und andere maligne Tumore) zur Beschreibung des Stadiums und damit in der Regel auch der Schwere der Erkrankung im TNM- oder FIGO-System (letzteres nur für gynäkologische Krebserkrankungen) klassifiziert werden. Das breiter gültige TNM-System klassifiziert Tumore vor allem nach drei Kategorien: T (Tumor), N (Nodus, lat. Knoten) und M (Metastasen). Mit dem Buchstaben T wird vor allem die räumliche Ausdehnung des Primärtumors auf der Skala T0-T4 beschrieben. Die Größenbereiche sind von der Tumorentität abhängig. N enthält Informationen über die An- oder Abwesenheit von Lymphknotenmetastasen in räumlicher Nähe zum Primärtumor. Bei Anwesenheit von Lymphknotenmetastasen wird der Befund auf der Skala N1-N3

einsortiert. Je höher der Zahlenwert ist, desto stärker ausgeprägt ist der Lymphknotenbefall. Den beiden Kategorien T und N kann der Zusatz „X“ angehangen werden, wenn keine Aussage zur jeweiligen Klassifizierung möglich ist. Die Angabe des Buchstabens M gibt Aufschluss über das Fehlen (M0) oder Vorhandensein (M1) von Fernmetastasen. In der aktuellen Fassung des TNM-Systems wurde der zusätzliche Deskriptor C gestrichen. Dieser zeigte in älteren Versionen die Zuverlässigkeit des Befundes an und konnte auf einer Skala von C1 (Röntgenaufnahme, allgemeine Untersuchungen) bis C5 (Autopsie) klassifiziert werden (6).

In Ergänzung zum TNM-System hat die Internationale Vereinigung für Gynäkologie und Geburtskunde (frz. FIGO) ein eigenes Klassifizierungssystem für gynäkologische Tumore veröffentlicht. Die Tumore werden in Stadien I-IV unterteilt, welche grob der T-Klassifizierung des TNM-Systems entspricht. Innerhalb der Stadien findet eine Feineinteilung mit den Buchstaben A-C statt. Das erste Stadium ist FIGO I, in welchem ein auf die Ovarien begrenzter Tumor vorliegt. Im Stadium IC können bereits beide Ovarien befallen sein und eine Schädigung bestimmter Strukturen (Ovarkapsel oder Tube) liegt vor. Außerdem sind Tumorzellen auf der Ovar- oder Tubenoberfläche nachweisbar. Handelt es sich um einen Tumor mit FIGO II, liegt bereits eine nachgewiesene Ausbreitung ins kleine Becken oder ein primäres Bauchfellkarzinom vor. Während im Stadium IIA eine Ausbreitung des Tumors auf Uterus und/oder Tuben beschränkt ist, sind im Stadium IIB weitere Strukturen des Bauchfells im Bereich des kleinen Beckens betroffen. Wird ein Ovarialkarzinom dem Stadium FIGO III zugeordnet, fand bereits eine Ausbreitung außerhalb des kleinen Beckens statt und/oder es konnten retroperitoneale Lymphknotenmetastasen nachgewiesen werden. Die detailliertere Klassifizierung innerhalb des Stadiums III basiert vorwiegend auf der Größe und Lokalisierung der (Lymphknoten-)Metastasen. Ein Tumor nach Stadium FIGO IV weist Fernmetastasen außerhalb des Peritoneums auf. Unterschieden wird nach IVA (Tumorzellen im Pleuraerguss nachweisbar) und IVB (Metastasen des parenchymalen Gewebes der Leber und/oder Milz oder Metastasen in Organen außerhalb des Abdomens) (4,7). Mit höherem FIGO-Stadium sinkt die Prognose der Patientinnen drastisch von rund 80 % in FIGO I auf 14 % in FIGO II, was sich in der 5-Jahres-Überlebensrate niederschlägt.

In Deutschland erkranken jährlich mehr als 7000 Frauen an Eierstockkrebs. Mit einem Anteil von 27 % ist das Ovarialkarzinom die zweithäufigste gynäkologische

Krebserkrankung nach Gebärmutterkrebs (40 %). Darüber hinaus sterben jedes Jahr mehr als 5000 Frauen an dieser Tumorerkrankung, sodass sie ursächlich für 50 % der Krebssterbefälle im gynäkologischen Bereich ist und damit die tödlichste gynäkologische Krebserkrankung in Deutschland darstellt. Diese Daten finden sich in Abbildung 2.

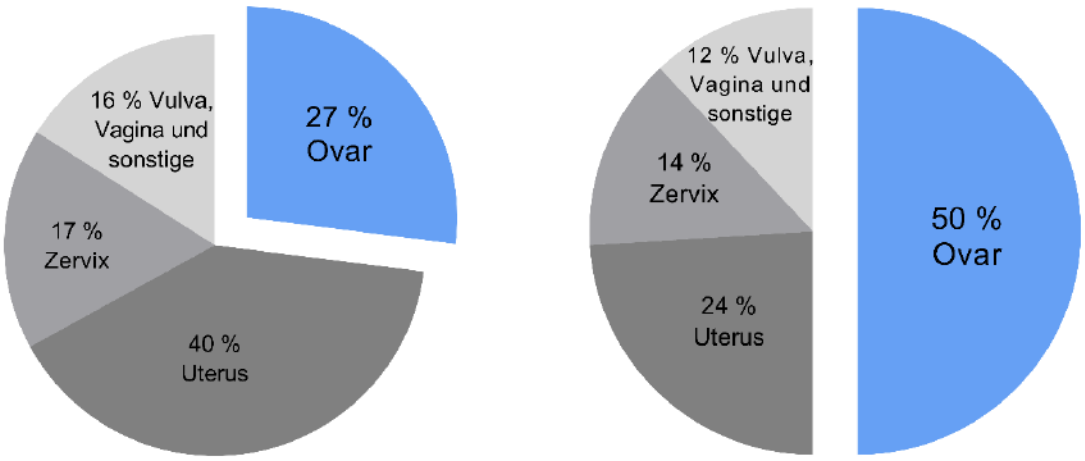

Abbildung 2: Anteil der einzelnen Krebsarten an jährlichen gynäkologischen Neuerkrankungen (links) und Sterbefällen (rechts).

Die Abbildung basiert auf Daten des RKI (8).

Statistisch erkrankt eine von 71 Frauen im Laufe ihres Lebens an Eierstockkrebs – die Erkrankungsraten steigen kontinuierlich mit steigendem Alter an und das mittlere Erkrankungsalter liegt bei 69 Jahren. Nur wenige seltene Eierstockkrebsarten wie zum Beispiel Keimzelltumore treten bereits bei Kindern und jungen Frauen auf. Mit einem Anteil von 54,8 % werden die meisten Erkrankungen als seröse Karzinome klassifiziert, welche überwiegend mäßig bis schlecht differenziert sind. Unter den klassifizierten Krebserkrankungen besitzt das seröse Karzinom mit einer relativen 5-Jahres-Überlebensrate von 40,5 % die schlechteste Prognose. Endometrioide und klarzellige Karzinome weisen mit 7,9 % und 2,7 % einen weitaus geringeren Anteil der gynäkologischen Krebserkrankungen auf. Zusätzlich ist die Prognose mit einer relativen 5-Jahres-Überlebensrate von 68,6 % und 64,4 % deutlich günstiger als bei den serösen Krebsformen. Die Daten zur Epidemiologie von Eierstockkrebserkrankungen in Deutschland wurden der aktuellsten Veröffentlichung des Robert-Koch-Instituts entnommen und haben Stand 2019 (8).

1.3 Therapie des Ovarialkarzinoms

Therapeutische Optionen ergeben sich gemäß der aktuellen Leitlinie der DGGG aus operativen Verfahren, einer systemischen Primärtherapie und einer eventuell notwendigen Rezidivtherapie (4). Im Folgenden werden zunächst operative Therapieoptionen und im Anschluss chemotherapeutische Ansätze, mit besonderem Fokus auf platinhaltige Möglichkeiten auf Basis der DGGG-Leitlinie dargestellt.

1.3.1 Operative Therapie

Sobald frühe Manifestationen einer potenziell hochgradig serösen Tumorerkrankung der Eierstöcke, sogenannte seröse tubare intraepitheliale Karzinome (STIC), nachweisbar sind, soll mit der Patientin die Möglichkeit einer Staging-Operation diskutiert werden. Im Rahmen dieser Staging-Operation kann das gesamte Abdomen inspiziert werden und es können bereits Biopsien verschiedener Gewebsstrukturen genommen werden. Weiterhin besteht die Möglichkeit bei makroskopisch auffälligem Befund sofort invasive Schritte wie die beidseitige Entfernung von Eierstöcken und Eileitern (Adnexexstirpation) durchzuführen, falls eine Fertilitätserhaltung im Rahmen der weiteren Therapie ausgeschlossen ist. Ist das Ovarialkarzinom bei Diagnosestellung allerdings bereits fortgeschritten, empfiehlt die Leitlinie eine makroskopisch vollständige Entfernung des Tumorgewebes im Rahmen einer Operation. Sollte dies nicht möglich sein, kommt eine Debulking-Operation zur möglichst starken Verringerung der Tumormasse zum Einsatz. Die klinische Prognose korreliert direkt mit der verbleidenden Tumormasse nach der Primäroperation. Nach erfolgter Primäroperation soll eine anschließende Chemotherapie durchgeführt werden.

1.3.2 Chemotherapeutische Optionen

Die Standard-Chemotherapie des fortgeschrittenen Ovarialkarzinoms besteht aus einer kombinierten Behandlung eines Platin-Zytostatikums und Paclitaxel (Mitosehemmstoff; hemmt den Abbau der Mikrotubuli während der Zellteilung). Als Platin-Zytostatikum wird bevorzugt Carboplatin verwendet, da es in der klinischen Anwendung ein besseres Profil hinsichtlich der unerwünschten Arzneimittelwirkungen als Cisplatin aufweist. Es wird allerdings auf die äquivalente Effektivität von

Carboplatin und Cisplatin hingewiesen. Bei HGS-Tumoren kann die duale Kombination um Bevacizumab erweitert werden. Dabei handelt es sich um einen therapeutischen Antiköper, der gegen VEGF (vaskulärer endothelialer Wachstumsfaktor) gerichtet ist. Somit wirkt Bevacizumab als Angiogenesehemmer. Damit konnte das Gesamtüberleben in Studien signifikant verbessert werden, wobei mit dieser Therapie auch eine geringe Verschlechterung der Lebensqualität einhergeht (9,10). Die Ursachen der Verringerung der Lebensqualität konnte durch systematische Befragung von Patientinnen im Rahmen einer Studie nicht vollständig geklärt werden und scheint daher multifaktoriell zu sein (11).

Sollte es bei einer erkrankten Patientin zu einer Rezidivbildung kommen, ist es für die weitere Therapie essenziell, ein platingeeignetes Rezidiv ohne bestehende Platin-Resistenz von einem nicht-platingeeignetem Rezidiv mit bestehender Platin-Resistenz zu unterscheiden. Früher wurde zur Klassifizierung der Zeitpunkt des Rezidivs nach der letzten Platin-Dosis (platin-freies Therapieintervall) verwendet und der Schwellenwert lag bei 6 Monaten. In die Entscheidung sollten nach momentanem Stand die Therapiepräferenz der Patientin, ihr Alter, ihre Belastbarkeit, genetische Faktoren und weitere tumorbiologische Aspekte einbezogen werden. Patientinnen, welche während der Primärtherapie nicht mit einem platinhaltigen Zytostatikum behandelt wurden, gelten stets als platinsensitiv und das Ziel der Rezidivtherapie ist die Verlängerung des progressionsfreien Überlebens. Liegt ein platinresistentes Rezidiv vor, sind Symptomkontrolle und Lebensqualitätserhaltung zentrale Therapieziele. Bei einem platinresistenten Rezidiv wird im Allgemeinen eine erneute Monochemotherapie mit Doxorubicin (DNA-Interkalator), Topotecan (Hemmstoff der Topoisomerase I), Gemcitabin (Antimetabolit) oder Paclitaxel erwogen. Zur zytostatischen Therapie eines platinsensitiven Rezidivs werden Carboplatin-haltige Kombinationstherapien empfohlen. Es kann mit Gemcitabin (+ Bevacizumab), Paclitaxel (+ Bevacizumab) oder Doxorubicin kombiniert werden. Durch die Addition von Bevacizumab zu den jeweiligen Dualkombinationen konnte das progressionsfreie Überleben gesteigert werden. Dieser Zusatz kommt allerdings nur für Patientinnen in Frage, welche ihr erstes Rezidiv erfahren und noch keine anti-VEGF-Therapie erhalten haben.

Liegen bei HGS-Tumorpatientinnen Mutationen der Gene BRCA1 bzw. BRCA2 (Brustkrebsgen 1/2) vor, kann grundsätzlich eine Therapie mit PARP-Inhibitoren (PARPi) in Betracht gezogen werden. Die meisten Daten liegen für den PARPi

Olaparib vor. Grundsätzlich sind BRCA1/2 Tumorsuppressorgene. Eine Funktionsverlustmutation oder Deletion eines dieser beiden Gene ist ein wichtiger Indikator für eine gestörte DNA-Reparatur der Zelle und befördert somit die Tumorinitiation. BRCA-Mutationen spielen bei gynäkologischen Tumoren eine wichtige Rolle. Eine verringerte Kapazität der Tumorzelle hinsichtlich der DNA-Reparatur ist grundsätzlich vorteilhaft für eine zytostatische Therapie mit platinhaltigen Chemotherapeutika wie Carboplatin oder Cisplatin (12,13). Die Tumorzelle reagiert auf diesen Stress mit der Aktivierung anderer DNA-Reparaturmechanismen wie beispielsweise der Aktivierung des Proteins PARP (Poly-ADP-Ribose-Polymerase). Zur Verhinderung dieses Umgehungsmechanismus werden PARPi bei Patientinnen mit platinsensitivem Primärtumor sowie vorhandener BRCA-Mutation als Erhaltungstherapie eingesetzt. Diese Empfehlung existiert ebenfalls für HGS-Patientinnen, welche ein Rezidiv erfahren, das auf eine platinhaltige Rezidivtherapie anspricht.

Platinhaltige Zytostatika haben einen hohen Stellenwert in der Therapie des hochgradig serösen Ovarialkarzinoms und dessen Rezidiven. Allerdings werden platinhaltige Regime niemals als Monotherapie appliziert, sondern stets als Komponente einer Kombinationstherapie. Für Cisplatin-sensitive Rezidive von Ovarialkarzinomen konnte in einer Metastudie gezeigt werden, dass sowohl das Gesamtüberleben als auch das progressionsfreie Intervall durch eine Kombinationstherapie verglichen mit einer Platin-Monotherapie verbessert wurde (14). Diese Kombinationstherapien weisen einige Vorteile auf. Zum einen besteht die Möglichkeit, bei vorliegendem Synergismus der Kombinationspartner die Dosen der einzelnen Komponenten zu verringern, was in der Regel mit einer geringeren Frequenz und Intensität der unterwünschten Arzneimittelwirkungen ohne Einbuße der Wirksamkeit einhergeht. Dieser Vorteil zeigt sich auch bei additiven Interaktionen der Komponenten, ist allerdings weniger stark ausgeprägt. Durch die Kombinationstherapien können mehrere Signaltransduktionswege gleichzeitig beeinflusst werden. Dies erschwert zum einen den Crosstalk zwischen unterschiedlichen Signalkaskaden, zum anderen können auf diese Art die Aktivierung von Umgehungs- oder Reparaturmechanismen erschwert oder gar inhibiert werden. Somit könnte die Resistenzbildung gegenüber den platinhaltigen Komponenten verhindert und ihre gute klinische Wirksamkeit erhalten werden.

1.4 Platinhaltige Therapieregime

Wie zuvor erwähnt, weisen Cisplatin und Carboplatin die gleiche klinische Effektivität hinsichtlich der chemotherapeutischen Therapie von Ovarialkarzinomen auf. Aufgrund des vorteilhafteren Profils hinsichtlich der unerwünschten Arzneimittelwirkungen, empfiehlt die aktuelle Leitlinie zur Diagnostik, Therapie und Nachsorge maligner Ovarialtumoren die Verwendung von Carboplatin (4). Ausschlaggebend ist hier die Lebensqualität der Patientinnen. Der Wirkmechanismus von Cisplatin und Carboplatin ist hinsichtlich ihrer Bildung von DNA-Addukten identisch und es besteht eine Kreuzresistenz (15–17). Die Studien im Rahmen dieser Dissertation wurden mit Cisplatin durchgeführt. Daher wird es im folgenden Kapitel fokussiert behandelt.

1.4.1 Cisplatin

1844 wurde die Verbindung *cis*-Diammindichloridoplatin-II $[Pt(NH_3)_2Cl_2]$ (Abbildung 3) vom italienischen Chemiker Michele Peyrone erstmals synthetisiert und ist heute unter dem Namen Cisplatin und der Abkürzung cDDP bekannt.

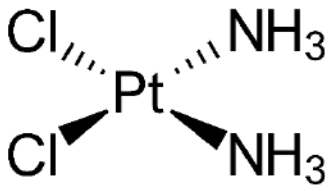

Abbildung 3: Cisplatin.

Die damalige Synthese erfolgte im Rahmen der Erforschung von komplexchemischen Vorgängen und hatte keinen medizinisch-therapeutischen Hintergrund. Die Entdeckung der zytostatischen Wirkung erfolgte rein zufällig Mitte der 1960er-Jahre durch den amerikanischen Biophysiker Barnett Rosenberg. Im Rahmen seines Experimentes setzte er *Escherichia coli* Bakterien einem elektrischen Wechselstromfeld mithilfe von Platinelektroden und Ammoniumchlorid-Puffer aus. Er stellte fest, dass die Bakterien auf das bis zu 300-fache ihrer üblichen Länge anwuchsen, ohne dass Zellteilung stattfand. Zunächst vermutete er ursächlich den Einfluss des elektrischen Feldes auf die Zellteilung. Dies erwies sich als inkorrekt. Er konnte beweisen, dass sich Platin der Elektroden ablöste und unter seinen Experimentalbedingungen zu dem zytostatischen Platinkomplex umsetzte. Ende der 1960er-Jahre konnte Rosenberg in Tierversuchen eine antitumorale Aktivität von

Cisplatin zeigen. Anfang der 1970er-Jahre wurden die ersten Studien in Amerika zur Behandlung von Hoden- und Eierstock-Krebs mit Cisplatin durchgeführt und 1978 wurde es von der FDA zur Behandlung ebendieser Krebsentitäten zugelassen. Cisplatin wurde damit weltweit zum ersten metallbasierenden chemotherapeutisch eingesetzten Arzneistoff. 1979 folgten Zulassungen in Großbritannien und Europa (18). In den folgenden Jahren bzw. Jahrzehnten wurde der Einsatz von Cisplatin stetig erweitert. Es zählt weiterhin zu den gängigsten Chemotherapeutika und ist auf der erweiterten komplementären Liste der unentbehrlichen Arzneimittel der WHO gelistet (Stand 2019, 21. Fassung der WHO-Liste).

Da Cisplatin infolge der im Gastrointestinaltrakt stattfindenden Hydrolyse oral nicht bioverfügbar ist wird es parenteral (intravenös) appliziert. Der Mechanismus der Aufnahme von Cisplatin in die Tumorzelle ist nicht abschließend geklärt. Zunächst wurde als maßgeblicher Influx-Mechanismus passive Diffusion angenommen, da die Aufnahme in die Zelle über die erste Zeit annähernd linear stattfindet (19). Da an Ovarialkarzinomzellen gezeigt werden konnte, dass es bei vorhandener Mutation des Kupfertransporters CTR1 zu einer Akkumulation von Cisplatin in der Zelle kommt, scheinen Influx und Efflux von Cisplatin in Verbindung mit der Kupfer-Homöostase der Zelle zu stehen (20). Das Bestreben Cisplatins mit seinen molekularen Zielstrukturen in Wechselwirkung zu treten wird durch diese Akkumulation allerdings nicht moduliert. So wurde beispielsweise gezeigt, dass eine intrazelluläre Akkumulation von Cisplatin nicht in direktem Zusammenhang mit dem Platinierungsgrad der DNA steht. Weiterhin konnte gezeigt werden, dass eine Überexpression von Kupfertransportern zu einer Cisplatin-Resistenz der Zelle führen. Prominente Efflux-Transporter sind ATP7B (Wilson-Protein, engl. *Copper-transporting P-type adenosine triphosphate*) (21) und MRP2 (engl. *Multidrug resistance-associated protein 2*) (22). Kupfer und Cisplatin behindern gegenseitig ihren Influx und verursachen die Degradierung bzw. Internalisierung von CTR1 (23–25).

Bei Cisplatin handelt es sich um ein Prodrug, das nach intrazellulärer Aufnahme aufgrund der dort niedrigeren Chloridionen-Konzentration bioaktiviert wird. Es bilden sich Mono- oder Di-Aqua-Komplexe ($[Pt(NH_3)_2Cl(OH_2)]^+$ bzw. $[Pt(NH_3)_2(OH_2)_2]^{2+}$) durch den Austausch der Chlorid-Liganden (Abbildung 4) (26).

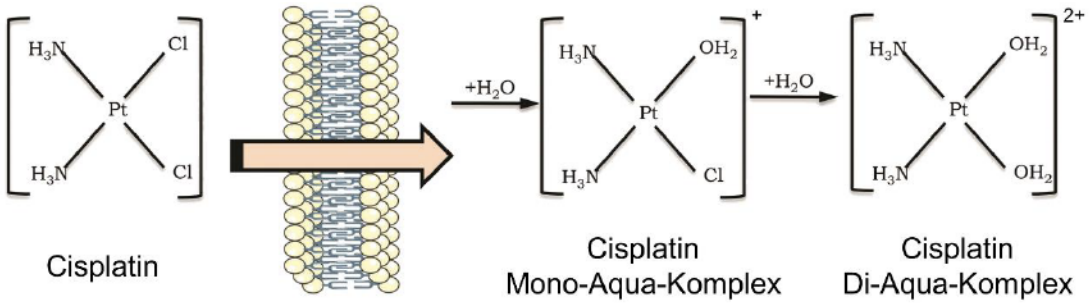

Abbildung 4: Intrazelluläre Aktivierung von Cisplatin.

Die Abbildung wurde aus (26) übernommen.

Die Aqua-Komplexe des Cisplatins sind gegenüber Nucleophilen wie der DNA, im Gegensatz zu nicht aktiviertem Cisplatin, reaktiv. Dies ist auf eine erhöhte Elektrophilie und dem damit verbundenen Elektronenmangel des Platin-Zentralatoms zurückzuführen. Die aktive Form von Cisplatin bildet mit den N^7-Stickstoffen der Purinbasen Adenin und Guanin Addukte und führt entsprechend zu Quervernetzungen. In rund 95 % der Fälle bilden sich mit 1,2- bzw. 1,3-Intrastrang-Addukten Quervernetzungen innerhalb eines DNA-Stranges. In den restlichen Fällen bilden sich Interstrang-Quervernetzungen zwischen zwei DNA-Strängen (Abbildung 5) (26).

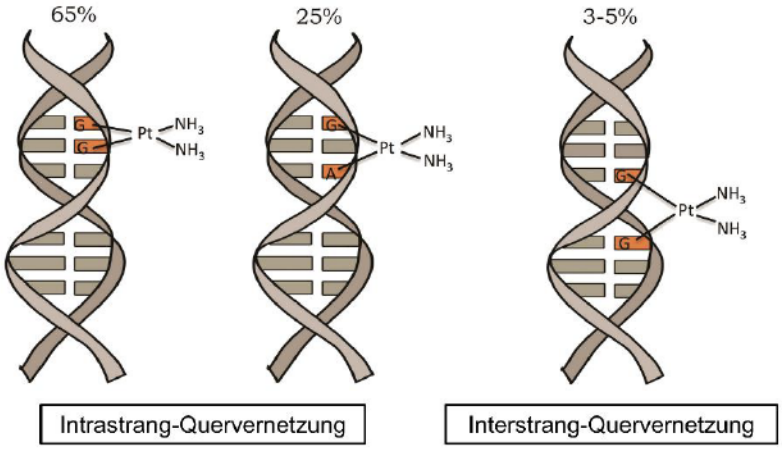

Abbildung 5: DNA-Addukte von Cisplatin.

Die Abbildung zeigt die Häufigkeiten des Auftretens der DNA-Addukte, welche sich mit Cisplatin bilden können. Diese sind als Prozentangaben über der jeweiligen Darstellung angegeben. Die Abbildung wurde übersetzt und aus (26) übernommen.

Cisplatin führt im Zuge der zellulären Reaktion auf die DNA-Schädigung (engl. *DNA Damage Response [DDR]*) über verschiedene Signalwege zur Apoptose der Zelle. Als Reaktion auf Cisplatin wird beispielsweise der Tumorsuppressor p53 aktiviert. Dies aktiviert DNA-Reparaturmechanismen, die bei irreparablen DNA-Schäden Apoptose auslösen. Als Konsequenz wird p21 aktiviert, was zu einem Zellzyklus-Arrest in der G_1-Phase mit anschließender Apoptose führt. Die Aktivierung

von p53 initiiert zusätzlich eine vermehrte Expression von PUMA (engl. *p53 upregulated modulator of apoptosis*), welches inhibierend auf antiapoptotische Proteine der Bcl-2-Familie (z.B. Bcl-xL) wirkt. Durch diesen Stimulus werden proapoptotische Proteine dieser Familie freigesetzt (z.B. BAK) und führen zum Verlust des Membranpotentials der Mitochondrien. Die Mitochondrienmembran wird permeabilisiert und Cytochrom C tritt aus. Freigesetztes Cytochrom C ist nun in der Lage, das cytosolische Protein APAF1 (engl. *Apoptotic protease activating factor 1*) zu aktivieren. APAF1 bildet das Apoptosom, welches zur Aktivierung der Caspase-Kaskade führt und damit ultimativ die Apoptose einleitet. Das antiapoptotische Protein Survivin wird durch die Aktivierung von p53 gehemmt und kann somit nicht mehr inhibierend auf verschiedene Caspasen wirken. In der Literatur sind zahlreiche weitere Signaltransduktionswege beschrieben, über welche Cisplatin zum Zelltod führt. So können diverse Kinasen wie AKT, c-ABL, MAPK, JNK oder ERK an der intrazellulären Transduktion des DNA-Schaden-Signals beteiligt sein (23). Auch wenn Cisplatin in extrem hohen Dosen zum Zelltod per Nekrose führen kann, ist die übliche Reaktion der Zelle unter therapeutischen Konzentrationen ein Niedergang durch Apoptose (23).

Gemäß den Angaben einer beispielhaften Fachinformation einer Cisplatin-Infusionslösung wird Cisplatin im menschlichen Körper schnell mit Ausnahme des zentralen Nervensystems in allen Geweben verteilt. Besonders hohe Konzentrationen werden demnach in Leber, Nieren, Blase, Muskelgewebe, Haut, Hoden, Prostata, Pankreas und Milz erreicht. Wie alle Zytostatika weist Cisplatin unerwünschte Arzneimittelwirkungen in erhöhter Frequenz und Intensität auf. Besonders hervorzuheben sind dosisabhängige Schädigungen der Nieren (Nephrotoxizität), der Ohren (Ototoxizität) und des Knochenmarks (Neurotoxizität), welche bei rund einem Drittel der Patienten gemeldet wurden. Vor allem die Nephrotoxizität bildet eine dosis- und damit unter Umständen auch eine therapielimitierende unerwünschte Arzneimittelwirkung. Bei mehr als 10 % der Behandelten führt die Therapie zu unerwünschten gastrointestinalen Wirkungen wie Übelkeit, Erbrechen und Durchfall. Cisplatin liegt zu 90 % an Plasmaproteine gebunden vor, wodurch die Halbwertszeit entsprechend erhöht wird. Die Elimination von Cisplatin verläuft dreiphasig und weist Halbwertszeiten von rund einer Viertelstunde (initiale Eliminierung) bis zu mehr als fünf Tagen (an Plasmaproteine gebundenes Cisplatin) auf. Die Eliminierung von Cisplatin erfolgt überwiegend renal. Es kann allerdings auch über die Gallenwege ausgeschieden werden (27).

1.4.2 Entwicklung einer Cisplatin-Resistenz

Neben den bereits erwähnten unerwünschten Arzneimittelwirkungen stellt die Resistenzentwicklung im Laufe einer Cisplatin-Therapie ein weiteres therapielimitierendes Problem dar. Wie am Anfang beschrieben wird die Einteilung eines Ovarialkarzinoms in Platin-sensitiv oder Platin-resistent im klinischen Kontext besonders wichtig, wenn es um die Behandlung von Rezidiven geht. Die Gynäkologische Onkologie Gruppe (GOG; US-amerikanische Non-Profit-Organisation) teilt die Chance auf Ansprechen eines Rezidivs auf eine Platin-haltige Chemotherapie auf Basis des Abstands des letzten Platin-haltigen Chemotherapiezyklus und der Rezidiv-Diagnose (Platin-freies Intervall) ein. Wird ein Rezidiv innerhalb von 4 Wochen diagnostiziert, liegt die Chance auf Erfolg mit einer Platin-haltigen Chemotherapie bei 0 %. Ein Ovarialkarzinom wird als Platin-resistenz klassifiziert, wenn es nach 6 Monaten zu einem Rezidiv kommt und die Erfolgsrate einer erneuten Platin-haltigen Chemotherapie wird auf unter 10 % geschätzt. Tritt ein Rezidiv im Zeitraum von 6 bis 12 Monaten nach dem letzten Platin-haltigen Zyklus auf, wird es zum einen als partiell Platin-resistent bezeichnet und zum anderen liegt die Ansprechrate auf eine erneute Platin-haltige Behandlung bei rund 30 %. Ein Platin-sensitives Rezidiv zeichnet sich dadurch aus, dass es frühestens 12 Monate nach der letzten Platin-haltigen Chemotherapie auftritt. Es weist mit mehr als 50 % die besten Erfolgschancen beim erneuten Einsatz einer Platin-haltigen Therapie auf (28). Als Konsequenz eines Ovarialkarzinoms, welches entweder intrinsisch schwierig mit Platin-haltigen Zytostatika zu behandeln ist (also ein frühes Rezidiv bildet) oder in einem kurzen Zeitabstand nach Platin-haltiger Chemotherapie ein Rezidiv ausbildet muss auf Second-Line-Therapien zurückgegriffen werden. Diese haben individuelle Nebenwirkungen und stellen nicht die gewünschte Therapieoption gemäß Leitlinie dar, wie zu Beginn bereits erläutert wurde (4). Rund 20-25 % der Patientinnen mit einem Ovarialkarzinom nach FIGO I-II erfahren einen Rückfall. Für Patientinnen, deren Primärtumor in FIGO III-IV einzuordnen war, liegt die Rezidiv-Quote bei etwa 70 %. Das mediane Intervall für das Auftreten eines ersten Rezidivs liegt bezogen auf Ovarialkarzinome zwischen 18 und 24 Monaten (29).

Die Resistenzentwicklung gegenüber Cisplatin stellt also bei Ovarialkarzinomen ein Problem mit potenziell schwerwiegenden therapeutischen Folgen dar. Galluzzi et al. definieren vier Kategorien von zellulären Mechanismen, die zu einer Cisplatin-Resistenz führen können:

- *pre-target:* Resistenzen, die vor Erreichen der DNA auftraten,
- *on-target:* Resistenzen, die in direktem Zusammenhang mit der (Reaktion auf die) DNA-Schädigung stehen,
- *post-target:* Resistenzen, die Veränderungen in der nachgeschalteten Signaltransduktion betreffen und
- *off-target:* Resistenzen, die durch eine Veränderung von zellulären Regelprozessen ausgelöst werden, die nicht direkt mit Cisplatin in Verbindung gebracht werden können (30,31).

Die detaillierte Beschreibung der verschiedenen Arten der Cisplatin-Resistenz richtet sich folgend nach der Einteilung von Galluzzi et al.

Pre-target Resistenzen lassen sich am besten dadurch beschreiben, dass die Tumorzelle über verschiedene Mechanismen versucht, entweder den Influx von Cisplatin zu verringern oder dessen Efflux bzw. Eliminierung zu erhöhen. Vor allem Veränderungen der zellulären Ausstattung an Influx-Transportern wie CTR1 oder Efflux-Transportern wie ATP7B oder MRP2 führen zu problematisch geringen Cisplatin-Konzentrationen innerhalb der Zelle. Auch wenn eine steigende Akkumulation von Cisplatin den zytotoxischen Effekt nicht endlos steigert (20), muss eine gewisse Konzentration überschritten werden, damit Eliminierungsprozesse der Zelle nicht zu viel Cisplatin inaktivieren oder entfernen. Sowohl die Veränderung der Expression der genannten Transporter als auch eine veränderte Lokalisation innerhalb der Zelle wurde mit einer Cisplatin-Resistenz in Verbindung gebracht. Weiterhin kann die Elimination von Cisplatin durch erhöhte Spiegel von Glutathion (GSH), Glutamatcysteinligase (GCL; Enzym, welches GSH-Bildung katalysiert) oder Glutathion-S-Transferasen (GST; Enzyme, welche Cisplatin und GSH verbinden) gesteigert werden (32,33). Während Veränderungen an CTR1 und ATP7B eine bewiesene klinische Relevanz besitzen, konnte diese für die anderen Transporter oder Enzyme bisher nicht gezeigt werden (20,25,30,34). Zeigen Tumore eine Überexpression von CTR1, verlängert sich das progressionsfreie Intervall und das Gesamtüberleben der Patientinnen signifikant (35). Analog weisen Patientinnen mit ATP7B-positiven Tumoren eine schlechtere klinische Prognose im Sinne einer schlechteren Gesamt-Überlebensrate und Verkürzung des progressionsfreien Intervalls auf (34).

Weist ein Tumor eine Cisplatin-Resistenz basierend auf einer *on-target* Resistenz auf, so liegen meist Veränderungen in der Reaktion auf den Cisplatin-induzierten DNA-Schaden vor. An der Detektion und dem Versuch der Reparatur dieser Schäden sind vor allem das NER-System (engl. *nucleotide excision repair*) (36) und das MMR-System (engl. *DNA mismatch repair*) (37) beteiligt. Eine Überaktivierung des NER-Systems (ausgedrückt durch eine Überexpression des DNA-Exzisionsreparaturproteins 1 [ERCC1]) zeigt klinische Relevanz, da sie mit einer verringerten Überlebensrate der Patienten einhergeht (38,39). Unter normalen Umständen ist das MMR-System nicht in der Lage den verursachten DNA-Schaden zu reparieren. Als Konsequenz werden proapoptotische Signalwege ausgelöst (40). Daher führt eine verringerte Expression der Komponenten der MMR in der Regel zu einer Cisplatin-Resistenz, da die verursachten DNA-Schäden nicht mehr unbedingt zur Auslösung der Apoptose führen. Cisplatin kann nach Bildung der DNA-Addukte zu Doppelstrangbrüchen führen, welche im Rahmen der DNA-Synthese oder der homologen Rekombination (HR) repariert werden sollten. Vor allem Veränderungen der Proteine BRCA1 und BRCA2, welche an der HR beteiligt sind, haben einen Einfluss auf die Cisplatin-Sensitivität der Zelle: während funktionseinschränkende Mutationen dieser Proteine zu einer Erhöhung der Cisplatin-Sensitivität führen, führen funktionssteigernde Mutationen zu einer Cisplatin-Resistenz (12,13,41).

Post-target Resistenzen sind in der Regel nicht spezifisch für Cisplatin. Die zugrundeliegenden Mechanismen lassen sich auch bei anderen DNA-schädigenden Verfahren (wie Bestrahlung) oder Zytostatika beobachten. Da eine maligne Zelle per Definition eine gewisse Resistenz gegenüber proapoptotischen Signalen aufweist (42), können die angesprochenen Mechanismen vermehrt festgestellt werden. Grundsätzlich wird eine Zelle zur Aufrechterhaltung der Zell-Homöostase zunächst versuchen, entstandene Schäden zu reparieren. Schlägt dies allerdings fehl, werden proapoptotische Signale weitergeleitet, um die Homöostase des gesamten Organismus aufrechtzuerhalten (43,44). Im Falle Cisplatins wechselt die MMR vom zytoprotektiven in den zytotoxischen Modus, was oft zu einer p53-abhängigen Einleitung der Apoptose und einer Akkumulation von reaktiven Sauerstoffspezies (ROS) führt. Beide Wege führen zum Zusammenbruch des Potentials der äußeren Mitochondrienmembran und ihrer Permeabilisation, was ein potenter apoptotischer Stimulus ist. Somit stellt beispielsweise eine funktionsmindernde Mutation von p53 eine Möglichkeit für eine *post-target* Resistenz dar, da die apoptotische

Signaltransduktion in diesem Fall früh gestört wird. Auch Veränderungen hinsichtlich der Expression von Proteinen der Bcl-2-Familie (z.B. Bcl-2, Bcl-xL und Mcl-1) oder Caspasen, welche eine wichtige Rolle in der finalen Ausführung der Apoptose spielen, stellen potenzielle Resistenzmechanismen dar. Das Protein Survivin, welches die Aktivität der Caspasen hemmt, ist als Reaktion auf Cisplatin-Stress bei manchen Tumorarten verstärkt exprimiert (30). Dies konnte zum Beispiel für Tumore des Magens, der Lunge und des Ösophagus gezeigt werden (45–47).

Unter *off-target* Resistenzen werden Überlebensmechanismen der Zelle kategorisiert, welche nicht direkt auf Cisplatin oder dessen ausgelösten Stress zurückzuführen sind. Ziel der malignen Zelle ist es eine verstärkte proliferative und anti-apoptotische Signaltransduktion aufrecht zu erhalten. Dies ist zum Beispiel durch die Überexpression von Wachstumsfaktorrezeptoren wie ErbB-2 und die damit verbundene verstärkte proliferationsfördernde Signaltransduktion über den PI3K-AKT-Signalweg möglich. Diese ErbB-2-Überexpression kann häufig in gynäkologischen Tumoren nachgewiesen werden (48). Auch ein verstärkter Abbau von ROS über die verstärkte Expression von Antioxidantien ist ein möglicher Mechanismus (30).

Die Entwicklung einer Cisplatin-Resistenz ist demnach ein multifaktorielles Geschehen. In der Regel findet sich in einer resistenten Zelle bzw. einem resistenten Tumor nicht nur ein aktivierter Resistenzmechanismus. So wird dem Tumor weiteres Wachstum trotz Einwirkens von Cisplatin ermöglicht, da diverse Umgehungsmechanismen in Kraft gesetzt werden können, um entweder eine Schädigung der DNA durch Cisplatin direkt zu verhindern, den eventuell verursachten Schaden zu reparieren oder den Zelltod über andere Wege zu verhindern. Aus dieser Erkenntnis ergibt sich die Rationale Cisplatin mit anderen Wirkstoffen zu kombinieren, welche einzelne oder mehrere Resistenzmechanismen adressieren und entsprechend inhibieren sollen.

Im Rahmen dieser Arbeit wurden verschiedene Ansätze zur Senkung der Cisplatin-Resistenz bzw. Erhöhung der Cisplatin-Sensitivität verschiedener Ovarialkarzinomzelllinien verfolgt. Ziel aller Kombinationsbehandlung war es, mehrere wichtige Punkte in der Ausbildung einer Cisplatin-Resistenz zu adressieren. Die verschiedenen Ansätze sind in Abbildung 6 dargestellt.

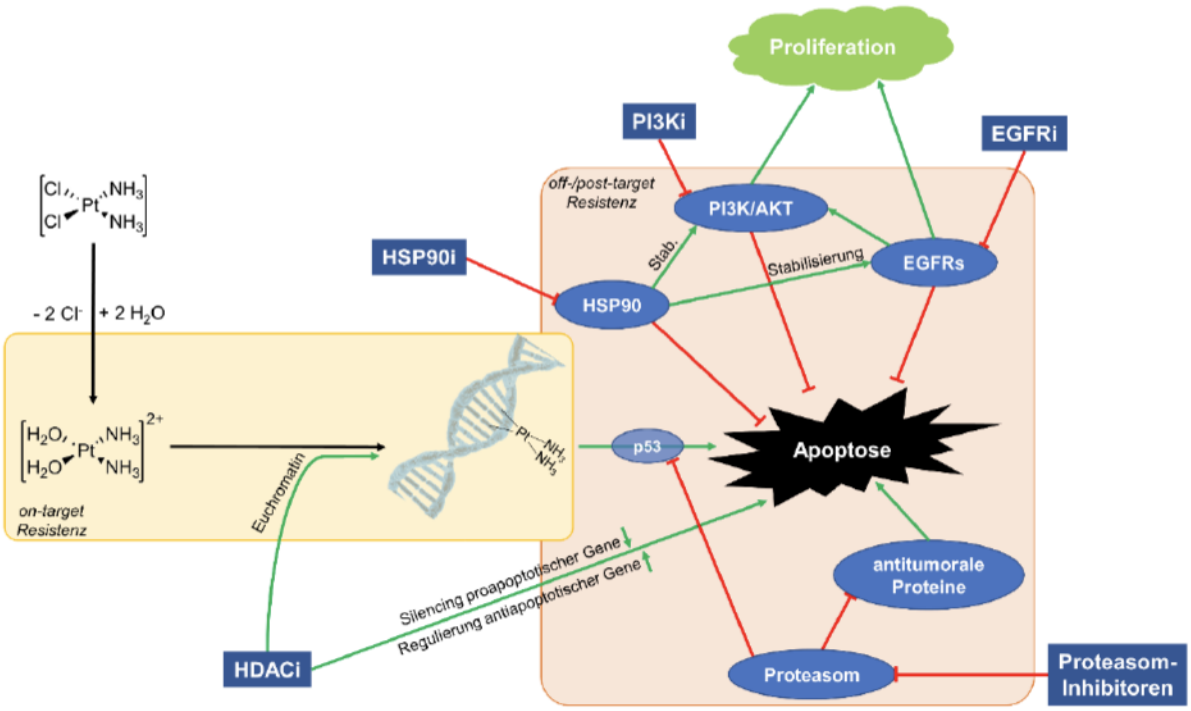

Abbildung 6: Darstellung wichtiger Angriffspunkte der Kombinationstherapien dieser Arbeit.

Die Abbildung zeigt verschiedene zelluläre Angriffspunkte, die im Rahmen dieser Arbeit als Teile von Kombinationstherapien adressiert wurden. Grüne Pfeile stehen für einen positiven/verstärkenden Effekt und rote Pfeile für einen inhibierenden/schwächenden Effekt.

Anhand der dargestellten multifaktoriellen Natur der Cisplatin-Resistenz, wurden Inhibitoren von Histondeacetylasen, Hitzeschockprotein 90, epidermalem Wachstumsfaktorrezeptoren, Phosphoinositid-3-Kinasen und des Proteasoms eingesetzt. So sollten sowohl *on-target* als auch *off-* bzw. *post-target* Resistenzen bekämpft werden. Die Inhibitoren sowie deren Einfluss auf die Modulation der Cisplatin-Resistenz von Ovarialkarzinomen sollen im Folgenden sowie im Ausblick näher erläutert werden.

1.5 *Targeted Therapies* zur Modulation der Cisplatin-Resistenz

1.5.1 Epigenetik

Der Begriff *Epigenetik* wurde in den 1940er-Jahren vom Entwicklungsbiologen und Genetiker Conrad H. Waddington geprägt. Er definierte Epigenetik als Veränderungen im Phänotyp eines Organismus, ohne dass eine entsprechende Änderung im Genotyp festgestellt werden konnte (49). Zur damaligen Zeit herrschte ein minimales Verständnis der zugrundeliegenden Mechanismen. Mehrere Jahrzehnte später ist klar, dass epigenetische Mechanismen regulatorisch auf die Genexpression wirken, indem sie Einfluss durch chemische Modifikationen auf das Chromatin bzw. Histone oder direkt auf die DNA ausüben (49–51).

Im Nukleosom werden DNA-Abschnitte zu jeweils 146 Basenpaare um ein Histon-Oktamer gewunden. Durch diese räumliche Komprimierung verringert sich die Länge des DNA-Abschnitts auf rund ein Siebtel. Ein Histon-Oktamer besteht aus jeweils zwei Proteinen der Histone H2A, H2B, H3 und H4. Eine Aneinanderreihung von mehreren Nucleosomen wird Chromatin genannt, welches sich räumlich zum Chromosom zusammenlagert. Die unterschiedlichen Zustände zwischen DNA und räumlich komprimierter DNA sind in Abbildung 7 dargestellt.

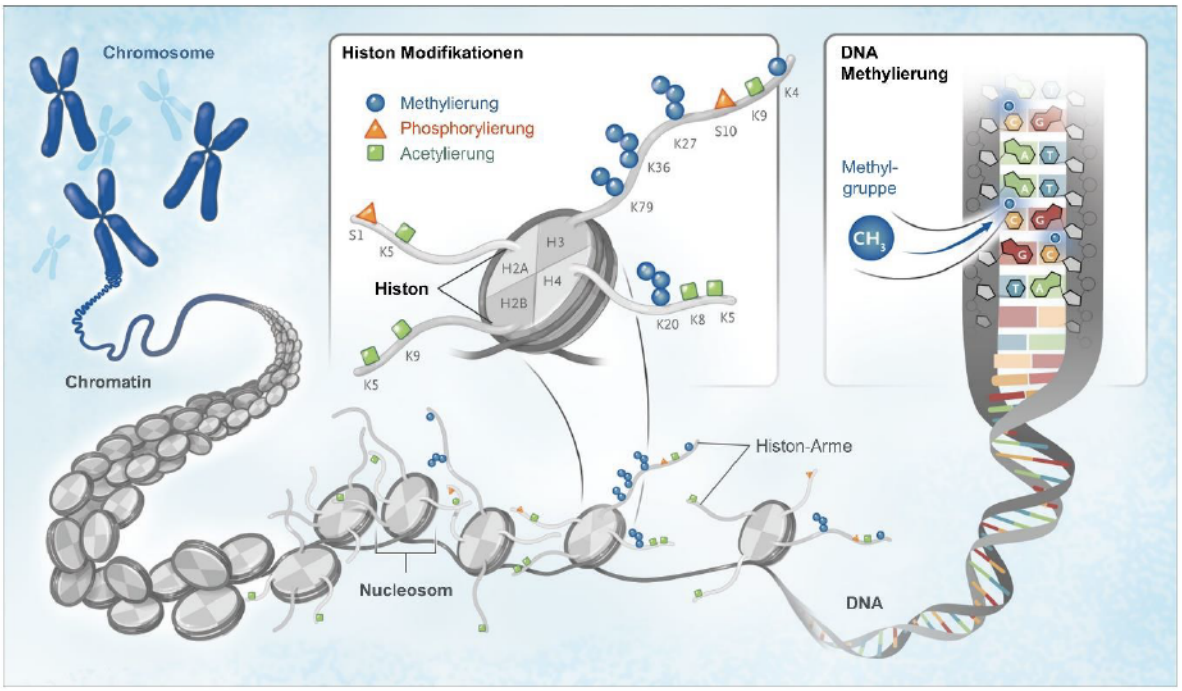

Abbildung 7: Räumlicher Aufbau des Chromatins und Modifikationen.

Die Abbildung wurde übersetzt uns aus (50) übernommen.

In Abbildung 7 sind ebenfalls die gängigsten epigenetischen Modifikationen der Histone bzw. der DNA dargestellt. Die Enzyme, welche an epigenetischen

Modifikationen beteiligt sind, werden in die vier folgenden Gruppen eingeteilt: *Writer* („Schreiber"), *Eraser* („Löscher"), *Reader* („Leser") und *Mover* („Beweger"). *Writer* fügen Modifikationen hinzu und bestehen zum Beispiel aus DNA-Methyltransferasen (DNMTs), Histonmethyltransferasen (HMTs) und Histonacetyltransferasen (HATs). Im Gegensatz dazu entfernen *Eraser* entsprechende Modifikationen und bestehen aus Histondemethylasen (HDMs) und Histondeacetylasen (HDACs). Zur Gruppe der *Reader* gehören Proteine, welche in der Lage sind, den Acetylierungsstatus der Histone (Bromodomain-Proteine) oder den Methylierungsstatus der DNA (Chromodomain-Proteine) zu lesen und in Signaltransduktion zu übersetzen. Eine Umstrukturierung des Chromatins durch Verschiebung von Nucleosomen kann durch Proteine der *Mover*-Gruppe vorgenommen werden. Dazu zählen zum Beispiel: ARID1A/1B/2 (*AT-rich interactive domain-containing protein 1A/1B/2)* oder die ATP-abhängigen Chromatin Umstrukturierungsproteine SMARCA2/A4/B1.

Der Methylierungsstatus der DNA und posttranslationale Modifikationen der Histone sind essentiell für die Regulation der Genexpression, da zum einen die Erreichbarkeit bestimmter Genabschnitte für die Transkriptions-Maschinerie gesteuert wird und zum anderen auch die direkte Funktionsfähigkeit der Gene beeinflusst werden kann (50).

Eine Hypermethylierung der DNA in entsprechenden Promoter-Regionen kann zur Inaktivierung von Tumorsuppressor-Genen oder dem Stilllegen diverser anderer Gene in malignen Zellen führen. Eine Methylierung der DNA findet in der Regel an Position 5 der Base Cytosin unter der Bildung von 5-Methylcytosin (5mC) statt. Besonders häufig kann die Bildung von 5mC in CpG-Inseln nachgewiesen werden, also Bereichen der DNA, in welchen das Dinukleotid aus Cytosin und Guanin gehäuft vorkommt. Gene, welche in Verbindung zum gynäkologischen Krebsgeschehen stehen und durch eine Hypermethylierung der CpG-Insel in der entsprechenden Promoter-Region stillgelegt werden können, codieren beispielsweise für BRCA1, CDKN2A/2B (Inhibitoren Cyclin-abhängiger Kinasen, welche als Tumorsuppressoren wirken (52)) oder den Estrogenrezeptor 1 (ESR1) (53). So zeichnen sich aggressive Karzinome des Endometriums (Typ II) durch eine verringerte Expression von ESR1 aus und zeigen eine schlechtere klinische Prognose (54,55). Als zugrundeliegender Mechanismus wird in der Literatur diskutiert, dass ESR1-negative Tumorzellen eines Endometriumkarzinoms vermehrte Resistenz gegenüber der Einleitung der Apoptose

aufweisen und eine erhöhte Tendenz zur Invasion benachbarten Gewebes zeigen (56–58).

Die Störungen der Homöostase epigenetischer Regulation ist daher eine Kerneigenschaft von malignen Zellen (59). Eine Rationale epigenetischer Therapieansätze besteht demnach in der Normalisierung von Methylierungsmustern der DNA bzw. des Modifikationszustandes der Histone, um die Eigenschaften eines malignen Phänotyps zu modulieren (49). Für die Beeinflussung von *Writer*- und *Eraser*-Proteinen sind momentan bereits Arzneistoffe in der Tumortherapie zugelassen (EMA- und FDA-Zulassung). Mit Azacitidin und Decitabin stehen zwei Arzneistoffe zur Verfügung, welche DNMTs (DNMT1/3A/3B) inhibieren und somit den Methylierungsstatus der DNA normalisieren sollen. Tazemetostat inhibiert die HMT EZH2, welche Histon H3 an Lysin-27 methyliert, um eine übermäßige bzw. krankhaft veränderte Methylierung von Histon H3 zu verhindern. Mit Ivosedenib und Enasidenib stehen zwei Arzneistoffe zur Verfügung, welche indirekt in die epigenetische Regulation eingreifen. Sie inhibieren Isocitratdehydrogenasen 1 und 2 (IDH1/2), welche bei einigen Krebserkrankungen mutiert vorliegen können und somit erhöhte Spiegel von 2-Hydroxyglutarat (2-HG) produzieren. 2-HG selbst ist ein Inhibitor von HDMs und des Enzyms Tet-Methylcytosindioxygenase 2 (TET2), welches an der Demethylierung von Cytosin beteiligt ist. Zuletzt existieren ebenfalls zugelassene Inhibitoren der HDACs: Vorinostat (keine EMA-Zulassung (60)), Belinostat, Panobinostat und Romidepsin (keine EMA-Zulassung (61)) (50,62).

Im Rahmen der Studien dieser Arbeit waren vor allem Histondeacetylasen und deren Inhibitoren relevant, da sie einen wichtigen Einfluss auf die Cisplatin-Sensitivität von Ovarialkarzinomzelllinien entfalten können, wie im folgenden Absatz erläutert wird.

1.5.1.1 Histondeacetylasen (HDACs)

Eine wichtige Untergruppe der *Eraser*-Proteine innerhalb der epigenetischen Modulierungsproteine sind Histondeacetylasen (HDACs). Im Zusammenspiel mit ihren Antagonisten, den Histonacetyltransferasen (HATs), erhalten sie die Homöostase des Acetylierungsstatus der Histone aufrecht. Basierend auf dem momentanen Acetylierungsstatus kann zwischen Heterochromatin und Euchromatin unterschieden werden. HATs sind in der Lage Acetylgruppen von Acetyl-Coenzym A (Acetyl-CoA) auf Lysin-Reste der Histone zu übertragen, während HDACs diese durch hydrolytische

Spaltung entfernen. Heterochromatin bezeichnet eine geschlossene Form des Chromatins, in welcher die DNA besonders eng um die Histone gewickelt ist. Dieser Zustand ist präsent, wenn ein geringer Acetylierungsgrad der Histone vorliegt. Es kommt zur Abnahme der Transkriptionsaktivität und Genexpression. Die Ausbildung des Heterochromatins wird durch eine erhöhte Aktivität von HDACs bzw. eine verringerte Aktivität von HATs befördert und ist in diversen Tumorproben nachweisbar. Liegt im Gegensatz dazu eine besonders offene Form des Chromatins, mit lockerer Bindung der DNA um die Histone vor, wird vom Euchromatin gesprochen. Dieser Zustand zeichnet sich durch einen hohen Acetylierungsgrad der Histone aus. Dies führt zu einer Steigerung der Transkriptionsaktivität und Genexpression (63–68).

In Säugetieren sind 18 HDAC-Isoenzyme bekannt, die sich in fünf Klassen unterteilen lassen: Klasse I (HDAC1/2/3/8), Klasse IIA (HDAC4/5/7/9), Klasse IIB (HDAC6/10), Klasse III (Sirtuine, SIRT1-7) und Klasse IV (HDAC11). Klasse I, IIA, IIB und IV HDACs weisen hohe strukturelle Ähnlichkeit auf und benötigen ein Zink-Ion als Cofaktor, während die Sirtuine aus Klasse III eine Strukturhomologie zum Protein Sir2 der Bäckerhefe (*Saccharomyces cerevisiae*) aufweisen und NAD^+ als Cofaktor benötigen. Somit sind klassische HDACi nicht in der Lage ihre Aktivität zu inhibieren. Zusätzlich ist bekannt, dass die HDACs der Klassen I, IIA, IIB und IV an der Organisation des Chromatins und der Aktivierung bzw. Inhibierung von Transkriptionsfaktoren beteiligt sind. Aufgrund dieser Unterschiede werden zumeist die 11 zinkabhängigen HDAC-Isoenzyme der Klassen I, IIA, IIB und IV gemeint, wenn im Hinblick auf maligne Erkrankungen HDACs betrachtet werden. Weiterhin ist die Rolle der Sirtuine im Rahmen der Karzinogenese nicht abschließend geklärt, da die Isoenzyme zum Teil duale Rolle erfüllen und somit sowohl als Tumorsuppressor, als auch Onkoproteine fungieren können (63,64).

Die HDAC-Isoenzyme weisen eine unterschiedliche intrazelluläre Lokalisation auf. Während HDAC1/2/8 vorwiegend nukleär vorkommen, befinden sich HDAC6/10/11 überwiegend im Zytoplasma. Die übrigen HDACs (HDAC3/4/5/7/9) können zwischen beiden Lokalisierungen wechseln. Weiterhin weisen die Isoenzyme unterschiedliche Neben-Substrate abseits der Histone auf. So interagiert HDAC1 beispielsweise mit dem Androgenrezeptor, dem Tumorsuppressor p53 oder dem intrazellulären Signal-Transkriptionsfaktor STAT3, während HDAC6 mit dem Stützprotein α-Tubulin und Hitzeschockprotein 90 (HSP90) interagieren kann. Der Acetylierungsgrad von Nicht-Histon-Proteinen hat Einfluss auf deren räumliche

Struktur und damit in der Regel auch auf die Funktion. So konnte zum Beispiel gezeigt werden, dass die Interaktion zwischen HDAC6 und α-Tubulin zu einer veränderten Zellmigration führt (68). Die Effekte von HDAC1, als Vertreter der Klasse I HDACs, und HDAC6 wurden im Rahmen dieser Arbeit in einzelnen Studien näher beleuchtet.

Für diverse Krebsarten konnte eine Überexpression von HDACs gezeigt werden. Dies konnte sowohl für urologische Tumorerkrankungen (Blase, Niere und Prostata) als auch für gynäkologische Tumorerkrankungen (Eierstöcke, Gebärmutter, Gebärmutterhals und Brust), respiratorische Tumorerkrankungen (Lunge) und Tumorerkrankungen des Gastrointestinaltraktes (Dickdarm, Gallenblase, Leber und Pankreas) gezeigt werden. Für Ovarialkarzinome ist besonders die Überexpression der Klasse I HDACs HDAC1-3 beschrieben, welche sowohl die Tumorinitiation als auch die Tumorprogression steigert. Eine Zunahme im Ausmaß der Überexpression ist im Übergang von benignen Tumoren über Grenzfälle zu Karzinomen feststellbar und besonders ausgeprägt bei HGS-, muzinösen oder endometrioiden Tumoren. Weiterhin ist die Überexpression von Klasse I HDACs mit einer schlechten klinischen Prognose verknüpft (63). Es konnte konkret gezeigt werden, dass HDAC1 die Zellproliferation erhöht, indem sie die Aktivität von Cyclin A steigert – Cyclin A reguliert den Zellzyklus am Übergang von der G_2-Phase in die M-Phase (69). Auch für HDAC4, ein prominentes Isoenzym der Klasse IIA, konnte die Relevanz als Zielstruktur in diversen Krebsarten über verschiedene Mechanismen gezeigt werden (70). Im speziellen Bezug zu Ovarialkarzinomzelllinien finden sich Hinweise in der Literatur auf proliferations- und migrationssteigernde Effekte. Diese Effekte beruhen unter anderem auf der Inhibierung von p21 (71,72).

Im Allgemeinen führt die verringerte Acetylierung der Histone und einiger Nicht-Histon-Proteine zu mannigfaltigen Effekten, welche das Krebsgeschehen befördern. So werden beispielsweise apoptotische Reize unterdrückt, indem die Expression antiapoptotischer Gene hochreguliert wird oder die Progression der Zelle durch den Zellzyklus sichergestellt, da arretierende Gene vermindert exprimiert werden. Zusätzlich können sich Effekte auf die DDR, die Angiogenese und die Reaktion der Zelle auf ROS auswirken (63,65).

Die Rationale in der Anwendung von HDAC-Inhibitoren im Rahmen einer Tumortherapie liegt also mindestens in der Wiederherstellung der Acetylierungs-Homöostase von Histonen und anderen Proteinen, oder noch besser im angestrebten

Zustand des Euchromatins, um beispielsweise die Expression proapoptotischer Gene intrinsisch zu steigern (63–68). Im Zuge der durchgeführten Studien wurde der Acetylierungsstatus verschiedener Proteine (z.B. α-Tubulin und Histon H3) mithilfe des Western Blots bestimmt.

1.5.1.2 Histondeacetylase-Inhibitoren (HDACi)

HDACi stellen eine diverse Arzneistoffgruppe dar, die sich strukturell in vier Untergruppen einteilen lässt: aliphatische kurzkettige Fettsäuren, zyklische Peptide, Hydroxamsäuren und Benzamide (63). Für HDACi vom Hydroxamsäure- und Benzamid-Typ lässt sich ein allgemeingültiges Pharmakophor-Modell beschreiben (Abbildung 8).

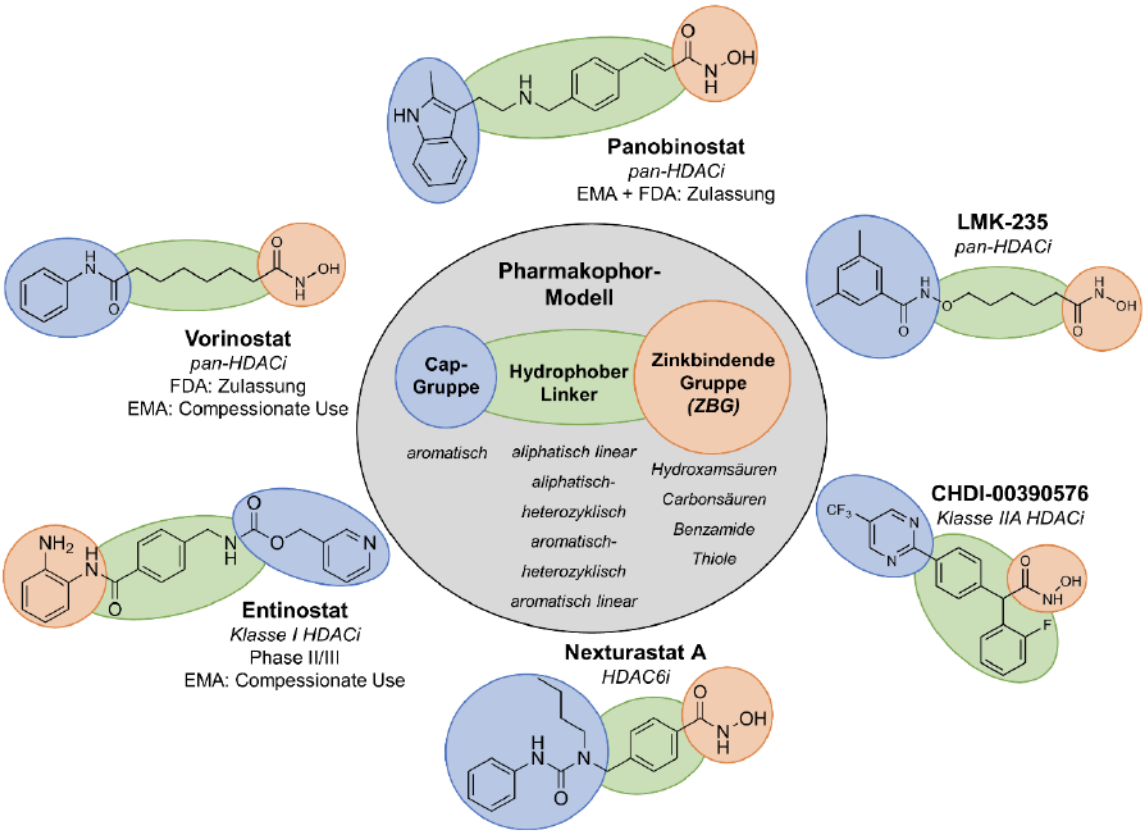

Abbildung 8: HDACi-Pharmakophor-Modell mit typischen Vertretern der einzelnen Strukturklassen.

Sie bestehen aus einer zinkbindenden Gruppe (ZBG, dargestellt in rot), welche in der Lage ist das Zinkion im katalytischen Zentrum der HDAC-Enzyme zu komplexieren und die Aktivität der Enzyme auf diese Art zu inhibieren. Gängige Strukturelemente sind Hydroxamsäuren (wie Panobinostat und Vorinostat) und Benzamide (wie Entinostat). Es finden sich in der Literatur allerdings auch Vertreter, welche Carbonsäuren (wie Valproinsäure) oder Thiole (wie Romidepsin nach Aktivierung) als

ZBG tragen (73). Zur Erkennung der Zielstruktur dient die, in blau dargestellte, Cap-Gruppe. Diese ist in der Regel aromatisch und enthält oft Stickstoff als Heteroatom und Wasserstoffbrücken-Akzeptor. Über die strukturelle Ausgestaltung der Cap-Gruppe lässt sich die Präferenz eines Inhibitors zu bestimmten HDAC-Enzymen oder -Klassen beeinflussen. So trägt der selektive HDACi Nexturastat A eine Butyl-Seitenkette, worin die präferierte Inhibierung von HDAC6 begründet ist (74). Die Bindungstasche von HDAC6 bietet mehr Raum und hat daher mehr verfügbaren Platz für Inhibitoren mit voluminöseren Cap-Gruppen (75). ZBG und Cap-Gruppe werden durch ein hydrophobes Verbindungsglied (Linker), dargestellt in grün, verbunden. Als Linker kommen diverse Strukturelemente in Frage. So tragen Vorinostat und LMK-235 beispielsweise einen aliphatisch-linearen Linker, während Panobinostat, Entinostat und Nexturastat A einen aromatisch-linearen Linker tragen. Die Rolle des Linkers bezüglich der Isoform-Selektivität ist nicht so gut erforscht wie die Rolle der Cap-Gruppe. Eine neuere Studie konnte allerdings Ansätze dafür erarbeiten, dass voluminöse Linker (aliphatisch oder aromatisch heterozyklischer Natur) die Selektivität eher in Richtung HDAC1 verschieben und aromatisch lineare Linker (wie Phenoxyacetate oder Thioacetate) die Selektivität eher Richtung HDAC6 dirigieren (76). Diese Ergebnisse sind allerdings nicht allgemeingültig und daher nicht auf alle HDACi anwendbar, sondern sollen vielmehr eine Tendenz zeigen.

Im Rahmen dieser Arbeit wurden die HDACi Panobinostat, LMK-235 und Vorinostat als nicht selektive Vertreter der pan-HDACi verwendet. Als selektive HDACi wurden das Benzamid Entinostat für Klasse I HDACs und die Hydroxamsäuren Nexturastat A für HDAC6 und CHDI für Klasse IIA HDACs eingesetzt. Die Strukturformeln der verwendeten HDACi inklusive ihrer Einordnung in das allgemeine Pharmakophor-Modell der Arzneistoffgruppe sind in Abbildung 8 dargestellt.

2006 wurde Vorinostat als erster HDACi von der FDA zur Behandlung von Patienten mit cutanem T-Zelllymphom (CTCL) zugelassen. In der Europäischen Union wurde Vorinostat von der EMA 2004 als Arzneistoff für seltene Leiden ausgewiesen. Der finale Zulassungsantrag wurde seitens des pharmazeutischen Unternehmens 2009 allerdings zurückgezogen, da der zuständige Ausschuss der EMA Bedenken geäußert und eine endgültige Zulassung als unwahrscheinlich eingestuft hatte. Vorinostat ist oral bioverfügbar und wird in den USA in Form von Kapseln vermarktet. Als zweiter pan-HDACi wurde 2015 Panobinostat sowohl von der FDA als auch von der EMA zur Behandlung von Patienten mit Multiplem Myelom im Rahmen einer

Kombinationsbehandlung mit dem Proteasom-Inhibitor Bortezomib und dem Glucocorticoid Dexamethason zugelassen. Auch Panobinostat ist oral bioverfügbar und wird in Form von Kapseln vermarktet. Entinostat wurde 2010 von der EMA als Arzneimittel für seltene Leiden (in diesem Fall zur Behandlung des Hodgkin Lymphoms) ausgewiesen und kann seitdem beispielsweise im Rahmen von Compessionate Use Programmen (engl. „Anwendung aus Mitgefühl“) Patienten zur Verfügung gestellt werden. Durch Compessionate Use Programme wird es Patienten mit seltenen Erkrankungen ermöglicht, von nicht zugelassenen Arzneimitteln zu profitieren, welche sich erst in Entwicklung oder klinischer Prüfung befinden. Allerdings ist eine Einschätzung der EMA (oder anderer zuständiger Arzneimittelbehörden) notwendig, dass der Wirkstoff vielversprechend ist und eine Zulassung in der Zukunft erwogen werden kann. Entinostat befindet sich zurzeit in zwei klinischen Phase III Studien (77,78). Es wird in Kombination mit dem Aromatasehemmer Exemestan zur Anwendung beim (rezidivierenden) Hormonrezeptor-positiven Brustkrebs untersucht. Auch Entinostat ist oral bioverfügbar. Als weitere HDACi wurden die Experimentalsubstanzen LMK-235 (Weiterentwicklung von Vorinostat (79)) als pan-HDACi, Nexturastat A als HDAC6i und CHDI als Klasse IIA HDACi verwendet.

1.5.2 Proteasom-Inhibitoren

Das Proteasom ist ein zentraler Teil der zellulären Qualitätskontrolle von Proteinen. Proteine, welche für den Abbau vorgesehen sind, werden durch Ubiquitinligasen mit dem Protein Ubiquitin verbunden und somit markiert. Die erste Ubiquitinierung eines Proteins ist ein Signal für weitere Ubiquitinligasen, die Ubiquitin-Kette zu verlängern. Diese polyubiquitinierten Proteine werden über ihre Ubiquitin-Kette an das Proteasom gebunden. Das Proteasom ist ein Proteinkomplex und die enzymatischen aktiven Proteasen bauen in der Folge die ubiquitinierten Proteine ab. Bei den Proteasen des Proteasoms handelt es sich um Endopeptidasen, welche in der Lage sind Bindungen zwischen nicht-terminalen Aminosäuren zu trennen. Es entstehen kurzkettige Peptide, welche durch Zellprozesse weiter abgebaut und somit erneut der Proteinbiosynthese zugeführt werden können. In Säugetier-Zellen wird das 26S-Proteasom exprimiert, welches aus einer proteolytisch aktiven 20S Untereinheit und zwei regulatorisch aktiven 19S-Untereinheiten besteht. Die beiden 19S-Untereinheiten sind ringförmig an entgegengesetzten Seiten der 20S-Untereinheit gelagert. An ihnen befinden sich Bindungsstellen für ATP und für die zuvor erwähnten

Polyubiquitin-Ketten. Der Kern des 26S-Proteasoms ist hohl. Proteinen wird es ermöglicht durch die entsprechenden Öffnungen einzutreten und zum proteolytisch aktiven Kern zu gelangen. Die ständige Qualitätskontrolle von Proteinen durch das Ubiquitin-Proteasom-System (UPS) ist eine Basis für die Aufrechterhaltung wichtiger Regulierungsprozesse und der Homöostase von Zellen. So wird beispielsweise der Zellzyklus reguliert oder der Übergang einer Zelle in die Apoptose begleitet (80–84).

Das Proteasom reguliert diverse Proteine. Hierzu zählen beispielsweise: Cycline, p21, p27 (Regulation des Zellzyklus); Bcl-2, Bax (anti- bzw. proapoptotische Proteine), p53 (Tumorsuppressor), NFκB (Tumorentwicklung, Metastasierung) und Wnt/β-Catenin (Adhäsionsmoleküle). Durch das Auftreten verschiedener Onkoproteine, die in Verbindung zum UPS stehen, kann eine erhöhte Ubiquitinierung und damit ein erhöhter Abbau von bestimmten antitumoralen Faktoren erfolgen. Dies konnte zum Beispiel für das Onkoprotein E6 gezeigt werden, welches zu einer verstärkten Ubiquitinierung des Tumorsuppressors p53 führt. Durch den erhöhten Abbau kann p53 seine tumorsupprimierenden Eigenschaften nicht mehr entfalten (85). Im Rahmen der regelhaft vorhandenen genetischen Instabilität von Krebszellen kommt es zu diversen genetischen Veränderungen gegenüber normalen Zellen (42). Bezogen auf das Proteasom konnte unter anderem an gynäkologischen Krebsarten gezeigt werden, dass die Gene für die Untereinheiten des Proteasoms häufig überexprimiert werden (86,87).

Mitte der 1990er-Jahre wurde der Proteasom-Inhibitor Bortezomib (Strukturformel siehe Abbildung 9) entwickelt und Ende dieser Dekade in klinischen Studien zur Behandlung des multiplen Myeloms untersucht.

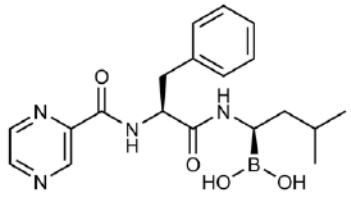

Abbildung 9: Bortezomib.

2003 wurde es von der FDA als erster Wirkstoff seiner Klasse zur Behandlung des Multiplen Myeloms zugelassen (88). Die Zulassung durch die EMA folgte Mitte 2004 (89). In beiden Regionen erfolgte die Zulassung zunächst zur Behandlung von Patienten, welche bereits eine Therapie durchlaufen haben und sich bereits einer Knochenmarktransplantation unterzogen haben oder für diese nicht geeignet sind. Beim Multiplen Myelom handelt es sich um eine Krebserkrankung der Plasmazellen

des Knochenmarks. Mehrere Jahre später erfolgte eine Erweiterung der Zulassung für die Initialbehandlung von Patienten mit Multiplem Myelom im Rahmen einer Kombinationsbehandlung mit dem Alkylans Melphalan und dem Glucocorticoid Prednison, die nicht für eine hochdosierte Chemotherapie inklusive Knochenmarktransplantation geeignet sind. Bortezomib steht seit 2019 auf der Liste der unentbehrlichen Arzneimittel der Weltgesundheitsorganisation (WHO) (90). Es ist nicht oral verfügbar und wird als Injektion verabreicht.

Bortezomib bindet über sein Bor-Atom an das katalytische Zentrum des Proteasoms (91). Weitere zugelassene Proteasom-Inhibitoren sind Carfilzomib, welches an der proteolytisch aktiven 20S-Untereinheit des Proteasoms bindet, und Ixazomib, welches oral verfügbar ist und den gleichen Wirkmechanismus wie Bortezomib aufweist.

Bisher zeigten sich vielversprechende präklinische Daten zur Anwendung von Proteasom-Inhibitoren in soliden Tumoren. Allerdings konnten sie in klinischen Studien bisher aufgrund ungünstiger Pharmakokinetik bezogen auf solide Tumore nicht überzeugen, da die notwendigen Plasmaspiegel mit (zu stark) erhöhter Toxizität einhergehen würden (92). Es finden sich im amerikanischen Register für klinische Studien (ClinicalTrials.gov) mehr als 40 Einträge über klinische Studien mit Bortezomib zur Anwendung bei soliden Tumoren. Eine einstellige Anzahl der Studien ist momentan aktiv und rekrutiert Probanden. Trotz der bisher eher mittelmäßigen klinischen Erfolge wird die Anwendung von Bortezomib bei soliden Tumorerkrankungen weiter untersucht. Beispielsweise wird momentan in Südkorea eine Phase II Studie zur Untersuchung der Anwendung von Bortezomib in Kombination mit dem DNA-Interkalator Doxorubicin bei platin-resistenten Ovarialkarzinomen, durchgeführt und es werden weiterhin Probandinnen rekrutiert (93).

In der Literatur finden sich weiterhin Hinweise, dass sich aus der Kombination von Proteasom-Inhibitoren und Klasse IIa-selektiven HDACi Behandlungsoptionen für Pankreaskarzinome ableiten lassen könnten (94). Die gezeigten Effekte beruhen auf einer gemeinsamen Induktion der Expression des Tumorsuppressors p21 und des proapoptotischen Gens FOXO3a.

1.5.3 Hitzeschockprotein 90-Inhibitoren (HSP90i)

Hitzeschockprotein 90 (HSP90) ist ein Chaperon und wird in Säugetierzellen nahezu ubiquitär exprimiert. Als Chaperon unterstützt es frisch synthetisierte Proteine bei der Faltung, die essenziell für die spätere Erfüllung ihrer jeweiligen Funktionen ist. Weitere Aufgaben erfüllt HSP90 im Rahmen des intrazellulären Transports und der Degradierung von Proteinen. Proteine, welche durch HSP90 beeinflusst werden, werden Clientproteine genannt. Die zytosolische Form von HSP90 ist HSP90A und wird in das konstitutiv exprimierte HSP90β und induzierbare HSP90α unterteilt, die eine 85 %-ige Sequenzidentität aufweisen (95–97). Werden beide Isoformen gemeint, wird allgemein nur von HSP90 gesprochen.

HSP90 liegt als Homodimer vor und wird ATP-abhängig in die aktive Form des HSP90-Dimers überführt (Abbildung 10).

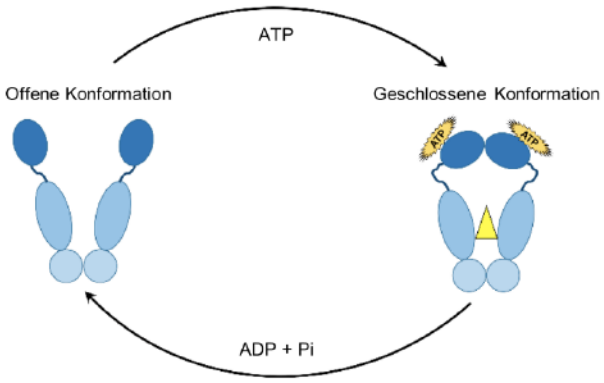

Abbildung 10: ATPase Zyklus von HSP90.

Pi steht für einen Phosphatrest nach Abspaltung von ATP.
Die Abbildung wurde übersetzt und aus (98) entnommen.

Strukturell betrachtet besteht HSP90 aus vier Domänen. Die N-terminale Domäne (NTD) enthält die ATP-Bindungsstelle und ist für die Bindung an Clientproteine notwendig. Außerdem stellt sie eine wichtige Bindungsstelle für niedermolekulare Inhibitoren von HSP90 (HSP90i), wie Geldanamycin, Luminespib oder HSP990 dar, welche in Konkurrenz zu ATP treten und somit die Ausbildung des Homodimers verhindern (Strukturformeln von Luminespib und HSP990: siehe Abbildung 11).

Abbildung 11: Luminespib (links) und HSP990 (rechts).

Als Verbindungsglied zur mittleren Domäne (MD) schließt sich eine geladene Linker-Region (CR) an die NTD an. Der Einfluss der CR auf die Chaperon-Aktivität von HSP90 wird kontrovers diskutiert (99,100). Nach der Spaltung von ATP in ADP und einen Phosphatrest wird dieser Phosphatrest an der MD gebunden. Als vierte Domäne existiert die C-terminale Domäne (CTD), welche vor allem für die Bildung des Homodimers wichtig ist (101). Allerdings kann sie auch als allosterer Modulator der NTD wirken (102) und stellt eine Zielstruktur für C-terminale HSP90i dar (103).

In malignen Zellen wird HSP90 exprimiert und kann verantwortlich für die Instandsetzung und Instandhaltung diverser Onkoproteine sein (98). Durch diese Involvierung von HSP90 in der Karzinogenese wird die bereits gesteigerte Zellproliferation sowie eine bereits verringerte Apoptose-Induktion zusätzlich verstärkt. Folgende HSP90-Clientproteine führen zu diesen Effekten: Wachstumsfaktor-Rezeptoren und andere Rezeptor-Tyrosin-Kinasen werden durch HSP90 stabilisiert, was zur angesprochenen unkontrollierten Proliferation beiträgt. Weiterhin sind PI3K und AKT Clientproteine von HSP90, welche maßgeblich für die Regulation des PI3K-AKT-Signalweges verantwortlich sind und unreguliert zu gesteigerter Zellproliferation und Angiogenese führen. Es finden sich außerdem apoptoserelevante Proteine wie p53, Survivin und APAF-1 unter den Proteinen, welche durch HSP90 in ihrer Aktivität reguliert werden. Eine gesteigerte HSP90 Expression führt in diesem Hinblick zur Unterdrückung von apoptotischen Signalen innerhalb der Krebszelle. Aufgrund dieser regulatorischen Eigenschaften ist HSP90 eine wichtige molekulare Zielstruktur für therapeutische Arzneistoffe im Rahmen einer Krebserkrankung (98).

Luminespib wurde bisher nur im Rahmen weniger präklinischer Studien zur Behandlung von Ovarialkarzinomen bzw. entsprechenden Zelllinien untersucht. Es lassen sich Erkenntnisse aus tierexperimentellen Xenotransplantations-Studien finden, die belegen, dass Luminespib den Wachstumsfaktor-Rezeptor ErbB-2 herunter reguliert (104) und positive Effekte durch Verringerung des Tumorwachstums, der Angiogenese und Metastasierung zeigt (105,106). Für HSP990 lassen sich keine präklinischen Daten aus Zell- und/oder Tierexperimenten finden. Folgend ergibt sich, dass bisher keine Daten zur Kombination der genannten HSP90i und Cisplatin und/oder HDACi an Ovarialkarzinomen bzw. entsprechenden Zelllinien veröffentlicht wurden. Für andere HSP90i wie Geldanamycin und dessen Derivate Tanespimycin (17-AAG [17-*N*-allylamino-17-demethoxygeldanamycin]) oder Alvespimycin (17-DMAG [17-Dimethylaminoethylamino-17-demethoxygeldanamycin]) konnte eine

positive Beeinflussung der Cisplatin-Sensitivität an verschiedenen Ovarialkarzinom-Zelllinien gezeigt werden (107). Für den positiven Effekt einer Kombination von HSP90i und Cisplatin lassen sich für andere Tumorentitäten als Ovarialkarzinome entsprechende Indikatoren finden. So konnte beispielsweise an Cisplatin-resistenten Kopf-Hals-Tumor-Zelllinien ein synergistischer Effekt zwischen Tanespimycin und Cisplatin gezeigt werden, welcher auf der Induktion von Apoptose beruht (108). Zusätzlich konnte für Tanespimycin und Alvespimycin gezeigt werden, dass die beiden HSP90i die Cisplatin-Sensitivität von Blasenkrebs-initiierenden Zellen erhöhen konnten. Auch in dieser Studie konnte eine gesteigerte Auslösung von Apoptose beobachtet werden (109). Eine Untersuchung der Dreifachkombination aus Cisplatin, HSP90i und HDACi wurde auch an anderen Tumorentitäten bisher nicht durchgeführt.

Mit Stand Dezember 2020 ist kein HSP90i zur Tumor-Behandlung oder in einer anderen Indikation zugelassen. In der Vergangenheit wurden laut ClinicalTrials.gov 28 klinische Phase I oder II Studien mit Luminespib (zu finden unter dem klinischen Prüfcode AUY-922) und zwei Phase I Studien mit HSP990 durchgeführt. Die entsprechenden Studien sind zum jetzigen Zeitpunkt beendet oder wurden abgebrochen. Explizite Studien an Patientinnen mit Ovarialkarzinomen wurden mit den beiden Inhibitoren nicht durchgeführt. Als einzige gynäkologische Krebserkrankung wurde in manchen Studien mit Luminespib Brustkrebs eingeschlossen. Einige wenige Studien befassten sich sehr breit mit der Anwendung bei diversen Tumorerkrankungen. Da für diese Studien noch keine Ergebnisse veröffentlicht wurden, ist nicht klar, ob auch Ovarialkarzinom-Patientinnen Teil des jeweiligen Patientenkollektivs waren. Momentan sind rund 18 klinische Studien (Phase I und II) mit anderen HSP90i zu diagnostischen oder therapeutischen Zwecken, aktiv und rekrutieren zum Teil Probanden. Diese Studien befassen sich sowohl mit soliden Tumoren als auch mit Leukämien und die Patientenkollektive bestehen zumeist aus Patienten, welche eine fortgeschrittene oder metastasierende Krebserkrankung aufweisen.

2 Zielsetzung

Aufgrund der besonderen Schwere einer Ovarialkarzinomerkrankung und schlechten klinischen Überlebensraten ist die Entwicklung und Bewertung von neuen Therapiemöglichkeiten ein wichtiges Forschungsgebiet. Im Zuge diverser Vorteile von Kombinationstherapien wie zum Beispiel der potenziellen Verringerung der Dosen der Einzelkomponenten und der damit einhergehenden Verringerung von unterwünschten Arzneimittelwirkungen, bietet sich eine fokussierte Forschung auf diesem Gebiet an.

Platinhaltige Zytostatika wie Cisplatin oder Carboplatin sind aus der Therapie des schwerwiegenden Ovarialkarzinoms nicht wegzudenken, da sie eine gute klinische Effektivität und Studienlage aufweisen. Eine Behandlung mit platinhaltigen Zytostatika geht allerdings oft mit gravierenden unerwünschten Wirkungen (wie Nephrotoxizität, Ototoxizität oder Nausea) einher und kann außerdem zu einer therapielimitierenden Entwicklung einer Platinresistenz führen. In den verschiedenen Studien dieser Arbeit sollten effektive Kombinationspartner für Cisplatin am zellulären Modell gefunden werden. Das Ziel dieser Kombinationsbehandlung sollte ein synergistischer Effekt zwischen Cisplatin und einer oder mehrerer weiterer Komponente sein. Aufgrund ihrer vielfältigen Effekte, welche theoretisch die zytostatischen Effekte von Cisplatin unterstützen sollten, lag der Fokus auf der Gruppe der Histondeacetylase-Inhibitoren (HDACi) als Kombinationspartner.

Im Rahmen der ersten Studie dieser Arbeit (*Class I-Histone Deacetylase (HDAC) Inhibition is Superior to pan-HDAC Inhibition in Modulating Cisplatin Potency in High Grade Serous Ovarian Cancer Cell Lines* [Bandolik et al.] (110)) sollte an verschiedenen hochgradig serösen Ovarialkarzinomzelllinien untersucht werden, welche Selektivität eines HDACi besonders vorteilhaft in der Kombination mit Cisplatin ist. Es wurden der unselektive HDACi Panobinostat mit dem Klasse I-selektiven HDACi Entinostat und dem HDAC6-selektiven HDACi Nexturastat A verglichen. Die Effektivität der Kombination wurde hinsichtlich der Auslösung von Apoptose und der Zytotoxizität beurteilt. Beide Effekte wurden hinsichtlich eines eventuell vorliegenden Synergismus bewertet.

Eine weitere Studie dieser Arbeit (*Priming with HDAC inhibitors Sensitizes Ovarian Cancer Cells to Treatment with Cisplatin and HSP90 Inhibitors* [Rodrigues-Moita, Bandolik et al.] (111)) hat sich mit der grundsätzlichen Bewertung einer denkbaren Dreifachkombination aus Cisplatin, den Hitzeschockprotein 90-Inhibitoren

(HSP90i) Luminespib und HSP990 sowie den unselektiven pan-HDACi Panobinostat und LMK-235 beschäftigt. Diese Studie wurde an verschiedenen cisplatinsensitiven und -resistenten Ovarialkarzinomzelllinien-Pärchen durchgeführt.

Im Zuge der weiteren Klärung der Effekte von selektiven HDACi hat sich eine zusätzliche Studie dieser Arbeit (*Synergism oft the Class IIa Selective Histone Deacetylase Inhibitor CHDI-00390576 and the Proteasome Inhibitor Bortezomib in Ovarian Cancer Cell Lines* [Bandolik et al.]) mit der Kombination des Klasse IIA-selektiven HDACi CHDI mit dem Proteasom-Inhibitor Bortezomib beschäftigt. Die Effekte sollten an cisplatinsensitiven und -resistenten Zelllinien durchgeführt werden, um zu klären, ob sich aus der Kombinationsbehandlung eine Behandlungsoption für Cisplatin-resistente Ovarialkarzinome ergeben kann. Bortezomib wird bisher an soliden Tumoren kaum eingesetzt und ist Gegenstand aktueller klinischer Studien. Es weist einen therapeutischen Fokus für hämatologische Tumore auf.

Die Bewertung der Effektivität von dualen Wirkstoffen, welche in einem Molekül sowohl alkylierende als auch Histondeacetylase-inhibierende Eigenschaften aufweisen, war die Zielsetzung der letzten Studie dieser Arbeit (*Hydroxamic Acids Immobilized on Resins (HAIRs): A Toolbox for the Synthesis of Dual-Targeting HDAC Inhibitors and HDAC Degraders (PROTACs)* [Sinatra, Bandolik et al.] (112,113)). Es wurden auf Seite der HDACi Strukturelemente von Vorinostat und Panobinostat verwendet um diese mit Strukturelementen der Alkylanzien Temozolomid, Chlorambucil und Mitozolomid zu kombinieren. Aufgrund der erhöhten klinischen Relevanz der verwendeten Alkylanzien für diese Tumorentitäten wurden die Experimente dieser Studie an Kopf-Hals-Tumor- bzw. Glioblastom-Zelllinien durchgeführt. Es wurde überprüft, ob die dualen Arzneistoffe in zellbasierten Experimenten vorteilhaft gegenüber der Anwendung beider Einzelkomponenten sind.

Zusammenfassend lag der Fokus dieser Arbeit auf der Entwicklung von Kombinationstherapien für Ovarialkarzinome, welche entweder Cisplatin oder HDACi beinhalteten. Nach der Entdeckung der Effekte sollten diese mechanistisch aufgeklärt werden.

3 Ergebnisse

3.1 Publikation 1

Class I-Histone Deacetylase (HDAC) Inhibition is Superior to pan-HDAC Inhibition in Modulating Cisplatin Potency in High Grade Serous Ovarian Cancer Cell Lines

Jan J. Bandolik[1], Alexandra Hamacher[1], Christian Schrenk[1], Robin Weishaupt[2], Matthias U. Kassack[1]

1 Institut für Pharmazeutische und Medizinische Chemie, Heinrich-Heine-Universität Düsseldorf
2 Institut für Informatik, Komplexitätstheorie und Kryptologie, Heinrich-Heine-Universität Düsseldorf

Veröffentlicht in: International Journal of Molecular Sciences, 22. Juni 2019

DOI: 10.3390/ijms20123052

Beitrag: Erstautorschaft. Durchführung der Experimente dieser Veröffentlichung (Ausnahme: isolierter Enzyminhibitionsassay). Auswertung der Daten und Verfassen der ersten Version des Manuskripts.

Zusammenfassung (übersetzt): Hochgradig seröser Ovarialkrebs (HGSOC) ist der verbreitetste und aggressivste Subtyp von Ovarialkrebs mit der schlechtesten klinischen Prognose aufgrund intrinsischer oder erworbener Arzneimittelresistenz. Die Standard-Behandlung beinhaltet Platin-Zytostatika. Die Entwicklung von Krebs und Ausbildung einer Chemoresistenz ist oft verbunden mit einer erhöhten Aktivität von Histondeacetylasen (HDAC). Das Ziel dieser Studie war die Untersuchung des Potentials von Histondeacetylase-Inhibitoren (HDACi) die Potenz von Cisplatin in HGSOC zu erhöhen. Vier HGSOC Zelllinien mit unterschiedlicher Cisplatin-Sensitivität wurden mit Kombination von Cisplatin und Entinostat (Klasse I HDACi), Panobinostat (pan-HDACi) oder Nexturastat A (Klasse IIb HDACi) behandelt. Die Inhibierung von Klasse I HDACs durch Entinostat zeigte sich bezüglich der Erhöhung der Potenz von Cisplatin in Zellviabilitäts-Assays (MTT), Apoptoseinduktion (subG1) und Caspase 3/7 Aktivierung überlegen gegenüber der pan-HDAC Inhibierung. Entinostat wirkte synergistisch mit Cisplatin in MTT- und Caspase-Aktivierungs-Assays bei allen Zelllinien. In den MTT-Assays ließen sich Kombinationsindices (*CI-Values*) < 0,9 nachweisen, was für eine synergistische Wirkung auszeichnet. Der Effekt der HDACi könnte mit der Hochregulierung von proapoptotischen Genen (*CDNK1A*, *APAF1*, *PUMA*, *BAK1*) und der Herunterregulierung von *Survivin* zusammenhängen. Zusammengefasst, ist die Kombination von Entinostat und Cisplatin synergistisch in HGSOC und könnte eine effektive Therapiestrategie beim aggressiven Ovarialkrebs darstellen.

International Journal of
Molecular Sciences

MDPI

Article

Class I-Histone Deacetylase (HDAC) Inhibition is Superior to pan-HDAC Inhibition in Modulating Cisplatin Potency in High Grade Serous Ovarian Cancer Cell Lines

Jan J. Bandolik [1], Alexandra Hamacher [1], Christian Schrenk [1], Robin Weishaupt [2] and Matthias U. Kassack [1,*]

[1] Institute for Pharmaceutical and Medicinal Chemistry, University of Duesseldorf, 40225 Duesseldorf, Germany; jan.bandolik@hhu.de (J.J.B.); alexandra.hamacher@hhu.de (A.H.); schrenc@hhu.de (C.S.)
[2] Institute for Computer Science, Computational Complexity and Cryptology, University of Duesseldorf, 40225 Duesseldorf, Germany; robin.weishaupt@hhu.de
* Correspondence: matthias.kassack@uni-duesseldorf.de

Received: 30 May 2019; Accepted: 20 June 2019; Published: 22 June 2019

Abstract: High grade serous ovarian cancer (HGSOC) is the most common and aggressive ovarian cancer subtype with the worst clinical outcome due to intrinsic or acquired drug resistance. Standard treatment involves platinum compounds. Cancer development and chemoresistance is often associated with an increase in histone deacetylase (HDAC) activity. The purpose of this study was to examine the potential of HDAC inhibitors (HDACi) to increase platinum potency in HGSOC. Four HGSOC cell lines with different cisplatin sensitivity were treated with combinations of cisplatin and entinostat (class I HDACi), panobinostat (pan-HDACi), or nexturastat A (class IIb HDACi), respectively. Inhibition of class I HDACs by entinostat turned out superior in increasing cisplatin potency than pan-HDAC inhibition in cell viability assays (MTT), apoptosis induction (subG1), and caspase 3/7 activation. Entinostat was synergistic with cisplatin in all cell lines in MTT and caspase activation assays. MTT assays gave combination indices (CI values) < 0.9 indicating synergism. The effect of HDAC inhibitors could be attributed to the upregulation of pro-apoptotic genes (*CDNK1A*, *APAF1*, *PUMA*, *BAK1*) and downregulation of *survivin*. In conclusion, the combination of entinostat and cisplatin is synergistic in HGSOC and could be an effective strategy for the treatment of aggressive ovarian cancer.

Keywords: cisplatin; high grade serous ovarian cancer (HGSOC); histone deacetylase inhibitors; caspase activity; antitumor platinum agents; combination treatment; panobinostat; entinostat; nexturastat A

1. Introduction

Ovarian cancer is one of the most lethal gynecological cancer subtypes, such as uterus, breast, cervical or vulva cancer. Compared to the other gynecological cancers, ovarian cancers have the worst survival rate over five years (47.6%, USA; 41%, Germany). In contrast, breast cancer has a 5 year survival rate of 89.9% in the USA and 88% in Germany [1–6]. Ovarian cancer can be divided into types I and II. Type I is usually less aggressive and contains the subtypes endometrioid carcinoma and clear cell carcinoma as well as mucinous carcinoma and low-grade serous carcinoma. However, cohort studies from the USA found out that 68% of ovarian cancer cases are type II diseases [7,8]. Type II ovarian cancer is clinically very aggressive and consists of high grade serous ovarian cancer (HGSOC). HGSOC is rapidly growing, shows genomic instability, and dysfunction in tumor suppressors [9,10]. Primary

options for treatment are surgery and a combination chemotherapy including platinum compounds like cisplatin or carboplatin and paclitaxel [11]. Initially, most ovarian cancers are chemosensitive. During the treatment, resistance develops and leads to relapse and therapeutic failure. The mechanisms behind a developing platinum resistance are multifactorial in nature and cannot be overcome by increasing the dose of a platinum drug given to a patient [12]. Furthermore, with increasing doses, patients suffer from increased frequency or intensity of side effects like nephrotoxicity or ototoxicity. Combination therapies with small molecule inhibitors are a widely used strategy to increase the platinum sensitivity of the tumor or to prevent/delay the development of therapeutic resistance [13,14]. It is well known that epigenetic modifications such as histone acetylation or DNA methylation are dysregulated in cancer and moreover in chemoresistance development [15,16]. The acetylation and deacetylation of proteins is regulated by histone acetyl transferases (HATs) and histone deacetylase (HDAC) enzymes. Eleven human zinc-dependent HDACs are known (HDAC1-11) which can be clustered into several classes: Class I: HDAC1, 2, 3, 8; class IIa: HDAC4, 5, 7, 9; class IIb: HDAC6, 10; and class IV: HDAC11. Class III comprises non-zinc-dependent HDAC enzymes, the so-called sirtuines which will not be considered in this paper [17]. There are several known overexpression patterns of histone deacetylase (HDAC) enzymes in different cancer subtypes leading to transcriptional repression [15]. For ovarian cancer, an overexpression of HDACs - especially of class I HDACs - is described and correlates with its aggressiveness. Furthermore, HDAC overexpression can serve as a marker of poor clinical outcome [18]. It is also described that chemotherapy leads to an upregulation of HDAC1 expression [19].

Thus, using HDAC inhibitors (HDACi) to normalize a dysregulated acetylation status of histone and non-histone proteins is an increasingly pursued strategy to increase the sensitivity of chemotherapeutic agents [20–22]. HDACi can act by regulating pro- and anti-apoptotic gene expression and thus promoting cell cycle arrest and induction of apoptosis [16]. However, the exact regulatory network of HDACi on apoptosis induction in a particular type of cancer is not fully understood. Further, it is not yet clear if subtype-selective HDACi or pan-HDAC inhibition is superior in increasing chemosensitivity of anticancer drugs such as platinum compounds.

The purpose of this study was to test the effect of HDACi with different subtype preferences on the chemosensitivity of cisplatin in HGSOC cell lines. Panobinostat was used as pan-HDACi, entinostat as class I selective HDACi, and nexturastat A as class IIb (HDAC6)-selective HDACi. Due to the intrinsic effect of HDACi regulating gene expression, all inhibitors were incubated 48 h prior to cisplatin treatment. CaOV3, Kuramochi, OVSAHO, and HEY cell lines were chosen as representatives for HGSOC based on literature recommendations [23–26]. Among these HGSOC cell lines, CaOV3, Kuramochi, and OVSAHO are described as very suitable cellular models for HGSOC [27]. In addition to the four HGSOC cell lines, A2780 was included as a comparison model for ovarian endometrioid adenocarcinoma (type I) [28,29]—a less aggressive type of ovarian cancer. HDACi—induced effects on cisplatin sensitivity were investigated using cell viability assays, apoptosis induction, caspase activation, and analysis of apoptosis-related gene expression. Notably, the class I HDACi entinostat turned out superior to panobinostat in increasing cisplatin potency in HGSOC and was synergistic with cisplatin. The chemosensitizing effect could be attributed to the upregulation of cell cycle arrest and pro-apoptotic genes.

2. Results

2.1. Characterization of the Human Ovarian Cancer Cell Lines

We chose the human ovarian cancer cell lines A2780, CaOV3, HEY, Kuramochi, and OVSAHO as cellular models for HGSOC (CaOV3, HEY, Kuramochi, and OVSAHO) and ovarian endometrioid adenocarcinoma type I (A2780). First, the cisplatin sensitivity of the cell lines and their HDAC expression profile (mRNA, protein) was analyzed. The results are shown in Figure 1.

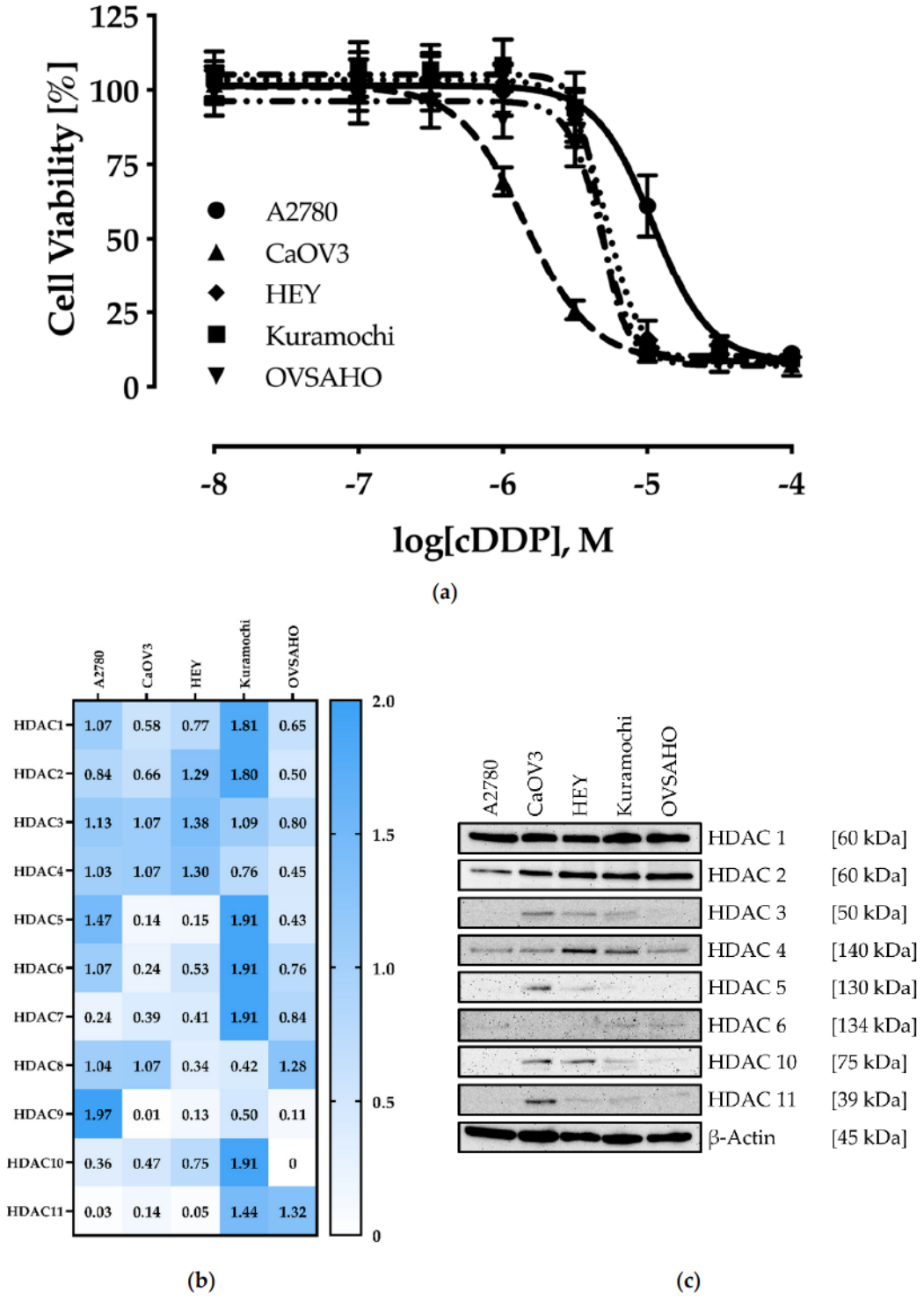

Figure 1. Characterization of the ovarian cancer cell lines. **(a)** Cell viability was measured by MTT assay after 72 h incubation with different concentrations of cisplatin. Data shown are mean ± SD of at least three independent experiments each carried out in triplicates, calculated as percentage of control. The cell line specific IC_{50} values are shown in Table 1. **(b)** Gene expression profile for HDAC enzymes was obtained by RT-PCR. Data shown are normalized to endogenous control gene expression of *HPRT1* (hypoxanthine-guanine phosphoribosyltransferase), *TBP* (TATA binding protein), and *GUSB* (beta-glucuronidase). **(c)** Representative immunoblot analysis of HDAC enzymes. One representative immunoblot with a protein molecular weight marker is shown in Figure S3.

IC_{50} values of the cell lines towards cisplatin ranged from 1.44 µM for CaOV3 up to 11.0 µM for A2780 (Figure 1A and Table 1). In literature, cisplatin plasma levels of 1.90 to 8.72 µM are reported in patients (c_{max} reached after 1–1.5 h) [30].

Table 1. IC_{50} and pIC_{50} for cisplatin after a 72h incubation.

Cell Line	IC_{50} [µM]	pIC_{50} ± SEM
A2780	11.0	4.96 ± 0.01
CaOV3	1.44	5.84 ± 0.01
HEY	5.25	5.28 ± 0.01
Kuramochi	4.68	5.33 ± 0.02
OVSAHO	4.83	5.32 ± 0.01

Data shown are the mean of pooled data from at least three experiments, each carried out in triplicate.

A2780 cells showed IC_{50}-values for cisplatin in the one-digit micromolar range in previous studies [20,21,31]. Nevertheless, under the experimental conditions chosen here, an IC_{50}-value of 11.0 µM was obtained. Based on the IC_{50}-values, CaOV3 cells can be classified as cisplatin-sensitive, while HEY, Kuramochi, and OVSAHO cells are mediocre sensitive and A2780 cisplatin-resistant.

Regarding the HDAC enzyme expression, different patterns were obtained. At mRNA level, the cell line Kuramochi showed the highest expression of *HDAC 1*, *2*, *5*, *6*, *7*, *10*, and *11* whereas A2780 revealed the highest expression of *HDAC9*. CaOV3, HEY, and OVSAHO generally showed a low expression of HDACs in comparison to Kuramochi (Figure 1B). Within a particular cell line, *HDAC1-4* showed a rather high expression except for Kuramochi and A2780.

Comparing the HDAC gene expression profile with the HDAC protein expression levels, some differences become evident (Figure 1C). HDAC1 and HDAC2 are well expressed in every cell line, whereas HDAC3 was only detected (protein) in CAOV, HEY, and Kuramochi. HDAC4 (class IIa HDAC) is expressed in every cell line with a slightly higher expression in HEY and Kuramochi. HDAC5 is only expressed in CaOV3 and slightly in HEY cells. For HDAC6 and HDAC10, members of class IIb, a more heterogenous expression profile occurred. While HDAC10 is strongly expressed in CaOV3 and HEY cells, it is weakly expressed especially in Kuramochi. For HDAC6 we observed a slight expression in A2780, Kuramochi, and OVSAHO. Expression levels for HDAC11 as representative of class III HDACs show some differences, too. CaOV3 expresses HDAC11 at a higher level, HEY, Kuramochi, and OVSAHO at a very weak level, and A2780 shows no expression. For HDAC4 and HDAC6 a good correlation between mRNA and protein expression levels could be observed. In conclusion, class I HDACs HDAC1 and HDAC2 were highly expressed throughout all ovarian cancer cell lines whereas the other HDAC isoforms are expressed at a much lower level and only in some but not all cell lines (Figure 1B,C).

2.2. Cytotoxic and HDAC-Inhibitory Effects of Entinostat, Panobinostat, and Nexturastat A

Next, we analyzed the antiproliferative effects of entinostat, panobinostat, and nexturastat A in the ovarian cancer cell lines. Incubation times applied for the investigation of HDACi alone (absence of cisplatin) were the same as later (chapter 2.3) used in combination experiments of HDACi with cisplatin. Results are shown in Table 2.

Panobinostat showed the highest cytotoxic effects against all five cell lines with IC_{50}-values in the low nanomolar range. Entinostat had moderate cytotoxicity with IC_{50}-values in the submicromolar range. Nexturastat A had micromolar IC_{50}-values. Thus, nexturastat A was not cytotoxic at concentrations where it displays HDAC6 selectivity (in the nanomolar range). To determine the HDAC inhibitory activity of entinostat, panobinostat, and nexturastat A, we performed a whole-cell HDAC inhibition assay. Results are shown in Table 3.

Table 2. Cytotoxic activity of entinostat, panobinostat, and nexturastat A.

Cell Line	HDACi					
	Entinostat		Panobinostat		Nexturastat A	
	IC_{50} [nM]	pIC_{50} ± SEM	IC_{50} [nM]	pIC_{50} ± SEM	IC_{50} [nM]	pIC_{50} ± SEM
A2780	606	6.22 ± 0.03	15.3	7.82 ± 0.02	7778	5.11 ± 0.09
CaOV3	1146	5.94 ± 0.03	7.62	8.12 ± 0.03	5291	5.28 ± 0.03
HEY	251	6.60 ± 0.02	2.68	8.57 ± 0.02	1724	5.76 ± 0.03
Kuramochi	485	6.31 ± 0.03	11.2	7.95 ± 0.02	5302	5.28 ± 0.02
OVSAHO	1828	5.74 ± 0.02	42.4	7.37 ± 0.05	16,218	4.79 ± 0.02

Cell viability was measured by MTT assay after 48 h preincubation followed by an additional 72 h incubation. Data shown are the mean of pooled data from at least three experiments each carried out in triplicates.

Table 3. HDAC inhibitory activity of entinostat, panobinostat, and nexturastat A.

Cell Line	HDACi					
	Entinostat		Panobinostat		Nexturastat A	
	IC_{50} [nM]	pIC_{50} ± SEM	IC_{50} [nM]	pIC_{50} ± SEM	IC_{50} [nM]	pIC_{50} ± SEM
A2780	313	6.50 ± 0.04	12.1	7.91 ± 0.06	3633	5.44 ± 0.04
CaOV3	333	6.48 ± 0.03	7.88	8.10 ± 0.05	3500	5.46 ± 0.03
HEY	219	6.60 ± 0.04	13.6	7.87 ± 0.03	3874	5.41 ± 0.03
Kuramochi	339	6.47 ± 0.04	9.87	8.01 ± 0.07	3733	5.43 ± 0.03
OVSAHO	326	6.49 ± 0.02	23.1	7.64 ± 0.04	5249	5.28 ± 0.02

Data shown are the mean of pooled data from at least three experiments each carried out in triplicates.

No significant differences were observed between the cell lines regarding the HDAC inhibitory potency of entinostat. The IC_{50}-values for entinostat ranged from 0.22 µM in HEY cells to 0.34 µM in Kuramochi cells. As expected, panobinostat showed IC_{50}-values in the nanomolar range. The IC_{50}-values were between 7.88 nM for CaOV3 cells and 23.1 nM for OVSAHO cells. For nexturastat A, we obtained IC_{50}-values in the low micromolar range and could not detect a large difference in the IC_{50}-values between the individual cell lines. The IC_{50}-values ranged from 3.63 µM for A2780 cells to 5.25 µM in OVSAHO cells. For confirmation of HDAC-inhibitory effects, α-tubulin and histone H3 acetylation were analyzed by western blot (Figure 2).

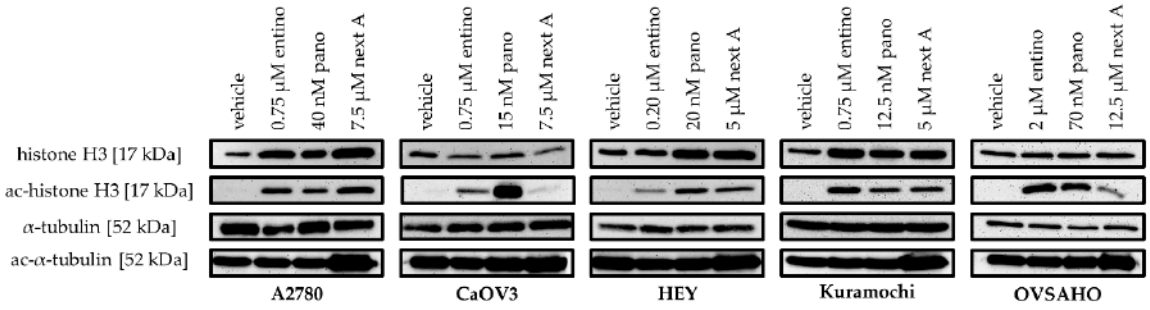

Figure 2. Effect of HDACi on acetylation level of α-tubulin and histone H3. Representative immunoblot analysis of histone H3, ac-histone H3, α-tubulin, and ac-α-tubulin in the different human ovarian cancer cell lines. Cells were treated with the indicated concentrations of HDACi. Control cells were incubated with vehicle. One representative immunoblot with a protein molecular weight marker is shown in Figure S3.

As can be seen, treatment with the HDACi was associated with a hyperacetylation of histone H3 indicating class I HDAC inhibitory effects. Hyperacetylation of α-tubulin is a marker for HDAC6

inhibition. Incubation with nexturastat A confirmed HDAC6 inhibition in every cell line by yielding increased levels of ac-α-tubulin.

2.3. Enhancement of Cisplatin-Induced Cytotoxicity

To investigate a possible effect of HDACi on the cisplatin sensitivity, the ovarian cancer cells were pretreated with HDACi for 48 h, respectively. After medium exchange, a 72 h treatment followed with freshly added HDACi and different concentrations of cisplatin. The concentrations of HDACi used in this combination experiment were adjusted to exert a maximum effect of 44–60% reduction of cell viability in the absence of cisplatin (i.e., a maximum reduction of the upper plateau of concentration-effect curves of 44–60%). Concentrations of HDACi used in combination treatments are shown in Table 4.

Table 4. HDACi concentrations used for combination treatment.

Cell Line	Entinostat [nM]	Panobinostat [nM]	Nexturastat A [nM]
A2780	750	40.0	7500
CaOV3	750	15.0	7500
HEY	200	20.0	5000
Kuramochi	750	12.5	5000
OVSAHO	2000	70.0	12,500

Whereas entinostat retained its class I-selective properties in the used concentration range, nexturastat A was likely to lose HDAC6 selectivity at 5–12.5 μM concentrations used in combinations with cisplatin. However, lower concentrations of nexturastat A did not have effects on the cisplatin sensitivity. To confirm the loss of selectivity of nexturastat A at high concentrations, we performed enzyme HDAC-inhibition assays with nexturastat on representative HDACs for class I, IIa, and IIb.

As can be seen in Table 5, nexturastat A is a nanomolar potency inhibitor at HDAC6 whereas the IC_{50}-value at HDAC2 is 1.99 μM. However, using nexturastat A in combination experiments with cisplatin in concentrations ranging from 5 to 12.5 μM (Table 4) is highly likely to lead to a loss of HDAC6 selectivity. Thus, nexturastat A effects may be attributed to class I and HDAC6 inhibition rather than HDAC6 inhibition only.

Table 5. IC_{50} and inhibitory constants (K_i) of nexturastat A on HDAC2, 4, 6, and 8.

Compd.	HDAC2		HDAC4		HDAC6		HDAC8	
	IC_{50} ± SD [μM]	K_i [μM]	IC_{50} ± SD [μM]	K_i [μM]	IC_{50} ± SD [μM]	K_i [μM]	IC_{50} ± SD [μM]	K_i [μM]
Nexturastat A	1.99 ± 0.25	1.25	12.0 ± 1.69	7.57	0.05 ± 0.01	0.03	22.6 ± 2.55	12.8

Data shown are the mean ± SD of pooled data from at least three experiments each carried out in triplicates.

Table 6 summarizes the effects of 48 h pretreatment of HDACi on the cisplatin concentration-effect curves in all ovarian cancer cell lines. Besides IC_{50}-values of cisplatin alone, IC_{50}-values of cisplatin in the combination with the respective HDACi are displayed. Further, shift factors (ratio of IC_{50}-value of cisplatin and the IC_{50}-value of the combination) were calculated and included in Table 6. Figure 3 shows the corresponding concentration-effect curves of those HDACi–cisplatin combinations that achieved the largest effect in each of the cell lines.

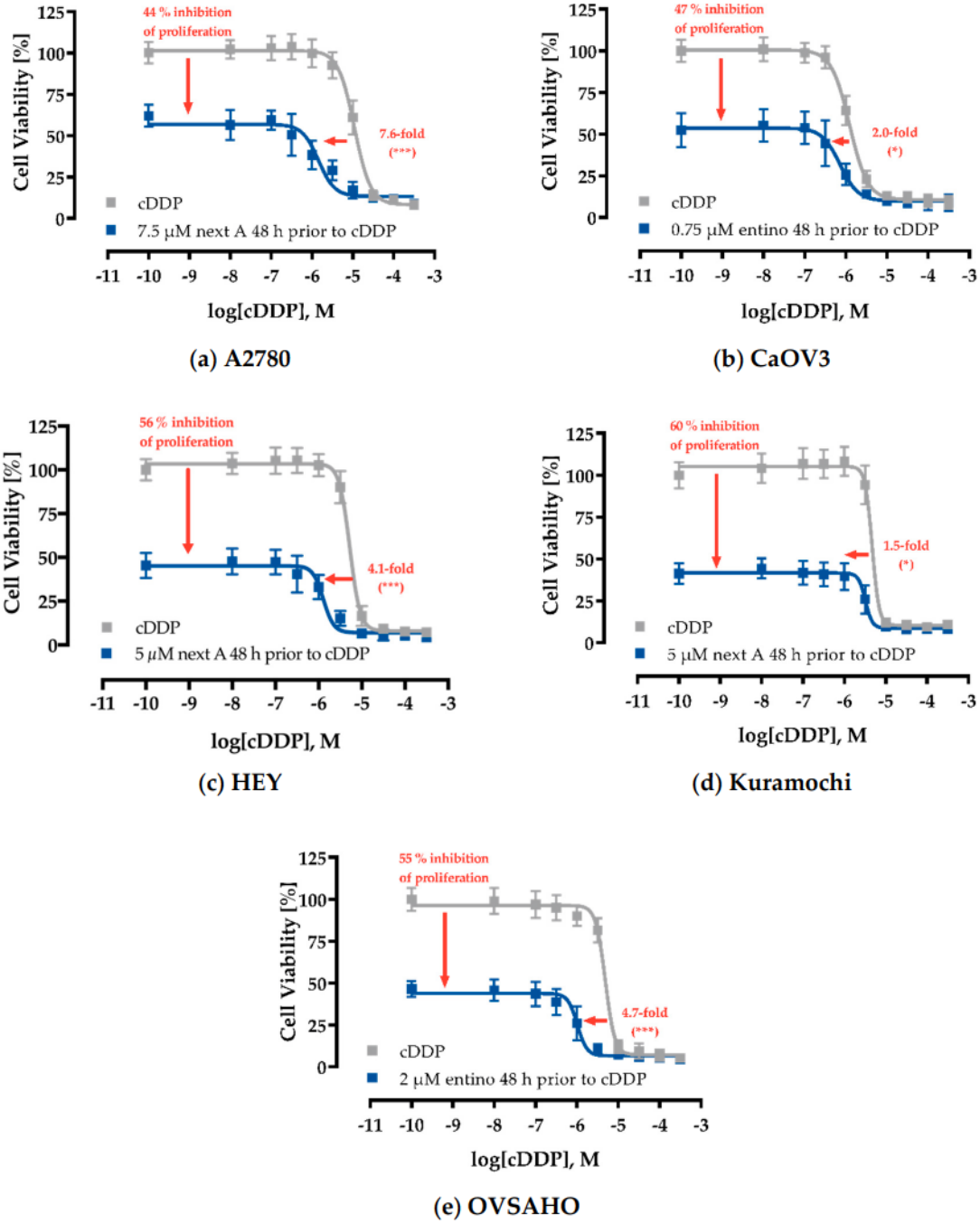

Figure 3. HDACi pretreatment enhances the cytotoxic effects of cisplatin. A2780 (**a**), CaOV3 (**b**), HEY (**c**), Kuramochi (**d**), and OVSAHO (**e**) were pretreated with the indicated HDACi 48 h prior to cisplatin (cDDP) administration. After another 72 h, IC_{50}-values were determined by MTT assay. Data shown are normalized to vehicle control and mean ± SD of at least three experiments each carried out in triplicates. The vertical arrows show the antiproliferative effects of HDACi in the absence of cisplatin and the horizontal arrows show the shifts of the IC_{50}-values of cisplatin (absence and presence of HDACi). Statistical analysis was performed using *t*-test. Levels of significance: ns ($p > 0.05$); * ($p \leq 0.05$); ** ($p \leq 0.01$); *** ($p \leq 0.001$).

Table 6. Effect of HDACi pretreatment on cisplatin-induced cytotoxicity (MTT assay).

Cell Line	Cisplatin	+ 48 h HDACi Pretreatment					
		Entinostat		Panobinostat		Nexturastat A	
	IC_{50}	IC_{50}	SF	IC_{50}	SF	IC_{50}	SF
A2780	11.0	4.99	2.2 (***)	2.58	5.6 (***)	1.44	7.6 (***)
CaOV3	1.44	0.72	2.0 (*)	0.74	2.0 (ns)	1.33	1.1 (ns)
HEY	5.25	1.39	3.8 (***)	2.75	1.9 (*)	1.28	4.1 (***)
Kuramochi	4.68	3.28	1.4 (*)	5.14	< 1 (ns)	3.22	1.5 (**)
OVSAHO	4.83	1.02	4.7 (***)	3.01	1.6 (**)	1.43	3.4 (***)

Data shown are the mean of pooled data from at least three experiments, each carried out in triplicate. Shift-factors (SF) were calculated by dividing the IC_{50}-values without and with HDACi-preincubation. pIC_{50} and SEM are shown in supplemental Table S1. Statistical analysis was performed using *t*-test. Levels of significance: ns ($p > 0.05$); * ($p \leq 0.05$); ** ($p \leq 0.01$); *** ($p \leq 0.001$).

Only class I-selective entinostat was able to increase cisplatin potency in each cell line in a significant manner (Table 6). Even in cisplatin-sensitive CaOV3 cells, entinostat was able to induce a slight, but significant enhancement of cisplatin potency (shift factor of 2.0, Figure 3B, Table 6). Within the HGSOC cell lines, entinostat gave the highest shift factors (except for HEY and Kuramochi cells where shift factors of entinostat and nexturastat A were not significantly different from each other). Entinostat showed the strongest effect in OVSAHO cells (SF = 4.7, Table 6, Figure 3E). Notably, a similar shift factor was achieved in HEY cells (SF = 3.8) with a remarkably low pretreatment-concentration of entinostat (200 nM) whereas the other cell lines were treated with 750 nM (A2780, CAOV, Kuramochi) or even 2000 nM (OVSAHO) entinostat. Surprisingly, the pan HDACi panobinostat was not superior but even less efficacious than entinostat to increase cisplatin potency except in A2780 cells. However, A2780 do not belong to HGSOC. Nexturastat A showed similar efficacy as entinostat. However, it needs to be considered that the concentrations used for nexturastat A (5 to 12.5 µM) lead to a loss of HDAC6 selectivity. Almost complete inhibition of class I HDACs can be assumed considering the K_i values presented in Table 5. Reducing nexturastat A concentration in pretreatment to 2.5 µM led to complete loss of chemosensitizing activity in HEY cells (Figure S2).

To analyze the type of interaction between HDACi and cisplatin, synergism studies according to Chou-Talalay were performed using MTT assay [32,33]. The cell lines were incubated with varying concentrations of HDACi and cisplatin. Cells were pretreated for 48 h with HDACi alone followed by 72 h treatment with HDACi and cisplatin (termed: "48 h + 72 h"). Concentrations were chosen to achieve a fraction affected (f_a; level of cell viability inhibition) between 0.2 and 0.9 in the Chou-Talalay-analysis. Combination indices (CI) were calculated and presented in Table 7.

Table 7. Synergism studies (CI-values) between HDACi entinostat, panobinostat, or nexturastat A and cisplatin.

	Cisplatin [µM]	Entinostat [µM]				Panobinostat [nM]				Nexturastat A [µM]			
		0.10	**0.25**	**0.50**	**0.75**	**10**	**20**	**30**	**40**	**1.25**	**2.50**	**5.00**	**7.50**
A2780	**0.50**	*	0.40	0.36	0.38	0.21	0.10	0.15	0.15	*	0.32	0.24	0.28
	1.00	0.64	0.38	0.35	0.39	0.25	0.12	0.17	0.18	*	0.36	0.28	0.32
	2.00	0.83	0.43	0.34	0.40	0.35	0.16	0.22	0.21	0.97	0.47	0.30	0.33
	4.00	0.73	0.44	0.34	0.38	0.35	0.21	0.27	0.25	>1.1	0.57	0.38	0.39
	6.00	0.59	0.35	0.32	0.37	0.29	0.23	0.26	0.26	0.83	0.52	0.37	0.40
		0.25	**0.50**	**0.75**	**1.00**	-	-	-	-	-	-	-	-
CaOV3	**0.20**	*	0.66	0.71	0.42	o	o	o	o	o	o	o	o
	0.40	*	0.56	0.59	0.33	o	o	o	o	o	o	o	o
	0.60	0.56	0.41	0.49	0.28	o	o	o	o	o	o	o	o
	0.80	0.33	0.30	0.31	0.23	o	o	o	o	o	o	o	o
	1.00	0.21	0.20	0.21	0.16	o	o	o	o	o	o	o	o

Table 7. *Cont.*

	Cisplatin [µM]	Entinostat [µM]				Panobinostat [nM]				Nexturastat A [µM]			
		0.10	0.25	0.50	0.75	10	20	30	40	1.25	2.50	5.00	7.50
		0.10	0.15	0.20	0.25	5.0	10.0	15.0	20.0	1.25	2.50	3.75	5.00
HEY	0.32	*	*	*	0.27	*	*	0.19	0.14	*	*	0.32	0.27
	0.50	*	*	*	0.26	*	*	0.21	0.15	*	*	0.33	0.29
	1.00	*	*	0.31	0.25	*	*	0.25	0.16	*	*	0.36	0.27
	2.00	*	0.37	0.29	0.24	*	0.41	0.25	0.17	*	0.63	0.33	0.26
	4.00	0.35	0.28	0.24	0.23	0.51	0.33	0.28	0.20	0.62	0.42	0.29	0.27
		0.25	0.50	0.75	1.00	-	-	-	-	1.25	2.50	3.75	5.00
Kuramochi	1.00	0.43	0.42	0.51	0.62	○	○	○	○	*	0.73	0.66	0.66
	2.00	0.42	0.43	0.49	0.60	○	○	○	○	*	0.78	0.74	0.72
	3.00	0.46	0.44	0.48	0.57	○	○	○	○	*	0.80	0.77	0.75
	4.00	0.44	0.42	0.44	0.53	○	○	○	○	0.84	0.79	0.77	0.74
	5.00	0.45	0.43	0.47	0.52	○	○	○	○	0.78	0.78	0.74	0.70
		0.50	1.00	1.50	2.00	40	50	60	70	5.00	7.50	10.0	12.5
OVSAHO	1.00	0.50	0.39	0.41	0.44	0.36	0.33	0.27	0.26	*	0.82	0.84	0.78
	2.00	0.41	0.29	0.34	0.37	0.25	0.23	0.21	0.21	0.87	0.77	0.75	0.67
	3.00	0.42	0.28	0.32	0.36	0.24	0.22	0.21	0.21	0.80	0.76	0.65	0.60
	4.00	0.39	0.28	0.31	0.35	0.23	0.22	0.21	0.21	0.72	0.69	0.61	0.57
	5.00	0.39	0.29	0.33	0.36	0.24	0.23	0.22	0.22	0.64	0.59	0.53	0.53

Data shown are combination indices (CI) calculated using CompuSyn 1.0 based on the Chou–Talalay method. CI > 1.1 indicates antagonism, CI = 1 indicates an additive effect, and CI < 0.9 indicates synergism. * means fraction affected is less than 0.20. Values are the mean of two experiments. SD is < 10 % of the mean. Combinations marked with ○ were not investigated because they did not show significant shift factors in combination treatment as can be seen in Table 6.

The interactions between cisplatin and entinostat, panobinostat, or nexturastat A, respectively, were synergistic as indicated by CI-values lower than 0.9. Most CI values were lower than 0.5 indicating strong synergism.

2.4. Enhancement of Cisplatin-Induced Cytotoxicity is Mediated via Apoptosis-Induction

Next, we investigated if the observed synergistic cytotoxic effect was mediated via apoptosis-induction. The cell lines were preincubated for 48 h with the same HDACi concentrations used for the MTT combination treatments (Figure 3, Table 6) followed by addition of cisplatin for another 24 h in an IC_{50} concentration. Then, cells were subjected to flow-cytometry-based subG1 analysis. Results are shown in Figure 4.

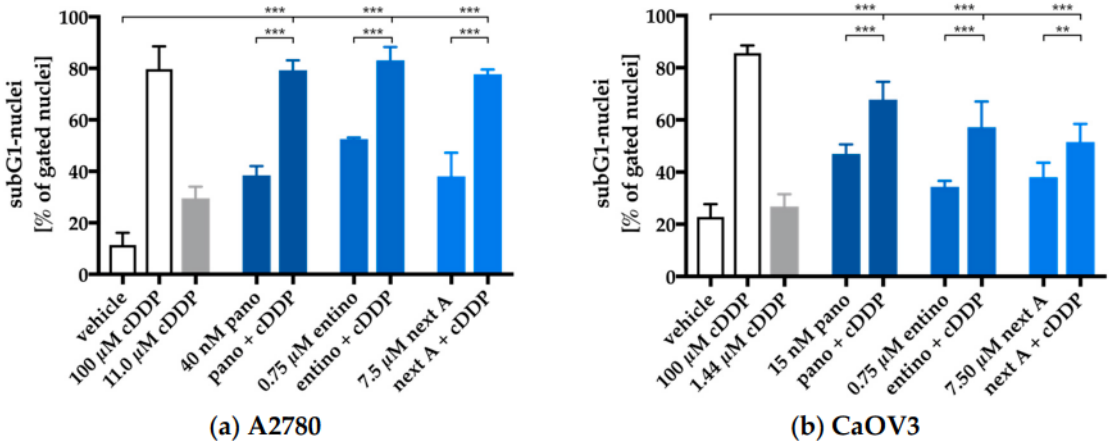

(a) A2780 (b) CaOV3

Figure 4. *Cont.*

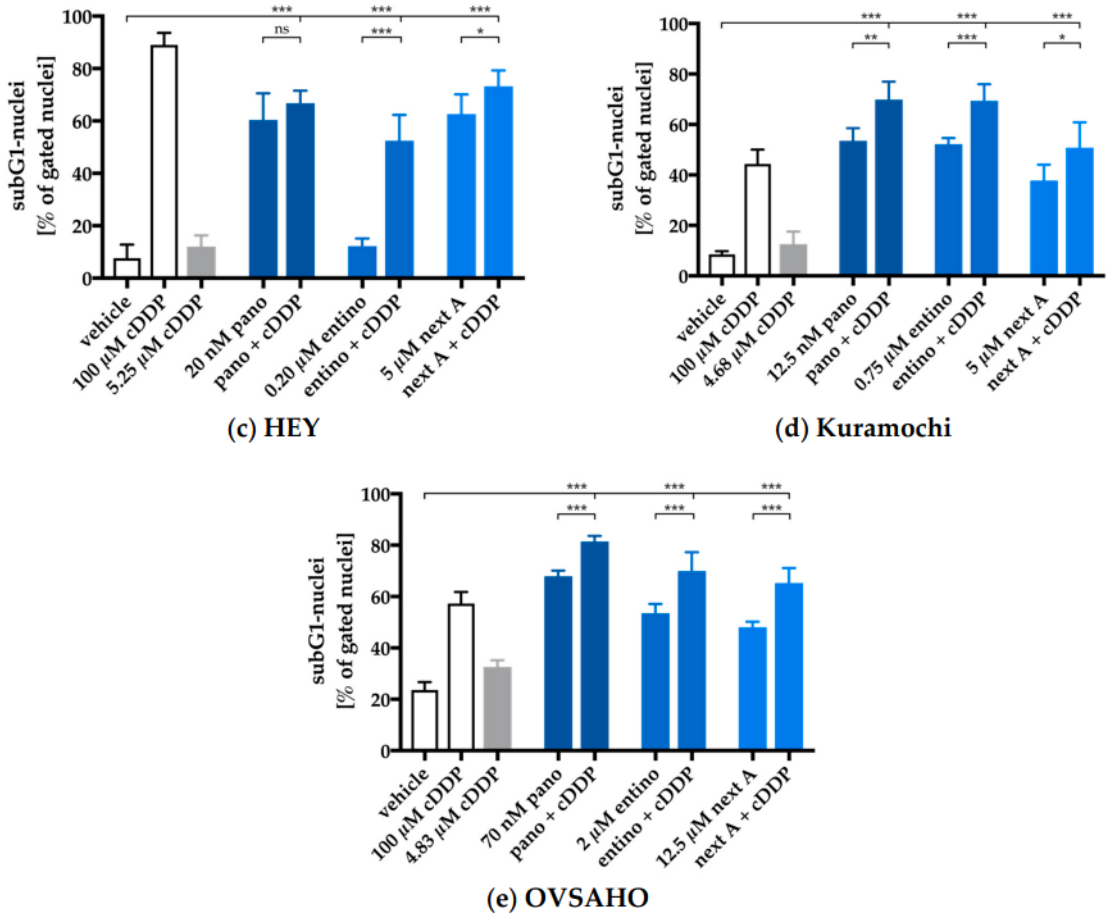

Figure 4. HDACi pretreatment enhances cisplatin-induced apoptosis. A2780 (**a**), CaOV3 (**b**), HEY (**c**), Kuramochi (**d**), and OVSAHO (**e**) cells were preincubated with HDACi for 48 h. Cisplatin was added in an IC_{50} concentration for each cell line for a further incubation period of 24 h. Apoptosis was analyzed by determining the sub-G1 cell fractions by flow cytometry analysis. 100 µM cisplatin served as positive control for apoptosis induction. 0.2% DMSO was added as a control for vehicle treated cells. All experimental conditions were incubated for same time periods. Data are the mean ± SD, n ≥ 2. Statistical analysis to compare the apoptosis induction by cisplatin or HDACi alone and the combination of HDACi and cisplatin was performed using *t*-test. Levels of significance: ns ($p > 0.05$); * ($p \leq 0.05$); ** ($p \leq 0.01$); *** ($p \leq 0.001$).

Single treatment with each HDACi had an equal or higher effect on apoptosis induction than treatment with cisplatin alone in each cell line. Every combination treatment showed a significant increase in apoptosis induction compared to cisplatin or HDACi alone. Only the combination of cisplatin and panobinostat in HEY cells showed no difference in apoptosis induction, possibly due to the unexpected high apoptotic effect of panobinostat alone. In order to determine whether the effects of HDACi and cisplatin combinations on apoptosis induction were hyperadditive (= synergistic), we compared the sum of the single treatment effects of HDACi and cisplatin (subG1 nuclei) with the results from the combination treatment (Figure 5). Data were only analyzed if there was a significant increase in subG1 induction in Figure 4.

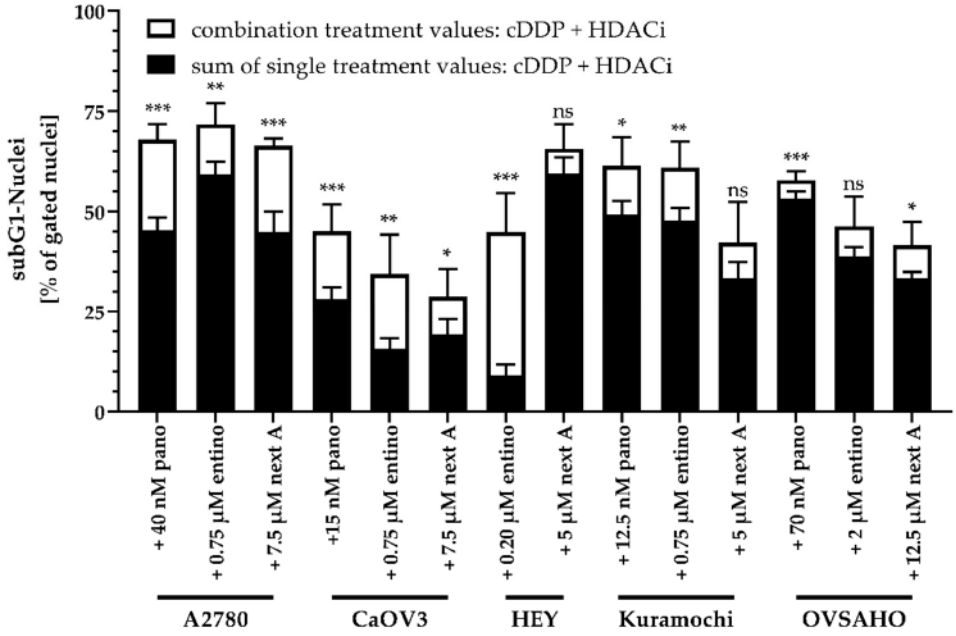

Figure 5. Synergistic effects of the combination of HDACi and cisplatin on apoptosis induction. The sum of single treatment effects (HDACi, cisplatin) are shown in black bars. The extended white bars show the difference (superadditive (= synergistic) part) between the sum of single treatment effects and the effect of combination treatments. Vehicle treated control was subtracted. Data are the mean ± SD. Statistical analysis was performed using *t*-test. Levels of significance: ns ($p > 0.05$); * ($p \leq 0.05$); ** ($p \leq 0.01$); *** ($p \leq 0.001$).

Interestingly, most combinations turned out to be synergistic. Only nexturastat A in HEY and Kuramochi and entinostat in OVSAHO showed no significant difference, probably due to the larger error of the entinostat data. Entinostat showed the strongest increase in subG1 nuclei in HEY cells. Overall, these combination treatment data from apoptosis induction confirm MTT data (Tables 6 and 7).

2.5. Apoptosis-Induction of the Combination Treatment is Caspase3/7-Driven

Here, we tested if apoptosis induction is caspase dependent. Caspase3/7-activation was measured by fluorescence imaging. Untreated controls, single compound and combined treatments of HDACi and cisplatin were analyzed. Figure 6 shows as an example fluorescence images for untreated control (vehicle), cisplatin, entinostat, and the combination of entinostat and cisplatin for each cell line.

Caspase3/7-activation images were monitored for all HDACi and cell lines and analyzed to obtain the results in Figure 7.

With exception of the panobinostat pretreatment in CaOV3 and HEY cells, every other experimental condition lead to an increase in caspase3/7-activation. Surprisingly, pan-HDAC-inhibition with panobinostat showed weaker effects than subtype-selective inhibition with entinostat or nexturastat A. In A2780, CaOV3, HEY, and Kuramochi cells, entinostat showed the strongest effect with exception of nexturastat A in OVSAHO. In order to determine whether the significant effects in caspase3/7-activation are synergistic, we compared the sum of the single treatment effects of HDACi and cisplatin (caspase3/7-activation) with the results from the combination treatments (Figure 8). Data were only analyzed if there was a significant increase in caspase3/7-activation in Figure 7.

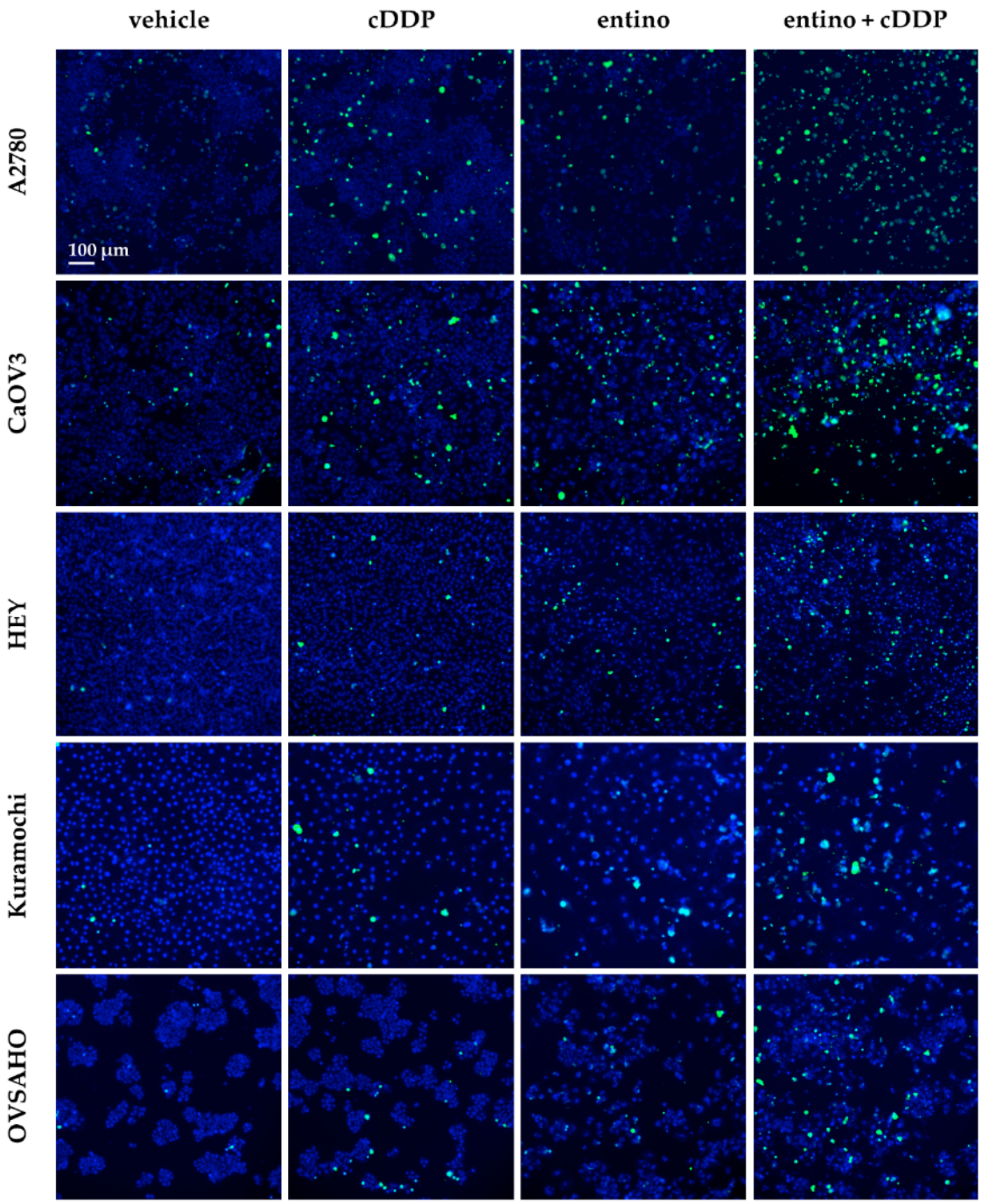

Figure 6. Representative fluorescent imaging pictures (10× magnification) are shown for each cell line for the treatment of cisplatin (IC_{50} concentration), entinostat, and the combination of cisplatin and entinostat. Cell nuclei were stained by Hoechst 33342 and appear blue while cells with activated caspases3/7 showed green fluorescence. Scale bar in upper left image is 100 µm and applies to all images.

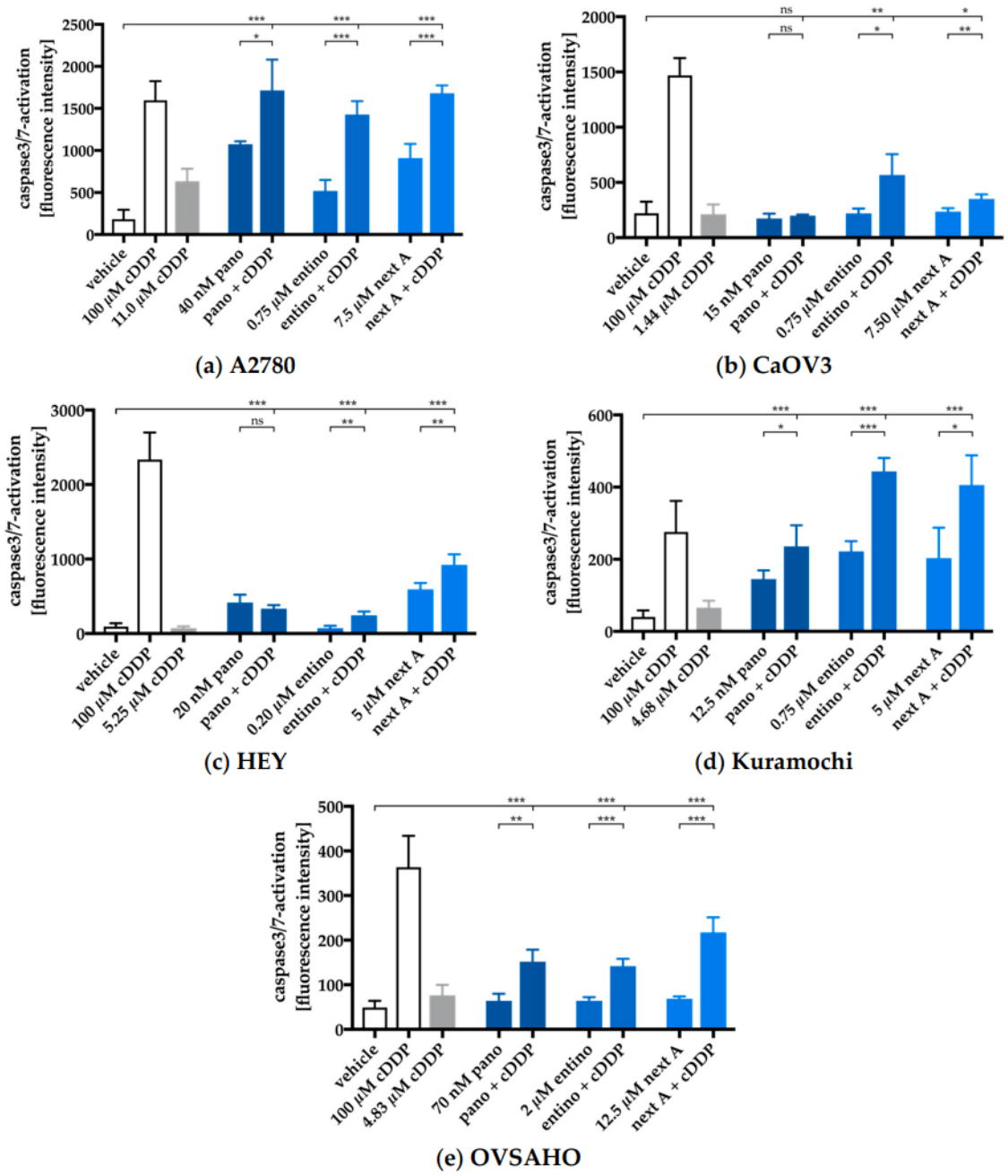

Figure 7. A2780 (**a**), CaOV3 (**b**), HEY (**c**), Kuramochi (**d**), and OVSAHO (**e**) cells were preincubated with HDACi for 48 h. Cisplatin was added in an IC_{50} concentration for each cell line for a further incubation period of 24 h. Caspase3/7-activation was analyzed by incubation with CellEvent Caspase-3/7 green detection reagent (Thermo Scientific, Germany) and visualized by ArrayScan XTI. Cisplatin 100 µM (24 h) was added as positive control for caspase3/7-activation. 0.2% DMSO was added as a control for vehicle treated cells. All experimental conditions were incubated for same time periods. To verify the involvement of caspases in the observed effects, 20 µM QVD was preincubated for 30 min prior to compound addition. No caspase3/7-activation was obtained (data not shown). Data are the mean ± SD. Statistical analysis to compare the caspase3/7-activation by cisplatin or HDACi alone and the combination of HDACi and cisplatin was performed using *t*-test. Levels of significance: ns ($p > 0.05$); * ($p \leq 0.05$); ** ($p \leq 0.01$); *** ($p \leq 0.001$).

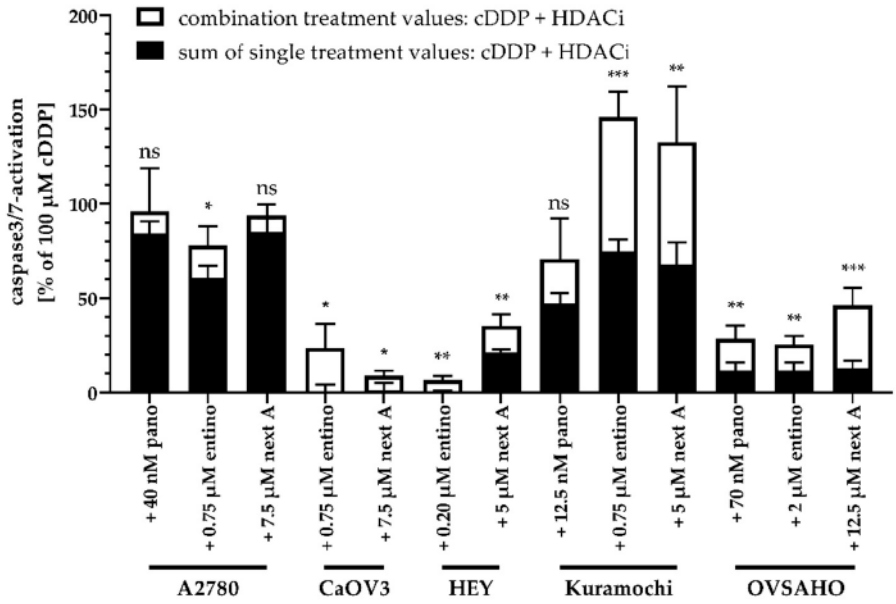

Figure 8. Synergistic effects of caspase3/7-activation upon combination treatment of HDACi and cisplatin. The sum of single treatment effects (HDACi, cisplatin) are shown in black bars. The extended white bars show the difference (superadditive (= synergistic) part) between the sum of single treatment effects and the effect of combination treatments. Results are shown for treatments significantly enhancing caspase3/7-activation (Figure 7). Before calculation, values were normalized to the effect of 100 µM cDDP and vehicle treated control was subtracted. Data shown are mean ± SD. Statistical analysis was performed using *t*-test. Levels of significance: ns ($p > 0.05$); * ($p \leq 0.05$); ** ($p \leq 0.01$); *** ($p \leq 0.001$).

Entinostat showed a significant synergistic effect on caspase3/7-activation in combination with cisplatin in every cell line. This synergism was mostly pronounced in Kuramochi cells as it reached the largest caspase3/7-activation. Caspase3/7-activation revealed a difference between the A2780 and the HGSOC cell lines. While in A2780 cells only entinostat triggered a synergistic effect (caspase3/7-activation) with cisplatin, both, entinostat and nexturastat A showed synergism with cisplatin in all HGSOC cell lines. However, it needs to be considered that nexturastat A was not HDAC6 selective in the concentrations used in this assay.

2.6. Alterations in Apoptosis-Related Gene Expression

To get insight into the mechanism by which HDACi increase the potency of cisplatin in MTT assays, apoptosis induction and caspase activation, we performed RT-PCR-based gene expression analysis of apoptosis and cell cycle related genes. *CDNK1A* (cyclin-dependent kinase inhibitor 1; p21) is a p53-mediated regulator of cell cycle progression at the transition of G_1- and S-phase and normally arrests the cell cycle in G_1-phase after DNA damage [34]. As proapoptotic factors we investigated the expression of *APAF1* (apoptotic protease activating factor 1), *PUMA* (p53 upregulated modulator of apoptosis), and *BAK1* (Bcl-2 homologous antagonist killer) genes. APAF1 is a key factor for the induction of apoptosis, while it forms the apoptosome leading to the activation of the caspase cascade via activation of caspase 9 [35]. PUMA and BAK1 are both proapoptotic members of the Bcl-2 family. As a response to DNA damage, p53 is activated leading to the upregulation of PUMA itself [36]. It is discussed that PUMA interacts with antiapoptotic members of the Bcl-2 family (like Mcl-1, Bcl-2) and inhibits their inhibitory interaction with proapoptotic Bak (coding gene: *BAK1*) and Bax (also members of Bcl-2 family) resulting in a proapoptotic effect [37]. Upon induction, Bak leads to a loss of mitochondrial membrane potential and thus to cytochrome c release and apoptosis. It is also published that Bak forms an oligomeric pore and leads to the permeabilization of the outer membrane of mitochondria [38]. *BIRC5* (baculoviral inhibitor of apoptosis repeat-containing 5; survivin) was

chosen as a representative antiapoptotic gene. It is a member of IAP (inhibitors of apoptosis) family and inhibits the activity of caspase 3/7 [39], which are downstream of caspase 9. BIRC5 leads to an inhibitory effect on apoptosis induction. Changes in apoptosis-related gene expression patterns are shown in Figure 9.

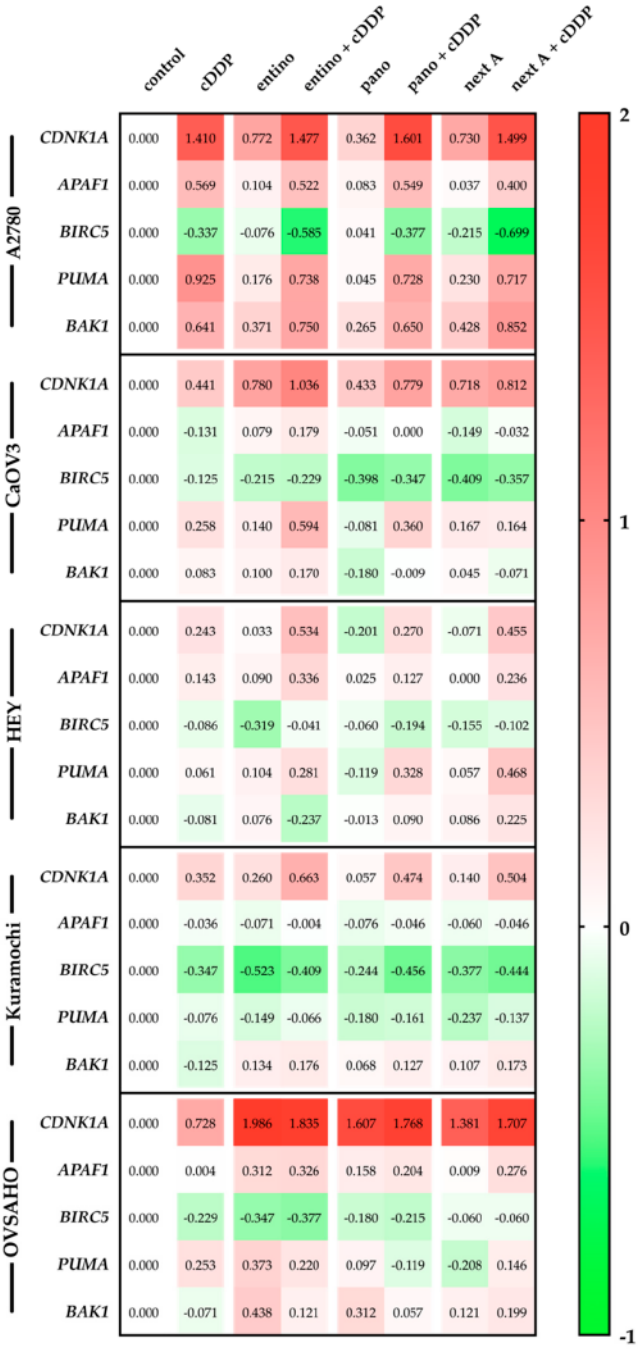

Figure 9. Gene expression data were obtained by RT-PCR and analyzed according to Vandesompele [40]. Cells were pretreated with concentrations of HDACi shown in Table 4 for 48 h followed by treatment with cisplatin for 24 h in an IC_{50} concentration. Data shown are normalized to endogenous control gene expression of *HPRT1* (hypoxanthine-guanine phosphoribosyltransferase), *TBP* (TATA binding protein), and *GUSB* (beta-glucuronidase) and rescaled to cell line specific control (72 h incubation with vehicle). Data are shown on a decadic logarithmic scale. Negative values marked in green show a lower expression compared to cell line specific control. Positive values marked in red show a higher expression compared to cell line specific control.

RT-PCR data showed varying levels of induction of *CDNK1A* (*p21*). While *p21* expression is strongly inducible by cisplatin and HDACi or combined treatment in A2780 and OVSAHO cells, the other cell lines showed a lower *p21* expression. Except for A2780 cells, the combination of HDACi and cisplatin showed a stronger induction of *p21* than cisplatin treatment alone. Interestingly, in OVSAHO cells, HDACi treatment alone had the same effect as the combination of HDACi and cisplatin on *p21* induction. In HEY and Kuramochi cell lines, HDACi only treatment had only moderate effects whereas the combination with cisplatin induces *p21*. In HEY cells, panobinostat and nexturastat A as single treatments led to slight downregulation of *p21*. Except for CaOV3 and Kuramochi cells, proapoptotic *APAF1* was upregulated by cisplatin and/or HDACi treatment. Mostly, combination treatments caused a higher upregulation than single treatment with HDACi. However, in A2780 cells, cisplatin single treatment was as effective in upregulating *APAF1* as combination treatments. The anti-apoptotic gene *survivin* (*BIRC5*) was downregulated as a result of the different treatment regimens. Mostly, the combination of HDACi with cisplatin caused a stronger downregulation of *survivin* gene than single treatments. Strongest downregulation of *survivin* was seen in A2780, CaOV3, and Kuramochi cells. Pro-apoptotic *PUMA* was upregulated under most treatment conditions except in Kuramochi cells. Whereas in A2780 cells combinations of HDACi and cisplatin were not superior to cisplatin alone, in CAOV3 and HEY cells combination treatments were more effective than cisplatin alone in upregulating *PUMA*. Pro-apoptotic *BAK1* expression was induced in A2780 cells upon cisplatin and HDACi treatment, however the combined treatment did only slightly increase *BAK1* expression. In the HGSOC cell lines, *BAK1* expression remained largely unaffected by cisplatin single treatment. HDACi mostly increased *BAK1* expression modestly. Combinations with cisplatin did not lead to additional *BAK1* expression in most cases—except for A2780 cells. As a general tendency, PCR studies showed an upregulation of *p21* and of proapoptotic genes *APAF1*, *PUMA*, *BAK1* as well as a downregulation of the antiapoptotic gene *survivin* (*BIRC5*) in ovarian cancer cell lines.

3. Discussion

Chemoresistance is the major problem in managing cancer. Among ovarian cancer, high grade serous ovarian carcinomas (HGSOC) have the lowest 5 year survival rate and do poorly respond to chemotherapy including platinum compounds [1,12]. Targeting epigenetic processes like DNA methylation or histone acetylation in tumors is a promising therapeutic strategy [20–22]. It is widely known that cancer cells exhibit hypoacetylation of histones (and other proteins) due to an overexpression of HDACs. Histone hypoacetylation leads to a more condensed heterochromatin structure of DNA with decreased expression of tumor suppressor genes and decreased access for DNA damaging agents like cisplatin [41]. HDACi are able to enhance the chemosensitivity of tumors for platinum-based drugs by normalizing the dysregulated process. Mechanisms behind this effect are among others alterations in the apoptosis-related gene expression pattern [42–44]. Studies with approved pan-HDACi like panobinostat and vorinostat (SAHA) explored their effects on gene expression [45,46], but there is still limited data available for cellular and transcriptional effects in solid tumors such as highly aggressive HGSOC. Furthermore, pan-HDACi have no selectivity towards an HDAC isoform or class and can cause severe side effects as known for panobinostat [47–49]. In our study, we compared the effects of one pan-HDACi and two isoform-selective HDACi on the cisplatin sensitivity of four HGSOC cell lines and—as control—one endometrioid adenocarcinoma type I (A2780). The aim was to explore if the use of a subtype-selective HDACi (entinostat, nexturastat A) has advantages over pan-HDACi (panobinostat).

The HDAC6-selective HDACi nexturastat A was efficacious in increasing cisplatin potency in the HGSOC and A2780 cells (Figure 3A,C,D, Table 6). However, the concentration needed to exert such effects was beyond HDAC6-selective concentrations. The K_i value of nexturastat A at HDAC6 was estimated as 0.03 µM whereas at HDAC2, the K_i was 1.25 µM. Even though this is a 42-fold selectivity for HDAC6, concentrations needed for nexturastat A to increase cisplatin potency were 5 µM and higher (Figure S2, Tables 4–6). In conclusion, effects seen with nexturastat A are in a concentration

range where this compound was no longer selective but turned into a class I and class IIb HDACi. Thus, HDAC6 inhibition does not seem to play a major role in sensitization of HGSOC cells against cisplatin.

The pan-HDACi panobinostat was able to increase the cisplatin sensitivity significantly in two out of the four HGSOC cell lines (HEY, OVSAHO) and in A2780 cells. However, in HGSOC cells, panobinostat was less efficacious in increasing cisplatin sensitivity than the class I-HDACi entinostat as seen by lower shift factors for panobinostat (Table 6). In contrast to panobinostat, entinostat was able to significantly increase cisplatin sensitivity in all four HGSOC cell lines (Figure 1B,E, Figure S1A,E,G, Table 6). Since entinostat remains a selective class I HDACi in all concentrations used in this study, it can be concluded that class I HDAC inhibition is sufficient to explain the observed effects and that pan-HDAC inhibition is not only not required but possibly detrimental due to severe side effects associated with pan-HDACi [47–49].

HDACi-mediated increase in cisplatin potency was first estimated in cell viability assays (MTT) and required a preincubation of the HDACi prior to addition of cisplatin (Figure 3, Tables 4 and 6). HDACi and cisplatin combinations were synergistic as shown by the Chou–Talalay analysis (Table 7). HDACi-mediated increase in cisplatin cytotoxicity (MTT) was shown to be associated with increased caspase3/7-activation and apoptosis induction (Figures 5–8). Whereas combinatorial effects of cisplatin and nexturastat A or panobinostat, respectively, were not significant in all cell lines, the combinatorial effects of entinostat and cisplatin were always significant and synergistic (caspase3/7-activation, apoptosis induction) except for apoptosis induction in OVSAHO cells (Figure 5). This leaves the class I-HDACi entinostat as the most promising chemosensitizing HDACi in this study. Based on the presented results and the use of the caspase inhibitor QVD (not shown), it can be assumed that apoptosis induction by entinostat (or the other HDACi) and cisplatin treatment is caspase-3/7-driven in HGSOC cell lines.

The next question was what changes are induced by HDACi in HGSOC cells leading to chemosensitization against cisplatin? It is known that HDACi stimulate apoptosis in ovarian cancer cell lines by alteration of gene expression related to cell growth, cell cycle progression and apoptosis [50]. In hepatocellular carcinomas, proapoptotic *APAF1* is upregulated by HDACi [51]. Overexpression of *survivin* is known for most types of cancer and an association with high grade cancers and poor disease prognosis is well described [52]. It was shown in gastric cancer that overexpression of *BAK1* is related to induction of apoptosis [53]. High expression of *p21* may be a predictor for cisplatin sensitivity in ovarian carcinoma [54]. Proapoptotic *PUMA* is normally upregulated by p53 [55]. These literature results prompted us to analyze the gene expression profile of the five apoptosis and survival-related genes *APAF1*, *survivin*, *BAK1*, *p21*, and *PUMA* by PCR in all ovarian cancer cells used in this study under single and combination treatments of HDACi with cisplatin (Figure 9). As a general summary, we found an upregulation of *p21* and proapoptotic genes and a downregulation of *survivin* upon HDACi treatment. However, variability within the different cell lines was rather large. Whereas *survivin* was downregulated in all cell lines upon entinostat treatment, *APAF1*, *PUMA*, and *BAK1* expression were upregulated in all cell lines except Kuramochi cells in which only *BAK1* was upregulated upon entinostat treatment. The same holds true for *PUMA* expression which is regulated by p53 [55]. Since p53-mutations are quite often observed in HGSOC cancer cell lines (e.g., CaOV3, Kuramochi, and OVSAHO [23,25,26]), it is not surprising that *PUMA* is less upregulated in these cells compared to p53 wt A2780 cells. Although literature describes a direct link between *p21* expression and cisplatin sensitivity [54], we could not establish a quantitative link in our cell lines (Figure 9, Table 6). Still, the gene expression analysis upon HDACi treatment of five apoptosis and survival-related genes can explain facilitated apoptosis upon cisplatin treatment in HGSOC and A2780 cells and is in full agreement with literature data on gene expression of proapoptotic genes presented above.

In conclusion, HDACi are able to increase the sensitivity of HGSOC cancer cell lines towards cisplatin. The class I-selective HDACi entinostat turned out superior in increasing cisplatin potency than pan-HDAC inhibition in cell viability assays (MTT), apoptosis induction (subG1), and caspase3/7-activation. Further, entinostat is synergistic with cisplatin in all cell lines in MTT and caspase

activation assays. Combination indices estimated according to Chou–Talalay were <0.9, indicating synergism. Mechanistically, HDACi induce an upregulation of cell cycle arrest and pro-apoptotic genes (*CDNK1A*, *APAF1*, *PUMA*, *BAK1*) and repression of prosurvival genes such as *survivin* which is in accordance with literature data for different types of cancer [56,57]. In conclusion, the combination of entinostat and cisplatin is synergistic in HGSOC and could be an effective strategy for the clinical treatment of this aggressive ovarian cancer subtype. Furthermore, studies on HDACi-induced gene expression changes (Figure 9) may lead to predictive biomarkers for cisplatin sensitivity in HGSOC.

4. Materials and Methods

4.1. Reagents

Cisplatin was purchased from Sigma (München, Germany) and dissolved in 0.9% sodium chloride solution, propidium iodide (PI) was purchased from PromoKine (Heidelberg, Germany). Stock solutions (10 mM) of entinostat, nexturastat A, and panobinostat (Selleckchem, Houston, Texas, USA) were prepared with DMSO and diluted to the desired concentrations with the appropriate medium. All other reagents were supplied by PAN Biotech (Aidenbach, Germany) unless otherwise stated.

4.2. Cell Lines and Cell Culture

The human ovarian carcinoma cell lines A2780 and HEY were obtained from European Collection of Cell Cultures (ECACC, Salisbury, UK). The cell lines Kuramochi and OVSAHO were obtained from Japanese Collection of Research Bioresources Cell Bank (JCRB Cell Bank, Osaka, Japan). CaOV3 cell line was obtained from ATCC/LGC Standards GmbH (Wesel, Germany). All cell lines were grown at 37 °C under humidified air supplemented with 5% CO_2 in RPMI 1640 (A2780, HEY, Kuramochi, OVSAHO) or DMEM (CaOV3) containing 10% heat inactivated fetal calf serum, 120 IU/mL penicillin, and 120 µg/mL streptomycin. The cells were grown to 80% confluency before being used in further assays.

4.3. MTT Cell Viability Assay

The rate of cell-survival under the action of test substances was evaluated by an improved MTT assay as previously described [20,31]. To investigate the effect of entinostat, panobinostat, and nexturastat A on cisplatin induced cytotoxicity, compounds were added 48 h before cisplatin administration. After 72 h, the cytotoxic effect was determined by MTT assay as described above (density of cell seeding for this incubation scheme: A2780 3000 cells/well (c/w), CaOV3 3000 c/w, HEY 3500 c/w, Kuramochi 4500 c/w, and OVSAHO 10,000 c/w), and shift factors were calculated by dividing the IC_{50} value of cisplatin alone by the IC_{50} value of the drug combinations. Incubation was ended after 72 h and cell survival was determined by addition of MTT (Serva, Heidelberg, Germany) solution (5 mg/mL in phosphate buffered saline). The formazan precipitate was dissolved in DMSO (VWR, Langenfeld, Germany). Absorbance was measured at 544 nm and 690 nm in a FLUOstar microplate-reader (BMG LabTech, Offenburg, Germany).

4.4. Whole-Cell HDAC Inhibition Assay

The cellular HDAC assay was based on an assay published by Heltweg and Jung [58], Ciossek et al. [59], and Bonfils et al. [60] with minor modifications as described in [20]. Briefly, human cancer cell lines A2780, CaOV3, HEY, Kuramochi, and OVSAHO were seeded in 96-well tissue culture plates (Corning, Kaiserslautern, Germany) at a density of 15,000 c/w, 15,000 c/w, 17,500 c/w, 22,500 c/w, and 50,000 c/w in a total volume of 90 µL of culture medium. After 24 h, cells were incubated for 18 h with increasing concentrations of test compounds. The reaction was started by adding 10 µL of 3 mM Boc-Lys(Ac)-AMC (Bachem, Bubendorf, Switzerland) to reach final concentration of 0.3 mM [61]. The cells were incubated with the Boc-Lys(Ac)-AMC for 3 h under cell culture conditions. After this incubation, 100 µL/well stop solution (25 mM Tris-HCl (pH 8), 137 mM NaCl, 2.7 mM KCl, 1 mM MgCl2, 1 % NP40, 2.0 mg/mL Trypsin, 10 µM Vorinostat) was added and the reaction was developed

for 3 h under cell culture conditions. Fluorescence intensity was measured at excitation of 320 nm and emission of 520 mm in a NOVOstar microplate reader (BMG LabTech, Offenburg, Germany).

4.5. Combination Experiments

For the investigation of the effect of HDACi on cisplatin induced cytotoxicity, the compounds were added 48 h before cisplatin administration. After 72 h, the cytotoxic effect was determined with a MTT cell viability assay. Calcusyn software 2.1 (Biosoft, Cambridge, UK) was used to calculate the combination index (CI) as a quantitative measure of the degree of drug interaction.

4.6. Enzyme HDAC Inhibition Assay

All human recombinant enzymes were purchased from Reaction Biology Corp. (Malvern, PA, USA). The HDAC activity assay HDAC2 (cat nr. KDA-21-277), HDAC4 (cat nr. KDA-21-279), HDAC6 (cat nr. KDA-21-213), and HDAC8 (cat nr. KDA-21-481) was performed in 96-well-plates (Corning, Kaiserslautern, Germany). Briefly 20 ng of HDAC2/8, 17.5 ng of HDAC6 and 2 ng of HDAC4 per reaction were used. Recombinant enzymes were diluted in assay buffer (50 mM Tris-HCl, pH 8.0, 137 mM NaCl, 2.7 mM KCl, 1 mM $MgCl_2$, and 1 mg/mL BSA). After a 5 min incubation step the reaction was started with 10 µL of 300 µM (HDAC2), 150 µM (HDAC6) Boc-Lys(Ac)-AMC (Bachem, Bubendorf, Switzerland) or 100 µM (HDAC4), 60 µM (HDAC8) Boc-Lys-(TFa)-AMC (Bachem, Bubendorf, Switzerland). The reaction was stopped after 90 min by adding 100 µL stop solution (16 mg/mL trypsin, 2 µM panobinostat for HDAC2/6/8, 2µM CHDI0039 (kindly provided by the CHDI Foundation Inc., New York, USA) for HDAC4 in 50 mM Tris-HCl, pH 8.0, and 100 mM NaCl. 15 min after the addition of the stop solution the fluorescence intensity was measured at excitation of 355 nm and emission of 460 nm in a NOVOstar microplate reader (BMG LabTech, Offenburg, Germany).

4.7. Measurement of Apoptotic Nuclei

A2780, CaOV3, HEY, Kuramochi, and OVSAHO cells were seeded at a density of 40,000 c/w, 50,000 c/w, 40,000 c/w, 60,000 c/w, and 100,000 c/w in 24-well plates (Sarstedt, Nürnbrecht, Germany). Cells were treated with entinostat, panobinostat, or nexturastat A and cisplatin alone or in combination for the indicated time points. Supernatant was removed after a centrifugation step and the cells were lysed in 500 µL hypotonic lysis buffer (0.1% sodium citrate, 0.1% Triton X-100, 100 µg/mL PI) at 4 °C in the dark overnight. The percentage of apoptotic nuclei with DNA content in sub-G1 was analyzed by flow cytometry using the CyFlow instrument (Partec, Norderstedt, Germany).

4.8. Caspase 3/7 Activation Assay

Compound-induced activation of caspases 3 and 7 was analyzed using the CellEvent Caspase-3/7 green detection reagent (Thermo Scientific, Wesel, Germany) according to the manufacturer's instructions. Briefly, A2780, CaOV3, HEY, Kuramochi, and OVSAHO cells were seeded in 96-well-plates (Corning, Kaiserslautern, Germany) at a density of 4000 c/w, 7500 c/w, 7500 c/w, 4500 c/w, and 10000 c/w. Cells were treated with entinostat, panobinostat, or nexturastat A 48 h prior to the addition cisplatin and another incubation period of 24 h. Then, medium was removed and 50 µL of CellEvent Caspase 3/7 green detection reagent (2 µM in PBS supplemented with 5% heat inactivated FBS) was added. Cells were incubated for 30 min at 37 °C in a humidified incubator before imaging by using the Thermo Fisher ArrayScan XTI high content screening (HCS) system with a 10× magnification (Thermo Scientific). Hoechst 33342 was used for nuclei staining. The pan caspase inhibitor QVD was used in a concentration of 20 µM diluted in the appropriate medium and incubated 30 min prior to compound addition.

4.9. Immunoblotting

Cells were treated with indicated concentrations of entinostat, panobinostat, or nexturastat A for 48h prior to cisplatin (24 h) or 72 h entinostat, panobinostat, or nexturastat A without cisplatin, or vehicle for 72 h. Cell pellets were dissolved with RIPA buffer (50 mM Tris-HCl pH8.0, 1% Triton X-100, 0.5% sodium deoxycholate, 0.1% SDS, 150 mM sodium chloride, 2 mM EDTA, supplemented with protease and phosphatase inhibitors (Pierce™ protease and phosphatase inhibitor mini tablets, Thermo Scientific, Wesel, Germany)) and clarified by centrifugation. Equal amounts of total protein (20 µg unless otherwise stated) were resolved by SDS-PAGE and transferred to polyvinylidene fluoride membranes (Merck Millipore, Darmstadt, Germany). PageRuler Prestained Protein Ladder, 10 to 180 kDa (Thermo Scientific, Wesel, Germany) was used as protein molecular weight marker. Blots were incubated with primary antibodies against acetylated α-tubulin (Cat. No. sc-23950), α-tubulin (Cat. No. sc-8035) (Santa Cruz Biotechnology, Heidelberg, Germany), histone H3 (Cat. No. MAB9448), acetyl histone H3 (Lys24, Cat. No. NBP2-54615), HDAC1 (Cat. No. NB100-56340), HDAC2 (Cat. No. MAB7679), HDAC3 (Cat. No. NB100-1669), HDAC4 (Cat. No. AF6205), HDAC5 (Cat. No. NBP2-22152), HDAC6 (Cat. No. NB100-56343), HDAC10 (Cat. No. NB100-91801), and HDAC11 (Cat. No. NBP2-16789) (Biotechne, Wiesbaden, Germany). Immunoreactive proteins were visualized using luminol reagent (Santa Cruz Biotechnology, Heidelberg, Germany) with an Intas Imager (Intas, Göttingen, Germany).

4.10. RT-PCR

Cells were treated with indicated concentrations of entinostat, panobinostat, or nexturastat a for 48 h prior to cisplatin (24 h) or 72 h entinostat, panobinostat, or nexturastat A without cisplatin, or cell culture medium for 72 h. RNA was isolated using RNeasy Mini Kit (Qiagen, Hilden, Germany). Afterwards transcription to cDNA was performed with High Capacity cDNA Reverse Transcription Kit (Thermo Scientific, Wesel, Germany). RT-PCR was performed with GoTaq qPCR Master Mix (Promega, USA) in a CFX96 Real-Time System (BIO-RAD, Hercules, California, USA). Relative changes in gene expression were normalized to endogenous control genes *GUSB* (beta-glucuronidase), *TBP* (TATA binding protein), and *HPRT1* (hypoxanthine-guanine phosphoribosyltransferase) by Vandesompele method [40] and if indicated normalized to vehicle treated control. Primers (Sigma Aldrich, Steinheim, Germany) with an efficacy between 80% and 115% were used (Table 8). They were designed by Primer-BLAST (NIH, Bethesda, Maryland, USA) [62] and efficacy was determined with a template isolated from HeLa cells.

Table 8. Primer sequences for RT-PCR.

Gene	Primer Forward	Primer Reverse	Efficacy [%]
HPRT1	CCTGGCGTCGTGATTAGTGA	CGAGCAAGACGTTCAGTCCT	93.6
TBP	GTGACCCAGCATCACTGTTTC	GAGCATCTCCAGCACACTCT	86.9
GUSB	ACCTCCAAGTATCCCAAGGGT	GTCTTGCTCCACGCTGGT	83.1
HDAC1	TGCAAAGAAGTCCGAGGCAT	ACCCTCTGGTGATACTTTAGCA	84.9
HDAC2	AATGGAAATATATAGGCCCC	GTTATCTGGTCTTATTGACCG	96.4
HDAC3	GGCAACTTCCACTACGGAGC	GCATATTGGTGGGGCTGACT	97.2
HDAC4	TTGGATGTCACAGACTCCGC	CCTTCTCGTGCCACAAGTCT	80.8
HDAC5	GGAGAGCTCAAGAATGGATTTGC	CTGCTGTAGGAGTTTTGCG	97.2
HDAC6	CTGGCGGAGTGGAAGAACC	TCTGCCTACTTCTTCGCTGC	104
HDAC7	TCTCGTGAGCTAAAGAATGG	CTGTTGAATGATCTGCATGG	96.5
HDAC8	CCACCTTCCACACTGATGCT	GCTGGGCAGTCATAACCTAGC	97.7
HDAC9	TGTAGCTGGTGGAGTTCCCT	CTCTGAGGCAAAGGTGCAGA	103
HDAC10	TGGCCTTTGAGTTTGACCCT	CCGATGGCTGAGTCAAATCCT	97.3
HDAC11	CGGAAAATGGGGCAAAGTGA	CAACAGCAAAGGACCACTTG	100
CDNK1A (p21)	TGCCGAAGTCAGTTCCTTGT	GTTCTGACATGGCGCCTCC	94.7
BIRC5 (Survivin)	TGAGAACGAGCCAGACTTGG	TGTTCCTCTATGGGGTCGTCA	108
APAF1	AGTGGAATAACTTCGTATGTAAGGA	AAACAACTGGCCTCTGTGGT	98.7
BAK1	TCATCGGGGACGACATCAAC	CAAACAGGCTGGTGGCAATC	111
PUMA	GAGCGGCGGAGACAAGAG	TAAGGGCAGGAGTCCCATGA	94.7

4.11. Data Analysis

Concentration-effect curves were constructed with Prism 7.0 (GraphPad, San Diego, CA, USA) by fitting the pooled data of at least three experiments performed in triplicate to the four-parameter logistic equation. Statistical analysis was performed using *t*-test or one-way ANOVA. To analyze the synergistic effects of apoptosis induction and caspase3/7-activation, the values of the single treatments were summed up and the standard deviation calculated. This value was compared with the actual measured value of the combination treatment using *t*-test.

Supplementary Materials: Supplementary materials can be found at http://www.mdpi.com/1422-0067/20/12/3052/s1.

Author Contributions: Conceptualization, M.U.K. and A.H.; Formal analysis, J.J.B. and R.W.; Funding acquisition, M.U.K.; Investigation, J.J.B. and C.S.; Project administration, M.U.K.; Resources, M.U.K.; Supervision, M.U.K. and A.H.; Visualization, J.J.B.; Writing—original draft, J.J.B.; Writing—review & editing: M.U.K. and A.H.

Funding: The Deutsche Forschungsgemeinschaft DFG is acknowledged for funds used to purchase the ArrayScan XTI High Content Platform used in this research (INST 208/690-1).

Conflicts of Interest: The authors declare no conflict of interest.

Abbreviations

HDAC	histone deacetylase
HDACi	histone deacetylase inhibitor
entino	entinostat
cDDP	*cis*-diamminedichloridoplatinum(II) (cisplatin)
pano	panobinostat
next A	nexturastat A
BIRC5, survivin	baculoviral inhibitor of apoptosis repeat-containing 5
PUMA	p53 upregulated modulator of apoptosis
BAK/Bak	Bcl-2 homologous antagonist killer
CDNK1A, p21	cyclin-dependent kinase inhibitor 1
APAF1	apoptotic protease activating factor 1
IAP	inhibitors of apoptosis
HPRT1	hypoxanthine-guanine phosphoribosyltransferase
GUSB	beta-glucuronidase
TBP	TATA binding protein
HGSOC	high grade serous ovarian cancer
MTT	3-(4,5-Dimethylthiazole-2-yl)-2,5-diphenyltetrazoliumbromide
CI	combination index
RT-PCR	reverse transcriptase polymerase chain reaction

References

1. Cancer of the Ovary - Cancer Stat Facts. Available online: https://seer.cancer.gov/statfacts/html/ovary.html (accessed on 24 April 2019).
2. Cancer of the Cervix Uteri - Cancer Stat Facts. Available online: https://seer.cancer.gov/statfacts/html/cervix.html (accessed on 24 April 2019).
3. Cancer of the Breast (Female) - Cancer Stat Facts. Available online: https://seer.cancer.gov/statfacts/html/breast.html (accessed on 24 April 2019).
4. Cancer of the Vulva - Cancer Stat Facts. Available online: https://seer.cancer.gov/statfacts/html/vulva.html (accessed on 24 April 2019).
5. Cancer of the Endometrium - Cancer Stat Facts. Available online: https://seer.cancer.gov/statfacts/html/corp.html (accessed on 24 April 2019).
6. Krebs – Datenbankabfrage. Available online: https://www.krebsdaten.de/Krebs/SiteGlobals/Forms/Datenbankabfrage/datenbankabfrage_stufe2_form.html (accessed on 14 May 2019).

7. Singh, N.; McCluggage, W.G.; Gilks, C.B. High-grade serous carcinoma of tubo-ovarian origin: recent developments. *Histopathology* **2017**, *71*, 339–356. [CrossRef] [PubMed]
8. Köbel, M.; Kalloger, S.E.; Huntsman, D.G.; Santos, J.L.; Swenerton, K.D.; Seidman, J.D.; Gilks, C.B. Cheryl Brown Ovarian Cancer Outcomes Unit of the British Columbia Cancer Agency, Vancouver BC Differences in tumor type in low-stage versus high-stage ovarian carcinomas. *Int. J. Gynecol. Pathol. Off. J. Int. Soc. Gynecol. Pathol.* **2010**, *29*, 203–211.
9. Kohn, E.C.; Ivy, S.P. Whence High-Grade Serous Ovarian Cancer. *Am. Soc. Clin. Oncol. Educ. Book Am. Soc. Clin. Oncol. Annu. Meet.* **2017**, *37*, 443–448. [CrossRef] [PubMed]
10. Koshiyama, M.; Matsumura, N.; Konishi, I. Subtypes of Ovarian Cancer and Ovarian Cancer Screening. *Diagnostics* **2017**, *7*. [CrossRef] [PubMed]
11. Eisenhauer, E.A. Real-world evidence in the treatment of ovarian cancer. *Ann. Oncol. Off. J. Eur. Soc. Med. Oncol.* **2017**, *28*, viii61–viii65. [CrossRef] [PubMed]
12. Ghosh, S. Cisplatin: The first metal based anticancer drug. *Bioorganic Chem.* **2019**, *88*, 102925. [CrossRef] [PubMed]
13. Ohmichi, M.; Hayakawa, J.; Tasaka, K.; Kurachi, H.; Murata, Y. Mechanisms of platinum drug resistance. *Trends Pharmacol. Sci.* **2005**, *26*, 113–116. [CrossRef]
14. Jain, A.; Jahagirdar, D.; Nilendu, P.; Sharma, N.K. Molecular approaches to potentiate cisplatin responsiveness in carcinoma therapeutics. *Expert Rev. Anticancer Ther.* **2017**, *17*, 815–825. [CrossRef]
15. Eckschlager, T.; Plch, J.; Stiborova, M.; Hrabeta, J. Histone Deacetylase Inhibitors as Anticancer Drugs. *Int. J. Mol. Sci.* **2017**, *18*, 1414. [CrossRef]
16. Kim, H.-J.; Bae, S.-C. Histone deacetylase inhibitors: molecular mechanisms of action and clinical trials as anti-cancer drugs. *Am. J. Transl. Res.* **2011**, *3*, 166–179.
17. Gregoretti, I.; Lee, Y.-M.; Goodson, H.V. Molecular Evolution of the Histone Deacetylase Family: Functional Implications of Phylogenetic Analysis. *J. Mol. Biol.* **2004**, *338*, 17–31. [CrossRef] [PubMed]
18. Yang, Q.; Yang, Y.; Zhou, N.; Tang, K.; Lau, W.B.; Lau, B.; Wang, W.; Xu, L.; Yang, Z.; Huang, S.; et al. Epigenetics in ovarian cancer: premise, properties, and perspectives. *Mol. Cancer* **2018**, *17*, 109. [CrossRef] [PubMed]
19. Yano, M.; Yasuda, M.; Sakaki, M.; Nagata, K.; Fujino, T.; Arai, E.; Hasebe, T.; Miyazawa, M.; Miyazawa, M.; Ogane, N.; et al. Association of histone deacetylase expression with histology and prognosis of ovarian cancer. *Oncol. Lett.* **2018**, *15*, 3524–3531. [CrossRef] [PubMed]
20. Marek, L.; Hamacher, A.; Hansen, F.K.; Kuna, K.; Gohlke, H.; Kassack, M.U.; Kurz, T. Histone deacetylase (HDAC) inhibitors with a novel connecting unit linker region reveal a selectivity profile for HDAC4 and HDAC5 with improved activity against chemoresistant cancer cells. *J. Med. Chem.* **2013**, *56*, 427–436. [CrossRef] [PubMed]
21. Stenzel, K.; Hamacher, A.; Hansen, F.K.; Gertzen, C.G.W.; Senger, J.; Marquardt, V.; Marek, L.; Marek, M.; Romier, C.; Remke, M.; et al. Alkoxyurea-Based Histone Deacetylase Inhibitors Increase Cisplatin Potency in Chemoresistant Cancer Cell Lines. *J. Med. Chem.* **2017**, *60*, 5334–5348. [CrossRef] [PubMed]
22. Krieger, V.; Hamacher, A.; Gertzen, C.G.W.; Senger, J.; Zwinderman, M.R.H.; Marek, M.; Romier, C.; Dekker, F.J.; Kurz, T.; Jung, M.; et al. Design, Multicomponent Synthesis, and Anticancer Activity of a Focused Histone Deacetylase (HDAC) Inhibitor Library with Peptoid-Based Cap Groups. *J. Med. Chem.* **2017**, *60*, 5493–5506. [CrossRef] [PubMed]
23. Cellosaurus Cell Line Caov-3 (CVCL_0201). Available online: https://web.expasy.org/cellosaurus/CVCL_0201 (accessed on 17 May 2019).
24. Cellosaurus Cell Line HEY (CVCL_0297). Available online: https://web.expasy.org/cellosaurus/CVCL_0297 (accessed on 17 May 2019).
25. Cellosaurus Cell Line Kuramochi (CVCL_1345). Available online: https://web.expasy.org/cellosaurus/CVCL_1345 (accessed on 17 May 2019).
26. Cellosaurus Cell Line OVSAHO (CVCL_3114). Available online: https://web.expasy.org/cellosaurus/CVCL_3114 (accessed on 17 May 2019).
27. Domcke, S.; Sinha, R.; Levine, D.A.; Sander, C.; Schultz, N. Evaluating cell lines as tumour models by comparison of genomic profiles. *Nat. Commun.* **2013**, *4*, 2126. [CrossRef]
28. Cellosaurus Cell Line A2780 (CVCL_0134). Available online: https://web.expasy.org/cellosaurus/CVCL_0134 (accessed on 17 May 2019).

29. Beaufort, C.M.; Helmijr, J.C.A.; Piskorz, A.M.; Hoogstraat, M.; Ruigrok-Ritstier, K.; Besselink, N.; Murtaza, M.; van IJcken, W.F.J.; Heine, A.A.J.; Smid, M.; et al. Ovarian Cancer Cell Line Panel (OCCP): Clinical Importance of In Vitro Morphological Subtypes. *PLoS ONE* **2014**, *9*, e103988. [CrossRef]
30. Panteix, G.; Beaujard, A.; Garbit, F.; Chaduiron-Faye, C.; Guillaumont, M.; Gilly, F.; Baltassat, P.; Bressolle, F. Population pharmacokinetics of cisplatin in patients with advanced ovarian cancer during intraperitoneal hyperthermia chemotherapy. *Anticancer Res.* **2002**, *22*, 1329–1336.
31. Engelke, L.H.; Hamacher, A.; Proksch, P.; Kassack, M.U. Ellagic Acid and Resveratrol Prevent the Development of Cisplatin Resistance in the Epithelial Ovarian Cancer Cell Line A2780. *J. Cancer* **2016**, *7*, 353–363. [CrossRef]
32. Chou, T.-C. Drug combination studies and their synergy quantification using the Chou-Talalay method. *Cancer Res.* **2010**, *70*, 440–446. [CrossRef] [PubMed]
33. Chou, T.-C.; Talalay, P. Quantitative analysis of dose-effect relationships: the combined effects of multiple drugs or enzyme inhibitors. *Adv. Enzyme Regul.* **1984**, *22*, 27–55. [CrossRef]
34. Waldman, T.; Kinzler, K.W.; Vogelstein, B. p21 Is Necessary for the p53-mediated G1 Arrest in Human Cancer Cells. *Cancer Res.* **1995**, *55*, 5187–5190. [PubMed]
35. Pop, C.; Timmer, J.; Sperandio, S.; Salvesen, G.S. The Apoptosome Activates Caspase-9 by Dimerization. *Mol. Cell* **2006**, *22*, 269–275. [CrossRef] [PubMed]
36. Han, J.; Flemington, C.; Houghton, A.B.; Gu, Z.; Zambetti, G.P.; Lutz, R.J.; Zhu, L.; Chittenden, T. Expression of bbc3, a pro-apoptotic BH3-only gene, is regulated by diverse cell death and survival signals. *Proc. Natl. Acad. Sci.* **2001**, *98*, 11318–11323. [CrossRef] [PubMed]
37. Nakano, K.; Vousden, K.H. PUMA, a Novel Proapoptotic Gene, Is Induced by p53. *Mol. Cell* **2001**, *7*, 683–694. [CrossRef]
38. McArthur, K.; Whitehead, L.W.; Heddleston, J.M.; Li, L.; Padman, B.S.; Oorschot, V.; Geoghegan, N.D.; Chappaz, S.; Davidson, S.; Chin, H.S.; et al. BAK/BAX macropores facilitate mitochondrial herniation and mtDNA efflux during apoptosis. *Science* **2018**, *359*, eaao6047. [CrossRef]
39. Shin, S.; Sung, B.-J.; Cho, Y.-S.; Kim, H.-J.; Ha, N.-C.; Hwang, J.-I.; Chung, C.-W.; Jung, Y.-K.; Oh, B.-H. An Anti-apoptotic Protein Human Survivin Is a Direct Inhibitor of Caspase-3 and -7. *Biochemistry* **2001**, *40*, 1117–1123. [CrossRef]
40. Vandesompele, J.; De Preter, K.; Pattyn, F.; Poppe, B.; Van Roy, N.; De Paepe, A.; Speleman, F. Accurate normalization of real-time quantitative RT-PCR data by geometric averaging of multiple internal control genes. *Genome Biol.* **2002**, *3*, RESEARCH0034. [CrossRef]
41. Benton, C.B.; Fiskus, W.; Bhalla, K.N. Targeting Histone Acetylation: Readers and Writers in Leukemia and Cancer. *Cancer J. Sudbury Mass* **2017**, *23*, 286–291. [CrossRef]
42. Pchejetski, D.; Alfraidi, A.; Sacco, K.; Alshaker, H.; Muhammad, A.; Monzon, L. Histone deacetylases as new therapy targets for platinum-resistant epithelial ovarian cancer. *J. Cancer Res. Clin. Oncol.* **2016**, *142*, 1659–1671. [CrossRef] [PubMed]
43. Spiegel, S.; Milstien, S.; Grant, S. Endogenous modulators and pharmacological inhibitors of histone deacetylases in cancer therapy. *Oncogene* **2012**, *31*, 537–551. [CrossRef] [PubMed]
44. Ozaki, K.; Kishikawa, F.; Tanaka, M.; Sakamoto, T.; Tanimura, S.; Kohno, M. Histone deacetylase inhibitors enhance the chemosensitivity of tumor cells with cross-resistance to a wide range of DNA-damaging drugs. *Cancer Sci.* **2008**, *99*, 376–384. [CrossRef] [PubMed]
45. Chen, S.; Zhao, Y.; Gou, W.; Zhao, S.; Takano, Y.; Zheng, H. The Anti-Tumor Effects and Molecular Mechanisms of Suberoylanilide Hydroxamic Acid (SAHA) on the Aggressive Phenotypes of Ovarian Carcinoma Cells. *PLoS ONE* **2013**, *8*, e79781. [CrossRef] [PubMed]
46. Ma, Y.-Y.; Lin, H.; Moh, J.-S.; Chen, K.-D.; Wang, I.-W.; Ou, Y.-C.; You, Y.-S.; Lung, C.-C. Low-dose LBH589 increases the sensitivity of cisplatin to cisplatin-resistant ovarian cancer cells. *Taiwan. J. Obstet. Gynecol.* **2011**, *50*, 165–171. [CrossRef] [PubMed]
47. Shah, R.R. Safety and Tolerability of Histone Deacetylase (HDAC) Inhibitors in Oncology. *Drug Saf.* **2019**, *42*, 235–245. [CrossRef] [PubMed]
48. Van Veggel, M.; Westerman, E.; Hamberg, P. Clinical Pharmacokinetics and Pharmacodynamics of Panobinostat. *Clin. Pharmacokinet.* **2018**, *57*, 21–29. [CrossRef]
49. Tzogani, K.; van Hennik, P.; Walsh, I.; De Graeff, P.; Folin, A.; Sjöberg, J.; Salmonson, T.; Bergh, J.; Laane, E.; Ludwig, H.; et al. EMA Review of Panobinostat (Farydak) for the Treatment of Adult Patients with Relapsed and/or Refractory Multiple Myeloma. *The Oncologist* **2018**, *23*, 631–636. [CrossRef]

50. Takai, N.; Narahara, H.; Narahara, T. Human Endometrial and Ovarian Cancer Cells: Histone Deacetylase Inhibitors Exhibit Antiproliferative Activity, Potently Induce Cell Cycle Arrest, and Stimulate Apoptosis. *Curr. Med. Chem.* **2007**, *14*, 2548–2553. [CrossRef]
51. Buurman, R.; Sandbothe, M.; Schlegelberger, B.; Skawran, B. HDAC inhibition activates the apoptosome via Apaf1 upregulation in hepatocellular carcinoma. *Eur. J. Med. Res.* **2016**, *21*, 26. [CrossRef]
52. Jaiswal, P.K.; Goel, A.; Mittal, R.D. Survivin: A molecular biomarker in cancer. *Indian J. Med. Res.* **2015**, *141*, 389–397. [PubMed]
53. Tong, Q.-S.; Zheng, L.-D.; Wang, L.; Liu, J.; Qian, W. BAK overexpression mediates p53-independent apoptosis inducing effects on human gastric cancer cells. *BMC Cancer* **2004**, *4*, 33. [CrossRef] [PubMed]
54. Rose, S.L.; Goodheart, M.J.; DeYoung, B.R.; Smith, B.J.; Buller, R.E. p21 expression predicts outcome in p53-null ovarian carcinoma. *Clin. Cancer Res. Off. J. Am. Assoc. Cancer Res.* **2003**, *9*, 1028–1032.
55. Yu, J.; Zhang, L. The transcriptional targets of p53 in apoptosis control. *Biochem. Biophys. Res. Commun.* **2005**, *331*, 851–858. [CrossRef] [PubMed]
56. Sanders, Y.Y.; Hagood, J.S.; Liu, H.; Zhang, W.; Ambalavanan, N.; Thannickal, V.J. Histone deacetylase inhibition promotes fibroblast apoptosis and ameliorates pulmonary fibrosis in mice. *Eur. Respir. J.* **2014**, *43*, 1448–1458. [CrossRef] [PubMed]
57. Glozak, M.A.; Seto, E. Histone deacetylases and cancer. *Oncogene* **2007**, *26*, 5420–5432. [CrossRef] [PubMed]
58. Heltweg, B.; Jung, M. A Microplate Reader-Based Nonisotopic Histone Deacetylase Activity Assay. *Anal. Biochem.* **2002**, *302*, 175–183. [CrossRef]
59. Ciossek, T.; Julius, H.; Wieland, H.; Maier, T.; Beckers, T. A homogeneous cellular histone deacetylase assay suitable for compound profiling and robotic screening. *Anal. Biochem.* **2008**, *372*, 72–81. [CrossRef]
60. Bonfils, C.; Kalita, A.; Dubay, M.; Siu, L.L.; Carducci, M.A.; Reid, G.; Martell, R.E.; Besterman, J.M.; Li, Z. Evaluation of the pharmacodynamic effects of MGCD0103 from preclinical models to human using a novel HDAC enzyme assay. *Clin. Cancer Res. Off. J. Am. Assoc. Cancer Res.* **2008**, *14*, 3441–3449. [CrossRef]
61. Hoffmann, K.; Brosch, G.; Loidl, P.; Jung, M. A non-isotopic assay for histone deacetylase activity. *Nucleic Acids Res.* **1999**, *27*, 2057–2058. [CrossRef]
62. Ye, J.; Coulouris, G.; Zaretskaya, I.; Cutcutache, I.; Rozen, S.; Madden, T.L. Primer-BLAST: A tool to design target-specific primers for polymerase chain reaction. *BMC Bioinform.* **2012**, *13*, 134. [CrossRef] [PubMed]

Supplemental Information

Table S1. Effect of HDACi pretreatment on cisplatin-induced cytotoxicity.

cell line	cisplatin	+ 48 h HDACi pretreatment					
		entinostat		panobinostat		nexturastat A	
	IC_{50} [pIC_{50} ± SEM]	IC_{50} [pIC_{50} ± SEM]	SF	IC_{50} [pIC_{50} ± SEM]	SF	IC_{50} [pIC_{50} ± SEM]	SF
A2780	11.0 [4.96 ± 0.01]	4.99 [5.30 ± 0.05]	2.2 ***	2.58 [5.59 ± 0.04]	5.6 ***	1.44 [5.84 ± 0.06]	7.6 ***
CaOV3	1.44 [5.84 ± 0.01]	0.72 [6.14 ± 0.05]	2.0 *	0.74 [6.13 ± 0.05]	2.0 ns	1.33 [5.88 ± 0.04]	1.1 ns
HEY	5.25 [5.28 ± 0.01]	1.39 [5.89 ± 0.03]	3.8 ***	2.75 [5.56 ± 0.04]	1.9 *	1.28 [5.89 ± 0.04]	4.1 ***
Kuramochi	4.68 [5.33 ± 0.02]	3.28 [5.48 ± 0.02]	1.4 *	5.14 [5.29 ± 0.04]	< 1 ns	3.22 [5.49 ± 0.02]	1.5 **
OVSAHO	4.83 [5.32 ± 0.01]	1.02 [5.99 ± 0.03]	4.7 ***	3.01 [5.52 ± 0.02]	1.6 **	1.43 [5.84 ± 0.05]	3.4 ***

Data shown are the mean of pooled data from at least three experiments each carried out in triplicates. Shift-factors (SF) were calculated by dividing the IC_{50}-values without and with HDACi-preincubation. Levels of significance: ns ($p > 0.05$); * ($p \leq 0.05$); ** ($p \leq 0.01$); *** ($p \leq 0.001$).

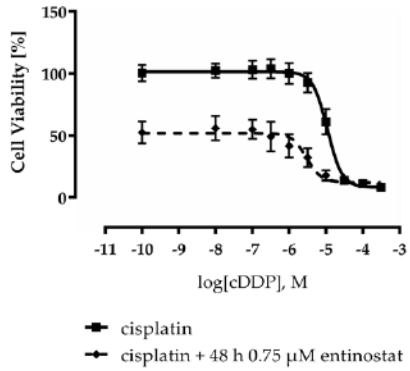
Cell Viability [%]
150
100
50
0
-11 -10 -9 -8 -7 -6 -5 -4 -3
log[cDDP], M
cisplatin
cisplatin + 48 h 0.75 μM entinostat

(a)

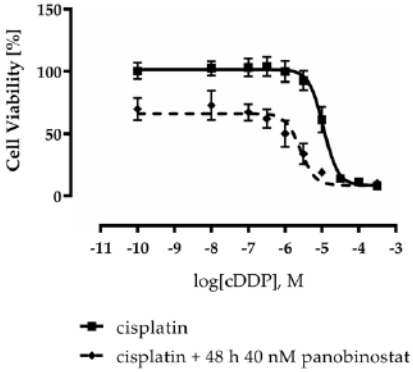
Cell Viability [%]
150
100
50
0
-11 -10 -9 -8 -7 -6 -5 -4 -3
log[cDDP], M
cisplatin
cisplatin + 48 h 40 nM panobinostat

(b)

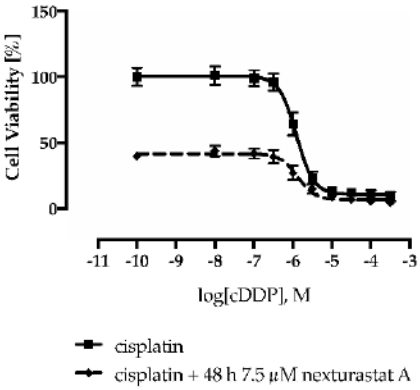
Cell Viability [%]
150
100
50
0
-11 -10 -9 -8 -7 -6 -5 -4 -3
log[cDDP], M
cisplatin
cisplatin + 48 h 7.5 μM nexturastat A

(c)

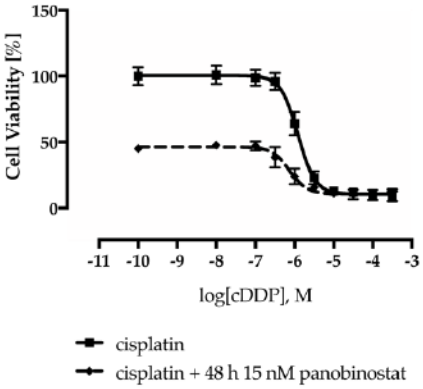
Cell Viability [%]
150
100
50
0
-11 -10 -9 -8 -7 -6 -5 -4 -3
log[cDDP], M
cisplatin
cisplatin + 48 h 15 nM panobinostat

(d)

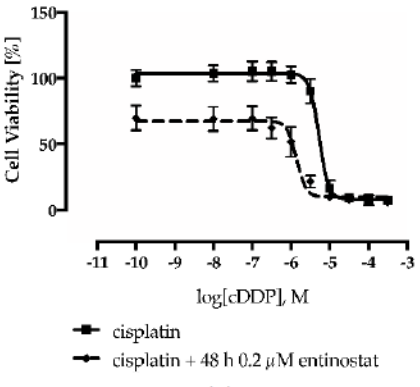
Cell Viability [%]
150
100
50
0
-11 -10 -9 -8 -7 -6 -5 -4 -3
log[cDDP], M
cisplatin
cisplatin + 48 h 0.2 μM entinostat

(e)

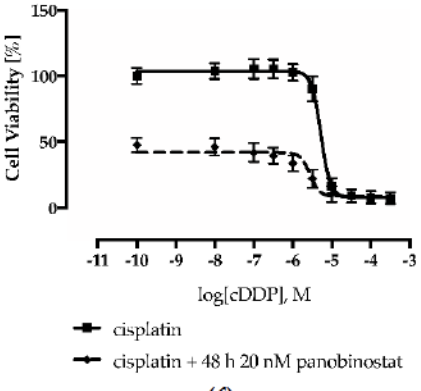
Cell Viability [%]
150
100
50
0
-11 -10 -9 -8 -7 -6 -5 -4 -3
log[cDDP], M
cisplatin
cisplatin + 48 h 20 nM panobinostat

(f)

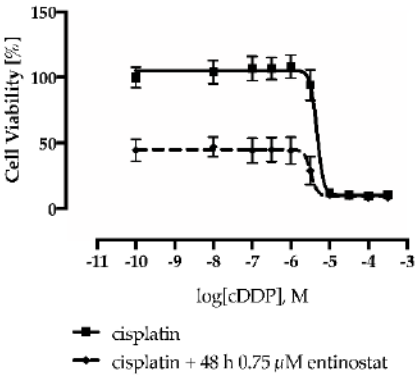
Cell Viability [%]
150
100
50
0
-11 -10 -9 -8 -7 -6 -5 -4 -3
log[cDDP], M
cisplatin
cisplatin + 48 h 0.75 μM entinostat

(g)

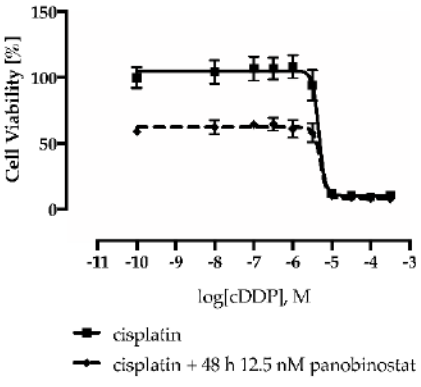
Cell Viability [%]
150
100
50
0
-11 -10 -9 -8 -7 -6 -5 -4 -3
log[cDDP], M
cisplatin
cisplatin + 48 h 12.5 nM panobinostat

(h)

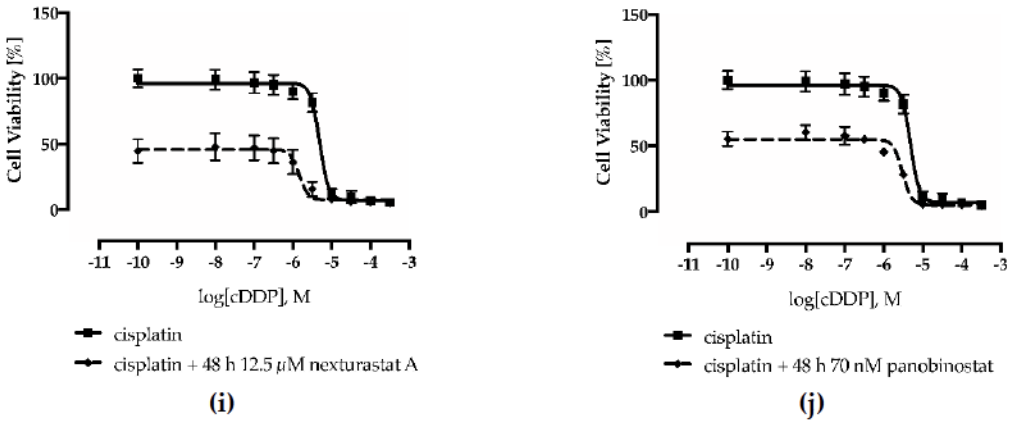

Figure S1. HDACi pretreatment enhance the cytotoxic effects of cisplatin. A2780 (a,b), CaOV3 (c,d), HEY (e,f), Kuramochi (g,h), and OVSAHO (i,j) were pretreated with the indicated HDACi 48 h prior to cisplatin (cDDP) administration. After another 72 h, IC_{50}-values were determined by MTT-assay. Data shown are normalized to vehicle control and pooled of at least two experiments each carried out in triplicates.

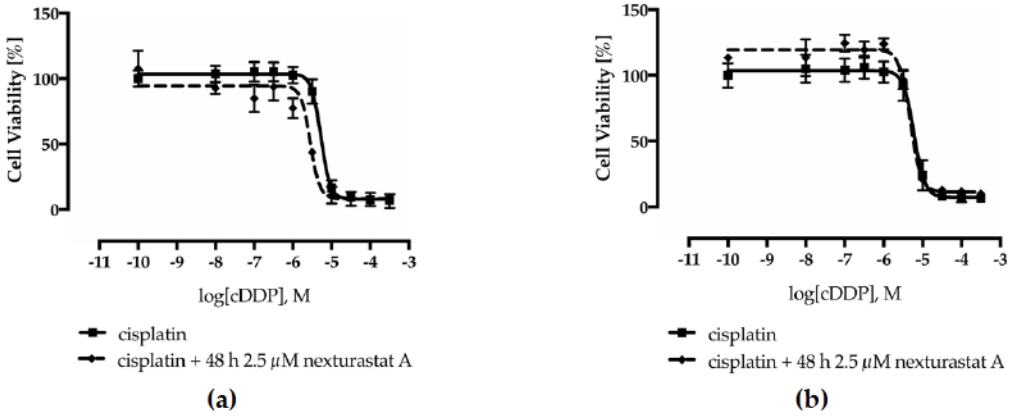

Figure S2. Pretreatment with nexturastat A in low concentrations did not enhance the cytotoxic effects of cisplatin. HEY (a) and CaOV3 (b) cells were pretreated with the indicated HDACi 48 h prior to cisplatin (cDDP) administration. After another 72 h, IC50-values were determined by MTT-Assay. Data shown are normalized to vehicle control and pooled of two (a) or one (b) experiment each carried out in triplicates.

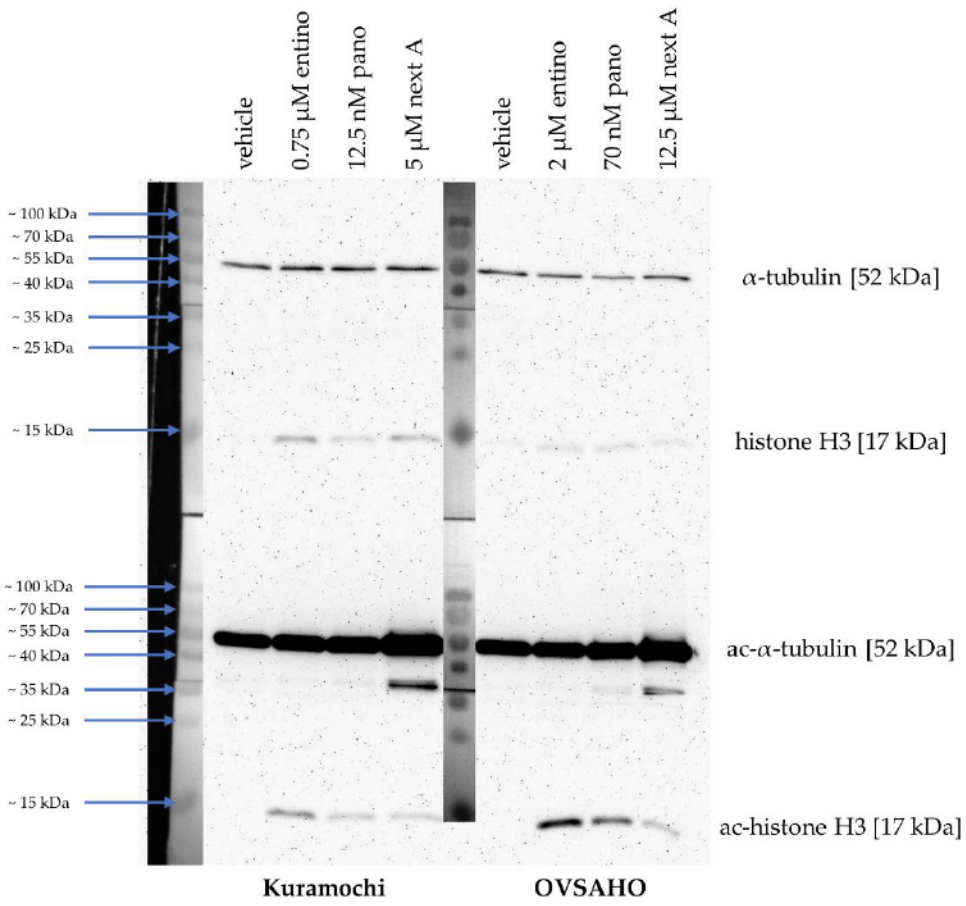

Figure S3. Effect of HDACi on acetylation level of α-tubulin and histone H3. Representative immunoblot analysis of histone H3, ac-histone H3, α-tubulin, and ac-α-tubulin in Kuramochi and OVSAHO cells. Cells were treated with the indicated concentrations of HDACi. Control cells were incubated with vehicle. Protein molecular weight marker is indicated on the left side.

3.2 Publikation 2

Hydroxamic Acids Immobilized on Resins (HAIRs): Synthesis of Dual-Targeting HDAC Inhibitors and HDAC Degraders (PROTACs)

Laura Sinatra[1], **Jan J. Bandolik[2]**, Martin Roatsch[1,3], Melf Sönnichsen[4], Clara T. Schoeder[5], Alexandra Hamacher[2], Andrea Schöler[1], Arndt Borkhardt[4], Jens Meiler[1,5], Sanil Bhatia[4], Matthias U. Kassack[2], Finn K. Hansen[1,6]

1 Institut für Pharmazie, Universität Leipzig
2 Institut für Pharmazeutische und Medizinische Chemie, Heinrich-Heine-Universität Düsseldorf
3 Zentrum für Biopharmazeutik, Universität Kopenhagen, Dänemark
4 Institut für Pädiatrische Onkologie, Heinrich-Heine-Universität / Universitätsklinikum Düsseldorf
5 Zentrum für Strukturbiologie, Universität Vanderbilt, USA
6 Pharmazeutisches Institut, Universität Bonn

Veröffentlicht in: Angewandte Chemie (International Edition), 11. August 2020

DOI: 10.1002/anie.202006725 (International Edition)
10.1002/ange.202006725 (Deutsche Version)

Beitrag: Zweitautorschaft. Durchführung der tiefergehenden biochemischen Evaluation dieser Veröffentlichung (Caspase-Assay, γ-H2AX-Assay, Western Blots, Kombinations-/Synergismus-Analysen) bzgl. der dualen HDAC-Inhibitoren und Alkylanzien. Auswertung der Daten und Verfassen der ersten Version des entsprechenden biochemischen Teils des Manuskripts.

Zusammenfassung (übersetzt): Die Hemmung von mehr als einem Signaltransduktionsweg im Rahmen einer Krebserkrankung durch Multi-Target-Arzneistoffe ist ein aufstrebender Ansatz in der modernen Wirkstoffforschung gegen Krebs. Basierend auf der gut erforschten Synergie zwischen Histondeacetylase-Inhibitoren (HDACi) und Alkylanzien, stellen wir hier die Entdeckung einer Reihe von alkylierenden HDACi unter Verwendung einer Pharmakophor-Verknüpfungsstrategie vor. Für die Parallelsynthese der Zielverbindungen entwickelten wir ein effizientes festphasengestütztes Protokoll unter Verwendung von auf Harzen immobilisierten Hydroxamsäuren (HAIRs) als stabile und vielseitige Bausteine für die Herstellung von funktionalisierten HDACi. Die vielversprechendste Verbindung, 3n, war signifikant aktiver bezüglich der Induktion von Apoptose, der Aktivierung von Caspase 3/7 und der Verursachung von DNA-Schäden (γ-H2AX) als die Summe der der Aktivitäten der isolierten einzelnen Wirkstoffe. Um den Nutzen unserer vorbeladenen Harze zu demonstrieren, wurde der HAIR-Ansatz darüber hinaus erfolgreich auf die Synthese einer Proof-of-Concept PROTAC (Proteolysis-Targeting Chimeras) ausgedehnt, die Histondeacetylase effizient abbaut.

How to cite: *Angew. Chem. Int. Ed.* **2020**, *59*, 22494–22499
International Edition: doi.org/10.1002/anie.202006725
German Edition: doi.org/10.1002/ange.202006725

Multi-Target Drugs | Hot Paper

Hydroxamic Acids Immobilized on Resins (HAIRs): Synthesis of Dual-Targeting HDAC Inhibitors and HDAC Degraders (PROTACs)

Laura Sinatra, Jan J. Bandolik, Martin Roatsch, Melf Sönnichsen, Clara T. Schoeder, Alexandra Hamacher, Andrea Schöler, Arndt Borkhardt, Jens Meiler, Sanil Bhatia, Matthias U. Kassack, and Finn K. Hansen**

In memory of Victoria Michler-Hansen

Abstract: *Inhibition of more than one cancer-related pathway by multi-target agents is an emerging approach in modern anticancer drug discovery. Here, based on the well-established synergy between histone deacetylase inhibitors (HDACi) and alkylating agents, we present the discovery of a series of alkylating HDACi using a pharmacophore-linking strategy. For the parallel synthesis of the target compounds, we developed an efficient solid-phase-supported protocol using hydroxamic acids immobilized on resins (HAIRs) as stable and versatile building blocks for the preparation of functionalized HDACi. The most promising compound,* ***3n****, was significantly more active in apoptosis induction, activation of caspase 3/7, and formation of DNA damage (γ-H2AX) than the sum of the activities of either active principle alone. Furthermore, to demonstrate the utility of our preloaded resins, the HAIR approach was successfully extended to the synthesis of a proof-of-concept proteolysis-targeting chimera (PROTAC), which efficiently degrades histone deacetylases.*

Difficulties in developing new drugs for multifactorial diseases like neurological disorders or cancer have led to rethinking of the "one disease—one target—one drug" paradigm to a "multi-target drug" concept.[1] Compared to combination therapies using two or more drugs, a single multi-target molecule has the advantages of no drug-drug interactions, a more predictable pharmacokinetic profile, and improved patient compliance.[2,3]

Histone acetyltransferases (HATs) and histone deacetylases (HDACs) are key enzymes controlling the acetylation level of histones and non-histone proteins.[4] Due to their repressive effect on gene transcription and their essential influence on drug resistance mechanisms of tumor cells,[5–7] HDACs are validated drug targets in epigenetic cancer therapy with four inhibitors already approved by the FDA.[8] Typically common HDAC inhibitors (HDACi) comprise a cap group, a linker region and a zinc binding group (ZBG), which is crucial for the chelation of the zinc ion inside the active site tunnel (Figure 1).[9] Fortunately, the cap group can be subjected to various structural modifications providing sufficient scope for hybridization approaches towards HDACi-based multi-target drugs.[10,11]

Recent preclinical results provide evidence that combinations of alkylating agents and HDACi exhibit efficacy against drug-resistant glioblastoma multiforme (GBM), the most common and aggressive primary brain tumor,[12,13] by increasing the DNA damage of alkylating agents via HDACi-mediated chromatin relaxation.[14,15] Consequently, the first-in-class nitrogen mustard-HDACi hybrid molecule tinostamustine (Figure 1) was developed by fusing the pharmacophores of the DNA-alkylating drug bendamustine and the HDACi vorinostat (SAHA).[16] Tinostamustine demonstrated superior *in vivo* activity compared to bendamustine, temozolomide and radiotherapy indicating that DNA/HDAC dual-targeting inhibitors could be promising drug candidates for cancer therapy.

[*] L. Sinatra, Dr. M. Roatsch, A. Schöler, Prof. Dr. J. Meiler, Prof. Dr. F. K. Hansen
Institute for Drug Discovery, Medical Faculty, Leipzig University
Brüderstraße 34, 04103 Leipzig (Germany)
J. J. Bandolik, Dr. A. Hamacher, Prof. Dr. M. U. Kassack
Institute of Pharmaceutical and Medicinal Chemistry, Heinrich-Heine-Universität Düsseldorf
40225 Düsseldorf (Germany)
E-mail: matthias.kassack@uni-duesseldorf.de
Dr. M. Roatsch
Center for Biopharmaceuticals, Department of Drug Design and Pharmacology, University of Copenhagen
Universitetsparken 2, 2100 Copenhagen (Denmark)
M. Sönnichsen, Prof. Dr. A. Borkhardt, Dr. S. Bhatia
Department of Pediatric Oncology, Hematology and Clinical Immunology, Medical Faculty, Heinrich Heine University Düsseldorf
Moorenstr. 5, 40225 Düsseldorf (Germany)
Dr. C. T. Schoeder, Prof. Dr. J. Meiler
Center for Structural Biology, Department of Chemistry, Vanderbilt University
Nashville, TN 37221 (USA)
Prof. Dr. F. K. Hansen
Pharmaceutical and Cell Biological Chemistry, Pharmaceutical Institute, University of Bonn
An der Immenburg 4, 53121 Bonn (Germany)
E-mail: finn.hansen@uni-bonn.de
Supporting information and the ORCID identification number(s) for the author(s) of this article can be found under: https://doi.org/10.1002/anie.202006725.

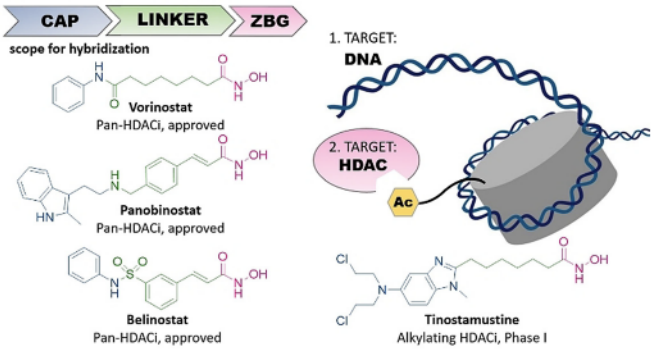

Figure 1. left: Selected HDAC inhibitors and their typical design; *right:* intended targets of this work and of the hybrid compound tinostamustine.

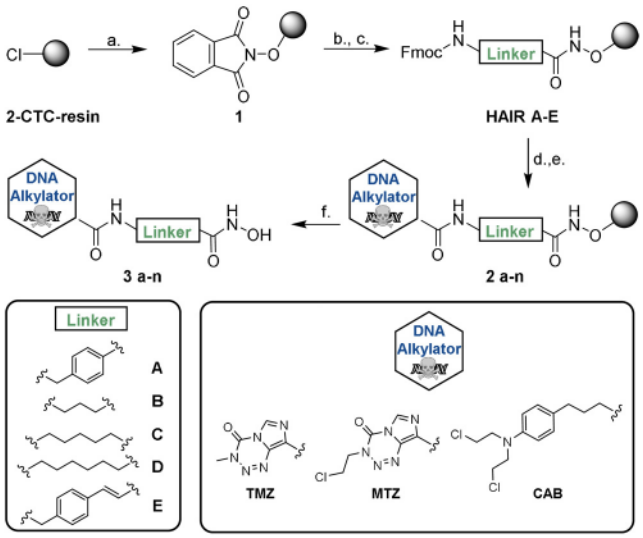

Scheme 1. Solid-phase supported strategy for the parallel synthesis of DNA-alkylating HDACi hybrid molecules. **a.)** PhthN-OH (3.5 equiv), Et_3N (3.5 equiv), DMF, r.t., 48 h. **b.)** 5% $N_2H_4 \cdot H_2O$ in MeOH, r.t., 2× 15 min. **c.)** Fmoc-NH-Linker-COOH (2.0 equiv), HATU (2.0 equiv), HOBt·H_2O (2.0 equiv), DIPEA (3.0 equiv), DMF, r.t., 20 h. **d.)** 20% piperidine in DMF, 2x 5 min. **e.)** Cap-COOH (3.0 equiv), HATU (3.0 equiv), DIPEA (5.0 equiv), DMF, r.t., 20 h, dark environment. **f.)** 5% TFA in CH_2Cl_2, r.t.,1 h.

Since HDACi-based multi-target drugs show great promise in preclinical and early clinical studies,[10,11] there is an urgent need for efficient synthetic protocols allowing the synthesis of focused compound libraries with linked or merged pharmacophores. Herein we present the development of a series of preloaded resins for solid-phase synthesis termed *hydroxamic acids immobilized on resins* (HAIRs). To demonstrate the utility of these HAIRs and to take advantage of the synergism between HDACi and alkylating agents, we successfully prepared a set of HDACi with DNA-alkylating properties via a fast and straightforward parallel synthesis approach. The scope of the HAIR technology was further extended to the synthesis of a proof-of-concept proteolysis-targeting chimera (PROTAC), that is, a protein degrader.

The preparation of HAIRs **A**–**E** as HDACi precursors is summarized in Scheme 1. Initially, we modified the commercially available 2-chlorotrityl chloride (2-CTC) resin with the immobilization of hydroxylamine by treatment of the resin with *N*-hydroxyphthalimide and triethylamine for 48 h. Next, after deprotection of the Phth-group using hydrazine hydrate, different Fmoc-protected HDACi linkers were loaded to the functionalized resin to provide the preloaded resins HAIRs **A**–**E**. For the linker a series of well-established HDACi linkers such as benzyl, alkyl and cinnamyl was selected. For all synthesized resins, high loadings between 0.81–0.90 mmol g^{-1} were achieved. All prepared HAIRs showed excellent crude purities and reproducible loadings (±5%). Furthermore, after storage for >6 months the weight and purity of all modified resins were retested after swelling and drying. All HAIRs showed stable weight (±5%) and high crude purities (>95% after >6 months of storage) (Table 1).

After establishing the preloaded HAIRs **A**–**E**, we utilized them to incorporate the DNA-alkylating part in the cap group region. Due to the synergistic activity of HDACi with alkylating agents, we chose the DNA-alkylating drugs temozolomide (TMZ), mitozolomide (MTZ), and chlorambucil (CAB) as suitable scaffolds for a hybridization approach. All three examples can be considered as challenging, because TMZ and MTZ are sensitive to base treatment, which leads to ring opening of the imidazotetrazinone ring system, whereas CAB contains a very reactive nitrogen mustard group.[17,18] For library synthesis, the Fmoc protecting group was removed and each linker was coupled with the three chosen alkylators in a concentration range of 0.5–1.0 M. Using a parallel synthesis strategy, we prepared a series of compounds combining each linker with each alkylator yielding a library comprising 15 hybrid molecules. This approach provided the target compounds in total yields of up to 83%. Purification by preparative HPLC afforded all compounds in >95% purity. Thus, only one purification step at the very end of the synthesis is required for each inhibitor allowing for rapid and time-efficient library expansion.

Compounds **3a–n** were tested in a fluorogenic assay for their in vitro inhibitory activity against HDAC1 (class I) and HDAC6 (class IIb). Results of the inhibition assay are shown in Table 2. Compounds containing a cinnamyl (**3l–n**) and hexyl (**3i–k**) linker showed inhibitory activity in the nanomolar range against both HDAC1 and HDAC6, which was comparable to the control compound vorinostat. Notably, inhibitors utilizing a benzyl linker revealed potent and preferential inhibition of HDAC6 with up to 17-fold selectivity over HDAC1 (see compound **3a**, Table 2). All compounds with a short propyl linker (**3d–f**) showed very low HDAC inhibition, which suggests that this linker length is too short to chelate the Zn^{2+} ion in the active site. To investigate the anticancer properties of the hybrid HDACi, the antiproliferative effects of **3a–n** were determined in three human cancer lines: the human tongue squamous cell carcinoma cell line Cal27 and the human primary glioblastoma cell lines U87 and U251. Results are summarized in Table 2. Based on data from MTT assays, compound **3n**, which contains a cinnamyl linker and CAB as cap group, emerged as the most promising compound. **3n** showed HDAC1 and 6 inhibition in a similar range as vorinostat and 3 to 5.6-fold weaker inhibition

Table 1: Loadings of synthesized HAIRs and stability after >6 months stored at 4 °C monitored by repetition of the loading and crude purity determination.

Entry	preloaded resin	Loading[a] (mmol g^{-1})	Loading[a] >6 months (mmol g^{-1})	Crude purity[b] >6 months
HAIR **A**	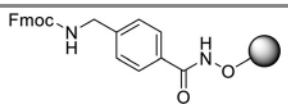	0.90	0.91	96 %
HAIR **B**	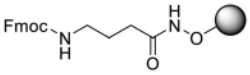	0.96	0.97	95 %
HAIR **C**	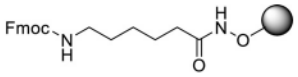	0.87	0.90	96 %
HAIR **D**	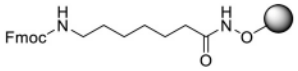	0.81	0.83	96 %
HAIR **E**	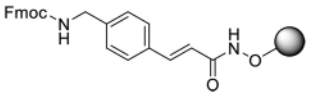	0.87	0.85	95 %

[a] Loadings were photometrically determined at 300 nm after deprotection of the Fmoc-group using 20 % piperidine in DMF. [b] Crude purities were analyzed by HPLC after test cleavage with 5 % TFA in dichloromethane for 1 h.

compared to the hybrid compound tinostamustine. Furthermore, **3n** demonstrated the most potent antiproliferative effect of all hybrid compounds against the three cancer cell lines (IC_{50} (Cal27): 2.68 μM, IC_{50} (U87): 19.8 μM, and IC_{50} (U251): 14.5 μM) and exceeded or was equal to the cytotoxicity of the reference compounds vorinostat, tinostamustine, TMZ, MTZ and CAB in the Cal27 cell line and with the exception of vorinostat and tinostamustine also in the glioblastoma cell lines. Notably, **3n** showed up to 10-fold improved antiproliferative effect in comparison to its parent compound CAB. Compounds bearing the cinnamyl linker (**3l–n**) showed the most effective combination of antiproliferative effect as well as HDAC inhibitory activity and were therefore chosen for evaluation of their DNA-damaging effects. **3l–n** were tested for induction of DNA double strand breaks by a γ-H2AX assay[19] using cisplatin, vorinostat, TMZ, MTZ, and CAB as controls (Figure 2A). Cal27 cells were treated with an IC_{50} or fivefold IC_{50} (from MTT assay) for 24 h. Among the cinnamyl linker-containing compounds **3l–n**, **3n** caused the largest increase in γ-H2AX levels in Cal27 cells. Using an IC_{50} from MTT assay, only **3n** achieved a significant increase in γ-H2AX formation, whereas **3l** and **3m** were not different from control. At fivefold IC_{50}, **3l–n** showed DNA damage with **3n** being significantly more active than **3l** and **3m**, Because **3l** and **3m** showed only weak DNA damage, they were excluded from further studies.

Based on these results, we investigated whether the nitrogen mustard moiety is contributing to the antiproliferative activity and DNA-damage of **3n**. We thus synthesized the control compound **3o** omitting the nitrogen mustard group (see Scheme S1, Supporting Information). The anti-

Table 2: *In vitro* inhibition of HDAC1 and 6 by the hybrid inhibitors with different combinations of linkers and cap groups and antiproliferative activity (MTT assay) against the human cancer cell lines Cal27, U87 and U251.

Compound	Linker	Cap Group	Target Inhibition[a] IC_{50} [μM]		Antiproliferative Effect[b] IC_{50} [μM]		
			HDAC1	HDAC6	Cal27	U87	U251
3a	A	TMZ	0.705 ± 0.077	0.035 ± 0.003	16.2 ± 2.86	165 ± 26.1	98.7 ± 10.0
3b	A	MTZ	0.394 ± 0.020	0.023 ± 0.002	16.8 ± 3.62	147 ± 19.7	44.5 ± 8.94
3c	A	CAB	0.518 ± 0.065	0.032 ± 0.003	6.89 ± 1.04	23.9 ± 3.41	22.0 ± 3.09
3d	B	TMZ	35.1 ± 5.32	4.99 ± 0.129	97.1 ± 16.3	323 ± 107	n.e.
3e	B	MTZ	16.2 ± 0.070	2.37 ± 0.086	87.8 ± 9.52	413 ± 77.7	461 ± 89.9
3f	B	CAB	8.21 ± 0.183	4.60 ± 0.082	8.67 ± 1.31	46.1 ± 5.71	20.1 ± 2.41
3g	C	MTZ	0.681 ± 0.015	0.094 ± 0.002	29.0 ± 3.73	262 ± 75.6	140 ± 17.8
3h	C	CAB	0.444 ± 0.053	0.121 ± 0.008	7.50 ± 0.62	43.9 ± 15.3	25.1 ± 3.27
3i	D	TMZ	0.161 ± 0.006	0.031 ± 0.002	10.2 ± 1.54	166 ± 33.6	86.2 ± 13.1
3j	D	MTZ	0.143 ± 0.005	0.038 ± 0.004	9.90 ± 1.24	122 ± 56.0	48.2 ± 7.35
3k	D	CAB	0.244 ± 0.041	0.063 ± 0.001	6.17 ± 0.51	39.2 ± 7.16	27.0 ± 3.55
3l	E	TMZ	0.146 ± 0.008	0.072 ± 0.008	15.4 ± 1.61	141 ± 20.7	97.8 ± 9.07
3m	E	MTZ	0.122 ± 0.009	0.051 ± 0.002	10.1 ± 0.99	84.3 ± 12.4	32.2 ± 3.55
3n	E	CAB	0.151 ± 0.021	0.062 ± 0.001	2.68 ± 0.31	19.8 ± 3.16	14.5 ± 1.59
vorinostat	–	–	0.097 ± 0.012	0.045 ± 0.008	3.26 ± 0.22	6.37 ± 0.51	7.49 ± 0.67
tinostamustine	–	–	0.047 ± 0.003	0.011 ± 0.001	2.94 ± 0.07	8.32 ± 0.55	10.2 ± 0.62
TMZ	–	–	–	-	56.8 ± 5.05	144 ± 15.6	457 ± 57.3
MTZ	–	–	–	–	3.56 ± 0.29	57.4 ± 9.51	84.5 ± 7.30
CAB	–	–	-	–	23.7 ± 2.26	86.3 ± 17.5	48.7 ± 11.9
3o	–	–	0.156 ± 0.008	0.066 ± 0.001	6.59 ± 0.44	27.7 ± 6.52	23.9 ± 3.51

[a] $n \geq 2$, each in duplicate wells. [b] $n \geq 3$, each in triplicate wells. n.e.: no effect up to 100 μM.

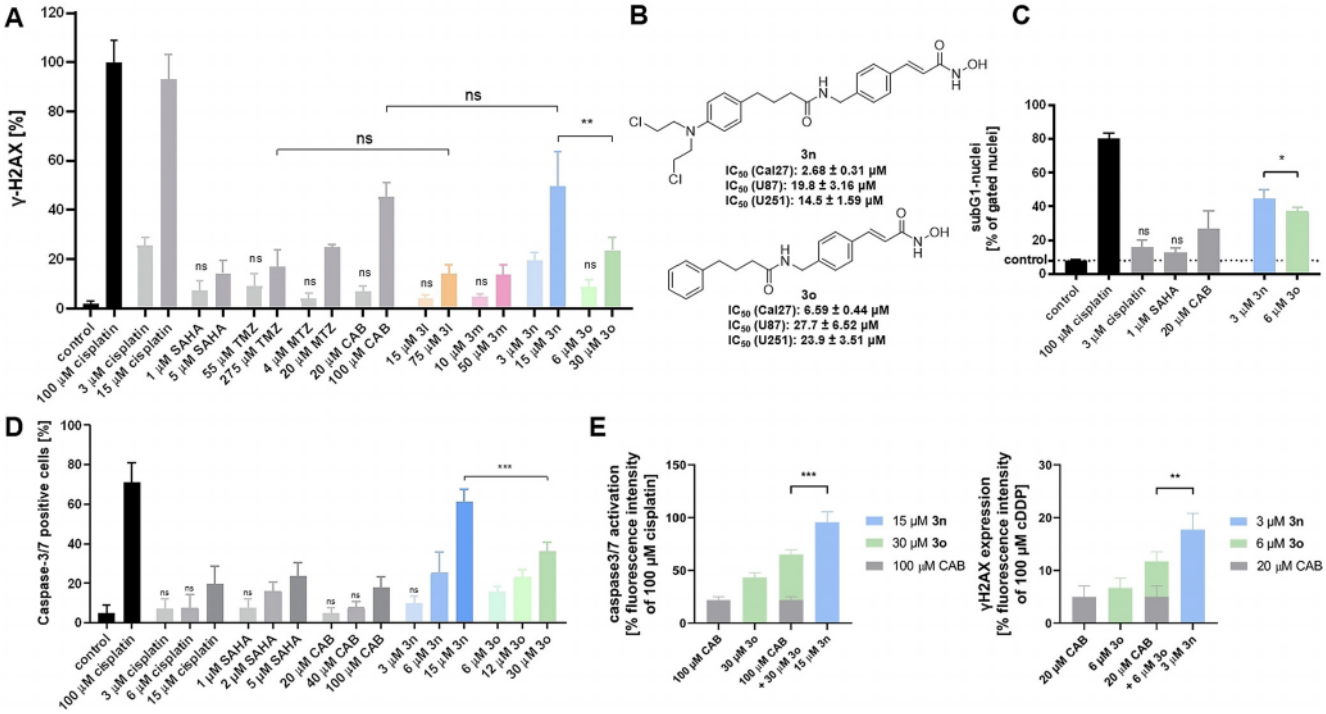

Figure 2. **A.** Compound-induced formation of γ-H2AX in Cal27 cells. Cells were treated with an IC_{50} or fivefold IC_{50} (from MTT assay) for 24 h. γ-H2AX formation was analyzed by immunohistochemistry. 100 µM cisplatin served as positive control and was set as 100%. "control" is vehicle control. Data are the mean ± SD, $n \geq 3$. T-test was used to analyse for significant differences between compounds and control or as indicated. ns ($p > 0.05$); ** ($p \leq 0.01$). **B.** Synthesized hit compound **3n** and its control compound without *N*-lost-functionality (**3o**) and their cytotoxicity. **C.** Induction of apoptosis shown as subG1 nuclei induced by **3n** and the nitrogen mustard-free compound **3o** in Cal27 cells. Cells were treated with indicated compounds and concentrations (MTT-IC_{50}) for 24 h, and sub-G1 cell fractions were analysed by flow cytometry. 100 µM cisplatin served as positive control for apoptosis induction. "control" is vehicle control. Data are the mean ± SD, $n = 3$. T-test was used to analyze for significant differences between compounds and control or as indicated. ns ($p > 0.05$); * ($p \leq 0.05$). **D.** Compound-induced caspase3/7 activation in Cal27 cells. Cells were treated with a single, double, or fivefold IC_{50} (from MTT assay) for 24 h. 100 µM Cisplatin was added as positive control. "control" is vehicle control. Data are the mean ± SD, $n = 3$. t-test was used to analyze for significant differences between compounds and control or as indicated. ns ($p > 0.05$); *** ($p \leq 0.001$). **E.** **3n** is significantly more effective than the sum of the effects of **3o** and CAB on caspase3/7 activation (left) and on formation of γH2AX (right). Compounds were used in concentrations reflecting the fivefold IC_{50} (MTT assay). Green and grey bars show sum of the effects of **3o** and CAB. Light blue bars show the effect of **3n**. Vehicle control was subtracted. Data are mean ± SD, $n = 3$. T-test was used to analyze for significant differences. ** ($p \leq 0.01$); *** ($p \leq 0.001$).The analysis was performed as previously described.[20]

proliferative potency of **3o** was slightly reduced compared to **3n** (Figure 2B). The most pronounced reduction in antiproliferative potency was observed in Cal27 cells (**3n** IC_{50}: 2.68 µM vs. **3o** IC_{50}: 6.59 µM). More importantly, **3n** caused significantly greater DNA damage (γ-H2AX assay) than **3o** at a concentration of five times its IC_{50} (Figure 2A) indicating an additive effect of the nitrogen mustard group. γ-H2AX formation is a marker for DNA damage, which usually results in induction of apoptosis.[19] Figure 2C displays apoptosis, shown as subG1 nuclei, induced by **3n** and the nitrogen mustard-free control **3o**. Notably, **3n** is more potent than **3o**, cisplatin, vorinostat, and CAB in inducing apoptosis at the respective IC_{50} values. Comparable results were observed in a caspase 3/7 activation-apoptosis assay demonstrating the superior utility of **3n** to kill cancer cells via induction of the programmed cell death (Figure 2D). Notably, although the combination of **3o** and CAB showed synergism in caspase activation assay as analysed by the method of *Chou-Talalay* (combination index (CI) values < 1), equal concentrations of compound **3n** demonstrated significantly stronger effects and lower CI values (< 0.9) (see Figure S1, Table S1, Supporting Information). In addition, the effect of 15 µM **3n** was significantly stronger than the sum of the effects of even 100 µM CAB and 30 µM **3o**, again indicating a superadditive effect of the dual-targeting compound **3n** (Figure 2E, left). The same holds true for results from the γ-H2AX assay (Figure 2E, right). The superior antiproliferative activity, apoptosis induction, activation of caspase 3/7, and formation of DNA damage of **3n** vs. **3o** could result from an altered HDAC inhibition profile. **3n** and **3o** were therefore screened for their inhibitory activity against all class I HDACs and HDAC6. However, **3n** showed similar or less potent HDAC inhibitory activity than **3o** (Figure 3A) highlighting the importance of the DNA-alkylating feature of the hit compound **3n** for its anticancer activity. Based on the biochemical HDAC inhibition data, it can be assumed that the nitrogen mustard in *p*-position of the cap group has little impact on the HDAC inhibitory activity of **3n**. To test the hypothesis that the DNA alkylating moiety fails to form specific interactions with the HDAC proteins, compounds **3n** and **3o** were docked into HDAC6. During the docking study the hydroxamic acid group was restrained in proximity to the zinc ion in the

A HDAC Inhibition, IC_{50}[μM]

Entry	3n	3o	control*
HDAC 1	0.151 ±0.021	0.156 ±0.008	0.097 ±0.012
HDAC 2	0.432 ±0.015	0.194 ±0.034	0.140 ±0.019
HDAC 3	0.187 ±0.009	0.117 ±0.020	0.096 ±0.012
HDAC 6	0.062 ±0.001	0.066 ±0.001	0.045 ±0.008
HDAC 8	4.04 ±0.28	0.82 0.11±	0.61 ±0.04

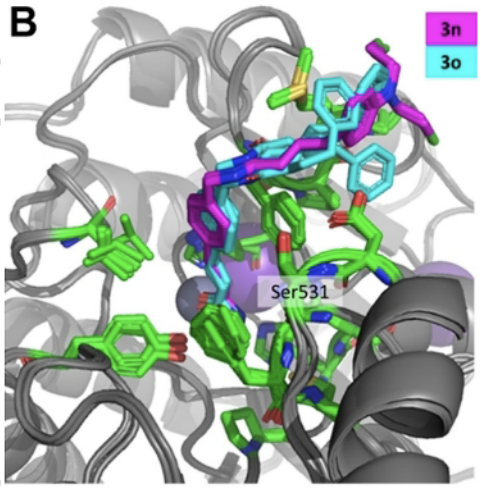

Figure 3. **A.** Inhibition of HDAC 1, 2, 3, 6, and 8 by the hit compound **3n** and compound **3o**. *Vorinostat was used as control compound except in the case of HDAC8, where panobinostat was used. $n \geq 2$, each in duplicate wells. **B.** Docking poses of **3n** and **3o** in the human HDAC6 (PDB: 5EDU). Both compounds were individually docked to human HDAC6 using RosettaLigand in iterative rounds of focused docking.

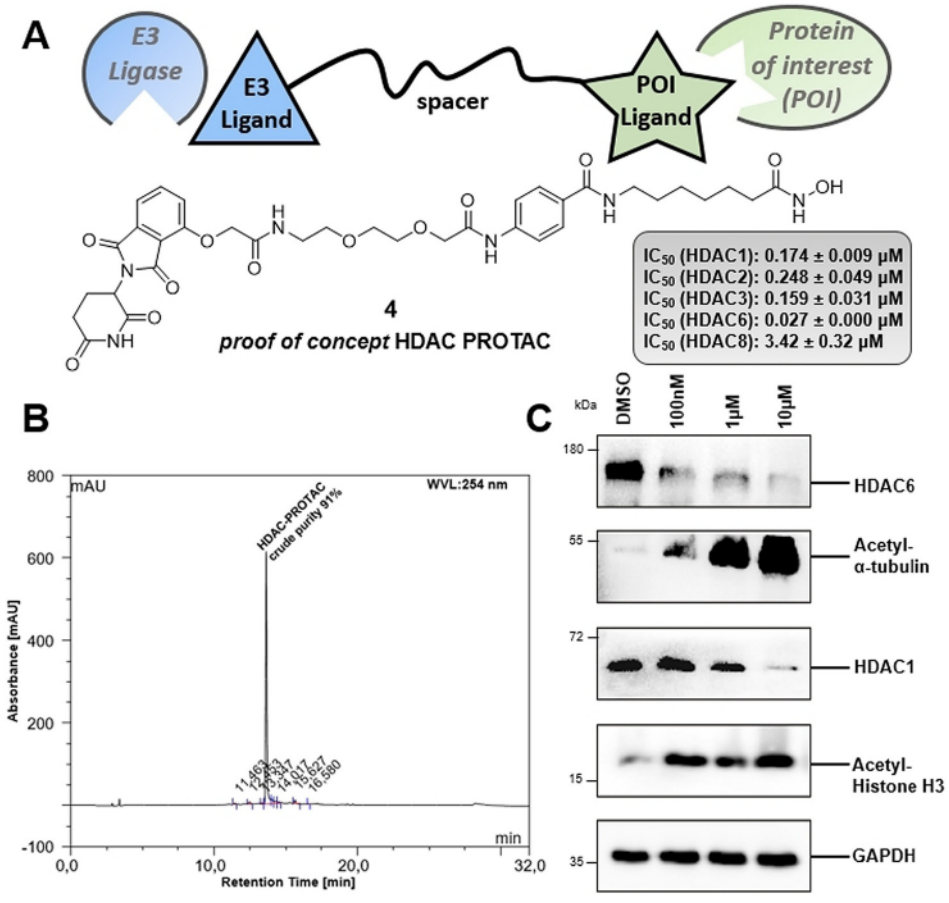

Figure 4. **A.** Synthesized proof of concept HDAC degrader **4** and inhibitory activities against HDAC1, 2, 3, 6, and 8. **B.** HPLC-chromatogram of the test cleavage of crude proof of concept PROTAC **4** (cleavage mix: 5% TFA in CH_2Cl_2, 1 h, r.t.). **C.** Immunoblot analysis of cell lysate after HL-60 cells were treated with **4** at various concentrations (0.1 μM, 1 μM and 10 μM).

catalytic center, resulting in very similar binding poses for both compounds (Figure 3B). The addition of the *N*-lost group did not alter the binding pose of the compounds as it points outwards and only interacts loosely with the protein surface. Taken together, our results demonstrate that the incorporation of a DNA-alkylating feature in the *p*-position of the cap group has little impact on the HDAC inhibition and can thus be utilized to enhance the anticancer effects of HDACi.

Encouraged by the successful and straightforward parallel synthesis of a focused library of DNA-alkylating HDACi, our aim was to extend the HAIR approach to a second class of chimeric small molecules: proteolysis-targeting chimeras (PROTACs). PROTACs are bifunctional small molecules that are able to hijack the cellular protein degradation system by recruiting the protein of interest (POI) to E3 ubiquitin ligases, which leads to polyubiquitinylation of the POI and induction of its proteasomal degradation.[21,22] Developments in PROTAC technology give new opportunities to address and study epigenetic targets such as HDACs, with already a few HDAC PROTACs reported recently.[23–26] However, due to their high molecular weight and bifunctional nature, the synthesis of HDAC PROTACs is usually cumbersome and involves multi-step protocols.[26] Consequently, we undertook the first reported solid-phase synthesis of an HDAC degrader. HAIR **D** was chosen as a suitable starting point for the preparation of the proof-of-concept HDAC PROTAC **4**. Iterative cycles of Fmoc deprotection and amide coupling allowed to introduce the HDAC cap, PROTAC linker, and thalidomide-based ubiquitin E3 ligase ligand in a modular fashion (see Scheme S2, Supporting Information for synthetic details) to generate PROTAC **4** (Figure 4A). This straightforward and rapid HAIR-supported synthesis provided **4** in an excellent crude purity of 91% (Figure 4B) and >95% after purification.

Biochemical HDAC inhibition assays highlighted **4** as a potent pan-HDAC inhibitor (Figure 4A). Pleasingly, PROTAC **4** turned out to be an efficient HDAC degrader. Western blot experiments using the AML cell line HL60 confirmed that **4** was able to degrade especially HDAC6 and also HDAC1 in a concentration dependent manner (Figure 4C). Furthermore, the treatment of HL60 cells with **4** led to a significant hyperacetylation of histone H3 (a marker of reduced HDAC1-3 activity) and α-tubulin (a marker of reduced HDAC6 activity) (Figure 4C). Thus, these results clearly confirm that PROTAC **4** is an efficient HDAC degrader, which is suitable for the *chemical knock-down* of histone deacetylases.

In conclusion, we have developed an efficient solid-phase synthesis protocol using *hydroxamic acids immobilized on resins* (HAIRs) to prepare novel dual-target epigenetic-cytotoxic compounds. The combination of potent class I/HDAC6 inhibition with established alkylating agents gave a series of active compounds, among which **3n** (derived from panobinostat and chlorambucil) showed the highest antiproliferative activity. **3n** was significantly more active in apoptosis induction, activation of caspase 3/7, and formation of DNA damage (γ-H2AX) than the sum of the activities of either control compounds alone, that is, chlorambucil and compound **3o**, an analogue of **3n** missing the nitrogen mustard. Thus, the combination of an HDACi and a DNA alkylating agent in **3n** indicates a superadditive effect. Finally, the HAIR technology was applied to synthesize the proof of concept HDAC degrader **4**. Indeed our proof of concept HDAC PROTAC showed efficient degradation of HDACs. The HAIR methodology is thus a versatile method for synthesis of HDACi-based chimeric small molecules.

Acknowledgements

We sincerely thank Dr. Christoph Selg for the design and preparation of the TOC artwork. M.U.K. acknowledges support from the Deutsche Forschungsgemeinschaft (DFG) for the Thermofisher Arrayscan XTI (INST 208/690-1 FUGG). The authors acknowledge excellent technical support from Nadine Horstick-Muche. Financial support by the Alexander von Humboldt Foundation is gratefully acknowledged. S.B. acknowledges the financial support by Forschungskommission (2018-04) and DSO-Netzwerkverbundes, HHU Düsseldorf. M.R. acknowledges a research fellowship from the Deutsche Forschungsgemeinschaft (DFG, RO5526/1-1). Open access funding enabled and organized by Projekt DEAL.

Conflict of interest

The authors declare no conflict of interest.

Keywords: DNA damage · histone deacetylase · multi-target drugs · PROTAC · solid-phase synthesis

[1] A. Anighoro, J. Bajorath, G. Rastelli, *J. Med. Chem.* **2014**, *57*, 7874–7887.
[2] R. Morphy, Z. Rankovic in *The Practise of Medicinal Chemistry, 4th ed.* (Eds.: C. Wermuth, D. Aldous, P. Raboisson, D. Rognan), Academic Press, Elsevier, **2015**, pp. 449–472.
[3] M. Rosini, *Future Med. Chem.* **2014**, *6*, 485–487.
[4] M. Haberland, R. L. Montgomery, E. N. Olson, *Nat. Rev. Genet.* **2009**, *10*, 32–34.
[5] O. Witt, H. E. Deubzer, T. Milde, I. Oehme, *Cancer Lett.* **2009**, *277*, 8–21.
[6] C. Wang, A. Hamacher, P. Petzsch, K. Köhrer, G. Niegisch, M. J. Hoffmann, W. A. Schulz, M. U. Kassack, *Cancers* **2020**, *12*, 337.
[7] V. Krieger, A. Hamacher, F. Cao, K. Stenzel, C. G. W. Gertzen, L. Schäker-Hübner, T. Kurz, H. Gohlke, F. J. Dekker, M. U. Kassack, F. K. Hansen, *J. Med. Chem.* **2019**, *62*, 11260–11279.
[8] Y. Li, E. Seto, *Cold Spring Harbor Perspect. Med.* **2016**, *6*, a026831.
[9] A. R. Maolanon, H. M. Kristensen, L. J. Leman, M. R. Ghadiri, C. A. Olsen, *ChemBioChem* **2017**, *18*, 5–49.
[10] A. Ganesan, *ChemMedChem* **2016**, *11*, 1227–1241.
[11] R. de Lera, A. Ganesan, *Clin. Epigenet.* **2016**, *8*, 105.
[12] C. Y. Lee, *Onco Targets Ther.* **2017**, *10*, 265–270.
[13] A. Urdiciain, E. Erausquin, B. Meléndez, J. A. Rey, M. A. Idoate, J. S. Castresana, *Int. J. Oncol.* **2019**, *54*, 1797–1808.
[14] S. Y. Lee, *Genes Dis.* **2016**, *3*, 198–210.
[15] L. Gatti, A. Sevko, M. De Cesare, N. Arrighetti, G. Manenti, E. Ciusani, P. Verderio, C. M. Ciniselli, D. Cominetti, N. Carenini, E. Corna, N. Zaffaroni, M. Rodolfo, L. Rivoltini, V. Umansky, P. Perego, *Oncotarget* **2014**, *5*, 4516–4528.
[16] C. Festuccia, A. Mancini, A. Colapietro, G. L. Gravina, F. Vitale, F. Marampon, S. Delle Monache, S. Pompili, L. Christiano, A. Vetuschi, V. Tombolini, Y. Chen, T. Mehrling, *J. Hematol. Oncol.* **2018**, *11*, 38.
[17] G. Hajós, Z. Riedl in *Comprehensive Heterocyclic Chemistry III*, *Vol. 11* (Eds.: A. Katritzky, C. Ramsden, E. F. V. Scriven, R. J. K Taylor), Elsevier, Amsterdam, **2008**, pp. 895–908.
[18] H. Setiyanto, V. Saraswaty, R. Hertadi, I. Noviandri, B. Buchari, *Int. J. Electrochem. Sci.* **2011**, *6*, 2090–2100.
[19] W. P. Roos, B. Kania, *Cancer Lett.* **2013**, *332*, 237–248.
[20] J. J. Bandolik, A. Hamacher, C. Schrenk, R. Weishaupt, M. U. Kassack, *Int. J. Mol. Sci.* **2019**, *20*, 3052.
[21] M. Toure, C. M. Crews, *Angew. Chem. Int. Ed.* **2016**, *55*, 1966–1973; *Angew. Chem.* **2016**, *128*, 2002–2010.
[22] M. Pettersson, C. M. Crews, *Drug Discovery Today* **2019**, *31*, 15–27.
[23] A. Vogelmann, D. Robaa, W. Sippl, M. Jung, *Curr. Opin. Chem. Biol.* **2020**, *57*, 8–16.
[24] K. Yang, Y. Song, H. Xie, H. Wu, Y.-T. Wu, E. D. Leisten, W. Tang, *Bioorg. Med. Chem. Lett.* **2018**, *28*, 2493–2497.
[25] J. P. Smalley, G. E. Adams, C. J. Millard, Y. Song, J. K. S. Norris, J. W. R. Schwabe, S. M. Cowley, J. T. Hodgkinson, *Chem. Commun.* **2020**, *56*, 4476–4479.
[26] H. Wu, K. Yang, Z. Zhang, E. D. Leisten, Z. Li, H. Xie, J. Liu, K. A. Smith, Z. Novakova, C. Barinke, W. Tang, *J. Med. Chem.* **2019**, *62*, 7042–7057.

Manuscript received: May 9, 2020
Revised manuscript received: July 30, 2020
Accepted manuscript online: August 11, 2020
Version of record online: October 9, 2020

Angewandte Chemie
Eine Zeitschrift der Gesellschaft Deutscher Chemiker

Supporting Information

Hydroxamic Acids Immobilized on Resins (HAIRs): Synthesis of Dual-Targeting HDAC Inhibitors and HDAC Degraders (PROTACs)

Laura Sinatra, Jan J. Bandolik, Martin Roatsch, Melf Sönnichsen, Clara T. Schoeder, Alexandra Hamacher, Andrea Schöler, Arndt Borkhardt, Jens Meiler, Sanil Bhatia, Matthias U. Kassack, and Finn K. Hansen**

anie_202006725_sm_miscellaneous_information.pdf

Table of Contents

Abbreviations

°C	degrees Celsius
Å	angstrom
aq.	aqueous
BSA	bovine serum albumin
c	concentration
calcd	calculated
d	doublet (spectral)
Da	dalton
DNA	deoxyribonucleic acid
DIPEA	*N,N*-Diisopropylethylamine
DMEM	Dulbecco's Modified Eagle Medium
DMF	*N,N*-Dimethylformamide
DMSO	dimethyl sulfoxide
EDTA	2,2',2",2"'-(Ethane-1,2-diyldinitrilo)tetraacetic acid
equiv.	equivalent
ESI	electrospray ionization (mass spectrometry)
et al.	and others
Fmoc	fluorenylmethoxycarbonyl
h	hour
H	histone
HAIR	hydroxamic acid immobilized on resin
HATU	[*O*-(7-Azabenzotriazol-1-yl)-*N,N,N',N'*-tetramethyluronium-hexafluorophosphate]
HDAC	histone deacetylase
HOBt	1-Hydroxybenzotriazole
HPLC	high performance liquid chromatography
HRMS	high-resolution mass spectrometry
Hz	hertz
IR	infrared spectroscopy
J	coupling constant (NMR spectrometry)
K	kelvin
lit	literature
M	molar (moles per liter)
m	multiplet (spectral)
m/z	mass-to-charge ratio
M+/M-	molecular ion
max.	maximum
MeOH	methanol
min	minutes
mL	milliliter
mm	millimeter
MS	mass spectrometry
MTT	3-(4,5-dimethylthiazol-2-yl)-2,5-diphenyltetrazolium bromide
nm	nanometer
NMR	nuclear magnetic resonance

PBS	phosphate-buffered saline
PDB	protein data bank
PE	polyethylene
PI	propidium iodide
PP	polypropylene
ppm	parts per million
PROTAC	protolysis targeting chimera
q	quartet (spectral)
QVD	5-(2,6-Difluorophenoxy)-3-[[3-methyl-1-oxo-2-[(2-quinolinylcarbonyl)amino]butyl]amino]-4-oxo-pentanoic acid hydrate
RIPA	Radioimmunoprecipitation assay
rpm	revolutions per minute
s	singlet (spectral)
sat.	saturated
SDS	sodium dodecyl sulfate
t	triplet (spectral)
TFA	trifluoroacetic acid
TLC	thin-layer chromatography
TNBS	2,4,6-trinitrobenzenesulfonic acid
TOF	time-of-flight (mass spectrometry)
t_R	retention time
TRIS	Tris(hydroxymethyl)-aminomethane
UV-vis	ultraviolet-visible
v/v	volume per volume
ZMAL	*N*-(4-Methyl-7-aminocoumarinyl)-*N*α-(t-butoxycarbonyl)-*N*ω-acetyllysineamide
δ	NMR chemical shift in parts per million downfield from a standard (tetramethylsilane)
ε	molar extinction coefficient

1 Supplementary tables, schemes and figures

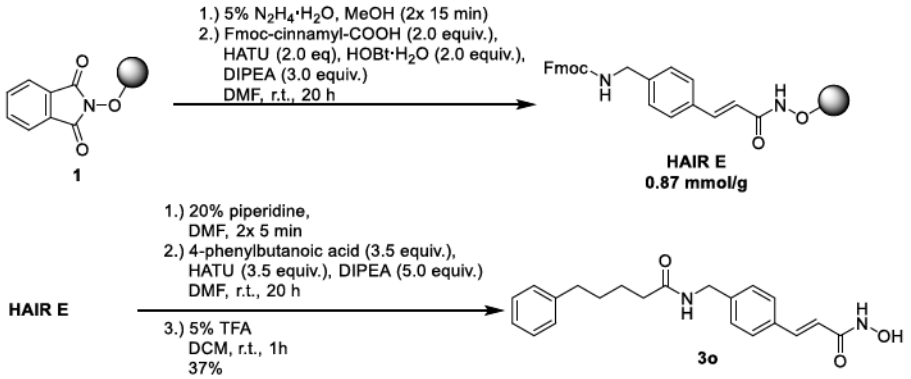

Scheme S1: Solid Phase supported Synthesis of control compound **3o** using HAIR E.

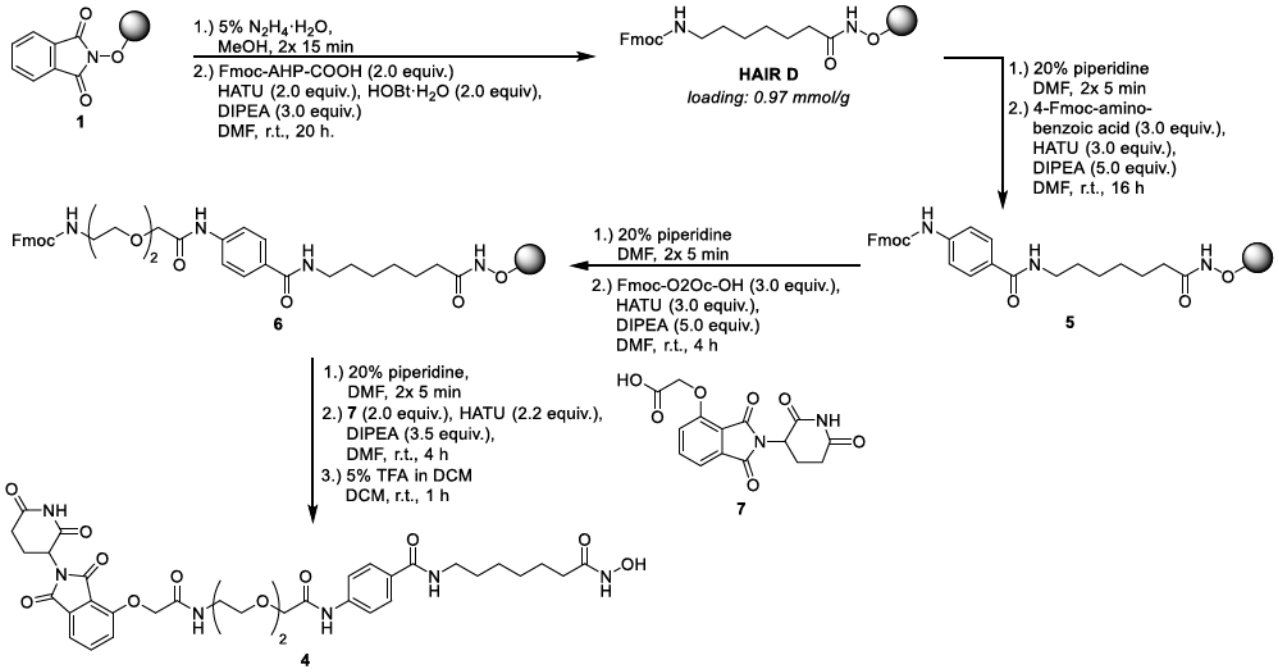

Scheme S2: Synthesis of proof of concept HDAC-PROTAC using solid phase supported HAIR approach. **7** was synthesized according to literature.[1]

Table S1: Data shown are combination indices (CI) calculated using CompuSyn 1.0 based on the Chou-Talalay method [2, 3]. CI > 1.0 indicates antagonism, CI = 1 indicates an additive effect, and CI < 1.0 indicates synergism. Cal27 cells were incubated with the drugs indicated for 24 h and caspase-3/7-positive cells were analyzed. The single drug effects of **3o** and CAB were compared to the effect of coincubation of "**3o** + CAB" and to the effect of **3n**. Values are the mean of three experiments. SD is < 10 % of the mean.

[3o], µM	[CAB], µM	CI-Values	
		3o + CAB	3n
6	6	0,93	0,92
9	9	0,90	0,69
12	12	0,96	0,70

SUPPORTING INFORMATION

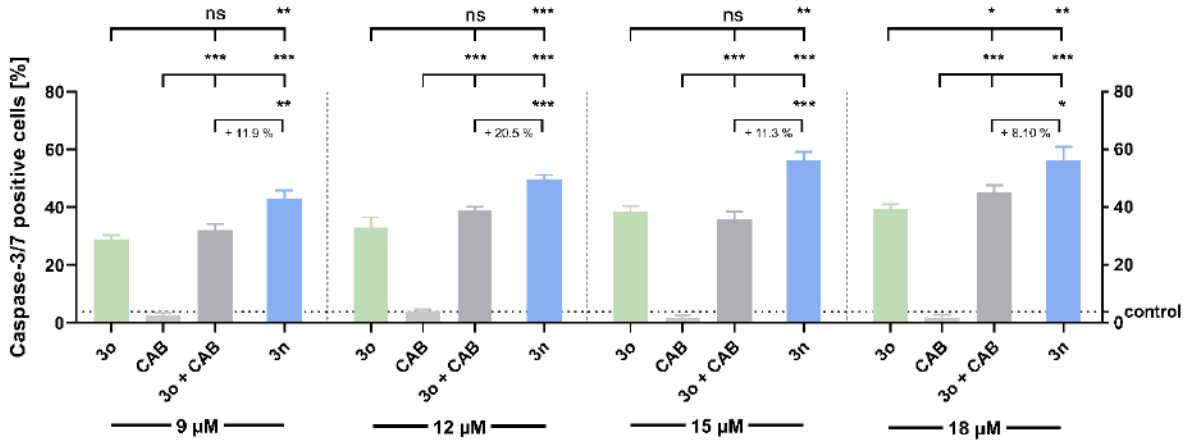

Figure S1: Compound-induced caspase-3/7 activation in Cal27 cells. Cells were treated with indicated concentrations for 24 h. 100 µM Cisplatin was added as positive control (data not shown). "control" is vehicle control (and showed 3.96 % caspase-3/7 positive cells). t-test was used to analyse for significant differences between **3o** or CAB single treatment and coincubation of **3o** and CAB or **3n** and the comparison of **3o** and CAB coincubation and **3n** single treatment as indicated. The increase in caspase-3/7 activation by **3n** single treatment over coincubation of **3o** and CAB is shown as percentage points below the respective bracket. Data are the mean ± SD, n = 3. ns ($p > 0.05$); * ($p \leq 0.05$); ** ($p \leq 0.01$); *** ($p \leq 0.001$).

2 Chemistry

2.1 General Remarks

Materials and Experimental Procedures

All chemicals were obtained from commercial suppliers (Sigma-Aldrich, Acros Organics, Carbolution Chemicals, Iris Biotech, TCI Chemicals) and used as purchased without further purification. 2-((2-(2,6-Dioxopiperidin-3-yl)-1,3-dioxoisoindolin-4-yl)oxy)acetic acid (**7**) was synthesized according to literature known procedures.[1] Solvents with technical grade were distilled prior to use. Acetonitrile in HPLC-grade quality (HiPerSolv CHROMANORM, *VWR*) was used for all HPLC purposes. Water was purified with a Milli-Q Simplicity 185 Water Purification System (Merck Millipore). All reactions with water- and/or air-sensitive starting materials were carried out in pre-dried glass wares under Argon atmosphere utilizing standard *Schlenk* techniques. All solid phase reactions were carried out in PP-reactors with PE frits (sizes: 2/5/10/20 mL, pore size 23 µm, *MultiSynTech GmbH*) and a 2-chlorotrityl chloride resin (200-400 mesh, 1.60 mmol/g, Iris Biotech) was used. Thin-layer chromatography (TLC) was carried out on prefabricated plates (silica gel 60, F254 with fluorescence indicator, *Merck*). Components were visualized by irradiation with ultraviolet light (254 nm, 366 nm) or by staining in potassium permanganate dip or ninhydrin dip followed by careful heating (~300 °C). Column Chromatography was either carried out on silica gel (NORMASIL 60®, 40-63 µm, *VWR*) or on a *Teledyne ISCO* Combi Flash NEXTGEN 300+ using prepacked silica columns (Redisep® normal phase, 35 to 70 microns, 230 to 400 mesh, 60 Å in the sizes 12 g or 24 g, *Teledyne ISCO*).

Figure 1 was partially created with BioRender.com.

Nuclear Magnetic Resonance Spectroscopy (NMR)

Proton (^{1}H) and carbon (^{13}C) NMR spectra were recorded either on a *Bruker* Avance III HD 400 MHz at a frequency of 400 MHz (^{1}H) and 100 MHz (^{13}C) or *Varian/Agilent* Mecury-plus-400 at a frequency of 400 MHz (^{1}H) and 100 MHz (^{13}C) or a *Varian/Agilent* Mecury-plus-300 at a frequency of 300 MHz (^{1}H) and 75 MHz (^{13}C). The residual solvent signal ($CDCl_3$: ^{1}H NMR: 7.26 ppm, ^{13}C NMR: 77.1 ppm, DMSO-d_6: ^{1}H NMR: 2.50 ppm, ^{13}C NMR: 39.52 ppm) was used for calibration referred to tetramethylsilane. As solvents deuterated chloroform ($CDCl_3$), deuterated methanol (MeOD) and deuterated dimethyl sulfoxide (DMSO-d_6) were used. The chemical shifts are given in parts per million (ppm). The multiplicity of each signal is reported as singlet (s), doublet (d), triplet (t), quartet (q), multiplet (m) or combinations thereof. Multiplicities are reported as they were measured, and they might disagree with the expected multiplicity of a signal.

Mass Spectrometry

High resolution electrospray ionisation mass spectra (HR-ESI-MS) were acquired either with a *Bruker Daltonik GmbH* micrOTOF coupled to a an *LC Packings* Ultimate HPLC system and controlled by micrOTOFControl3.4 and HyStar 3.2-LC/MS or with a *Bruker Daltonik GmbH* ESI-qTOF Impact II coupled to a *Dionex* UltiMate™ 3000 UHPLC system and controlled by micrOTOFControl 4.0 and HyStar 3.2-LC/MS.

High Performance Liquid Chromatography (HPLC)

For analytical purposes either a *Thermo Fisher Scientific* UltiMate™ 3000 UHPLC system or a *Gynkotek* Gina 50 HPLC system (Detector: Gynkotek UVD340U, Pump: Dionex P680 HPLC pump, column oven: Dionex STH 585) with a Nucleodur 5 u C18 100 Å (250 x 4.6 mm, Macherey Nagel) column were used. In the process a flow rate of 1 mL/min and a temperature of 25° C were set. For preparative purposes a *Varian* ProStar system with either a Jupiter 5 u C18 100 Å-column (250 x 10 mm, Phenomenex) with 4 mL/min or a Nucleodur 5 u C18 HTec (150 x 32 mm, Macherey Nagel) column with 15 mL/min were used. Detection was implemented by UV absorption measurement at a wavelength of λ = 220 nm and λ =254 nm. Bidest. H_2O (A) and MeCN (B) were used as eluents with an addition of 0.1% TFA for eluent A. For analytical as well as preparative purposes after column equilibration for 5 min a linear gradient from 5% A to 95% B in 15 min followed by an isocratic regime of 95% B for 5 min was used.

UV-VIS and Infrared Spectroscopy (IR)

Loading determinations were performed on a *Shimadzu* UV-160A spectrometer at room temperature. All measurements were performed in a 3500 µL quartz cuvette (100-QS, Hellma Analytics) with a path lengths of 10 mm. Infrared spectroscopy measurements were performed on a PerkinElmer SpectrumTwo FT-IR spectrometer at room temperature.

Determination of the Loading

A small part of the different HAIRs (~5 mg) was weighed and treated with 500 µL of the deprotection solution (20% piperidine in DMF) for 5 min. The solution was collected and the procedure was repeated once. The concentration of the cleaved Fmoc-group was determined photometrically ($\varepsilon_{300\,nm}$(dibenzofulvene)= 7800 $M^{-1}cm^{-1}$). With the concentration of the cleaved dibenzofulvene determined by using Lambert-Beer law and the mass of the resin the loading could be determined.

$$A = \varepsilon \cdot c \cdot l$$

where A = absorbance; ε = molar extinction coefficient; c = concentration; l = optical path length.

2.2 General Procedures

General Procedure A

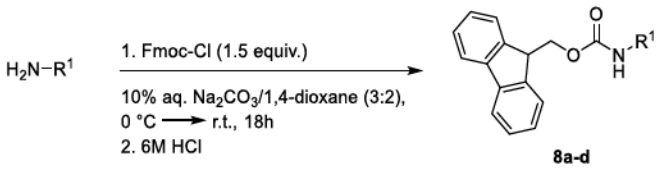

The amounts of reagents and solvents used in the following synthesis protocol correspond to 6.00 – 8.00 mmol scale. To a cooled (0 °C) solution of the appropriate amine (1.00 equiv.) in 10% aq. Na_2CO_3/1,4-dioxane (3:2, 20mL/mmol) was added Fmoc-Cl (1.50 equiv.) in five portions over a period of 20 min. The mixture was then allowed to warm to room temperature and stirred for 18 h. Upon completion of the reaction, the reaction solution was diluted with dest. H_2O (50 mL) and washed with Et_2O (3 x 150 mL). Subsequently the aqueous phase was acidified to pH 1 with 6 M HCl. Filtration of the resulting precipitate, followed by washing with dest. H_2O (200 mL) and drying *in vacuo* afforded the desired products **8a-d**.

General Procedure B

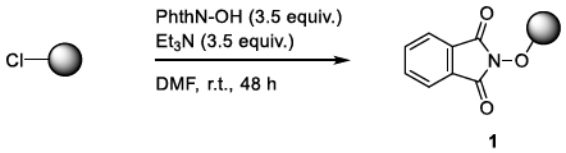

The amounts of reagents and solvents used in the following synthesis protocol correspond to a 3.00 – 4.00 mmol scale. This reaction step was carried out based on a procedure of Khan *et. al.*[4] After resin swelling for 30 min in DMF, a solution of *N*-hydroxyphthalimide (3.50 equiv) and Et_3N (3.50 equiv.) in DMF (1.5 mL/g resin) was added to the resin and reacted for 48 h. Afterwards the resin was washed with DMF (10 x 5 mL) and CH_2Cl_2 (10 x 5 mL). Capping of the modified resin was performed by treatment with capping solution (10 mL, CH_2Cl_2/MeOH/DIPEA, 80:15:5) two times for 15 min. Subsequently, the resin was washed with DMF (5 x 5 mL) and CH_2Cl_2 (10 x 5 mL) and dried *in vacuo* to afford the modified resin **1**.

General Procedure C

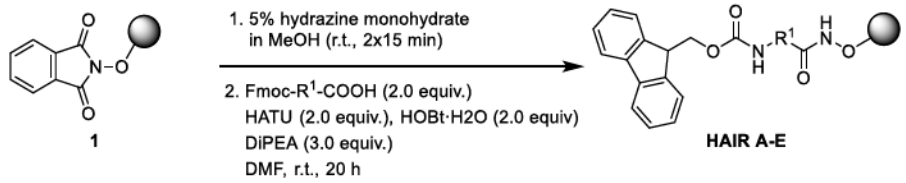

The amounts of reagents and solvents used in the following synthesis protocol correspond to a 1.50 – 2.00 mmol scale. After swelling of the modified resin **1** (estimated loading 1.50 mmol/g) for 30 min in DMF, the resin was washed with MeOH (3 x 5 mL). The phthaloyl protecting group was removed by treatment with 5% hydrazine monohydrate in MeOH for 15 min (2 x 5 mL). Afterwards the resin was washed with DMF (5 x 5 mL), MeOH (5 x 5 mL), CH_2Cl_2 (5 x 5 mL) and DMF (5 x 5 mL). For the subsequent amide coupling reaction a solution of the respective acid (2.00 equiv.), HATU (2.00 equiv.), HOBt·H_2O (2.00 equiv.) and DIPEA (3.00 equiv.) in DMF (1 mL/mmol acid) was agitated for 5 min and then added to the resin. The amide coupling was performed for 20 h at room temperature. Afterwards the resin was washed with DMF (5 x 5 mL) and CH_2Cl_2 (5 x 5 mL). Completion of the reaction was monitored via TNBS-test. The preloaded resins **HAIR A-E** were dried *in vacuo* and stored at 4 °C. Determination of the loading capacity was conducted photometrically.

General Procedure D

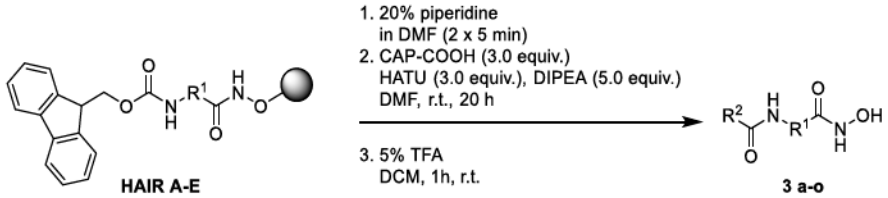

The amounts of reagents and solvents used in the following synthesis protocol correspond to 0.30 – 0.50 mmol scale. After swelling of the appropriate **HAIR** in DMF for 30 min, Fmoc deprotection was performed by treatment with 20% piperidine in DMF for 5 min (2 x 3 mL). Afterwards the resin was washed with DMF (5 x 3 mL), CH_2Cl_2 (5 x 3 mL) and DMF (5 x 3 mL). For the subsequent amide coupling reaction a solution of the respective acid (3.00 equiv.), HATU (3.00 equiv.), and DIPEA (5.00 equiv.) in DMF (1 mL/mmol acid) was agitated for 5 min and then added to the resin. The amide coupling was performed in dark environment for 20 h at room temperature. Afterwards the resin was washed with DMF (5 x 3 mL) and CH_2Cl_2 (5 x 3 mL). Completion of the reaction was monitored via TNBS-test on a few resin beads. The resin was dried *in vacuo* followed by the cleavage of the crude products from the resin by treatment with cleavage solution (5% TFA in CH_2Cl_2, 1 mL/40 mg resin) for 1 h at room temperature. The filtrates were concentrated *in vacuo* and the crude products **3a-o** were purified by preparative HPLC. Lyophilization of the respective fractions yielded the desired products **3a-o** in >95% purity.

2.3 Synthesis

Building block synthesis

*4-((((9H-Fluoren-9-yl)methoxy)carbonyl)amino)butanoic acid (**8a**)*

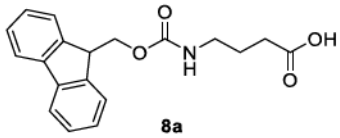

8a

Synthesized from 4-aminobutanoic acid (2.00 g, 19.4 mmol, 1.00 equiv.) and 9-fluorenylmethoxycarbonyl chloride (7.53 g, 29.1 mmol, 1.50 equiv.) according to general procedure A. Filtration and drying *in vacuo* afforded **8a** as a white solid (5.04 g, 15.5 mmol, 80%). **^{1}H-NMR** (400 MHz, MeOD): δ= 7.79 (d, *J* = 7.6 Hz, 2H), 7.65 (d, *J* = 7.5 Hz, 2H), 7.39 (t, *J* = 7.4 Hz, 2H), 7.31 (t, *J* = 7.4 Hz, 2H), 4.35 (d, *J* = 6.8 Hz, 2H), 4.20 (t, *J* = 6.9 Hz, 1H), 3.15 (t, *J* = 6.8 Hz, 2H), 2.31 (t, *J* = 7.5 Hz, 2H), 1.84 – 1.69 (m, 2H) ppm, -COO*H* signal could not be detected due to solvent exchange. **HRMS-ESI (*m/z*)**: [*M* + Na]$^+$ calcd for $C_{19}H_{19}NO_4$: 348.1206; found: 348.1204. The analytical data are in accordance with the literature.[5]

*7-((((9H-Fluoren-9-yl)methoxy)carbonyl)amino)heptanoic acid (**8b**)*

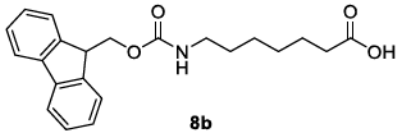

8b

Synthesized from 4-aminoheptanoic acid (1.00 g, 6.90 mmol, 1.00 equiv.) and 9-fluorenylmethoxycarbonyl chloride (2.67 g, 10.3 mmol, 1.50 equiv.) according to general procedure A. Filtration and drying *in vacuo* afforded **8b** as a white solid (2,26 g, 6.14 mmol, 89%). **^{1}H-NMR** (400 MHz, DMSO-d_6): δ= 7.88 (dt, *J* = 7.6, 1.0 Hz, 2H), 7.68 (d, *J* = 7.4 Hz, 2H), 7.41 (td, *J* = 7.5, 1.2 Hz, 2H), 7.32 (td, *J* = 7.4, 1.2 Hz, 2H), 7.24 (t, *J* = 5.7 Hz, 1H), 4.29 (d, *J* = 6.9 Hz, 2H), 4.20 (t, *J* = 6.9 Hz, 1H), 2.98 – 2.92 (m, *J* = 6.6 Hz, 2H), 2.18 (t, *J* = 7.4 Hz, 2H), 1.48 (p, *J* = 7.4 Hz, 2H), 1.38 (p, *J* = 6.9 Hz, 2H), 1.25 (h, *J* = 4.2, 3.1 Hz, 4H) ppm, -COO*H* signal could not be detected due to solvent exchange. **^{13}C-NMR** (101 MHz, DMSO-d_6): δ= 174.6, 156.1, 144.0, 140.8, 127.6, 127.1, 125.2, 121.4, 120.1, 65.2, 46.8, 33.8, 29.2, 28.3, 26.0, 24.5 ppm. **HRMS-ESI (*m/z*)**: [*M* - H]$^-$ calcd for $C_{22}H_{25}NO_4$: 366.1711, found: 366.1722. **IR**: $\tilde{\nu}$= 3222 (br), 2935 (br), 1743 (vs), 1640 (vs), 1579 (s), 1518 (s), 1455 (vs),1249 (s), 1087 (s), 956 (m), 735 (s) cm^{-1}.

*tert-Butyl (4-bromobenzyl)carbamate (**9**)*

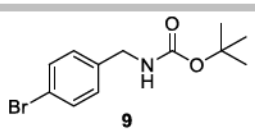

9

To a cooled (0 °C) solution of 4-bromobenzylamine (1.00 g, 5.38 mmol, 1.00 equiv.) and triethylamine (822 µL, 5.91 mmol, 1.10 equiv.) in CH_2Cl_2 (15 mL), a solution of di-*tert*-butyl dicarbonate (1.29 g, 5.91 mmol, 1.10 equiv.) in CH_2Cl_2 (10 mL) was added dropwise. The mixture was then allowed to warm to room temperature and stirred for 18 h. Upon completion of the reaction, the solvent was removed *in vacuo* and the crude product was dissolved in EtOAc (20 mL). The organic phase was acidified to pH 4 with anhydrous citric acid. The organic phase was washed with dest. H_2O (3 x 20 mL) and sat. $NaHCO_3$ (3 x 20 mL). Drying over anhydrous $MgSO_4$ and removal of the solvent *in vacuo* afforded the crude product **9**, which was purified by flash column chromatography (cyclohexane/EtOAc, 4:1) to afford the desired product **9** (1.15 g, 4.04 mmol, 75%). **^{1}H-NMR** (400 MHz, $CDCl_3$): δ= 7.60 – 7.39 (m, 2H), 7.15 (d, *J* = 8.0 Hz, 2H), 4.85 (s, 1H), 4.26 (d, *J* = 6.0 Hz, 2H), 1.45 (s, 9H) ppm. **^{13}C-NMR** (75 MHz, $CDCl_3$): δ= 156.0, 138.2, 131.8, 129.3, 121.3, 58.4, 44.2, 28.5 ppm. **HRMS-ESI (*m/z*)**: [*M* + Na]$^+$ calcd for $C_{12}H_{16}BrNO_2$: 308.0257, found: 308.0253. **IR**: $\tilde{\nu}$= 3363 (m), 3340 (m), 2976 (m), 2931 (w), 1682 (vs), 1534 (s), 1504 (vs), 1486 (s), 1362 (s), 1281 (m), 1244 (vs), 1157 (vs), 1068 (m), 1047 (vs), 1010 (s), 877 (m), 808 (m), 798 (m), 623 (m), 479 (s) cm^{-1}.

*tert-Butyl (E)-3-(4-(((tert-butoxycarbonyl)amino)methyl)phenyl)acrylate (**10**)*

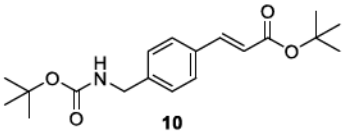

10

To a mixture of tert-butyl (4-bromobenzyl)carbamate (600 mg, 2.10 mmol, 1.00 equiv.), $[PdCl_2(PPh_3)_2]$ (73.5 mg, 0.11 mmol, 5 mol%), LiCl (177 mg, 4.20 mmol, 2.00 equiv.) and DIPEA (714 µL, 4.20 mmol, 2.00 equiv.) in DMF (7 mL) was added *tert*-Butyl acrylate (609 µL, 4.20 mmol, 2.00 equiv.). The reaction was heated up to 100 °C under argon atmosphere for 16 h. Upon completion of the reaction, the solvent was removed *in vacuo* and coevaporated with toluene (3 x 15 mL). The residue war dissolved in EtOAc (20 mL) and washed with 1 M HCl (5 x 20 mL), sat. aq. $NaHCO_3$ (3 x 20 mL) and brine (3 x 20 mL). The organic phase was dried over anhydrous $MgSO_4$ and the solvent was removed under reduced pressure. Purification by flash column chromatography (cyclohexane/EtOAc, 9:1) afforded the desired product **10** as white solid (574 mg, 1.72 mmol, 82%). **^{1}H-NMR** (400 MHz, $CDCl_3$): δ= 7.56 (d, *J* = 16.0 Hz, 1H), 7.46 (d, *J* = 8.0 Hz, 2H), 7.28 (d, *J* = 8.1 Hz, 2H), 6.34 (d, *J* = 16.0 Hz, 1H), 4.88 (s, 1H), 4.32 (d, *J* = 6.0 Hz, 2H), 1.53 (s, 9H), 1.46 (s, 9H) ppm. **^{13}C-NMR** (101 MHz, $CDCl_3$): δ= 166.5, 156.0, 143.2, 141.2, 133.9, 128.4, 127.9, 120.2, 80.7, 79.8, 44.5, 28.5, 28.3 ppm. **HRMS-ESI (*m/z*)**: [*M* + Na]$^+$ calcd for $C_{19}H_{27}NO_4$: 356.1832, found: 356.1828. **IR**: $\tilde{\nu}$= 3362 (br), 2977 (m), 2930 (m), 1703 (vs), 1513 (br), 1367 (m), 1151 (vs), 845 (br) cm^{-1}.

*(E)-3-(4-(((((9H-Fluoren-9-yl)methoxy)carbonyl)amino)methyl)phenyl)acrylic acid (**8c**)*

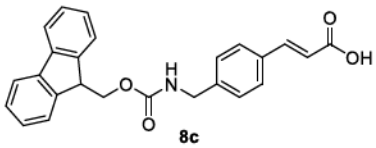

8c

TFA (7.5 mL) was added dropwise to a cooled (0 °C) solution of **10** (511 mg, 1.55 mmol, 1.00 equiv.) in CH_2Cl_2 (22.5 mL). After stirring for 15 min, the solution was allowed to warm to room temperature and stirred for further 2 h. Upon completion of the reaction, the solvent was removed *in vacuo*. The crude product was further reacted with 9-fluorenylmethoxycarbonyl chloride (481mg, 1.86 mmol, 1.20 equiv.) following general procedure A yielding the desired product **8c** as white solid (482 mg, 1.20 mmol, 77%). **^{1}H-NMR** (400 MHz, DMSO-d_6): δ= 12.39 (s, 1H), 7.89 -7.82 (m, 3H), 7.70 (d, *J* = 7.5 Hz, 2H), 7.63 (d, *J* = 8.0 Hz, 2H), 7.57 (d, *J* = 16.0 Hz, 1H), 7.42 (t, *J* = 7.5 Hz, 2H), 7.33 (t, *J* = 7.4 Hz, 2H), 7.25 (d, *J* = 7.9 Hz, 2H), 6.51 (d, *J* = 16.0 Hz, 1H), 4.36 (d, *J* = 6.8 Hz, 2H), 4.23 (t, *J* = 6.7 Hz, 1H), 4.20 (d, *J* = 6.2 Hz, 2H) ppm. **^{13}C-NMR** (101 MHz, DMSO-d_6): δ= 167.9, 156.4, 143.9, 143.2, 142.0, 140.8, 133.0, 128.1, 127.6, 127.4, 127.1, 125.2, 120.1, 119.4, 65.3, 46.8, 43.5 ppm. **HRMS-ESI (*m/z*)**: [*M* - H]$^-$ calcd for $C_{25}H_{21}NO_4$: 398.1398, found:398.1398. **IR**: $\tilde{\nu}$= 3310 (br), 1686 (vs), 31 (m), 1532 (m), 1427 (w), 1254 (s), 1142 (m), 984 (m), 757 (m), 737 (s), 533 (m) cm^{-1}.

*4-((((9H-Fluoren-9-yl)methoxy)carbonyl)amino)benzoic acid (**8d**)*

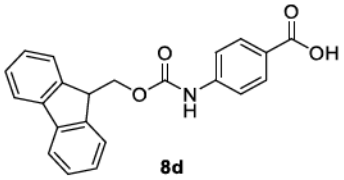

8d

Synthesized from 4-aminobenzoic acid (1.00 g, 7.30mmol, 1.00 equiv.) and 9-fluorenylmethoxycarbonyl chloride (2.83 g, 11.0 mmol, 1.50 equiv.) according to general procedure A. Filtration and drying *in vacuo* afforded the desired product **8d** as white solid (2.32 g, 6.46 mmol, 88%). **^{1}H-NMR** (400 MHz, DMSO-d_6): δ= 12.67 (s, 1H, broad signal), 10.06 (s, 1H), 7.91 (dt, *J* = 7.6, 0.9 Hz, 2H), 7.85 (d, *J* = 8.5 Hz, 2H), 7.76 (dd, *J* = 7.4, 1.2 Hz, 2H), 7.55 (d, *J* = 8.1 Hz, 2H), 7.48 – 7.39 (m, 2H), 7.35 (td, *J* = 7.4, 1.2 Hz, 2H), 4.53 (d, *J* = 6.5 Hz, 2H), 4.33 (t, *J* = 6.5 Hz, 1H) ppm. **HRMS-ESI (*m/z*)**: [*M* + Na]$^+$ calcd for $C_{22}H_{17}NO_4$: 382.1050, found: 382.1049. The analytical data are in accordance with the literature.[6]

*4-Diazo-4H-imidazole-5-carboxamide (**11**)*

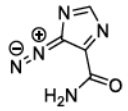

11

A solution of 5-amino-1*H*-imidazole-4-carboxamide hydrochloride (3.50 g,21.5 mmol, 1.00 equiv.) in 1 M HCl (28 mL) was slowly added dropwise to a solution of sodium nitrite (1.63 g, 23.7 mmol, 1.10 equiv.) in water (42 mL) at 0°C in an ice-bath. With every drop, the orange-reddish color of the suspension intensified and more and more precipitate formed. After completion of the addition, the dark red suspension was stirred for further 15 min at 0°C, before the solids were collected by suction filtration and thoroughly washed with water. Drying in a desiccator over $CaCl_2$ under vacuum for several days afforded **11** as a deep-red powder (3.02 g, 22.0 mmol, 79%). **^{1}H-NMR** (400 MHz, DMSO-d_6): δ= 7.99 (s, 1H), 7.80 (s, 1H), 7.61 (s, 1H) ppm. **^{13}C-NMR** (101 MHz, DMSO-d_6): δ= 161.3, 155.4, 149.7, 102.3 ppm. **MS-ESI (*m/z*)**: [*M* + Na]$^+$ calcd for $C_4H_3N_5O$: 160.023, found: 160.024; [*M* - H]$^-$ calcd for $C_4H_3N_5O$: 136.026, found: 136.027. Synthesized according to literature.[7]

*3-(2-Chloroethyl)-4-oxo-3,4-dihydroimidazo[5,1-d][1,2,3,5]tetrazine-8-carboxamide (**12**)*

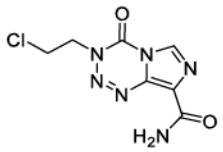

12

To a suspension of 4-diazo-4*H*-imidazole-5-carboxamide (2.00 g, 14.6 mmol, 1.00 equiv.) in dry EtOAc (70 mL) were slowly added via syringe 6.60 mL (8.16 g, 77.3 mmol, 5.30 equiv.) chloroethyl isocyanate. The dark red suspension was stirred for 72 h in the dark at room temperature, before being diluted with diethyl ether (180 mL). More solid material formed, which was collected by suction filtration and dried, yielding **12** as a red powder (2.84 g, 11.7 mmol, 80%). **^{1}H-NMR** (400 MHz, DMSO-d_6): δ= 8.87 (s, 1H), 7.83 (s, 1H), 7.70 (s, 1H), 4.64 (t, *J* = 6.1 Hz, 2H), 4.03 (t, *J* = 6.1 Hz, 2H) ppm. **^{13}C-NMR** (101 MHz, DMSO-d_6): δ= 161.4, 139.1, 134.0, 131.2, 129.1, 50.0, 41.5 ppm. **MS-ESI (*m/z*)**: [*M* + Na]$^+$ calcd for $C_7H_7ClN_6O_2$: 265.021, found: 265.021.

*3-(2-Chloroethyl)-4-oxo-3,4-dihydroimidazo[5,1-d][1,2,3,5]tetrazine-8-carboxylic acid (**13**)*

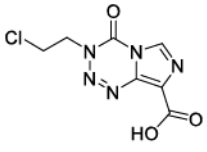

13

A solution of sodium nitrite (2.56 g, 37.1 mmol, 3.60 equiv.) in 7.50 mL water was added very slowly and under vigorous stirring to a suspension of 2.50 g (10.30 mmol, 1.00 equiv.) **12** in concentrated sulfuric acid (15 mL) at 0°C in an ice-bath. Under heavy evolution of gases, the suspension became lighter in color and more precipitate formed, while the temperature was maintained at max. 10°C. After completion of the addition (ca. 1 h), the mixture was warmed to room temperature and vigorously stirred for further 3 h, before being poured into crushed ice (ca. 100 g). An off-white solid formed, which was collected by suction filtration and dried *in vacuo* to yield **13** as a peach-colored powder (1.76 g, 7.23 mmol, 70%). **^{1}H-NMR** (400 MHz, DMSO-d_6): δ= 8.86 (s, 1H), 4.65 (t, *J* = 6.1 Hz, 2H), 4.02

(t, *J* = 6.1 Hz, 2H) ppm. **^{13}C-NMR** (101 MHz, DMSO-d_6): δ= 161.7, 138.9, 135.9, 129.7, 128.4, 50.1, 41.4 ppm. **HRMS-ESI (*m/z*)**: [*M* + Na]$^+$ calcd for $C_7H_6ClN_5O_3$: 266.005, found: 266.005. Synthesized according to literature.[8]

*3-Methyl-4-oxo-3,4-dihydroimidazo[5,1-*d*][1,2,3,5]tetrazine-8-carboxylic acid (**14**)*

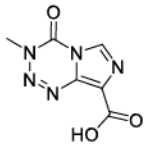

14

A solution of sodium nitrite (2.56 g (37.1 mmol, 3.60 equiv.) in 20 mL water was added very slowly and under vigorous stirring to a suspension of 2.00 g (10.3 mmol, 1.00 equiv.) temozolomide in concentrated sulfuric acid (20 mL) at 0°C in an ice-bath. Under heavy evolution of gases, the suspension became lighter in color and more precipitate formed, while the temperature was maintained at max. 10°C. After completion of the addition within 45 min the mixture was warmed to room temperature and vigorously stirred for further 2 h, before being poured into crushed ice (ca. 100 g). An off-white solid formed, which was collected by suction filtration and dried *in vacuo* to yield **14** as a white powder (1.52 g, 7.77 mmol, 76%). **^{1}H-NMR** (400 MHz, DMSO-d_6): δ= 8.80 (s, 1H), 3.87 (s, 3H) ppm. **^{13}C-NMR** (101 MHz, DMSO-d_6): δ= 161.8, 139.0, 136.4, 129.0, 127.8, 36.3 ppm. **MS-ESI (*m/z*)**: [*M* + Na]$^+$ calcd for $C_6H_5N_5O_3$: 218.028 found: 218.028; [*M* - H]$^-$ calcd for $C_6H_5N_5O_3$: 194.032, found: 194.032. Synthesized according to literature.[8]

HAIR synthesis

HAIR A

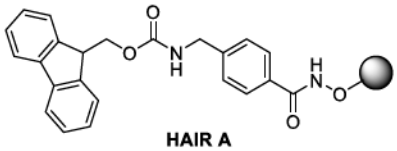

HAIR A

Synthesized according to general procedure C using modified resin **1** (1.00 g, 1.50 mmol, estimated loading 1.50 mmol), 4-(Fmoc-aminomethyl)benzoic acid (1.12 g, 3.00 mmol, 2.00 equiv.), HOBt·H_2O (459 mg, 3.00 mmol, 2.00 equiv.), HATU (1.14 g, 3.00 mmol, 2.00 equiv.) and DIPEA (790 µL, 4.50 mmol, 3.00 equiv.) following general procedure C. Upon completion of the reaction and washing, the resin was dried *in vacuo* and a loading of 0.90 mmol/g was photometrically determined for **HAIR A**.

HAIR B

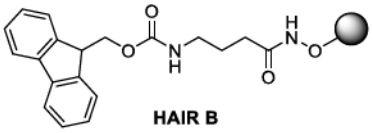

HAIR B

Synthesized according to general procedure C using modified resin **1** (1.00 g, 1.50 mmol, estimated loading 1.50 mmol), 4-Fmoc-aminobutanoic acid (1.12 g, 3.00 mmol, 2.00 equiv.), HOBt·H_2O (459 mg, 3.00 mmol, 2.00 equiv.), HATU (1.14 g, 3.00 mmol, 2.00 equiv) and DIPEA (790 µL, 4.50 mmol, 3.00 equiv) following general procedure C. Upon completion of the reaction and washing, the resin was dried *in vacuo* and a loading of 0.96 mmol/g was photometrically determined for **HAIR B**.

HAIR C

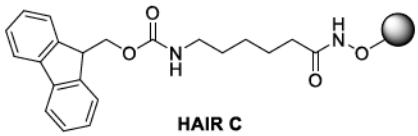

HAIR C

Synthesized according to general procedure C using modified resin **1** (1.19 g, 1.79 mmol, estimated loading 1.50 mmol), 6-Fmoc-aminohexanoic acid (1.26 g, 3.57 mmol, 2.00 equiv.), HOBt·H_2O (547 mg, 3.57 mmol, 2.00 equiv.), HATU (1.36 g, 3.57 mmol, 2.00 equiv.) and DIPEA (933 µL, 5.35 mmol, 3.00 equiv.) following general procedure C. Upon completion of the reaction and washing, the resin was dried *in vacuo* and a loading of 0.87 mmol/g was photometrically determined for **HAIR C**.

HAIR D

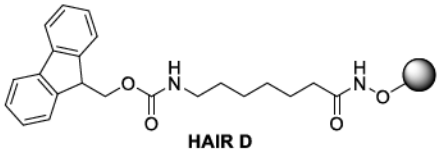

HAIR D

Synthesized according to general procedure C using modified resin **1** (1.22 g, 1.83 mmol, estimated loading 1.50 mmol), 7-Fmoc-aminoheptanoic acid **8b** (1.34 g, 3.65 mmol, 2.00 equiv), HOBt·H_2O (560 mg, 3.65 mmol, 2.00 equiv.), HATU (1.39 g, 3.65 mmol, 2.00 equiv.) and DIPEA (960 µL, 5.50 mmol, 3.00 equiv.) following general procedure C. Upon completion of the reaction and washing, the resin was dried *in vacuo* and a loading of 0.81 mmol/g was photometrically determined for **HAIR D**.

HAIR E

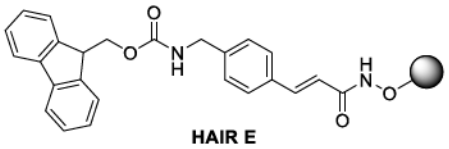

HAIR E

Synthesized according to general procedure C using modified resin **1** (66.6 mg, 0.10 mmol, estimated loading 1.50 mmol), 4-(Fmoc-aminomethyl)phenylacrylic acid **8c** (79.8 mg, 0.20 mmol, 2.00 equiv.), HOBt·H_2O (30.6 mg, 0.20 mmol, 2.00 eq), HATU (76.0 mg, 0.20 mmol, 2.00 equiv.) and DIPEA (51.0 µL, 0.30 mmol, 3.00 equiv.) following general procedure C. Upon completion of the reaction and washing, the resin was dried *in vacuo* and a loading between 0.80 and 0.87 mmol/g was photometrically determined for different batches **HAIR E**.

Library Synthesis

*N-(4-(Hydroxycarbamoyl)benzyl)-3-methyl-4-oxo-3,4-dihydroimidazo[5,1-d][1,2,3, 5] tetrazine-8-carboxamide (**3a**)*

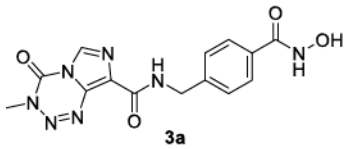

3a

Synthesized according to general procedure D with different equivalents for the reagents using **HAIR A** (200 mg, 0.30 mmol, 1.00 equiv.), HATU (171 mg, 0.45 mmol, 1.50 equiv.), DIPEA (116 mg, 0.90 mmol, 3.00 equiv.) and **14** (88.0 mg, 0.45 mmol, 1.50 equiv.). Purification by preparative HPLC afforded **3a** as beige colored powder (5.0 mg, 14.6 mmol, 5%). **HPLC**: t_R= 12.70 min, **^{1}H-NMR** (400 MHz, DMSO-d_6): δ= 11.16 (s, 1H), 9.13 (t, *J* = 6.3 Hz, 1H), 8.99 (s, 1H), 8.87 (s, 1H), 7.70 (d, *J* = 8.1 Hz, 2H), 7.39 (d, *J* = 8.0 Hz, 2H), 4.53 (d, *J* = 6.3 Hz, 2H), 3.87 (s, 3H) ppm. **^{13}C-NMR** (101 MHz, DMSO-d_6): δ= 164.1, 159.8, 142.8, 139.2, 134.6, 131.3, 130.2, 128.5, 127.1, 126.9, 41.9, 36.1 ppm. **HRMS-ESI (*m/z*)**: [*M* + H]$^+$ calcd for $C_{14}H_{13}N_7O_4$: 344.1102, found: 344.1101. **IR**: $\tilde{\nu}$= 3281 (br), 1756 (m), 1641 (vs), 1557 (m), 1517 (vs), 1455 (m), 1350 (m), 1251 (s), 1015 (m), 952 (m), 732 (s), 586 (s) cm^{-1}.

*3-(2-Chloroethyl)-N-(4-(hydroxycarbamoyl)benzyl)-4-oxo-3,4-dihydroimidazo[5,1-d][1,2,3,5]tetrazine-8-carboxamide (**3b**)*

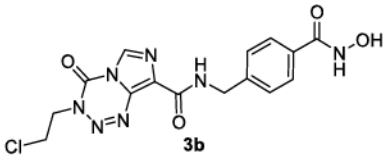

3b

Synthesized according to general procedure D with different equivalents for the reagents using **HAIR A** (400 mg, 0.60 mmol, 1.00 equiv.), HATU (342 mg, 0.90 mmol, 1.50 equiv.), DIPEA (233 mg, 1.80 mmol, 3.00 equiv.) and **13** (219 mg, 0.90 mmol, 1.50 equiv.). Purification by preparative HPLC afforded **3b** as beige coloured powder (56.0 mg, 0.14 mmol, 24%). **HPLC**: t_R= 14.22 min. **^{1}H-NMR** (400 MHz, DMSO-d_6): δ= 11.16 (s, 1H), 9.18 (t, *J* = 6.3 Hz, 1H), 8.96 (s, 1H, broad signal), 8.93 (s, 1H), 7.71 (d, *J* = 8.1 Hz, 2H), 7.40 (d, *J* = 8.0 Hz, 2H), 4.64 (t, *J* = 6.1 Hz, 2H), 4.54 (d, *J* = 6.3 Hz, 2H), 4.03 (t, *J* = 6.1 Hz, 2H) ppm. **^{13}C-NMR** (101 MHz, DMSO-d_6): δ= 164.1, 159.7, 142.7, 139.0, 134.0, 131.3, 130.9, 129.3, 127.1, 126.9, 50.0, 42.0, 41.4 ppm. **HRMS-ESI (*m/z*)**: [*M* + H]$^+$ calcd for

$C_{15}H_{14}ClN_7O_4$: 392.0869, found 392.0866. **IR**: $\tilde{\nu}$= 3413 (w), 3286 (br), 3128 (w), 2869 (br), 1766 (s), 1644 (vs), 1580 (s), 1519 (s), 1456 (s), 1316 (m), 1255 (s), 1246 (s), 1077 (m), 954 (s), 902 (m), 729 (m), 654 (s), 600 (s), 572 (vs), 554 (s) cm^{-1}.

*4-((4-(4-(Bis(2-chloroethyl)amino)phenyl)butanamido)methyl)-N-hydroxybenz-amide (**3c**)*

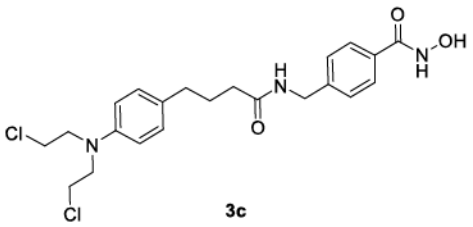

3c

Synthesized according to general procedure D with different equivalents for the reagents using **HAIR A** (200 mg, 0.30 mmol, 1.00 equiv.), HATU (171 mg, 0.45 mmol, 1.50 equiv.), DIPEA (116 mg, 0.90 mmol, 3.00 equiv.) and chlorambucil (137 mg, 0.45 mmol, 1.50 equiv.). Purification by preparative HPLC afforded **3c** as white powder (25.0 mg, 0.06 mmol, 18%). **HPLC**: t_R= 18.17 min. **^{1}H-NMR** (300 MHz, DMSO-d_6): δ= 11.14 (br s, 1H), 8.35 (t, *J* = 5.9 Hz, 1H), 7.69 (d, *J* = 8.2 Hz, 2H), 7.29 (d, *J* = 8.2 Hz, 2H), 7.02 (d, *J* = 8.6 Hz, 2H), 6.69 – 6.63 (m, 2H), 4.29 (d, *J* = 5.9 Hz, 2H), 3.69 (s, 8H), 2.45 (d, *J* = 7.6 Hz, 2H), 2.15 (t, *J* = 7.5 Hz, 2H), 1.76 (p, *J* = 7.6 Hz, 2H) ppm. **APT** (75 MHz, DMSO-d_6): δ= 172.0, 164.0, 144.4, 143.0, 131.2, 129.9, 129.3, 127.0, 126.9, 111.9, 52.2, 41.7, 41.2, 34.8, 33.6, 27.4 ppm. **HRMS-ESI (*m/z*)**: [*M* + H]$^+$ calcd for $C_{22}H_{27}Cl_2N_3O_3$: 452.1502, found 452.1367. **IR**: $\tilde{\nu}$= 3281 (br), 1756 (br), 1640 (s), 1613 (s), 1552 (m), 1432 (br), 1176 (vs), 1153 (vs), 1015 (m), 799 (m), 703 (m) cm^{-1}.

*N-(4-(Hydroxyamino)-4-oxobutyl)-3-methyl-4-oxo-3,4-dihydroimidazo[5,1-d][1,2,3,5]tetrazine-8-carboxamide (**3d**)*

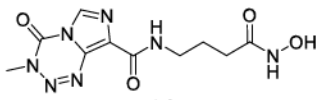

3d

Synthesized according to general procedure D using **HAIR B** (400 mg, 0.36 mmol, 1.00 equiv.), HATU (407 mg, 1.07 mmol, 3.00 equiv.), DIPEA (302 µL, 1.78 mmol, 5.00 equiv.) and **14** (209 mg, 1.07 mmol, 3.00 equiv.). Purification by preparative HPLC afforded **3d** as beige coloured solid (80.7 mg, 0.27 mmol, 76%). **HPLC**: t_R= 11.33 min. **^{1}H-NMR** (400 MHz, DMSO-d_6): δ= 10.39 (s, 1H), 8.84 (s, 1H), 8.55 (t, *J* = 6.0 Hz, 1H), 3.87 (s, 3H), 3.29 (q, *J* = 6.7 Hz, 2H), 2.01 (dd, *J* = 8.4, 6.7 Hz, 2H), 1.82 – 1.70 (m, 2H) ppm, , -C-N*H*-OH signal could not be detected due to solvent exchange. **^{13}C-NMR** (101 MHz, DMSO-d_6): δ= 168.8, 159.7, 139.2, 134.4, 130.5, 128.4, 38.3, 36.1, 30.0, 25.5 ppm. **HRMS-ESI (*m/z*)**: [*M* + Na]$^+$ calcd for $C_{10}H_{13}N_7O_4$: 318.0921 found:318.0927. **IR**: $\tilde{\nu}$= 3223 (br), 3127 (br), 2935 (br), 1742 (vs), 1641 (s), 1579 (s), 1518 (m), 1455 (vs), 1351 (w), 1248 (m), 1170 (s), 945 (br), 735 (vs), 595 (br) cm^{-1}.

*3-(2-Chloroethyl)-N-(4-(hydroxyamino)-4-oxobutyl)-4-oxo-3,4-dihydroimidazo [5,1-d][1,2,3,5]tetrazine-8-carboxamide (**3e**)*

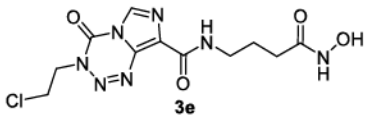

3e

Synthesized according to general procedure D using **HAIR B** (400 mg, 0.36 mmol, 1.00 equiv.), HATU (407 mg, 1.07 mmol, 3.00 equiv.), DIPEA (302 µL, 1.78 mmol, 5.00 equiv.) and **13** (260 mg, 1.07 mmol, 3.00 equiv.). Purification by preparative HPLC afforded **3e** as beige coloured solid (73.4 mg, 0.21 mmol, 59%). **HPLC**: t_R= 13.10 min. **1H-NMR** (400 MHz, DMSO-d6): δ= 10.40 (s, 1H), 8.90 (s, 1H), 8.61 (t, *J* = 6.1 Hz, 1H),4.64 (t, *J* = 6.1 Hz, 2H), 4.03 (t, *J* = 6.1 Hz, 2H), 3.29 (q, *J* = 6.7 Hz, 2H), 2.01 (t, *J* = 7.6 Hz, 2H), 1.76 (p, *J* = 7.2 Hz, 2H) ppm, -C-N*H*-OH signal could not be detected due to solvent exchange. **^{13}C-NMR** (101 MHz, DMSO-d6): δ= 168.8, 159.5, 139.1, 133.8, 131.2, 129.1, 49.9, 41.5, 38.3, 30.0, 25.5 ppm. **HRMS-ESI (*m/z*)**: [*M* + H]$^+$ calcd for $C_{11}H_{14}ClN_7O_4$: 344.0869, found 344.0864. **IR**: $\tilde{\nu}$= 3224 (br), 3129 (br), 2935 (br), 1743 (vs), 1642 (s), 1579 (m), 1455 (s), 1247 (m), 1157 (s), 1076 (m), 735 (vs) cm^{-1}.

*4-(4-(Bis(2-chloroethyl)amino)phenyl)-N-(4-(hydroxyamino)-4-oxobutyl)butanamide (**3f**)*

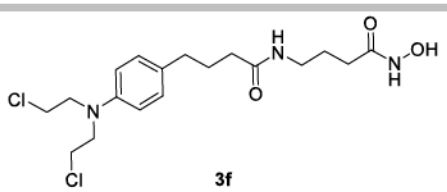

3f

Synthesized according to general procedure D using **HAIR B** (270 mg, 0.24 mmol, 1.00 equiv.), HATU (273 mg, 0.72 mmol, 3.00 equiv.), DIPEA (210 µL, 1.20 mmol, 5.00 equiv.) and chlorambucil (219 mg, 0.72 mmol, 3.00 equiv.). Purification by preparative HPLC afforded **3f** as beige coloured solid (59.5 mg, 0.15 mmol, 63%). **HPLC**: t_R= 17.38 min. **^{1}H-NMR** (300 MHz, DMSO-d_6): δ= 10.35 (s, 1H), 7.77 (t, *J* = 5.6 Hz, 1H), 7.01 (d, *J* = 8.6 Hz, 2H), 6.66 (d, *J* = 8.7 Hz, 2H), 3.69 (s, 8H), 3.01 (q, *J* = 6.9 Hz, 2H), 2.42 (t, *J* = 7.6 Hz, 2H), 2.04 (t, *J* = 7.5 Hz, 2H), 1.94 (dd, *J* = 8.3, 6.8 Hz, 2H), 1.72 (qd, *J* = 8.3, 6.6 Hz, 2H), 1.66 – 1.53 (m, 2H) ppm, -C-N*H*-OH signal could not be detected due to solvent exchange. **^{13}C-NMR** (75 MHz, DMSO-d_6): δ= 171.9, 168.8, 144.4, 130.0, 129.3, 111.9, 52.2, 41.2, 38.1, 34.9, 33.7, 29.9, 27.4, 25.4 ppm. **HRMS-ESI (*m/z*)**: [*M* - H]$^-$ calcd for $C_{18}H_{27}Cl_2N_3O_3$: 402.1357 found: 402.1356. **IR**: $\tilde{\nu}$= 3222 (br), 2935 (br), 1742 (vs), 1639 (vs), 1579 (s), 1518 (s), 1350 (w), 1248 (m), 1173 (s), 947 (m), 735 (vs), 596 (m) cm^{-1}.

*3-(2-Chloroethyl)-N-(6-(hydroxyamino)-6-oxohexyl)-4-oxo-3,4-dihydroimidazo[5,1-d][1,2,3,5]tetrazine-8-carboxamide (**3g**)*

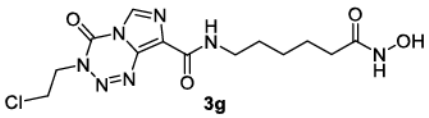

3g

Synthesized according to general procedure D using **HAIR C** (450 mg, 0.38 mmol, 1.00 equiv.), HATU (437 mg, 1.15 mmol, 3.00 equiv.), DIPEA (326 µL, 1.92 mmol, 5.00 equiv.) and **13** (279 mg, 1.15 mmol, 3.00 equiv.). Purification by preparative HPLC afforded **3g** as beige coloured solid (83.4 mg, 0.22 mmol, 58%). **HPLC**: t_R= 13.87 min. **^{1}H-NMR** (400 MHz, DMSO-d_6): δ= 10.32 (s, 1H), 8.89 (s, 1H), 8.51 (t, *J* = 6.0 Hz, 1H), 4.63 (t, *J* = 6.1 Hz, 2H), 4.03 (t, *J* = 6.1 Hz, 2H), 3.28 (q, *J* = 6.8 Hz, 2H), 1.94 (t, *J* = 7.4 Hz, 2H), 1.52 (h, *J* = 7.1 Hz, 4H), 1.27 (qd, *J* = 9.4, 8.9, 6.1 Hz, 2H) ppm, -C-N*H*-OH signal could not be detected due to solvent exchange. **^{13}C-NMR** (101 MHz, DMSO-d_6): δ= 169.0, 159.4, 139.1, 133.8, 131.3, 129.1, 49.9, 41.5, 38.5, 32.2, 28.9, 26.0, 24.9 ppm. **HRMS-ESI (*m/z*)**: [*M* + H]$^+$ calcd for $C_{13}H_{18}ClN_7O_4$: 372.1182, found: 372.1177. **IR**: $\tilde{\nu}$= 3334 (br), 3273 (br), 2941 (br), 2866 (br), 1753 (m), 1682 (m), 1629 (m), 1257 (m), 1452 (m), 1251 (s), 1200 (m), 733 (vs) cm^{-1}.

*6-(4-(4-(Bis(2-chloroethyl)amino)phenyl)butanamido)-N-hydroxyhexanamide (**3h**)*

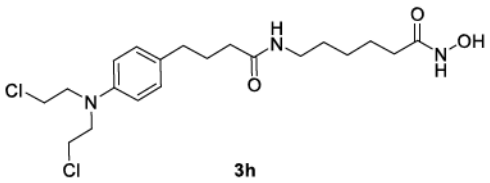

3h

Synthesized according to general procedure D using **HAIR C** (450 mg, 0.38 mmol, 1.00 equiv.), HATU (437 mg, 1.15 mmol, 3.00 equiv.), DIPEA (326 µL, 1.92 mmol, 5.00 equiv.) and chlorambucil (349 mg, 1.15 mmol, 3.00 equiv). Purification by preparative HPLC afforded **3h** as beige coloured solid (84.5 mg, 0.20 mmol, 51%). **HPLC**: t_R= 17.86 min. **^{1}H-NMR** (400 MHz, DMSO-d_6): δ= 10.32 (s, 1H), 7.72 (t, *J* = 5.6 Hz, 1H), 7.01 (d, *J* = 8.7 Hz, 2H), 6.66 (d, *J* = 8.7 Hz, 2H), 3.75 – 3.60 (m, 8H), 3.00 (td, *J* = 7.0, 5.6 Hz, 2H), 2.42 (t, *J* = 7.6 Hz, 2H), 2.04 (t, *J* = 7.5 Hz, 2H), 1.92 (t, *J* = 7.4 Hz, 2H), 1.78 – 1.65 (m, 2H), 1.47 (p, *J* = 7.5 Hz, 2H), 1.36 (p, *J* = 7.3 Hz, 2H), 1.28 – 1.14 (m, 2H) ppm, -C-N*H*-OH signal could not be detected due to solvent exchange. **^{13}C-NMR** (101 MHz, DMSO-d_6): δ= 171.7, 169.0, 144.4, 130.0, 129.3, 111.9, 52.2, 41.2, 38.3, 34.9, 33.7, 32.2, 28.9, 27.4, 26.0, 24.9 ppm. **HRMS-ESI (*m/z*)**: [*M* + H]$^+$ calcd for $C_{20}H_{31}Cl_2N_3O_3$: 432.1815, found 432.1816. **IR**: $\tilde{\nu}$= 3223 (br), 2934 (br), 1743 (vs), 1639 (vs), 1579 (s), 1518 (s), 1455 (vs), 1173 (s), 946 (m), 735 (vs) cm^{-1}.

*N-(7-(Hydroxyamino)-7-oxoheptyl)-3-methyl-4-oxo-3,4-dihydroimidazo[5,1-d][1,2,3,5]tetrazine-8-carboxamide (**3i**)*

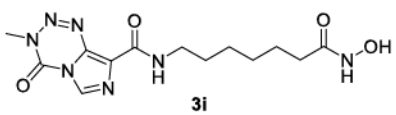

3i

Synthesized according to general procedure D using **HAIR D** (500 mg, 0.41 mmol, 1.00 equiv.), HATU (468 mg, 1.23 mmol, 3.00 equiv.), DIPEA (349 µL, 2.05 mmol, 5.00 equiv.) and **14** (242 mg, 1.23 mmol, 3.00 equiv.). Purification by preparative HPLC afforded **3i** as colorless powder (114 mg, 0.34 mmol, 83%). **HPLC**: t_R= 12.25 min. **^{1}H-NMR** (400 MHz, DMSO-d_6): δ= 10.32 (s, 1H), 8.82 (s, 1H), 8.46 (t, *J* = 6.0 Hz, 1H), 3.86 (s, 3H), 3.28 (q, *J* = 6.7 Hz, 2H), 1.93 (t, *J* = 7.3 Hz, 2H), 1.50 (dp, *J* = 14.5, 6.9 Hz, 4H), 1.27

(dq, *J* = 9.0, 5.2, 4.5 Hz, 4H) ppm, -C-N*H*-OH signal could not be detected due to solvent exchange. **^{13}C-NMR** (101 MHz, DMSO-d_6): δ= 169.1, 159.6, 139.2, 134.4, 130.6, 128.4, 38.5, 36.1, 32.2, 29.1, 28.4, 26.1, 25.1 ppm. **HRMS-ESI (*m/z*)**: [*M* + Na]$^+$ calcd for $C_{13}H_{19}N_7O_4$: 360.1391, found: 360.1401. **IR**: $\tilde{\nu}$= 3301 (br), 3195 (br), 2911 (br), 2847 (br), 1736 (vs), 1622 (m), 1580 (s), 1255 (m), 1044 (m), 948 (s) cm^{-1}.

*3-(2-Chloroethyl)-N-(7-(hydroxyamino)-7-oxoheptyl)-4-oxo-3,4-dihydroimidazo [5,1-d][1,2,3,5]tetrazine-8-carboxamide (**3j**)*

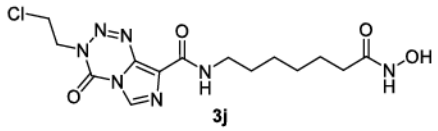

3j

Synthesized according to general procedure D using **HAIR D** (500 mg, 0.41 mmol, 1.00 equiv.), HATU (468 mg, 1.23 mmol, 3.00 equiv.), DIPEA (349 µL, 2.05 mmol, 5.00 equiv.) and **13** (300 mg, 1.23 mmol, 3.00 equiv.). Purification by preparative HPLC afforded **3j** as colorless powder (108 mg, 0.28 mmol, 68%). **HPLC**: t_R= 13.63 min. **^{1}H-NMR** (400 MHz, DMSO-d_6): δ= 10.32 (s, 1H), 8.88 (s, 1H), 8.50 (t, *J* = 6.0 Hz, 1H), 4.64 (t, *J* = 6.1 Hz, 2H), 4.03 (t, *J* = 6.1 Hz, 2H), 3.28 (q, *J* = 6.7 Hz, 2H), 1.93 (t, *J* = 7.4 Hz, 2H), 1.50 (m, *J* = 17.5, 7.1 Hz, 4H), 1.27 (m, *J* = 10.9, 9.3, 4.4 Hz, 4H) ppm, -C-N*H*-OH signal could not be detected due to solvent exchange. **^{13}C-NMR** (101 MHz, DMSO-d_6): δ= 169.1, 159.4, 139.1, 133.8, 131.3, 129.1, 49.9, 41.5, 38.5, 32.2, 29.1, 28.3, 26.1, 25.1 ppm. **HRMS-ESI (*m/z*)**: [*M* + Na]$^+$ calcd for $C_{14}H_{20}ClN_7O_4$: 408.1158, found: 408.1158. **IR:** $\tilde{\nu}$= 3251 (br), 2927 (br), 2854 (br), 1736 (vs), 1630 (vs), 1580 (s), 1519 (m), 1456 (s), 1318 (m), 1250 (m), 1088 (m), 926 (m), 737 (m), 643 (m) cm^{-1}.

*7-(4-(4-(Bis(2-chloroethyl)amino)phenyl)butanamido)-N-hydroxyheptanamide (**3k**)*

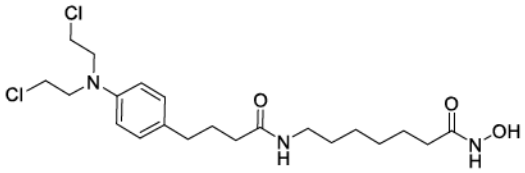

3k

Synthesized according to general procedure D using **HAIR D** (500 mg, 0.41 mmol, 1.00 equiv.), HATU (468 mg, 1.23 mmol, 3.00 equiv.), DIPEA (349 µL, 2.05 mmol, 5.00 equiv.) and chlorambucil (374 mg, 1.23 mmol, 3.00 equiv.). Purification by preparative HPLC afforded **3k** as colorless powder (93.0 mg, 0.21 mmol, 51%). **HPLC**: t_R= 17.53 min. **^{1}H-NMR** (300 MHz, DMSO-d_6): δ= 10.31 (s, 1H), 7.71 (t, *J* = 5.6 Hz, 1H), 7.01 (d, *J* = 8.6 Hz, 2H), 6.66 (d, *J* = 8.7 Hz, 2H), 3.69 (s, 8H), 3.10 – 2.90 (m, 2H), 2.42 (t, *J* = 7.5 Hz, 2H), 2.04 (t, *J* = 7.4 Hz, 2H), 1.92 (t, *J* = 7.3 Hz, 2H), 1.80 – 1.65 (m, 2H), 1.48 (q, *J* = 7.2 Hz, 2H), 1.35 (q, *J* = 6.8 Hz, 2H), 1.22 (p, *J* = 3.5 Hz, 4H) ppm, -C-N*H*-OH signal could not be detected due to solvent exchange. **^{13}C-NMR** (101 MHz, DMSO-d_6): δ= 171.7, 169.1, 144.4, 130.0, 129.3, 111.9, 52.2, 41.2, 38.3, 34.9, 33.6, 32.2, 29.1, 28.3, 27.4, 26.2, 25.1 ppm. **HRMS-ESI (*m/z*)**: [*M* + H]$^+$ calcd for $C_{21}H_{33}Cl_2N_3O_3$: 446.1972, found: 446.1971. **IR**: $\tilde{\nu}$= 3262 (br), 2928 (br), 2852 (br), 1614 (s), 1564 (s), 1517 (vs), 1354 (m), 1178 (m), 804 (m), 740 (s) cm^{-1}.

*(E)-N-(4-(3-(Hydroxyamino)-3-oxoprop-1-en-1-yl)benzyl)-3-methyl-4-oxo-3,4-dihydro-imidazo[5,1-d][1,2,3,5]tetrazine-8-carboxamide (**3l**)*

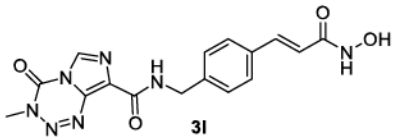

3l

Synthesized according to general procedure D using **HAIR E** (500 mg, 0.41 mmol, 1.00 equiv.), HATU (468 mg, 1.23 mmol, 3.00 equiv.), DIPEA (349 µL, 2.05 mmol, 5.00 equiv.) and **14** (242 mg, 1.23 mmol, 3.00 equiv.). Purification by preparative HPLC afforded **3l** as white coloured powder (63.0 mg, 0.17 mmol, 41%). **HPLC**: t_R= 13.05 min. **^{1}H-NMR** (300 MHz, DMSO-d_6): δ= 10.72 (s, 1H), 9.09 (t, *J* = 6.3 Hz, 1H), 8.86 (s, 1H), 7.52 (d, *J* = 8.1 Hz, 2H), 7.42 (d, *J* = 15.9 Hz, 1H), 7.37 (d, *J* = 8.2 Hz, 2H), 6.43 (d, *J* = 15.8 Hz, 1H), 4.51 (d, *J* = 6.3 Hz, 2H), 3.87 (s, 3H) ppm, -C-N*H*-OH signal could not be detected due to solvent exchange. **^{13}C-NMR** (75 MHz, DMSO-d_6): δ= 162.8, 159.8, 141.1, 139.2, 138.1, 134.6, 133.4, 130.3, 128.5, 127.9, 127.5, 118.6, 41.9, 36.2 ppm. **HRMS-ESI (*m/z*)**: [*M* + H]$^+$ calcd for $C_{16}H_{15}N_7O_4$: 392.1078, found: 392.1060. **IR**: $\tilde{\nu}$= 3209 (br), 3028 (br), 2854 (br), 1745 (vs), 1651 (s), 1582 (m), 1454 (m), 1250 (m), 1054 (m), 943 (m), 734 (s), 568 (m), 509 (s) cm^{-1}.

*(E)-3-(2-Chloroethyl)-N-(4-(3-(hydroxyamino)-3-oxoprop-1-en-1-yl)benzyl)-4-oxo-3,4-dihydroimidazo[5,1-d][1,2,3,5]tetrazine-8-carboxamide (**3m**)*

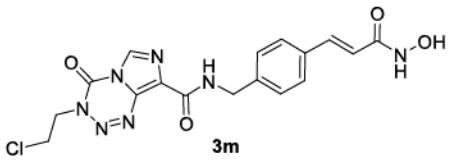

3m

Synthesized according to general procedure D using **HAIR E** (600 mg, 0.41 mmol, 1.00 equiv.), HATU (470 mg, 1.24 mmol, 3.00 equiv.), DIPEA (350 µL, 2.06 mmol, 5.00 equiv.) and **13** (301 mg, 1.24 mmol, 3.00 equiv.). Purification by preparative HPLC afforded **3m** as white coloured powder (94.1 mg, 0.23 mmol, 56%). **HPLC**: t_R= 14.38 min. **^{1}H-NMR** (400 MHz, DMSO-d_6): δ= 10.73 (s, 1H), 9.14 (t, *J* = 6.3 Hz, 1H), 8.92 (s, 1H), 7.52 (d, *J* = 8.0 Hz, 2H), 7.43 (d, *J* = 15.8 Hz, 1H), 7.37 (d, *J* = 8.3 Hz, 2H), 6.43 (d, *J* = 15.8 Hz, 1H), 4.64 (t, *J* = 6.1 Hz, 2H), 4.52 (d, *J* = 6.3 Hz, 2H), 4.03 (t, *J* = 6.1 Hz, 2H) ppm, -C-N*H*-OH signal could not be detected due to solvent exchange. **^{13}C-NMR** (101 MHz, DMSO-d_6): δ= 162.7, 159.7, 141.0, 139.1, 138.1, 134.0, 133.4, 130.9, 129.3, 127.8, 127.5, 118.6, 50.0, 41.9, 41.5 ppm. **HRMS-ESI (*m/z*)**: [*M* + H]$^+$ calcd for $C_{17}H_{16}ClN_7O_4$: 418.1025, found: 418.1025. **IR**: $\tilde{\nu}$= 3387 (br), 3226 (br), 3032 (br), 1738 (vs), 1657 (vs), 1622 (m), 1582 (m), 1519 (m), 1251 (m), 1056 (m), 780 (m), 733 (s), 612 (m), 496 (m) cm^{-1}.

*(E)-4-(4-(Bis(2-chloroethyl)amino)phenyl)-N-(4-(3-(hydroxyamino)-3-oxoprop-1-en-1-yl)benzyl)butanamide (**3n**)*

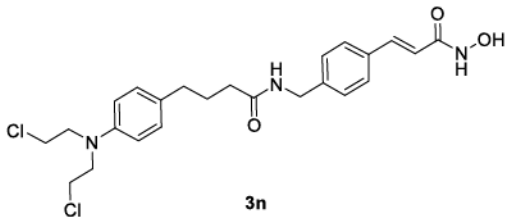

3n

Synthesized according to general procedure D using **HAIR E** (500 mg, 0.40 mmol, 1.00 equiv.), HATU (456 mg, 1.20 mmol, 3.00 equiv.), DIPEA (340 µL, 2.00 mmol, 5.00 equiv.) and chlorambucil (365 mg, 1.20 mmol, 3.00 equiv.). Purification by preparative HPLC afforded **3n** as white coloured powder (48.5 mg, 0.10 mmol, 25%). **HPLC**: t_R= 18.00 min. **^{1}H-NMR** (400 MHz, DMSO-d_6): δ= 10.73 (s, 1H), 8.32 (t, *J* = 5.9 Hz, 1H), 7.50 (d, *J* = 7.9 Hz, 2H), 7.42 (d, *J* = 15.8 Hz, 1H), 7.27 (d, *J* = 8.0 Hz, 2H), 7.02 (d, *J* = 8.6 Hz, 2H), 6.66 (d, *J* = 8.7 Hz, 2H), 6.43 (d, *J* = 15.8 Hz, 1H), 4.27 (d, *J* = 5.9 Hz, 2H), 3.69 (d, *J* = 3.2 Hz, 8H), 2.45 (t, *J* = 7.6 Hz, 2H), 2.14 (t, *J* = 7.5 Hz, 2H), 1.87 – 1.68 (m, 2H) ppm, -C-N*H*-OH signal could not be detected due to solvent exchange.**^{13}C-NMR** (101 MHz, DMSO-d_6): δ= 172.0, 162.7, 144.4, 141.3, 138.0, 133.3, 129.9, 129.3, 127.7, 127.4, 118.6, 111.9, 52.2, 41.8, 41.1, 34.9, 33.6, 27.4 ppm. **HRMS-ESI (*m/z*)**: [*M* + H]$^+$ calcd for $C_{24}H_{29}Cl_2N_3O_3$: 478.1659, found: 478.1654. **IR**: $\tilde{\nu}$= 3227 (br), 3030 (br), 2856 (br), 1745 (w), 1641 (m), 1614 (m), 1517 (s), 1349 (m), 802 (m), 736 (m) cm^{-1}.

*(E)-N-(4-(3-(Hydroxyamino)-3-oxoprop-1-en-1-yl)benzyl)-4-phenylbutanamide (**3o**)*

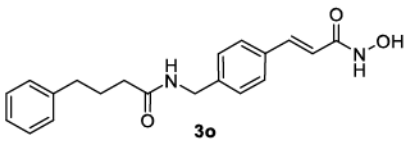

3o

Synthesized according to general procedure D with different equivalents for the reagents using **HAIR E** (170 mg, 0.14 mmol, 1.00 equiv.), HATU (186 mg, 0.49 mmol, 3.50 equiv.), DIPEA (122 µL, 0.70 mmol, 5.00 equiv.) and 4-phenylbutanoic acid (80.0 mg, 0.49 mmol, 3.50 equiv.). Purification by preparative HPLC afforded **3o** as white coloured powder (17.6 mg, 0.05 mmol, 37%). **HPLC**: t_R= 15.72 min, **^{1}H-NMR** (400 MHz, DMSO-d_6): δ= 10.72 (s, 1H), 9.00 (s, 1H, broad signal), 8.34 (t, *J* = 5.9 Hz, 1H), 7.50 (d, *J* = 8.0 Hz, 2H), 7.42 (d, *J* = 15.8 Hz, 1H), 7.32 – 7.23 (m, 4H), 7.22 – 7.13 (m, 3H), 6.42 (d, *J* = 15.8 Hz, 1H), 4.27 (d, *J* = 6.0 Hz, 1H), 2.59 – 2.53 (m, 2H), 2.16 (t, *J* = 7.5 Hz, 2H), 1.89 – 1.73 (m, 2H) ppm. **^{13}C-NMR** (101 MHz, DMSO-d_6): δ= 171.9, 162.8, 141.7, 141.3, 138.1, 133.3, 128.3, 128.3, 127.7, 127.4, 125.7, 118.6, 41.8, 34.8, 34.7, 27.1 ppm. **HRMS-ESI (*m/z*)**: [*M* + H]$^+$ calcd for $C_{20}H_{22}N_2O_3$: 339.1703, found: 339.1705. **IR**: $\tilde{\nu}$= 3288 (br), 2924 (br), 1641 (vs), 1556 (s), 1418 (w), 1350 (w), 1069 (m), 973 (m), 741 (s), 697 (vs), 590 (br), 521 (m), 488 (m) cm^{-1}.

*4-(2-(2-(2-(2-((2-(2,6-Dioxopiperidin-3-yl)-1,3-dioxoisoindolin-4-yl)oxy)acetamido)ethoxy)ethoxy)acetamido)-N-(7-(hydroxyamino)-7-oxoheptyl)benzamide (**4**)*

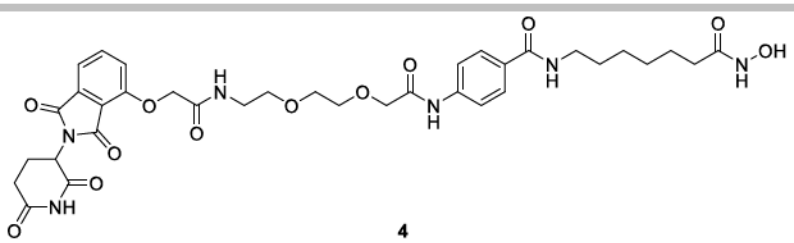

4

After swelling **HAIR E** (156 mg, 0.15 mmol, 1.00 eq) in DMF for 30 min, Fmoc deprotection was performed by treatment with deprotection solution (20% piperidine in DMF, 2 x 15 min). Afterwards the resin was washed with DMF (3 x 5 mL), CH_2Cl_2 (3 x 5 mL) and DMF (3 x 5 mL). For the subsequent amide coupling reaction a solution of 4-(Fmoc-amino)benzoic acid **8d** (162 mg, 0.45 mmol, 3.00 equiv.), HATU (171 mg, 0.45 mmol, 3.00 equiv.), and DIPEA (105 µL, 0.60 mmol, 4.00 equiv.) in DMF (0.5 mL) was agitated for 5 min and then added to the resin. The amide coupling was performed for 16 h at room temperature. Afterwards the resin was washed with DMF (3 x 5 mL), CH_2Cl_2 (3 x 5 mL) and DMF (3 x 5 mL). Completion of the reaction was monitored via TNBS-test. Coupling of the PEG-linker was performed starting with Fmoc deprotection, subsequent washing and coupling using Fmoc-O2Oc-OH (173 mg, 0.45 mmol, 3.00 equiv., supplied by Iris Biotech), HATU (171 mg, 0.45 mmol, 3.00 equiv.), and DIPEA (105 µL, 0.60 mmol, 4.00 equiv.) in DMF (0.5 mL) for 4 h at room temperature. After washing with DMF (3 x 5 mL), CH_2Cl_2 (3 x 5 mL) and DMF (3 x 5 mL) the coupling cycle was repeated using 2-((2-(2,6-dioxopiperidin-3-yl)-1,3-dioxoisoindolin-4-yl)oxy)acetic acid **7** (99.7 mg, 0.30 mmol, 2.00 equiv), HATU (125 mg, 0.33 mmol, 2.20 equiv.), DIPEA (92 µL, 0.53 mmol, 3.50 equiv.) in DMF (500 µL). Amide coupling was performed for 4 h at room temperature. Afterwards the resin was washed with DMF (3 x 5 mL) and CH_2Cl_2 (3 x 5 mL). The resin was dried *in vacuo* followed by the cleavage of the crude products from the resin by treatment with cleavage solution (5% TFA in CH_2Cl_2, 1 mL/40 mg resin) for 1 h at room temperature. The filtrates were concentrated *in vacuo* and the crude product **4** was purified by preparative HPLC. Lyophilization of the respective fractions yielded the desired product **4** (63.5 mg, 86.0 µmol, 57%) in >95% purity. **HPLC**: t_R= 13.65 min. **^{1}H-NMR** (400 MHz, DMSO-d_6): δ= 11.11 (s, 1H), 10.32 (s, 1H), 9.79 (s, 1H), 8.29 (t, *J* = 5.6 Hz, 1H), 8.00 (t, *J* = 5.7 Hz, 1H), 7.89 – 7.73 (m, 3H), 7.68 (d, *J* = 8.8 Hz, 2H), 7.48 (d, *J* = 7.2 Hz, 1H), 7.38 (d, *J* = 8.6 Hz, 1H), 5.10 (dd, *J* = 12.9, 5.4 Hz, 1H), 4.77 (s, 2H), 4.10 (s, 2H)*, 3.73 – 3.65 (m, 2H), 3.66 – 3.59 (m, 2H), 3.52 (t, *J* = 5.6 Hz, 2H), 3.35 (q, *J* = 5.6 Hz, 2H), 3.21 (q, *J* = 6.7 Hz, 2H), 2.95 – 2.83 (m, 1H), 2.69 – 2.52 (m, 2H), 2.10 – 1.98 (m, 1H), 1.94 (t, *J* = 7.3 Hz, 2H), 1.49 (p, *J* = 6.6, 6.1 Hz, 4H), 1.27 (tq, *J* = 8.2, 4.7, 3.3 Hz, 4H) ppm, -N*H* signal could not be detected due to solvent exchange. **^{13}C-NMR** (101 MHz, DMSO-d_6): δ= 172.7, 169.9, 169.1, 168.6, 166.9, 166.7, 165.5, 165.5, 154.9, 140.7, 136.9, 133.0, 129.5, 127.9, 120.3, 118.7, 116.8, 116.0, 70.3, 70.2, 69.4, 68.9, 67.5, 48.8, 39.1*, 38.3, 32.2, 31.0, 29.1, 28.4, 26.2, 25.1, 22.0 ppm, *overlapping with DMSO signal, confirmed by HSQC. **HRMS-ESI (*m/z*)**: [*M* + H]$^+$ calcd for $C_{35}H_{42}N_6O_{12}$: 739.2933, found: 739.2936. **IR**: $\tilde{\nu}$= 3333 (br), 2930 (br), 1707 (s), 1527 (m), 1394 (m), 1262 (m), 1196 (m), 1116 (m), 747 (m), 602 (m), 466 (m) cm^{-1}.

*N-(6-(Hydroxyamino)-6-oxohexyl)-3-methyl-4-oxo-3,4-dihydroimidazo[5,1-d][1,2,3,5]tetrazine-8-carboxamide (**3p**)*

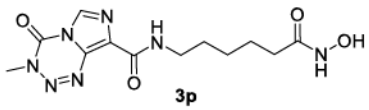

3p

Synthesized according to general procedure D using **HAIR C** (450 mg, 0.38 mmol, 1.00 equiv.), HATU (437 mg, 1.15 mmol, 3.00 equiv.), DIPEA (326 µL, 1.92 mmol, 5.00 equiv.) and **14** (226 mg, 1.15 mmol, 3.00 equiv). This compound turned out to be unstable, already during lyophillization and thus could not be characterized and was excluded from the biological evaluation.

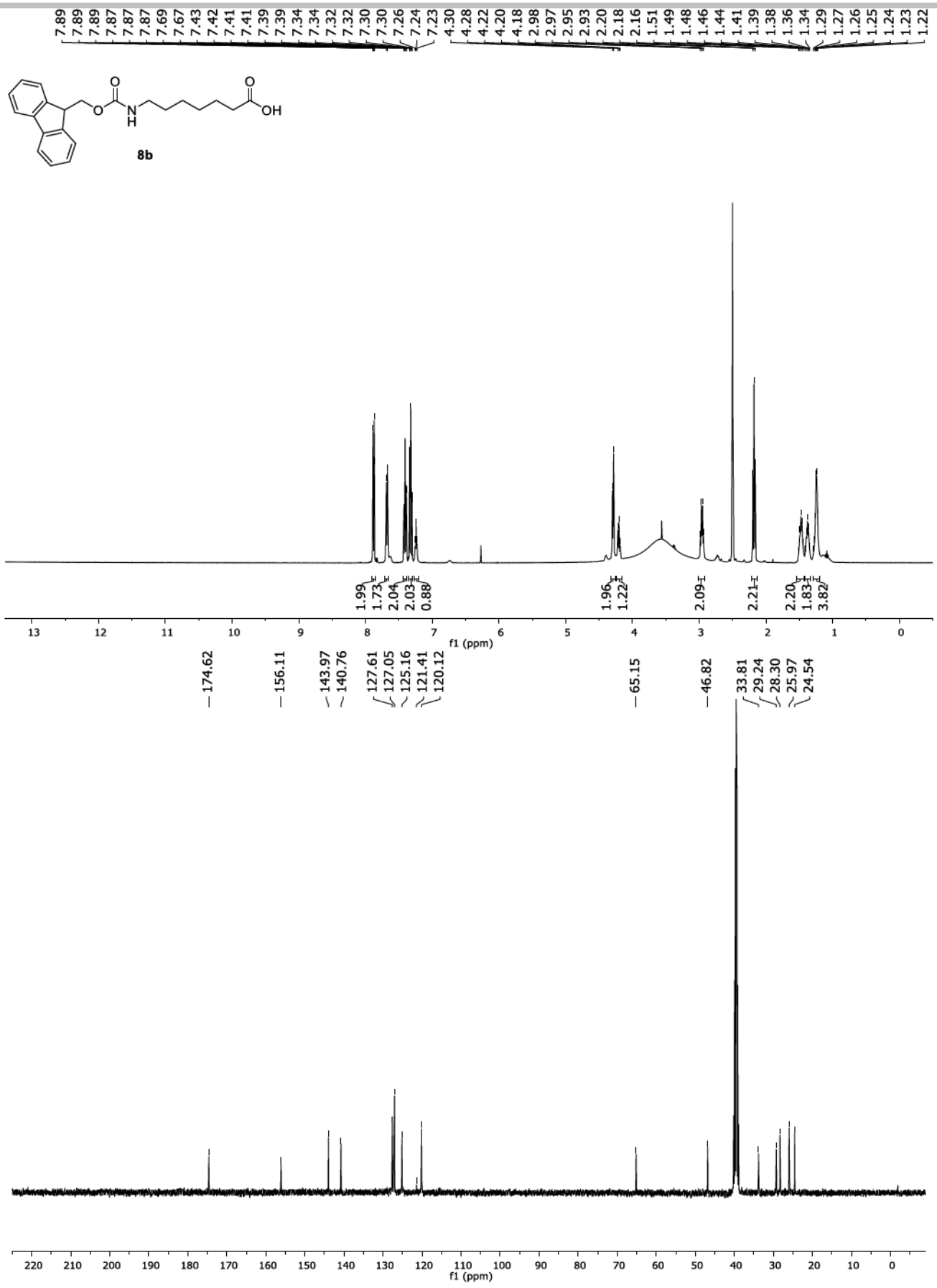

Figure S2: ^{1}H and ^{13}C-NMR spectra of **8b** in DMSO-d_6.

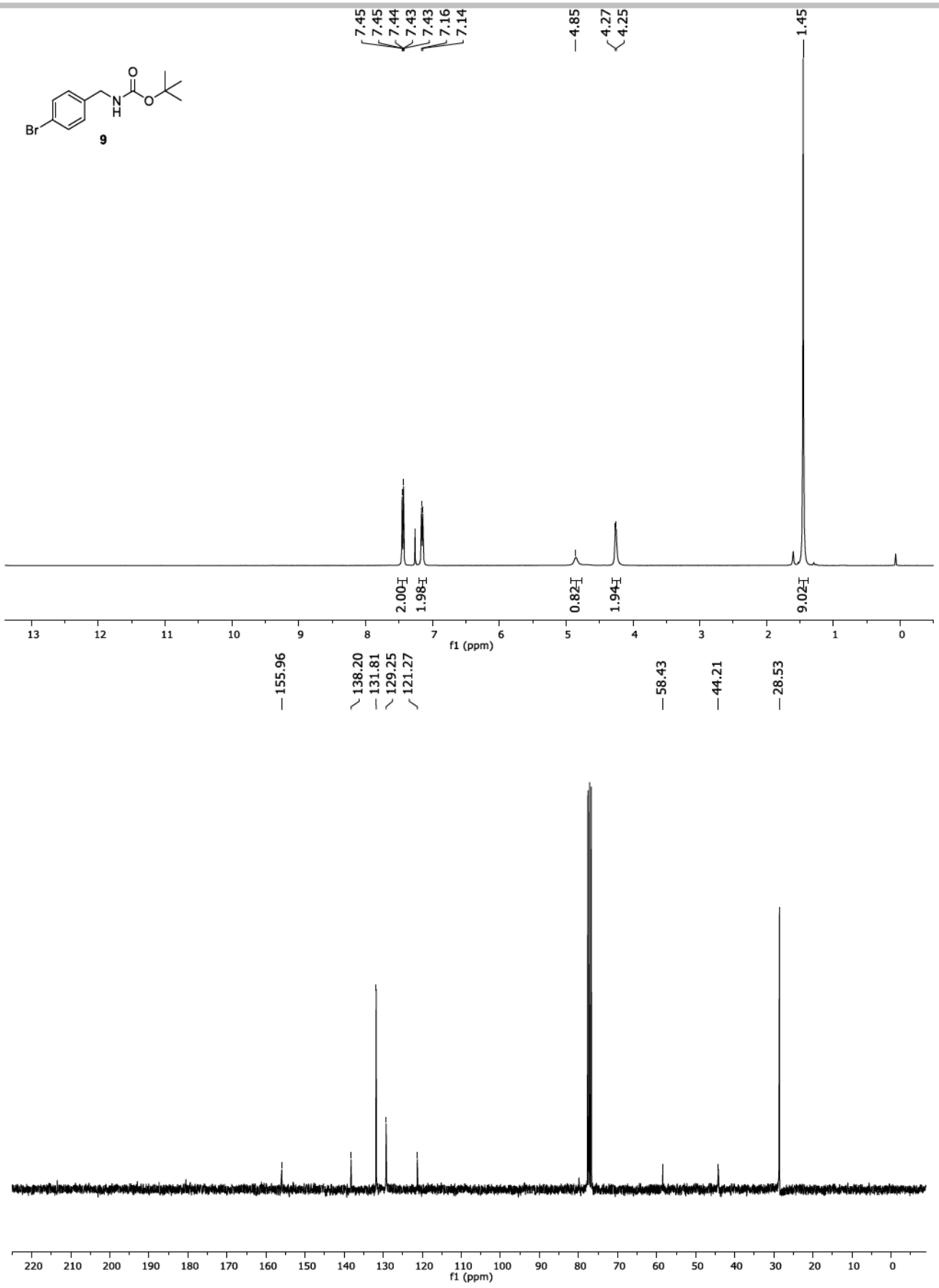

Figure S3: ^{1}H and ^{13}C-NMR spectra of **9** in DMSO-d_6.

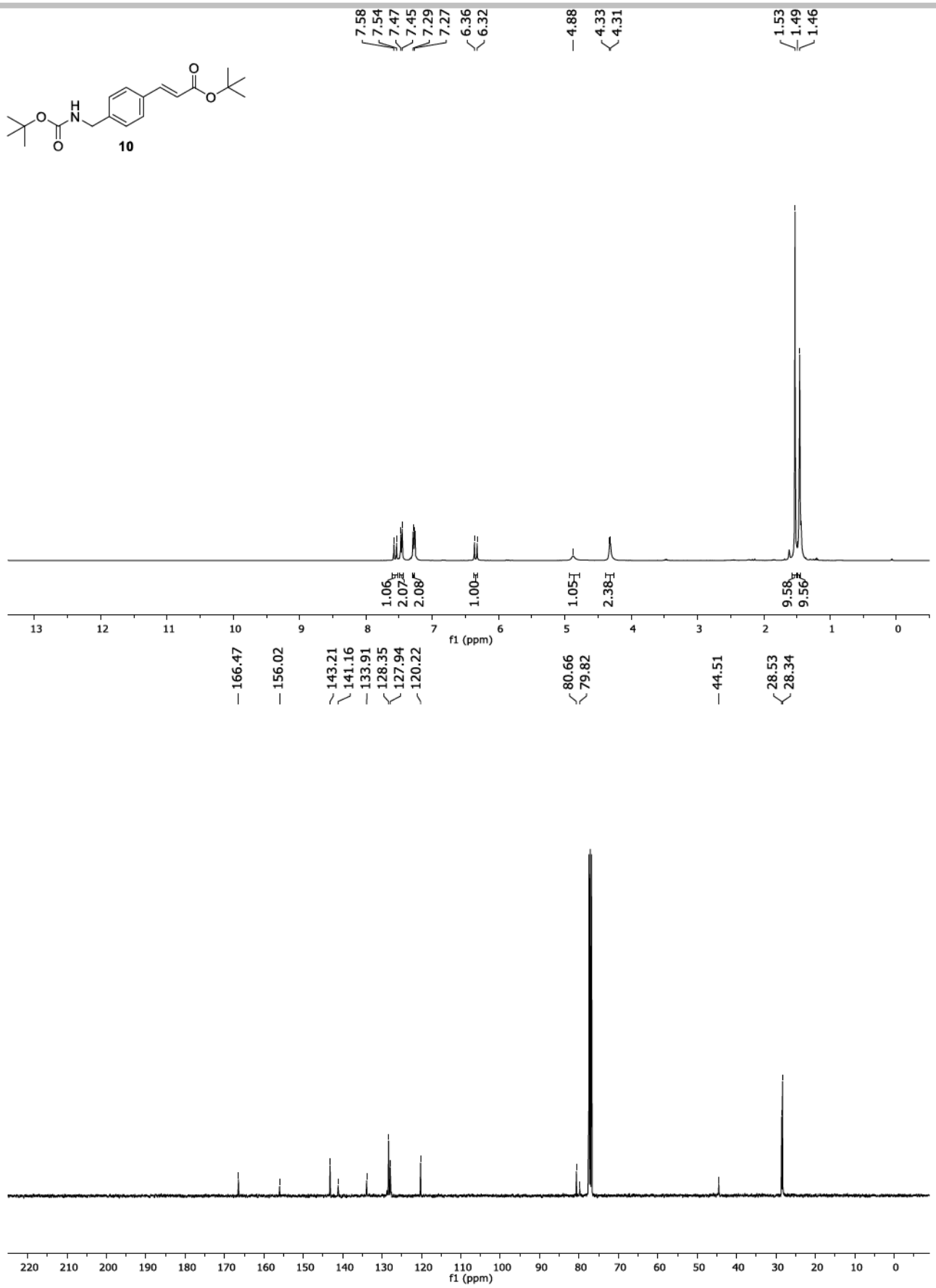

Figure S4: ^{1}H and ^{13}C-NMR spectra of **10** in $CDCl_3$.

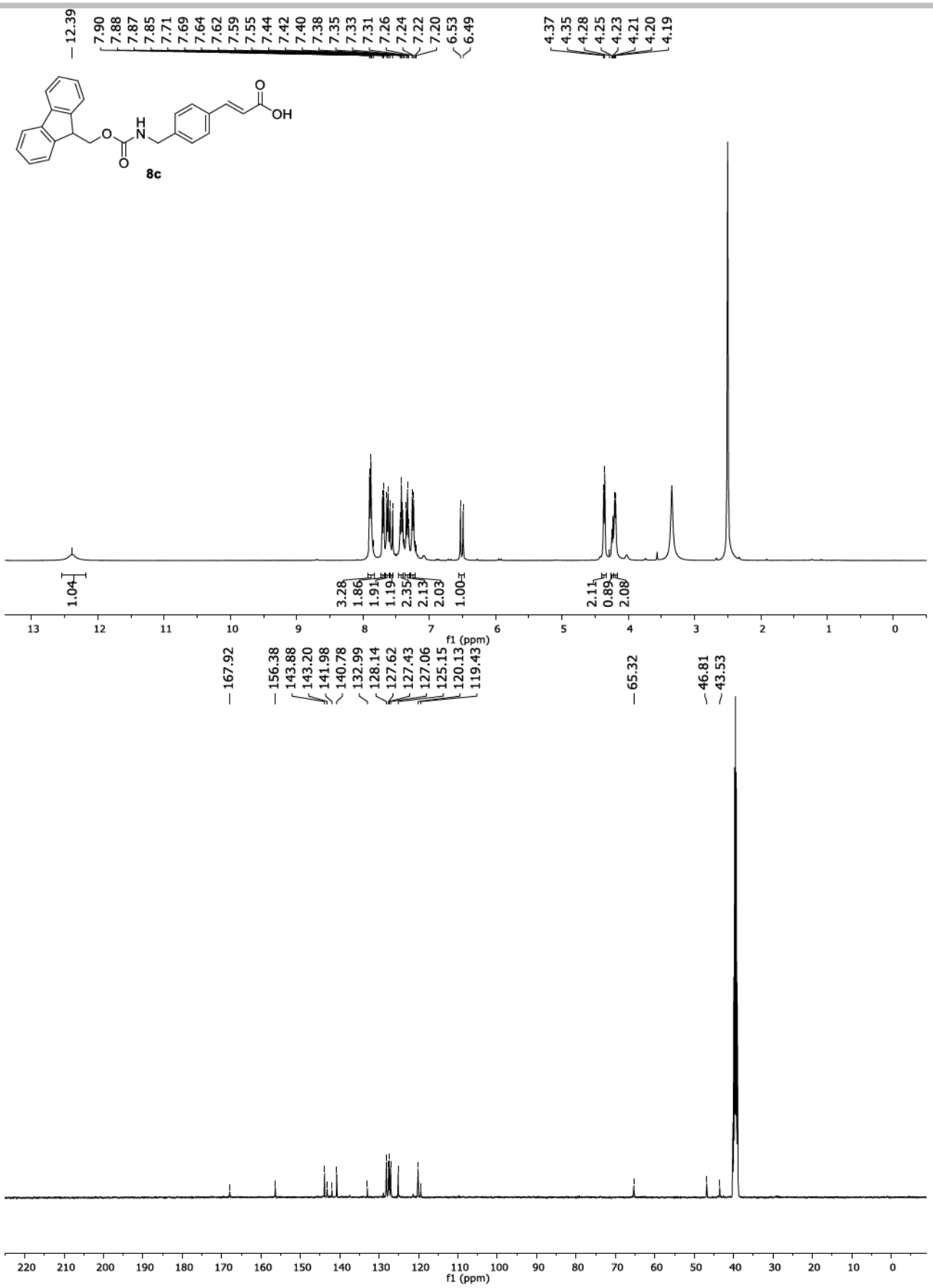

Figure S5: ^{1}H and ^{13}C-NMR spectra of **8c** in DMSO-d_6.

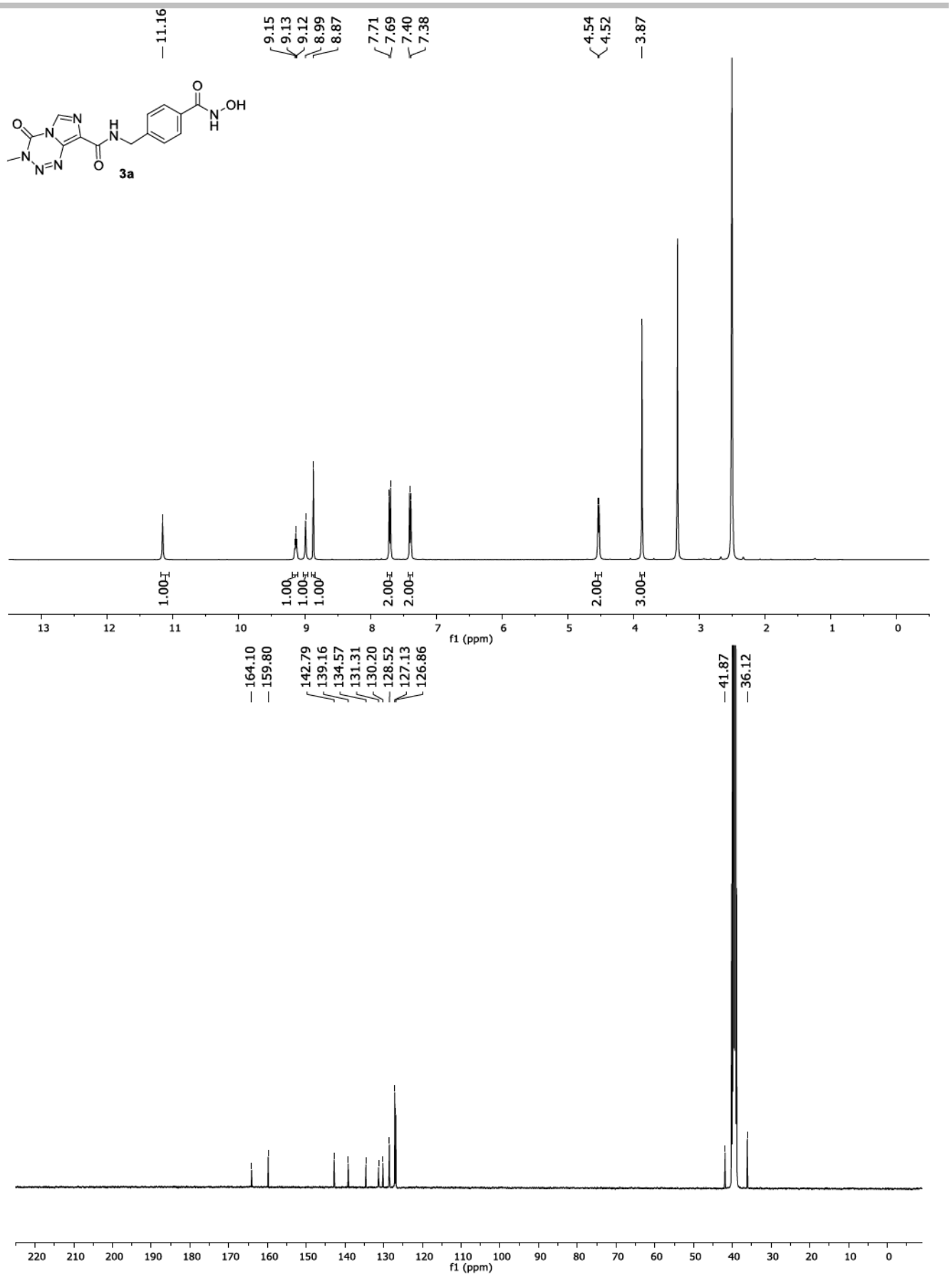

Figure S6: ^{1}H and ^{13}C-NMR spectra of **3a** in DMSO-d_6.

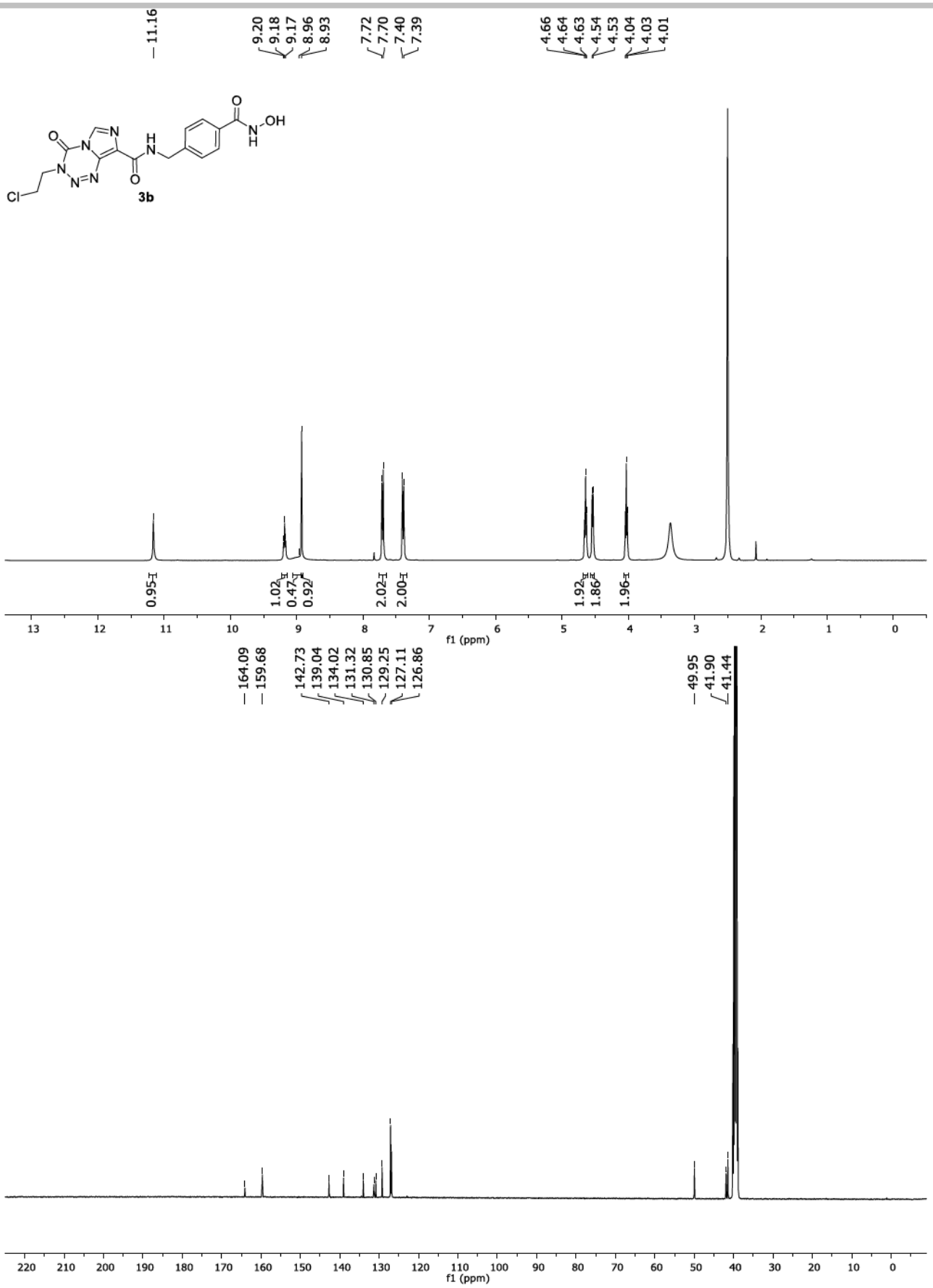

Figure S7: ^{1}H and ^{13}C-NMR spectra of **3b** in DMSO-d_6.

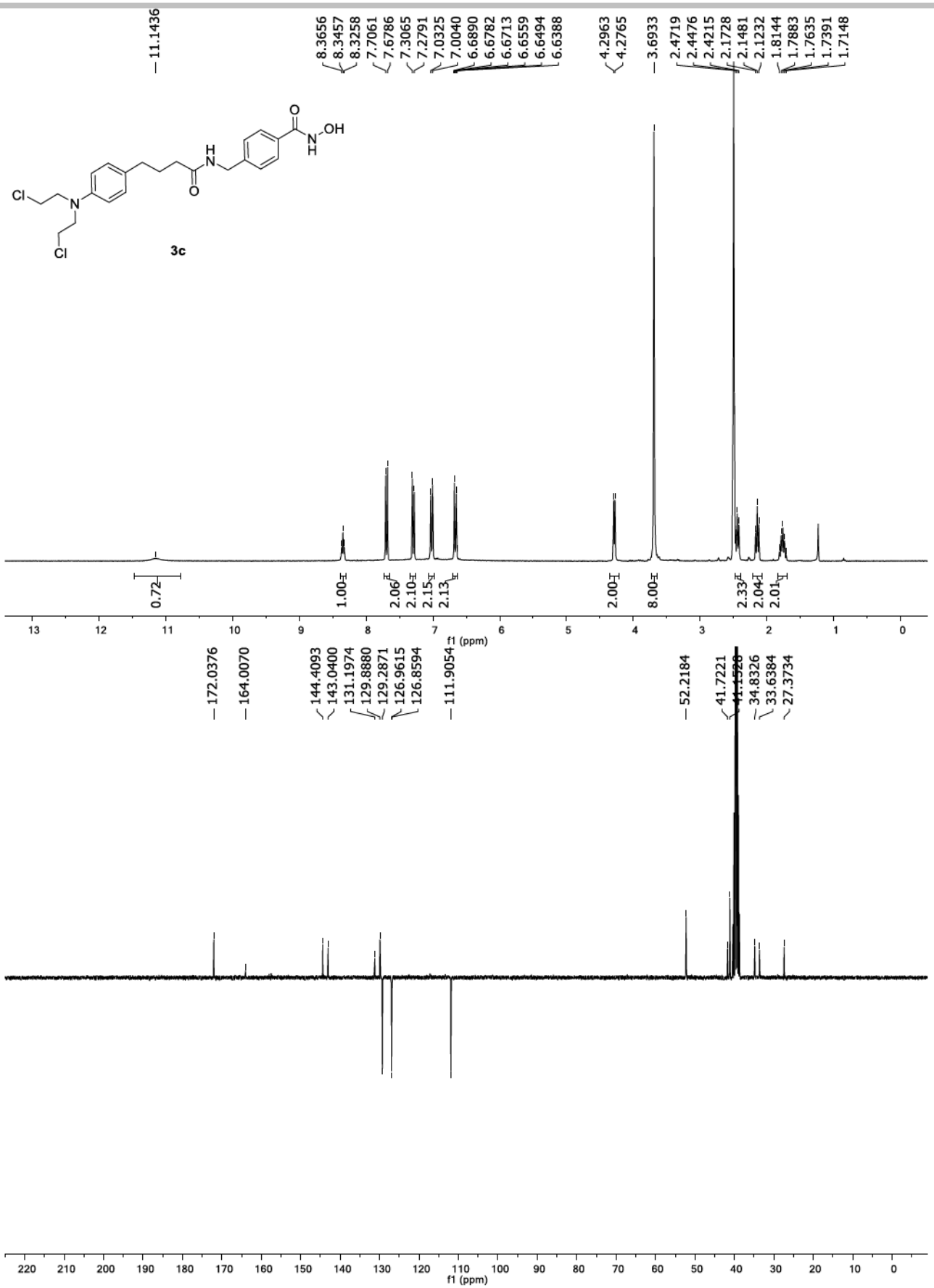

3c

Figure S8: ^{1}H and APT spectra of **3c** in DMSO-d_6.

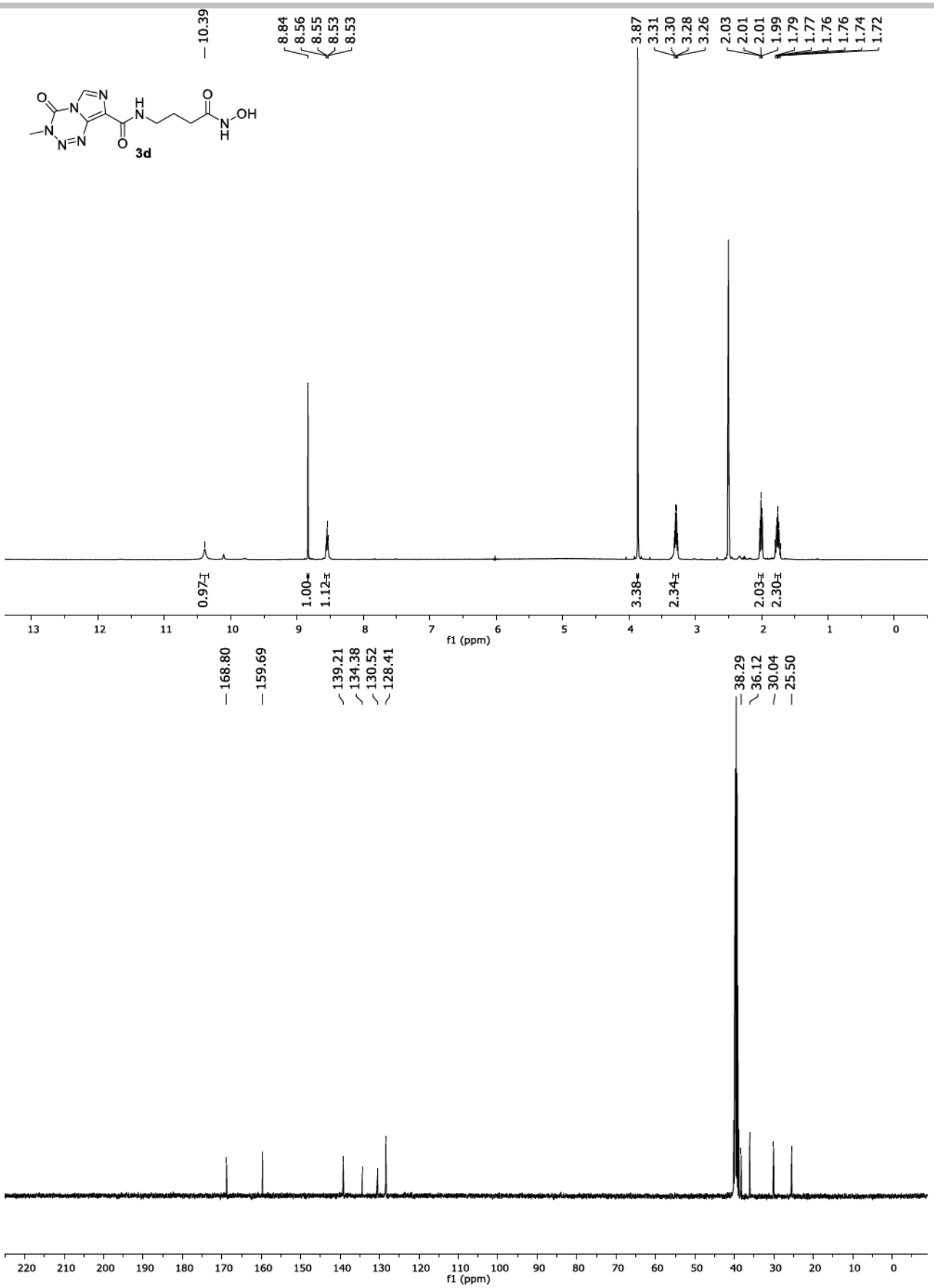

Figure S9: ^{1}H and ^{13}C-NMR spectra of **3d** in DMSO-d_6.

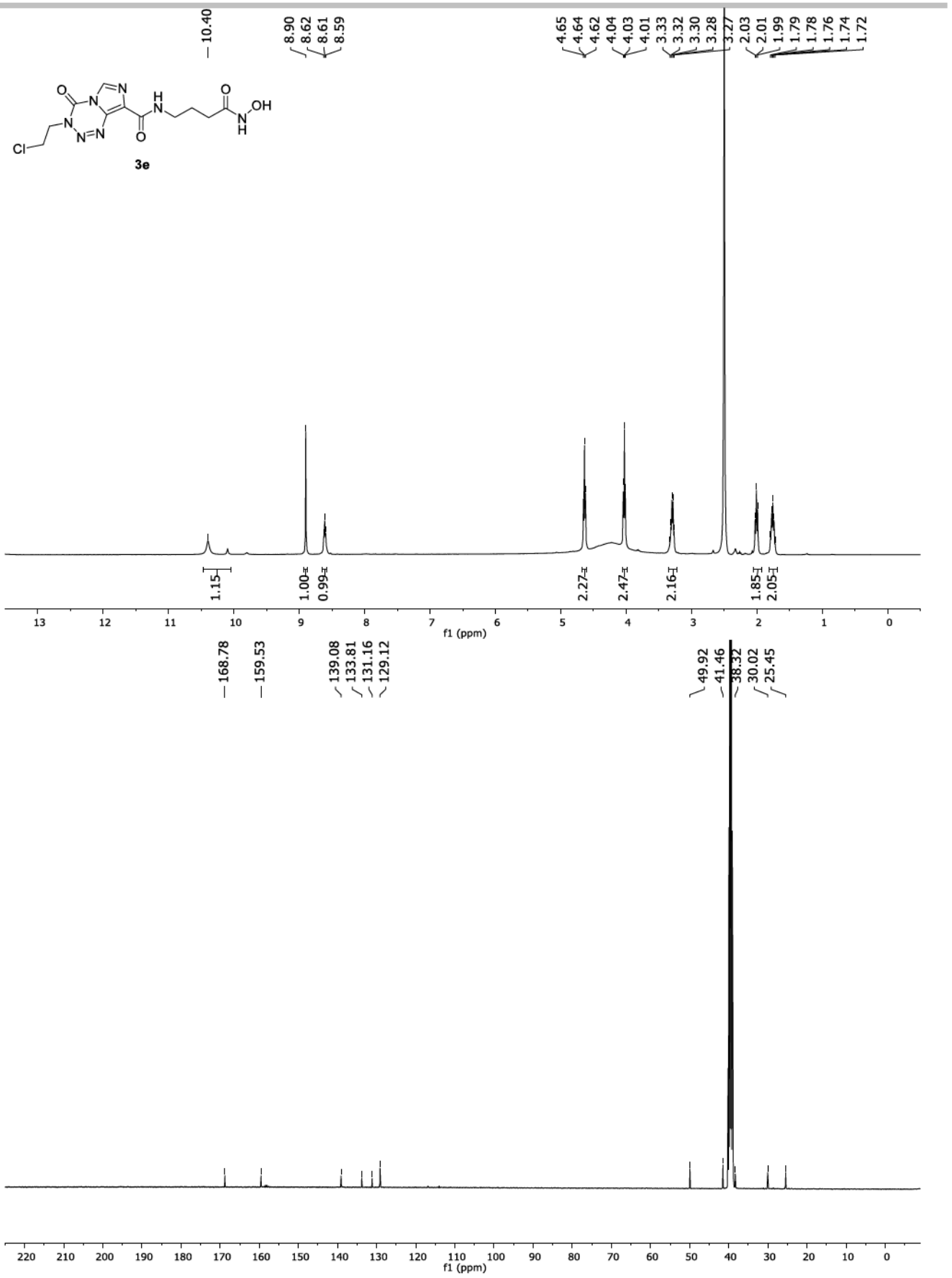

Figure S10: ^{1}H and ^{13}C-NMR spectra of **3e** in DMSO-d_6.

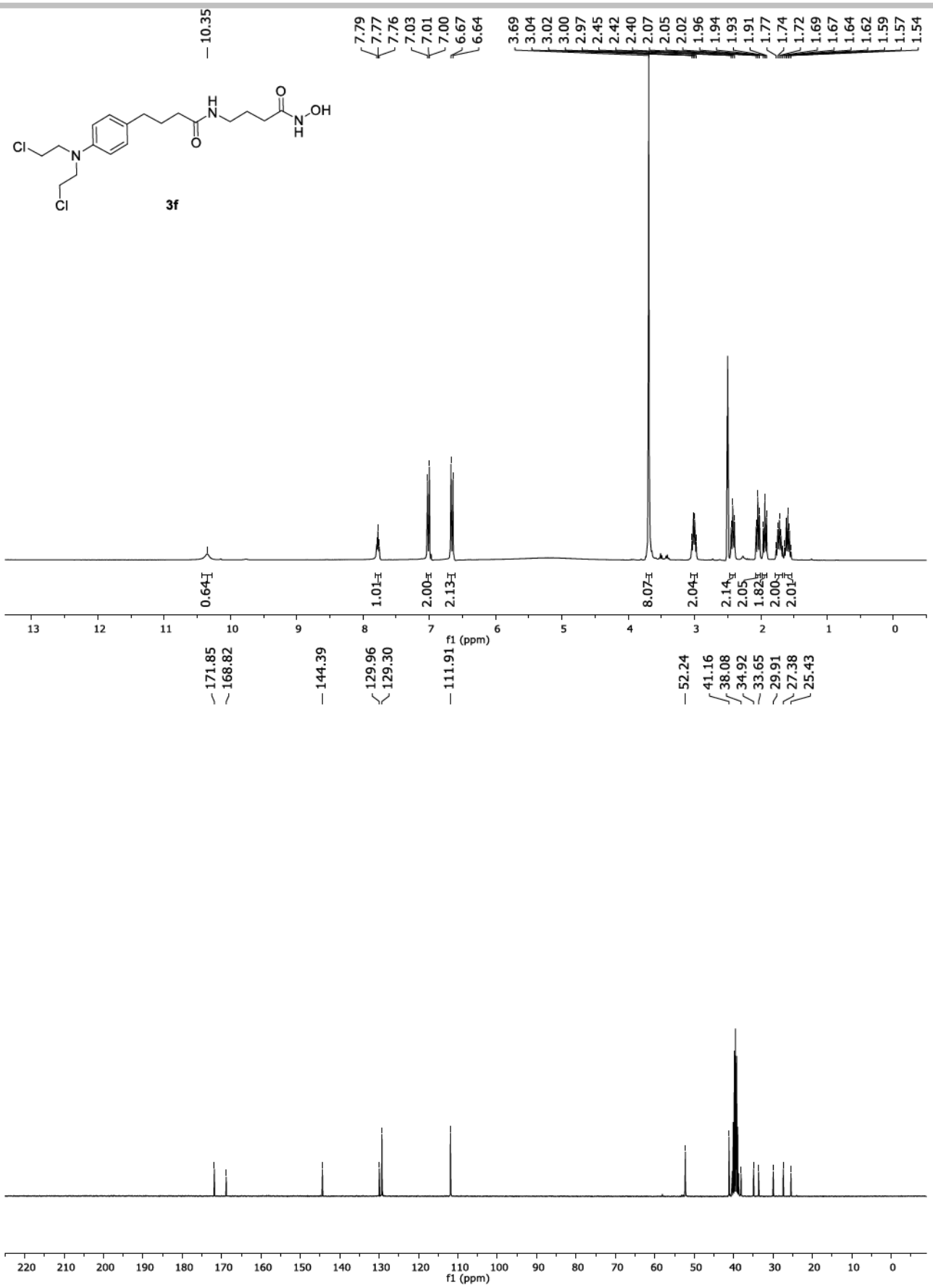

Figure S11: ^{1}H and ^{13}C-NMR spectra of **3f** in DMSO-d_6.

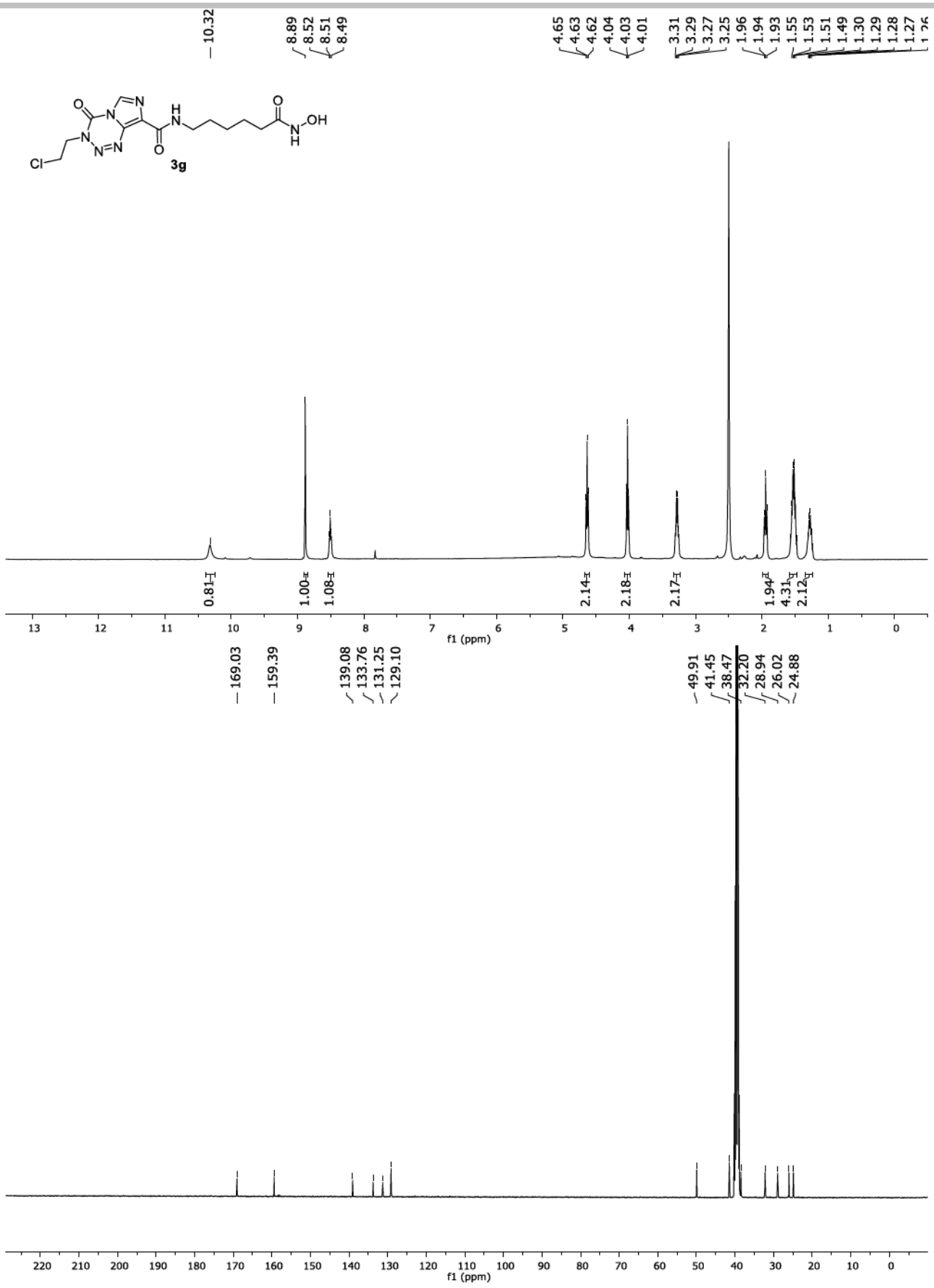

Figure S12: ^{1}H and ^{13}C-NMR spectra of **3g** in DMSO-d_6.

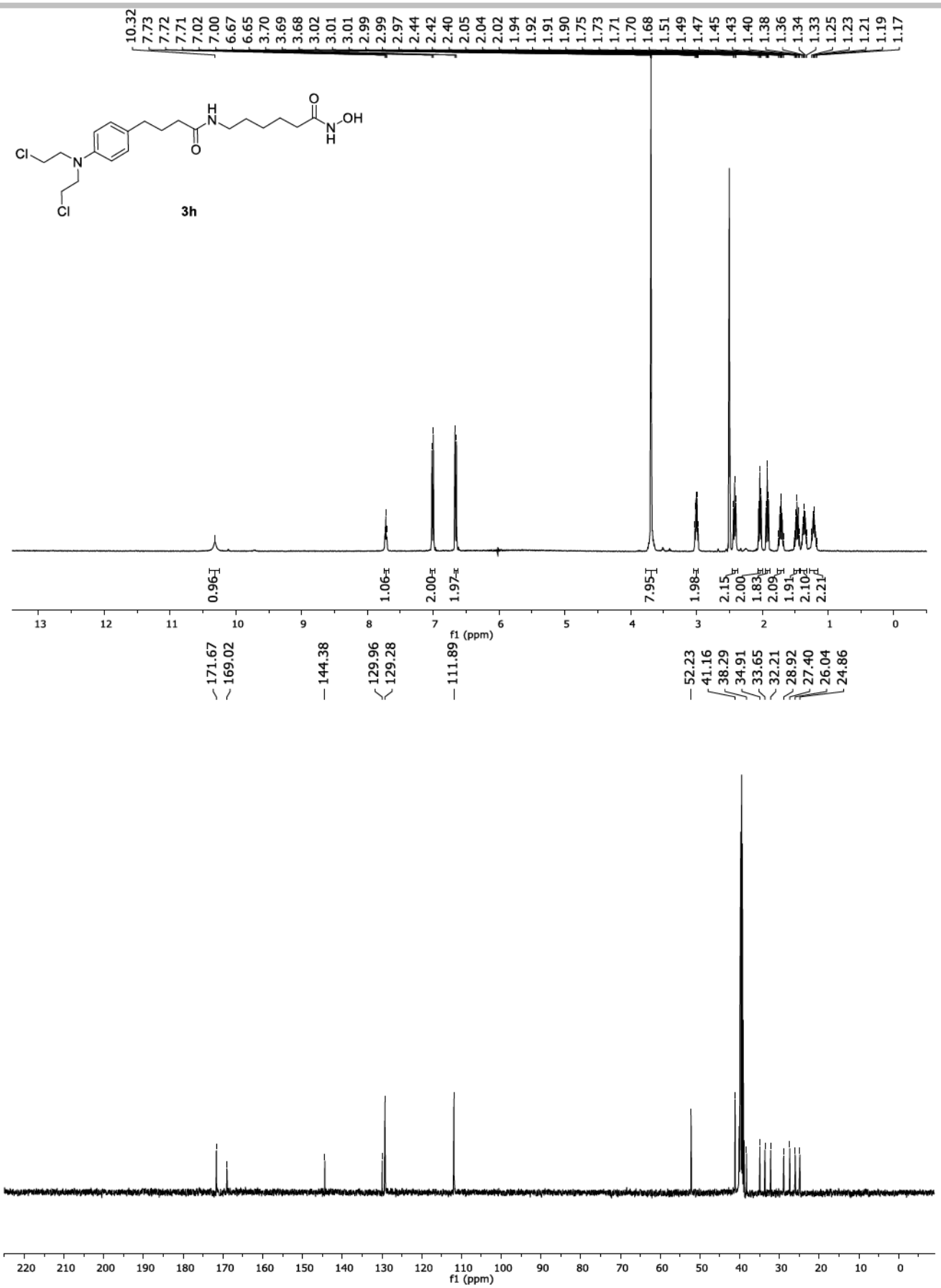

Figure S13: ^{1}H and ^{13}C-NMR spectra of **3h** in DMSO-d_6.

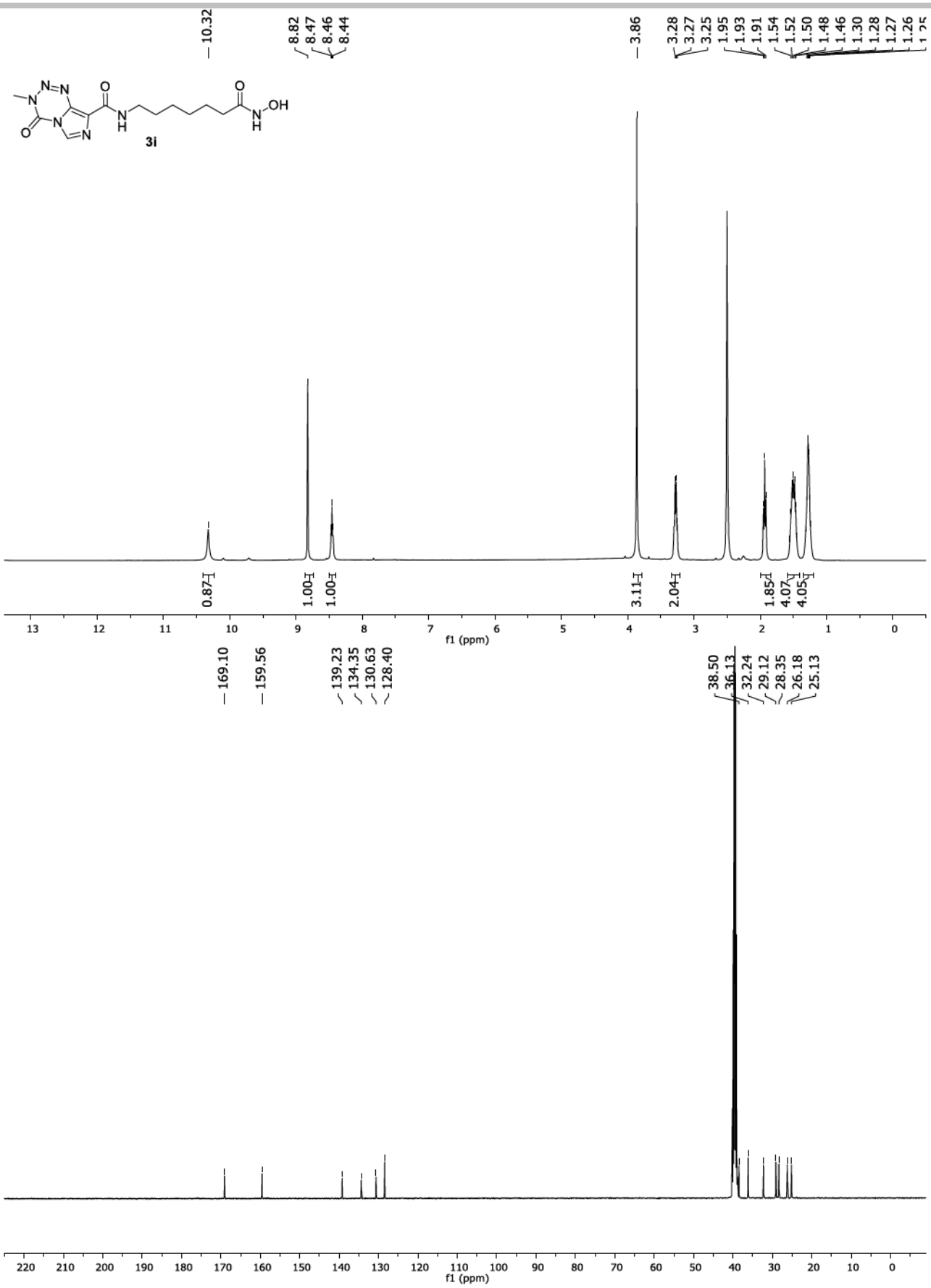

Figure S14: ^{1}H and ^{13}C-NMR spectra of **3i** in DMSO-d_6.

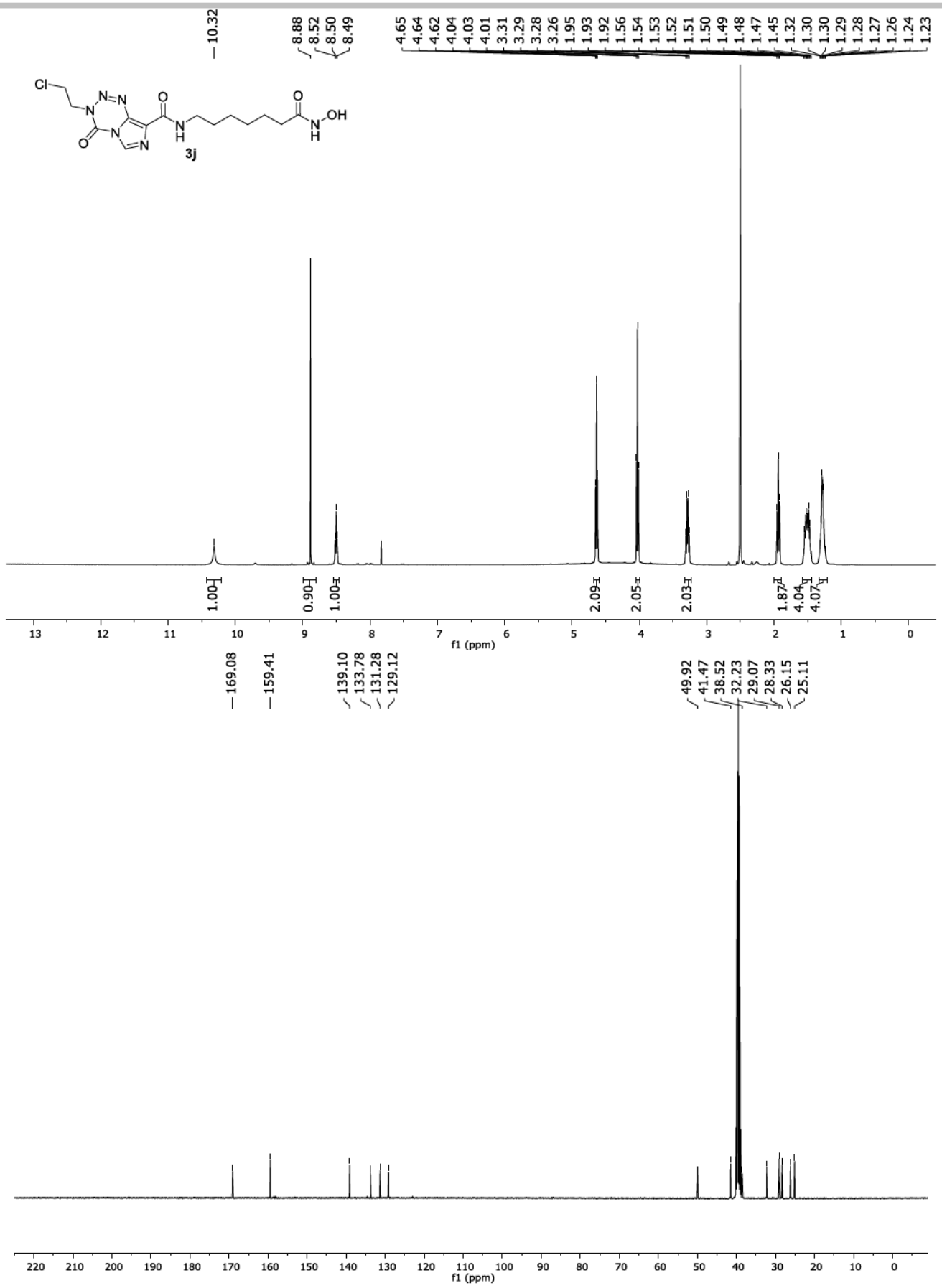

Figure S15: ^{1}H and ^{13}C-NMR spectra of **3j** in DMSO-d_6.

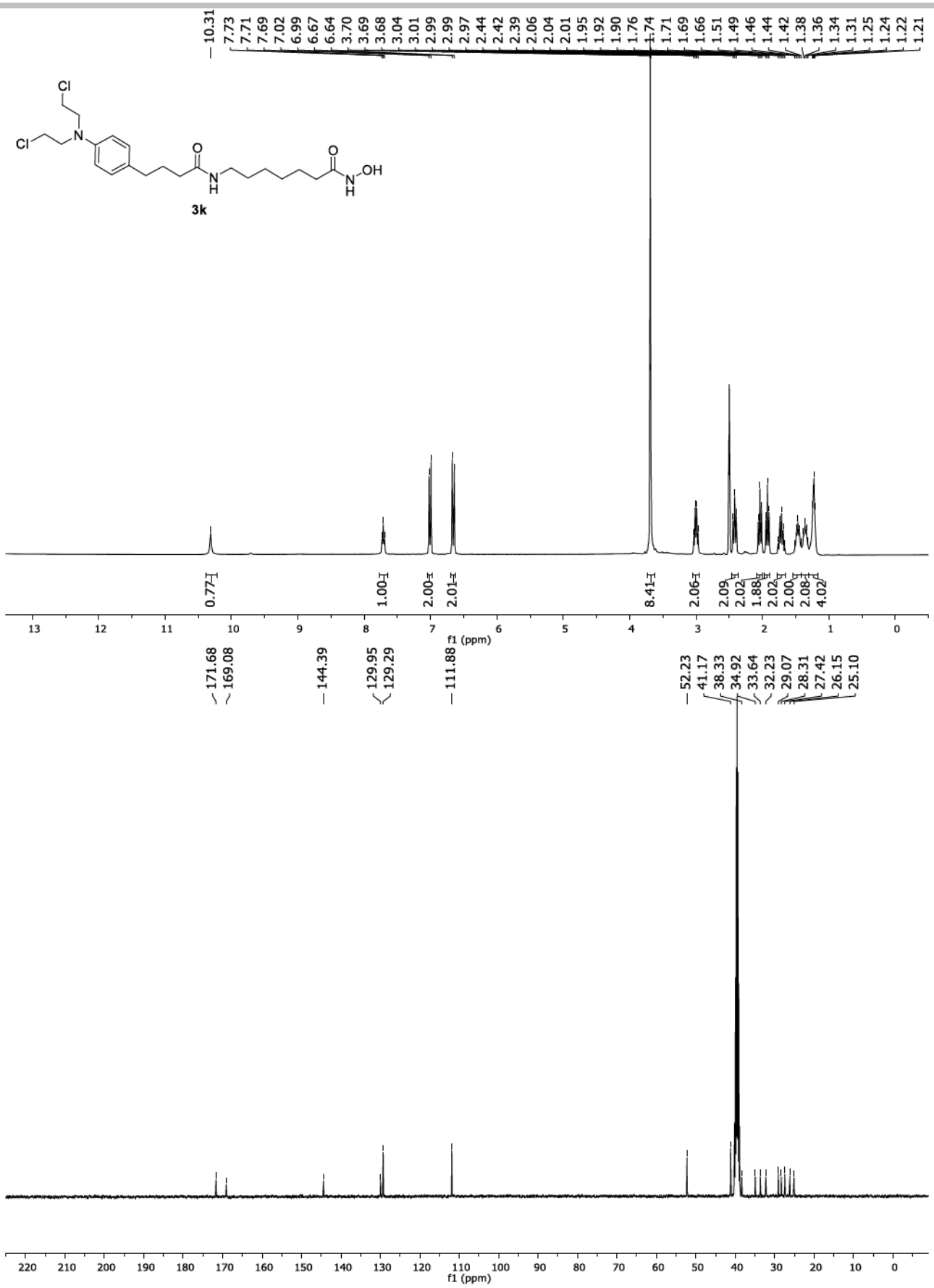

Figure S16: ^{1}H and ^{13}C-NMR spectra of **3k** in DMSO-d_6.

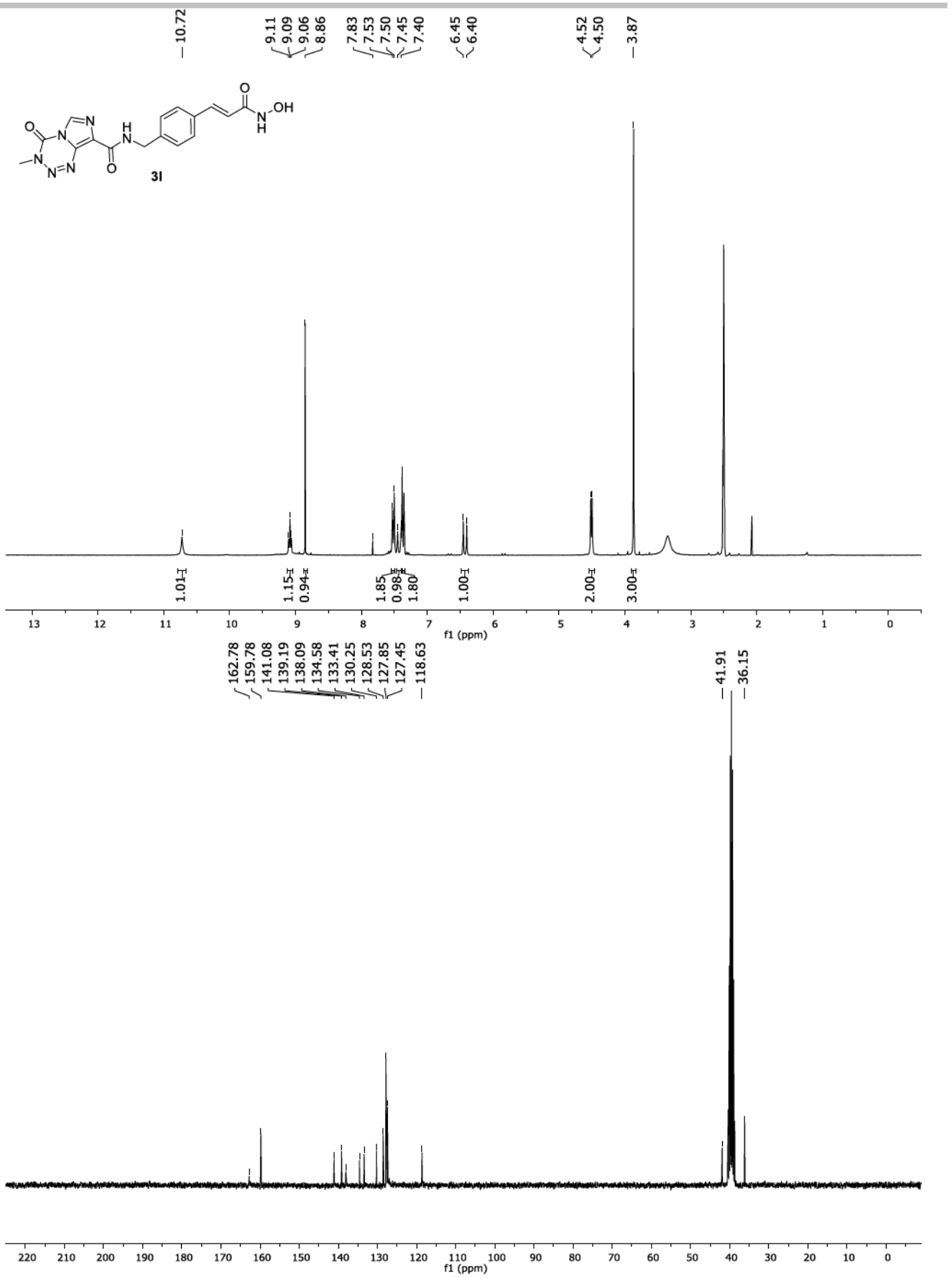

Figure S17: ^{1}H and ^{13}C-NMR spectra of **3l** in DMSO-d_6.

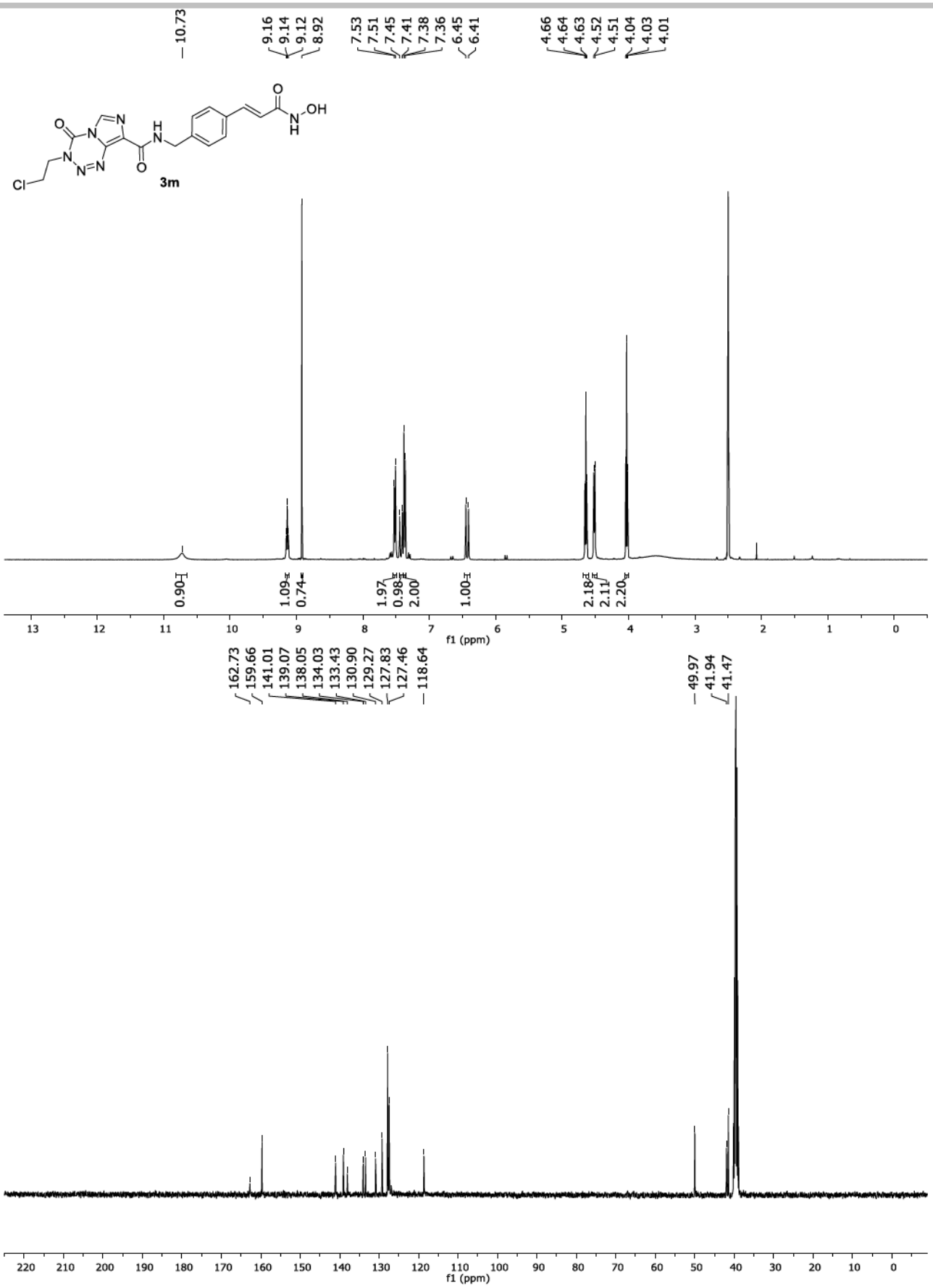

Figure S18: ^{1}H and ^{13}C-NMR spectra of **3m** in DMSO-d_6.

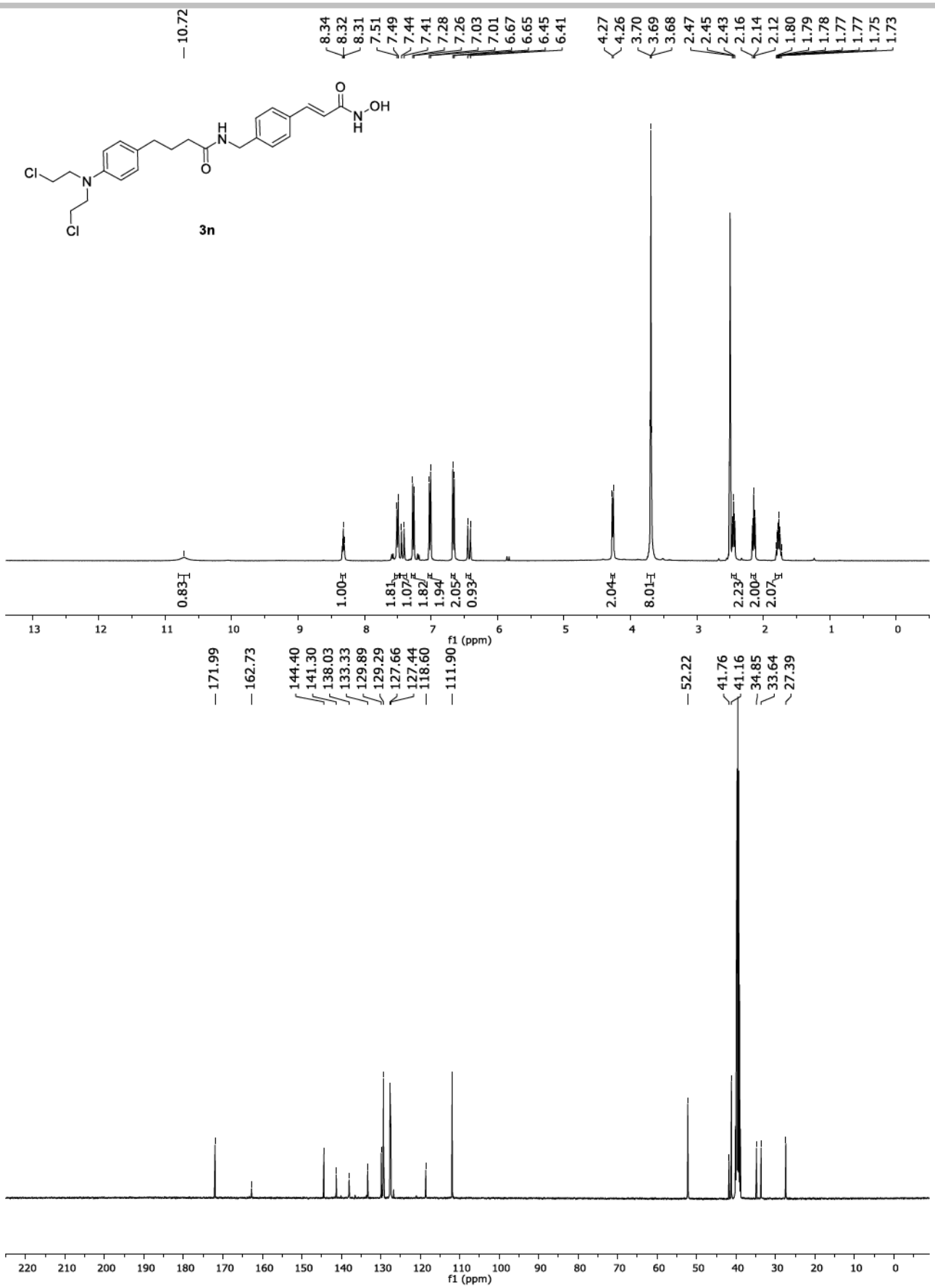

Figure S19: ^{1}H and ^{13}C-NMR spectra of **3n** in DMSO-d_6.

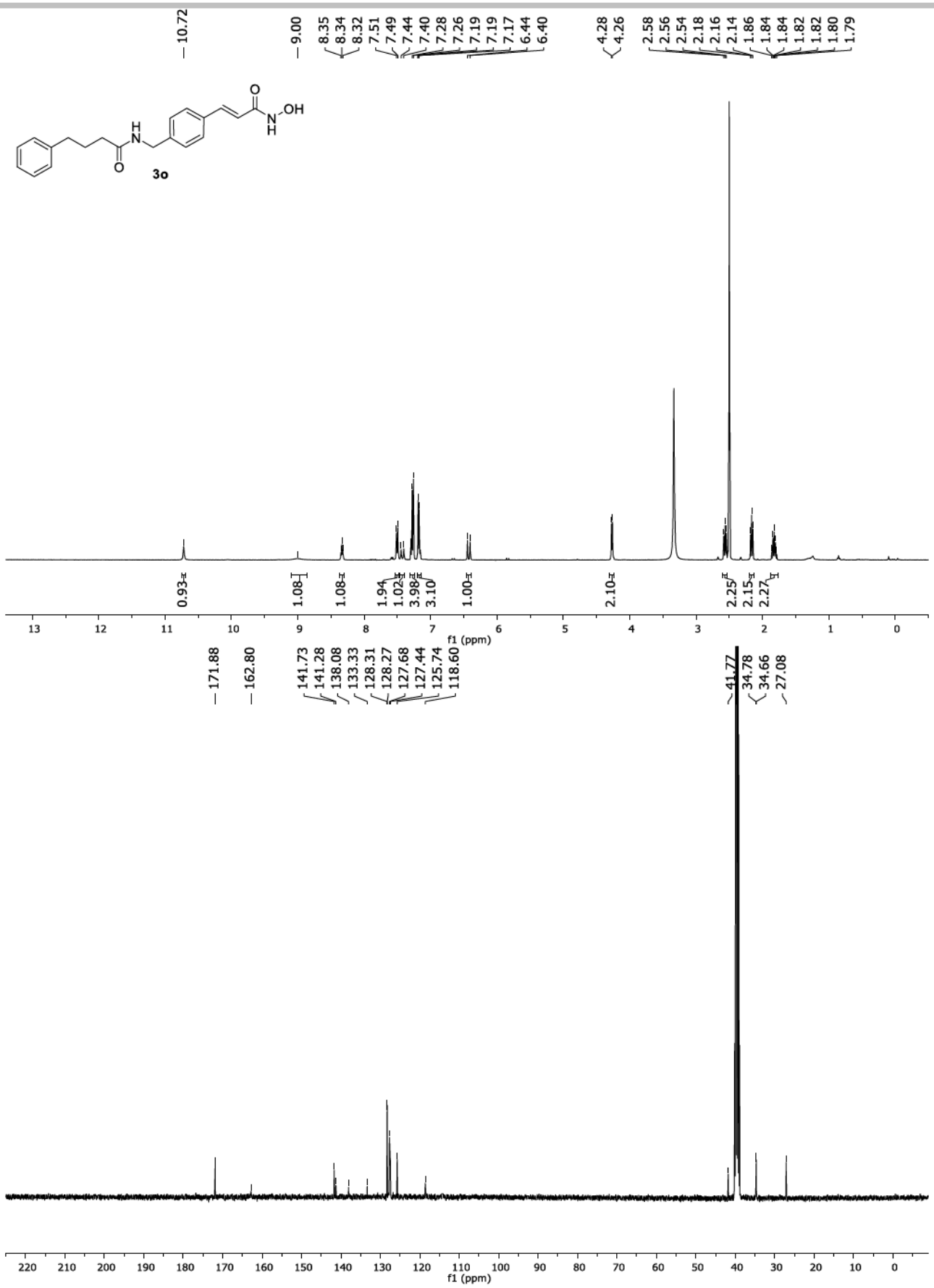

Figure S20: ^{1}H and ^{13}C-NMR spectra of **3o** in DMSO-d_6.

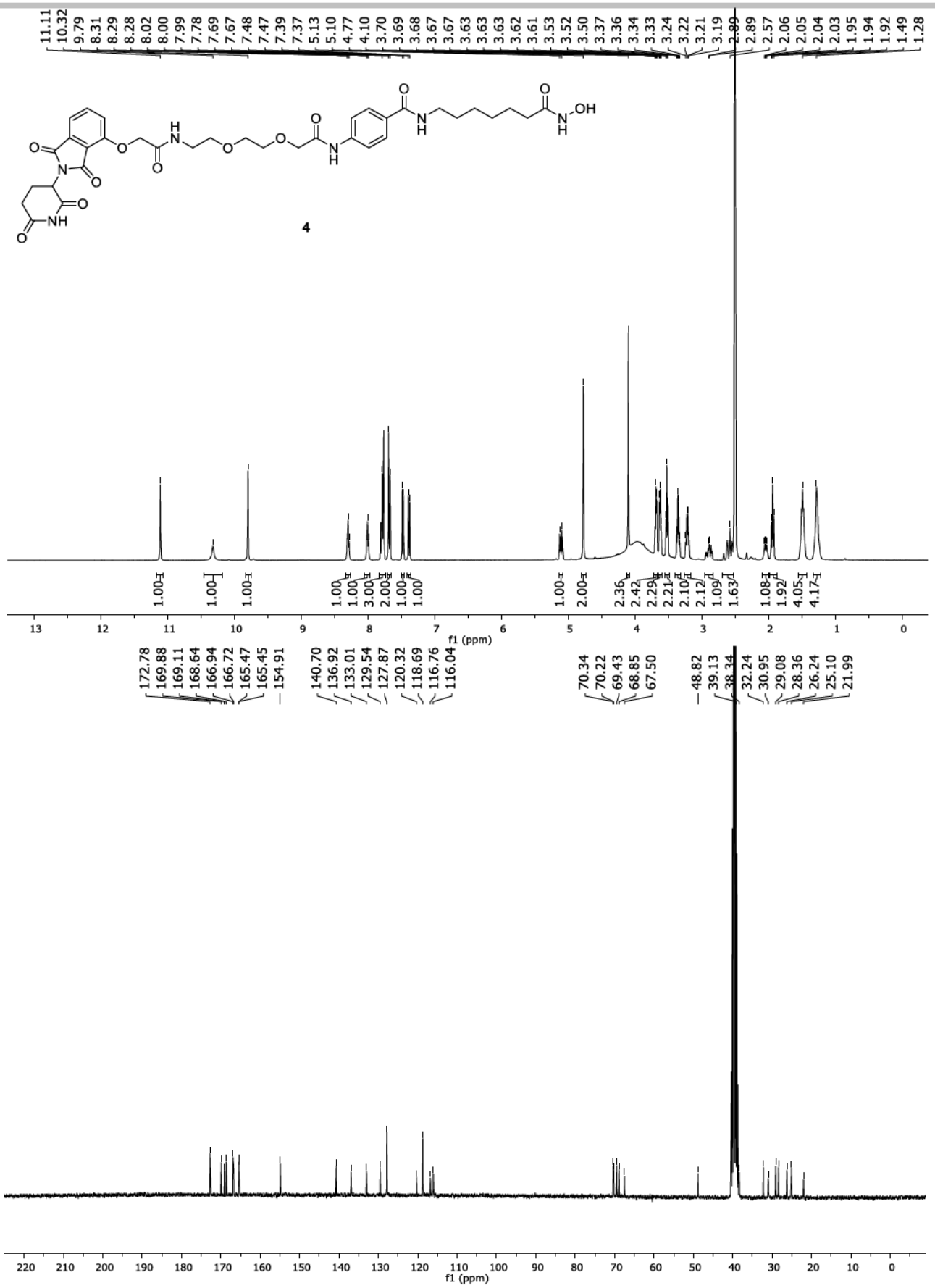

Figure S21: ^{1}H and ^{13}C-NMR spectra of **4** in DMSO-d_6.

3 Biological Evaluation

3.1 Reagents

Cisplatin was purchased from Sigma (München, Germany) and dissolved in 0.9% sodium chloride solution, propidium iodide (PI) was purchased from PromoKine (Heidelberg, Germany). Stock solutions (10 mM) of vorinostat, nexturastat A (Selleckchem, Houston, Texas, USA), chlorambucil (Sigma Aldrich, Germany), temozolomide (TCI Chemicals) and mitozolomide (synthesized, see compound **12**), were prepared with DMSO and diluted to the desired concentrations with DMEM. All other reagents were supplied by PAN Biotech (Aidenbach, Germany) unless otherwise stated.

3.2 Cell Lines and Cell Culture

The human tongue squamous cell carcinoma cell line Cal27 and the human primary glioblastoma cell lines U87 and U251 were obtained from Merck KGaA (Darmstadt, Germany). All cell lines were grown at 37 °C under humidified air supplemental with 5 % CO_2 in DMEM containing 10% heat inactivated fetal calf serum, 120 IU/mL penicillin, and 120 µg/mL streptomycin. The cells were grown to 80 % confluency before being used in further assays.

3.3 MTT Cell Viability Assay

The rate of cell survival under the action of test compounds was evaluated by an improved MTT assay as previously described.[9-11] Briefly, cells were plated out (Cal27 2,500 c/w, U87 4,000 c/w, and U251 2,500 c/w) and incubated with the compounds in different concentrations. After 72 hours, the incubation was ended by addition of MTT (Serva, Heidelberg, Germany) solution (5 mg/mL in PBS). The formazan precipitate was dissolved in DMSO (VWR, Langenfeld, Germany). Absorbance was measured at 544 nm and 690 nm in a FLUOstar microplate-reader (BMG LabTech, Offenburg, Germany).

3.4 γ-H2AX Expression DNA Damage Assay

The γ-H2AX DNA damage assay was based on an assay published by Ziegler et al. with minor modifications.[12] Briefly, Cal27 cells were seeded in 96-well tissue culture plates (Corning, Kaiserslautern, Germany) at a density of 2,500 c/w. Cells were treated with indicated concentrations and compounds for 24 hours. Cells were fixed with 4 % formaldehyde solution followed by incubation with ice-cold methanol and blocking in blocking buffer (5 % BSA, 0.3 % Triton X-100 in PBS). Cells were incubated with primary antibody (Cat. No. 05-636, Merck Millipore, Darmstadt, Germany) overnight at 4°C and secondary fluorophore-labeled antibody (Northern Light Anti Mouse, Cat. No. NL007, Biotechne, Wiesbaden, Germany) for 2 hours in the dark. Cell nuclei were counterstained with Hoechst 33342. Analysis was performed with Thermo Fischer ArrayScan XTI (Thermo Scientific, Wesel, Germany).

3.5 Measurement of Apoptotic Nuclei

Cal27 cells were seeded at a density of 32,000 c/w in 24-well plates (Sarstedt, Nürnbrecht, Germany). Cells were treated with indicated compounds for 24 hours. Supernatant was removed after a centrifugation step and the cells were lysed in 500 µL hypotonic lysis buffer (0.1 % sodium citrate, 0.1 % Triton X-100, 100 µg/mL propidium iodide) at 4°C overnight in the dark. The percentage of apoptotic nuclei with DNA content in sub-G1 was analyzed by flow cytometry using the CyFlow instrument (Partec, Norderstedt, Germany).

3.6 Caspase 3/7 Activation Assay

Compound-induced activation of caspases 3 and 7 was analyzed using the CellEvent Caspase-3/7 green detection reagent (Thermo Scientific, Wesel, Germany) according to the manufacturer´s instructions. Briefly, Cal27 cells were seeded in 96-well plates (Corning, Kaiserslautern, Germany) at a density of 2,500 c/w. Cells were treated with indicated compounds for 24 hours. Then, medium was removed and 50 µL of CellEvent Caspase 3/7 green detection reagent (2.0 µM in PBS supplemented with 5 % heat inactivated FBS) was added. Cells were incubated for 30 min at 37 °C in a humidified incubator before imaging by using the *Thermo Fisher* ArrayScan XTI high content screening (HCS) system with a 10X magnification (Thermo Scientific). Hoechst 33342 was used for nuclei staining. The pan caspase inhibitor QVD was used in a concentration of 20 µM diluted in DMEM and incubated 30 min prior to compound addition.

3.7 Immunoblotting

Cells were treated with the indicated concentration of the compound or vehicle (DMSO) for 48 hours. Cell pellets were dissolved with RIPA buffer (50 mM Tris-HCl pH 8.0, 1 % Triton X-100, 0.5 % sodium deoxycholate, 0.1% SDS, 150 mM sodium chloride, 2 mM EDTA, supplemented with protease and phosphatase inhibitors (Pierce protease and phosphatase inhibitor mini tablets, Thermo Scientific, Wesel, Germany) and clarified by centrifugation. Equal amount of total protein were resolved by SDS-PAGE and transferred to polyvinylidene fluoride membranes (Merck Millipore, Darmstadt, Germany). PageRuler Prestained Protein Ladder, 10 to 180 kDa (Thermofisher Scientific, Wesel, Germany) was used as protein molecular weight marker. Blots were incubated with antibodies against acetylated α-tubulin (Cat. No. #5335), HDAC6 (Cat. No. #7558), HDAC1 (Cat. No. #2062), acetyl histone H3 (Cat. No. # 9677) and GAPDH (Cat. No. #97166), obtained from Cell Signaling Technology, Danvers, MA.

3.8 Data Analysis

Concentration-effect curves were constructed with Prism 7.0 (GraphPad, San Diego, CA, USA) by fitting the pooled data of at least three experiments performed in triplicates to the four-parameter logistic equation. Statistical analysis was performed using t-test or one-way ANOVA. To analyze the superadditive effects of chlorambucil and **3o** on caspase3/7-activation and DNA damage, the values of single treatments were summed up and the standard deviation calculated according to Bandolik et al.[11] This value was compared with the effects of **3n** using t-test.

3.9 In-vitro human HDAC1/2/3/6 assay

All reactions were performed in OptiPlate-96 black microplates (Perkin Elmer) with duplicate series in at least two independent experiments. An assay end volume of 50 µL was set for each experiment and all reactions were carried out in assay buffer (50 mM Tris-HCl, pH 8.0, 137 mM NaCl, 2.7 mM KCl, 1.0 mM $MgCl_2$, 0.1 mg/mL BSA) with appropriate concentrations of substrate and inhibitors obtained by dilution from 10 mM stock solutions. Control wells without enzyme and control wells with vorinostat as reference were included in each plate. After addition of 5 µL test compound or control in assay buffer, 35 µL of the fluorogenic substrate ZMAL (21.43 µM in assay buffer) and 10 µL of human recombinant HDAC1 (1.2 ng/µL in assay buffer; BPS Bioscience, Catalog# 50051) or HDAC2 (1.0 ng/µL, BPS Bioscience Catalog# 50052) or HDAC3 (1.0 ng/µL, BPS Bioscience Catalog# 50003) or HDAC6 (2.0 ng/µL in assay buffer; BPS Bioscience, Catalog# 50006) the reaction were incubated at 37 °C for 90 min. Afterwards 50 µL of 0.4 mg/mL trypsin in trypsin buffer (50 mM Tris-HCl, pH 8.0, 100 mM NaCl) was added, followed by further incubation at 37 °C for 30 min. Plates were analyzed using a Fluoroskan Ascent microplate reader (Thermo Scientific) and fluorescence was measured with an excitation wavelength of 355 nm and an emission wavelength of 460 nm.

3.10 In-vitro human HDAC8 assay

HDAC8 recombinant enzyme was purchased from Reaction Biology Corp. (Cat Nr. KDA-21-481; Malvern, PA, USA). The HDAC activity assay was performed in 96-well-plates (Corning, Kaiserslautern, Germany). Briefly 20 ng of HDAC8 per reaction were used. HDAC8 was diluted in assay buffer (50 mM Tris-HCl, pH 8.0, 137 mM NaCl, 2.7 mM KCl, 1.0 mM $MgCl_2$, and 1.0 mg/mL BSA). After a 5 min incubation step the reaction was started with 10 µL of 60 µM Boc-Lys-(TFa)-AMC (Bachem, Bubendorf, Switzerland). The reaction was stopped after 90 min by adding 100 µL stop solution (16 mg/mL trypsin, 2.0 µM panobinostat in 50 mM Tris-HCl, pH 8.0, and 100 mM NaCl). 15 min after the addition of the stop solution the fluorescence intensity was measured at excitation of 355 nm and emission of 460 nm in a NOVOstar microplatereader (BMG LabTech, Offenburg, Germany).

4. Docking Studies

Docking of 3n and 3o to human HDAC6 with RosettaLigand

The crystal structure of human HDAC6 (PDB: 5EDU)[13] was obtained from the Protein Data Bank (PDB, www.rcsb.org). Residues 114-478 of chain A corresponding to the maltose-binding periplasmatic protein, which was used to facilitate crystallization, and a second copy of the protein in the crystallographic unit, chain B, were deleted. All heteroatom records were removed, except for all metal ions (one zinc atom and two potassium atoms). The zinc bound water was positioned based on crystal structure PDB: 6CW8.[14] Throughout the calculation a metal ion restraint was applied. The structure was optimized to the closest local energy minimum using the RosettaRelax application with coordinate constraints on the backbone.[15] Ligand input files for **3n** and **3o** were created with ChemDraw. An initial 3D conformer with hydrogen atoms was constructed in Corina[16] and subsequently an ensemble of 1000 low-energy conformers was produced by using the BCL:ConformerGenerator.[17] One conformer was placed in the binding pocket of HDAC6 and aligned to the known binding pose of hydroxamic acids in PDB: 6CW8.[11] A constraint file was constructed using the known distance measures between hydroxamic acid, zinc ion and water molecule as described by Porter *et al.*[18] Ligand docking was performed for an initial 10,000 models and subsequently three rounds of focused refinement using RosettaLigand were applied to identify the best scoring models by predicted binding energy.[19-21] A final ensemble of models was selected for **3n** from three clusters containing 640 models and for **3o** from seven clusters containing 315 models of ligand poses by root mean square deviation. Only such models were considered that complied with the observed binding pose of the hydroxamic acid residue and the hydrogen bond between the amide group and serine 531, a known interaction of this compound class.[14,18]

The following commands were executed throughout the modeling process.

Relax input starting structures:

```
/dors/meilerlab/apps/rosetta/rosetta-3.11/main/source/bin/relax.default.linuxgccrelease -s
5edu_align_A.pdb -database /dors/meilerlab/apps/rosetta/rosetta-3.11/main/database/ -
in:auto_setup_metals -constrain_relax_to_start_coords -ignore_waters False -out:prefix
relax_ -nstruct 25
```

Options for RosettaLigand:

```
-packing
    -ex1
    -ex2
    -no_optH false
    -flip_HNQ true
    -ignore_ligand_chi true

-parser
    -protocol
/dors/meilerlab/home/schoedct/Documents/Versuche/HDAC_docking_chlorambucil_derivates/dock_to
_human_HDAC6/docking/docking-LOST/dock.xml

-mistakes
    -restore_pre_talaris_2013_behavior true

-constraints:cst_file
/dors/meilerlab/home/schoedct/Documents/Versuche/HDAC_docking_chlorambucil_derivates/dock_to
_human_HDAC6/docking/docking-LOST/constraint.cst
```

RosettaScripts protocol for executing RosettaLigand:

```
<ROSETTASCRIPTS>

        <SCOREFXNS>
            <ScoreFunction name="ligand_soft_rep" weights="ligand_soft_rep">
            </ScoreFunction>
            <ScoreFunction name="hard_rep" weights="ligand">
            </ScoreFunction>
        </SCOREFXN  S>

        <LIGAND_AREAS>
            <LigandArea name="inhibitor_dock_sc" chain="X" cutoff="6.0" add_nbr_radius="true"
all_atom_mode="false"/>
```

```
            <LigandArea name="inhibitor_final_sc" chain="X" cutoff="6.0" add_nbr_radius="true"
all_atom_mode="false"/>
            <LigandArea name="inhibitor_final_bb" chain="X" cutoff="7.0"
add_nbr_radius="false" all_atom_mode="true" Calpha_restraints="0.3"/>
        </LIGAND_AREAS>

        <INTERFACE_BUILDERS>
            <InterfaceBuilder name="side_chain_for_docking"
ligand_areas="inhibitor_dock_sc"/>
            <InterfaceBuilder name="side_chain_for_final" ligand_areas="inhibitor_final_sc"/>
            <InterfaceBuilder name="backbone" ligand_areas="inhibitor_final_bb"
extension_window="3"/>
        </INTERFACE_BUILDERS>

        <MOVEMAP_BUILDERS>
            <MoveMapBuilder name="docking" sc_interface="side_chain_for_docking"
minimize_water="false"/>
            <MoveMapBuilder name="final" sc_interface="side_chain_for_final"
bb_interface="backbone" minimize_water="false"/>
        </MOVEMAP_BUILDERS>

        <SCORINGGRIDS ligand_chain="X" width="25">
            <ClassicGrid grid_name="classic" weight="1.0"/>
        </SCORINGGRIDS>

        <MOVERS>
            <ConstraintSetMover name="coordinate" add_constraints="true"
cst_file="/dors/meilerlab/home/schoedct/Documents/Versuche/HDAC_docking_chlorambucil_derivat
es/dock_to_human_HDAC6/docking/docking-LOST/constraint.cst"/>
            <Transform name="transform" chain="X" box_size="7.0" move_distance="0.2" angle="20"
cycles="500" repeats="1" temperature="5"/>
            <HighResDocker name="high_res_docker" cycles="6" repack_every_Nth="3"
scorefxn="ligand_soft_rep" movemap_builder="docking"/>
            <FinalMinimizer name="final" scorefxn="hard_rep" movemap_builder="final"/>
            <InterfaceScoreCalculator name="add_scores" chains="X" scorefxn="hard_rep" />
        </MOVERS>

        <PROTOCOLS>
            <Add mover_name="coordinate"/>
            <Add mover_name="transform"/>
            <Add mover_name="high_res_docker"/>
            <Add mover_name="final"/>
            <Add mover_name="add_scores"/>
        </PROTOCOLS>

</ROSETTASCRIPTS>
```

Executing RosettaLigand:

```
#!/bin/tcsh

 foreach a (`cat templates.ls`)
     /dors/meilerlab/apps/rosetta/rosetta-
3.10/main/source/bin/rosetta_scripts.default.linuxgccrelease -s $a -database
/dors/meilerlab/apps/rosetta/rosetta-3.10/main/database/ -ignore_waters False -
in:auto_setup_metals
@/dors/meilerlab/home/schoedct/Documents/Versuche/HDAC_docking_chlorambucil_derivates/dock_t
o_human_HDAC6/docking/docking-LOST/docking.options -in:file:extra_res_fa
/dors/meilerlab/home/schoedct/Documents/Versuche/HDAC_docking_chlorambucil_derivates/dock_to
_human_HDAC6/docking/docking-LOST/Los.params -out:prefix dock_ -nstruct 400 -out:path:all
/dors/meilerlab/home/schoedct/Documents/Versuche/HDAC_docking_chlorambucil_derivates/dock_to
_human_HDAC6/docking/docking-LOST/output_run_01/ &
end
```

SUPPORTING INFORMATION

Calculation of binding energy

```
/dors/meilerlab/apps/rosetta/rosetta-
3.10/main/source/bin/rosetta_scripts.default.linuxgccrelease -l run_01_models.ls -database
/dors/meilerlab/apps/rosetta/rosetta-3.10/main/database/ -in:file:extra_res_fa nLo.params -
parser:protocol interface.xml -ignore_waters False -in:auto_setup_metals -
out:file:score_only
```

RMSD versus binding energy (interface delta) plots for **3n** and **3o**

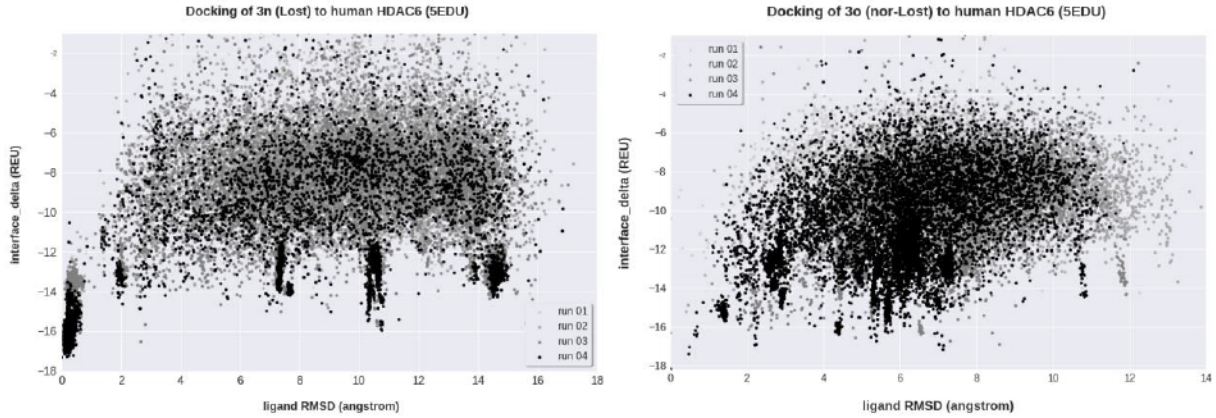

Figure S22: Ligand RMSD versus interface_delta plots for **3n** and **3o**. Both compounds were docked over four consecutive rounds, always taking the best 1000 models by interface_delta forward and redocking the ligand.

References

[1] J. Lohbeck, A. Miller, *Bioorg Med Chem Lett.* **2016**, *21*, 5260-5262.
[2] T.-C. Chou, *Cancer Res.* **2010**, 70, 440-446.
[3] T.-C. Chou, P. Talalay, *Adv. Enzyme Regul.* **1984**, 22, 27-55.
[4] S. I. Khan, M. W. Grinstaff, *Tetrahedron Lett.* **1998**, *39*, 8031-8034.
[5] H. Aloysius, L. Hu, *Chem Biol Drug Des* **2015**, *4*, 837-848.
[6] H. Seyler, A. Kilbinger, *Tetrahedron Lett.* **2013**, *8*, 753-756.
[7] J. F. Shealy, R. F. Struck, L. B. Holum, J. A. Montgomery, *J. Org. Chem.* **1961**, *26*, 7, 2396-2401.
[8] K. R. Horspool, M. F. G. Stevens, C. G. Newton, E. Lunt, R. J. A. Walsh, B. L. Pedgrift, G. U. Baig, F. Lavelle, C. Fizames, *J. Med. Chem* **1990**, 33, 1393-1399.
[9] L. Marek, A. Hamacher, F. K. Hansen, K. Kuna, H. Gohlke, M. U. Kassack, T. Kurz, *J. Med. Chem.* **2013**, *56*, 427-436.
[10] L. H. Engelke, A. Hamacher, P. Proksch, M. U. Kassack, *J. Cancer.* **2016**, *7*, 353-363.
[11] J. J. Bandolik, A. Hamacher, C. Schrenk, R. Weishaupt, M. U. Kassack, *Int J Mol Sci.* **2019**, *20*, 3052.
[12] V. Ziegler, A. Albers, G. Fritz, *Biochim Biophys Acta.* **2016**, *1863*, 1082-1092.
[13] Y. Hai, D. W. Christianson, *Nat Chem Biol* **2016**, *12*, 741-747.
[14] S. Bhatia, V. Krieger, M. Groll, J. D. Osko, N. Ressing, H. Ahlert, A. Borkhardt, T. Kurz, D. W. Christianson, J. Hauer, F. K. Hansen, *J Med Chem* **2018**, *61*, 10299-10309.
[15] L. G. Nivon, R. Moretti, D. A. Baker, *PLoS One* **2013**, *8*, e59004.
[16] C. Schwab, *Drug Discov Today Technol* **2010**, *7*, e203-70.
[17] S. Kothiwale, J. L. Mendenhall, J. Meiler, *J Cheminform* **2015**, *7*, 47.
[18] N. J. Porter, J. D. Osko, D. Diedrich, T. Kurz, J. M. Hooker, F. K. Hansen, D. W. Christianson, *J Med Chem* **2018**, *61* (17), 8054-8060.
[19] S. DeLuca, K. Khar, J. Meiler, *PLoS One* **2015**, *10* (7), e0132508.
[20] K. W. Kaufmann, J. Meiler, *PLoS One* **2012**, *7* (12), e50769.
[21] J. Meiler, D. Baker, *Proteins* **2006**, *65*, 538-548.

3.3 Publikation 3

Priming with HDAC Inhibitors Sensitizes Ovarian Cancer Cells to Treatment with Cisplatin and HSP90 Inhibitors

Ana J. Rodrigues Moita[1,*], **Jan J. Bandolik**[1,*], Finn K. Hansen[2], Thomas Kurz[1], Alexandra Hamacher[1,*], Matthias U. Kassack[1,*]

1 Institut für Pharmazeutische und Medizinische Chemie, Heinrich-Heine-Universität Düsseldorf
2 Pharmazeutisches Institut, Universität Bonn

* Ana J. Rodrigues Moita und **Jan J. Bandolik** haben zu gleichen Teilen als geteilte Erstautoren und Alexandra Hamacher und Matthias U. Kassack haben zu gleichen Teilen als geteilte Senior-Autoren beigetragen

Veröffentlicht in: International Journal of Molecular Sciences, 05. November 2020

DOI: 10.3390/ijms21218300

Beitrag: Geteilte Erstautorenschaft mit Dr. Ana J. Rodrigues Moita. Durchführung der Apoptose-bezogenen Experimente (Western Blot, PCR, Caspase-Assay). Auswertung der Daten und Verfassen der überarbeiteten Version des Manuskriptes.

Zusammenfassung (übersetzt): Ovarialkrebs ist die fünfthäufigste Todesursache unter Krebstoden. Chemoresistenz, insbesondere gegen Platinverbindungen, trägt zu einer schlechten Prognose bei. Es ist bekannt, dass Histondeacetylase-Inhibitoren (HDACi) und Hitzeschockprotein 90-Inhibitoren (HSP90i) die an der Chemoresistenz beteiligten Signalwege modulieren. Diese Studie untersuchte die Auswirkungen von HDACi (Panobinostat, LMK235) und HSP90i (Luminespib, HSP990) auf die Wirksamkeit von Cisplatin in Ovarialkarzinom-Zelllinien (A2780, CaOV3, OVCAR3 und deren Cisplatin-resistente Subklone). Die Präinkubation mit HDACi erhöhte die zytotoxische Potenz von HSP90i, während die Präinkubation mit HSP90i keinen Effekt hatte. Die 48-stündige Präinkubation mit HSP90i oder HDACi vor Cisplatin-Behandlung, erhöhte die Cisplatin-Potenz in allen Zelllinien via Apoptoseinduktion signifikant und beeinflusste die Expression apoptoserelevanter Gene und Proteine. Bei CaOV3CisR und A2780CisR führte eine Präinkubation mit HDACi für 48 bis 72 Stunden zu einer vollständigen Revertierung der Cisplatin-Resistenz. Darüber hinaus verhinderte die permanente Anwesenheit von HDACi in subzytotoxischen Konzentrationen die Entwicklung einer Cisplatin-Resistenz bei A2780 Zellen. Dreifachkombinationen von HDACi, HSP90i und Cisplatin waren jedoch den Doppelkombinationen nicht überlegen. Insgesamt sensibilisiert das Priming mit HDACi die Ovarialkarzinomzelllinien für die Behandlung mit HSP90i oder Cisplatin und hat einen Einfluss auf die Entwicklung einer Cisplatin-Resistenz – beide Effekte können zu einer verbesserten Behandlung des Ovarialkarzinoms beitragen.

International Journal of
Molecular Sciences

MDPI

Article

Priming with HDAC Inhibitors Sensitizes Ovarian Cancer Cells to Treatment with Cisplatin and HSP90 Inhibitors

Ana J. Rodrigues Moita [1,†], Jan J. Bandolik [1,†], Finn K. Hansen [2], Thomas Kurz [1], Alexandra Hamacher [1,†] and Matthias U. Kassack [1,*,†]

1 Institute for Pharmaceutical and Medicinal Chemistry, University of Duesseldorf, 40225 Duesseldorf, Germany; ana.rodrigues.moita@hhu.de (A.J.R.M.); jan.bandolik@hhu.de (J.J.B.); thomas.kurz@hhu.de (T.K.); alexandra.hamacher@hhu.de (A.H.)

2 Pharmaceutical Institute, University of Bonn, 53121 Bonn, Germany; finn.hansen@uni-bonn.de

* Correspondence: matthias.kassack@hhu.de

† A.J.R.M. and J.J.B. equally contributed as first co-authors, A.H. and M.U.K equally contributed as senior authors.

Received: 9 September 2020; Accepted: 2 November 2020; Published: 5 November 2020

Abstract: Ovarian cancer is the fifth leading cause of cancer deaths. Chemoresistance, particularly against platinum compounds, contributes to a poor prognosis. Histone deacetylase inhibitors (HDACi) and heat shock protein 90 inhibitors (HSP90i) are known to modulate pathways involved in chemoresistance. This study investigated the effects of HDACi (panobinostat, LMK235) and HSP90i (luminespib, HSP990) on the potency of cisplatin in ovarian cancer cell lines (A2780, CaOV3, OVCAR3 and cisplatin-resistant sub-clones). Preincubation with HDACi increased the cytotoxic potency of HSP90i, whereas preincubation with HSP90i had no effect. Preincubation with HSP90i or HDACi 48h prior to cisplatin enhanced the cisplatin potency significantly in all cell lines via apoptosis induction and affected the expression of apoptosis-relevant genes and proteins. For CaOV3CisR and A2780CisR, a preincubation with HDACi for 48–72 h led to complete reversal of cisplatin resistance. Furthermore, permanent presence of HDACi in sub-cytotoxic concentrations prevented the development of cisplatin resistance in A2780. However, triple combinations of HDACi, HSP90i and cisplatin were not superior to dual combinations. Overall, priming with HDACi sensitizes ovarian cancer cells to treatment with HSP90i or cisplatin and has an influence on the development of cisplatin resistance, both of which may contribute to an improved ovarian cancer treatment.

Keywords: ovarian cancer; chemoresistance; HSP90 inhibitors; luminespib; HSP990; epigenetics; HDAC inhibitors; panobinostat; LMK235; cisplatin

1. Introduction

Ovarian cancer is among the five most deadly types of cancer in women [1]. Although therapeutic options have improved in the last decades, the five-year survival rate remains at around 48% for ovarian cancer in the USA [2] and 40–43% in Germany [3,4]. When comparing the different cancers of the female genital tract, ovarian cancer shows the highest death rate (6.9 per 100,000 US or German citizen) compared to cervical cancer (2.3 per 100,000 in USA and 2.4 per 100,000 in Germany) and uterine cancer (4.8 per 100,000 in USA and 3.0 per 100,000 in Germany). In 2020, about 22,000 new cases of ovarian cancer are predicted in the USA with around 14,000 deaths [3,5]. First line therapy includes taxane- and platinum-based chemotherapy after cytoreductive surgery [6]. A major obstacle of this therapy is the development of resistance against platinum-based drugs eventually leading to death. Resistance is multifactorial and can be intrinsic or acquired [7]. In addition, there is the

possibility of neoadjuvant chemotherapy (NACT) to further reduce the tumor mass before debulking surgery [8]. Randomized studies have shown that NACT before debulking was "non-inferior" to primary tumor removal [9,10]. However, there is currently no consensus on which patients are best suited for this type of therapy. Mutations and altered gene expression are the most common reasons for resistance, leading to altered mismatch repair, DNA methylation, histone acetylation and reduced apoptosis [11,12]. Modulators to overcome platinum resistance have not yet entered clinical routine, possibly due to multiple mutations in resistant cells and heterogeneous cell populations [13]. Heat shock protein 90 (HSP90) is an abundantly found molecular chaperone with over 280 client proteins and influences their activity through various regulatory mechanisms [14,15]. Many HSP90 client proteins such as Akt, MEK, receptor tyrosine kinases or estrogen receptors are members of proliferative and antiapoptotic pathways activated in drug-resistant ovarian cancers [16]. HSP90 inhibitors (HSP90i) could therefore interfere in many pathways by inducing degradation of HSP90 client proteins through the ubiquitin-proteasome pathway [17]. Moreover, the expression of HSP90 is increased in most cancer types [18]. For that reason, HSP90i are widely tested in different cancers such as colon, melanoma, prostate or ovarian cancer as single drug or as part of combination therapies [19–24]. In the past, HSP90i such as luminespib, SNX-5422, onalespib or ganetespib have entered phase II clinical trials (NLM identifier NCT01854034, NCT02612285, NCT2535338, and NCT01551693). Most of them are finished now. HSP90 was identified as a promising target in epithelial ovarian cancer [16]. Our group has previously shown that increased expression and phosphorylation of the HSP90 clients IGFR, ErbB2, and ErbB3 play a pivotal role in the development of resistance in ovarian cancer [25,26]. Thus, we investigated in this study whether HSP90i such as luminespib and HSP990 could serve as treatment options to address cisplatin resistance.

Another widely tested approach to address chemoresistance is epigenetic modulation [27,28]. Specifically, histone deacetylase inhibitors (HDACi) are currently under investigation. HDACi increase the acetylation status of histones and non-histone proteins such as transcription factors or HSP90 [13,29]. Furthermore, HDACi influence cell proliferation, cell cycle regulation and apoptosis of ovarian cancer cells [30]. We and others demonstrated that HDACi, e.g., the broad spectrum HDACi vorinostat, panobinostat, and LMK235 or class I selective HDACi entinostat, sensitize ovarian cancer cells to DNA-damaging drugs such as cisplatin [31–33]. HDACi increase the acetylation of HSP90 and lead to a loss of chaperone activity [34,35]. Thus, the combination of HSP90i and HDACi seems to be intriguing for the treatment of cancer. The combination of HSP90i and HDACi has indeed been tested: a combination of the HSP90i luminespib and the HDACi belinostat increased cell death in anaplastic thyroid carcinoma cells in a synergistic manner [34]. Based on this study, the detected synergism was investigated further, and it was found that the HSP90i SNX-5422 is also synergistic in combination with belinostat, vorinostat, and trichostatin A [36]. There is further evidence for a synergistic cytotoxic effect of the combination panobinostat or vorinostat with luminespib or HSP990 [29,37]. Part of the effect was shown to be mediated through inactivation of the PI3K/AKT signaling pathway, which was previously shown by us to contribute to cisplatin resistance in ovarian cancer and triple negative breast cancer [25,38]. Similar effects were obtained by combining luminespib and the HDACi vorinostat in multiple myeloma cells [29]. To the best of our knowledge, the combination of HSP90i and HDACi has not yet been tested in ovarian cancer cells together with a cytotoxic platinum agent. Thus, we decided to include the HSP90i luminespib and HSP990, as well as the non-selective HDACi panobinostat and LMK235 [39] in our study and to investigate their effect in a combination therapy with cisplatin in ovarian cancer. The rationale of this project was to compare single and combined effects of the HDACi and HSP90i and cisplatin in the ovarian cancer cell lines A2780 and A2780CisR to contribute to improved therapies addressing chemoresistance in ovarian cancer. The best combination was further tested in CaOV3, OVCAR3, and their cisplatin-resistant sub-cell lines to extend the impact of our findings on high grade serous ovarian cancer cell lines.

2. Results

2.1. HDACi and HSP90i Mediated Biological Effects in Ovarian Cancer Cells

First, we characterized the HSP90i luminespib and HSP990 and the HDACi panobinostat and LMK235 for their biological effects in the ovarian cancer cell lines A2780 and A2780CisR. MTT assays were used to determine the compound-induced cytotoxicity and revealed IC_{50} values in the two-digit nanomolar range for both HSP90i and panobinostat. LMK235 showed three-digit nanomolar IC_{50} values against A2780 (847 nM) and A2780CisR (644 nM) (Table 1 and Figure S2A,B).

Table 1. Cytotoxic activity of panobinostat, LMK235, luminespib and HSP990.

Cell Line	HDACi				HSP90i			
	Panobinostat		LMK235		Luminespib		HSP990	
	IC_{50} [nM]	pIC_{50} ± SEM	IC_{50} [nM]	pIC_{50} ± SEM	IC_{50} [nM]	pIC_{50} ± SEM	IC_{50} [nM]	pIC_{50} ± SEM
A2780	28.0	7.55 ± 0.02	847	6.07 ± 0.03	11.2	7.95 ± 0.06	20.1	7.70 ± 0.06
A2780CisR	28.2	7.55 ± 0.03	644	6.19 ± 0.02	16.4	7.78 ± 0.04	29.8	7.53 ± 0.02

Cell viability was determined by MTT assay after a 72 h incubation. Data shown are the mean of pooled data from at least three experiments each carried out in triplicate. Concentration effect curves are shown in Figure S2A,B.

To analyze the influence of the observed cytotoxicity on the growth kinetics of A2780 and A2780CisR, we analyzed the doubling times with or without inhibitor treatment after 24, 48, and 72 h. The results are shown in Figure 1A,B. Luminespib and HSP990 led to a slight increase in the doubling time of A2780 and A2780CisR. This effect was statistically significant for all four compounds in A2780CisR but only for two compounds (HSP990 and LMK235) in A2780 (Figure 1A). Further, both HDACi reduced the growth of A2780 and A2780CisR, as indicated by an increase in the doubling time (Figure 1B). In accordance to HSP90i, the effect seemed stronger in A2780CisR. The effect of HSP90i and HDACi on the protein expression, protein phosphorylation (HSP90i) and protein acetylation was analyzed by Western blot. The results are shown in Figure 1C,D. Both HSP90i reduced the expression and phosphorylation of the client protein and proto-oncogene AKT in both cell lines in a concentration- and time-dependent manner (luminespib in Figure 1C and HSP990 in Figure S3). This is consistent with the mechanisms of HSP90 inhibition. Cellular activity of both HDACi was demonstrated by a concentration-dependent increase in acetylated tubulin in A2780 and A2780CisR analyzed by Western blot (Figure 1D).

2.2. Treatment Order of HDACi and HSP90i Affects Increase in Cytotoxic Activity and Apoptosis Induction in A2780 and A2780CisR

Because of the known interplay between HSP90 and HDACs [13,29,34,36,37], we were interested in analyzing the cytotoxic effects of a combination treatment with HDACi and HSP90i. MTT experiments for this combination study used longer incubation times than standard 72 h MTT assays. A 48 h preincubation with one inhibitor (HDACi or HSP90i) was followed by 72 h coincubation with HDACi or HSP90i resulting in a total incubation time of 120 h. Therefore, IC_{50} values for inhibitors obtained in this experimental setup were substantially higher (Table S1 and Figure 2A–D) and not comparable to those obtained with a 72 h MTT (Figure S2). A 48 h preincubation with HSP90i (luminespib or HSP990, respectively) had no effect on the cytotoxic activity of panobinostat or LMK235 (Figure S4). In contrast, 48 h preincubation with panobinostat or LMK235 increased the potency of HSP990 and luminespib by factors up to 3.2-fold (Figure 2A–D and Figure S4 and Table S1). The effects on the potency of HSP90i were significant in A2780 and for panobinostat in A2780CisR. For LMK235, no significant interaction in A2780CisR was observed. Therefore, we analyzed apoptosis induction only for the combination of panobinostat with both HSP90i. The results are shown in Figure S5. The enhancement of the HSP90i-induced cytotoxicity by HDACi pretreatment seen in MTT assays was mediated by apoptosis

induction. A 24 h preincubation with HSP90i followed by 24 h coincubation with panobinostat had no effect on the number of apoptotic cells, whereas, vice versa, a 24 h preincubation with panobinostat followed by 24 h coincubation with HSP90i significantly increased the rate of apoptosis in A2780 and A2780CisR cells (Figure S5).

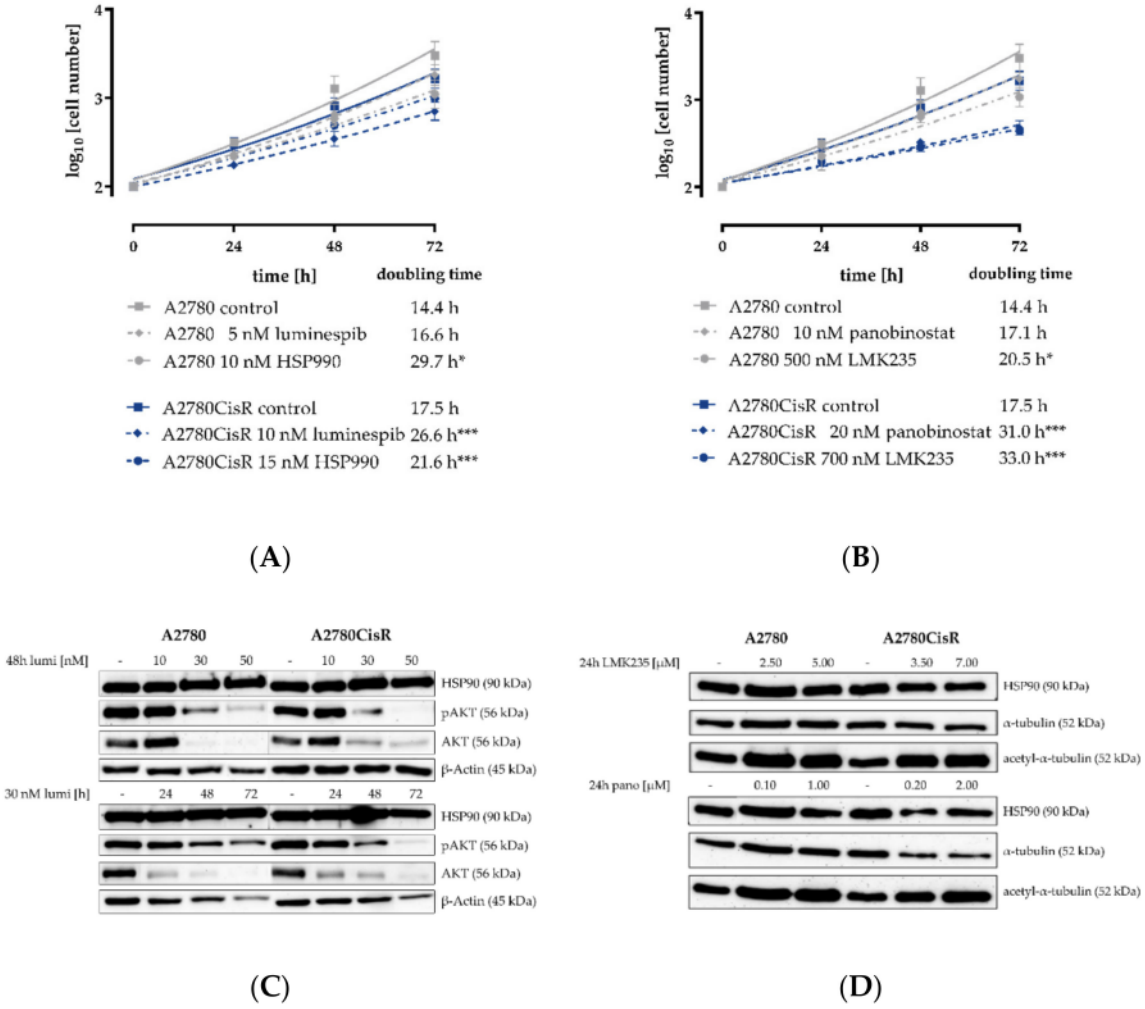

Figure 1. Effects of HSP90i and HDACi on cell growth and protein expression in A2780 and A2780CisR cells. (**A**) A 72 h incubation with the HSP90i luminespib and HSP990 showed a slight decrease in cell proliferation for A2780CisR cells. In A2780, this effect was only achieved with HSP990. (**B**) A 72 h incubation with the HDACi panobinostat or LMK235 slightly reduced the cellular growth of A2780 and A2780CisR cells. (**C**) A 48 h incubation with luminespib with IC_{50}, three-fold IC_{50} and five-fold IC_{50} or time-dependent incubation with three-fold IC_{50} of luminespib led to a decrease in the expression of the HSP90 client protein AKT and its phosphorylation (pAKT). The uncropped and labeled immunoblots are shown in Figure S1. (**D**) A 24 h incubation with panobinostat or LMK235 increased the acetylation of α-tubulin in both cell lines. Data shown are mean ± SEM of three independent experiments or one representative immunoblot out of three. Statistical analysis was performed using t-test. Levels of significance: * $p \leq 0.05$, *** $p \leq 0.001$.

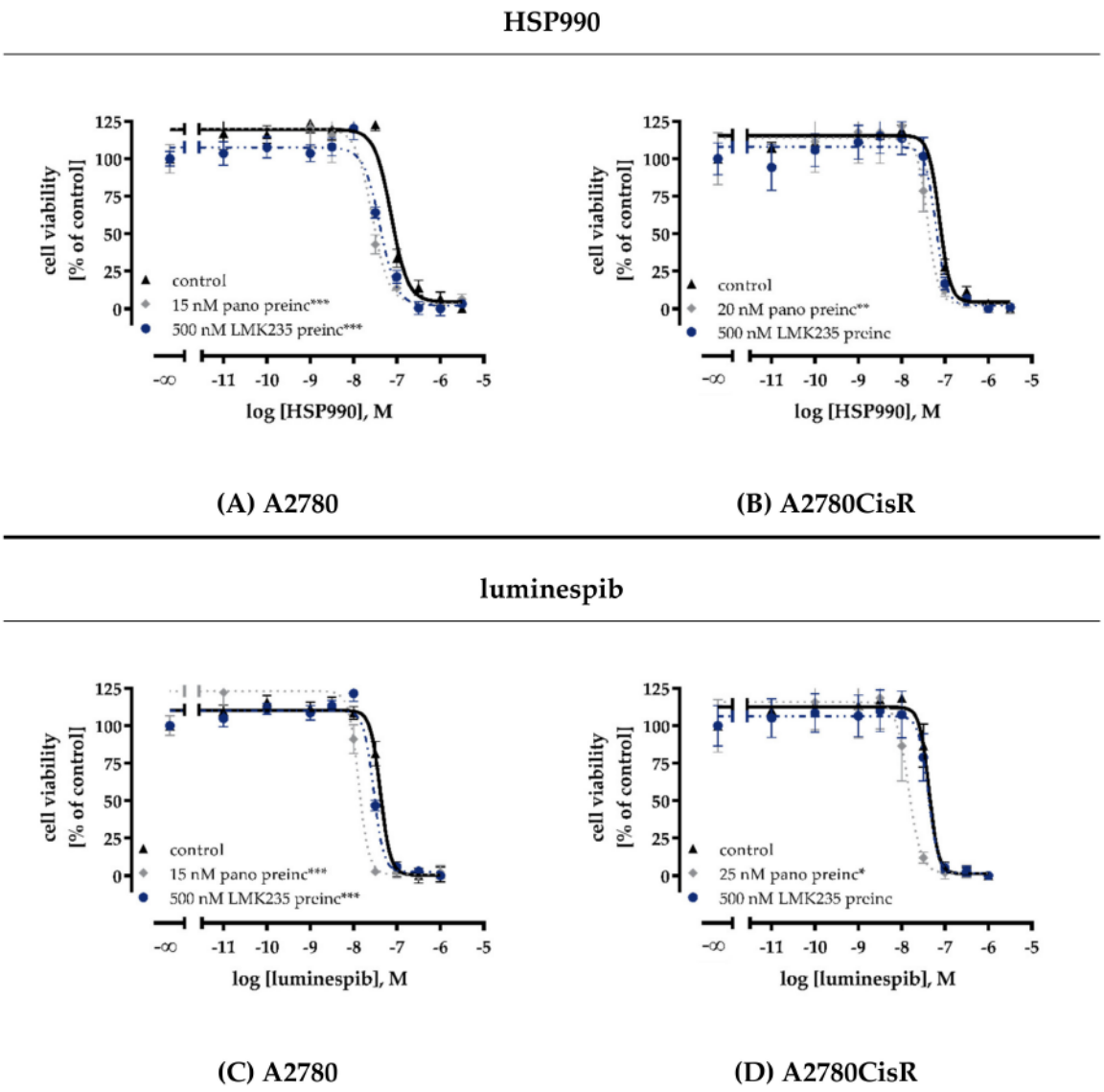

Figure 2. Preincubation with HDACi increase cytotoxic potency of HSP90i. A 48 h preincubation (preinc) with panobinostat or LMK235 with the indicated concentrations decreased IC_{50} values of HSP990 (**A**,**B**) and luminespib (**C**,**D**) in A2780 (**A**,**C**) and A2780CisR cells (**B**,**D**). IC_{50} values, pIC_{50} and SEM are shown in Table S1. Data shown are mean ± SEM of three independent experiments each carried out in triplicate. Statistical analysis was performed using t-test. Levels of significance: * $p \leq 0.05$, ** $p \leq 0.01$, *** $p \leq 0.001$.

To gain a first idea of the mechanisms behind the observed enhancement of cytotoxicity and apoptosis induction after preincubation with HDACi, the effects of panobinostat and luminespib on the gene expression of apoptosis-relevant factors in A2780 and A2780CisR cells were investigated. Both inhibitors (luminespib and panobinostat) were chosen based on their highest effects in the MTT assays shown in Figure 2A–D. Expression of the tumor suppressor gene *p21*; the proapoptotic genes *BAK*, *BAX*, and *APAF-1*; and the antiapoptotic genes *survivin*, *Bcl-xL*, and *Mcl-1* was analyzed by PCR. A2780 and A2780CisR cells were treated with panobinostat or luminespib alone for the indicated time points followed by analysis of gene expression. The results are shown in Figure 3.

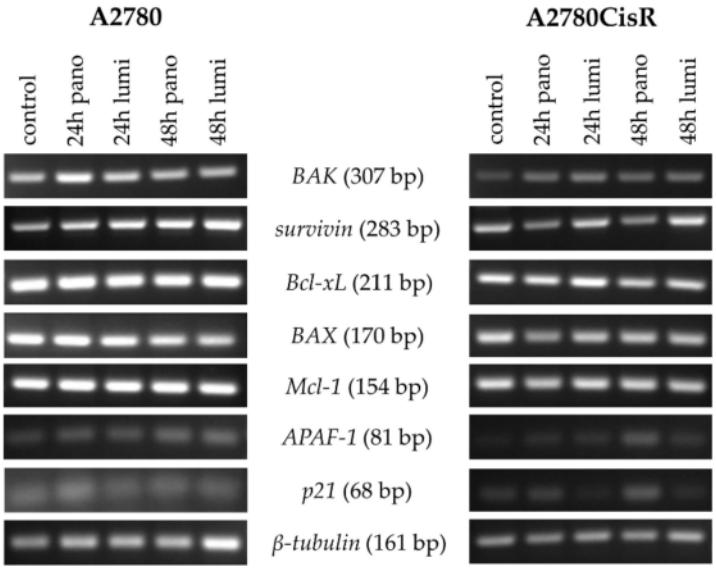

Figure 3. Effects of HDACi or HSP90i incubation on apoptosis-related genes. Gene expression data were obtained by PCR. Cells were treated with 10 nM (A2780) or 20 nM (A2780CisR) panobinostat or 5 nM (A2780) or 10 nM (A2780CisR) luminespib for 24 or 48 h.

In A2780, the expression of pro- and antiapoptotic genes remained largely unaffected by the treatment with the exception of *survivin*. Surprisingly, both inhibitors increased the mRNA level in a time-dependent manner. In A2780CisR, panobinostat reduced *survivin* expression and increased *APAF-1* and *p21* expression.

2.3. Effects of HDACi and HSP90i on Cisplatin Induced Cytotoxicity and Apoptosis

HDACi showed a priming effect on the cytotoxic activity of HSP90i. This prompted us to explore a possible influence of HSP90i or HDACi treatment alone or in combination on the potency of cisplatin in ovarian cancer cells. First, MTT assays were performed in A2780 and A2780CisR with a 48 h inhibitor preincubation prior to cisplatin administration or a coincubation of inhibitor and cisplatin (Figure S6A–D, IC_{50} values in Table 2 and pIC_{50} values in Table S2A). Coincubation of inhibitors with cisplatin (dual combination) showed no or only small increases in the potency of cisplatin in A2780/A2780CisR except for LMK235 (Figure S6C and Table 2). A 48 h preincubation with the inhibitors prior to cisplatin administration however markedly increased the potency of cisplatin with shift factors up to 6.7 (e.g., calculated for A2780, $IC_{50\ (cisplatin)}$: 3.34 µM; $IC_{50\ (cisplatin\ +\ 48h\ HSP990\ preincubation)}$: 0.5 µM; Figure S6A and Table 2). Notably, the effects were more pronounced in A2780 cells. HDACi and HSP90i showed equal effects in increasing the cisplatin potency in A2780 (Figure S6A,C).

In A2780CisR, HDACi were slightly but not significantly superior to HSP90i (Figure S6B,D). The best effect was observed with a 48 h preincubation with 20 nM panobinostat, decreasing the cisplatin IC_{50} from 19.7 to 6.53 µM (shift factor 3). Despite this relatively large effect, a complete resensitization by reaching the cisplatin IC_{50} of the parental cell line was not achieved (Figure S6D and Table 2). Notably, even though HDACi and HSP90i were equally effective in increasing cisplatin potency in MTT assays in A2780 (Figure S6A,C), only HDACi, but not HSP90i, showed a significant increase in apoptosis induction in the absence or presence of cisplatin (Figure S6E).

Table 2. Influence of dual or triple combinations with HDACi or HSP90i on the cytotoxic activity of cisplatin in A2780 and A2780CisR cells.

A – Dual Combination (inhibitor + cDDP)									
cell line		**cDDP IC50 [μM]**							
	Control (cDDP only)	**HSP90i**				**HDACi**			
		Luminespib		**HSP990**		**Panobinostat**		**LMK235**	
		Coinc	**preinc**	**coinc**	**preinc**	**coinc**	**preinc**	**coinc**	**preinc**
A2780	3.34	2.41	0.71	2.22	0.50	1.63	0.57	0.69	0.57
A2780CisR	19.7	24.9	13.2	25.7	11.8	16.6	6.53	11.0	7.05

B – Triple Combination I (HSP90i prior to HSP90i + HDACi + cDDP)							
		A2780 cDDP IC_{50} [μM]			**A2780CisR cDDP IC_{50} [μM]**		
		cDDP	**HDACi/cDDP**		**cDDP**	**HDACi/cDDP**	
			pano	**LMK235**		**pano**	**LMK235**
HSP90i	**lumi**	0.71	0.65	0.63	13.2	12.3	9.69
	HSP990	0.50	0.70	0.95	11.8	7.78	7.07

C – Triple Combination II (HDACi prior to HDACi + HSP90i + cDDP)							
		A2780 cDDP IC_{50} [μM]			**A2780CisR cDDP IC_{50} [μM]**		
		cDDP	**HSP90i/cDDP**		**cDDP**	**HSP90i/cDDP**	
			lumi	**HSP990**		**lumi**	**HSP990**
HDACi	**pano**	0.57	0.91	0.84	6.53	6.07	5.91
	LMK235	0.57	0.70	0.84	7.05	9.23	9.26

Data shown are IC_{50} values in μM obtained from three independent experiments each carried out in triplicate: (**A**) dual combinations in A2780 and A2780CisR; and (**B**,**C**) triple combinations in A2780 and A2780CisR. Preincubation means a 48 h preincubation with the indicated inhibitor followed by a 72-h incubation with cisplatin (**A**) or cisplatin plus indicated HDACi/HSP90i (**B**,**C**). pIC_{50} and SEM are shown in Table S2. Control denotes the IC_{50} value for cisplatin without inhibitor treatment. Concentrations used are 5 nM luminespib, 10 nM HSP990, 500 nM LMK235, and 10 nM panobinostat in A2780 and 10 nM luminespib, 15 nM HSP990, 700 nM LMK235, and 20 nM panobinostat in A2780CisR. (**A**) IC_{50} values are derived from the results in Figure S6A–D.

Preincubation with HDACi or HSP90i increased the potency of cisplatin. Next, we were interested in whether a triple combination of HDACi, HSP90i, and cisplatin had an even more pronounced effect regarding chemosensitivity against cisplatin. Data are presented in Figure S7A,B and Table 2. HSP90i were incubated for 48 h prior to addition of cisplatin plus HDACi (Table 2). In a further experiment, the HDACi were incubated for 48 h prior to addition of cisplatin plus HSP90i (Table 2). pIC_{50} values and errors are shown in Table S2. All triple combinations (HDACi panobinostat or LMK235 plus HSP90i luminespib or HSP990 plus cisplatin) resulted in significant increases in the potency of cisplatin in A2780 and A2780CisR (Figure S7A,B). The increase in potency yielded shift factors for triple combinations not significantly superior to those obtained by dual combinations (i.e., HDACi or HSP90i plus cisplatin). As an example, the triple combination consisting of a 48 h preincubation with panobinostat followed by 72 h of HSP990 plus cisplatin gave the lowest IC_{50} for cisplatin in A2780CisR (5.91 μM, Figure S7B). However, cisplatin potency was not significantly different from a dual combination of panobinostat with cisplatin which gave an IC_{50} of 6.53 μM (Figure S6D). Shift factors from dual (HDACi plus cisplatin) and triple combination MTT assays are listed in Table S3.

The effect of inhibitors was more pronounced in A2780 than in A2780CisR indicated by shift factors up to 6.7 in A2780 and up to 3.3 in A2780CisR. We conclude that a triple combination has no benefit over a dual combination treatment with regard to the cytotoxicity of cisplatin.

Similar to the dual combinations, the observed increase in cytotoxic activity of the triple combinations was mediated via apoptosis induction. A 48 h preincubation with HDACi in combination with HSP90i induced apoptosis in a similar range as a single pretreatment with HDACi (absence of cisplatin; Figures S6E and S7C). Further, pretreatment with HDACi plus HSP90i increased the

cisplatin-mediated induction of apoptosis (Figure S7C). However, this effect was not superior to dual combinations of HDACi and cisplatin (Figure S6E). To confirm that the observed effects in the apoptosis assay were mediated via caspase activation, the activity of caspase 3 and 7 was measured with a fluorescence-based assay for single treatment and combinations of panobinostat, luminespib, and cisplatin. The results are shown in Figure 4.

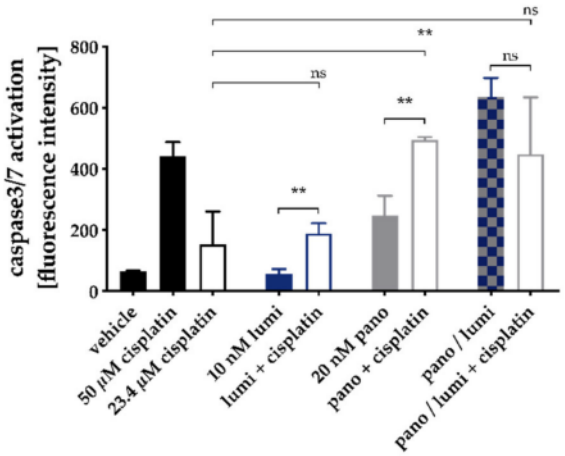

Figure 4. Caspase 3/7 activation by single treatment and combinations of panobinostat, luminespib, and cisplatin in A2780CisR cells. A2780CisR cells were preincubated with panobinostat and/or luminespib (lumi) for 48h. Cisplatin (23.4 µM, corresponding to the IC_{50}) or buffer control were added for a further incubation period of 24 h. Caspase 3/7 activation was analyzed by ArrayScan XTI. Cisplatin 50 µM (24 h) served as positive control for caspase 3/7 activation, 0.2% DMSO as vehicle control. Data are the mean ± SD. Statistical analysis to compare the caspase 3/7 activation of the two indicated treatments was performed using t-test. Levels of significance: ns $p > 0.05$, ** $p \leq 0.01$.

Whereas 10 nM luminespib did not lead to caspase 3/7 activation, 20 nM panobinostat was as effective as the IC_{50} of cisplatin (23.4 µM). The combination of luminespib with cisplatin resulted in a caspase 3/7 activation not significantly different from cisplatin alone. The HSP90i luminespib did not increase cisplatin efficacy for caspase 3/7 activation, which is in agreement with the results from apoptosis activation (Figure S6E). However, preincubation with panobinostat significantly increased caspase 3/7 activation of cisplatin (Figure 4). In agreement with our results from MTT and apoptosis assays (Figures S6 and S7), the triple combination of HSP90i, HDACi, and cisplatin showed no advantages over dual combinations of HDACi and cisplatin. Again, in agreement with results from MTT and apoptosis induction (Figure 2 and Figure S5), the combination of panobinostat and luminespib led to a massive caspase 3/7 activation which could not further be increased by cisplatin.

Notably, the antiproliferative and chemosensitizing effects of HSP90i and HDACi alone or in combination were not associated with changes in the cell cycle distribution of A2780 or A2780CisR (Figure S8).

2.4. Effects of HDACi and/or HSP90i Plus Cisplatin Incubation on mRNA and Protein Expression of Pro-/Antiapoptotic Key Genes

To identify genes that are altered by dual or triple combinations, we performed a PCR analysis. The tumor suppressor gene *p21*, the proapoptotic gene *APAF-1*, and antiapoptotic gene *survivin* were analyzed (Figure 5).

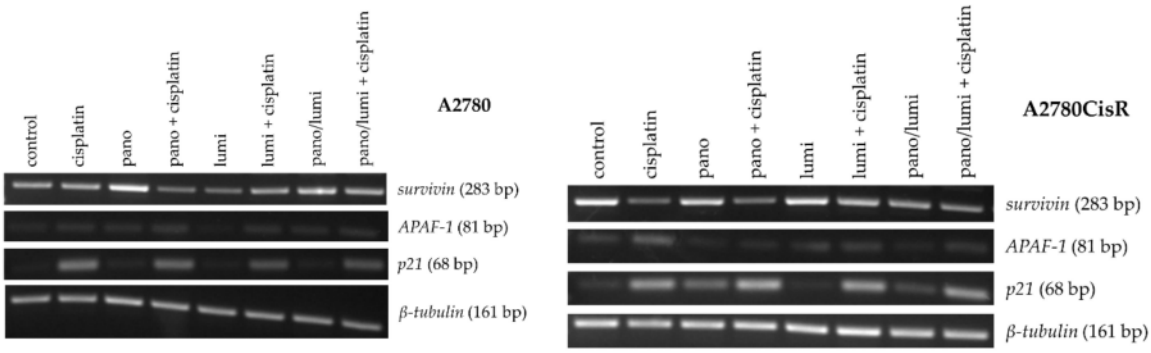

(A) **(B)**

Figure 5. Effects of HDACi or HSP90i preincubation prior to cisplatin on apoptosis-related genes. Gene expression data were obtained by PCR. (**A**,**B**) A2780 and A2780CisR cells were treated with the indicated inhibitors or their combinations. For combination treatments panobinostat and/or luminespib were administrated 48 h prior to 24 h cisplatin treatment in an IC_{50}. Cell line specific untreated controls were obtained by 72 h incubation with cell culture medium. The concentrations used (**A**,**B**) were the same as for cytotoxicity combination studies (Figure S6 and Table 2). One representative agarose gel is shown. Densitometric evaluation can be found in Figure S10B,C.

In A2780, the expression of *survivin* was reduced by the combination of panobinostat and cisplatin and by luminespib alone. Panobinostat alone and the combination of panobinostat and luminespib with or without cisplatin increased the expression of *survivin*. Only treatment with luminespib alone did not increase the expression of *APAF-1*; all other treatments resulted in a small increase in expression. The expression of the tumor suppressor gene *p21* was generally increased by each treatment. Treatment with panobinostat or luminespib alone (including the combination of both) had only a weak effect on the expression of *p21*. The expression of *p21* was strongly induced by any treatment regimen containing cisplatin (Figure 5A). In A2780CisR, the expression of *survivin* was reduced by cisplatin alone and cisplatin in combination with panobinostat or luminespib. Combination treatment with panobinostat and luminespib (also with cisplatin) also led to a significant reduction in *survivin* expression. A significant increase in the expression of *APAF-1* could only be achieved by treatment with cisplatin alone. *p21* Expression was increased in A2780CisR for all treatment regimens containing either cisplatin or panobinostat. Luminespib alone had no effect on the expression of *p21* (Figure 5B). To confirm the results of mRNA gene expression, protein expression of *p21*, *APAF-1*, and *survivin* was analyzed by Western blot (Figure 6).

APAF-1, *p21*, and *survivin* expressions were strongly influenced by our treatments. Dual or triple combinations containing panobinostat resulted in both cell lines in downregulation of survivin and upregulation of *p21* and *APAF-1* in comparison to a single treatment with cisplatin. In contrast, dual combinations with luminespib were clearly less effective and showed the desired effects only in combination with panobinostat.

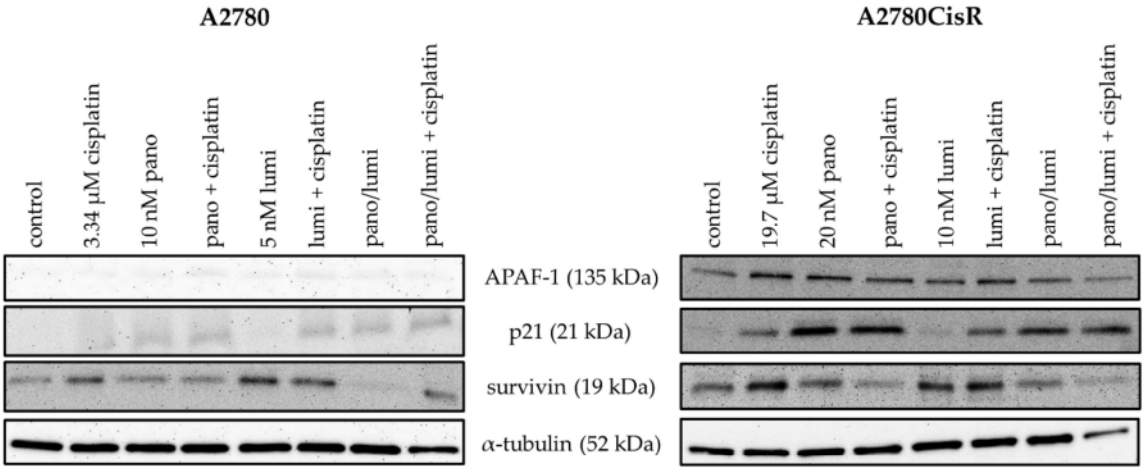

Figure 6. Effects of HDACi and HSP90i incubation or preincubation prior to cisplatin on protein expression levels of pro-/antiapoptotic proteins. Representative immunoblot analysis of APAF-1, *p21*, survivin and α-tubulin (as loading control) in A2780 and A2780CisR cells is shown. For combination treatments, panobinostat (pano) and/or luminespib (lumi) were administrated 48 h prior to 24 h cisplatin treatment with respective IC_{50} concentrations. Cell line specific control was treated with vehicle for 72 h. Densitometric analysis of the Western blots are shown in Figure S11.

2.5. Effects of Panobinostat or HSP990 Plus Cisplatin on Cell Viability in High Grade Serous Ovarian Cancer Cell Lines CaOV3 and OVCAR3 and Their Cisplatin-Resistant Sub-Cell Lines

To demonstrate that our findings are not limited to the ovarian cancer cell pair A2780/A2780CisR, the experimental conditions yielding the largest shift factors in MTT assays consisting of dual combinations panobinostat plus cisplatin and HSP990 plus cisplatin (Table 2) were applied to the high grade serous ovarian cancer (HGSOC) cell lines CaOV3 and OVCAR3, as well as their cisplatin resistant sublines. Table S3 shows IC_{50} values from single treatments with panobinostat and HSP990. IC_{50} values of panobinostat and HSP990 in CaOV3, OVCAR3 and their cisplatin-resistant sub-lines (Table 3) are in a similar range as IC_{50} values at A2780 and A2780CisR cell lines (Table 1).

Table 3. Cytotoxic activity of panobinostat and HSP990 in sensitive and cisplatin-resistant HGSOC cell lines CaOV3 and OVCAR3.

Cell Line	Panobinostat		HSP990	
	IC_{50} [nM]	pIC_{50} ± SEM	IC_{50} [nM]	pIC_{50} ± SEM
CaOV3	15.9	7.80 ± 0.02	40.9	7.39 ± 0.03
CaOV3CisR	16.9	7.77 ± 0.02	55.6	7.26 ± 0.02
OVCAR3	41.3	7.38 ± 0.02	27.6	7.56 ± 0.03
OVCAR3CisR	30.5	7.52 ± 0.01	25.0	7.60 ± 0.02

Cell viability was determined by MTT assay after a 72 h incubation. Data shown are the mean of pooled data from at least three experiments each carried out in triplicate. Concentration effect curves are shown in Figure S2C–F.

The applied dual combinations increased the cisplatin potency significantly in all cell lines with shift factors up to 4.7 except HSP990 plus cisplatin in OVCAR3 where no significant shift was observed (Table 4 and Table S4). Notably, 10 nM panobinostat was able to completely reverse the cisplatin resistance of CaOV3CisR (CaOV3, $IC_{50\,(cisplatin)}$: 1.92 µM; CaOV3CisR, $IC_{50\,(cisplatin + 48h\ panobinostat\ preincubation)}$: 1.38 µM; Table 4 and Table S4).

Table 4. Influence of dual combinations with panobinostat or HSP990 on the cytotoxic activity of cisplatin in CaOV3, OVCAR3, and their cisplatin resistant sublines.

Cell Line	Control (Cisplatin Only)	+ 48h Pretreatment			
		HSP990		Panobinostat	
		Cisplatin IC_{50} [μM]	SF	Cisplatin IC_{50} [μM]	SF
CaOV3	1.92	0.79	2.4 ***	1.04	1.8 ***
CaOV3CisR	4.80	3.20	1.5 **	1.38	3.5 ***
OVCAR3	3.94	2.77	1.4 ns	1.50	2.6 **
OVCAR3CisR	37.7	12.6	3.0 *	8.03	4.7 ***

Data shown are IC_{50} values and shift factors (SF) obtained from three independent experiments each carried out in triplicate. The concentrations used were 10 nM for panobinostat and 10 nM HSP990. SF were calculated as the ratio of IC_{50} of cisplatin and the IC_{50} of the corresponding drug combination. pIC_{50} and SEM are shown in Table S4. Statistical analysis was performed using t-test. Levels of significance: ns $p > 0.05$, * $p \leq 0.05$, ** $p \leq 0.01$, *** $p \leq 0.001$.

2.6. Effects of HDACi or HSP90i and Cisplatin on the Non-Cancer Cell Line HEK293

Next, to investigate if the observed effects were tumor specific in nature, we treated the non-cancerous cell line HEK293 with a combination of HDACi or HSP90i with cisplatin (Figure 7). Both HSP90i did not affect the cell viability, whereas the HDACi reduced the cell viability around 50%, which can be recognized by the lowering of the top plateau of the concentration effect curves. Notably, none of the inhibitors significantly increased the potency of cisplatin in HEK293 cells, except LMK235 which slightly (1.7 fold) reduced the IC_{50} of cisplatin (Figure 7 and Table S6). Therefore, we assume that the observed effects of HSP90i and HDACi on cisplatin have a certain selectivity for ovarian cancer cells over non-tumor cells.

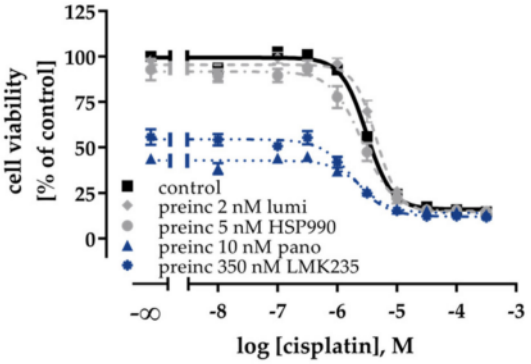

Figure 7. 48 h preincubation with luminespib, HSP990, panobinostat or LMK235 prior to 72 h cisplatin treatment did not affect cisplatin sensitivity of the non-cancerous cell line HEK293. Data shown are mean ± SEM of three independent experiments. Results (IC_{50}, pIC_{50}, SEM, and shift factors) are summarized in Table S6.

2.7. Long Term Treatment with Low-Dose HDACi or HSP90i can Overcome and Prevent the Development of Cisplatin Resistance in A2780 Ovarian Cancer Cells.

The development of cisplatin resistance is a major obstacle in the therapy of ovarian cancer. We observed favorable effects with dual combinations (HSP90i or HDACi and cisplatin) on the cisplatin sensitivity in A2780 cells. In A2780CisR cells, the chemosensitizing effect on cisplatin was less pronounced. Therefore, we were interested in whether a prolongation of the incubation time of HDACi or HSP90i had an influence on cisplatin sensitivity in A2780CisR. Instead of 48 h, we applied a 72 h preincubation with HDACi followed by 48-h cisplatin incubation or 48 h preincubation with HDACi followed by 24 h preincubation with HDACi plus HSP90i and subsequent addition of cisplatin for 48 h. The results of MTT assays for A2780CisR with this incubation scheme are shown in Figure 8.

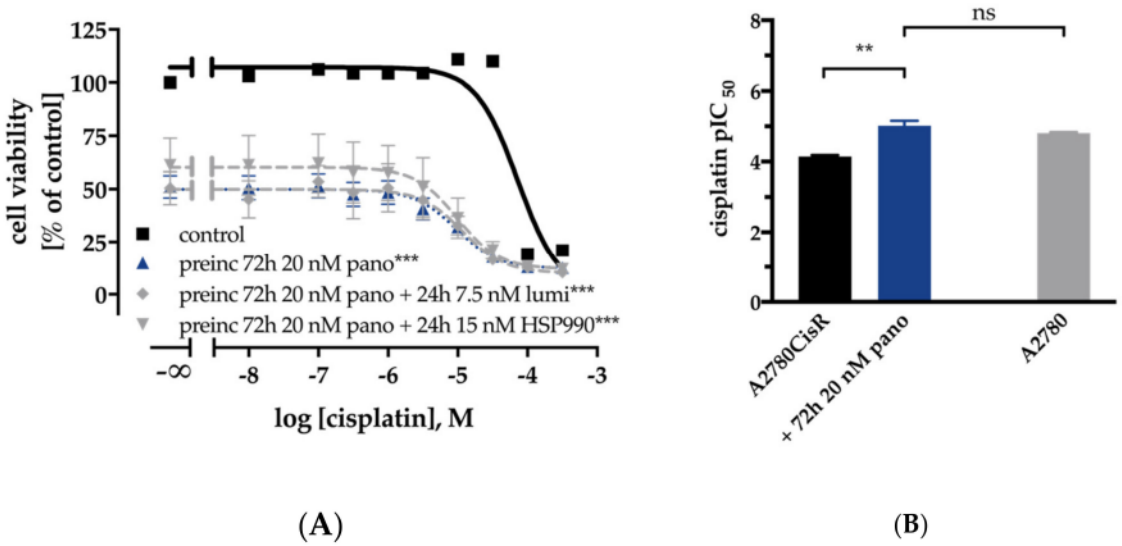

Figure 8. Effects of prolonged (72 h instead of 48 h) preincubation with HDACi / HSP90i on cisplatin sensitivity in A2780CisR ovarian cancer cells. 72 h preincubation with panobinostat or combination of 72 h of panobinostat with 24 h of luminespib or HSP990 prior to 48 h cisplatin treatment increased cisplatin sensitivity in A2780CisR (**A**). pIC_{50} ± SEM values of cisplatin in A2780CisR using 72 h preincubation with panobinostat compared to A2780 (**B**). Results (IC_{50}, pIC_{50}, SEM, and shift factor) are summarized in Table S5. Statistical analysis was performed using t-test. Levels of significance: ns $p > 0.05$, ** $p \leq 0.01$, *** $p \leq 0.001$.

Extension of the preincubation time of HDACi from 48 (as applied in Figures S6 and S7) to 72 h resulted in only slightly decreased shift factors in A2780 cells (Figure S9, Table S5). In contrast, prolongation of the incubation time increased shift factors in A2780CisR cells and reduced the cell viability (Figure 8 and Figure S9A,B and Table S5B). As a result of the prolonged incubation scheme, cisplatin IC_{50} control values differed from those reported in Figures S6 and S7.

The prolonged incubation scheme resulted in an IC_{50} for cisplatin of 72.7 µM for A2780CisR. Preincubation for 72 h of panobinostat enhanced the cisplatin potency 7.6-fold, resulting in a cisplatin IC_{50} of 9.56 µM (Figure 8B). This indicates complete reversal of cisplatin resistance, as can be seen from the cisplatin IC_{50} of 15.4 µM for A2780 cells using the prolonged MTT pretreatment scheme (Figure 8B). The complete reversal of cisplatin resistance by panobinostat preincubation in A2780CisR and the observed hypersensitization in A2780 cells prompted us to investigate the effect of a permanent presence of the HDACi panobinostat or LMKM235 or the HSP90i luminespib on cisplatin sensitivity. This was studied in short-term cisplatin-treated A2780 cells (Figure 9A, single cisplatin treatment cycle) as well as in long-term cisplatin-treated cells (Figure 9B, 16–21 cisplatin treatment cycles).

Treatment cycle means that A2780 cells were exposed to cisplatin in an IC_{50} for 6 h followed by washout, a two-day recovery and subsequent determination of cisplatin IC_{50} by MTT. Single cisplatin treatment cycle applied to A2780 cells resulted in approximately the same IC_{50} value of cisplatin as obtained without cisplatin stress. Notably, the same cisplatin treatment cycle applied to A2780 cells in permanent presence of 3 nM luminespib, 5 nM panobinostat or 200 nM LMK235 resulted in reduced IC_{50} values indicating (hyper)sensitization towards cisplatin (Figure 9, "resistance" factors of less than 1). Increased sensitivity towards cisplatin was significant for both HDACi (5 nM panobinostat and 200 nM LMK235; Figure 9), confirming the data shown in Figure 2 and Figure S5 where we were able to sensitize A2780 cells towards cisplatin by HDACi pretreatment. Long-term intermittent treatment with IC_{50} of cisplatin (16-21 treatment cycles) resulted in the resistant subclone A2780CisR with a resistance factor of around 4.5. When this long-term intermittent treatment with cisplatin was performed in the presence of HDACi or HSP90i, resistance development was moderately (but not significantly) reduced by 3 nM luminespib. Notably, in permanent presence of 5 nM panobinostat or 200 nM LMK235, a

significant reduction of the resistance development was achieved. After 21 weekly treatment cycles, the resistance factor of cisplatin was only 1.7 in presence of LMK235, demonstrating that the development of cisplatin resistance was almost completely abrogated in the presence of HDACi.

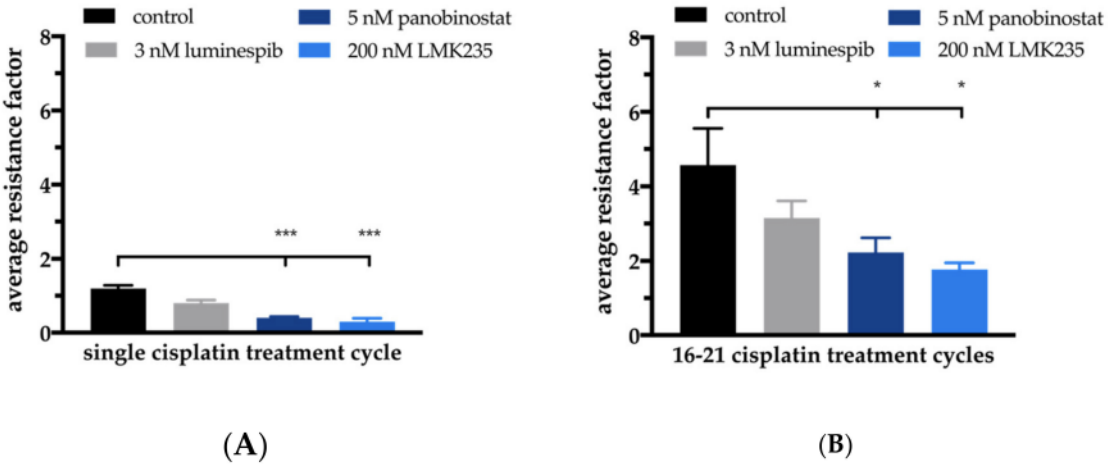

(**A**) (**B**)

Figure 9. Effects of HDACi or HSP90i on short-term (**A**) or long-term (**B**) cisplatin stress-induced changes of cisplatin sensitivity in A2780 ovarian cancer cells. Average resistance factors of cisplatin after single cisplatin treatment cycle ("cisplatin stress") (A) or after 16–21 cisplatin treatment cycles (averaged data over Treatment Cycles 16–21) in A2780 cells. Cisplatin treatment cycle means treatment for 6 h with an IC_{50} of cisplatin alone ("control") or in permanent presence of 3 nM luminespib, 5 nM panobinostat or 200 nM LMK235. Resistance factors were calculated by dividing the IC_{50} of cisplatin obtained after a treatment cycle ("stressed" cells) by the IC_{50} of cisplatin from unstressed A2780 cells. Statistical analysis was performed using t-test. Levels of significance: * $p \leq 0.05$, *** $p \leq 0.001$.

3. Discussion

This study reports on single and combined effects of HDACi and HSP90i with cisplatin in human ovarian cancer cell lines and offers a strategy to address chemoresistance in ovarian cancer that is urgently needed [13]. In 2007, Solár et al. reported that geldanamycin, one of the first discovered HSP90i, increased the sensitivity to cisplatin of the cisplatin-resistant ovarian cancer cell line A2780CisR [40]. Similarly, HSP90i have recently been shown to reverse cisplatin resistance in human ovarian cancer cells [21]. However, these findings have not yet led to clinical approval of drugs for reversal of chemoresistance. HDACi are approved epigenetic drugs for the treatment of specific lymphomas, e.g., cutaneous T cell lymphoma or multiple myeloma. Their potential to reverse chemoresistance of DNA-damaging drugs is currently explored by many groups including ours [31–33,41,42]. Weberpals et al. could show that the increase in cisplatin sensitivity by HDACi could be caused by a decrease in the expression of BRCA1 [43]. This reduced expression is achieved by HDACi alone or more strongly in combination with cisplatin. This suggests a therapeutic option for patients with tumors expressing significant levels of BRCA1. Additionally, there is the possibility to combine different epigenetic therapy strategies. For example, another group has been successful in overcoming cisplatin resistance of an ovarian cancer cell line by combining DNA methyltransferase inhibitors (DNMTi) and HDACi [44]. Furthermore, it has been shown that this combination leads to cell cycle arrest and increased apoptosis rate [45]. For the DNMTi decitabine, a BRCA1 related mechanism of action is discussed. These and our results in the field of epigenetic therapy of ovarian cancer in cellular models underline the importance of research in this field. To the best of our knowledge, the combination of HSP90i with HDACi and cisplatin has not yet been thoroughly studied in ovarian cancer and was thus the aim of this project.

We could confirm the results from previous studies [21,40] that pretreatment with HSP90i led to an increase in cisplatin potency (Figure S6A,B and Table 2, Table S3A and Table 4). However,

in contrast to Zhang et al., the sensitizing effect of HSP90i was only seen in A2780 but not in the cisplatin-resistant cell line A2780CisR although HSP90 inhibition led to a decrease in AKT expression and phosphorylation in both cell lines (Figure 1C) which is in accordance with literature reports [46]. In contrast to A2780/A2780CisR cells, we observed a larger cisplatin-sensitizing effect after HSP990 preincubation in cisplatin-resistant OVCAR3CisR than in OVCAR3 cells (Table 2, Table S3A and Table 4). Further, we could demonstrate that the sequence of inhibitor incubation matters: only pretreatment with HSP90i prior to cisplatin addition but not coincubation with cisplatin increased cisplatin potency (Figure S6A,B and Table 2 and Table S3).

Protein levels of HDAC isoforms in A2780 cells were not different in our previously shown studies [33] compared to those of Khabele et al. [30]. Consequently, combinations of the pan-HDACi panobinostat or LMK235 with cisplatin had similar synergistic effects as recently reported [32,33,42] (Figure S6C,D and Table 2 and Table S3A). Panobinostat and LMK235 showed no major differences, and, in addition to synergistic effects with cisplatin (Figure S6), both HDACi reduced cell proliferation significantly in A2780CisR but not in A2780 (Figure 1A,B), although an increase in acetylation was observed in both cell lines (Figure 1D). This is however in accordance with reports that resistant cancer cells undergo further epigenetic changes and might thus be more susceptible to HDACi [47]. Combinations of HDACi and cisplatin were synergistic as shown by the gold standard method of Chou-Talalay [32,33,48]. Of note, both coincubation of HDACi with cisplatin and 48 h preincubation with HDACi prior to addition of cisplatin increased cisplatin potency. However, preincubation was more effective in resistant A2780CisR, CaOV3CisR and OVCAR3CisR (Tables 2 and 4), which is somewhat different from the results of Ong et al. who showed marked increases in sensitivity to cisplatin by coincubation of vorinostat with cisplatin [49].

The importance of the sequence of inhibitor addition in combination experiments was further explored when combining HDACi and HSP90i. Preincubation with HDACi prior to addition of HSP90i increased HSP90i potency in A2780 and A2780CisR (Figure S7) up to three-fold, whereas, vice versa, preincubation with HSP90i prior to addition of HDACi did not or only slightly increase the potency of HDACi (Figure 2A–D and Figure S4 and Table S1). These results are in accordance with data from Kaiser et al. (myeloma cells) and Kim et al. (anaplastic thyroid carcinoma cells) showing that luminespib was more potent and synergistic after preincubation with HDACi [29,34]. Synergy improves the efficiency of a therapy and could also help to reduce employed concentrations, thus avoiding side effects limiting clinical application [50]. Maximum concentrations used in our study (10 nM luminespib, 15 nM HSP990, and 25 nM panobinostat) were far below the maximum plasma levels resulting from application of the maximum tolerated dose (2.4 μM for luminespib, 1.3 μM for HSP990 and 721 nM for panobinostat) [51–53]. Preincubation with HDACi leads to hyperacetylation of histone and non-histone proteins, including HSP90 [54], mediated at least by HDAC6 and HDAC10 [35]. Increase in HSP90 acetylation then results in HSP90 inhibition, which is further boosted by addition of HSP90i [54], thus explaining the synergistic behavior of combinations of HDACi and HSP90i (Figure 2 and Figure S5). Since the contribution of different HDAC subtypes to the effect of HSP90i is not completely understood and an HDAC6-selective inhibitor showed no superior effect over pan-HDACi in increasing the chemosensitivity of cisplatin [33,41], we decided to use the pan-HDACi panobinostat and LMK235 [32].

Based on the promising results of dual combinations of HDACi and HSP90i in ovarian cancer, we evaluated the potential of triple combinations of HDACi, HSP90i and cisplatin. As can be seen in Figure S7 and Table 2 and Table S3B,C, triple combinations were not superior to dual combinations of HSP90i and cisplatin or HDACi and cisplatin, regardless of the order of application of HDACi, HSP90i and cisplatin. Between almost all applied combinations (dual and triple combinations) were no significant differences in IC_{50} values of cisplatin in A2780 or A2780CisR (Table 2). However, the best effects of HDACi in increasing cisplatin potency (highest shift factors) were observed in A2780 and not in A2780CisR (Table S3B,C). In A2780 cells, the largest increase in cisplatin potency was obtained by 48 h preincubation with HSP990 (shift factor: 6.7), panobinostat (shift factor: 5.9)

or LMK235 (shift factor: 5.9). In A2780CisR cells, neither combination led to a complete reversal of cisplatin resistance, except if the preincubation time of HDACi was extended from 48 to 72 h (Figure 8 and Table S5). In contrast, 48 h preincubation with panobinostat was sufficient for complete reversal of cisplatin resistance in the HGSOC cell line CaOV3CisR (Table 3). HSP90i increased cisplatin sensitivity but did not overcome (completely reverse) cisplatin resistance in A2780CisR, CaOV3CisR or OVCAR3CisR. High HSP90 expression is associated with drug resistance [55], however, A2780CisR cells did not show increased HSP90 expression compared to A2780 (Figure 1C,D). In addition, in a previous study, we were also not able to reverse a fully established cisplatin resistance by various kinase inhibitors [26]. Since an extended preincubation time of panobinostat (72 h instead of 48 h) led to a complete reversal of cisplatin resistance (Figure 8), we were interested in studying the effects of long-term, sub-cytotoxic concentrations of panobinostat on the development of chemoresistance against cisplatin. For comparison, the HSP90i luminespib was included. Chemoresistance against cisplatin was induced as previously described [26,38,56]. Cells were exposed to IC_{50} of cisplatin for 6h followed by washout and recovery for one week (termed as "treatment cycle"). We demonstrated that one treatment cycle in continuous presence of low concentrations of HDACi (5 nM panobinostat or 200 nM LMK235) significantly increased the potency of cisplatin as noticed by a resistance factor of less than 1 (Figure 9A). The HSP90i luminespib also led to an increase in cisplatin potency but this effect was not significant. Of note, long-term incubation of low concentrations of HDACi for up to 21 treatment cycles prevented almost completely the development of cisplatin resistance (Figure 9B). Permanent presence of 200 nM LMK235 gave a resistance factor of 1.7, whereas, in the absence of LMK235, a resistance factor of 4.5 was obtained. This shows that epigenetic modulation by HDACi is able to prevent the development of chemoresistance against cisplatin. Interestingly, these data are in accordance with results previously published by us using resveratrol or ellagic acid (which have also been described as HDACi) to prevent the development of resistance against cisplatin [26].

HDACi are known to induce apoptosis in ovarian cancer cells by modulating the expression of genes regulating cell growth, cell cycle progression or apoptosis [57]. Apoptosis induction by HSP90i has also been described for various cancers [58]. We were thus interested in the regulation of key genes of apoptosis, cell survival, and cell cycle by HSP90i, HDACi, and cisplatin. Proapoptotic *APAF-1* is upregulated by HDACi in hepatocellular carcinomas [59]. Overexpression of *survivin* is known to be associated with poor prognosis and high-grade cancers [60]. A high expression of *p21* could be a predictor of cisplatin sensitivity in ovarian cancer [61]. We thus examined expression of the key genes *APAF-1*, *survivin*, and *p21* in PCR and Western blot (Figures 3–6).

Effects were most pronounced in A2780CisR in Western blot. Survivin expression was even increased upon treatment with cisplatin or luminespib (or their combination) in A2780CisR (Figure 5), possibly explaining the lower effect of HSP90i in cisplatin resistant cells (Table 2). However, panobinostat and any combination thereof, reduced expression of survivin, giving a further hint to the stronger effect of HDACi over HSP90i. p21 expression was increased upon panobinostat (or panobinostat-containing combinations) but unaffected by luminespib and only slightly increased under cisplatin treatment, again explaining superior effects of HDACi in inducing cell cycle arrest via p21 followed by apoptosis or caspase 3/7 activation (Figure 4, Figures S6E, S7C and S8). *APAF-1* regulation was affected by the modulators similar as p21. Luminespib gave almost no increase in *APAF-1*, whereas panobinostat and cisplatin increased APAF-1 in A2780CisR cells (Figures 3, 5 and 6). Taken together, the effects of HDACi on gene expression of survivin, p21, and APAF-1 may explain increased apoptosis and caspase activation including synergy with the DNA-damaging agent cisplatin. Further, effects on gene expression by panobinostat observed in this study are in accordance with previous results from our group [33]. Interestingly, the triple combination of HDACi, HSP90i and cisplatin is less advantageous than the dual combination HDACi and cisplatin regarding increase in *APAF-1* and *p21* and decrease in survivin. The dual combination HSP90i and cisplatin is not favorable at all regarding gene expressions of *APAF-1*, *p21* and *survivin*.

In conclusion, this study revealed that preincubation with HDACi increase the potency of HSP90i in sensitive and cisplatin-resistant ovarian cancer cells but not vice versa. Further, preincubation with HDACi or HSP90i prior to cisplatin increase cisplatin sensitivity and act synergistically. HDACi are more effective than HSP90i in cisplatin-resistant cell lines. Surprisingly, triple combinations of HSP90i, HDACi and cisplatin were not superior to dual combinations of HDACi and cisplatin. Finally, permanent presence of low concentrations of HDACi significantly impedes the development of cisplatin resistance. Thus, combinations of HDACi and HSP90i as well as combinations of HDACi and cisplatin may improve the therapeutic outcome of ovarian cancer, in particular of HGSOC.

4. Materials and Methods

4.1. Materials

Materials and reagents for cell culture were purchased from PAN Biotech (Aidenbach, Germany) unless otherwise stated. Cisplatin was from Sigma-Aldrich (Steinheim, Germany) and 3-(4,5-dimethylthiazol-2-yl)-2,5-diphenyltetrazolium bromide (MTT) from Serva (Heidelberg, Germany). Luminespib and HSP990 were gifts from Novartis, Basel, Switzerland. Panobinostat was purchased from Selleckchem (Eching, Germany). LMK235 was synthesized in the group of Prof. T. Kurz, Heinrich Heine University, Duesseldorf, Germany.

4.2. Cell Lines

The human embryonic kidney cells HEK293 was obtained from the German Collection of Microorganism and Cell Cultures (DSMZ, Braunschweig, Germany). The human ovarian carcinoma cell lines CaOV3 and OVCAR3 were obtained from American Type Culture Collection (ATCC, Manassas, Virginia, USA). The human ovarian carcinoma cell line A2780 was obtained from European Collection of Cell Cultures (ECACC, Salisbury, UK). The cisplatin resistant sublines A2780CisR, CaOV3CisR, and OVCAR3CisR were generated by exposing the parental cell line to weekly cycles of cisplatin in an IC_{50} concentration according to Gosepath et al. [56]. Results of STR analysis of A2780 and A2780CisR can be found in Table S7. Both cell lines have been previously characterized in our group [25,26]. Cisplatin resistant cell lines in the presence of an inhibitor were generated in an analogous manner in the permanent presence of 3 nM luminespib, 5 nM panobinostat or 200 nM LMK235.

Cells were grown at 37 °C under humidified air supplemented with 5% CO_2 in RPMI 1640 (A2780, CaOV3 and, OVCAR3) or DMEM (HEK293) containing 10% heat inactivated fetal calf serum, 120 IU/mL penicillin, and 120 µg/mL streptomycin.

4.3. Cell Viability Assay

The cytotoxic activity of the inhibitors and cisplatin was evaluated by an MTT assay as previously described [26,32,33]. To analyze the interactions between HSP90i and HDACi, cells were preincubated with one of these inhibitors for 48h followed by treatment for 72 h together with the second inhibitor. To determine the effect of HSP90i and HDACi on cisplatin sensitivity, inhibitors were coincubated for 72 h with cisplatin or preincubated for 48 h prior to cisplatin addition. Total incubation time of cells never exceeded 120 h. All experiments were performed at least three times in triplicates. Shift factors (SF) were calculated by dividing the IC_{50} value from single agent-treated cells by the IC_{50} value of combined treated cells. Resistance factors (RF) were calculated as the ratio between IC_{50} values of cisplatin-resistant cells and the sensitive subline.

4.4. Doubling Time

A2780 and A2780CisR cells were plated in 24-well plates (Sarstedt AG, Nürmbrecht, Germany) and incubated under culture conditions for 24 h. After 24 h, initial cell number was determined and cells were incubated with HSP90i or HDACi for additional 24, 48, and 72 h. After each time point, cells were harvested by trypsin-EDTA, diluted in 0.9% NaCl with 0.1% NaN_3 (Acros Organics, Geel,

Belgium) and counted by flow cytometry (Partec GmbH, Muenster, Germany). Doubling time was calculated using GraphPad Prism v. 4.0 (GraphPad Software Inc, San Diego, USA).

4.5. Analysis of Apoptosis Induction

To determine the number of apoptotic cells, A2780 and A2780CisR cells were treated in 24-well plates with the indicated concentrations of the inhibitors for 24 or 48 h. If mentioned, cells were first treated for 48 h with indicated inhibitor and then treated for 6 h with the IC_{50} of cisplatin. Next, cells recovered for 24 h. After total incubation time, cells were lysed overnight in hypotonic staining buffer (0.1% Triton X-100, 0.1% sodium citrate in sterile water) containing 100 µg/mL propidium iodide (PI, PromoCell, Heidelberg, Germany) and analyzed by flow cytometry (Partec GmbH, Muenster, Germany). Ten percent DMSO incubated for 24 h served as positive control for apoptosis induction.

4.6. Immunoblotting

Cells were treated with the inhibitors for the indicated time periods. After treatment, cells were lysed by using Lysis Buffer 6 (R&D Systems Inc, Minneapolis, MN, USA). Protein concentration was determined with the bicinchoninic acid (BCA) protein assay. From 20 to 30 µg of protein were separated by SDS-PAGE (8% polyacrylamide gel for AKT and pAKT, 12% polyacrylamide gel for α-Tubulin and Acetyl-α-Tubulin) and transferred to PVDF membrane (Millipore Corporation, Billerica, MA, USA). Blots were incubated with primary antibodies against HSP90 α/β (Cat. No. sc-7947), AKT (Cat. No. sc-8312), phospho AKT (5.Ser 473, Cat. No. sc-293125), β-actin (Cat. No. sc-47778), α-tubulin (Cat. No. sc-8035) (Santa Cruz Biotechnology, Heidelberg, Germany), APAF-1 (Cat. No. MAB868), survivin (Cat. No. AF886) and p21 (AF1047) (Bio-Techne GmbH, Wiesbaden-Nordenstadt, Germany). Membranes were incubated with the corresponding HRP-conjugated secondary antibody (R&D Systems Inc, Minneapolis, MN, USA). Proteins were visualized using luminol reagent (Santa Cruz Biotechnology, Heidelberg, Germany) and an INTAS Science Imaging Instrument (Chemo Imager INTAS, Goettingen, Germany).

4.7. RNA Extraction and PCR

Cells were treated with the indicated conditions and harvested at 70–80% confluence. Total RNA extraction was performed using RNeasy Mini Kit with DNase treatment according to the manufacturer's instructions (Qiagen, Hilden, Germany). Total RNA (µg) was reverse transcribed using the High Capacity cDNA Reverse Transcription Kit (Thermo Scientific, Wesel, Germany). Thermocycler program setting was initiated for 10 min at 25 °C, followed by 120 min at 37 °C. In total, 20 µg cDNA were diluted in 100 µL TE buffer (1 mM Tris-HCl, 0.1 mM EDTA in distilled water; pH 7.50). Specific primers (Sigma Aldrich, Steinheim, Germany, Table 5) were designed by Primer-BLAST (NIH, Bethesda, Maryland, USA) [62]. The PCR program consisted of an initial denaturation step at 95 °C for 2 min for the first cycle then continued with 94 °C for 20 s, 57 °C for 30 s and 72 °C for 60 s for 40 cycles. The PCR products were separated using 2% agarose gel in TAE buffer (2.42 g Tris, 0.57 mL acetic acid and 185 mg EDTA disodium salt in 500 mL distilled water). DNA bands were stained using GelRed (New England Biolabs, Frankfurt, Germany) and detected with an Intas Gel iX Imager UV system (INTAS, Goettingen, Germany). GeneRuler 50 bp (Thermo Scientific, Wesel, Germany) was used as DNA ladder and *β-tubulin* served as housekeeping gene.

Table 5. Primer sequences for PCR.

Gene.	Primer Forward	Primer Reverse	Size [bp]
BAK	GAACAGGAGGCTGAAGGGGT	TCAGGCCATGCTGGTAGACG	307
survivin	CGAGGCTGGCTTCATCCACT	ACGGCGCACTTTCTTCGCA	283
Bcl-xL	CTGAATCGGAGATGGAGACC	TGGGATGTCAGGTCACTGAA	211
BAX	GATGCGTCCACCAAGAAGCT	CGGCCCCAGTTGAAGTTG	170
β-tubulin (TUBB)	TCTACCTCCCTCACTCAGCT	CCAGAGTCAGGGGTGTTCAT	161
Mcl-1	GGACATCAAAAACGAAGACG	GCAGCTTTCTTGGTTTATGG	154
APAF-1	ACAATGCTCTACTACATGAAGGATATAAAGA	CACTGGAAGAAGAGACAACAGGAA	81
p21	CCTAATCCGCCCACAGGAA	AAGATGTAGAGCGGGCCTTTG	68

4.8. Caspase 3/7 Activation Assay

Compound-induced activation of caspases 3 and 7 was analyzed using the CellEvent Caspase-3/7 green detection reagent (Thermo Scientific, Wesel, Germany) according to the manufacturer´s instructions. Briefly, A2780CisR cells were seeded in 96-well plates (Corning, Kaiserslautern, Germany) at a density of 4000 *c/w*. Cells were treated with panobinostat or LMK235 and/or HSP990 or luminespib (as indicated) for a maximum treatment duration of 48 h. Then, medium was removed and 50 µL of CellEvent Caspase 3/7 green detection reagent (2 µM in PBS supplemented with 5% heat inactivated FBS) was added. Cells were incubated for 30 min at 37 °C in a humidified incubator before imaging by using the Thermo Fisher ArrayScan XTI high content screening (HCS) system with a 10 X magnification (Thermo Scientific). Hoechst 33342 was used for nuclei staining.

4.9. Statistical Methods

Assays were performed at least in three independent experiments. Concentration–effect curves were obtained using Prism 4.0 from GraphPad, San Diego, CA, USA, by fitting the pooled data to the four-parameter logistic equation with variable hill slope. Flow cytometry data were analyzed using FloMax 2.82 (Partec, Muenster, Germany). Statistical significance was assessed by two-tailed Student´s t-test.

Supplementary Materials: The following are available online at http://www.mdpi.com/1422-0067/21/21/8300/s1, Figure S1: Effects of HSP90i and HDACi on cell growth and protein expression, Figure S2: Antiproliferative activity of HDACi and HSP90i against ovarian cancer cell lines, Figure S3: Concentration-dependent 48 h incubation with HSP990 (IC50, three-fold and five-fold IC50) and time-dependent incubation with three-fold IC50 of HSP990, Figure S4: Influence on the cytotoxicity of HSP90i and HDACi on each other, Figure S5: Apoptosis induction was analyzed in A2780 and A2780CisR after a 24 h incubation with an HSP90i or panobinostat followed by a 24 h incubation with both inhibitors in combination, Figure S6: HSP90i and HDACi treatment enhance the activity of cisplatin in A2780 and A2780CisR, Figure S7: Triple combination treatment (HDACi, HSP90i, cisplatin) is not superior to dual combination of HDACi and cisplatin with regard to cisplatin cytotoxicity and apoptosis induction, Figure S8: Effect of HDACi, HSP90i and drug combinations on cell cycle distribution, Figure S9: A 72 h preincubation with LMK235 (350 nM for A2780 and 500 nM for A2780CisR) (A,B) or panobinostat (10 nM for A2780 and 20 nM for A2780CisR) (C) or 48 h preincubation with HDACi followed by 24 h incubation together with HDACi and HSP90i increased cisplatin sensitivity after 48 h cisplatin treatment at A2780 (C) and A2780CisR (A,B) cells, Figure S10: Effects of HDACi or HSP90i incubation or preincubation prior to cisplatin on apoptosis related genes, Figure S11: Effects of HDACi or HSP90i incubation or preincubation prior to cisplatin on protein expression levels, Table S1: Influence on the cytotoxicity of HSP90i and HDACi on each other, Table S2: Influence of dual or triple combinations with HDACi or HSP90i on the cytotoxic activity of cisplatin in A2780 and A2780CisR cells, Table S3: Shift factors of dual or triple combinations with HDACi or HSP90i on the cytotoxic activity of cisplatin in A2780 and A2780CisR cells, Table S4: Influence of dual combinations with panobinostat or HSP990 on the cytotoxic activity of cisplatin in CaOV3, CaOV3CisR, OVCAR3, and OVCAR3CisR cells, Table S5: Effects of short-term treatment with HDACi or HSP90i on cisplatin sensitivity of A2780/A2780CisR ovarian cancer cells, Table S6: Influence of HDACi/HSP90i preincubation on cisplatin sensitivity of non-tumor cell line HEK293, Table S7: Results of STR analysis of A2780 and A2780CisR.

Author Contributions: Conceptualization, M.U.K and A.H.; formal analysis, A.J.R.M. and J.J.B..; investigation, A.J.R.M. and J.J.B.; resources, M.U.K., T.K. and F.K.H.; writing—original draft preparation, A.J.R.M. and J.J.B..; writing—review and editing, M.U.K. and A.H.; visualization, A.J.R.M. and J.J.B.; supervision, M.U.K. and A.H.; and funding acquisition, M.U.K. All authors have read and agreed to the published version of the manuscript.

Funding: This research was funded by Deutsche Forschungsgemeinschaft (DFG), grant number KA 1942/1-1 and from the DFG grant (INST208/690-1) for purchasing the Thermofisher Arrayscan XTI High Content Platform used in this study.

Acknowledgments: We acknowledge support from Heinrich-Heine-University Düsseldorf.

Conflicts of Interest: The authors declare no conflict of interest.

Abbreviations

(p)Akt/AKT	(phosphorylated) protein kinase B
APAF-1	apoptotic protease activating factor 1
BAK	Bcl-2 homologous antagonist killer
BAX	Bcl-2-associated X protein
Bcl-xL	B-cell lymphoma-extra large
cDDP	*cis*-diamminedichloroplatinum(II) (cisplatin)
coinc	coincubation
HDAC	histone deacetylase
HDACi	histone deacetylase inhibitor
HSP90	heat shock protein 90
HSP90i	heat shock protein 90 inhibitor
HSP990	NVP-HSP990
lumi	luminespib; NVP-AUY922
pano	panobinostat
PCR	polymerase chain reaction
preinc	preincubation

References

1. Ward, E.M.; Sherman, R.L.; Henley, S.J.; Jemal, A.; Siegel, D.A.; Feuer, E.J.; Firth, A.U.; Kohler, B.A.; Scott, S.; Ma, J.; et al. Annual Report to the Nation on the Status of Cancer, Featuring Cancer in Men and Women Age 20–49 Years. *J. Natl Cancer Inst.* **2019**, *111*, 1279–1297. [CrossRef] [PubMed]
2. Cancer of the Ovary—Cancer Stat Facts. Available online: https://seer.cancer.gov/statfacts/html/ovary.html (accessed on 1 March 2020).
3. Krebs—Datenbankabfrage—RKI. Available online: https://www.krebsdaten.de/Krebs/SiteGlobals/Forms/Datenbankabfrage/datenbankabfrage_stufe2_form.html (accessed on 1 March 2020).
4. Buttmann-Schweiger, N.; Kraywinkel, K. Epidemiologie von Eierstockkrebs in Deutschland. *Onkologe* **2019**, *25*, 92–98. [CrossRef]
5. Home | American Cancer Society—Cancer Facts & Statistics. Available online: https://cancerstatisticscenter.cancer.org/#!/ (accessed on 18 October 2020).
6. Wagner, U.; Harter, P.; Hilpert, F.; Mahner, S.; Reuß, A.; du Bois, A.; Petru, E.; Meier, W.; Ortner, P.; König, K.; et al. S3-Guideline on Diagnostics, Therapy and Follow-up of Malignant Ovarian Tumours: Short version 1.0—AWMF registration number: 032/035OL, June 2013. *Geburtshilfe Frauenheilkd* **2013**, *73*, 874–889. [CrossRef] [PubMed]
7. Pchejetski, D.; Alfraidi, A.; Sacco, K.; Alshaker, H.; Muhammad, A.; Monzon, L. Histone deacetylases as new therapy targets for platinum-resistant epithelial ovarian cancer. *J. Cancer Res. Clin. Oncol* **2016**, *142*, 1659–1671. [CrossRef] [PubMed]
8. Eisenhauer, E.A. Real-world evidence in the treatment of ovarian cancer. *Ann. Oncol.* **2017**, *28*, viii61–viii65. [CrossRef] [PubMed]
9. Kehoe, S.; Hook, J.; Nankivell, M.; Jayson, G.C.; Kitchener, H.; Lopes, T.; Luesley, D.; Perren, T.; Bannoo, S.; Mascarenhas, M.; et al. Primary chemotherapy versus primary surgery for newly diagnosed advanced ovarian cancer (CHORUS): An open-label, randomised, controlled, non-inferiority trial. *Lancet* **2015**, *386*, 249–257. [CrossRef]
10. Vergote, I.; Tropé, C.G.; Amant, F.; Kristensen, G.B.; Ehlen, T.; Johnson, N.; Verheijen, R.H.M.; van der Burg, M.E.L.; Lacave, A.J.; Panici, P.B.; et al. Neoadjuvant Chemotherapy or Primary Surgery in Stage IIIC or IV Ovarian Cancer. *New Engl. J. Med.* **2010**, *363*, 943–953. [CrossRef]

11. Balch, C.; Huang, T.H.-M.; Brown, R.; Nephew, K.P. The epigenetics of ovarian cancer drug resistance and resensitization. *Am. J. Obstet. Gynecol.* **2004**, *191*, 1552–1572. [CrossRef]
12. Galluzzi, L.; Senovilla, L.; Vitale, I.; Michels, J.; Martins, I.; Kepp, O.; Castedo, M.; Kroemer, G. Molecular mechanisms of cisplatin resistance. *Oncogene* **2012**, *31*, 1869–1883. [CrossRef] [PubMed]
13. Khabele, D. The Therapeutic Potential of Class I Selective Histone Deacetylase Inhibitors in Ovarian Cancer. *Front. Oncol.* **2014**, 4. [CrossRef]
14. Eckl, J.M.; Richter, K. Functions of the Hsp90 chaperone system: Lifting client proteins to new heights. *Int J. Biochem Mol. Biol.* **2013**, *4*, 157–165.
15. Prodromou, C. Mechanisms of Hsp90 regulation. *Biochem J.* **2016**, *473*, 2439–2452. [CrossRef] [PubMed]
16. Liu, H.; Xiao, F.; Serebriiskii, I.G.; O'Brien, S.W.; Maglaty, M.A.; Astsaturov, I.; Litwin, S.; Martin, L.P.; Proia, D.A.; Golemis, E.A.; et al. Network analysis identifies an HSP90-central hub susceptible in ovarian cancer. *Clin. Cancer Res.* **2013**, *19*, 5053–5067. [CrossRef]
17. Maloney, A.; Clarke, P.A.; Naaby-Hansen, S.; Stein, R.; Koopman, J.-O.; Akpan, A.; Yang, A.; Zvelebil, M.; Cramer, R.; Stimson, L.; et al. Gene and protein expression profiling of human ovarian cancer cells treated with the heat shock protein 90 inhibitor 17-allylamino-17-demethoxygeldanamycin. *Cancer Res.* **2007**, *67*, 3239–3253. [CrossRef] [PubMed]
18. Richter, K.; Hendershot, L.M.; Freeman, B.C. The cellular world according to Hsp90. *Nat. Struct. Mol. Biol.* **2007**, *14*, 90–94. [CrossRef]
19. Mielczarek-Lewandowska, A.; Hartman, M.L.; Czyz, M. Inhibitors of HSP90 in melanoma. *Apoptosis* **2020**, *25*, 12–28. [CrossRef]
20. Vasilevskaya, I.A.; Rakitina, T.V.; O'Dwyer, P.J. Quantitative effects on c-Jun N-terminal protein kinase signaling determine synergistic interaction of cisplatin and 17-allylamino-17-demethoxygeldanamycin in colon cancer cell lines. *Mol. Pharmacol.* **2004**, *65*, 235–243. [CrossRef]
21. Zhang, Z.; Xie, Z.; Sun, G.; Yang, P.; Li, J.; Yang, H.; Xiao, S.; Liu, Y.; Qiu, H.; Qin, L.; et al. Reversing drug resistance of cisplatin by hsp90 inhibitors in human ovarian cancer cells. *Int J. Clin. Exp. Med.* **2015**, *8*, 6687–6701.
22. Hoter, A.; Rizk, S.; Naim, H.Y. The Multiple Roles and Therapeutic Potential of Molecular Chaperones in Prostate Cancer. *Cancers (Basel)* **2019**, *11*, 1194. [CrossRef]
23. Kryeziu, K.; Bruun, J.; Guren, T.K.; Sveen, A.; Lothe, R.A. Combination therapies with HSP90 inhibitors against colorectal cancer. *Biochim Biophys Acta Rev. Cancer* **2019**, *1871*, 240–247. [CrossRef]
24. Dutta Gupta, S.; Bommaka, M.K.; Banerjee, A. Inhibiting protein-protein interactions of Hsp90 as a novel approach for targeting cancer. *Eur J. Med. Chem* **2019**, *178*, 48–63. [CrossRef]
25. Eckstein, N.; Servan, K.; Hildebrandt, B.; Pölitz, A.; von Jonquières, G.; Wolf-Kümmeth, S.; Napierski, I.; Hamacher, A.; Kassack, M.U.; Budczies, J.; et al. Hyperactivation of the insulin-like growth factor receptor I signaling pathway is an essential event for cisplatin resistance of ovarian cancer cells. *Cancer Res.* **2009**, *69*, 2996–3003. [CrossRef] [PubMed]
26. Engelke, L.H.; Hamacher, A.; Proksch, P.; Kassack, M.U. Ellagic Acid and Resveratrol Prevent the Development of Cisplatin Resistance in the Epithelial Ovarian Cancer Cell Line A2780. *J. Cancer* **2016**, *7*, 353–363. [CrossRef]
27. Eckschlager, T.; Plch, J.; Stiborova, M.; Hrabeta, J. Histone Deacetylase Inhibitors as Anticancer Drugs. *Int J. Mol. Sci* **2017**, *18*, 1414. [CrossRef]
28. Kim, H.-J.; Bae, S.-C. Histone deacetylase inhibitors: Molecular mechanisms of action and clinical trials as anti-cancer drugs. *Am. J. Transl Res.* **2011**, *3*, 166–179.
29. Kaiser, M.; Lamottke, B.; Mieth, M.; Jensen, M.R.; Quadt, C.; Garcia-Echeverria, C.; Atadja, P.; Heider, U.; von Metzler, I.; Türkmen, S.; et al. Synergistic action of the novel HSP90 inhibitor NVP-AUY922 with histone deacetylase inhibitors, melphalan, or doxorubicin in multiple myeloma. *Eur. J. Haematol.* **2010**, *84*, 337–344. [CrossRef]
30. Khabele, D.; Son, D.-S.; Parl, A.K.; Goldberg, G.L.; Augenlicht, L.H.; Mariadason, J.M.; Rice, V.M. Drug-induced inactivation or gene silencing of class I histone deacetylases suppresses ovarian cancer cell growth: Implications for therapy. *Cancer Biol. Ther.* **2007**, *6*, 795–801. [CrossRef]
31. Ozaki, K.; Kishikawa, F.; Tanaka, M.; Sakamoto, T.; Tanimura, S.; Kohno, M. Histone deacetylase inhibitors enhance the chemosensitivity of tumor cells with cross-resistance to a wide range of DNA-damaging drugs. *Cancer Sci.* **2008**, *99*, 376–384. [CrossRef]

32. Marek, L.; Hamacher, A.; Hansen, F.K.; Kuna, K.; Gohlke, H.; Kassack, M.U.; Kurz, T. Histone deacetylase (HDAC) inhibitors with a novel connecting unit linker region reveal a selectivity profile for HDAC4 and HDAC5 with improved activity against chemoresistant cancer cells. *J. Med. Chem.* **2013**, *56*, 427–436. [CrossRef]
33. Bandolik, J.J.; Hamacher, A.; Schrenk, C.; Weishaupt, R.; Kassack, M.U. Class I-Histone Deacetylase (HDAC) Inhibition is Superior to pan-HDAC Inhibition in Modulating Cisplatin Potency in High Grade Serous Ovarian Cancer Cell Lines. *IJMS* **2019**, *20*, 3052. [CrossRef] [PubMed]
34. Kim, S.H.; Kang, J.G.; Kim, C.S.; Ihm, S.-H.; Choi, M.G.; Yoo, H.J.; Lee, S.J. Novel Heat Shock Protein 90 Inhibitor NVP-AUY922 Synergizes With the Histone Deacetylase Inhibitor PXD101 in Induction of Death of Anaplastic Thyroid Carcinoma Cells. *J. Clin. Endocrinol. Metab.* **2015**, *100*, E253–E261. [CrossRef]
35. New, M.; Olzscha, H.; La Thangue, N.B. HDAC inhibitor-based therapies: Can we interpret the code? *Mol. Oncol* **2012**, *6*, 637–656. [CrossRef]
36. Kim, S.H.; Kang, J.G.; Kim, C.S.; Ihm, S.-H.; Choi, M.G.; Yoo, H.J.; Lee, S.J. The heat shock protein 90 inhibitor SNX5422 has a synergistic activity with histone deacetylase inhibitors in induction of death of anaplastic thyroid carcinoma cells. *Endocrine* **2016**, *51*, 274–282. [CrossRef]
37. Lamottke, B.; Kaiser, M.; Mieth, M.; Heider, U.; Gao, Z.; Nikolova, Z.; Jensen, M.R.; Sterz, J.; von Metzler, I.; Sezer, O. The novel, orally bioavailable HSP90 inhibitor NVP-HSP990 induces cell cycle arrest and apoptosis in multiple myeloma cells and acts synergistically with melphalan by increased cleavage of caspases. *Eur. J. Haematol.* **2012**, *88*, 406–415. [CrossRef] [PubMed]
38. Gohr, K.; Hamacher, A.; Engelke, L.H.; Kassack, M.U. Inhibition of PI3K/Akt/mTOR overcomes cisplatin resistance in the triple negative breast cancer cell line HCC38. *Bmc Cancer* **2017**, *17*, 711. [CrossRef]
39. Kaletsch, A.; Pinkerneil, M.; Hoffmann, M.J.; Jaguva Vasudevan, A.A.; Wang, C.; Hansen, F.K.; Wiek, C.; Hanenberg, H.; Gertzen, C.; Gohlke, H.; et al. Effects of novel HDAC inhibitors on urothelial carcinoma cells. *Clin. Epigenet* **2018**, *10*, 100. [CrossRef] [PubMed]
40. Solár, P.; Horváth, V.; Kleban, J.; Koval', J.; Solárová, Z.; Kozubík, A.; Fedorocko, P. Hsp90 inhibitor geldanamycin increases the sensitivity of resistant ovarian adenocarcinoma cell line A2780cis to cisplatin. *Neoplasma* **2007**, *54*, 127–130.
41. Diedrich, D.; Hamacher, A.; Gertzen, C.G.W.; Alves Avelar, L.A.; Reiss, G.J.; Kurz, T.; Gohlke, H.; Kassack, M.U.; Hansen, F.K. Rational design and diversity-oriented synthesis of peptoid-based selective HDAC6 inhibitors. *Chem. Commun. (Camb.)* **2016**, *52*, 3219–3222. [CrossRef] [PubMed]
42. Pflieger, M.; Hamacher, A.; Öz, T.; Horstick-Muche, N.; Boesen, B.; Schrenk, C.; Kassack, M.U.; Kurz, T. Novel α,β-unsaturated hydroxamic acid derivatives overcome cisplatin resistance. *Bioorganic Med. Chem.* **2019**, *27*, 115036. [CrossRef]
43. Weberpals, J.I.; O'Brien, A.M.; Niknejad, N.; Garbuio, K.D.; Clark-Knowles, K.V.; Dimitroulakos, J. The effect of the histone deacetylase inhibitor M344 on BRCA1 expression in breast and ovarian cancer cells. *Cancer Cell Int* **2011**, *11*, 29. [CrossRef]
44. Steele, N.; Finn, P.; Brown, R.; Plumb, J.A. Combined inhibition of DNA methylation and histone acetylation enhances gene re-expression and drug sensitivity in vivo. *Br. J. Cancer* **2009**, *100*, 758–763. [CrossRef]
45. Chen, M.-Y.; Liao, W.S.-L.; Lu, Z.; Bornmann, W.G.; Hennessey, V.; Washington, M.N.; Rosner, G.L.; Yu, Y.; Ahmed, A.A.; Bast, R.C. Decitabine and suberoylanilide hydroxamic acid (SAHA) inhibit growth of ovarian cancer cell lines and xenografts while inducing expression of imprinted tumor suppressor genes, apoptosis, G2/M arrest, and autophagy. *Cancer* **2011**, *117*, 4424–4438. [CrossRef]
46. Zitzmann, K.; Ailer, G.; Vlotides, G.; Spoettl, G.; Maurer, J.; Göke, B.; Beuschlein, F.; Auernhammer, C.J. Potent antitumor activity of the novel HSP90 inhibitors AUY922 and HSP990 in neuroendocrine carcinoid cells. *Int. J. Oncol.* **2013**, *43*, 1824–1832. [CrossRef]
47. Brown, R.; Curry, E.; Magnani, L.; Wilhelm-Benartzi, C.S.; Borley, J. Poised epigenetic states and acquired drug resistance in cancer. *Nat. Rev. Cancer* **2014**, *14*, 747–753. [CrossRef]
48. Chou, T.-C. Drug combination studies and their synergy quantification using the Chou-Talalay method. *Cancer Res.* **2010**, *70*, 440–446. [CrossRef]
49. Ong, P.-S.; Wang, X.-Q.; Lin, H.-S.; Chan, S.-Y.; Ho, P.C. Synergistic effects of suberoylanilide hydroxamic acid combined with cisplatin causing cell cycle arrest independent apoptosis in platinum-resistant ovarian cancer cells. *Int. J. Oncol.* **2012**, *40*, 1705–1713. [CrossRef]

50. Sidera, K.; Patsavoudi, E. HSP90 inhibitors: Current development and potential in cancer therapy. *Recent Pat. Anticancer Drug Discov* **2014**, *9*, 1–20. [CrossRef]
51. Johnson, M.L.; Yu, H.A.; Hart, E.M.; Weitner, B.B.; Rademaker, A.W.; Patel, J.D.; Kris, M.G.; Riely, G.J. Phase I/II Study of HSP90 Inhibitor AUY922 and Erlotinib for EGFR-Mutant Lung Cancer With Acquired Resistance to Epidermal Growth Factor Receptor Tyrosine Kinase Inhibitors. *J. Clin. Oncol.* **2015**, *33*, 1666–1673. [CrossRef]
52. Spreafico, A.; Delord, J.-P.; De Mattos-Arruda, L.; Berge, Y.; Rodon, J.; Cottura, E.; Bedard, P.L.; Akimov, M.; Lu, H.; Pain, S.; et al. A first-in-human phase I, dose-escalation, multicentre study of HSP990 administered orally in adult patients with advanced solid malignancies. *Br. J. Cancer* **2015**, *112*, 650–659. [CrossRef]
53. Sharma, S.; Beck, J.; Mita, M.; Paul, S.; Woo, M.M.; Squier, M.; Gadbaw, B.; Prince, H.M. A phase I dose-escalation study of intravenous panobinostat in patients with lymphoma and solid tumors. *Invest. New Drugs* **2013**, *31*, 974–985. [CrossRef]
54. Kovacs, J.J.; Murphy, P.J.M.; Gaillard, S.; Zhao, X.; Wu, J.-T.; Nicchitta, C.V.; Yoshida, M.; Toft, D.O.; Pratt, W.B.; Yao, T.-P. HDAC6 regulates Hsp90 acetylation and chaperone-dependent activation of glucocorticoid receptor. *Mol. Cell* **2005**, *18*, 601–607. [CrossRef] [PubMed]
55. Whitesell, L.; Lindquist, S.L. HSP90 and the chaperoning of cancer. *Nat. Rev. Cancer* **2005**, *5*, 761–772. [CrossRef]
56. Gosepath, E.M.; Eckstein, N.; Hamacher, A.; Servan, K.; von Jonquieres, G.; Lage, H.; Györffy, B.; Royer, H.D.; Kassack, M.U. Acquired cisplatin resistance in the head-neck cancer cell line Cal27 is associated with decreased DKK1 expression and can partially be reversed by overexpression of DKK1. *Int. J. Cancer* **2008**, *123*, 2013–2019. [CrossRef] [PubMed]
57. Takai, N.; Narahara, H. Human Endometrial and Ovarian Cancer Cells: Histone Deacetylase Inhibitors Exhibit Antiproliferative Activity, Potently Induce Cell Cycle Arrest, and Stimulate Apoptosis. Available online: http://www.eurekaselect.com/59959/article (accessed on 14 May 2019).
58. Rong, B.; Yang, S. Molecular mechanism and targeted therapy of Hsp90 involved in lung cancer: New discoveries and developments (Review). *Int. J. Oncol.* **2018**, *52*, 321–336. [CrossRef] [PubMed]
59. Buurman, R.; Sandbothe, M.; Schlegelberger, B.; Skawran, B. HDAC inhibition activates the apoptosome via Apaf1 upregulation in hepatocellular carcinoma. *Eur. J. Med. Res.* **2016**, *21*, 26. [CrossRef]
60. Jaiswal, P.K.; Goel, A.; Mittal, R.D. Survivin: A molecular biomarker in cancer. *Indian J. Med. Res.* **2015**, *141*, 389–397. [CrossRef]
61. Rose, S.L.; Goodheart, M.J.; DeYoung, B.R.; Smith, B.J.; Buller, R.E. p21 expression predicts outcome in p53-null ovarian carcinoma. *Clin. Cancer Res.* **2003**, *9*, 1028–1032.
62. Ye, J.; Coulouris, G.; Zaretskaya, I.; Cutcutache, I.; Rozen, S.; Madden, T.L. Primer-BLAST: A tool to design target-specific primers for polymerase chain reaction. *Bmc Bioinform.* **2012**, *13*, 134. [CrossRef]

Supplemental Information

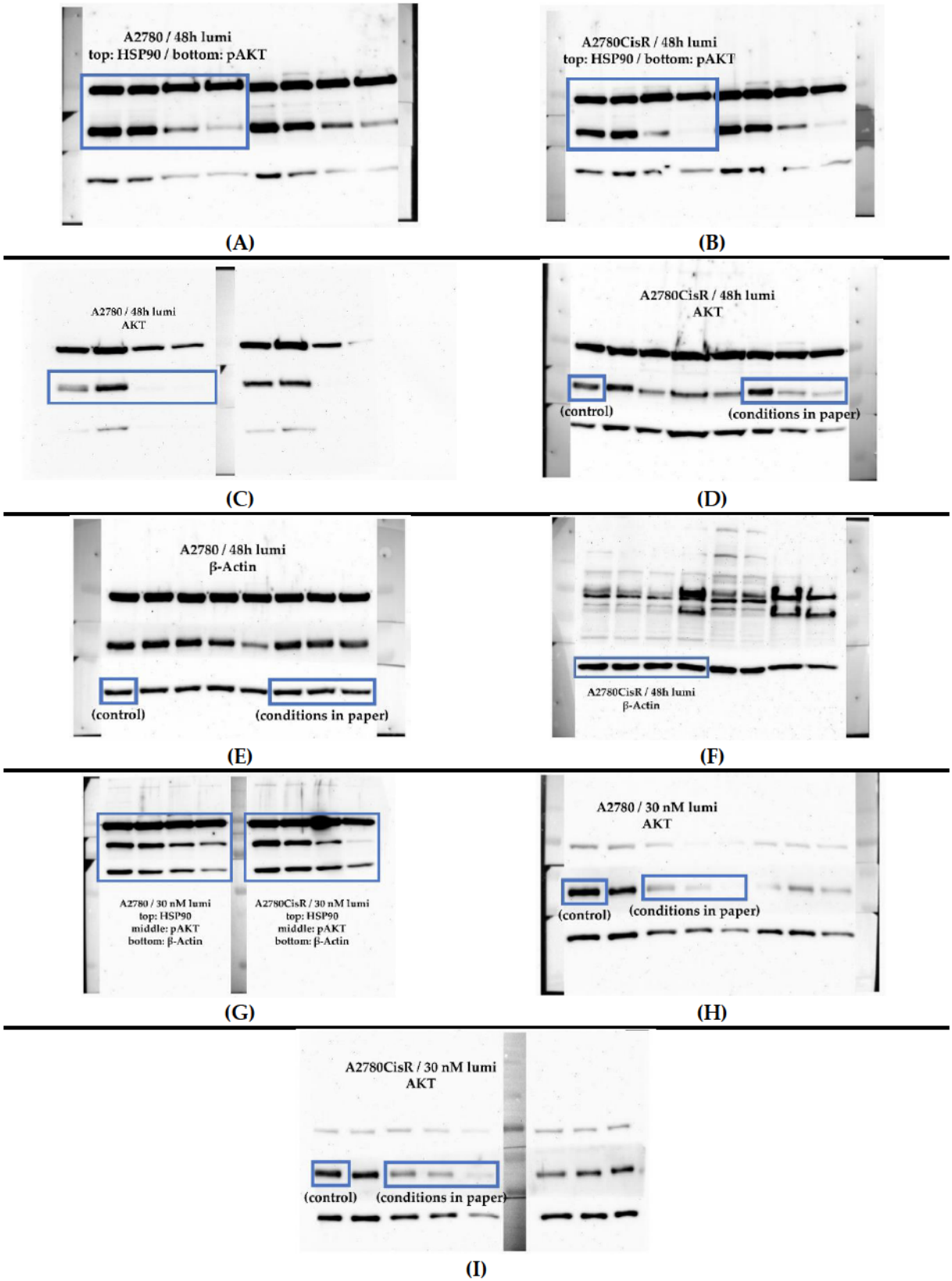

Figure S1. Effects of HSP90i and HDACi on cell growth and protein expression in A2780 and A2780CisR cells. Shown are the uncropped, labeled, and representative immunoblots from which Figure 1C was assembled.

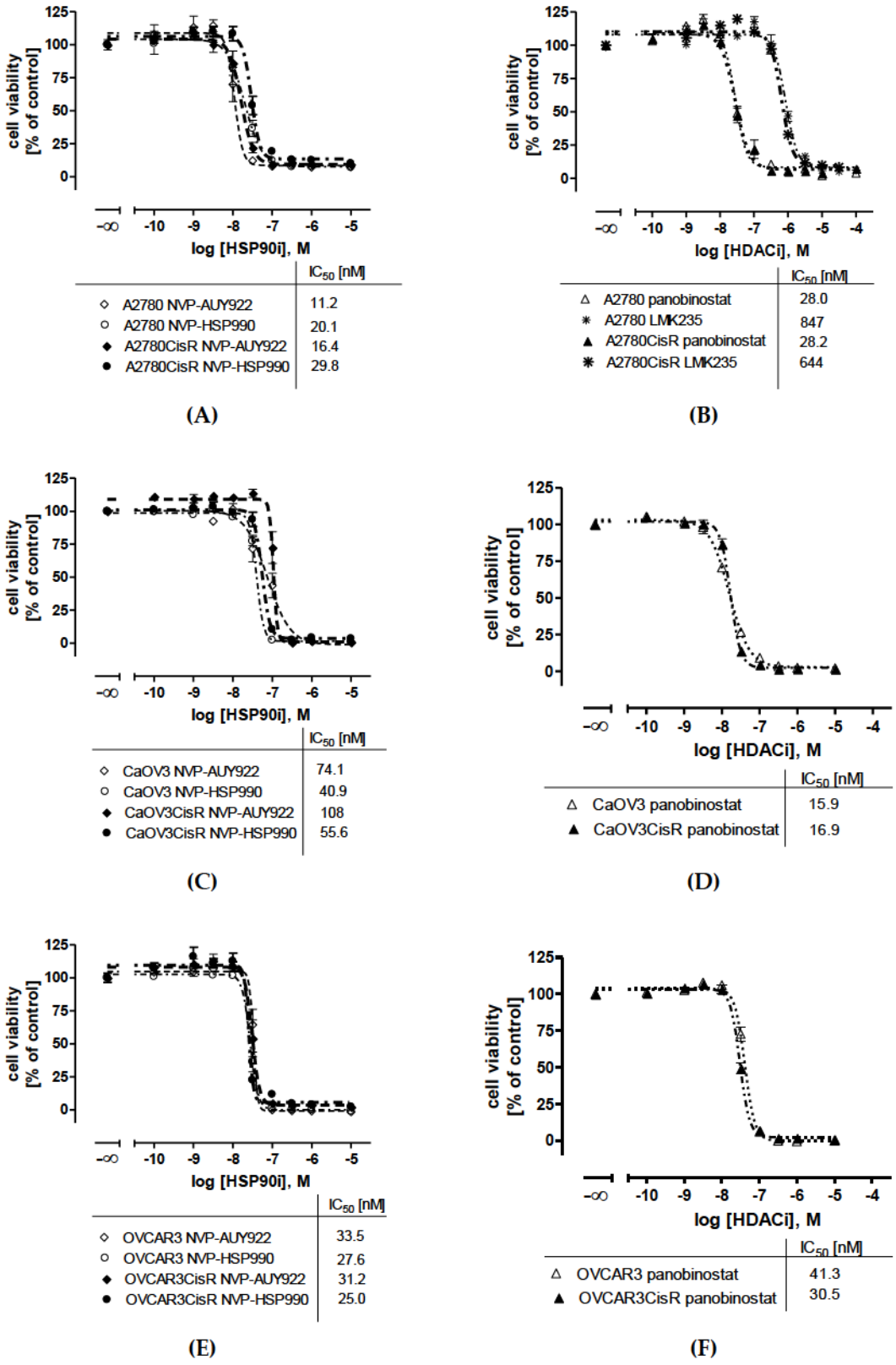

Figure S2. Antiproliferative activity of HDACi and HSP90i against ovarian cancer cell lines. The cytotoxic activity of the HSP90i luminespib and NVP-HSP990 and the HDACi panobinostat was determined against A2780 **(A,B)**, CaOV3 **(C,D)**, OVCAR3 **(E,F)** and their cisplatin resistant sublines with a MTT assay after a 72h incubation. The HDACi LMK235 was characterized at A2780 and A2780CisR **(A,B)**. Data shown were determined in at least three independent experiments each performed in triplicates. Graphs show average ± SD. IC_{50}, pIC_{50}, and SEM were summarized in Table 1.

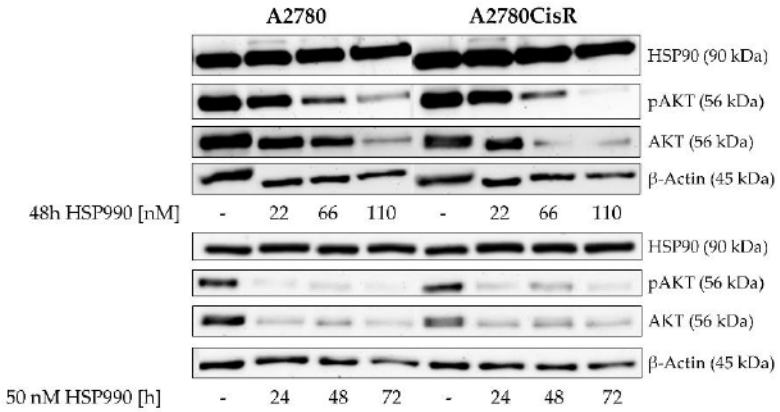

Figure S3. Concentration-dependent 48h incubation with HSP990 (IC_{50}, 3-fold and 5-fold IC_{50}) and time-dependent incubation with 3-fold IC_{50} of HSP990 led to a decrease in AKT expression and AKT phosphorylation. Shown is a representative experiment out of three.

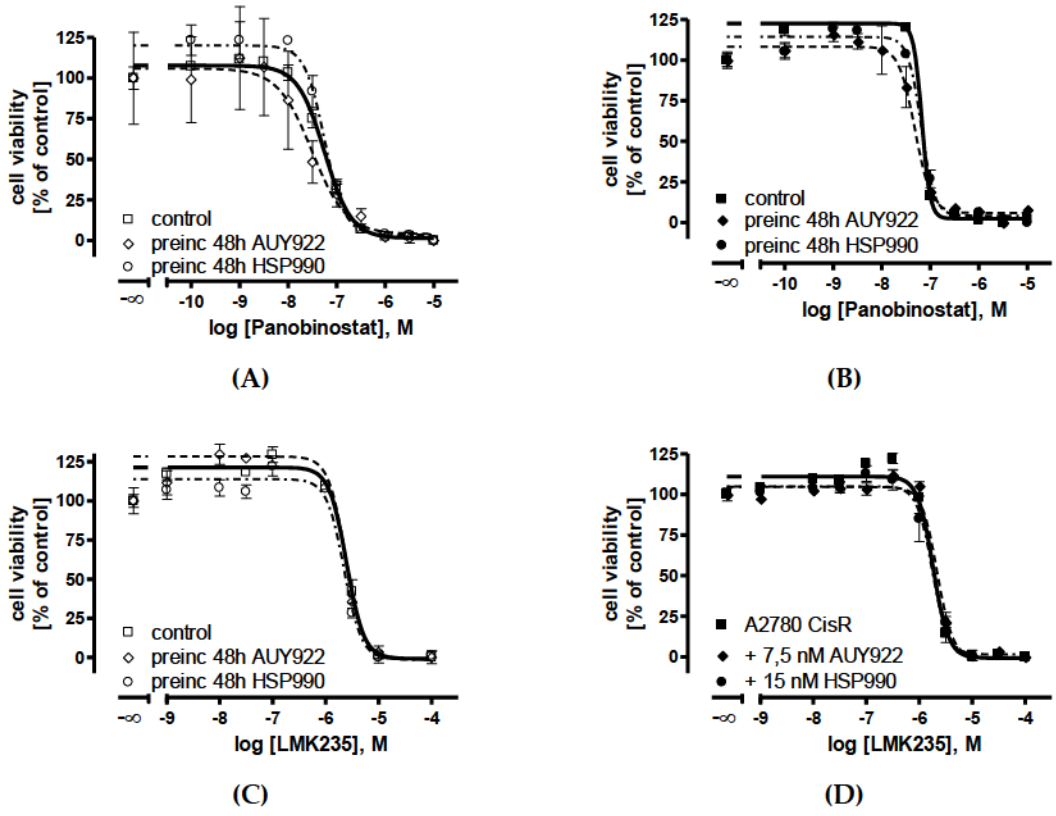

Figure S4. Influence on the cytotoxicity of HSP90i and HDACi on each other. A 48h preincubation with the HSP90i (luminespib or HSP990 did not influence the cytotoxic activity of panobinostat **(A,B)** or LMK235 **(C,D)** in A2780 **(A,C)** and A2780CisR **(B,D)**. Concentrations used were 5 nM luminespib and 10 nM NVP-HSP990 for A2780; 7.5 nM luminespib and 15 nM NVP-HSP990 for A2780CisR. Graphs shown are average ± SD from at least three independent experiments each performed in triplicates. Control is the concentration effect curve of cisplatin with the indicated cell line without any pretreatment. IC_{50} (pIC_{50} ± SEM) and significances are shown in Table S1.

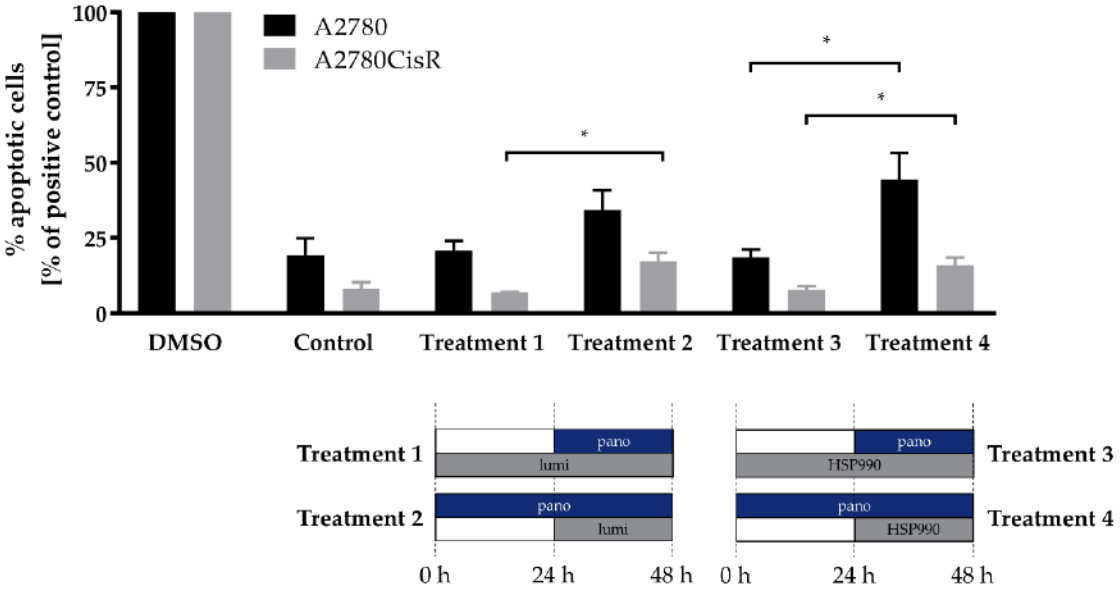

Figure S5. Apoptosis induction was analyzed in A2780 and A2780CisR after a 24h incubation with an HSP90i or panobinostat followed by a 24h incubation with both inhibitors in combination. Maximum incubation time did not exceed 48h. Concentrations used were 10 nM panobinostat, 5 nM luminespib and 10 nM HSP990 in A2780 and 20 nM panobinostat, 7.5 luminespib and 15 nM HSP990 in A2780CisR. 10% DMSO for 24h was used as positive control for apoptosis induction. Values were normalized to the effect of 10% DMSO. Experimental treatment schemes 1-4: To analyze the effect of panobinostat (pano) on HSP90i (luminespib = lumi) and vice versa, one inhibitor was preincubated for 24h before the other was applied for an additional 24h incubation. Data shown are mean ± SEM of three independent experiments each carried out in triplicates. Statistical analysis was performed using t-test. Levels of significance: * ($p \leq 0.05$); ** ($p \leq 0.01$); *** ($p \leq 0.001$).

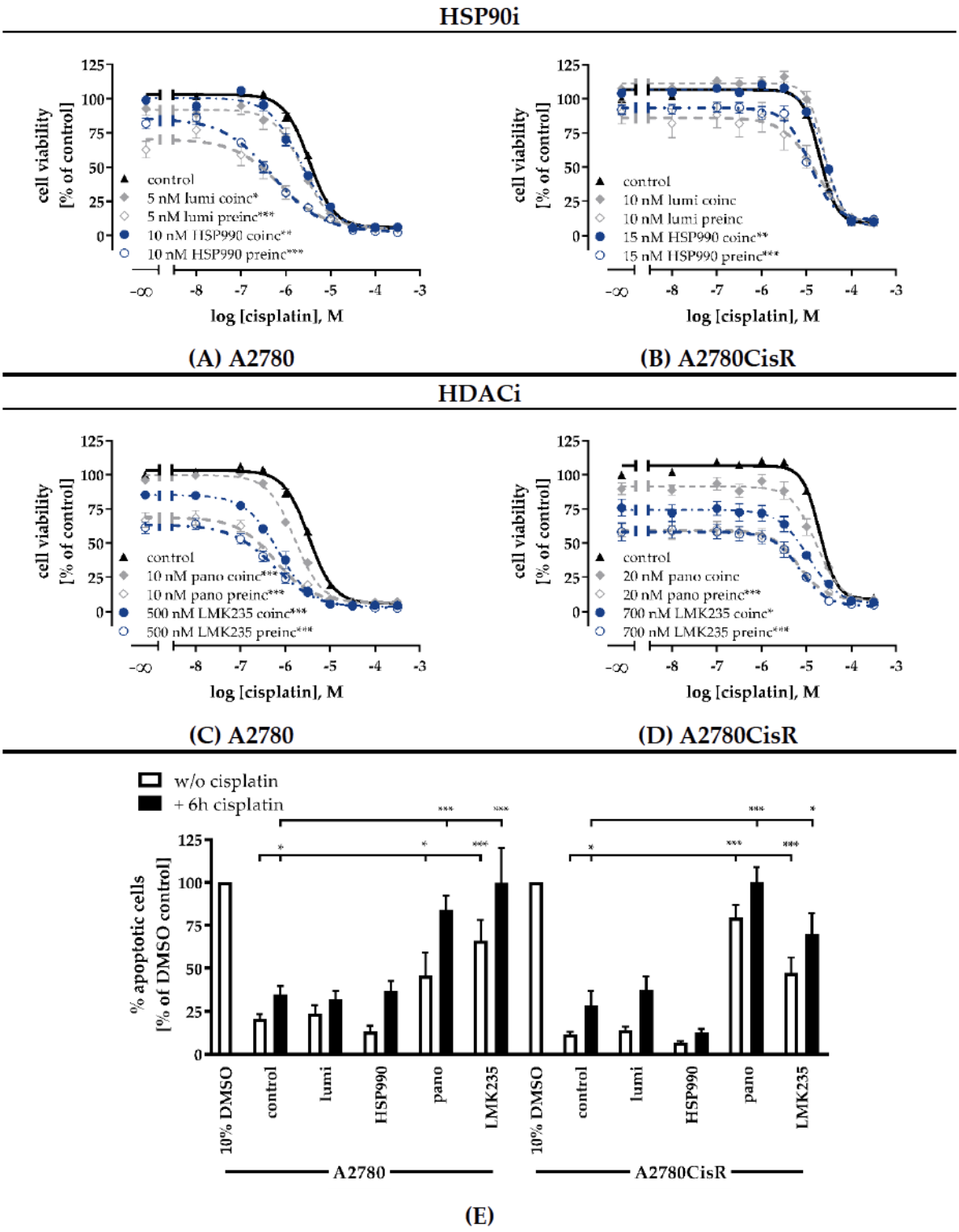

Figure S6. HSP90i and HDACi treatment enhance the activity of cisplatin in A2780 and A2780CisR. Coincubation of cisplatin (coinc) or a 48h preincubation prior to cisplatin treatment (preinc) with HSP90i luminespib (lumi) or HSP990 (**A, B**) or HDACi panobinostat (pano) or LMK235 (**C, D**) enhanced the cytotoxic activity of cisplatin in A2780 and A2780CisR cells, respectively. **(E)** Apoptosis induction in A2780 and A2780CisR cells by HDACi or HSP90i with or without (w/o) cisplatin. HSP90i or HDACi were preincubated for 48h prior to cisplatin treatment for 6h with an IC_{50} followed by 24h recovery (without cisplatin). Concentrations used of HSP90i and HDACi were the same as denoted in (A-D). 10% DMSO was used as positive control for apoptosis induction. Data shown are mean ± SEM of three independent experiments. Corresponding IC_{50} values for A-D are shown in Table 2A. Statistical analysis was performed using t-test. Levels of significance: * ($p \leq 0.05$); ** ($p \leq 0.01$); *** ($p \leq 0.001$).

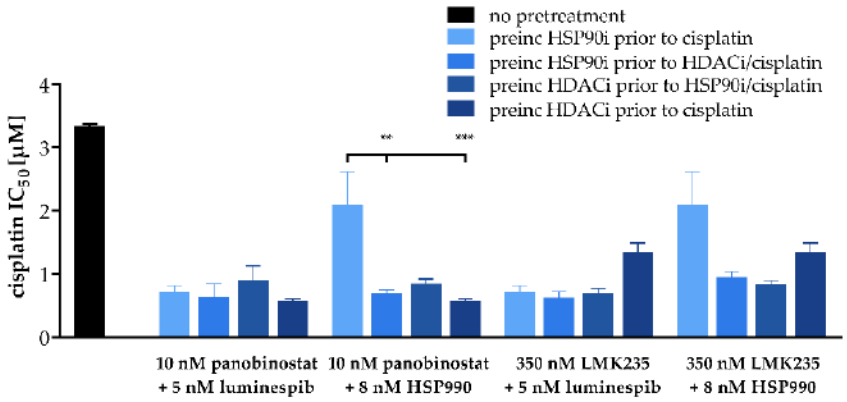

(A) A2780

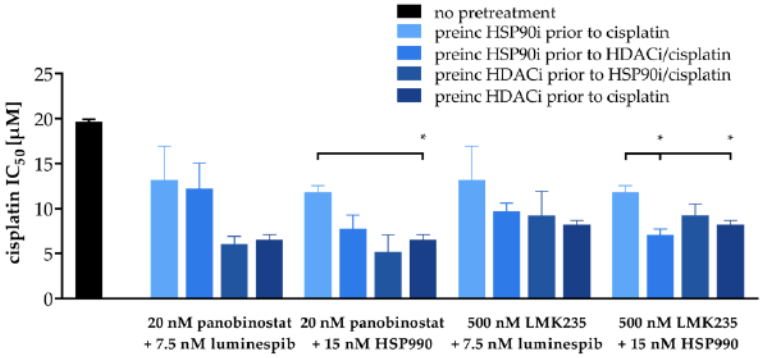

(B) A2780CisR

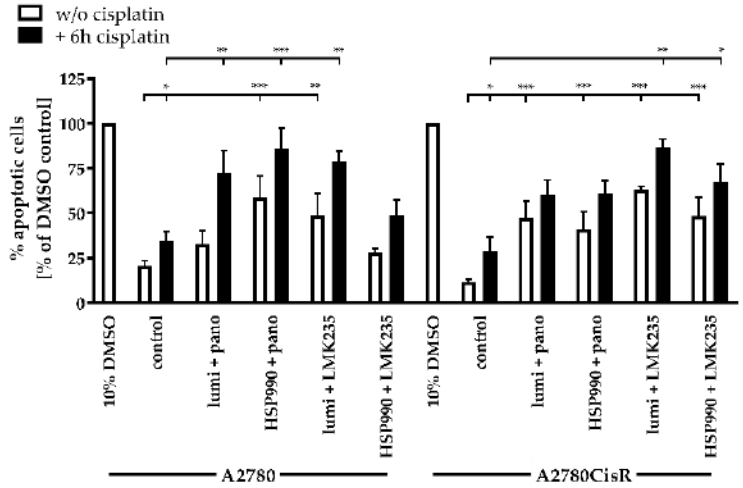

(C)

Figure S7. Triple combination treatment (HDACi, HSP90i, cisplatin) is not superior to dual combination of HDACi and cisplatin with regard to cisplatin cytotoxicity and apoptosis induction. 48h preincubation of luminespib or HSP990 prior to addition of panobinostat or LMK235 plus cisplatin increased cisplatin sensitivity up to 5-fold in A2780 **(A)** and A2780CisR **(B)**. Cells were preincubated for 48h with an HSP90i or HDACi prior to 72h cisplatin plus HDACi or HSP90i. Corresponding results are also shown in Table 2B/C. **(C)** Apoptosis induction in A2780 and A2780CisR upon 48h pretreatment with HDACi and/or HSP90i followed by 6h cisplatin treatment (with an IC_{50} concentration) or solvent control (w/o cisplatin) and 24h recovery without cisplatin. Concentrations used for apoptosis assay were the same as for cell viability assay (**A, B**) except for panobinostat in A2780CisR (25 nM). 10% DMSO was used as positive control for apoptosis induction. Data shown are mean ± SEM of three independent experiments. Statistical analysis was performed using t-test. Levels of significance: * ($p \leq 0.05$); ** ($p \leq 0.01$); *** ($p \leq 0.001$).

Supplemental Method: Analyzing of cell cycle distribution. Cells were seeded in 6-well plates and treated with HSP90i or HDACi for 48h. After treatment, cells were fixed and permeabilized in 70% ethanol at -20°C for at least 24h. After washing cells with PBS, cells were stained with 1 µg/mL propidium iodide containing 0.1 % Triton-X100 and 0.2 mg/mL DNAse-free RNAse A (AppliChem, Darmstadt, Germany). After 15 minutes incubation at 37 °C in the dark, cells were analyzed for DNA content by flow cytometry (Partec GmbH, Münster, Germany).

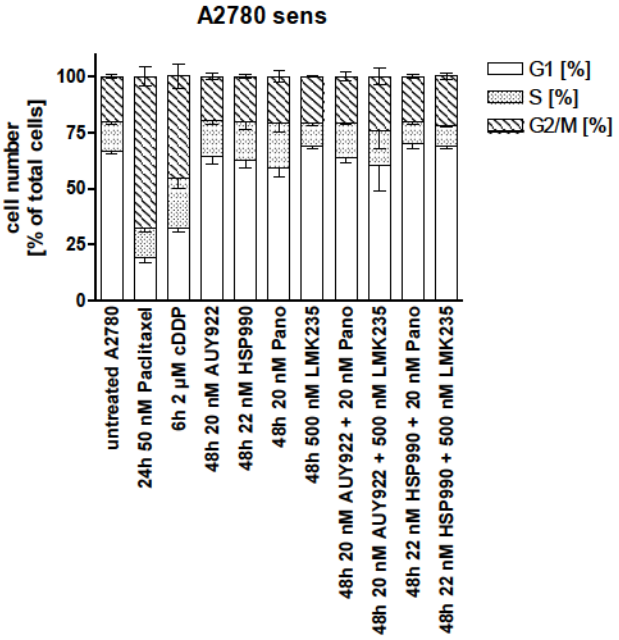

(A)

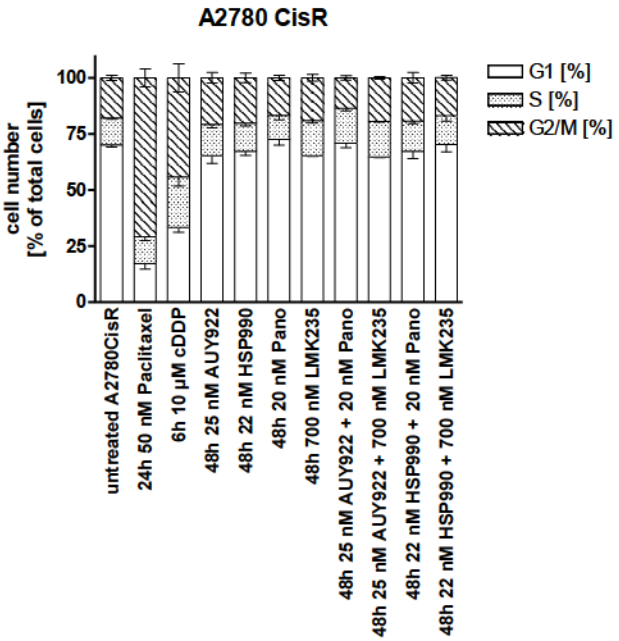

(B)

Figure S8. Effect of HDACi, HSP90i and drug combinations on cell cycle distribution of A2780 **(A)** and A2780CisR **(B)**. Cells were incubated for 48h with HDACi or HSP90i alone or in combination and stained with PI. For G2/M arrest control, 50 nM paclitaxel was incubated for 24h. Graphs show average ± SEM from three independent experiments.

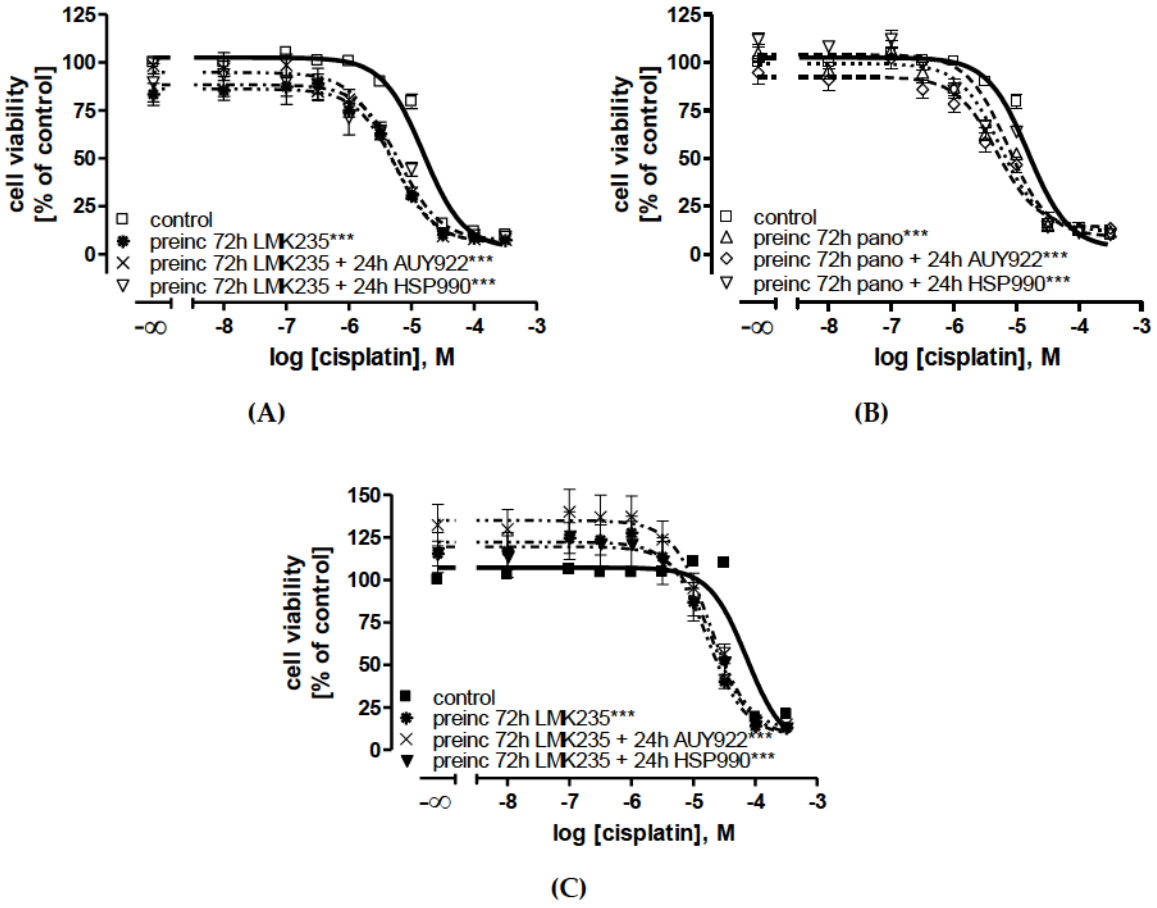

Figure S9. A 72 hour preincubation with LMK235 (350 nM for A2780 and 500 nM for A2780CisR) **(A,B)** or panobinostat (10 nM for A2780 and 20 nM for A2780CisR) **(C)** or 48h preincubation with HDACi followed by 24h incubation together with HDACi and HSP90i increased cisplatin sensitivity after 48h cisplatin treatment at A2780 **(C)** and A2780CisR **(A,B)** cells. Data shown are average ± SD from three independent experiments each carried out in triplicates. Control is the concentrations effect curve of cisplatin without any pretreatment. Statistical analysis was performed using t-test. Levels of significance: *** ($p \leq 0.001$).

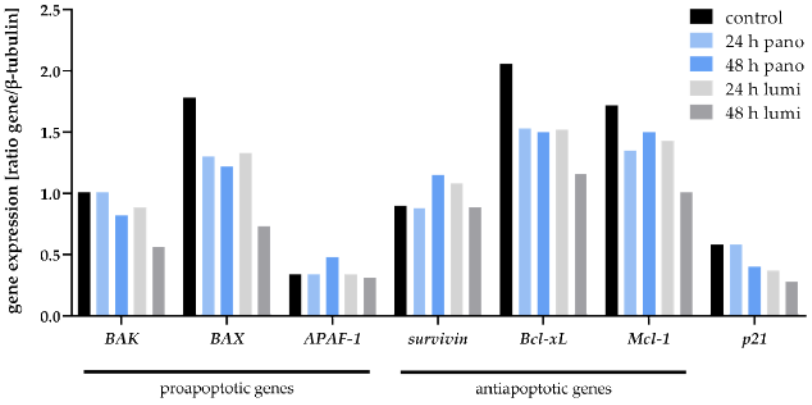

(A1) A2780

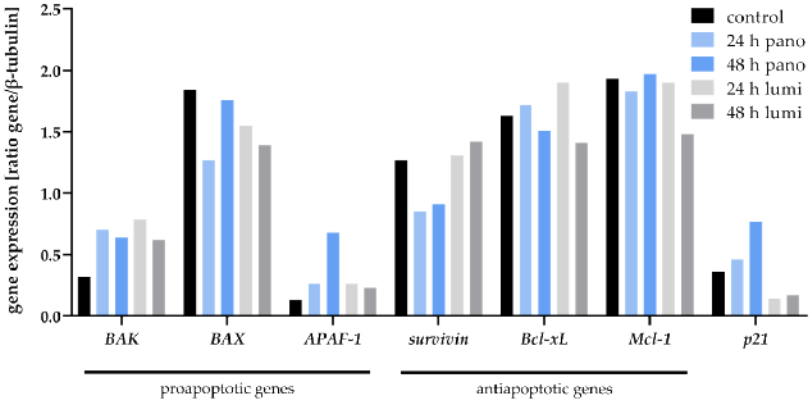

(A2) A2780CisR

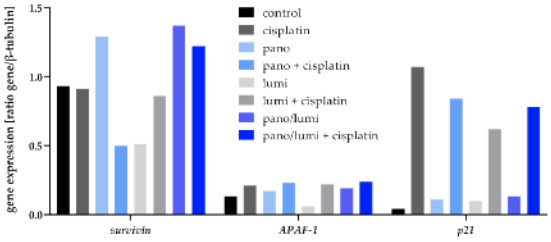

(B) A2780

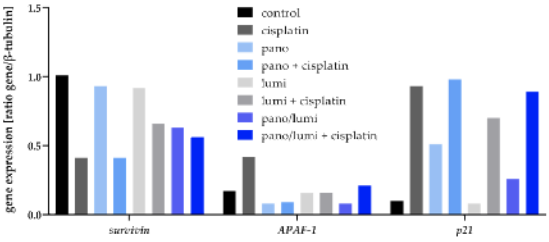

(C) A2780CisR

Figure S10. Effects of HDACi or HSP90i incubation or preincubation prior to cisplatin on apoptosis-related genes. Ratios of integrated densities of genes of interest and β-tubulin corresponding to PCR results shown in Figure 5.

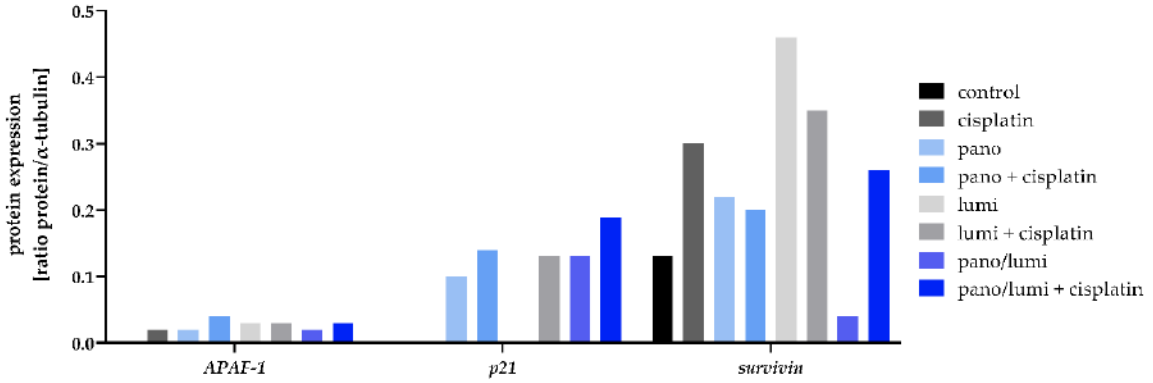

(A) A2780

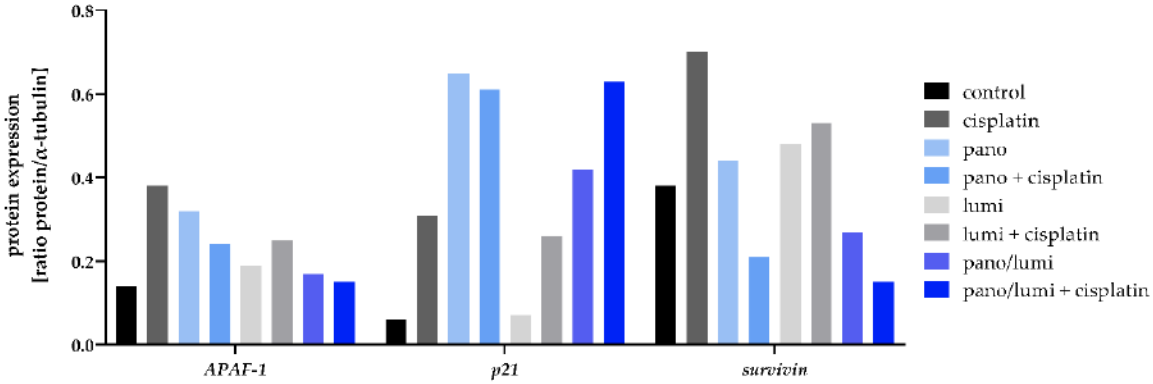

(B) A2780CisR

Figure S11. Effects of HDACi or HSP90i incubation or preincubation prior to cisplatin on protein expression levels. Ratios of integrated densities of genes of interest and α-tubulin corresponding to Western Blot results shown in Figure 6.

Table S1. Influence on the cytotoxicity of HSP90i and HDACi on each other.

A2780				
	lumi		**HSP990**	
	IC_{50} (pIC_{50} ± SEM)	**SF**	**IC_{50} (pIC_{50} ± SEM)**	**SF**
control	41.6 (7.38 ± 0.03)	-	74.0 (7.13 ± 0.04)	-
pano preinc	13.2 (7.88 ± 0.04)	3.2 ***	26.9 (7.57 ± 0.07)	2.8 ***
LMK235 preinc	29.1 (7.54 ± 0.02)	1.4 ***	40.8 (7.39 ± 0.05)	1.8 ***
	pano		**LMK235**	
control	56.2 (7.25 ± 0.03)	-	2,490 (5.60 ± 0.04)	-
lumi preinc	28.6 (7.54 ± 0.23)	2.0 (ns)	2,420 (5.62 ± 0.05)	1.0 (ns)
HSP990 preinc	58.8 (7.23 ± 0.07)	1.0 (ns)	2,240 (5.65 ± 0.04)	1.1 (ns)
A2780CisR				
	lumi		**HSP990**	
	IC_{50} (pIC_{50} ± SEM)	**SF**	**IC_{50} (pIC_{50} ± SEM)**	**SF**
control	44.2 (7.35 ± 0.03)	-	74.6 (7.13 ± 0.02)	-
pano preinc	13.6 (7.87 ± 0.10)	3.3 *	39.9 (7.40 ± 0.08)	1.9 **
LMK235 preinc	42.2 (7.38 ± 0.08)	1.0 (ns)	61.7 (7.21 ± 0.08)	1.2 (ns)
	pano		**LMK235**	
control	67.4 (7.17 ± 0.06)	-	1,830 (5.74 ± 0.04)	-
lumi preinc	48.6 (7.31 ± 0.05)	1.4 *	2,190 (5.66 ± 0.02)	0.8 (ns)
HSP990 preinc	65.5 (7.18 ± 0.04)	1.0 (ns)	1,770 (5.75 ± 0.05)	1.0 (ns)

IC_{50} values [nM] of MTT assays with HSP90i or HDACi incubation (72h) at A2780 and A2780CisR after 48h with indicated preincubation (preinc) of HDACi or HSP90i shown in Figures 2A-D and S3. Data shown is pooled data from three independent experiments. Statistical analysis was performed using t-test. Levels of significance: (ns) ($p > 0.05$); * ($p \leq 0.05$); ** ($p \leq 0.01$); *** ($p \leq 0.001$).

Table S2. Influence of dual or triple combinations with HDACi or HSP90i on the cytotoxic activity of cisplatin in A2780 and A2780CisR cells.

A – Dual Combination (inhibitor + cisplatin)

cell line	Control (cisplatin only)	cisplatin pIC_{50} ± SEM							
		HSP90i				HDACi			
		luminespib		HSP990		panobinostat		LMK235	
		Coinc	preinc	coinc	preinc	coinc	preinc	coinc	preinc
A2780	5.48 ± 0.02	5.62 ± 0.06	6.15 ± 0.13	5.65 ± 0.05	6.30 ± 0.06	5.79 ± 0.03	6.24 ± 0.08	6.16 ± 0.04	6.25 ± 0.08
A2780CisR	4.71 ± 0.02	4.60 ± 0.03	4.88 ± 0.09	4.59 ± 0.02	4.93 ± 0.05	4.78 ± 0.07	5.19 ± 0.09	4.96 ± 0.09	5.15 ± 0.10

B – Triple Combination I (HSP90i prior to HSP90i + HDACi + cisplatin)

		A2780 cisplatin pIC_{50} ± SEM			A2780CisR cisplatin pIC_{50} ± SEM		
		cisplatin	HDACi/cisplatin		cisplatin	HDACi/cisplatin	
			pano	LMK235		pano	LMK235
HSP90i	lumi	6.15 ± 0.13	6.19 ± 0.20	6.20 ± 0.11	4.88 ± 0.09	4.91 ± 0.18	5.01 ± 0.08
	HSP990	6.30 ± 0.06	6.16 ± 0.05	6.02 ± 0.07	4.93 ± 0.05	5.11 ± 0.14	5.15 ± 0.07

C – Triple Combination II (HDACi prior to HDACi + HSP90i + cisplatin)

		A2780 cisplatin pIC_{50} ± SEM			A2780CisR cisplatin pIC_{50} ± SEM		
		cisplatin	HSP90i/cisplatin		cisplatin	HSP90i/cisplatin	
			lumi	HSP990		lumi	HSP990
HDACi	pano	5.79 ± 0.03	6.04 ± 0.16	6.07 ± 0.07	5.19 ± 0.09	5.22 ± 0.10	5.23 ± 0.11
	LMK235	6.25 ± 0.08	6.16 ± 0.08	6.08 ± 0.05	5.15 ± 0.10	5.04 ± 0.19	5.03 ± 0.11

(A) Dual combinations in A2780 and A2780CisR (data and concentrations from Figures S5/S6). **(B)** Triple combinations in A2780 and A2780CisR. Preincubation (preinc) means a 48h preincubation with the indicated inhibitor followed by a 72h incubation with cisplatin **(A)** and additionally if indicated with a HDACi/HSP90i **(C)**.

Table S3. Shift factors of dual or triple combinations with HDACi or HSP90i on the cytotoxic activity of cisplatin in A2780 and A2780CisR cells.

A – Dual Combination (inhibitor + cisplatin)

cell line	HSP90i				HDACi			
	luminespib		HSP990		panobinostat		LMK235	
	coinc	preinc	coinc	preinc	coinc	preinc	coinc	preinc
A2780	1.4 *	4.7 ***	1.5 **	6.7 ***	2.0 ***	5.9 ***	4.8 ***	5.9 ***
A2780CisR	0.8 *	1.5 ns	0.8 **	1.7 ***	1.2 ns	3.0 ***	1.8 *	2.8 ***

B – Triple Combination I (HSP90i prior to HSP90i + HDACi + cisplatin)

		A2780			A2780CisR		
		cisplatin	HDACi/cisplatin		cisplatin	HDACi/cisplatin	
			pano	LMK235		pano	LMK235
HSP90i	lumi	4.7 ***	5.1 ***	5.3 ***	1.5 ns	1.6 ns	2.0 ***
	HSP990	6.7 ***	4.8 ***	3.5 ***	1.7 ***	2.5 *	2.8 ***

C – Triple Combination II (HDACi prior to HDACi + HSP90i + cisplatin)

		A2780			A2780CisR		
		cisplatin	HSP90i/cisplatin		cisplatin	HSP90i/cisplatin	
			lumi	HSP990		lumi	HSP990
HDACi	pano	5.9 ***	3.7 ***	4.0 ***	3.0 ***	3.2 ***	3.3 *
	LMK235	5.9 ***	4.8 ***	4.0 ***	2.8 ***	2.1 *	2.1 **

Data shown are shift factors (SF) corresponding to drug combinations from Table 2. which were calculated as the ratio of IC_{50} of cisplatin and the IC_{50} of the corresponding drug combination. IC_{50} values are shown in Table 2, pIC_{50} and SEM are shown in Table S2. Statistical analysis was performed using t-test. Levels of significance: ns ($p > 0.05$); * ($p \leq 0.05$); ** ($p \leq 0.01$); *** ($p \leq 0.001$).

Table S4. Influence of dual combinations with panobinostat or HSP990 on the cytotoxic activity of cisplatin in CaOV3, CaOV3CisR, OVCAR3, and OVCAR3CisR cells.

cell line	cisplatin	+ 48 h pretreatment	
		HSP990	panobinostat
	pIC_{50} ± SEM	pIC_{50} ± SEM	pIC_{50} ± SEM
CaOV3	5.72 ± 0.01	6.10 ± 0.02	5.98 ± 0.05
CaOV3CisR	5.32 ± 0.02	5.50 ± 0.03	5.86 ± 0.15
OVCAR3	5.40 ± 0.02	5.56 ± 0.12	5.82 ± 0.09
OVCAR3CisR	4.42 ± 0.02	4.90 ± 0.24	5.10 ± 0.10

Data shown are pIC_{50} ± SEM (SF) from three independent experiments each carried out in triplicates. Dual combinations in CaOV3, OVCAR3, and their cisplatin resistant sublines. The concentrations used were 10 nM for panobinostat and 10 nM HSP990. IC_{50} values are shown in Table 4.

Table S5. Effects of short-term treatment with HDACi or HSP90i on cisplatin sensitivity of A2780/A2780CisR ovarian cancer cells.

A – A2780			
	IC$_{50}$ (pIC$_{50}$ ± SEM) [SF]		
	without inhibitor	**+ 24h 5 nM lumi**	**+ 24h 8 nM HSP990**
control (48h cisplatin)	15.4 (4.81 ± 0.03)	-	-
72h 10 nM pano	5.61 (5.25 ± 0.06) [2.7 ***]	4.88 (5.31 ± 0.08) [3.2 ***]	7.23 (5.14 ± 0.06) [2.1 ***]
72h 350 nM LMK235	5.55 (5.26 ± 0.06) [2.8 ***]	4.78 (5.32 ± 0.06) [3.2 ***]	6.52 (5.19 ± 0.12) [2.4 ***]
B – A2780CisR			
	IC$_{50}$ (pIC$_{50}$ ± SEM) [SF]		
	without inhibitor	**+ 24h 7.50 nM lumi**	**+ 24h 15 nM HSP990**
control (48h cisplatin)	72.7 (4.14 ± 0.04)	-	-
72h 20 nM pano	9.56 (5.02 ± 0.14) [7.6 ***]	11.7 (4.93 ± 0.23) [6.2 ***]	9.88 (5.01 ± 0.27) [7.4 ***]
72h 500 nM LMK235	17.0 (4.77 ± 0.09) [4.3 ***]	18.7 (4.73 ± 0.10) [3.9 ***]	20.5 (4.69 ± 0.13) [3.5 ***]

Data shown are IC$_{50}$ values in µM and pIC$_{50}$ ± SEM of cisplatin (48h incubation) determined by MTT assays against A2780 **(A)** and A2780CisR **(B)** with inhibitor incubation. Data were obtained from three independent experiments each carried out in triplicates. Shift factors (SF) were calculated as the ratio of IC$_{50}$ of cisplatin and the IC$_{50}$ of the corresponding drug combination. Lumi means luminespib and pano means panobinostat. Concentrations used as described in Figure 8. Corresponding Curves are shown in Figure 4A/S8. Statistical analysis was performed using t-test. Levels of significance: *** ($p \leq 0.001$).

Table S6. Influence of HDACi/HSP90i preincubation on cisplatin sensitivity of non-tumor cell line HEK293.

preincubation condition	**IC$_{50}$ (pIC$_{50}$ ± SEM)**	**SF**
control	3.09 (5.51 ± 0.02)	-
2 nM luminespib	4.47 (5.35 ± 0.03)	0.7
5 nM HSP990	2.60 (5.59 ± 0.05)	1.2
10 nM panobinostat	2.54 (5.60 ± 0.07)	1.2
350 nM LMK235	1.85 (5.73 ± 0.07)	1.7

Data shown are IC$_{50}$ values in µM and pIC$_{50}$ ± SEM of cisplatin after a 72h incubation determined with MTT assays against HEK293 cells. HEK293 cells were preincubated with the indicated inhibitors for 48h prior to cisplatin administration. Shift factors (SF) were calculated as the ratio of IC$_{50}$ of cisplatin ("control") and the IC$_{50}$ of the corresponding drug combination. Graphs are shown in Figure 7. Data were obtained from three independent experiments each carried out in triplicates. The shift factors shown were not significantly different from control. Statistical analysis was performed using t-test.

Table S7. Results of STR analysis of A2780 and A2780CisR

Loci	A2780	A2780 (ECACC)	A2780CisR	A2780CisR (ECACC)
D5S818	11, 12	11, 12	11, 12	11
D16S539	11, 13	11, 13	11, 13	11, 13
vWA	15, 16	15, 16	15, 16	15, 16
D13S317	12, 13	12, 13	13	13
CSF1PO	10, 11	10, 11	10, 11	10, 11
TPOX	8, 10	8, 10	8	8, 10
TH01	6	6	6	6
D21S11	28	-	28	-
D7S820	10	10	10	10
AMEL	X	X	X	X

Shown are the results of the short tandem repeat (STR) analysis of the cell lines A2780 and A2780CisR. The results were compared with the data of the cell bank ECACC and it can be stated that A2780 and A2780CisR were successfully authenticated.

3.4 Publikation 4 (Manuskript)

Synergism of the Class IIa Selective Histone Deacetylase Inhibitor CHDI-00390576 and the Proteasome Inhibitor Bortezomib in Ovarian Cancer Cell Lines

Jan J. Bandolik[1], Alexander J. Skerhut[1], A. Hamacher[1], Matthias U. Kassack[1]

1 Institut für Pharmazeutische und Medizinische Chemie, Heinrich-Heine-Universität Düsseldorf

Veröffentlicht in: eingereicht bei *Cancers* am 05.03.2021

Beitrag: Erstautorenschaft. Durchführung der Experimente (Ausnahme: isolierter Enzyminhibitonsassay) dieser (eingereichten) Veröffentlichung. Auswertung der Daten und Verfassen der ersten Version des Manuskripts.

Zusammenfassung (übersetzt): Das Ovarialkarzinom hat die mit Abstand schlechteste klinische Prognose unter den gynäkologischen Krebserkrankungen. Ein großes Problem ist die intrinsische oder erworbene Resistenz gegen Zytostatika wie Platinverbindungen. Dies macht die Erforschung neuartiger Behandlungsstrategien für platinresistente Karzinome notwendig. Es ist bekannt, dass epigenetische Störungen, wie eine erhöhte Aktivierung von Histondeacetylasen (HDACs), zur Chemoresistenz von Krebs beitragen. Das Ziel dieser Studie war es, den Beitrag der Klasse IIa HDACs zur Chemoresistenz von Ovarialkarzinomen zu untersuchen. In einem Panel von 10 Ovarialkarzinom-Zelllinien – bestehend aus fünf Paaren von Cisplatin-sensitiven und Cisplatin-resistenten Zelllinien - untersuchten wir die Kombination des Klasse IIa selektiven HDAC-Inhibitors CHDI-00390576 (CHDI) mit dem Proteasom-Inhibitor Bortezomib (BTZ). Diese Kombination war in A2780- und TOV21GcisR-Zellen hoch synergistisch, wie die Synergieanalyse nach Chou und Talalay (MTT-Assay) zeigte. CHDI verstärkte die Apoptoseinduktion von BTZ durch Aktivierung von Caspase3/7. Darüber hinaus verstärkte CHDI die BTZ-induzierte DNA-Schädigung (γH2AX-BIldung) und erhöhte die Expression von proapoptotischen Genen wie *APAF1*, *BAD*, *BAK*, *p21* und *FOXO*. Zusammenfassend lässt sich sagen, dass CHDI und BTZ eine hochsynergistische Kombination darstellen, die über die Caspase3/7-induzierte Apoptoseinduktion durch erhöhte Expression von proapoptotischen Genen wirkt und somit das Potenzial einer neuartigen Behandlungsstrategie für Eierstockkrebs bietet.

Synergism of the Class IIa Selective Histone Deacetylase Inhibitor CHDI-00390576 and the Proteasome Inhibitor Bortezomib in Ovarian Cancer Cell Lines

Jan J. Bandolik, Alexander J. Skerhut, Alexandra Hamacher, Matthias U. Kassack

Institute for Pharmaceutical and Medicinal Chemistry,
Department of Pharmaceutical Biochemistry, University of Duesseldorf,
40225 Duesseldorf, Germany

Simple Summary

Ovarian cancer has the worst clinical prognosis among gynecological cancers. Intrinsic or acquired resistance against cytostatic drugs such as platinum compounds is a major problem and requires novel therapeutic strategies. Epigenetic dysregulations, such as increased histone deacetylase (HDAC) activity contributes to the development of chemoresistance. Whereas the contribution of class I HDACs is widely accepted, the role of class IIa HDACs in ovarian cancer chemosensitivity is less well understood. The aim of this study was to investigate class IIa HDACs as novel therapeutic targets in ovarian cancer. Selective and potent inhibition of class IIa HDACs by CHDI-00390576 increased the potency of the proteasome inhibitor bortezomib in a synergistic manner. The combination of CHDI-00390576 and bortezomib increased pro-apoptotic gene expression and induced caspase3/7-mediated apoptosis. Class IIa HDAC plus proteasome inhibition is highly synergistic and may constitute a novel treatment combination particularly in chemoresistant ovarian cancer.

Abstract

Ovarian cancer has the poorest clinical prognosis among gynecologic cancers. A major problem is intrinsic or acquired resistance to cytostatic drugs such as platinum compounds. This warrants the investigation of novel treatment strategies for platinum-resistant cancers. Epigenetic disturbances such as increased activation of histone deacetylases (HDACs) are known to contribute to cancer chemoresistance. The aim of this study was to investigate the contribution of class IIa HDACs to ovarian cancer chemoresistance. In a panel of 10 ovarian cancer cell lines - five pairs of cisplatin-sensitive and cisplatin-resistant cell lines – we evaluated the combination of the class IIa selective HDAC inhibitor CHDI-00390576 (CHDI) with the proteasome inhibitor bortezomib (BTZ). This combination was highly synergistic in A2780 and TOV21GcisR cells as shown by synergy analysis (Chou-Talalay, MTT assay). CHDI enhanced apoptosis induction of BTZ by activation of caspase3/7. In addition, CHDI augmented BTZ-induced DNA damage (γH2AX staining) and increased expression of pro-apoptotic genes such as *APAF1*, *BAD*, *BAK*, *p21*, and *FOXO*. In conclusion, class II HDAC and proteasome inhibition by CHDI and BTZ are a highly synergistic combination acting via caspase3/7-induced apoptosis induction through increased expression of pro-apoptotic genes, thus offering the potential of a novel treatment strategy for (chemoresistant) ovarian cancer.

Keywords

ovarian cancer, histone deacetylase (HDAC) inhibition, proteasome inhibitor, bortezomib, CHDI-00390576, cisplatin, cisplatin resistance, epigenetics, class IIa HDAC inhibition

Introduction

Ovarian cancer is by far the most lethal cancer within the group of gynecologic cancers (uterine, breast, cervical, vulvar, and ovarian cancer). Comparing five-year survival rates within this group, ovarian cancer shows the worst prognosis (47.6 %, USA; 43 %, Germany), while breast cancer shows the best prognosis (89.9 %, USA; 88 %, Germany) [1–7]. Ovarian cancers can be broadly divided into two groups: type I and II. Type I is typically less aggressive and consists of subtypes endometrioid carcinoma, clear cell carcinoma, mucinous carcinoma, and low-grade serous carcinoma (LGSOC). Type II ovarian cancers clinically show an aggressive progression and mainly include high-grade serous ovarian cancers (HGSOC). HGSOCs are rapidly growing, exhibit genomic instability, and regularly show dysfunctional tumor suppressors [8,9]. In cohort studies conducted in the USA, it has been shown that 68 % of ovarian cancer cases are type II diseases [10,11]. Primary treatment options include surgical excision of the tumor and combined chemotherapy that includes platinum-containing cytostatic agents such as cisplatin or carboplatin and paclitaxel [12]. At the beginning, most ovarian cancers are chemosensitive. In many cases, drug resistance develops during therapy and leads to therapeutic failure and relapse. The mechanisms leading to platinum resistance are multifactorial and cannot be countered by increasing the dose of cis-/carboplatin given to the patient [13–15], mainly since increasing platinum doses lead to intolerable side effects (nephron-, oto-, neurotoxicity). Epigenetic aberrations are meanwhile well known to contribute to chemoresistance of cancer cells [16]. Approaches to address chemoresistance include synergistic combination therapies to increase platinum sensitivity or to prevent or delay the development of drug resistance [17,18]. In this context, epigenetic modulators such as histone deacetylase inhibitors (HDACi) are subject of preclinical and clinical research and show promising effects in hematological and solid cancers [19–24]. On the other hand, the strategy of treating a cisplatin-resistant tumor with other cytostatic drugs is also an approach with good prospects. In a previous study, we have examined the use of pan- and class I HDACi to investigate the reversal of cisplatin chemoresistance in HGSOC cells [19]. In the current study, the approach will be pursued to treat ovarian cancer cell lines (pairs of parental and cisplatin-resistant subclones) with a combination of the class IIa selective HDACi CHDI-00390576 (CHDI) and the proteasome inhibitor bortezomib (BTZ). The rationale behind this approach is that a combination of class IIa HDACi and proteasome inhibitors has been successfully identified as synergistic in cancer cells such as multiple myeloma and pancreatic cancer but not yet in ovarian cancer [25,26].

Homeostasis of the acetylation level of histones and non-histone proteins is maintained by histone deacetylases (HDACs) and histone acetyltransferases (HATs). There are eleven known zinc-dependent HDAC isozymes (HDAC1-11), which can be divided into four classes: class I (HDAC1-3/8), class IIa (HDAC4/5/7/9), class IIb (HDAC6/10), and class IV (HDAC11). Class III consists of non-zinc-dependent HDAC enzymes, known as sirtuins [27–29]. HDAC enzymes are known to be overexpressed in diverse cancers, generally leading to transcriptional repression [30]. Normalization of the dysregulated acetylation status of histones and non-histone proteins using HDACi is an emerging strategy to increase the sensitivity of tumor cells to other cytostatic drugs [19–24]. Class IIa HDACs have been less investigated so far compared to class I HDACs. There is however increasing knowledge that class IIa HDACs can also contribute to cancer proliferation and chemoresistance [31,32]. The mechanism of action of HDACi may be based on downregulation of anti-apoptotic genes and upregulation of proapoptotic genes [19,20]. Furthermore, HDACi could lead to cell cycle arrest, which would result in apoptosis. However, the exact mechanism of action is not fully understood and is the subject of current research. For ovarian cancer, overexpression of HDACs, especially HDAC1,

is associated with a poor clinical prognosis, as the increased expression leads to an increase in tumor aggressiveness [33].

The proteasome is a central part of protein quality control in cells. Proteins intended for degradation are enzymatically linked to the protein ubiquitin and thus labeled. Polyubiquitinated proteins are bound to the proteasome via their ubiquitin chain and degraded. The degradation is carried out by endopeptidases. In mammalian cells, the 26S proteasome is expressed consisting of a proteolytically active 20S subunit and two regulatory active 19S subunits. The constant quality control of proteins by the ubiquitin proteasome system (UPS) is a basis for the maintenance of important regulatory processes and cell homeostasis such as the cell cycle or the initiation of apoptosis [34–38]. Overexpression of genes encoding subunits of the proteasome has been shown for gynecologic cancers leading to increased degradation of antitumor factors in cancer cells [39,40]. The proteasome inhibitor bortezomib was the first drug in its class to be approved by the FDA in the U.S. and by the EMA in Europe for the treatment of multiple myeloma [41,42]. While proteasome inhibitors show good clinical efficacy in hematologic cancers, this has not yet been confirmed for solid tumors despite promising preclinical data [43]. However, a phase II clinical trial in South Korea is currently investigating the use of BTZ in patients with cisplatin-resistant ovarian cancer in combination with the DNA intercalator doxorubicin [44].

Based on the results of studies in other cancer entities [25,26], we investigated in this study whether a therapeutic benefit would result from the combination of the class IIa selective HDACi CHDI and the proteasome inhibitor BTZ. Although the effect of combining the class I/II selective HDACi trichostatin A with BTZ has already been studied in ovarian cancer [45,46], the use of a highly selective and potent class IIa HDACi in combination with BTZ has, to the best of our knowledge, not yet been investigated. Strong synergistic effects of CHDI and BTZ were observed in A2780 and TOV21GcisR and led to caspase-mediated apoptosis induction with increased DNA double strand breaks.

Results

Characterization of the Human Ovarian Cancer Cell Lines

We chose human ovarian cancer cell lines A2780, CaOV3, HEY, OVCAR3, and TOV21G as cellular models for different ovarian cancer types. While A2780 and TOV21G represent type I diseases, CaOV3, HEY, and OVCAR3 represent the more aggressive type II diseases (Table 1). In addition, cisplatin-resistant subclones (cisR) of the five cell lines were also included in this study. CisR clones were generated according to methods previously published mimicking the clinical treatment situation [47].

Table 1. Overview of ovarian cancer cell lines.

Cell Line	Grade	Cell Type	References
A2780	-	endometrioid carcinoma (derived from primary tumor)	(48–52)
CaOV3	-	high grade serous adenocarcinoma (derived from primary tumor)	(48,53–55)
HEY	-	high grade serous adenocarcinoma (derived from papillary deposit)	(52–54,56)
OVCAR3	III	high grade serous adenocarcinoma (derived from ascites)	(48,52,57)
TOV21G	III	clear cell carcinoma (hypermutated, derived from primary tumor)	(48,54,58,59)

Information shown were gathered from different literature references as indicated.

First, the cisplatin sensitivity of the cell lines and the resistance factor between sensitive parental cell lines and their cisplatin-resistant subclones were determined (Figure 1, Table 2).

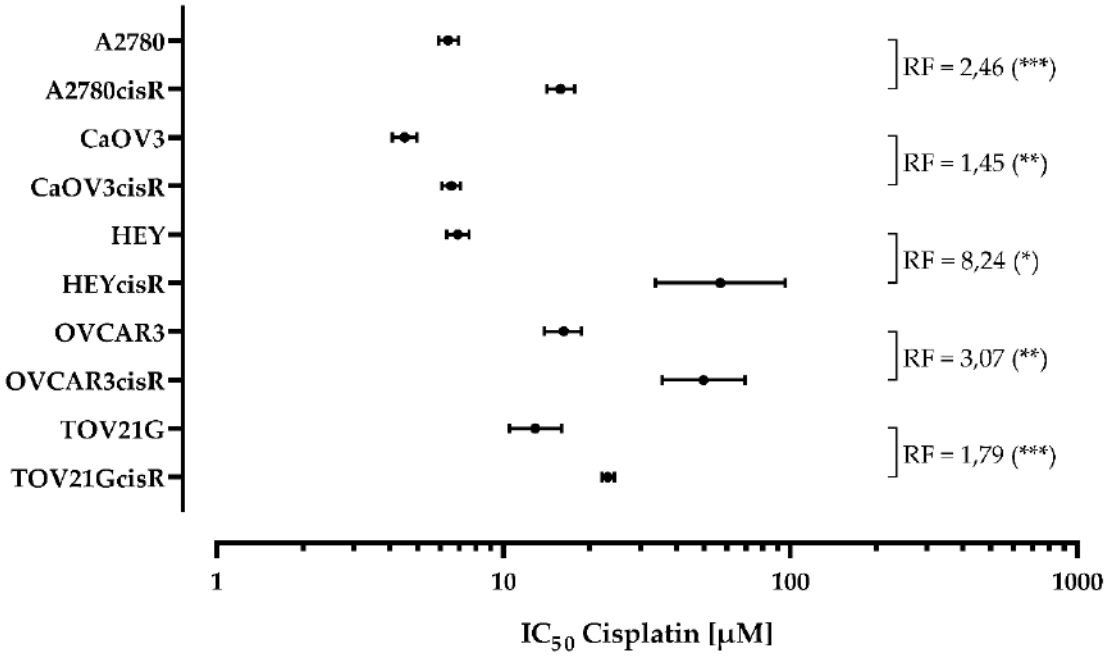

Figure 1. Cisplatin sensitivity of the ovarian cancer cell lines. Cell viability was measured by MTT assay after 72 h incubation with different concentrations of cisplatin. Data shown are the mean ± 95 % confidence interval of at least two independent experiments each carried out in at least triplicates. The cell line specific IC_{50} values are shown in Table **2**. Resistance factors were calculated by dividing the IC_{50} values of the resistant cell lines by the IC_{50} values of the parental cell lines. Statistical analysis was performed using t-test.
Levels of significance: * ($p \leq 0.05$); ** ($p \leq 0.01$); *** ($p \leq 0.001$).

The IC_{50} values of the parental cell lines to cisplatin range from 4.52 µM for CaOV3 to 16.2 µM for OVCAR3, while the cisplatin-resistant subclones show cisplatin IC_{50} values from 6.57 for CaOV3cisR to 57.0 µM for HEYcisR. The highest resistance factor (8.24) within a pair of cell lines was achieved for HEY and HEYcisR cells. The data are summarized in Table 2. In literature, cisplatin plasma levels of 1.90 to 8.72 µM are reported in patients (c_{max} reached after 1-1.5 h) [69].

Table 2. IC_{50}, pIC_{50}, and resistance factors for cisplatin after 72 h incubation.

Cell Line	IC_{50} [µM]	pIC_{50} ± SEM	Cell Line	IC_{50} [µM]	pIC_{50} ± SEM	RF
A2780	6.42	5.19 ± 0.02	**A2780cisR**	15.8	4.80 ± 0.02	2.46
CaOV3	4.52	5.35 ± 0.02	**CaOV3cisR**	6.57	5.18 ± 0.02	1.45
HEY	6.92	5.16 ± 0.02	**HEYcisR**	57.0	4.24 ± 0.11	8.24
OVCAR3	16.2	4.79 ± 0.03	**OVCAR3cisR**	49.8	4.30 ± 0.07	3.07
TOV21G	12.9	4.89 ± 0.05	**TOV21GcisR**	23.1	4.64 ± 0.01	1.79

Data shown are the mean of pooled data from at least two experiments, each carried out in at least triplicates.

In terms of parental cell lines, it appears that initial cisplatin sensitivity does not necessarily depend on the type of ovarian cancer. Considering above-mentioned clinically achievable plasma concentrations of cisplatin, all parental cell lines show only moderate cisplatin sensitivity or even cisplatin resistance, particularly OVCAR3 and TOV21G. Treatment with intermittent concentrations of cisplatin allows acquired cisplatin resistance to develop in all five cell lines. Except for CaOV3cisR, all subclones now exhibit IC_{50} values for cisplatin that are outside clinically achievable concentrations, meaning a patient would appear as chemoresistant. In a previous paper, we could demonstrate a sensitization of ovarian cancer cells against cisplatin by treatment with class I HDAC inhibitors. Here, we tested the combination of cisplatin and CHDI which however yielded only very low shift factors (less than 2) and did not turn out as synergistic - in contrast to class I HDACi (data not shown). We thus looked for alternative treatments for cisplatin-resistant ovarian cancer cells. Literature reports on promising combinations of class IIa HDACi and proteasome inhibitors that have been identified as synergistic in multiple myeloma and pancreatic cancer but not yet tested in ovarian cancer [25,26]. We thus followed up on that approach and applied a combination of the class IIa HDACi CHDI and BTZ to our ovarian cancer cell lines.

Cytotoxic Effects of CHDI-00390576 (CHDI) and bortezomib

We first analyzed the antiproliferative and cytotoxic effect of CHDI and BTZ using MTT assay after a 72 h incubation period. Results are shown in Table 3 for CHDI and in Table 4 for BTZ.

Table 3. IC_{50} and pIC_{50} for CHDI after 72 h incubation.

Cell Line	IC_{50} [µM]	pIC_{50} ± SEM	Cell Line	IC_{50} [µM]	pIC_{50} ± SEM	Sig
A2780	16.4	4.79 ± 0.03	**A2780cisR**	8.58	5.07 ± 0.01	**
CaOV3	37.2	4.43 ± 0.02	**CaOV3cisR**	13.6	4.87 ± 0.02	***
HEY	39.7	4.40 ± 0.04	**HEYcisR**	7.89	5.10 ± 0.06	**
OVCAR3	16.7	4.78 ± 0.09	**OVCAR3cisR**	21.1	4.68 ± 0.08	ns
TOV21G	4.95	5.31 ± 0.05	**TOV21GcisR**	18.0	4.75 ± 0.12	*

Data shown are the mean of pooled data from at least two experiments, each carried out in at least triplicates. The column *Sig* indicates whether there is a significant difference between the IC_{50} values for CHDI of the parental cell line and the cisplatin resistant subclone. Statistical analysis was performed using t-test. Levels of significance: ns ($p > 0.05$); * ($p \leq 0.05$); ** ($p \leq 0.01$); *** ($p \leq 0.001$).

IC_{50} values of CHDI for the five parental cell lines vary from 4.95 µM for TOV21G to 39.7 µM for HEY. Compared with their cisplatin resistant subclones, it can be seen that acquired cisplatin resistance has an impact on CHDI sensitivity (up or down) except for OVCAR3/OVCAR3cisR: IC_{50} values for CHDI at A2780 (A2780cisR: 8.58 µM), CaOV3 (CaOV3cisR: 13.6 µM), and HEY (HEYcisR: 7.89 µM) decreased after the development of cisplatin resistance. Only for TOV21G, the IC_{50} value increased from 4.96 µM (parental) to 18.0 µM in TOV21GcisR cells. There is a tendency for the ovarian cancer type I cell lines A2780 and TOV21G to show lower IC_{50} values towards CHDI than the type II cell lines used.

Table 4. IC_{50} and pIC_{50} for BTZ after 72 h incubation.

Cell Line	IC_{50} [nM]	pIC_{50} ± SEM	Cell Line	IC_{50} [nM]	pIC_{50} ± SEM	Sig
A2780	42.1	7.38 ± 0.02	**A2780cisR**	97.7	7.01 ± 0.09	**
CaOV3	22.6	7.65 ± 0.03	**CaOV3cisR**	15.9	7.80 ± 0.04	*
HEY	50.5	7.30 ± 0.03	**HEYcisR**	24.5	7.61 ± 0.12	**
OVCAR3	18.5	7.73 ± 0.04	**OVCAR3cisR**	180	6.75 ± 0.16	*
TOV21G	21.0	7.68 ± 0.05	**TOV21GcisR**	49.8	7.30 ± 0.04	**

Data shown are the mean of pooled data from at least two experiments, each carried out in at least triplicates. The column *Sig* indicates whether there is a significant difference between the IC_{50} values for BTZ of the parental cell line and the cisplatin resistant subclone. Statistical analysis was performed using t-test. Levels of significance: * ($p \leq 0.05$); ** ($p \leq 0.01$).

For BTZ, IC_{50} values of the parental ovarian cancer cell lines range from 18.5 nM for OVCAR3 to 50.5 nM for HEY. The IC_{50} values of BTZ in the cisplatin resistant subclones varied from 15.9 nM for CaOV3cisR to 180 nM for OVCAR3cisR. Literature data show plasma concentrations of BTZ of around 500 nM after intravenous and 55 nM after subcutaneous application (c_{max}) [70]. An efficient clinical inhibition by BTZ is not clear considering the high IC_{50} values of BTZ, particularly in A2780cisR and OVCAR3cisR cells. For all five cell line pairs, BTZ sensitivity was significantly affected by acquired cisplatin resistance. In the case of CaOV3 and HEY, the IC_{50} of BTZ decreased and in A2780, OVCAR3, and TOV21G it increased. Whereas BTZ sensitivity decreased in cisplatin-resistant type I cell lines (A2780, TOV21G), cisplatin-resistant type II cell lines (CAOV3, HEY, OVCAR3) displayed a mixed BTZ sensitivity.

Investigation of the Cytotoxic Effect of the Combination of CHDI and BTZ

To investigate a potential superadditive or synergistic effect of a combination treatment with CHDI and BTZ, the ten ovarian cancer cell lines were incubated for 72 h with BTZ and CHDI in concentrations based on their IC_{10} to IC_{50} values. For CHDI, this generally resulted in concentrations in the single-digit micromolar range and for BTZ in the mid-double-digit nanomolar range. Figure 2A shows the superadditive effect of 4 µM / 6 µM CHDI with different concentrations of BTZ in A2780 cells. Figure 2D shows similar data for TOV21GcisR cells. Similar effects, but to a lesser extent, were obtained for A2780cisR (Figure 2B) and TOV21G (Figure 2C) as well as the HGSOC cell lines CaOV3cisR, HEY, and OVCAR3 (SFigure 1, STable 1), but not for CaOV3, HEYcisR, and OVCAR3cisR (data not shown).

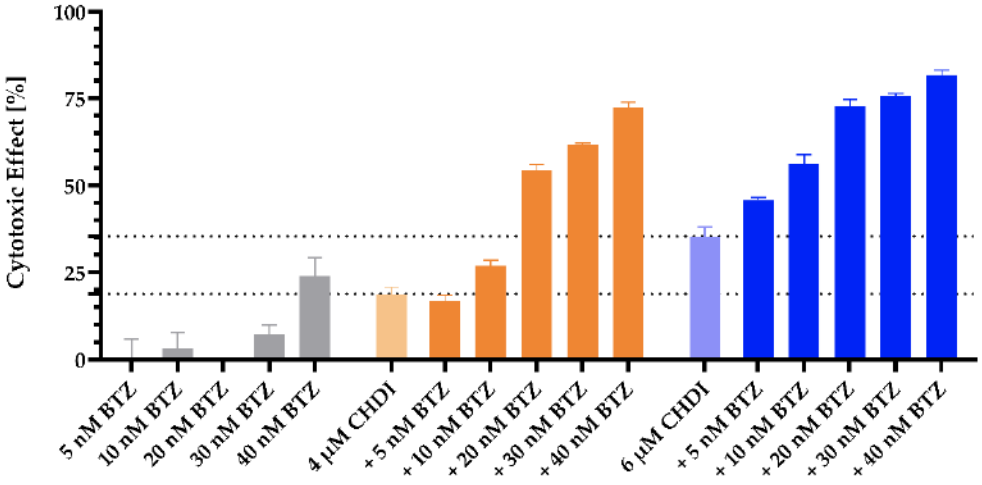

(A) A2780

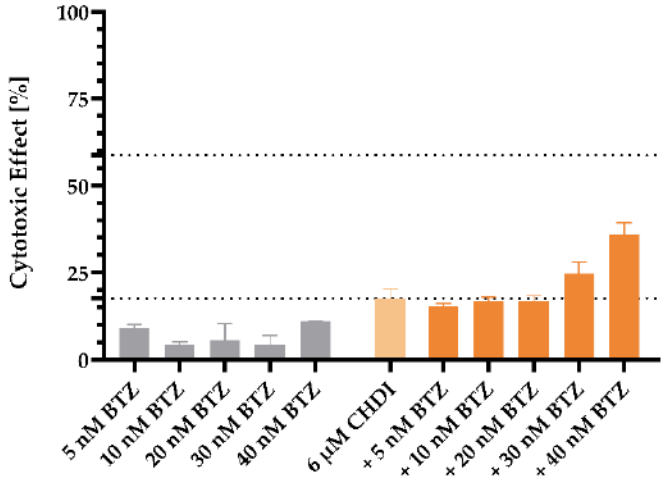

(B) A2780cisR

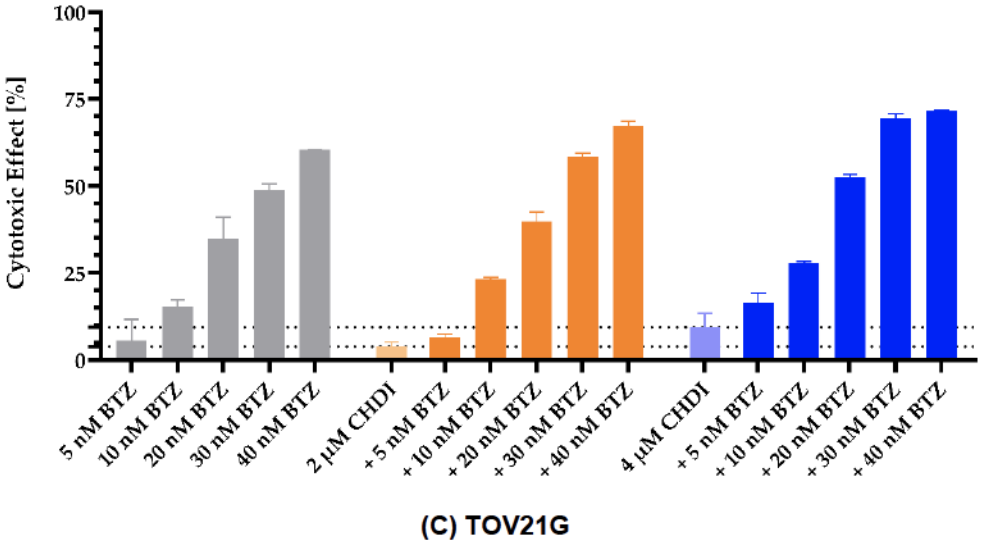

(C) TOV21G

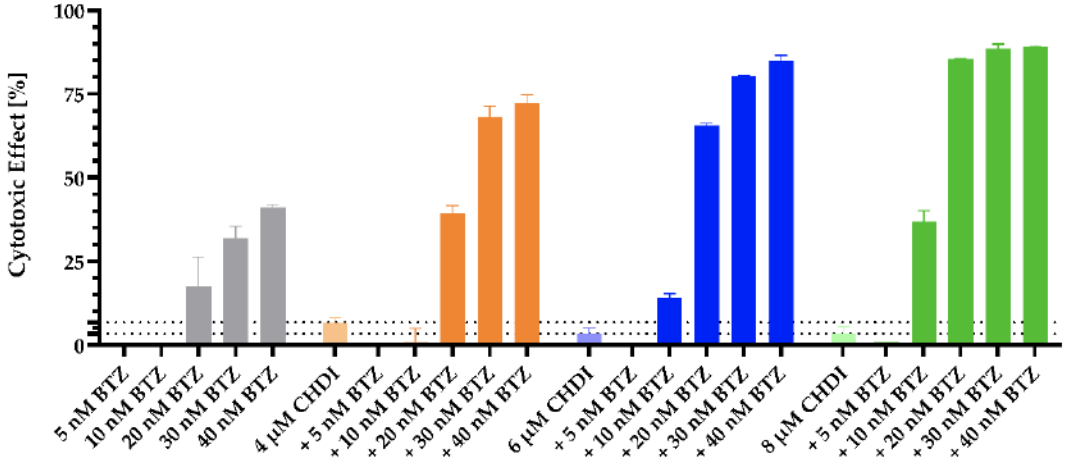

(D) TOV21GcisR

Figure 2. Combined cytotoxic effects of BTZ and CHDI. A2780 (A), A2780cisR (B), TOV21G (C), and TOV21GcisR (D) cells were treated for 72 h with the indicated concentrations of BTZ and/or CHDI. Data shown are the cytotoxic effect normalized to vehicle (untreated) control (mean ± SD; n ≥ 3).

The quantified superadditive cytotoxic effect is shown in Table 5.

Table 5. Superadditive cytotoxic effect of BTZ and CHDI in A2780/cisR and TOV21G/cisR.

A2780		CHDI [µM]	
		4	6
BTZ [nM]	5	0.6 %	6.6 %
	10	7.3 %	16 %
	20	42 %	32 %
	30	38 %	31 %
	40	34 %	18 %

TOV21G		CHDI [µM]	
		2	4
BTZ [nM]	5	*	1.3 %
	10	3.9 %	2.9 %
	20	1.1 %	8.5 %
	30	5.5 %	11 %
	40	3.0 %	1.8 %

A2780cisR		CHDI [µM]
		6
BTZ [nM]	5	*
	10	*
	20	*
	30	2.9 %
	40	7.4 %

TOV21GcisR		CHDI [µM]		
		4	6	8
BTZ [nM]	5	*	*	1.9 %
	10	*	16 %	39 %
	20	15 %	45 %	64 %
	30	30 %	45 %	53 %
	40	25 %	40 %	44 %

Data shown are superadditive cytotoxic effect of the combination treatments with BTZ and CHDI corresponding to the results shown in Figure 2. Effects were adjusted to vehicle control. * indicated calculated superadditive effects < 0 %. Data shown are mean with n ≥ 3.

Next, the cell lines obtaining the highest superadditive effects (A2780 and TOV21GcisR (Figure 2A/D, Table 5)) were used to analyze if there is drug synergism between CHDI and BTZ according to the method of Chou-Talalay using MTT assay [71,72]. Concentrations of CHDI and BTZ were chosen to achieve a fraction affected (f_a; level of cell viability inhibition) between 0.1 and 0.9 in the Chou-Talalay-analysis. Combination indices (CI) were calculated and are presented in Table 6 for A2780 and TOV21GcisR cells.

Table 6. Synergism studies (CI values) between CHDI and BTZ in A2780 and TOV21GcisR.

		BTZ [nM]									
		A2780					TOV21GcisR				
		2.5	5	10	20	30	5	10	20	30	40
CHDI [µM]	2	*	*	*	0.35	0.30	*	*	*	0.51	0.43
	4	0.47	0.49	0.53	0.36	0.31	*	*	0.64	0.55	0.48
	6	0.59	0.56	0.49	0.38	0.38	*	*	0.75	0.65	0.59
	8	0.60	0.56	0.48	0.45	0.45	0.91	0.90	0.75	0.69	0.64

Data shown are combination indices (CI) calculated using Calcusyn 2.1 based on the Chou-Talalay method. CI > 1.1 indicates antagonism, 0.9 < CI < 1.1 indicates an additive effect, and CI < 0.9 indicates synergism. * means fraction affected is less than 0.10. Values are the mean of three experiments. SD is < 10 % of the mean.

Considering the CI values obtained, it can be seen that the cytotoxic effect of the combination of the HDACi CHDI and the proteasome inhibitor BTZ proved to be synergistic in both cell lines A2780 and TOV21GcisR. CI values of even less than 0.50 are seen for some combinations, indicating strong synergism.

Potentiating Effect of a Fixed Concentration of CHDI on the Cytotoxicity of BTZ

To investigate the effect of co-incubation of the class IIa HDACi CHDI on the cytotoxic potency of BTZ, concentration-effect curves of BTZ were determined in the absence and in the presence of CHDI in A2780 and TOV21G cells (parental and cisplatin-resistant). Results are shown in Figure 3.

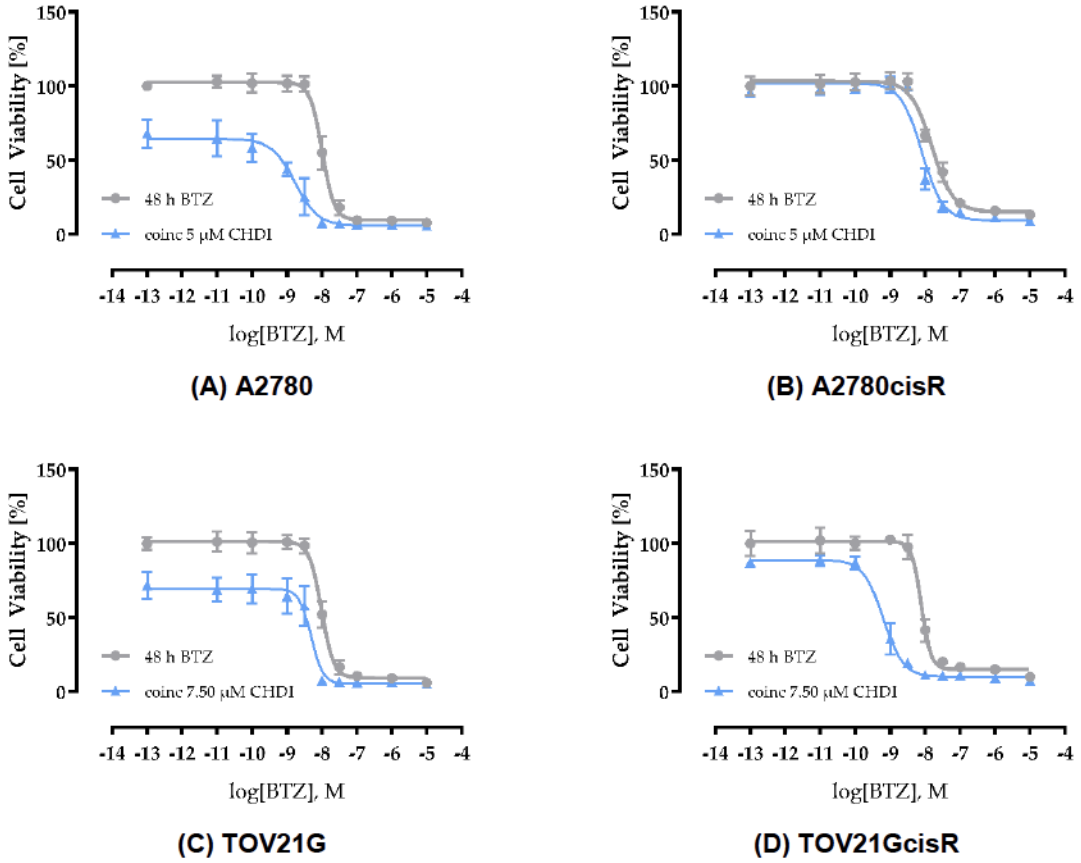

Figure 3. Effect of coincubation with CHDI on the cytotoxicity of BTZ. A2780 (A), A2780cisR (B), TOV21G (C), and TOV21GcisR (D) cells were treated with increasing concentrations of BTZ for 48 h. As indicated the cells were treated with different concentrations of BTZ and co-incubated with the indicated concentration of CHDI. Data shown are normalized to vehicle control and mean ± SD of at least two experiments each carried out in at least triplicates. IC_{50} values derived from these curves are shown in Table 7.

Based on the obtained concentration-effect curves, IC_{50} values were calculated for BTZ with and without CHDI co-incubation. From these IC_{50} values, a shift factor (SF) was calculated describing the degree to which CHDI could increase the potency of BTZ. The calculated IC_{50} values, pIC_{50} ± SEM, and shift factors are shown in Table 7.

Table 7. Influence of co-incubation with CHDI on BTZ cytotoxicity.

Cell Line	Treatment	BTZ		SF	Sig.
		IC_{50} [nM]	pIC_{50} ± SEM		
A2780	48 h BTZ	10.1	8.00 ± 0.01	6.05	***
	coinc 5 µM CHDI	1.67	8.78 ± 0.07		
A2780cisR	48 h BTZ	15.5	7.81 ± 0.02	1.93	**
	coinc 5 µM CHDI	8.03	8.10 ± 0.04		
TOV21G	48 h BTZ	9.64	8.02 ± 0.01	1.98	*
	coinc 7.50 µM CHDI	4.88	8.31 ± 0.04		
TOV21GcisR	48 h BTZ	7.78	8.11 ± 0.02	12.3	***
	coinc 7.50 µM CHDI	0.63	9.20 ± 0.04		

Data shown are the mean of pooled data from at least three experiments, each carried out in at least triplicates. Shift factors (SF) were calculated by dividing the IC_{50} values without and with CHDI co-incubation. Statistical analysis was performed using t-test. Level of significance: *** ($p \leq 0.001$).

In A2780 and TOV21G cells (parental and cisplatin-resistant), CHDI was able to significantly enhance the cytotoxicity of BTZ in a 48 h co-incubation. Highest shift factors were obtained in A2780 and TOV21GcisR cells. In A2780 cells, 5 µM CHDI decreased the IC_{50} value of BTZ from 10.1 nM to 1.67 nM (SF = 6.05). 7.50 µM CHDI reduced the IC_{50} value of BTZ from 7.78 nM to 0.63 nM (SF = 12.3) in TOV21GcisR cells.

To test whether the results found were dependent on the cisplatin resistance status of the cell lines, we performed corresponding experiments on A2780cisR and TOV21G (Table 7). In A2780cisR cells, co-incubation with 5 µM CHDI reduced the 48 h IC_{50} value of BTZ from 15.5 nM to 8.03 nM (SF = 1.93). Co-incubation with 7.50 µM CHDI decreased the 48 h IC_{50} value of BTZ on TOV21G from 9.64 nM to 4.88 nM (SF = 1.98). Despite statistical significance, the shift factors achieved are substantially lower than those obtained with A2780 (SF = 6.05) and TOV21GcisR (SF = 12.3) cells, indicating that the cisplatin resistance status does not predict the effect of the class IIa HDACi CHDI.

HDAC-Enzyme Inhibition Profile of CHDI

Next, we wanted to ensure that CHDI exerts its synergistic effects with BTZ (increase of BTZ cytotoxicity) by inhibition of class IIa and not class I HDACs. We thus investigated the HDAC inhibitory profile of CHDI on nine HDAC isoenzymes and re-confirmed the literature-known HDAC inhibition profile [73]. Results are shown in Table 8.

Table 8. IC_{50} of CHDI on HDAC isoenzymes.

Class	Isoenzyme	IC_{50} [µM]	pIC_{50} ± SEM
I	1	120	3.92 ± 0.10
	2	300	3.52 ± 0.15
	3	45.6	4.34 ± 0.10
	8	24.8	4.61 ± 0.02
IIa	4	0.10	7.01 ± 0.03
	5	0.11	6.97 ± 0.04
	7	0.13	6.90 ± 0.07
IIb	6	5.98	5.22 ± 0.04
IV	11	45.6	4.34 ± 0.10

Data shown are the mean of at least three experiments. SD is < 10 % of the mean.

The results confirm that CHDI is a potent and selective class IIa HDACi with an IC_{50} of around 100 nM at HDAC4, 5, and 7. The selectivity index for class IIa HDACs versus HDAC6 is 47. Selectivity indices versus class I HDACs are > 195. Against HDAC1 and HDAC2, CHDI has no detectable inhibitory activity. These data confirm the excellent selectivity of CHDI for class IIa HDACs which is important since inhibition of class I HDACs is known to increase chemosensitivity [19].

In addition to HDAC enzyme inhibition data, whole cell HDAC inhibition assays were performed in those cell lines showing the highest shift factors for the combination of CHDI and BZT, A2780 and TOV21GcisR. Whole cell HDAC assays were performed with the HDAC substrate Boc-Lys(Ac)-AMC (all HDACs except class IIa) and the HDAC class IIa (and HDAC8) selective substrate Boc-Lys(Tfa)-AMC. Data obtained are presented in Table 9.

Table 9. HDAC inhibitory activity of CHDI in whole cell HDAC inhibition assay.

Cell Line	Boc-Lys(Ac)-AMC		Boc-Lys(Tfa)-AMC		SI
	IC_{50} [µM]	pIC_{50} ± SEM	IC_{50} [µM]	pIC_{50} ± SEM	
A2780	26.4	4.58 ± 0.06	0.26	6.58 ± 0.05	102 (***)
TOV21G	36.3	4.44 ± 0.04	0.12	6.94 ± 0.08	303 (***)

Data shown are the mean of pooled data from three experiments each carried out in triplicates. Selectivity index (SI) is calculated by dividing the IC_{50} of unselective Ac-substrate by the IC_{50} of class IIa selective Tfa-substrate. Statistical analysis was performed using t-test. Levels of significance: *** ($p \leq 0.001$).

The whole cell HDAC inhibition assay with the pan (except class IIa) substrate Boc-Lys(Ac)-AMC showed IC_{50} values for CHDI of 26.4 µM and 36.3 µM for A2780 and TOV21GcisR, respectively. Using the class IIa HDAC selective substrate, IC_{50} values of 0.26 µM (A2780) and 0.12 µM (TOV21GcisR) were obtained. This confirms a high selectivity of CHDI for class IIa in the cellular environment. Selectivity indices (class IIa HDAC inhibition vs. pan-HDAC inhibition) were around 100 for A2780 and around 300 for TOV21GcisR. Furthermore, the cellular HDAC assay confirms cellular activity and thus uptake of CHDI into the respective cells. Based on these results, we can exclude an effect of CHDI on class I HDACs.

Effect of CHDI + BTZ Combination Treatment on the Induction of Apoptosis

In the following, we investigated if the observed synergistic cytotoxic effects of CHDI and BTZ were mediated via apoptosis-induction. A2780 and TOV21GcisR cell lines were co-incubated for 24 or 48 h with CHDI and BTZ. The concentrations of CHDI used were the same for both cell lines and are based on the IC_{50} value of CHDI against HDAC4 isoenzyme (Table 8). Thus, 1.25 µM (12.5-fold IC_{50}), 2.50 µM (25-fold IC_{50}), and 5.00 µM (50-fold IC_{50}) of CHDI were used. In this concentration range, CHDI is still clearly selective for class IIa HDACs (Table 9). For BTZ, concentrations were chosen based on the cytotoxic effect detected in MTT assays (Table 4). Concentrations corresponding to 1/2, 1/4, 1/8, and 1/16 of the respective IC_{50} values were used. Apoptosis was quantified by a modified Nicoletti assay analyzing subG1 fraction. Results are presented in Figure 4.

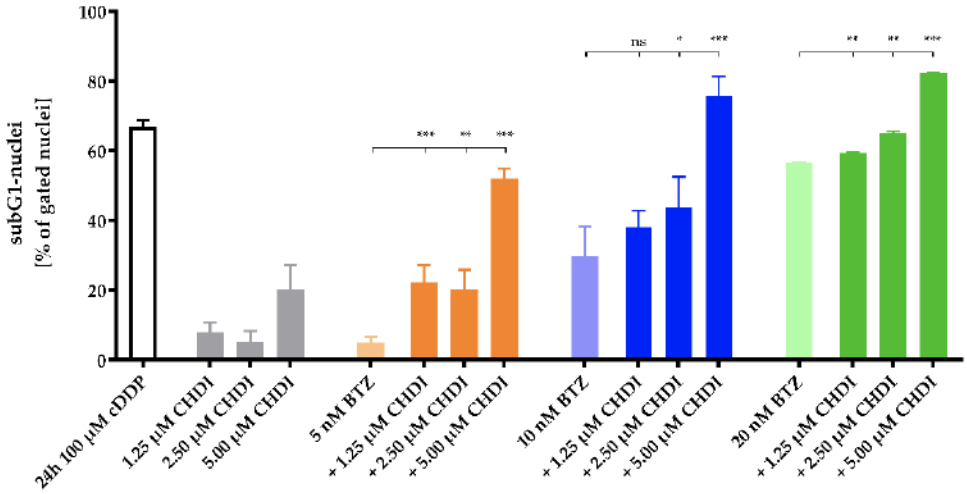

(A) A2780 – 24 h

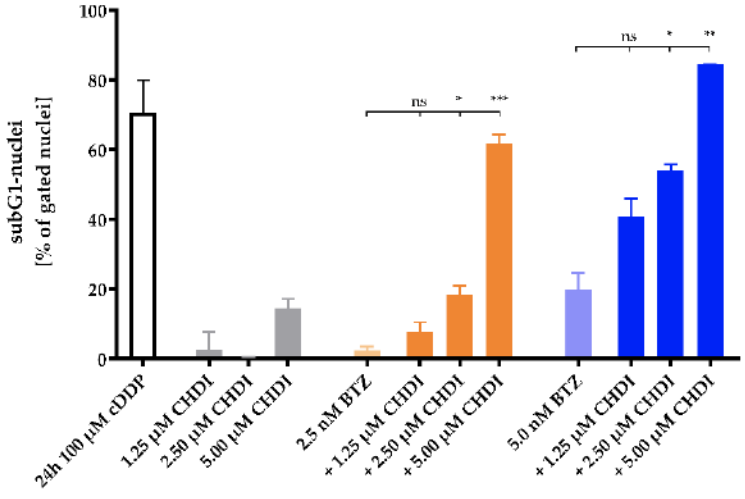

(B) A2780 – 48 h

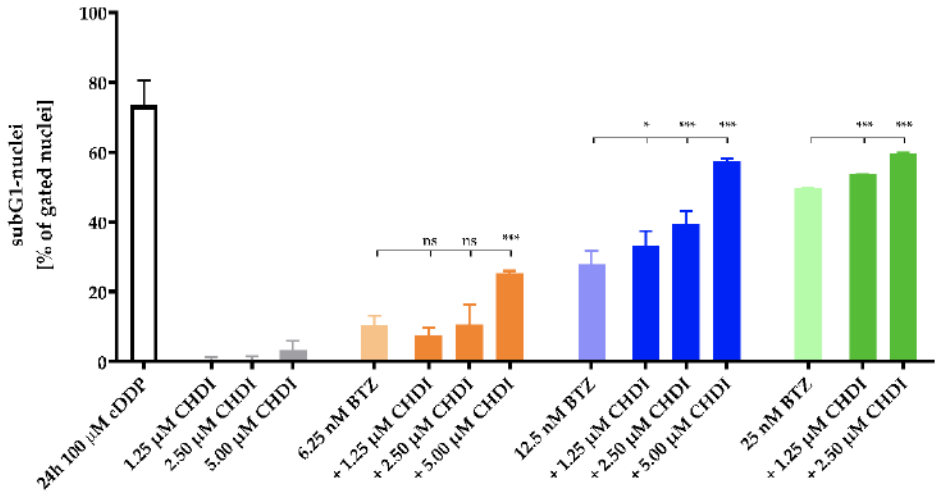

(C) TOV21GcisR – 24 h

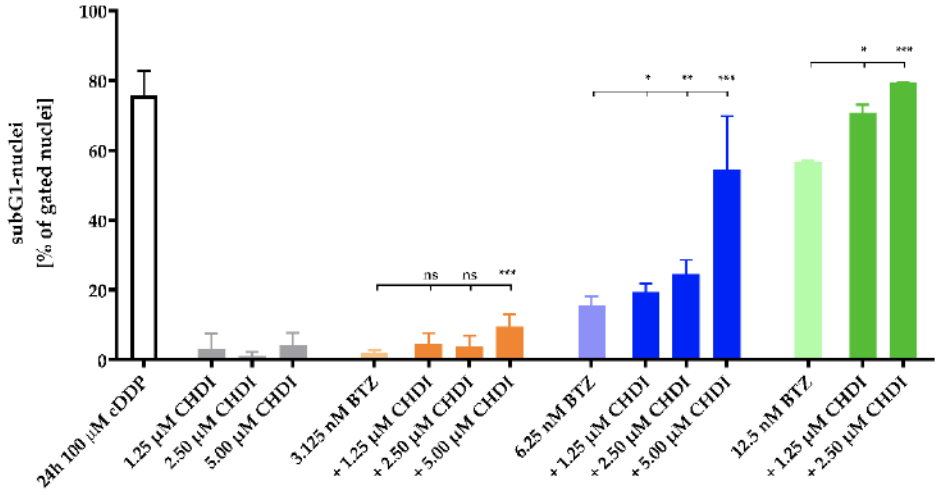

(D) TOV21GcisR – 48 h

Figure 4. Apoptosis induction by combination treatment with CHDI and BTZ. A2780 (A,B) and TOV21GcisR (C,D) cells were treated for 24 h (A,C) or 48 h (B,D) with the indicated concentrations of CHDI and BTZ. Apoptosis was analyzed by determining the subG1 cell fractions by flow cytometry analysis. 100 µM cisplatin (cDDP) served as positive control for apoptosis induction. 0.2 % DMSO was added as a control for vehicle treated cells. Effect of vehicle treated control was subtracted. Data are the mean ± SD, n ≥ 2. Raw data for (A), (B), (C), and (D) can be found in SFigure 2, SFigure 3, SFigure 4, and SFigure 5, respectively. Statistical analysis was performed using t-test. Levels of significance: ns ($p > 0.05$); * ($p \leq 0.05$); ** ($p \leq 0.01$); *** ($p \leq 0.001$).

In both cell lines, CHDI was able to significantly increase apoptosis induction of BTZ. However, in A2780 cells, 1.25 µM CHDI could not increase apoptosis induction of 24 h 10 nM, 48 h 2.5 nM, and 48 h 5 nM BTZ. The highest increase in the rate of apoptotic cells in A2780 was shown for 48 h incubation with 5 nM BTZ and 5 µM CHDI. In TOV21GcisR, the BTZ low-dose combinations 24 h 6.25 nM BTZ + 1.25 or 2.50 µM CHDI and 48 h 3.125 nM BTZ + 1.25 or 2.50 µM CHDI did not increase apoptosis induction. The combination of 48 h 6.25 nM BTZ and 5 µM CHDI gave the highest increase in apoptosis induction TOV21GcisR.

To determine whether the effects of BTZ and CHDI combinations on apoptosis induction were superadditive (= synergistic), we compared the sum of the single treatment effects of BTZ and CHDI (subG1 nuclei) with the results from the combination treatment (Figure 5). Data were only analyzed if there was a significant increase in subG1 induction in Figure 4.

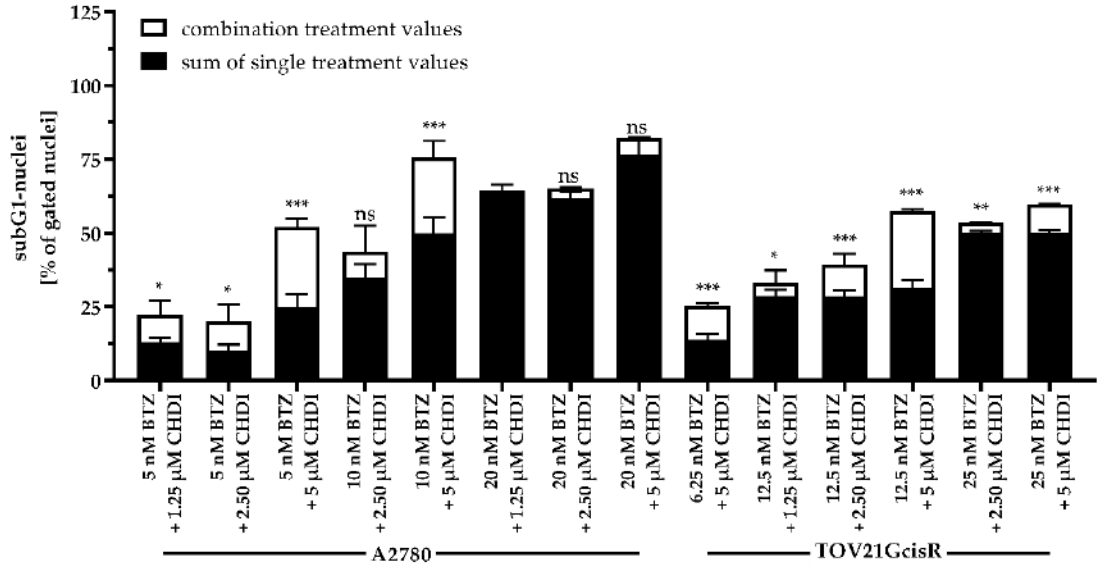

(A) 24 h

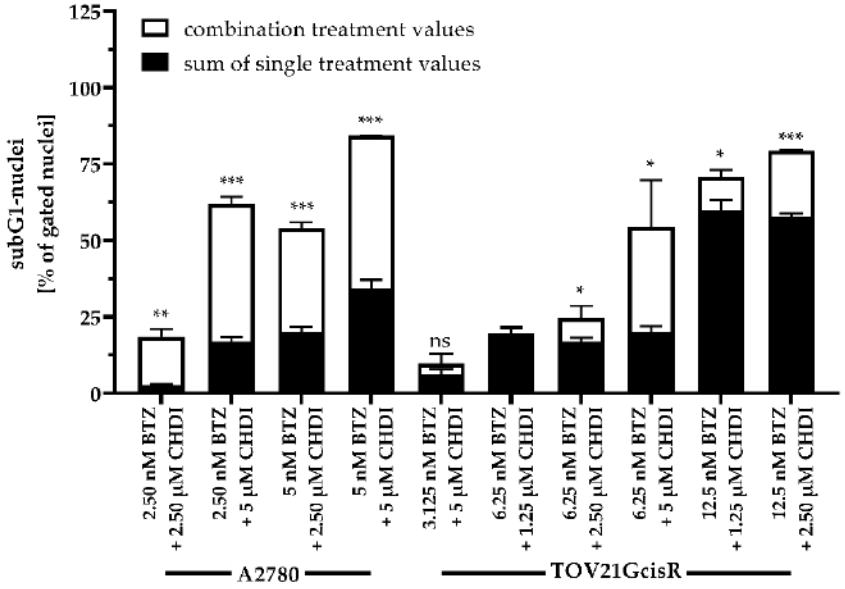

(B) 48 h

Figure 5. Synergistic effects of the combination of BTZ and CHDI on apoptosis induction. The sum of single treatment effects (BTZ, CHDI) are shown in black bars. The extended white bars show the difference (superadditive (= synergistic) part) between the sum of single treatment effects and the effect of combination treatments. Vehicle treated control was subtracted. Data are the mean ± SD. Statistical analysis was performed as previously described (19,65) and using t-test.
Levels of significance: ns ($p > 0.05$); * ($p \leq 0.05$); ** ($p \leq 0.01$); *** ($p \leq 0.001$).

Figure 5 revealed that most combinations are synergistic. Non-synergistic combinations in A2780 cells were 10 nM BTZ + 2.50 µM CHDI, as well as all 20 nM BTZ combinations. The strongest hyperadditive effects during 24 h incubation were obtained in A2780 cells for 5 nM / 10 nM BTZ + 5 µM CHDI and in TOV21GcisR cells for 12.5 nM BTZ + 5 µM CHDI. When incubated for 48 h, only the combination of 3.125 nM BTZ + 5 µM CHDI was not synergistic in TOV21GcisR cells. The strongest hyperadditive effects were obtained in A2780 cells with the combination of 2.50 nM / 5 nM BTZ + 5 µM CHDI and in TOV21GcisR cells with 6.25 nM BTZ + 5 µM CHDI.

Apoptosis Induction of the Combination Treatment is Caspase3/7-Driven

Next, we tested whether the observed apoptosis induction by the combination treatment of CHDI and BTZ was caspase-dependent. CHDI was used at 10- and 50-fold concentrations of its IC_{50} value against the HDAC4 isoenzyme in both cell lines (Table 8). BTZ was used in the respective cell line at concentrations corresponding to one-, two-, and five-fold IC_{50} from MTT assay (Table 4). The caspase3/7-activation of untreated controls, single compounds, and combination treatments were analyzed by fluorescent imaging. Results are shown in Figure 6.

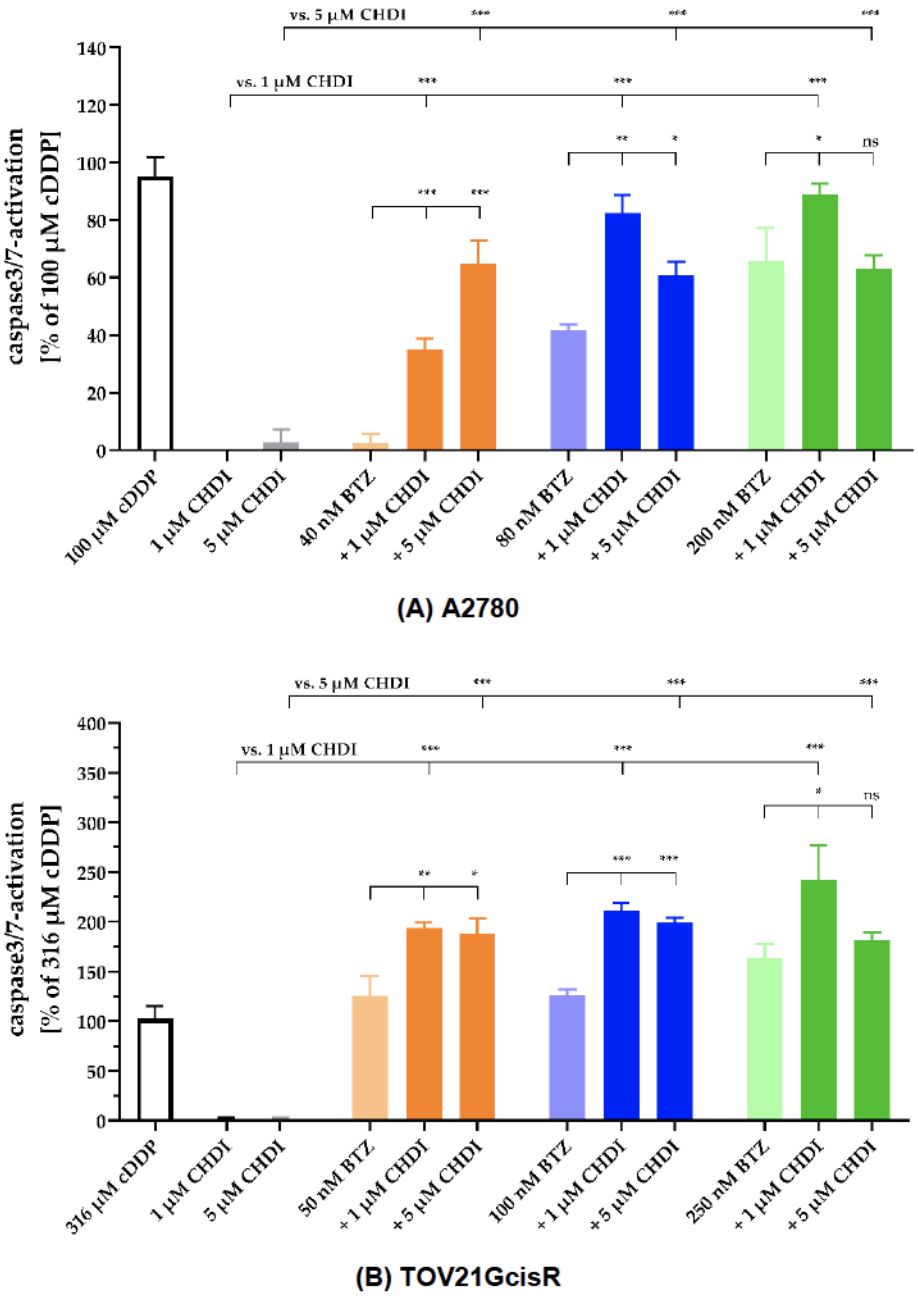

Figure 6. Caspase3/7-activation by combination treatment of CHDI and BTZ. A2780 (A) and TOV21GcisR (B) cells were treated with the indicated concentrations of CHDI and BTZ for 24 h. 100 µM (A2780) or 316 µM (TOV21GcisR) cisplatin (cDDP) was added as positive control for caspase3/7-activation. 0.2 % DMSO was added as a control for vehicle treated cells. Effect of vehicle treated control was subtracted. Experiment was carried out in triplicates. Data are the mean ± SD. Statistical analysis was performed using t-test. Levels of significance: ns ($p > 0.05$); * ($p \leq 0.05$); ** ($p \leq 0.01$); *** ($p \leq 0.001$).

In A2780 cells, all combinations of CHDI and BTZ showed significantly increased activation of caspase3/7 compared with the effects of the single compounds at the respective concentrations. An exception is the combination of 200 nM BTZ and 5 µM CHDI. 5 µM CHDI and 40 nM BTZ individually show no significant activation of caspase3/7 in A2780 cells. The combination, however, achieves an effect of about 60% of the effect of 100 µM cisplatin. Thus, it shows the strongest enhancement related to caspase3/7 activation of BTZ. TOV21G cells also show good effects upon combination treatment with CHDI and BTZ related to caspase3/7 activation. All combinations examined led to a significant increase in the activation rate of caspase3/7 compared with the effects of the single compounds. An exception in TOV21GcisR, similar to A2780, is the combination of 250 nM BTZ with 5 µM CHDI. The greatest increase in caspase3/7 activation compared to the individual compounds, is achieved with the combination of 100 nM BTZ and 1 µM CHDI.

In order to determine whether the significant effects in caspase3/7 activation are synergistic, we compared the sum of the single treatment effects of BTZ and CHDI (caspase3/7 activation) with the results from the combination treatments (Figure 7). Data were only analyzed if there was a significant increase in caspase3/7 activation in Figure 6.

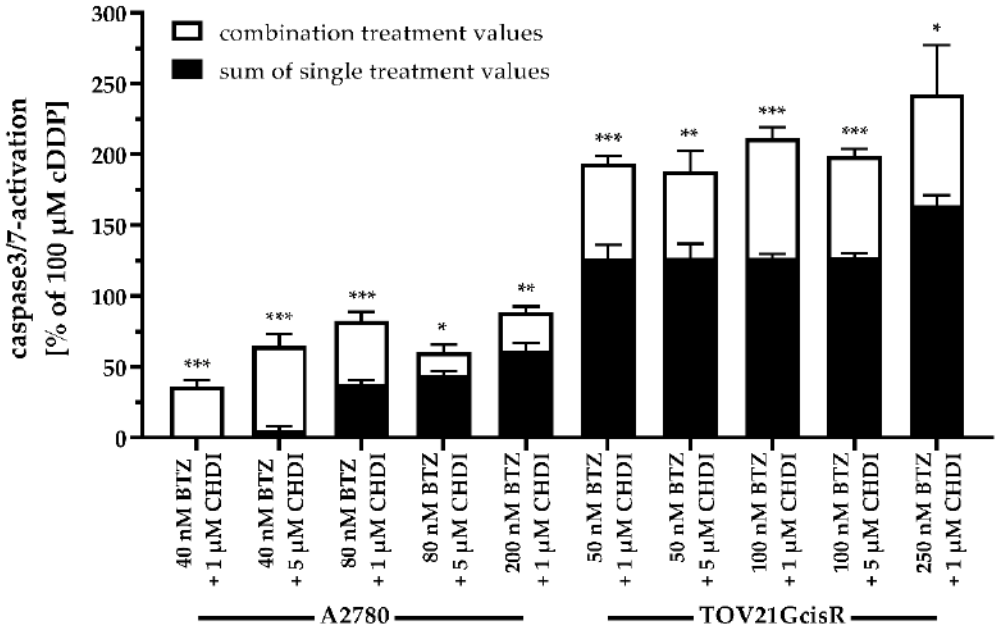

Figure 7. Synergistic effects of caspase3/7 activation upon combination treatment of BTZ and CHDI. The sum of single treatment effects (BTZ, CHDI) are shown in black bars. The extended white bars show the difference (superadditive (= synergistic) part) between the sum of single treatment effects and the effect of combination treatments. Vehicle treated control was subtracted. Data are the mean ± SD. Statistical analysis was performed as previously described (19,65) and using t-test.
Levels of significance: * ($p \leq 0.05$); ** ($p \leq 0.01$); *** ($p \leq 0.001$).

All combinations investigated were synergistic regarding their effects on caspase3/7 activation in both cell lines. The strongest hyperadditive effects were obtained in A2780 cells with the combination 40 nM BTZ + 5 µM CHDI and in TOV21GcisR cells with 100 nM BTZ + 1 µM CHDI.

Detection of Increased γH2AX Expression as Evidence for DNA Damage Caused by the Combination of CHDI and BTZ

To further understand the synergistic action between CHDI and BTZ observed in MTT assay, apoptosis induction and caspase3/7 activation, DNA damage induced by CHDI and BTZ and their combination was analyzed. As a marker for DNA double-strand breaks serves the analysis of γH2AX foci [74]. Thus, a fluorescence-based γH2AX assay was performed. Since the focus of this assay was to understand the synergistic action between CHDI and BTZ regardless of the cell lines, we chose exemplary A2780 cells to detect potential DNA damage by CHDI and BTZ. The same incubation conditions as for the caspase3/7 activation assay were used. Results are shown in Figure 8.

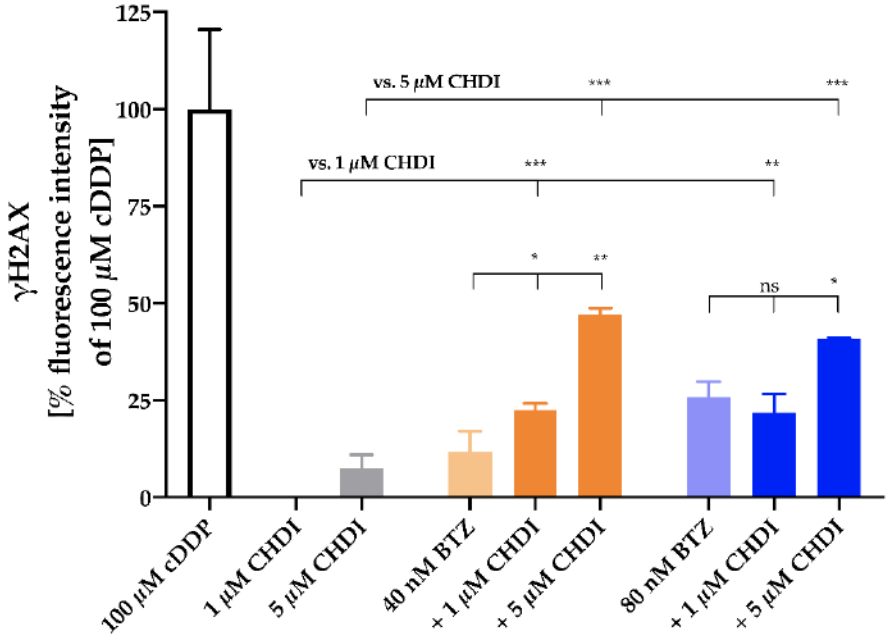

Figure 8. γH2AX formation induced by combination of CHDI and BTZ in A2780 cells. A2780 cells were treated with an IC_{50}, double IC_{50}, or fivefold IC_{50} of BTZ (from MTT assay) and indicated concentrations of CHDI for 24 h. γH2AX formation was analyzed by immunohistochemistry. 100 µM cisplatin (cDDP) served as a positive control and was set as 100 % effect. 0.2 % DMSO was added as vehicle control. Vehicle treated control was subtracted. Data are the mean ± SD. Experiment was carried out in triplicates. Statistical analysis was performed using t-test. Levels of significance: ns ($p > 0.05$);
* ($p \leq 0.05$); ** ($p \leq 0.01$); *** ($p \leq 0.001$).

Figure 8 demonstrates that the rather small induction of γH2AX foci by 40 and 80 nM BTZ (11.4 % and 25.1 % γH2AX foci of 100 µM cisplatin control) could be significantly enhanced by 5 µM CHDI. The highest level of γH2AX foci induced by 40 nM BTZ in the presence of 5 µM CHDI was almost 50% of the level of 100 µM cisplatin.

To determine whether the effects of BTZ and CHDI combinations on formation of γH2AX were superadditive (= synergistic), we compared the sum of single treatment effects of BTZ and CHDI (γH2AX formation) with the results of the combination treatment (Figure 9). Data were only analyzed if there was a significant increase in γH2AX formation in Figure 8.

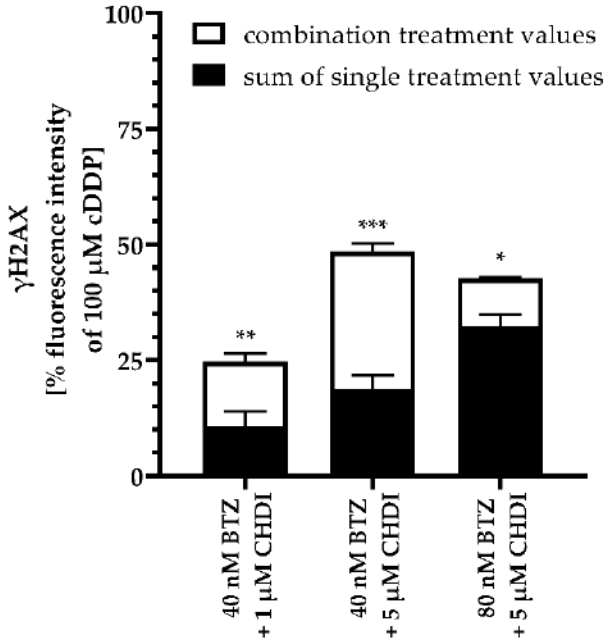

Figure 9. Synergistic effects of the combination of BTZ and CHDI on γH2AX formation. The sum of single treatment effects (BTZ, CHDI) are shown in black bars. The extended white bars show the difference (superadditive (= synergistic) part) between the sum of single treatment effects and the effect of combination treatments. Vehicle treated control was subtracted. Data are the mean ± SD. Statistical analysis was performed as previously described **(19,65)** and using t-test.
Levels of significance: * ($p \leq 0.05$); ** ($p \leq 0.01$); *** ($p \leq 0.001$).

Concerning the formation of γH2AX, all three investigated combinations in A2780 cells of BTZ and CHDI proved to be synergistic. The strongest superadditive effect regarding induced DNA damage could be achieved with the combination of 40 nM BTZ + 5 µM CHDI.

Gene Expression of Pro- and Antiapoptotic Proteins in Untreated, CHDI-Treated, BTZ-Treated and CHDI plus BTZ-Treated A2780 and TOV21GcisR Cells

Using quantitative RT-PCR, we investigated the influence of selected treatments on the expression of *CCND1* (coding gene for cyclin D1) and *HDAC4*, as well as the pro-apoptotic genes *APAF1*, *BAD*, *BAK1*, *BCL2L11* (Bim), *CDKN1A* (p21), *FOXO1*, *FOXO3*, *PTEN*, *TP53*, and the anti-apoptotic genes *BCL2*, *BCL2L1* (Bcl-xL), *MCL1*, *BIRC5* (survivin), and *XIAP* in A2780 and TOV21GcisR cells. Results are shown in Figure 10.

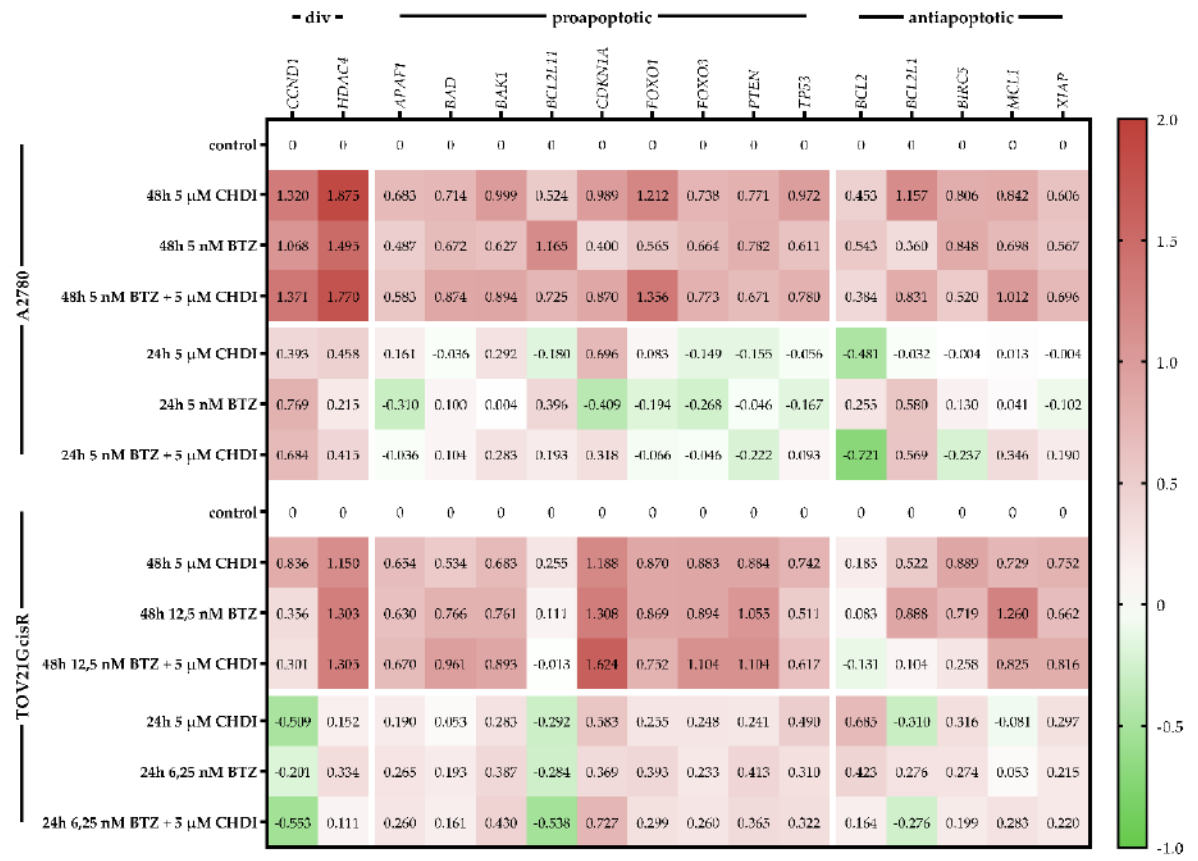

Figure 10. Expression of pro- and antiapoptotic genes in A2780 and TOV21GcisR cells. Gene expression data were obtained by RT-PCR and analyzed according to Vandesompele (67). Cells were (co-)incubated with the indicated inhibitors. Data shown are normalized to endogenous control gene expression of *HPRT1* (hypoxanthine-guanine phosphoribosyltransferase), *TBP* (TATA binding protein), and *GUSB* (beta-glucuronidase) and rescaled to cell line specific control (48 h incubation with vehicle). Data are shown on a decadic logarithmic scale. Negative values marked in green show a lower expression compared to cell line specific control. Positive values marked in red show a higher expression compared to cell line specific control.

Overall, treatment-induced expression changes are similar in A2780 and TOV21GcisR cells. Further, differences in gene expression between 24 h and 48 h incubations are also similar in both cell lines. Interestingly, after 24h incubation, almost 50% of the genes in A2780 and around 20% of the genes in TOV21GcisR were downregulated (green areas). In contrast, 48h incubation led to upregulation only in A2780 and upregulation of all except two genes in combination treatment in TOV21GcisR cells. Surprisingly, 48h incubation affected upregulation of both, pro- and anti-apoptotic genes although upregulation of pro-apoptotic genes seems to be stronger than upregulation of anti-apoptotic genes (darker red among pro-apoptotic than among anti-apoptotic genes). Notably, in TOV21GcisR, anti-apoptotic *Bcl2* is downregulated after combination treatment. In general, an increase in expression of anti-apoptotic genes after 48h treatment may be an attempt of the cancer cells to counteract the strong pro-apoptotic signals which however superimpose anti-apoptotic signaling as is evident from results of the caspase and apoptosis assays. Another observed feedback mechanism is the strong upregulation of HDAC4 after 48h treatment with CHDI and/or BTZ.

In A2780 cells, pro-apoptotic *BAD* and *FOXO1* were stronger upregulated after combination treatment with CHDI plus BTZ than after respective single treatments. The same holds true in TOV21GcisR cells for the upregulation of *BAD*, *BAK1*, *CDKN1A*, *FOXO3*, and *PTEN* and the downregulation of *BCL2*. In addition, the upregulation of anti-apoptotic genes *BCL2L1*

(TOV21GcisR), *BIRC5* (TOV21GcisR, A2780), and *BCL2* (A2780) is remarkably lower under combination treatment (CHDI plus BTZ) than under respective single treatments.

Discussion

Ovarian cancer generally has a poor clinical prognosis and the lowest 5-year survival rate among gynecologic cancers [2]. HGSOC has the poorest prognosis among the ovarian cancers. Platinum drugs such as carboplatin (or cisplatin) are part of the chemotherapeutic regime in ovarian cancers. Particularly HGSOCs have a low responsiveness to platinum drugs, however also endometrioid and clear cell ovarian cancers may acquire resistance. Chemoresistant ovarian cancer poses a major therapeutic challenge. Thus, strategies to regain chemosensitivity or prevent resistance development are urgently needed. Epigenetic disturbances such as increased expression of HDACs lead to hypoacetylation, condensed DNA, and impaired expression of tumor suppressor genes [75]. Further, a dysregulated acetylation status of histones and non-histone proteins can play an important role in chemoresistance [16]. Thus, HDAC inhibitors (HDACi) are intensively investigated to reestablish a normal acetylation homeostasis [76–78]. In a previous study, we could show that class I HDACi are superior in reversing chemoresistance than pan-HDACi in various HGSOC cell lines [19]. However, class IIa HDACi were not investigated in that previous study. Yet, we have shown that also class IIa HDACs, and in particular HDAC4, are expressed in HGSOCs and in A2780 cells [19]. Class IIa HDACs are known to play an important role in cancer and contribute to chemoresistance [31]. Thus, this study aims to investigate the role of class IIa HDACs and their inhibitors in cisplatin-resistant ovarian cancer. Initially, we investigated if the potent class IIa inhibitor CHDI is able to revert cisplatin resistance. This however yielded resistance shift factors of maximum 2 (data not shown). Another class of chemotherapeutic drugs undergoing clinical trials in (chemoresistant) ovarian cancer are proteasome inhibitors [44,79–81]. Protein quality control is a central function of the ubiquitin proteasome system (UPS) and crucial for the maintenance of cell homeostasis such as regulation of the cell cycle and apoptosis [34–38]. Overexpression of UPS genes is associated with an increased degradation of antitumor factors and has been described for ovarian carcinomas [39,40]. The idea behind the use of proteasome inhibitors is therefore to normalize the activity of the UPS and prevent the degradation of antitumor factors. We thus shifted the aim of our study and investigated the combination of the class IIa HDACi CHDI and the proteasome inhibitor bortezomib (BTZ) in parental and cisplatin-resistant ovarian cancer cell lines (Table 1, Figure 1).

Simultaneous treatment of the non-HGSOC cell lines A2780 and TOV21GcisR with BTZ and CHDI resulted in a strong synergistic cytotoxic effect (Figure 2, Figure 3, Table 5, Table 6, Table 7). Of note, concentrations of CHDI used in this study (up to 8 µM) were still highly selective for class IIa HDACs (except for HDAC6 (Table 8)), excluding an effect of class I HDAC inhibition and thus supporting the use of class IIa HDACi in combination with BTZ. A partial inhibition of HDAC6 is unlikely to play a major role sine HDAC6 inhibition did not reveal significant effects in improving chemosensitivity in ovarian cancer as previously shown [19]. In HGSOC cell lines (CaOV3cisR, HEY, OVCAR3), we found some hyperadditive effects (SFigure 1) but synergism according to Chou-Talalay could not be proven (data not shown). Subsequent studies were thus performed in parental and cisplatin-resistant A2780 and TOV21G cells. Incubation of CHDI in the presence of increasing concentrations of BTZ resulted in significant shifts of the corresponding BTZ concentration-effect curves (shift factors up to 12.3, Table 7). CHDI is thus able to increase the cytotoxic potency of BTZ. This effect was clearly more pronounced in parental A2780 and cisplatin-resistant TOV21GcisR (Figure

3). Cisplatin sensitivity (or resistance) is thus not a predictor for a synergistic effect of CHDI and BTZ. Synergy was proven with the method according to Chou-Talalay (Table 5) [71,72]. Combination indices (CI values) below 0.9 indicate synergism. If CI is < 0.5, which was the case for a majority of data in A2780 cells (Table 5), strong synergism can be assumed. Notably, strong synergism was observed for BTZ concentrations which are clearly below clinically observed plasma concentrations of BTZ. Literature data show plasma concentrations of BTZ of around 500 nM after intravenous and 55 nM after subcutaneous application (c_{max}) [70]. Thus, combinations of class IIa HDACi with BTZ (or other proteasome inhibitors) may allow reducing doses and by that, toxic side effects of the proteasome inhibitors.

CHDI induced very little apoptosis (Figure 4). However, CHDI in combination with even very low concentrations of BTZ (such as 2.50 / 5 nM for A2780 and 6.25 / 12.5 nM for TOV21GcisR, respectively) strongly enhanced apoptosis in a caspase3/7 dependent manner in A2780 and TOV21GcisR cells. This effect was synergistic in apoptosis assays (Figure 4, Figure 5) and caspase3/7 activation assays (Figure 6, Figure 7). Notably, 48 h co-incubation of 2.5 nM or 5 nM BTZ plus 5 µM CHDI gave apoptosis induction in A2780 cells at least as strong as 24 h 100 µM cisplatin (Figure 4). The same is true for the combination of 6.25 nM or 12.5 nM BTZ plus 5 µM CHDI in TOV21GcisR cells. Caspase3/7 activation assays thus confirm that the subG1 cells found in apoptosis assays are indeed apoptotic cells (Figure 6). The potential for inducing apoptosis by BTZ is consistent with the literature [82,83]. Furthermore, the combination of BTZ and CHDI was synergistic in inducing DNA damage analyzed by γH2AX staining (Figure 8, Figure 9). Even though BTZ and CHDI are not primarily DNA-damaging agents, a combination of 40 nM BTZ plus 5 µM CHDI for 24 h achieved around 50% of the DNA damage induced by 100 µM cisplatin. These results are in accordance with literature data reporting BTZ-induced DNA damage [84].

qPCR-based gene expression analysis supports our data on CHDI-increased apoptosis induction by BTZ. Gene expression data suggest that the class IIa HDACi CHDI enhanced pro-apoptotic gene expression (Figure 10), assumingly responsible for increased caspase3/7-dependent apoptosis induction. This is in accordance with the general mechanism of action of HDACi and confirms gene expression analyses of previous studies conducted by us [19,20]. Combination treatments particularly affected upregulation of pro-apoptotic *BAD, BAK1*, *CDKN1A*, *FOXO1, FOXO3*, and *PTEN* and downregulation of anti-apoptotic *BCL2* (in TOV21GcisR cells) or diminished expression of anti-apoptotic *BCL2L1* (TOV21GcisR) and *BIRC5* (TOV21GcisR, A2780) under combination treatment (BTZ plus CHDI) compared to single treatment (BTZ or CHDI). Especially the pro-apoptotic *BAD* gene seems to be affected by our combination treatments. It is well known that *BAD* is a crucial factor during the induction of apoptosis, which is also described for ovarian cancer [85,86].

Conclusions

This study aimed to investigate the contribution of class IIa HDACs in ovarian cancer chemoresistance. In conclusion, we could demonstrate that selective class IIa HDAC inhibition increases the potency of the proteasome inhibitor BTZ in a synergistic manner in parental and cisplatin-resistant non-HGSOC cells. The highly potent and selective class IIa HDACi CHDI shifts gene expression to a more apoptotic phenotype, thus explaining increased caspase-mediated apoptosis of the combination CHDI plus BTZ. This opens a new strategy for treatment of platinum-resistant ovarian cancers by using low-toxic class IIa HDACi in combination with proteasome inhibitors. HGSOC cancer cells may have more benefit from class I HDACi as shown by our previous study [19].

Materials and Methods

Reagents

Cisplatin was purchased from Sigma (München, Germany) and dissolved in 0.9 % sodium chloride solution, propodium iodide (PI) was purchased from PromoKine (Heidelberg, Germany). Stock solutions (10 mM) of bortezomib (Selleckchem, Houston, Texas, USA) and CHDI-00390576 (Tocris Bioscience, Bristol, UK) were prepared with DMSO and diluted to the desired concentrations with the appropriate medium. All other reagents were supplied by PAN Biotech (Aidenbach, Germany) unless otherwise stated.

Cell Lines and Cell Culture

The human ovarian carcinoma cell lines A2780 and HEY were obtained from European Collection of Cell Cultures (ECACC, Salisbury, UK). CaOV3, OVCAR3, and TOV21G cell lines were obtained from ATCC/LGC Standards GmbH (Wesel, Germany). The cisplatin resistant sublines A2780cisR, CaOV3cisR, HEYcisR, OVCAR3cisR, and TOV21GcisR were generated by exposing the parental cell line to weekly cycles of cisplatin in an IC_{50} concentration according to Gosepath et al. (47). All cell lines were grown at 37 °C under humidified air supplemental with 5 % CO_2 in RPMI-1640 (A2780, HEY, OVCAR3, TOV21G) or DMEM (CaOV3) containing 10 % heat inactivated fetal calf serum, 120 IU/mL penicillin, and 120 µg/mL streptomycin. The cells were grown to 80 % confluency before used in further assays.

MTT Cell Viability Assay

The rate of cell-survival under the action of test substances was evaluated by an improved MTT assay as previously described (21,80). For an incubation period of 72 h cell lines were seeded in 96-well tissue culture plates (Corning, Kaiserslautern, Germany) in the following concentrations: OVCAR3 – 7,000 c/w; A2780, CaOV3, CaOV3cisR, HEY, HEYcisR, OVCAR3cisR – 8,000 c/w; A2780cisR, TOV21G, TOV21GcisR – 10,000 c/w. For an incubation period of 24 or 48 h A2780 and TOV21GcisR cells were seeded at a density of 15,000 c/w. Incubation was ended after the indicated period and cell survival was determined by addition of MTT (Serva, Heidelberg, Germany) solution (5 mg/mL in phosphate buffered saline). The formazan precipitate was dissolved in DMSO (VWR, Langenfeld, Germany). Absorbance was measured at 544 nm and 690 nm in a ThermoFisher Multiskan FC Microplate Photometer (Thermo Scientific, Wesel, Germany).

Whole-Cell HDAC Inhibition Assay

The cellular HDAC assay was based on an assay published by Heltweg and Jung (81), Ciossek et al. (82), and Bonfils et al. (83) with minor modifications as described in (21). Briefly, human cancer cell lines A2780 and TOV21GcisR were seeded in 96-well tissue culture plates (Corning, Kaiserslautern, Germany) at a density of 25,000 c/w and 22,500 c/w in a total volume of 90 µL of culture medium. After 24 h, cells were incubated for 18 h with increasing concentrations of test compound CHDI-00390576. The reaction was started by adding 10 µL of 3 mM Boc-Lys(Ac)-AMC or 1 mM Boc-Lys(Tfa)-AMC (Bachem, Bubendorf, Switzerland) to reach final concentration of 0.3 mM or 0.1 mM (84). The cells were incubated with the respective substrate for 3 h under cell culture conditions. After this incubation, 100 µL/well stop solution (25 mM Tris-HCl (pH 8), 127 mM NaCl, 2.7 mM KCl, 1 mM MgCl2, 1 % NP40, 2 mg/mL Trypsin, 10 µM Panobinostat) was added and the reaction was developed for 3 h under cell culture conditions. Fluorescence intensity was measured at excitation of 320 nm and emission of 520 nm in a NOVOstar microplate reader (BMG LabTech, Offenburg, Germany).

Combination Experiments

For the investigation of the effect of a combination treatment with bortezomib and CHDI-00390576 the cells were coincubated with the compounds for the indicated period of time. After the incubation the cytotoxic effect was determined with a MTT cell viability assay. Calcusyn software 2.1 (Biosoft, Cambridge, UK) was used to calculate the combination index (CI) as a quantitative measure of the degree of drug interaction.

Enzyme HDAC Inhibition Assay

All human recombinant enzymes were purchased from Reaction Biology Corp. (Malvern, PA, USA). The HDAC activity assay HDAC1 (cat nr. KDA-21-365), HDAC2 (cat nr. KDA-21-277), HDAC3 (cat nr. KDA-22-278), HDAC4 (cat nr. KDA-21-279), HDAC5 (cat nr. KDA-21-280), HDAC6 (cat nr. KDA-21-213), HDAC7 (cat nr. KDA-21-281), and HDAC8 (cat nr. KDA-21-481) was performed in 96-well-plates (Corning, Kaiserslautern, Germany). Briefly 20 ng of HDAC1/2/3/8, 17.5 ng of HDAC6, 30 ng of HDAC11, and 2 ng of HDAC4/5/7 per reaction were used. Recombinant enzymes were diluted in assay buffer (50 mM Tris-HCl, pH 8.0, 137 mM NaCl, 2.7 mM KCl, 1 mM MgCl2, and 1 mg/mL BSA). After a 5 min incubation step the reaction was started with 10 µL of 15 µM (HDAC6), 30 µM (HDAC2), 40 µM (HDAC1), 50 µM (HDAC3) Boc-Lys(Ac)-AMC (Bachem, Bubendorf, Switzerland) or 6 µM (HDAC8), 10 µM (HDAC4/5/7), 25 µM (HDAC11) Boc-Lys-(Tfa)-AMC (Bachem, Bubendorf, Switzerland). The reaction was stopped after 90 min by adding 100 µL stop solution (16 mg/mL trypsin, 4 µM panobinostat for HDAC8/11, 2 µM CHDI-00390576 for HDAC4, 4 µM vorinostat for HDAC1/2/3, 4 µM tubastatin a for HDAC6 in 50 mM Tris-HCl, pH 8.0, and 100 mM NaCl. 15 min after the addition of the stop solution the fluorescence intensity was measured at excitation of 355 nm and emission of 460 nm in a NOVOstar microplate reader (BMG LabTech, Offenburg, Germany).

Measurement of Apoptotic Nuclei

A2780 and TOV21GcisR cells were seeded at a density of 30,000 c/w in 24-well plates (Sarstedt, Nürnbrecht, Germany). Cells were treated with bortezomib and/or CHDI-00390576 as indicated for 24 or 48 h. Supernatant was removed after a centrifugation step and the cells were lysed in 500 µL hypotonic lysis buffer (0.1 % sodium citrate, 0.1 % Triton X-100, 100 µg/mL propidium iodide) at 4 °C in the dark overnight. The percentage of apoptotic nuclei with DNA content in sub-G1 was analyzed by flow cytometry using the CyFlow instrument (Partec, Norderstedt, Germany).

Caspase3/7 Activation Assay

Compound-induced activation of caspase3/7 was analyzed using the CellEvent Caspase-3/7 green detection reagent (Thermo Scientific, Wesel, Germany) according to the manufacturer´s instructions. Briefly, A2780 and TOV21GcisR cells were seeded in 96-well-plates (Corning, Kaiserslautern, Germany) at a density of 8,000 c/w. Cells were treated with bortezomib and/or CHDI-00390576 for 24 h. Then, medium was removed and 50 µL of CellEvent Caspase3/7 green detection reagent (2 µM in PBS supplemented with 5 % heat inactivated FCS) was added. Cells were incubated for 30 min at 37 °C under cell culture conditions before imaging by using the Thermo Fisher ArrayScan XTI high content screening (HCS) system with a 10X magnification (Thermo Scientific, Wesel, Germany). Hoechst 33342 was used for nuclei staining. The pan caspase inhibitor QVD was used in a concentration of 20 µM diluted in the appropriate medium and incubated 30 min prior to compound addition.

γH2AX-Assay

The γH2AX DNA damage assay was based on an assay published by Ziegler et al. (85) with minor modifications. Briefly, A2780 cells were seeded in 96-well tissue culture plates (Corning, Kaiserslautern, Germany) at a density of 6,000 c/w. Cells were treated with the indicated concentrations and compounds for 24 h. Cells were fixed with 4 % formaldehyde solution followed by incubation with ice-cold methanol and blocking buffer (5 % BSA, 0.3 % Triton X-100 in PBS). Cells were incubated with primary antibody (Cat. No. 05-636, Merck Millipore, Darmstadt, Germany) overnight at 4 °C and secondary fluorophore-labeled antibody (Northern Light Anti Mouse, Cat. No. NL007, Biotechne, Wiesbaden, Germany) for 2 hours in the dark. Cell nuclei were counterstained with Hoechst 33342. Analysis was performed with Thermo Fisher ArrayScan XTI (Thermo Scientific, Wesel, Germany).

RT-PCR

Cells were (co-)incubated with the indicated concentrations of CHDI and/or BTZ for 24 or 48 h. RNA was isolated using RNeasy Mini Kit (Qiagen, Hilden, Germany). Afterwards transcription to cDNA was performed with High Capacity cDNA Reverse Transcription Kit (Thermo Scientific, Wesel, Germany). RT-PCR was performed with GoTaq qPCR Master Mix (Promega, USA) in a CFX96 Real-Time System (BIO-RAD, Hercules, California, USA). Relative changes in gene expression were normalized to endogenous control genes *HPRT1* (hypoxanthine-guanine phosphoribosyltransferase), *TBP* (TATA binding protein), and *GUSB* (beta-glucuronidase) by Vandesompele method (67) and normalized to vehicle treated control. Primers (Sigma Aldrich, Steinheim, Germany) with an efficacy between 80.4 % and 111.3 % were used (Table 10). They were designed by Primer-BLAST (NIH, Bethesda, Maryland, USA) (86) and efficacy was determined with a template isolated from HeLa cells.

Table 10. Primer sequences for RT-PCR.

Gene	Primer Forward	Primer Reverse	Efficacy [%]
APAF1	AGTGGAATAACTTCGTATGTAAGGA	AAACAACTGGCCTCTGTGGT	98.7
BAD	TTGTGGACTCCTTTAAGAAGG	CACCAGGACTGGAAGACTCG	87.6
BAK1	TCATCGGGGACGACATCAAC	CAAACAGGCTGGTGGCAATC	111.3
BCL2	GATAACGGAGGCTGGGATGC	TCACTTGTGGCCCAGATAGG	82.9
BCL2L1	CAGTAAAGCAAGCGCTGAGG	CCACAAAAGTATCCTGTTCAAAGC	86.5
BCL2L11	AGACAGAGCCACAAGCTTCC	CAATACGCCGCAACTCTTGG	106.9
BIRC5	TGAGAACGAGCCAGACTTGG	TGTTCCTCTATGGGGTCGTCA	108.4
CCND1	ATCAAGTGTGACCCGGACTG	CTTGGGGTCCATGTTCTGCT	80.4
CDKN1A	TGCCGAAGTCAGTTCCTTGT	GTTCTGACATGGCGCCTCC	94.7
FOXO1	ATGTGTTGCCCAACCAAAGC	AGTGTAACCTGCTCACTAACCC	97.1
FOXO3	AAGGATCACTGAGGAAGGG	GTGTCAGTTTGAGGGTCTGC	90.3
GUSB	ACCTCCAAGTATCCCAAGGGT	GTCTTGCTCCACGCTGGT	83.1
HDAC4	TTGGATGTCACAGACTCCGC	CCTTCTCGTGCCACAAGTCT	80.8
HPRT1	CCTGGCGTCGTGATTAGTGA	CGAGCAAGACGTTCAGTCCT	93.6
MCL1	GTTAAACAAAGAGGCTGGGATGG	AGCAGCACATTCCTGATGCC	92.4
PTEN	ACTTGCAATCCTCAGTTTGTGG	TCGTGTGGGTCCTGAATTGG	90.1
TBP	GTGACCCAGCATCACTGTTTC	GAGCATCTCCAGCACACTCT	86.9
TP53	AGTCAGATCCTAGCGTCG	TCAGGAAGTAGTTTCCATAGG	102.9
XIAP	TTGGAAGCCCAGTGAAGACC	CAGATATTTGCACCCTGGATACC	97.7

Data Analysis

Concentration-effect curves were constructed with Prism 7.0 (GraphPad, San Diego, CA, USA) by fitting the pooled data of at least three experiments performed in triplicates (or stated otherwise) to the four-parameter logistic equation. Statistical analysis was performed using t-test. To analyze the synergistic effects of apoptosis induction, caspase3/7 activation, and formation of γH2AX, the values of the single treatments were summed up and the standard deviation was calculated. This value was compared with the value of the combination treatment using t-test as previously described (19,65).

Funding

We acknowledge support by the Deutsche Forschungsgemeinschaft (DFG) for grant KA 1942/1-1. Further, the DFG is acknowledged for funds used to purchase the ArrayScan XTI High Content Platform used in this research (INST 208/690-1).

Conflicts of Interest

The authors declare no conflict of interest.

Acknowledgements

The authors thank Ana J. Rodrigues Moita for establishing the cisplatin resistant “cisR” cell lines. We acknowledge support by the Heinrich Heine University Düsseldorf.

Abbreviations

BTZ	Bortezomib
Boc-Lys(Ac)-AMC	tert-Butyloxycarbonyl-acetyl-lysine-7-amido-4-methylcoumarin
Boc-Lys(Tfa)-AMC	tert-Butyloxycarbonyl-trifluoroacetyl-lysine-7-amido-4-methylcoumarin
cDDP	*cis*-diamminedichloridoplatinum(II) (cisplatin)
CHDI	CHDI-00390576
CI	combination index
DSB	double-strand breaks (DNA damage)
EMA	European Medicines Agency
FDA	Food and Drug Administration
HDAC(i)	histone deacetylase (inhibitor)
HGSOC	high grade serous ovarian cancer
LGSOC	low grade serous ovarian cancer
UPS	ubiquitin proteasome system

References

1. Buttmann-Schweiger N, Kraywinkel K. Epidemiologie von Eierstockkrebs in Deutschland. Onkol. 2019 Feb 1;25(2):92–8.

2. Cancer of the Ovary - Cancer Stat Facts [Internet]. SEER. [cited 2019 Apr 24]. Available from: https://seer.cancer.gov/statfacts/html/ovary.html

3. Cancer of the Cervix Uteri - Cancer Stat Facts [Internet]. SEER. [cited 2019 Apr 24]. Available from: https://seer.cancer.gov/statfacts/html/cervix.html

4. Cancer of the Breast (Female) - Cancer Stat Facts [Internet]. SEER. [cited 2019 Apr 24]. Available from: https://seer.cancer.gov/statfacts/html/breast.html

5. Cancer of the Vulva - Cancer Stat Facts [Internet]. SEER. [cited 2019 Apr 24]. Available from: https://seer.cancer.gov/statfacts/html/vulva.html

6. Cancer of the Endometrium - Cancer Stat Facts [Internet]. SEER. [cited 2019 Apr 24]. Available from: https://seer.cancer.gov/statfacts/html/corp.html

7. Krebs - Datenbankabfrage [Internet]. [cited 2019 May 14]. Available from: https://www.krebsdaten.de/Krebs/SiteGlobals/Forms/Datenbankabfrage/datenbankabfrage_stufe2_form.html

8. Kohn EC, Ivy SP. Whence High-Grade Serous Ovarian Cancer. Am Soc Clin Oncol Educ Book Am Soc Clin Oncol Annu Meet. 2017;37:443–8.

9. Koshiyama M, Matsumura N, Konishi I. Subtypes of Ovarian Cancer and Ovarian Cancer Screening. Diagnostics [Internet]. 2017 Mar 2 [cited 2019 May 21];7(1). Available from: https://www.ncbi.nlm.nih.gov/pmc/articles/PMC5373021/

10. Singh N, McCluggage WG, Gilks CB. High-grade serous carcinoma of tubo-ovarian origin: recent developments. Histopathology. 2017;71(3):339–56.

11. Köbel M, Kalloger SE, Huntsman DG, Santos JL, Swenerton KD, Seidman JD, et al. Differences in tumor type in low-stage versus high-stage ovarian carcinomas. Int J Gynecol Pathol Off J Int Soc Gynecol Pathol. 2010 May;29(3):203–11.

12. Eisenhauer EA. Real-world evidence in the treatment of ovarian cancer. Ann Oncol Off J Eur Soc Med Oncol. 2017 Nov 1;28(suppl_8):viii61–5.

13. Ghosh S. Cisplatin: The first metal based anticancer drug. Bioorganic Chem. 2019 Apr 11;88:102925.

14. Galluzzi L, Senovilla L, Vitale I, Michels J, Martins I, Kepp O, et al. Molecular mechanisms of cisplatin resistance. Oncogene. 2012 Apr;31(15):1869–83.

15. Galluzzi L, Vitale I, Michels J, Brenner C, Szabadkai G, Harel-Bellan A, et al. Systems biology of cisplatin resistance: past, present and future. Cell Death Dis. 2014 May;5(5):e1257–e1257.

16. Morel D, Jeffery D, Aspeslagh S, Almouzni G, Postel-Vinay S. Combining epigenetic drugs with other therapies for solid tumours - past lessons and future promise. Nat Rev Clin Oncol. 2020 Feb;17(2):91–107.

17. Ohmichi M, Hayakawa J, Tasaka K, Kurachi H, Murata Y. Mechanisms of platinum drug resistance. Trends Pharmacol Sci. 2005 Mar 1;26(3):113–6.

18. Jain A, Jahagirdar D, Nilendu P, Sharma NK. Molecular approaches to potentiate cisplatin responsiveness in carcinoma therapeutics. Expert Rev Anticancer Ther. 2017;17(9):815–25.

19. Bandolik JJ, Hamacher A, Schrenk C, Weishaupt R, Kassack MU. Class I-Histone Deacetylase (HDAC) Inhibition is Superior to pan-HDAC Inhibition in Modulating Cisplatin Potency in High Grade Serous Ovarian Cancer Cell Lines. Int J Mol Sci. 2019 Jun 22;20(12):3052.

20. Rodrigues Moita AJ, Bandolik JJ, Hansen FK, Kurz T, Hamacher A, Kassack MU. Priming with HDAC Inhibitors Sensitizes Ovarian Cancer Cells to Treatment with Cisplatin and HSP90 Inhibitors. Int J Mol Sci. 2020 Jan;21(21):8300.

21. Marek L, Hamacher A, Hansen FK, Kuna K, Gohlke H, Kassack MU, et al. Histone deacetylase (HDAC) inhibitors with a novel connecting unit linker region reveal a selectivity profile for HDAC4 and HDAC5 with improved activity against chemoresistant cancer cells. J Med Chem. 2013 Jan 24;56(2):427–36.

22. Krieger V, Hamacher A, Cao F, Stenzel K, Gertzen CGW, Schäker-Hübner L, et al. Synthesis of Peptoid-Based Class I-Selective Histone Deacetylase Inhibitors with Chemosensitizing Properties. J Med Chem. 2019 Dec 26;62(24):11260–79.

23. Stenzel K, Hamacher A, Hansen FK, Gertzen CGW, Senger J, Marquardt V, et al. Alkoxyurea-Based Histone Deacetylase Inhibitors Increase Cisplatin Potency in Chemoresistant Cancer Cell Lines. J Med Chem. 2017 Jul 13;60(13):5334–48.

24. Krieger V, Hamacher A, Gertzen CGW, Senger J, Zwinderman MRH, Marek M, et al. Design, Multicomponent Synthesis, and Anticancer Activity of a Focused Histone Deacetylase (HDAC) Inhibitor Library with Peptoid-Based Cap Groups. J Med Chem. 2017 Jul 13;60(13):5493–506.

25. Usami M, Kikuchi S, Takada K, Ono M, Sugama Y, Arihara Y, et al. FOXO3a Activation by HDAC Class IIa Inhibition Induces Cell Cycle Arrest in Pancreatic Cancer Cells: Pancreas. 2020 Jan;49(1):135–42.

26. Kikuchi S, Suzuki R, Ohguchi H, Yoshida Y, Lu D, Cottini F, et al. Class IIa HDAC inhibition enhances ER stress-mediated cell death in multiple myeloma. Leukemia. 2015 Sep;29(9):1918–27.

27. Gregoretti I, Lee Y-M, Goodson HV. Molecular Evolution of the Histone Deacetylase Family: Functional Implications of Phylogenetic Analysis. J Mol Biol. 2004 Apr 16;338(1):17–31.

28. Bates SE. Epigenetic Therapies for Cancer. Longo DL, editor. N Engl J Med. 2020 Aug 13;383(7):650–63.

29. Sanaei M, Kavoosi F. Histone Deacetylases and Histone Deacetylase Inhibitors: Molecular Mechanisms of Action in Various Cancers. Adv Biomed Res. 2019;8:63.

30. Eckschlager T, Plch J, Stiborova M, Hrabeta J. Histone Deacetylase Inhibitors as Anticancer Drugs. Int J Mol Sci. 2017 Jul 1;18(7).

31. Asfaha Y, Schrenk C, Alves Avelar LA, Hamacher A, Pflieger M, Kassack MU, et al. Recent advances in class IIa histone deacetylases research. Bioorg Med Chem. 2019 Nov;27(22):115087.

32. Asfaha Y, Schrenk C, Alves Avelar LA, Lange F, Wang C, Bandolik JJ, et al. Novel alkoxyamide-based histone deacetylase inhibitors reverse cisplatin resistance in chemoresistant cancer cells. Bioorg Med Chem. 2019 Sep 13;115108.

33. Yang Q, Yang Y, Zhou N, Tang K, Lau WB, Lau B, et al. Epigenetics in ovarian cancer: premise, properties, and perspectives. Mol Cancer. 2018 Jul 31;17(1):109.

34. Nandi D, Tahiliani P, Kumar A, Chandu D. The ubiquitin-proteasome system. J Biosci. 2006 Mar;31(1):137–55.

35. Adams J, Palombella VJ, Sausville EA, Johnson J, Destree A, Lazarus DD, et al. Proteasome inhibitors: a novel class of potent and effective antitumor agents. Cancer Res. 1999 Jun 1;59(11):2615–22.

36. Collins GA, Goldberg AL. The Logic of the 26S Proteasome. Cell. 2017 May 18;169(5):792–806.

37. Bard JAM, Goodall EA, Greene ER, Jonsson E, Dong KC, Martin A. Structure and Function of the 26S Proteasome. Annu Rev Biochem. 2018 20;87:697–724.

38. Budenholzer L, Cheng CL, Li Y, Hochstrasser M. Proteasome Structure and Assembly. J Mol Biol. 2017 10;429(22):3500–24.

39. Medina-Martinez I, Barrón V, Roman-Bassaure E, Juárez-Torres E, Guardado-Estrada M, Espinosa AM, et al. Impact of Gene Dosage on Gene Expression, Biological Processes and Survival in Cervical Cancer: A Genome-Wide Follow-Up Study. PLoS ONE [Internet]. 2014 May 30 [cited 2020 Nov 16];9(5). Available from: https://www.ncbi.nlm.nih.gov/pmc/articles/PMC4039463/

40. Dressman MA, Baras A, Malinowski R, Alvis LB, Kwon I, Walz TM, et al. Gene Expression Profiling Detects Gene Amplification and Differentiates Tumor Types in Breast Cancer. Cancer Res. 2003 May 1;63(9):2194–9.

41. Bortezomib Monograph for Professionals [Internet]. Drugs.com. [cited 2020 Nov 22]. Available from: https://www.drugs.com/monograph/bortezomib.html

42. Anonymous. Velcade [Internet]. European Medicines Agency. 2018 [cited 2020 Nov 22]. Available from: https://www.ema.europa.eu/en/medicines/human/EPAR/velcade

43. Manasanch EE, Orlowski RZ. Proteasome inhibitors in cancer therapy. Nat Rev Clin Oncol. 2017 Jul;14(7):417–33.

44. Seoul National University Hospital. A Phase II Trial to Evaluate the Efficacy of Bortezomib and Pegylated Liposomal Doxorubicin in Patients With BRCA Wild-type Platinum-resistant Recurrent Ovarian Cancer [Internet]. clinicaltrials.gov; 2020 Jan [cited 2020 Nov 24]. Report No.: NCT03509246. Available from: https://clinicaltrials.gov/ct2/show/NCT03509246

45. Fang Y, Hu Y, Wu P, Wang B, Tian Y, Xia X, et al. Synergistic efficacy in human ovarian cancer cells by histone deacetylase inhibitor TSA and proteasome inhibitor PS-341. Cancer Invest. 2011 May;29(4):247–52.

46. Jin X, Fang Y, Hu Y, Chen J, Liu W, Chen G, et al. Synergistic activity of the histone deacetylase inhibitor trichostatin A and the proteasome inhibitor PS-341 against taxane-resistant ovarian cancer cell lines. Oncol Lett. 2017 Jun;13(6):4619–26.

47. Gosepath EM, Eckstein N, Hamacher A, Servan K, von Jonquieres G, Lage H, et al. Acquired cisplatin resistance in the head-neck cancer cell line Cal27 is associated with decreased DKK1 expression and can partially be reversed by overexpression of DKK1. Int J Cancer. 2008 Nov 1;123(9):2013–9.

48. Beaufort CM, Helmijr JCA, Piskorz AM, Hoogstraat M, Ruigrok-Ritstier K, Besselink N, et al. Ovarian Cancer Cell Line Panel (OCCP): Clinical Importance of In Vitro Morphological Subtypes. PLoS ONE [Internet]. 2014 Sep 17 [cited 2019 May 6];9(9). Available from: https://www.ncbi.nlm.nih.gov/pmc/articles/PMC4167545/

49. Cellosaurus cell line A2780 (CVCL_0134) [Internet]. [cited 2020 Dec 20]. Available from: https://web.expasy.org/cellosaurus/CVCL_0134

50. Hallas-Potts A, Dawson JC, Herrington CS. Ovarian cancer cell lines derived from non-serous carcinomas migrate and invade more aggressively than those derived from high-grade serous carcinomas. Sci Rep. 2019 Dec;9(1):5515.

51. Eva A, Robbins KC, Andersen PR, Srinivasan A, Tronick SR, Reddy EP, et al. Cellular genes analogous to retroviral onc genes are transcribed in human tumour cells. Nature. 1982 Jan;295(5845):116–9.

52. Hernandez L, Kim MK, Lyle LT, Bunch KP, House CD, Ning F, et al. Characterization of ovarian cancer cell lines as in vivo models for preclinical studies. Gynecol Oncol. 2016 Aug;142(2):332–40.

53. Buick RN, Pullano R, Trent JM. Comparative properties of five human ovarian adenocarcinoma cell lines. Cancer Res. 1985 Aug;45(8):3668–76.

54. Domcke S, Sinha R, Levine DA, Sander C, Schultz N. Evaluating cell lines as tumour models by comparison of genomic profiles. Nat Commun. 2013 Jul 9;4:2126.

55. Cellosaurus cell line Caov-3 (CVCL_0201) [Internet]. [cited 2020 Dec 20]. Available from: https://web.expasy.org/cellosaurus/CVCL_0201

56. Cellosaurus cell line HEY (CVCL_0297) [Internet]. [cited 2020 Dec 20]. Available from: https://web.expasy.org/cellosaurus/CVCL_0297

57. Cellosaurus cell line OVCAR-3 (CVCL_0465) [Internet]. [cited 2020 Dec 20]. Available from: https://web.expasy.org/cellosaurus/CVCL_0465

58. Provencher DM, Lounis H, Champoux L, Tétrault M, Manderson EN, Wang JC, et al. Characterization of four novel epithelial ovarian cancer cell lines. Vitro Cell Dev Biol - Anim. 2000 Jun 1;36(6):357–61.

59. Cellosaurus cell line TOV-21G (CVCL_3613) [Internet]. [cited 2020 Dec 20]. Available from: https://web.expasy.org/cellosaurus/CVCL_3613

60. Panteix G, Beaujard A, Garbit F, Chaduiron-Faye C, Guillaumont M, Gilly F, et al. Population pharmacokinetics of cisplatin in patients with advanced ovarian cancer during intraperitoneal hyperthermia chemotherapy. Anticancer Res. 2002 Apr;22(2B):1329–36.

61. Tan CRC, Abdul-Majeed S, Cael B, Barta SK. Clinical Pharmacokinetics and Pharmacodynamics of Bortezomib. Clin Pharmacokinet. 2019 Feb;58(2):157–68.

62. Chou T-C. Drug combination studies and their synergy quantification using the Chou-Talalay method. Cancer Res. 2010 Jan 15;70(2):440–6.

63. Chou T-C, Talalay P. Quantitative analysis of dose-effect relationships: the combined effects of multiple drugs or enzyme inhibitors. Adv Enzyme Regul. 1984 Jan 1;22:27–55.

64. Luckhurst CA, Aziz O, Beaumont V, Bürli RW, Breccia P, Maillard MC, et al. Development and characterization of a CNS-penetrant benzhydryl hydroxamic acid class IIa histone deacetylase inhibitor. Bioorg Med Chem Lett. 2019 Jan;29(1):83–8.

65. Sinatra L, Bandolik JJ, Roatsch M, Sönnichsen M, Schoeder CT, Hamacher A, et al. Hydroxamic Acids Immobilized on Resins (HAIRs): Synthesis of Dual-Targeting HDAC Inhibitors and HDAC Degraders (PROTACs). Angew Chem Int Ed Engl. 2020 Dec 7;59(50):22494–9.

66. Roos WP, Kaina B. DNA damage-induced cell death: From specific DNA lesions to the DNA damage response and apoptosis. Cancer Lett. 2013 May;332(2):237–48.

67. Vandesompele J, De Preter K, Pattyn F, Poppe B, Van Roy N, De Paepe A, et al. Accurate normalization of real-time quantitative RT-PCR data by geometric averaging of multiple internal control genes. Genome Biol. 2002 Jun 18;3(7):RESEARCH0034.

68. Benton CB, Fiskus W, Bhalla KN. Targeting Histone Acetylation: Readers and Writers in Leukemia and Cancer. Cancer J Sudbury Mass. 2017 Oct;23(5):286–91.

69. Pchejetski D, Alfraidi A, Sacco K, Alshaker H, Muhammad A, Monzon L. Histone deacetylases as new therapy targets for platinum-resistant epithelial ovarian cancer. J Cancer Res Clin Oncol. 2016 Aug;142(8):1659–71.

70. Spiegel S, Milstien S, Grant S. Endogenous modulators and pharmacological inhibitors of histone deacetylases in cancer therapy. Oncogene. 2012 Feb 2;31(5):537–51.

71. Ozaki K, Kishikawa F, Tanaka M, Sakamoto T, Tanimura S, Kohno M. Histone deacetylase inhibitors enhance the chemosensitivity of tumor cells with cross-resistance to a wide range of DNA-damaging drugs. Cancer Sci. 2008 Feb;99(2):376–84.

72. Jandial DA, Brady WE, Howell SB, Lankes HA, Schilder RJ, Beumer JH, et al. A phase I pharmacokinetic study of intraperitoneal bortezomib and carboplatin in patients with persistent or recurrent ovarian cancer: An NRG Oncology/Gynecologic Oncology Group study. Gynecol Oncol. 2017 May;145(2):236–42.

73. Ramirez PT, Landen CN, Coleman RL, Milam MR, Levenback C, Johnston TA, et al. Phase I trial of the proteasome inhibitor bortezomib in combination with carboplatin in patients with platinum- and taxane-resistant ovarian cancer. Gynecol Oncol. 2008 Jan;108(1):68–71.

74. Aghajanian C, Blessing JA, Darcy KM, Reid G, DeGeest K, Rubin SC, et al. A phase II evaluation of bortezomib in the treatment of recurrent platinum-sensitive ovarian or primary peritoneal cancer: a Gynecologic Oncology Group study. Gynecol Oncol. 2009 Nov;115(2):215–20.

75. Bonvini P, Zorzi E, Basso G, Rosolen A. Bortezomib-mediated 26S proteasome inhibition causes cell-cycle arrest and induces apoptosis in CD-30+ anaplastic large cell lymphoma. Leukemia. 2007 Apr;21(4):838–42.

76. Mpakou V, Papadavid E, Kontsioti F, Konsta E, Vikentiou M, Spathis A, et al. Apoptosis Induction and Gene Expression Profile Alterations of Cutaneous T-Cell Lymphoma Cells following Their Exposure to Bortezomib and Methotrexate. PLoS ONE [Internet]. 2017 Jan 20 [cited 2020 Nov 18];12(1). Available from: https://www.ncbi.nlm.nih.gov/pmc/articles/PMC5249051/

77. Palanca A, Casafont I, Berciano MT, Lafarga M. Proteasome inhibition induces DNA damage and reorganizes nuclear architecture and protein synthesis machinery in sensory ganglion neurons. Cell Mol Life Sci. 2014 May;71(10):1961–75.

78. Stickles XB, Marchion DC, Bicaku E, Al Sawah E, Abbasi F, Xiong Y, et al. BAD-mediated apoptotic pathway is associated with human cancer development. Int J Mol Med. 2015 Apr;35(4):1081–7.

79. Liu Z, Zhang G, Huang S, Cheng J, Deng T, Lu X, et al. Induction of apoptosis in hematological cancer cells by dorsomorphin correlates with BAD upregulation. Biochem Biophys Res Commun. 2020 Feb 12;522(3):704–8.

80. Engelke LH, Hamacher A, Proksch P, Kassack MU. Ellagic Acid and Resveratrol Prevent the Development of Cisplatin Resistance in the Epithelial Ovarian Cancer Cell Line A2780. J Cancer. 2016;7(4):353–63.

81. Heltweg B, Jung M. A Microplate Reader-Based Nonisotopic Histone Deacetylase Activity Assay. Anal Biochem. 2002 Mar 15;302(2):175–83.

82. Ciossek T, Julius H, Wieland H, Maier T, Beckers T. A homogeneous cellular histone deacetylase assay suitable for compound profiling and robotic screening. Anal Biochem. 2008 Jan 1;372(1):72–81.

83. Bonfils C, Kalita A, Dubay M, Siu LL, Carducci MA, Reid G, et al. Evaluation of the pharmacodynamic effects of MGCD0103 from preclinical models to human using a novel HDAC enzyme assay. Clin Cancer Res Off J Am Assoc Cancer Res. 2008 Jun 1;14(11):3441–9.

84. Hoffmann K, Brosch G, Loidl P, Jung M. A non-isotopic assay for histone deacetylase activity. Nucleic Acids Res. 1999 May 1;27(9):2057–8.

85. Ziegler V, Albers A, Fritz G. Lovastatin protects keratinocytes from DNA damage-related pro-apoptotic stress responses stimulated by anticancer therapeutics. Biochim Biophys Acta. 2016 Jun;1863(6 Pt A):1082–92.

86. Ye J, Coulouris G, Zaretskaya I, Cutcutache I, Rozen S, Madden TL. Primer-BLAST: A tool to design target-specific primers for polymerase chain reaction. BMC Bioinformatics. 2012 Jun 18;13(1):134.

Supplemental Information

STable 1. Superadditive cytotoxic effect of BTZ and CHDI in CaOV3cisR, HEY, and OVCAR3.

CaOV3cisR		CHDI [µM]		HEY		CHDI [µM]		OVCAR3		CHDI [µM]	
		6	8			5	10			4	6
BTZ [nM]	5	*	1.4 %	BTZ [nM]	20	2.3 %	2.1 %	BTZ [nM]	5	6.6 %	4.2 %
	10	7.8 %	9.1 %		30	6.9 %	9.3 %		10	9.6 %	3.0 %
	-	-	-		40	*	1.2 %		20	3.6 %	*
	-	-	-		50	*	*		30	*	*
	-	-	-		60	*	*		40	1.7 %	*

Data shown are superadditive cytotoxic effect of the combination treatments with BTZ and CHDI corresponding to the results shown in SFigure 1. Effects were adjusted to vehicle control. * indicates calculated superadditive effects < 0 %. Data shown are the mean, n ≥ 3.

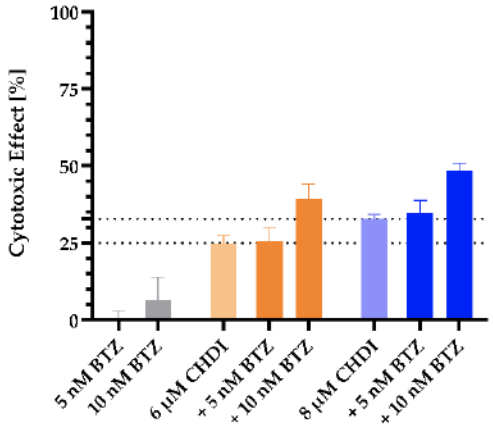

(A) CaOV3cisR

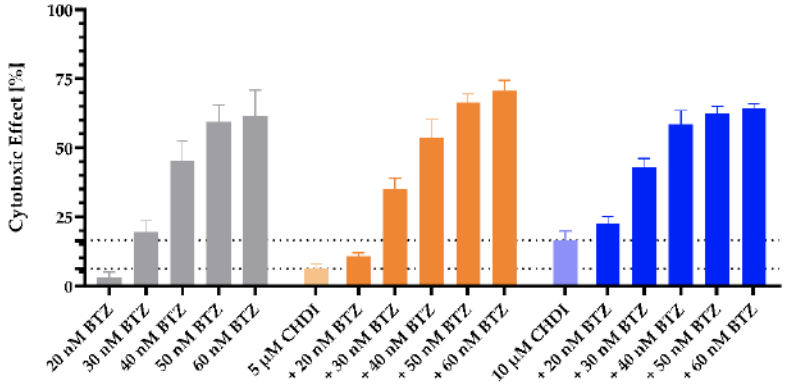

(B) HEY

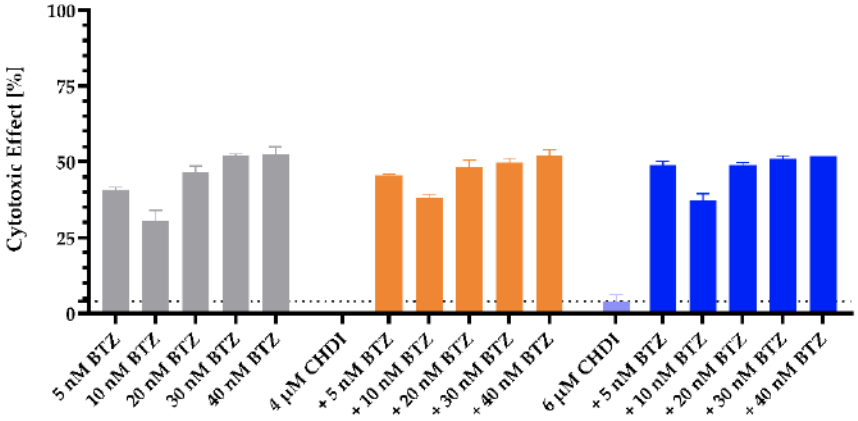

(C) OVCAR3

SFigure 1. Combined cytotoxic effect of BTZ and CHDI on CaOV3cisR, HEY, and OVCAR3 cells. CaOV3cisR (A), HEY (B), and OVCAR3 (C) cells were treated for 72 h with the indicated concentrations of BTZ and/or CHDI. Data shown are the cytotoxic effect normalized to vehicle control (mean ± SD, n ≥ 3).

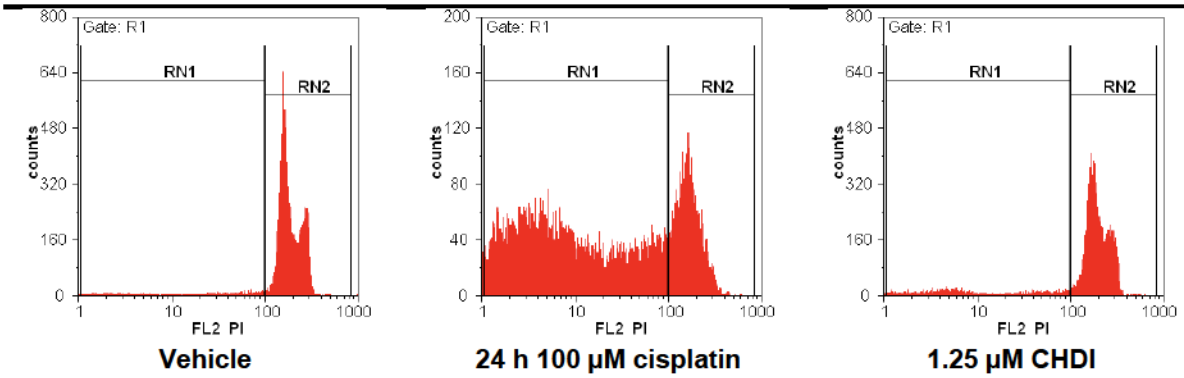

Vehicle | 24 h 100 µM cisplatin | 1.25 µM CHDI

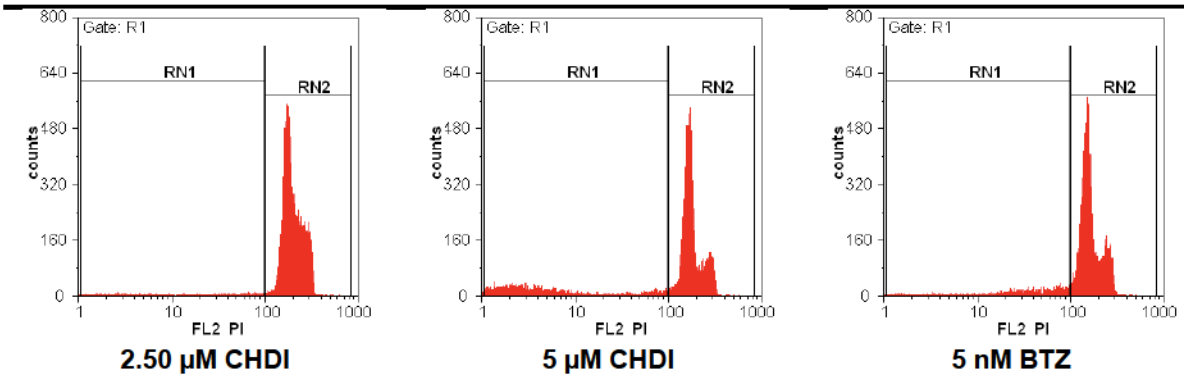

2.50 µM CHDI | 5 µM CHDI | 5 nM BTZ

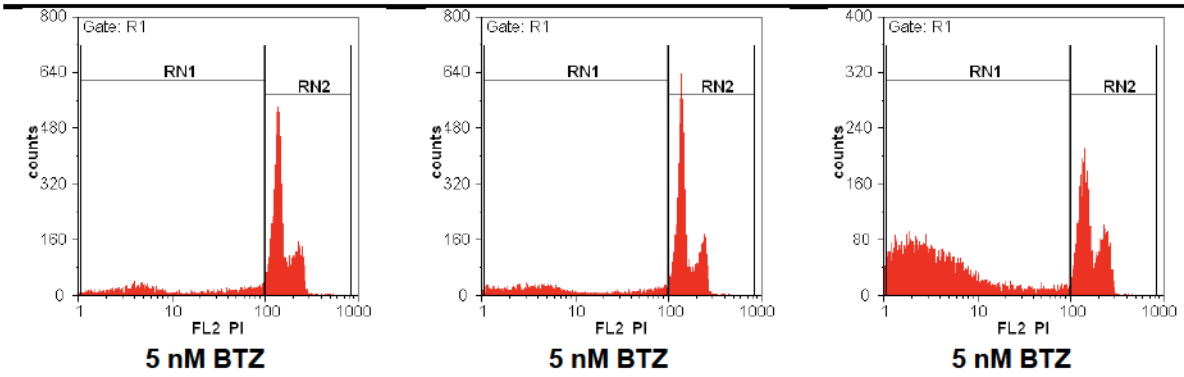

5 nM BTZ + 1.25 µM CHDI | 5 nM BTZ + 2.50 µM CHDI | 5 nM BTZ + 5 µM CHDI

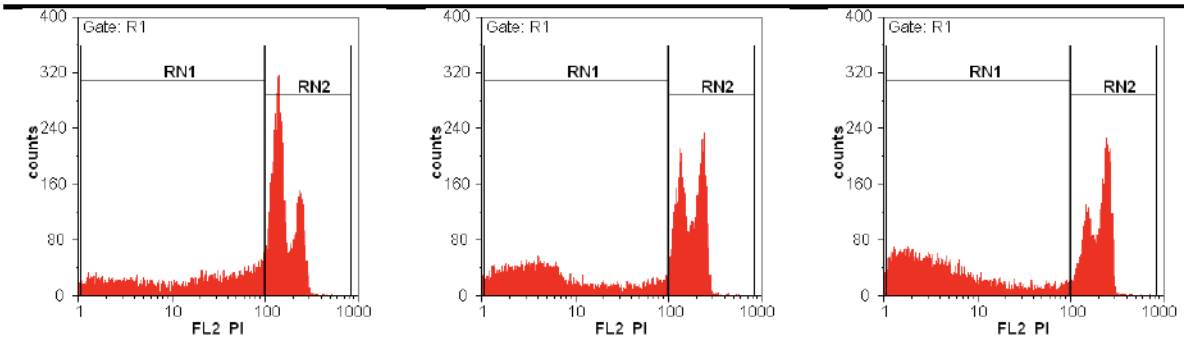

10 nM BTZ | 10 nM BTZ + 1.25 µM CHDI | 10 nM BTZ + 2.50 µM CHDI

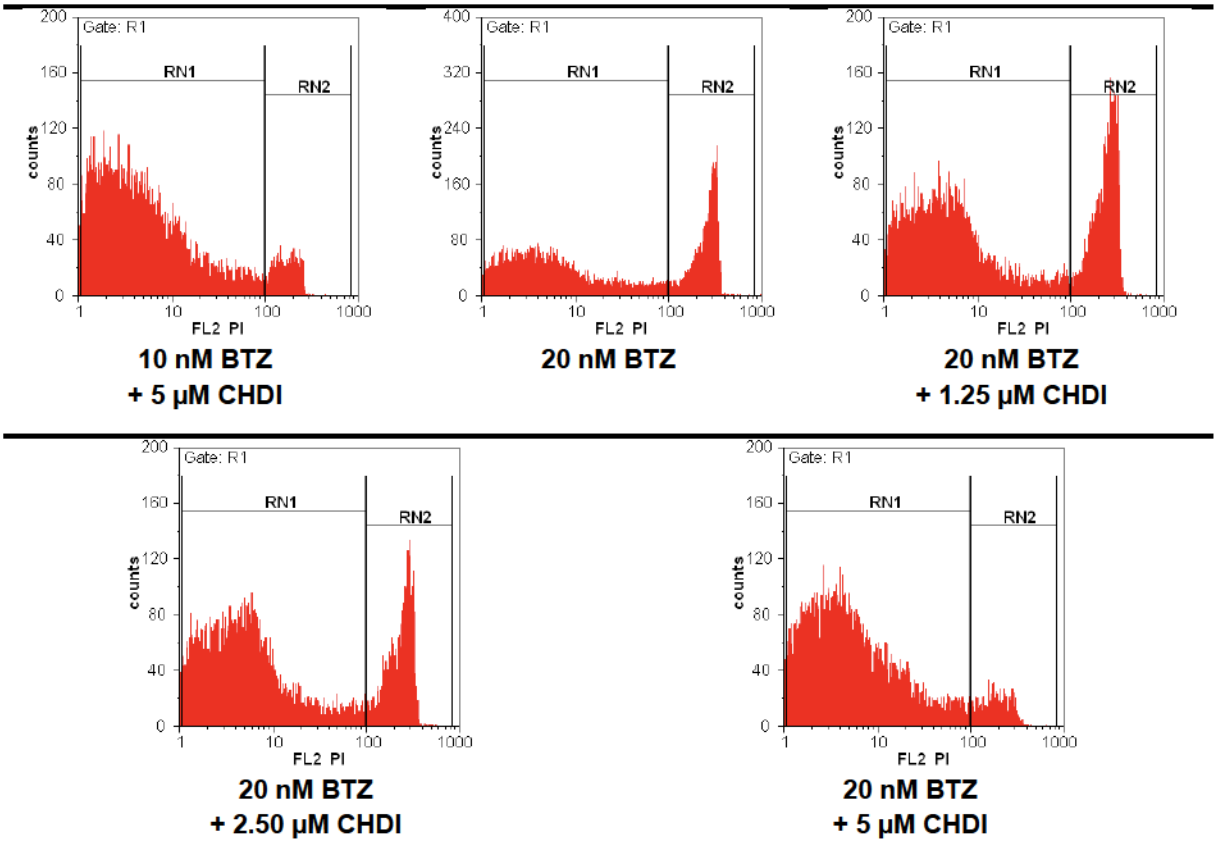

SFigure 2. Raw data of flow cytometry analysis (apoptosis assay) - A2780 cells with 24 h incubation time. The data shown are exemplary for the treatment indicated under the respective plot and correspond to Figure 4A. Cells counted in the RN1 region were classified as subG1. A2780 cells were treated for 24 h with the indicated inhibitors unless otherwise stated.

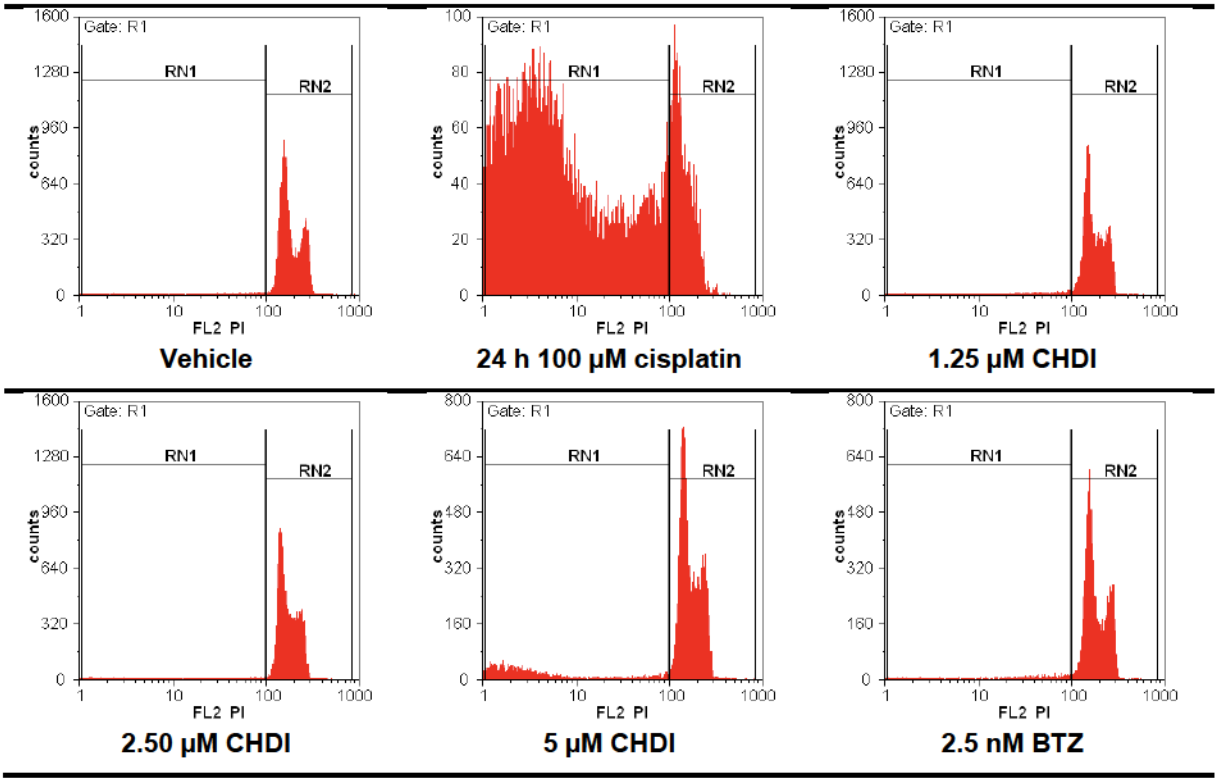

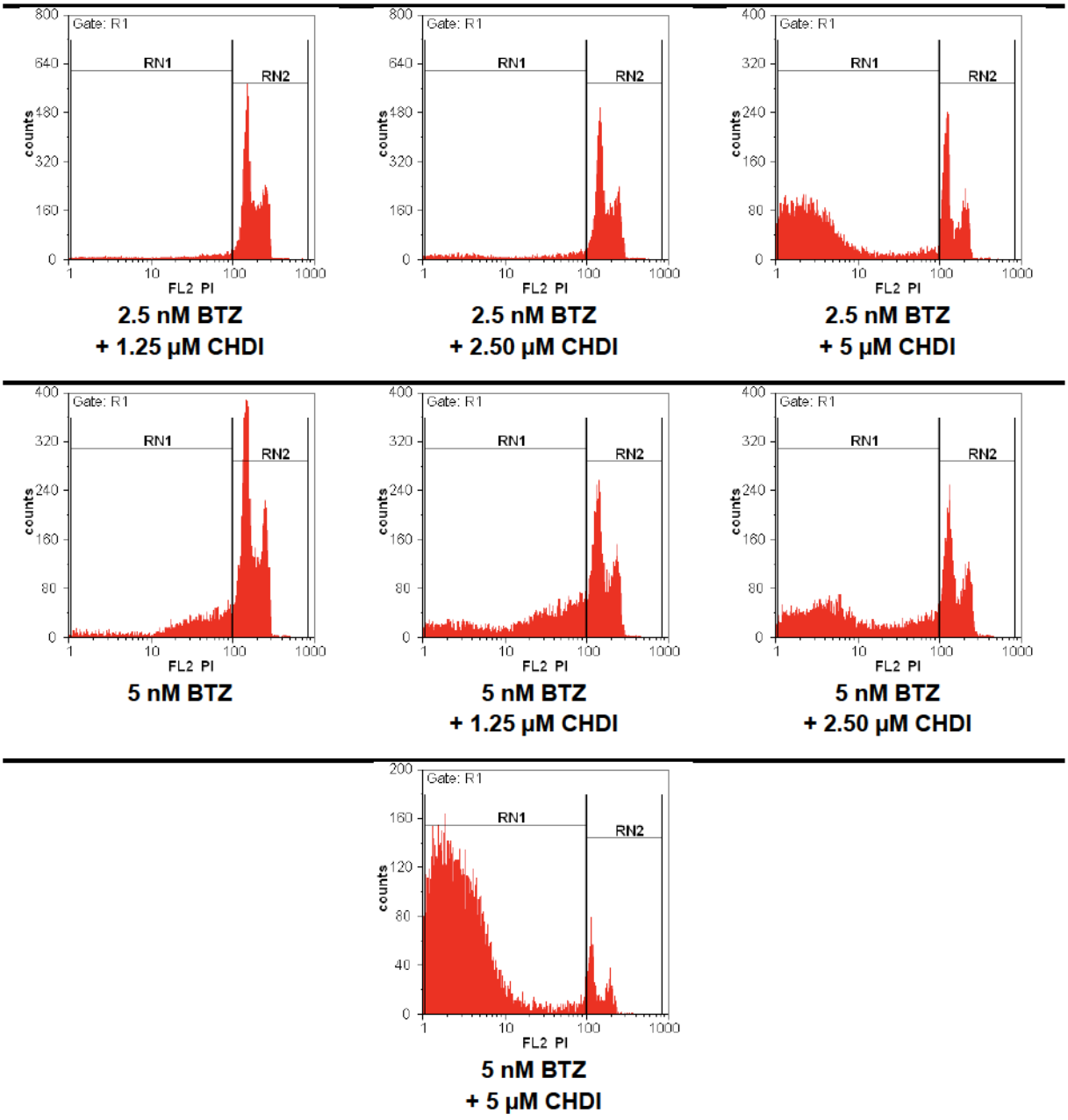

SFigure 3. Raw data of flow cytometry analysis (apoptosis assay) - A2780 cells with 48 h incubation time. The data shown are exemplary for the treatment indicated under the respective plot and correspond to Figure 4B. Cells counted in the RN1 region were classified as subG1. A2780 cells were treated for 48 h with the indicated inhibitors unless otherwise stated.

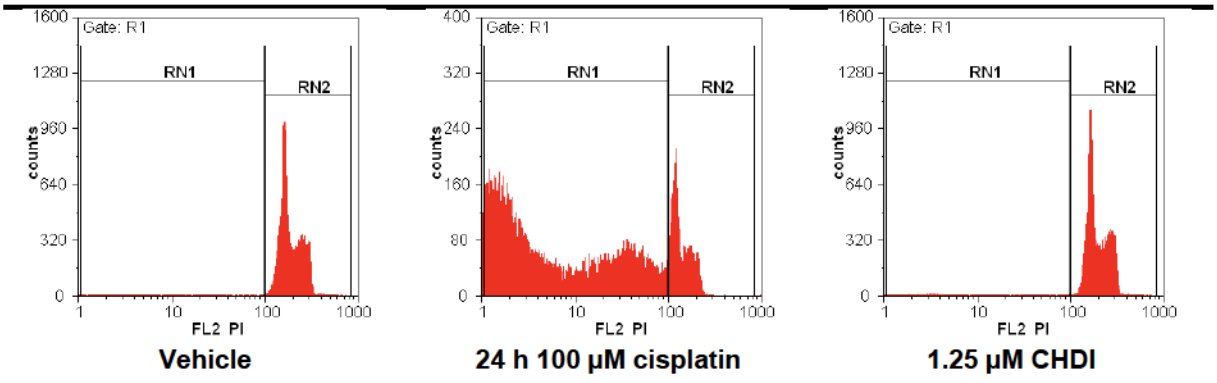

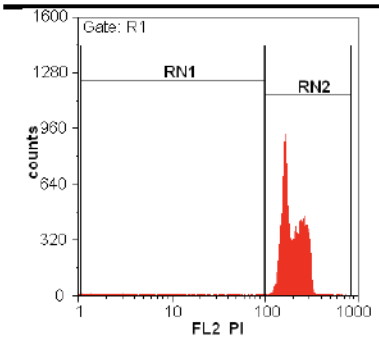

2.50 µM CHDI

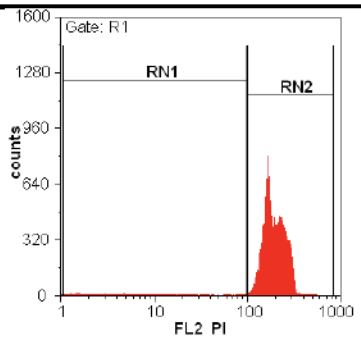

5 µM CHDI

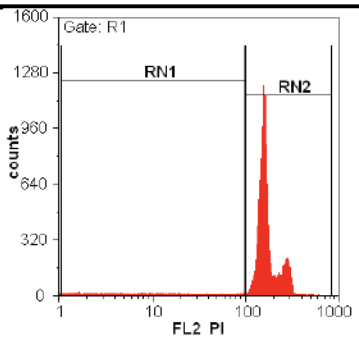

6.25 nM BTZ

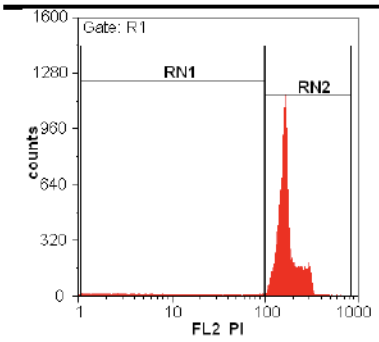

6.25 nM BTZ
+ 1.25 µM CHDI

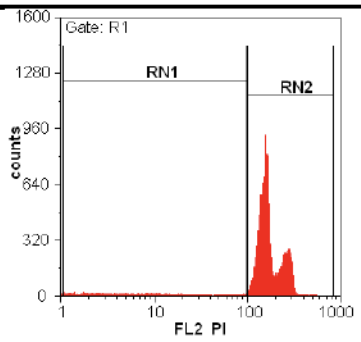

6.25 nM BTZ
+ 2.50 µM CHDI

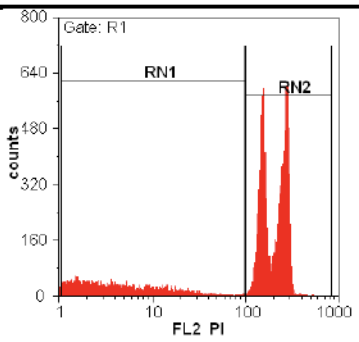

6.25 nM BTZ
+ 5 µM CHDI

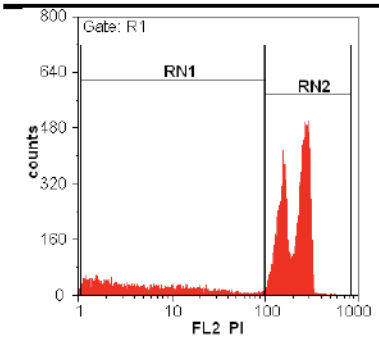

12.5 nM BTZ

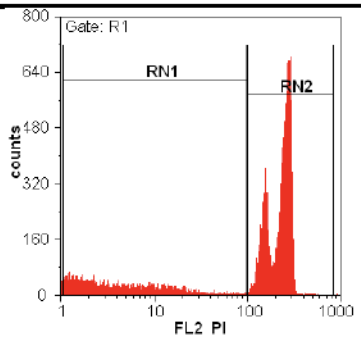

12.5 nM BTZ
+ 1.25 µM CHDI

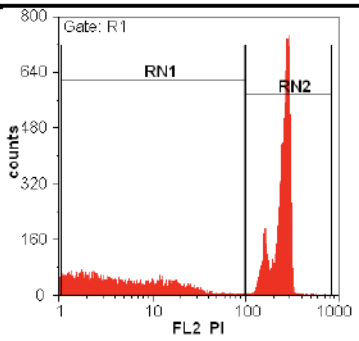

12.5 nM BTZ
+ 2.50 µM CHDI

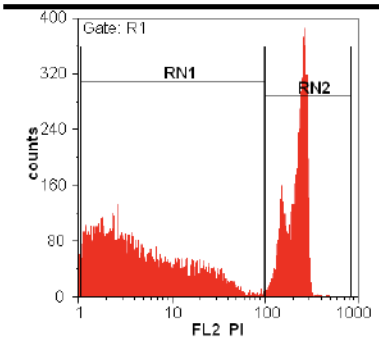

12.5 nM BTZ
+ 5 µM CHDI

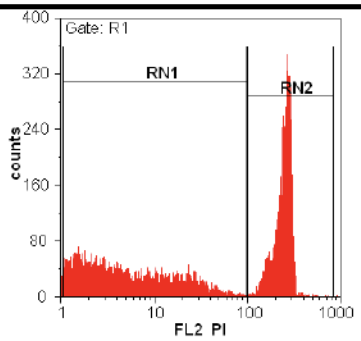

25 nM BTZ

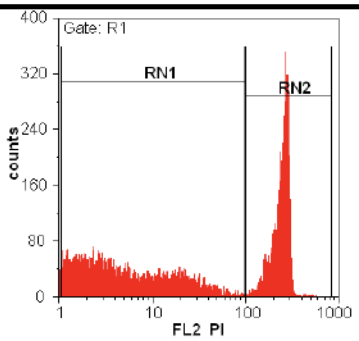

25 nM BTZ
+ 1.25 µM CHDI

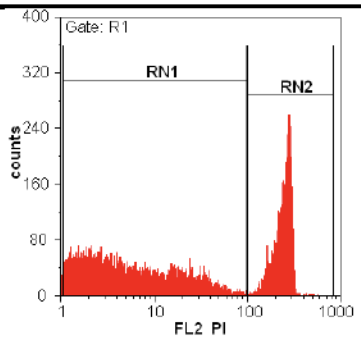

25 nM BTZ
+ 2.50 µM CHDI

SFigure 4. Raw data of flow cytometry analysis (apoptosis assay) - TOV21GcisR cells with 24 h incubation time. The data shown are exemplary for the treatment indicated under the respective plot and correspond to Figure 4C. Cells counted in the RN1 region were classified as subG1. TOV21GcisR cells were treated for 24 h with the indicated inhibitors unless otherwise stated.

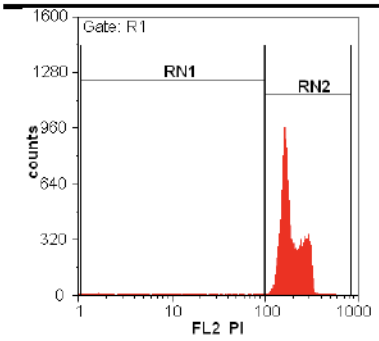

Vehicle

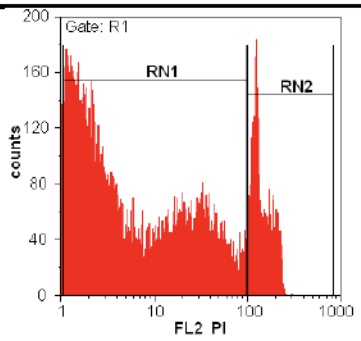

24 h 100 µM cisplatin

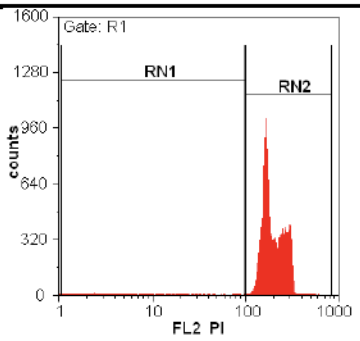

1.25 µM CHDI

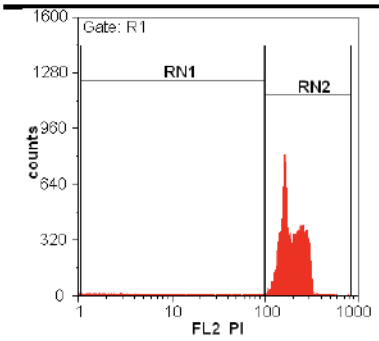

2.50 µM CHDI

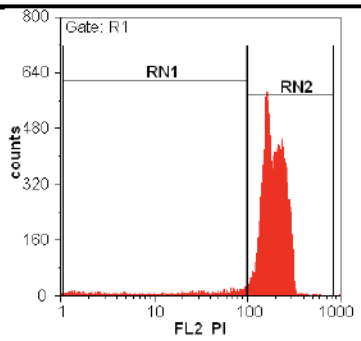

5 µM CHDI

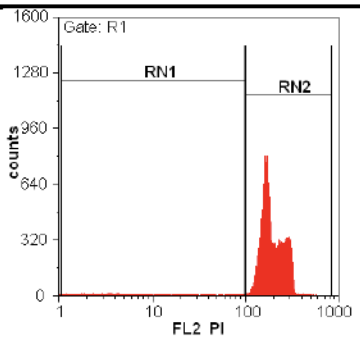

3.125 nM BTZ

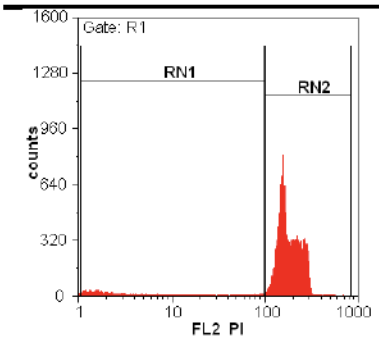

3.125 nM BTZ
+ 1.25 µM CHDI

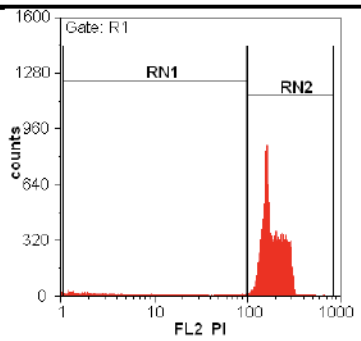

3.125 nM BTZ
+ 2.50 µM CHDI

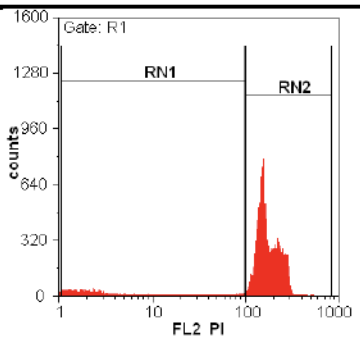

3.125 nM BTZ
+ 5 µM CHDI

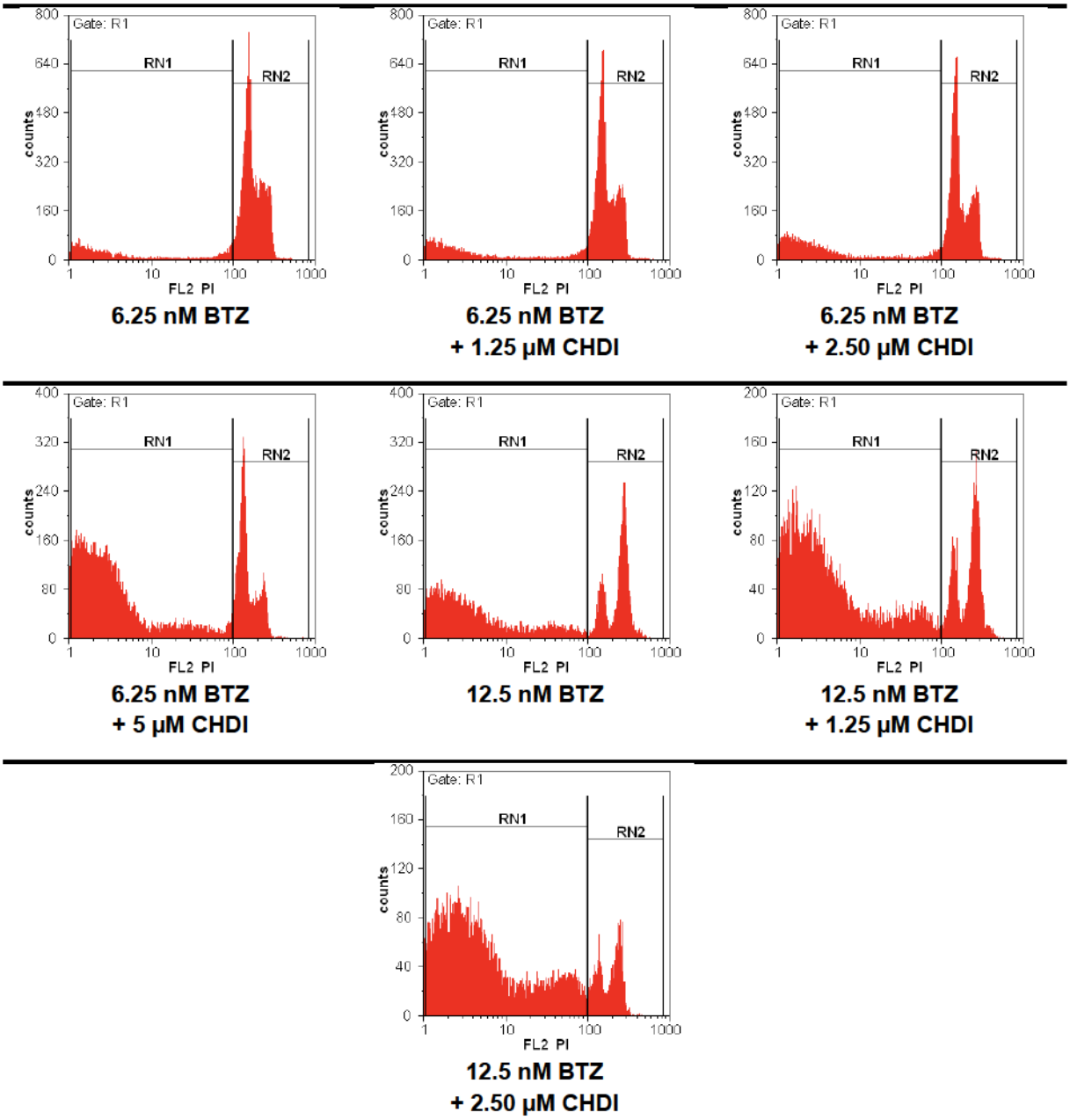

SFigure 5. Raw data of flow cytometry analysis (apoptosis assay) - TOV21GcisR cells with 48 h incubation time. The data shown are exemplary for the treatment indicated under the respective plot and correspond to Figure 4D. Cells counted in the RN1 region were classified as subG1. TOV21GcisR cells were treated for 48 h with the indicated inhibitors unless otherwise stated.

3.5 Dreifachkombination aus Cisplatin, HDACi und Kinaseinhibitoren

Nach den vielversprechenden Ergebnissen der dualen Kombination von Cisplatin und dem Klasse I selektiven HDACi Entinostat in Bandolik et al. (110) wurden Möglichkeiten zur Erweiterung der Kombinationstherapie um einen dritten Wirkstoff (*small molecule inhibitor*) analysiert. Ziele dieser Strategie waren zum einen eine Reduktion der eingesetzten Konzentrationen der jeweiligen Wirkstoffe infolge eines möglichen synergistischen Effektes. Dies könnte in klinischer Hinsicht zu einer Verringerung des Auftretens bzw. der Intensität von unerwünschten Arzneimittelwirkungen der einzelnen Wirkstoffe führen. Zum anderen könnte die gleichzeitige Inhibition verschiedener Signaltransduktionswege neue Therapieoptionen von chemoresistenten Ovarialkarzinomen eröffnen. Im Zuge dieses Versuchs der Weiterentwicklung der Kombinationsbehandlung haben sich zwei Wirkstoffgruppen als besonders beachtenswert herausgestellt: Inhibitoren der epidermalen Wachstumsfaktorrezeptoren (EGFRi) und Inhibitoren der Phosphoinositid-3-Kinasen (PI3Ki).

Die beiden Wirkstoffgruppen wurden aufgrund der dargestellten Zusammenhänge in Abbildung 6 bezüglich verschiedener Angriffspunkte im Rahmen der Bekämpfung einer Cisplatin-Resistenz als Kombinationspartner von Interesse ausgewählt. Durch die Erweiterung der Kombinationstherapie von Entinostat und Cisplatin mit diesen beiden Wirkstoffgruppen, wurde eine gegenseitige Verstärkung der Wirkung hinsichtlich der Auslösung von Apoptose erwartet. Während Entinostat das apoptotische Geschehen über Änderungen in der Expression pro- und antiapoptotischer Gene unterstützt, verhindern aktive EGFR- und PI3K-Signalwege die Auslösung von Apoptose. Durch eine Inhibierung dieser Strukturen erscheint ein verstärkender Effekt möglich. Auf die genauen Mechanismen, welche der Signaltransduktion durch EGFRs und PI3Ks zugrunde liegen und wie diese mit der Auslösung von Apoptose zusammenhängen, wird im Folgenden erläutert.

3.5.1 Erweiterung der Kombinationstherapie von Cisplatin und Entinostat durch Inhibitoren von epidermalen Wachstumsfaktorrezeptoren (EGFRi)

Der *epidermal growth factor receptor* (EGFR) ist eine transmembranäre Rezeptor-Tyrosinkinase. Liganden aus der epidermalen Wachstumsfaktorfamilie wie beispielsweise der epidermale Wachstumsfaktor EGF oder der transformierende Wachstumsfaktor TGFα können an EGFR binden und den Rezeptor aktivieren (114). Er ist Teil der ErbB- bzw. EGF-Rezeptorfamilie, was auch durch seine synonyme Bezeichnung ErbB-1 deutlich wird. Ebenfalls Teil der ErbB-Rezeptorfamilie sind die Wachstumsfaktorrezeptoren ErbB-2, ErbB-3 und ErbB-4. Sie weisen strukturelle Ähnlichkeit zum EGFR auf. Die Bindungsstelle für Liganden liegt extrazellulär, während das enzymatische Zentrum intrazellulär lokalisiert ist. Das enzymatische Zentrum bildet eine Bindestelle für ATP, welche von Wirkstoffen wie Lapatinib oder Gefitinib zur Inhibierung der Signaltransduktion genutzt werden kann. Nach extrazellulärer Ligandbindung wird eine Rezeptor-Dimerisierung induziert, die zu einer gegenseitigen Phosphorylierung von Tyrosin-Resten der beiden Rezeptor-Monomere führt (Autophosphorylierung). Für die Autophosphorylierung wird ATP als Cofaktor benötigt. Es werden verschiedene Signalmoleküle unter Bildung eines Signalkomplexes rekrutiert, welche durch ihre nachgeschalteten Bindungspartner die Signaltransduktion weiter in den Zellkern leiten. Nach Dissoziation des Signalkomplexes wird das Rezeptordimer per Endozytose internalisiert und entweder über Lysosomen degradiert oder wiederverwendet. Die Rezeptoren der EGF-Familie sind in der Lage, Heterodimere (z.B. aus EGFR und ErbB-2) zu bilden. Diese sind in der Regel weniger stabil, zerfallen nach der Rezeptorinternalisierung leichter und werden erneut verwendet, während Homodimere (z.B. aus zwei EGFR) stabiler sind und mit erhöhter Wahrscheinlichkeit degradiert werden. Für ErbB-2 sind keine natürlichen Liganden bekannt und somit kann dieser Rezeptor seine Signaltransduktion lediglich durch Heterodimerisierung mit anderen Mitgliedern der EGFR-Familie entfalten (115,116). Die Aktivierung der Rezeptoren führt zu diversen Effekten, unter anderem DNA-Synthese, Zellproliferation, Zellmigration, Adhäsion und Verhinderung der Apoptose (117).

EGF-Rezeptoren sind in verschiedenen Krebsarten exprimiert oder mutiert (118). Auch für Ovarialkarzinome konnte eine (Über-)Expression von EGFR und anderen Mitgliedern der Rezeptorfamilie gezeigt werden (119–121). Eine Überexpression von EGF-Rezeptoren führt zu einer Verstärkung der proliferativen Signaltransduktion

sowie der Abschwächung von apoptotischen Signalen, was in Kombination ein unkontrolliertes Zellwachstum unterstützt (42). Es sind verschiedene Mutationen von EGFR bekannt, welche vor allem bei der Behandlung von Lungenkrebs eine gesteigerte Rolle spielen (122), da sie dort häufiger auftreten und Zielstrukturen für Wirkstoffe darstellen können.

Im Rahmen der Untersuchung einer möglichen Dreierkombination von Cisplatin, Entinostat und EGFRi wurden die drei Wirkstoffe Lapatinib, Afatinib und AZD-3759 in die Experimente einbezogen. Die Strukturformeln sind in Abbildung 12 dargestellt.

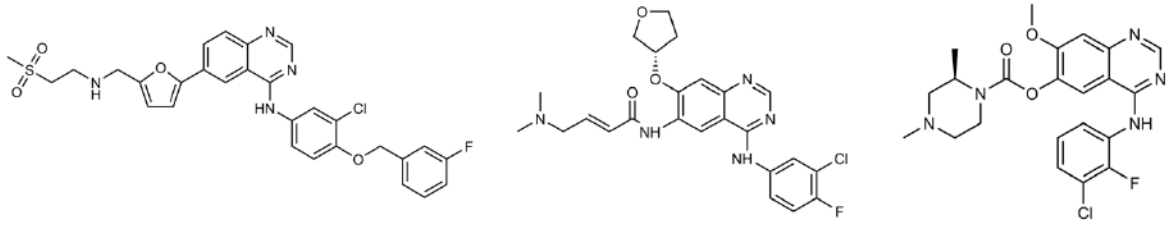

Abbildung 12: Lapatinib (links), Afatinib (zentral) und AZD-3759 (rechts).

Lapatinib ist ein reversibler Inhibitor von EGFR und ErbB-2 und tritt aufgrund struktureller Ähnlichkeit durch Bindung an der intrazellulären ATP-Bindungsstelle in Konkurrenz zu ATP, was die Autophosphorylierung im Rahmen der Rezeptoraktivierung hemmt (123). Es ist zur Behandlung von ErbB-2 positivem Brustkrebs im Rahmen einer Kombinationstherapie zugelassen. Bei Afatinib handelt es sich um einen peroral verfügbaren und irreversiblen Inhibitor von EGFR, ErbB-2 und ErbB-4. Die irreversible Hemmung kommt durch kovalente Bindung durch eine Michael-Addition (Afatinib trägt eine α,β-ungesättigte Carbonylverbindung, welche als Michael-Akzeptor dient) an einen Cystein-Rest der Rezeptoren zustande (124–126). Da es auch mutierte EGFR inhibieren kann, ist es zur Behandlung von nicht-kleinzelligem Lungenkrebs mit aktivierenden EGFR-Mutationen zugelassen. Als Vertreter der neuesten Generation von EGFR-Inhibitoren wurde AZD-3759 in die Untersuchungen eingeschlossen. Es ist aus der Leitstruktur des ATP-kompetitiven Inhibitors Gefitinib entstanden, ist oral bioverfügbar und ZNS-gängig, was sein Anwendungsgebiet zum Beispiel auf Hirnmetastasen von EGFR-positiven bzw. EGFR-mutierten Tumorarten erweitert (127). In diesem Kontext wird es momentan in verschiedenen klinischen Studien hinsichtlich Sicherheit und Wirksamkeit untersucht (128,129). Die drei Inhibitoren weisen unterschiedliche Profile hinsichtlich ihrer inhibitorischen Aktivität gegenüber den verschiedenen EGFR-Subtypen auf. Lapatinib inhibiert in ähnlichem Ausmaß EGFR (IC_{50}: 9,2 nM) und ErbB-2 (IC_{50}: 10,8 nM) und schwächer auch ErbB-4 (IC_{50}: 367 nM) (130). Afatinib inhibiert ebenfalls EGFR (IC_{50}:

0,5 nM), ErbB-2 (IC_{50}: 14 nM) und ErbB-4 (IC_{50}: 1 nM), sowie zwei Mutationen von EGFR im nanomolaren Bereich (L858R und L858R/T790M) (125,131). Die Experimentalsubstanz AZD-3759 inhibiert sowohl nicht mutierte EGFR (IC_{50}: 0,3 nM), als auch mutierte EGFR (L858R und Exon 19Del) im subnanomolaren Bereich (127). Die angegebenen IC_{50}-Werte beziehen sich auf Messungen am isolierten Enzym. Im zellulären Kontext sind in der Regel höhere Konzentrationen erforderlich. Der Mutationsstatus der EGF-Rezeptoren der verwendeten Zelllinien wurde in den durchgeführten Studien nicht bestimmt. Allerdings finden sich in der Literatur Hinweise auf eine Expression von EGFR bzw. ErbB-2 sowohl in A2780 als auch in HEY Zellen (132,133), was durch bisher unveröffentlichte Expressionsanalysen aus unserem Arbeitskreis bestätigt werden konnte.

Eine Kombinationsbehandlung bestehend aus Entinostat (oder anderen HDACi), EGFRi und Cisplatin an Ovarialkarzinomen bzw. entsprechenden Zelllinien ist bisher nicht in der Literatur beschrieben und wurde im Rahmen dieser Arbeit aufgrund der möglichen positiven Kombinationseffekte in ersten Experimenten untersucht.

Der verstärkende Einfluss von Entinostat auf die Behandlung von Ovarialkrebs-Zelllinien mit Cisplatin durch Steigerung der Apoptoserate konnte bereits gezeigt werden (110). Durch die Erweiterung der Behandlung mit einem EGFRi könnte zusätzlich zur verstärkten Apoptoseinduktion ein weiterer Impuls zur Hemmung der Zellproliferation gegeben werden. Außerdem verhindern aktive EGFR in gewissem Ausmaß die Einleitung der Apoptose. Zielsetzung dieser Folgeexperimente war die Überprüfung der These, ob sich die verstärkte Apoptoseinduktion der Kombinationsbehandlung von Entinostat und Cisplatin durch Hemmung von EGFR noch weiter steigern lässt.

In ersten Experimenten konnte gezeigt werden, dass eine gemeinsame 48-stündige Präinkubation von Entinostat und den EGFRi Lapatinib und Afatinib an den Zelllinien A2780 und HEY zu einer deutlichen Erhöhung der Zytotoxizität von Cisplatin führen konnte. Beispielhaft sind die Ergebnisse an A2780 Zellen der Kombination von Entinostat, Lapatinib und Cisplatin in Abbildung 13 dargestellt.

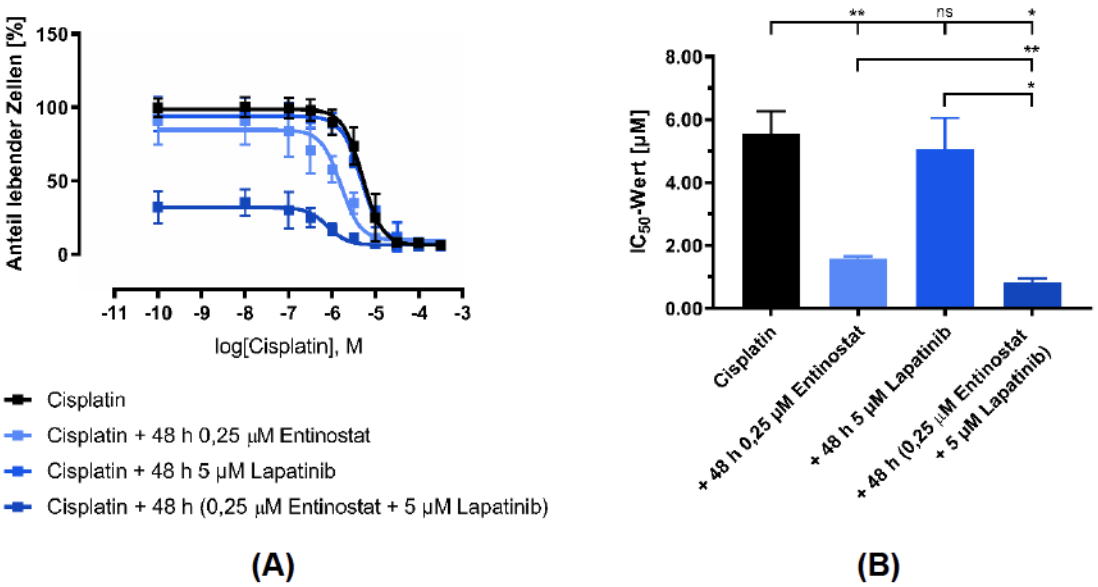

Abbildung 13: Einfluss von Entinostat und Lapatinib auf die Zytotoxizität von Cisplatin an A2780.

*A2780 Zellen wurden für 48 Stunden mit Entinostat und/oder Lapatinib präinkubiert. Anschließend wurden die Zellen für 72 Stunden mit verschiedenen Konzentrationen Cisplatin behandelt. Die Bestimmung der Zellviabilität per MTT-Assay und die Auswertung der erhaltenen Daten wurde nach Bandolik et al. (110) durchgeführt. Die dargestellten Ergebnisse stammen aus mindestens drei voneinander unabhängigen Experimenten, vermessen in Triplikaten, und zeigen den Mittelwert und die Standardabweichung (A) bzw. den Standardfehler (B) der einzelnen Datenpunkte. Signifikanzniveaus (t-Test): ns ($p > 0,05$); * ($p \leq 0,05$); ** ($p \leq 0,01$).*

Durch gleichzeitige Präinkubation mit 0,25 µM Entinostat und 5 µM Lapatinib konnte in A2780 der IC_{50}-Wert von Cisplatin von 5,54 µM auf 0,83 µM (Shift-Faktor (SF) = 6,67) signifikant gesenkt werden. Entinostat allein konnte den IC_{50}-Wert auf 1,59 µM (SF = 3,48) senken, während Lapatinib einen IC_{50}-Wert für Cisplatin von 5,06 µM (SF = 1,09) hervorrufen konnte. Für HEY Zellen konnte gezeigt werden, dass eine gleichzeitige Präinkubation mit 175 nM Entinostat (SF = 2,34) und Lapatinib (SF = 1,82) den IC_{50}-Wert für Cisplatin von 7,12 µM auf 0,99 µM (SF = 7,17) senken konnte. Im Gegensatz zu A2780 konnte an HEY Zellen ein ähnlicher Effekt auch für 0,25 µM Afatinib gezeigt werden. Afatinib allein zeigte einen Shift-Faktor von 1,71, während in der kombinierten Anwendung von Entinostat und Afatinib die Cisplatin-Sensitivität auf 1,22 µM (SF = 5,84) gesenkt werden konnte. Für die Kombination von Entinostat, AZD-3759 und Cisplatin konnten keine vergleichbaren Effekte hinsichtlich der Zytotoxizität von Cisplatin gezeigt werden. Sowohl für die Experimente mit A2780, als auch mit HEY konnten die eingesetzten Konzentrationen von Entinostat im Vergleich zur dualen Kombination mit Cisplatin in Bandolik et al. (110) zum Teil deutlich verringert werden.

Da für den verstärkenden Effekt von Entinostat auf Cisplatin maßgeblich die erhöhte Aktivierung von Caspasen 3/7 verantwortlich gemacht werden konnte (110), wurde auch zur Beurteilung der Kombinationsbehandlung aus Entinostat, EGFRi und

Cisplatin ein Caspase 3/7-Aktivierungs-Assay durchgeführt. Die Ergebnisse für A2780 sind in Abbildung 14 dargestellt.

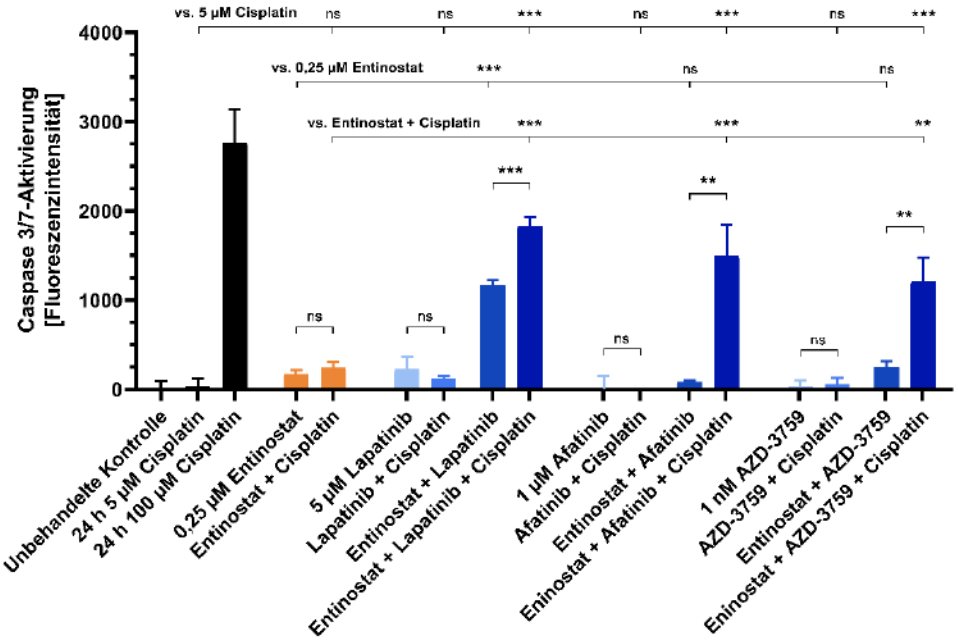

Abbildung 14: Einfluss der Kombination von Entinostat, EGFRi und Cisplatin an A2780 auf die Aktivierung von Caspase3/7.

*A2780 Zellen wurden für 48 Stunden mit Entinostat und/oder EGFRi (Lapatinib, Afatinib oder AZD-3759) präinkubiert. Anschließend wurden die Zellen für 24 Stunden mit 5 µM Cisplatin behandelt. Die Bestimmung der Caspase 3/7-Aktivität per fluoreszenzbasiertem Caspase-Assay und die Auswertung der erhaltenen Daten wurde nach Bandolik et al. (110) durchgeführt. Die dargestellten Ergebnisse haben explorativen Charakter, stammen aus einem Experiment (mindestens in Triplikaten vermessen) und zeigen den Mittelwert und die Standardabweichung der einzelnen Datenpunkte. Die Fluoreszenzintensität der unbehandelten Kontrolle wurde von allen Werten abgezogen. Signifikanzniveaus (t-Test): ns ($p > 0,05$); * ($p \leq 0,05$); ** ($p \leq 0,01$), *** ($p \leq 0,001$).*

Wie zu erkennen ist, verursachen weder 5 µM Cisplatin noch 0,25 µM Entinostat oder die eingesetzten EGFRi in ihren jeweiligen Konzentrationen eine signifikante Steigerung der Caspase-Aktivität. Auch die dualen Kombinationen aus Cisplatin und einem weiteren Inhibitor (entweder Entinostat oder EGFRi) zeigen keine erhöhte Caspase-Aktivität in A2780 Zellen. Innerhalb der dualen Kombinationen aus Entinostat und einem EGFRi, war die Kombination aus Entinostat und Lapatinib in der Lage eine signifikant erhöhte Caspase-Aktivität verglichen mit den beiden Einzelkomponenten zu verursachen. Alle untersuchten Triple-Kombinationen aus Entinostat, einem EGFRi und Cisplatin vermochten eine deutlich erhöhte Caspase-Aktivität auszulösen. Im Falle von Afatinib und AZD-3759 ist zu unterstreichen, dass jede beliebige duale Kombination aus diesen beiden EGFRi mit Entinostat und/oder Cisplatin nicht in der Lage war eine signifikante Aktivierung von Caspase 3/7 zu verursachen und somit nur die entsprechende Triple-Kombination effektiv war. An HEY Zellen ließ sich nach bisherigen Erkenntnissen kein analoger Effekt der Dreifachkombination hinsichtlich der

Caspase 3/7-Aktivität zeigen. Eine Steigerung der Caspase 3/7-Aktivität durch die Lapatinib enthaltene Dreifachkombination konnte in CaOV3-Zellen gezeigt werden.

Zusammenfassend ist festzuhalten, dass im Rahmen erster Experimente vielversprechende Ergebnisse für die Triple-Kombination aus Cisplatin, Entinostat und einem EGFRi generiert werden konnten. Es zeigt sich außerdem eine Tendenz für die Möglichkeit, die einzelnen Komponenten in geringeren Konzentrationen als in dualen Kombinationen einzusetzen. Würde sich ein solcher Sachverhalt auch in vivo oder im klinischen Alltag zeigen, bestünde wie einleitend erwähnt, die Möglichkeit, eine deutlich verringerte Häufigkeit bzw. Intensität der unerwünschten Wirkungen der Wirkstoffe festzustellen.

3.5.2 Erweiterung der Kombinationstherapie von Cisplatin und Entinostat durch Inhibitoren von Phosphoinositid-3-Kinasen (PI3Ki)

Der zusammenhängende Signaltransduktionsweg von Phosphoinositid-3-Kinasen (PI3K), Proteinkinase B (AKT oder PKB) und des *mechanistic/mammalian target of rapamcyin* (mTOR, dt. Ziel des Rapamycins im Säugetier) spielt im Krebsgeschehen eine zentrale Rolle (134,135) und wird im Rahmen verschiedener Krebsarten, wie zum Beispiel Karzinome des Ovars (136,137), der Brust (138) oder der Prostata (139), auch in Zusammenhang mit der Entwicklung von Therapieresistenzen untersucht. Der klinische Erfolg konnte zum Teil allerdings noch nicht ausreichend gezeigt werden. Grundsätzlich gibt es vier Klassen (I-IV) von PI3K – da die drei Wirkstoffe dieser Studie PI3Ks der Klasse I adressieren, wird im Folgenden vorwiegend auf diese eingegangen. Innerhalb von Klasse I werden weiterführend die Klassen IA und IB unterschieden. Klasse I PI3Ks katalysieren die Umsetzung von PIP_2 (Phosphatidylinositol-4,5-bisphosphat) zu PIP_3 (Phosphatidylinositol-3,4,5-trisphosphat) und werden im Fall von Klasse IA durch Rezeptor-Tyrosinkinasen (wie Kinasen der EGFR-Familie) oder durch GPCRs (G-Protein gekoppelte Rezeptoren) im Fall von Klasse IB, aktiviert. Klasse I PI3K sind Heterodimere und bestehen aus einer p85 (Klasse IA) bzw. p101 (Klasse IB) regulatorischen Untereinheit und einer p110 katalytischen Untereinheit. Für die katalytische Untereinheit gibt es vier unterschiedliche codierende Gene. Je nachdem, welche katalytische Untereinheit exprimiert wird und Teil des jeweiligen Heterodimers ist, werden PI3K α, β, γ (Klasse IA) oder δ (Klasse ID) unterschieden. Daraus ergibt

sich für diese Untereinheiten die jeweilige Schreibweise p110α, p110β, p110γ oder p110δ. Die Aktivierung von PI3K führt zur Aktivierung durch Phosphorylierung von AKT. mTOR kann in vivo als Teil zweier Komplexe vorliegen: mTOR-Komplex 1 (mTORC1) oder mTOR-Komplex 2 (mTORC2). Die Aktivierung von mTORC1 oder mTORC2 führt zu einer Steigerung der Translation von Proteinen, was zu gesteigertem Zellwachstum und damit Zellproliferation führt (140,141). Aktiviertes AKT aktiviert mTORC1 durch Phosphorylierung von mTOR. In der Literatur ist außerdem eine Aktivierung von mTORC2 direkt durch PI3K beschrieben (142). Aktivierung von mTORC2 führt indirekt, über Aktivierung von AKT ebenfalls zur Aktivierung mTORC1. Der wichtigste Regulator des PI3K/AKT/mTOR-Signalweges ist der Tumorsuppressor PTEN (*phosphatase and tensin homolog*). PTEN wandelt PIP_3 zu PIP_2 um und verhindert somit die PIP_3-abhängige Aktivierung von AKT (143). Eine Senkung der Aktivität oder ein vollständiges Fehlen von PTEN durch genetische Mutationen führt auf der anderen Seite zu einer Ansammlung von PIP_3 und damit zu einer verlängerten und nicht mehr regulierten Aktivierung von AKT (137). Für Ovarialkarzinome konnte gezeigt werden, dass eine Funktionsbeeinträchtigung von PTEN in einer gewissen Anzahl von Fällen stattfindet (144).

Die Aktivierung des PI3K/AKT/mTOR-Signalweges führt alles in allem also zu einer gesteigerten Proliferation der Zellen und unterdrückt damit apoptotische Signale. Auf Basis dieser Eigenschaften wurden im Rahmen der folgenden Studien Inhibitoren dieses Signalweges in Kombination mit Cisplatin und Entinostat untersucht. Eine Dreierkombination dieser Wirkstoffe bzw. Wirkstoffklassen ist bisher nicht in der Literatur beschrieben. Allerdings ist beschrieben, dass A2780 Zellen, welche als Testsystem dienten, eine Deregulation des PI3K/AKT/mTOR-Signalweges aufgrund einer PTEN-Mutation (145–147) und einer Mutation in PI3Kα (146) aufweisen. Für HEY- und CaOV3-Zellen, an welchen Teile der Studie ebenfalls durchgeführt wurden, weisen laut Literatur derartige Deregulationen oder Mutationen nicht auf (146,147).

In die folgenden Untersuchungen wurden die PI3Ki Buparlisib (BKM-120), BGT-226 und Dactolisib (BEZ-235) eingeschlossen. Die Strukturformeln sind in Abbildung 15 dargestellt.

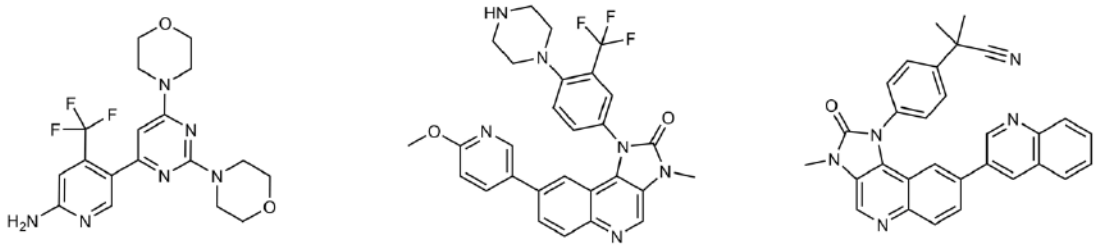

Abbildung 15: Buparlisib (links), BGT-226 (zentral) und Dactolisib (rechts).

Buparlisib ist vorwiegend ein nanomolarer und oral verfügbarer Inhibitor aller PI3Ks der Klasse I und zeigt nur schwache inhibitorische Wirkung auf mTOR im mittleren mikromolaren Bereich (145). Es war zuletzt Teil von Phase I Studien zur Klärung der klinischen Sicherheit und pharmakokinetischer Eigenschaften bei Patientinnen mit Ovarialkarzinomen und anderen soliden Tumoren (148,149). Weiterhin wurde es im Rahmen von Phase III Studien an Patientinnen mit fortgeschrittenem oder metastasierendem Brustkrebs, zumeist als Teil einer Kombinationstherapie, untersucht (150,151). Eine weitere Phase III Studie an Patienten mit Kopf-Hals-Tumoren ist geplant (152). BGT-226 inhibiert sowohl PI3Ks der Klasse I als auch mTOR im nanomolaren Bereich (153). Auch BGT-226 wurde bisher in Phase I Studien untersucht, allerdings nicht explizit an Ovarialkarzinomen, sondern entweder an fortgeschrittenen Brustkarzinomen (154) oder breiter an verschiedenen fortgeschrittenen soliden Tumoren (155). Dactolisib ist oral verfügbar, inhibiert ebenfalls PI3Ks der Klasse I und mTOR im nanomolaren Bereich. Mechanistisch wirkt es über ATP-Konkurrenz an der entsprechenden Bindungsstelle der PI3Ks (156). Es war der erste PI3Ki, welcher in klinischen Studien untersucht wurde. So wurde es im Rahmen einer abgeschlossenen Phase IB/II Studie an HER2-negativem Brustkrebs untersucht (157). Dactolisib wurde auch an anderen Krebsformen (Pankreastumore (158) und Nierenkarzinome (159)) untersucht. Diese Studien wurden allerdings aufgrund hoher Toxizität bzw. geringer klinischer Effizienz abgebrochen.

Es konnte gezeigt werden, dass eine gemeinsame 48-stündige Präinkubation mit Entinostat und Buparlisib (PI3Ki) oder BGT-226 (PI3Ki/mTORi) zu einer deutlichen Steigerung der Cisplatin-Sensitivität von A2780 Zellen führen konnte. Diese Daten sind in Abbildung 16 dargestellt.

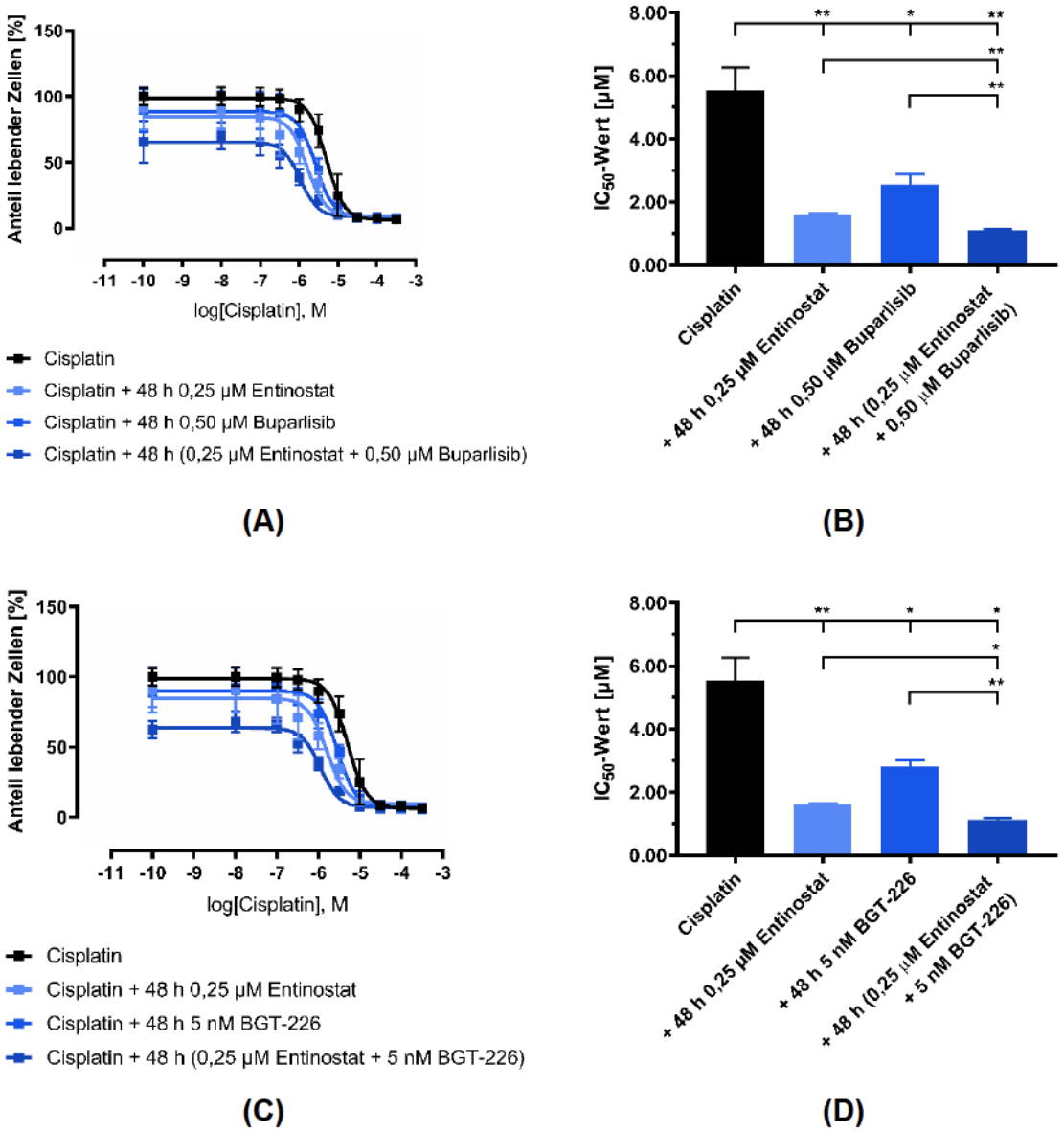

Abbildung 16: Einfluss von Entinostat und Buparlisib bzw. BGT-226 auf die Zytotoxizität von Cisplatin an A2780.

*A2780 Zellen wurden für 48 Stunden mit Entinostat und/oder Buparlisib (A/B) bzw. BGT-226 (C/D) präinkubiert. Anschließend wurden die Zellen für 72 Stunden mit verschiedenen Konzentrationen Cisplatin behandelt. Die Bestimmung der Zellviabilität per MTT-Assay und die Auswertung der erhaltenen Daten wurde nach Bandolik et al. (110) durchgeführt. Die dargestellten Ergebnisse stammen aus mindestens drei voneinander unabhängigen Experimenten, vermessen in Triplikaten, und zeigen Mittelwerte und Standardabweichung (A/C) bzw. Standardfehler (B/D). Signifikanzniveaus (t-Test): ns ($p > 0,05$); * ($p \leq 0,05$); ** ($p \leq 0,01$).*

Eine 48-stündige Präinkubation mit 0,25 µM Entinostat konnte den IC_{50}-Wert von Cisplatin an A2780 von 5,54 µM auf 1,59 µM (SF = 3,48) senken. Sowohl ein Zusatz von Buparlisib als auch von BGT-226 konnte diesen Effekt verstärken. Wurde nur mit 0,50 µM Buparlisib präinkubiert, sank der IC_{50}-Wert von Cisplatin auf 2,57 µM (SF = 2,16). In Kombination mit Entinostat allerdings konnte der IC_{50}-Wert von Cisplatin auf 1,09 µM (SF = 5,08) gesenkt werden. Damit liegt er signifikant niedriger als nach einer alleinigen Vorbehandlung mit Entinostat oder Buparlisib. Ähnliches zeigt sich für BGT-

226. Eine alleinige Vorbehandlung vermochte es, den IC_{50}-Wert von Cisplatin auf 2,82 µM (SF = 1,96) zu senken. In Kombination mit Entinostat wurde der IC_{50}-Wert von Cisplatin auf 1,12 µM (SF = 4,95) signifikant gesenkt. Auch in diesem Fall liegt dieser IC_{50}-Wert signifikant niedriger als nach Vorbehandlung mit den beiden Inhibitoren allein. Für HEY Zellen konnte dies in ersten explorativen Experimenten für eine gemeinsame Präinkubation aus Entinostat und BGT-226 gezeigt werden – hier konnte der IC_{50}-Wert von Cisplatin von ungefähr 7 µM auf rund 1 µM gesenkt werden, was in etwa einem Shift-Faktor von 7 entsprechen würde. Für Dactolisib konnte weder ein alleiniger noch in Kombination mit Entinostat sensitivierender Effekt gegenüber Cisplatin festgestellt werden.

Zur Klärung, ob dieser beobachtete Effekt auf der erhöhten Induktion von Apoptose beruht, wurde der subG1-Anteil der Zellpopulation nach entsprechender Behandlung bestimmt. Die Ergebnisse in A2780 Zellen sind in Abbildung 17 dargestellt.

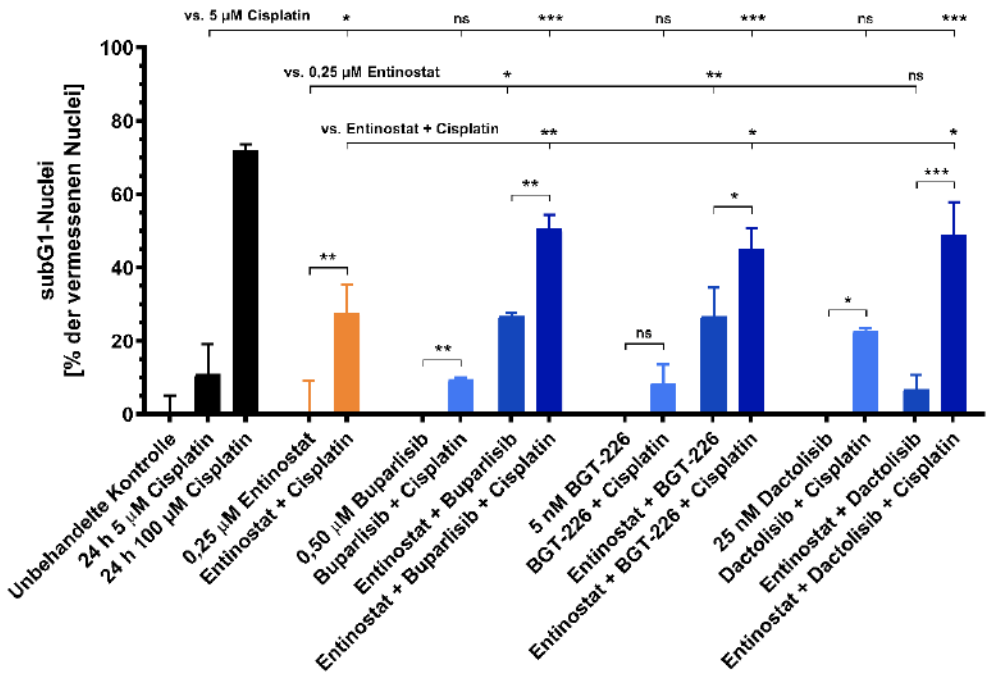

Abbildung 17: Einfluss der Kombination von Entinostat, PI3Ki und Cisplatin an A2780 auf den Anteil von subG1-Zellen.

*A2780 Zellen wurden für 48 Stunden mit Entinostat und/oder PI3Ki (Buparlisib, BGT-226 oder Dactolisib) präinkubiert. Anschließend wurden die Zellen für 24 Stunden mit 5 µM Cisplatin behandelt. Die Bestimmung des Anteils von subG1-Zellen wurde per Durchflusszytometrie bestimmt und die Auswertung der erhaltenen Daten wurde nach Bandolik et al. (110) durchgeführt. Die dargestellten Ergebnisse haben explorativen Charakter, stammen aus zwei Experimenten (mindestens in Duplikaten vermessen) und zeigen den Mittelwert und die Standardabweichung der einzelnen Datenpunkte. Die Rate von subG1-Zellen der unbehandelten Kontrolle wurde von allen Werten abgezogen. Signifikanzniveaus (t-Test): ns ($p > 0,05$); * ($p \leq 0,05$); ** ($p \leq 0,01$), *** ($p \leq 0,001$).*

Es ist zu erkennen, dass weder 5 µM Cisplatin noch Entinostat oder die eingesetzten PI3Ki in alleiniger Anwendung eine signifikante Erhöhung der Rate von subG1-Zellen verursachen. Nur Entinostat konnte in dualer Kombination mit 5 µM Cisplatin dessen erreichte subG1-Raten signifikant steigern. Buparlisib und BGT-226 konnten in dualer Kombination mit Entinostat signifikant höhere subG1-Raten erreichen als Entinostat allein. Verglichen mit der Kombinationsbehandlung aus 5 µM Cisplatin und Entinostat, konnte eine Erweiterung des Behandlungsschemas mit einem beliebigen PI3Ki die Rate an subG1-Zellen darüber hinaus signifikant steigern. An HEY Zellen konnten ähnliche Effekte bzgl. BGT-226 und Dactolisib bzw. deren Dreierkombinationen mit Cisplatin und Entinostat gezeigt werden.

Um zu verifizieren, ob es sich bei den gemessenen subG1-Zellen um apoptotische Zellen handelt, wurde unter den gleichen Bedingungen ein Caspase 3/7-Aktivierungs-Assay durchgeführt. Die exemplarischen Ergebnisse für A2780 Zellen sind in Abbildung 18 dargestellt.

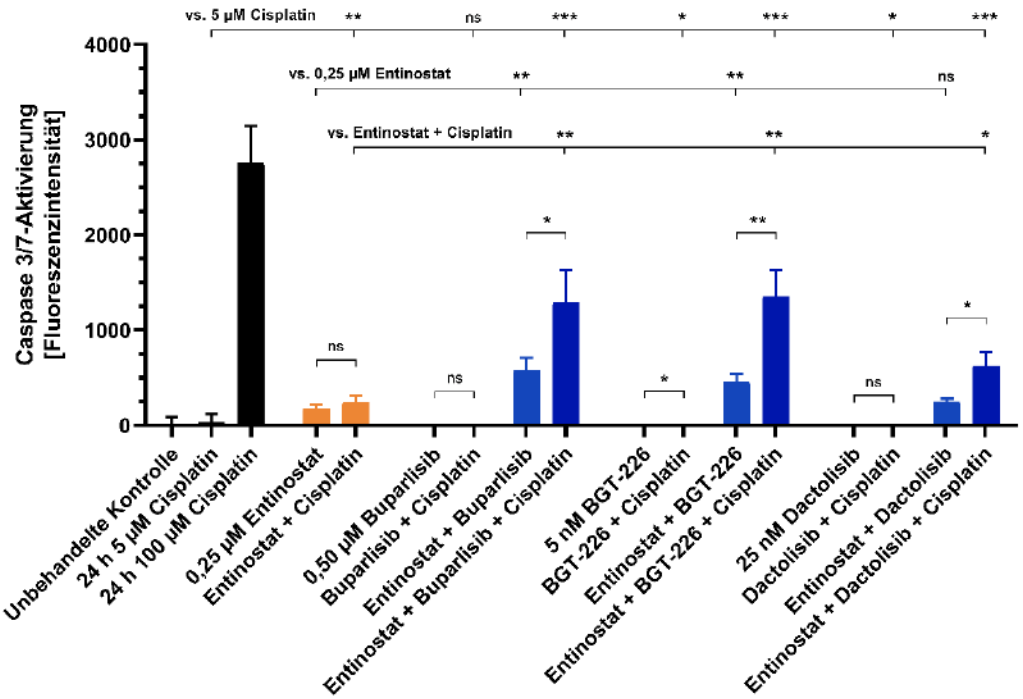

Abbildung 18: Einfluss der Kombination von Entinostat, PI3Ki und Cisplatin in A2780 auf die Aktivierung von Caspase 3/7.

*A2780 Zellen wurden für 48 Stunden mit Entinostat und/oder EGFRi (Lapatinib, Afatinib oder AZD-3759) präinkubiert. Anschließend wurden die Zellen für 24 Stunden mit 5 µM Cisplatin behandelt. Die Bestimmung der Caspase 3/7-Aktivität per fluoreszenzbasiertem Caspase-Assay und die Auswertung der erhaltenen Daten wurde nach Bandolik et al. (110) durchgeführt. Die dargestellten Ergebnisse haben explorativen Charakter, stammen aus einem Experiment (mindestens in Triplikaten vermessen) und zeigen den Mittelwert und die Standardabweichung der einzelnen Datenpunkte. Die Fluoreszenzintensität der unbehandelten Kontrolle wurde von allen Werten abgezogen. Signifikanzniveaus (t-Test): ns ($p > 0,05$); * ($p \leq 0,05$); ** ($p \leq 0,01$), *** ($p \leq 0,001$).*

Es zeigte sich, dass weder 5 µM Cisplatin noch Entinostat oder einer der eingesetzten PI3Ki in alleiniger Behandlung nach insgesamt 72-stündiger Inkubationszeit eine signifikante Aktivierung von Caspase 3/7 verursachten. Dies gilt mit einer Einschränkung für Entinostat auch für die dualen Kombinationen mit Cisplatin. Die Kombination aus Cisplatin und Entinostat konnte zwar die Caspase 3/7-Aktivierung von Cisplatin signifikant steigern, liegt allerdings nicht signifikant höher als unter alleiniger Anwendung von Entinostat. Unter Verwendung der dualen Kombination von Entinostat und einem der drei PI3Ki konnte keine erhöhte Caspase 3/7-Aktivität im Vergleich zur unbehandelten Kontrolle festgestellt werden. Die dualen Kombinationen von Entinostat und PI3Ki konnten, mit Ausnahme von Dactolisib, die verursachte Caspase 3/7-Aktivität von Entinostat signifikant erhöhen. Für alle drei untersuchten Dreifachkombinationen aus 5 µM Cisplatin, Entinostat und PI3Ki konnte eine deutlich erhöhte Caspase 3/7-Aktivität gezeigt werden. Diese war in jedem Fall signifikant höher im Vergleich zu 5 µM Cisplatin allein oder der dualen Kombination aus Cisplatin und Entinostat. Auch bei der Auswertung des Caspase 3/7-Aktivierungs-Assays konnten an HEY Zellen im Wesentlichen analoge Ergebnisse für Buparlisib und Dactolisib beinhaltende Dreifachkombinationen erzielt werden. An CaOV3-Zellen konnten schwache, aber signifikante Effekte durch die Dreifachkombination von Cisplatin, Entinostat und BGT-226 hinsichtlich der Aktivierung von Caspase 3/7 gezeigt werden.

Zusammenfassend zeigt sich, dass im Rahmen dieser ersten explorativen Experimente vielversprechende Ergebnisse für die Dreierkombination aus Cisplatin, Entinostat und einem der eingesetzten PI3Ki gezeigt werden konnten. Zunächst wurde festgestellt, dass Buparlisib bzw. BGT-226 zusammen mit Entinostat die Zytotoxizität von Cisplatin deutlich verstärken konnten. Folgend konnte gezeigt werden, dass die Rate an subG1-Zellen unter den Dreifachkombinationen erhöht war und diese Beobachtung, nach zusätzlicher Durchführung eines Caspase 3/7-Aktivierungs-Assays auf eine gesteigerte Auslösung von Apoptose zurückzuführen sein dürfte. Auch mit diesen Experimenten konnte gezeigt werden, dass verminderte Konzentrationen der einzelnen Komponenten in Kombination wirkungsvoll sein können.

4 Diskussion und Schlussfolgerung

Allgemeines

Aufgrund der besonderen Schwere einer Ovarialkrebs-Erkrankung, die sich durch eine schlechte klinische Prognose und hohe Rezidiv-Raten auszeichnet, ist es von besonderer Wichtigkeit neue Therapiestrategien gegen diese Krebsentität zu entwickeln. Erkenntnisse, die in präklinischen Zellkultur-Studien gewonnen werden, können wertvolle Impulse für die klinische Therapie von Ovarialkarzinomen generieren. Zellkultur-Studien bieten die Möglichkeit viele verschiedene Experimentalkonditionen zu untersuchen, was im Rahmen einer klinischen Studie am Patienten (auch aus ethischen Gründen) in diesem Ausmaß und dieser Vielfalt schwer umsetzbar wäre. Im Rahmen dieser Arbeit wurde die Bedeutung von HDACi für die Behandlung von Ovarialkarzinomen genauer herausgearbeitet. Dafür wurden Studien mit unterschiedlichen Zielsetzungen und an verschiedenen zellulären Testsystemen durchgeführt, die im Folgenden in einen gemeinsamen Kontext gesetzt werden sollen.

Kombinationen mit pan-HDACi und HSP90i

Im Rahmen der Studie *Priming with HDAC inhibitors Sensitizes Ovarian Cancer Cells to Treatment with Cisplatin and HSP90 Inhibitors* (Rodrigues-Moita, Bandolik et al.) bezüglich der möglichen Kombination von HDACi, HSP90i und Cisplatin, konnten wichtige Erkenntnisse bezüglich des grundsätzlichen Zusammenspiels von HDACi und Cisplatin an Ovarialkarzinom-Zelllinien generiert werden (111). In diese Studie waren die pan-HDACi Panobinostat und LMK-235 eingeschlossen. Im Fokus stand die Zelllinie A2780 und ihr Cisplatin-resistenter Subklon A2780cisR – A2780 gilt als zelluläres Modellsystem für Ovarialkarzinome vom EC-Typ (147,160–163). Allerdings wurden Teile dieser Studie auch an den Zelllinien CaOV3 und OVCAR3, inklusive ihrer Cisplatin-resistenten Subklone, durchgeführt. Sie gelten als zelluläre Modellsysteme für Ovarialkarzinome vom aggressiven HGS-Typ (146,147,163–166). Insgesamt konnte gezeigt werden, dass die Anwendung von pan-HDACi sensitivierend auf die untersuchten Zelllinien bezüglich Cisplatin wirkte. Dies konnte für EC- und HGS-Zelllinien, eingeschlossen ihrer Cisplatin-resistenten Subklone (an CaOV3, CaOV3cisR, OVCAR3 und OVCAR3cisR nur für Panobinostat bewiesen), gezeigt werden. Die Basis der gefunden Effekte beruht auf einer verstärkten Induktion von Apoptose, was mit einer Beeinflussung der Expression Apoptose-relevanter Gene

begründet werden konnte. Als besonders wichtig stellten sich Änderungen der Expression von *Survivin*, *APAF1* und *p21* heraus, die letztendlich in einem proapoptotischen Effekt resultieren und besonders durch die Kombination von Panobinostat und Cisplatin ausgelöst wurden. Diese Ergebnisse konnten auf Proteinebene im Wesentlichen bestätigt werden. Zur Rolle von HSP90i ist zusammenfassend zu sagen, dass sie zwar geeignete Kombinationspartner für Cisplatin sein können, aber die Dreifachkombination aus pan-HDACi, HSP90i und Cisplatin keinen signifikanten Vorteil ergibt.

Kombinationen mit Klasse I HDACi und pan-HDACi

Auf Basis der vielversprechenden Ergebnisse, welche mit pan-HDACi erzielt wurden, wurde die folgende Studie *Class I-Histone Deacetylase (HDAC) Inhibition is Superior to pan-HDAC Inhibition in Modulating Cisplatin Potency in High Grade Serous Ovarian Cancer Cell Lines* (Bandolik et al.) entworfen (110). Der Fokus dieser Studie lag auf den HGS-Zelllinien CaOV3, HEY, Kuramochi und OVSAHO (146,147,165,167–169), die mit der EC-Zelllinie A2780 verglichen wurden. Ziel war es Erkenntnisse darüber zu sammeln, ob für die Effekte der vorherigen Studie die Anwendung eines pan-HDACi notwendig ist oder ob sich eine bestimmte HDAC-Klasse oder sogar ein einzelnes Isoenzym als besonders wichtig erweisen würde. Im Rahmen der Experimente dieser Studie wurden die beiden selektiven HDACi Entinostat (Klasse I) und Nexturastat A (HDAC6) mit dem pan-HDACi Panobinostat verglichen. Es wurde gezeigt, dass eine Vorbehandlung der Zellen mit Entinostat die Cisplatin-Sensitivität jeder untersuchten Zelllinie maximal um Faktor 4,7 steigern konnte. Panobinostat konnte zwar die Cisplatin-Sensitivität von A2780 Zellen erhöhen, was in Einklang mit den Ergebnissen der vorherigen Studie steht, jedoch nur von zwei der vier HGS-Zelllinien, und zwar um maximal Faktor 1,9. Nexturastat A zeigte an drei der vier HGS-Zelllinien gute Ergebnisse (Steigerung der Cisplatin-Sensitivität um maximal Faktor 4,1), musste dafür allerdings in Konzentrationen eingesetzt werden, in deren Höhe es nicht mehr selektiv für HDAC6 ist, sondern auch Klasse I HDACs inhibiert. Kontroll-Experimente mit Nexturastat A Konzentrationen im HDAC6-selektiven Bereich wurden durchgeführt und es konnten keine Cisplatin-sensitivierenden Effekte festgestellt werden. Für alle Kombinationen aus Cisplatin und HDACi, die eine signifikante Steigerung der Cisplatin-Sensitivität auslösten, konnte mit Hilfe der Chou-Talalay-

Methode bewiesen werden, dass es sich um eine synergistische Beziehung zwischen den HDACi und Cisplatin handelte. In der sich anschließenden Versuchsreihe der Studie konnte gezeigt werden, dass eine erhöhte Auslösung von Apoptose die Ursache für die synergistische zytotoxische Wirkung zwischen HDACi und Cisplatin ist. Die Kombinationen, welche eine synergistische Steigerung der Apoptose zeigten, wurden zur Verifizierung der Ergebnisse auf eine erhöhte Aktivierung von Caspase 3/7 untersucht. Allein Entinostat konnte in allen fünf Zelllinien, sowohl die Cisplatin-Sensitivität als auch die Cisplatin-induzierte Apoptose und die Caspase 3/7 Aktivierung von Cisplatin signifikant steigern. Für Nexturastat A zeigten sich hinsichtlich der Caspase 3/7 Aktivierung ähnliche Ergebnisse, was die Resultate von Entinostat bestätigte, da Nexturastat A in den eingesetzten Konzentrationen auch HDACs der Klasse I hemmt. Im Zuge einer explorativen qPCR-Genexpressions-Analyse konnten die Ergebnisse der Vorgängerstudie bestätigt werden. Eine Kombinationsbehandlung aus Cisplatin und HDACi führte an A2780 als EC-Zelllinie und den vier HGS-Zelllinien zu einer verringerten Expression des antiapoptotischen Gens *Survivin* und einer verstärkten Expression der proapoptotischen Gene *p21*, *APAF1*, *BAK1* und *PUMA*. Diese Erkenntnisse lassen sich mit Genexpressions-Analysen aus andren Veröffentlichungen bezogen auf unterschiedliche Krebsarten in Einklang bringen (170,171). Alles in Allem ließen sich durch diese Studie die Ergebnisse der Vorgängerstudie in wichtigen Punkten hinsichtlich der allgemeinen Effekte der Kombination von HDACi und Cisplatin bestätigen. Darüber hinaus konnte anhand verschiedener Kriterien gezeigt werden, dass für HGS- (und mit Einschränkungen auch für EC-) Zelllinien eine selektive Inhibierung von HDACs der Klasse I Vorteile gegenüber einer Inhibition aller HDAC Isoenzyme zeigt. Projiziert auf die klinische Anwendung von HDACi könnte dies die Notwendigkeit der Anwendung von pan-HDACi einschränken, was Vorteile hinsichtlich der Vermeidung von teils schwerwiegenden unerwünschten Arzneimittelwirkungen haben könnte (172–174).

Erweiterung der Kombination von Cisplatin und Entinostat um Kinaseinhibitoren

Nachdem sich in der Studie *Class I-Histone Deacetylase (HDAC) Inhibition is Superior to pan-HDAC Inhibition in Modulating Cisplatin Potency in High Grade Serous Ovarian Cancer Cell Lines* (Bandolik et al.) Arbeit Entinostat als vielversprechender Kombinationspartner für Cisplatin herauskristallisiert hat, wurden erste Experimente durchgeführt, die zum Ziel hatten, diese duale Kombination (Cisplatin + Entinostat) um einen dritten Wirkstoff zu erweitern (vgl. Kapitel 4 Ausblick). Der Vorteil in Kombinationsbehandlungen besteht im Allgemeinen darin die eingesetzten Konzentrationen der einzelnen Substanzen zu senken. Daraus ergibt sich in der Regel, dass die Patienten unter einer geringeren Häufigkeit an (potenziell schwerwiegenden) unerwünschten Arzneimittelwirkungen leiden müssen. Als mögliche Kandidaten wurden Inhibitoren von epidermalen Wachstumsfaktorrezeptoren (EGFRi) und Inhibitoren von Phosphoinositid-3-Kinasen (PI3Ki) ausgewählt.

Die Aktivierung der Rezeptoren der EGFR-Familie führt unter anderem zu einer Steigerung der DNA-Synthese, erhöhter Zellproliferation, Zellmigration, Zelladhäsion und Verhinderung der Apoptose (117). Für Ovarialkarzinome konnte eine Expression von EGFR und anderen Mitgliedern der EGFR-Familie gezeigt werden (119–121). Eine Expression und aktive Signaltransduktion dieser Rezeptoren unterstützt die wesentlichen Charakteristika einer Krebszelle (42) und stehen im Zusammenhang mit der Ausbildung einer *off-* bzw. *post-target* Cisplatin-Resistenz (30,31). Die Experimente wurden mit den drei EGFRi Lapatinib (reversibler Inhibitor von EGFR und ErbB-2; zugelassen für die Behandlung von ErbB-2 positivem Brustkrebs), Afatinib (irreversibler Inhibitor von EGFR, ErbB-2 und ErbB-4; zugelassen für die Behandlung von NSCLC mit aktivierenden EGFR-Mutationen) und AZD-3759 (EGFRi; Gegenstand aktueller klinischer Studien) durchgeführt. Als Modellsysteme wurden A2780 und zum Teil HEY Zellen verwendet. Es konnte gezeigt werden, dass eine gemeinsame Vorbehandlung mit low-dose Entinostat und Lapatinib die Cisplatin-Sensitivität beider Zelllinien signifikant verbessern konnte (Faktor 6,67 für A2780 und Faktor 7,17 für HEY). An HEY Zellen zeigte sich ein ähnlicher Effekt auch unter analoger Verwendung von Afatinib. AZD-3759 konnte hinsichtlich der Beeinflussung der Zytotoxizität von Cisplatin keine vergleichbaren Ergebnisse zeigen. An A2780 Zellen konnte ein vorteilhafter und synergistischer Effekt der Dreifachkombinationen hinsichtlich der Aktivierung von Caspase 3/7 gezeigt werden. Grundsätzlich lässt sich, bezogen auf

die bisherigen Ergebnisse, die Einbeziehung von EGFRi ins Behandlungsschema als vielversprechend bewerten.

Der PI3K/AKT/mTOR-Signalweg ist bezogen auf das Krebsgeschehen von zentraler Bedeutung (134,135) und wird unter anderem an Ovarialkarzinomen im Zusammenhang mit der Entwicklung von Therapieresistenzen untersucht (136,137). Eine Aktivierung dieses Signalwegs führt zu einer gesteigerten Proliferation der Zelle und unterdrückt damit apoptotische Signale (140,141). Eine Dreierkombination von Cisplatin, Entinostat und PI3Ki ist in der Literatur bisher nicht beschrieben. In die Experimente für diesen explorativen Ansatz wurden die PI3Ki Buparlisib (pan-PI3Ki für Klasse I; geringe inhibitorische Wirkung auf mTOR), BGT-226 (pan-PI3Ki für Klasse I und mTORi) und Dactolisib (pan-PI3Ki für Klasse I und mTORi) einbezogen. Keiner der drei Wirkstoffe ist bisher zugelassen; sie befinden sich in unterschiedlichen Phasen der klinischen Entwicklung. Es konnte gezeigt werden, dass eine gemeinsame Präinkubation mit low-dose Entinostat und Buparlisib bzw. BGT-226 die Cisplatin-Sensitivität von A2780 Zellen signifikant um Faktor 5,08 bzw. 4,95 erhöhen konnte. An HEY Zellen konnte BGT-226 in Kombination mit Entinostat die Cisplatin-Sensitivität etwa um Faktor 7 erhöhen. Hinsichtlich der Auslösung von Apoptose konnten die Dreifachkombinationen überzeugen. Sie wiesen eine starke Steigerung der Rate apoptotischer Zellen auf. An HEY Zellen konnten ähnliche Effekte mit BGT-226 und Dactolisib erzielt werden. Ein Caspase 3/7 Aktivierungs-Assay bestätigte die Ergebnisse im Wesentlichen. Die apoptose-steigernden Effekte waren besonders ausgeprägt für die Dreierkombinationen, die Buparlisib oder BGT-226 (A2780) bzw. Buparlisib oder Dactolisib (HEY) enthielten. Auch für die Einbeziehung von PI3Ki in ein Kombinationsschema von Cisplatin und Entinostat lassen sich vielversprechende Zwischenergebnisse erkennen.

Es konnte damit gezeigt werden, dass sowohl EGFRi als auch PI3Ki eine potenzielle Erweiterung der Kombinationstherapie aus Cisplatin und Entinostat sein können. Damit konnte hervorgehoben werden, dass die Adressierung dieser beiden Zielstrukturen im Rahmen der Bekämpfung einer Cisplatin-Resistenz an Ovarialkarzinomen von besonderer Wichtigkeit sein können. Der Apoptose-steigernde Effekt von Entinostat auf Cisplatin konnte durch die Inhibierung Proliferations-steigernder Impulse zusätzlich unterstützt werden.

Kombinationen mit Klasse IIa HDACi

In der Studie *Synergism of the Class IIa Selective Histone Deacetylase Inhibitor CHDI-00390576 and the Proteasome Inhibitor Bortezomib in Ovarian Cancer Cell Lines* (Bandolik et al.) wurde ein Panel von insgesamt zehn HGS-, EC- und CC-Zellinien (fünf Zelllinien inklusive ihrer Cisplatin-resistenten Subklone [„cisR"]) hinsichtlich eines Therapieansatzes zur Kombination eines Klasse IIa selektiven HDACi und eines Proteasom-Inhibitors untersucht. Als HDACi wurde CHDI-00390576 (CHDI) eingesetzt und als Proteasom-Inhibitor Bortezomib (BTZ). Für Klasse IIa HDACs finden sich verschiedene Hinweise in der Literatur, dass sie eine gewisse Rolle im Krebsgeschehen spielen können und werden an anderen Krebsentitäten untersucht (70,94). Das Proteasom ist ein wichtiger Teil des Ubiquitin-Proteasom-Systems (UPS). Wenn die Qualitätskontrolle von Zellen im Rahmen einer malignen veränderten Zelle aus den Fugen gerät, werden gezielt antitumorale Proteine abgebaut, um beispielsweise die Auslösung von Apoptose zu verhindern (86,87). Im Rahmen dieser Studie konnte gezeigt werden, dass CHDI und BTZ im Allgemeinen antiproliferative Effekte auf alle zehn Zelllinien entfalten konnten. Synergistische zytotoxische Effekte ließen sich allerdings, bewiesen per Chou-Talalay-Methode, nur für die EC-Zelllinie A2780 und die Cisplatin-resistente CC-Zelllinie TOV21GcisR zeigen. Beide Zelllinien repräsentieren eher weniger aggressive Unterarten von Ovarialkarzinomen. Nichtsdestotrotz ist es wichtig auch Therapieoptionen für weniger aggressive Ovarialkarzinome zu entwickeln, da nicht jedes dieser Ovarialkarzinome automatisch gut auf eine Standardbehandlung mit beispielsweise Platin-basierten Zytostatika anspricht. Außerdem besteht grundsätzlich ein großes Problem in der Therapie von Platin-resistenten Ovarialkarzinomen. Die weiteren Untersuchungen der Studie wurden daher fokussiert an A2780 und TOV21GcisR durchgeführt. Es konnte gezeigt werden, dass CHDI die von BTZ ausgelöste Rate an apoptotischen Zellen in beiden Zelllinien sowohl nach 24- als auch 48-stündiger gemeinsamer Inkubation steigern konnte. Diese Ergebnisse ließen sich im Allgemeinen im Caspase 3/7 Aktivierungs-Assay bestätigen. An A2780 Zellen wurde zusätzlich ein γH2AX-Assay durchgeführt, um die Kombinationsbehandlung hinsichtlich möglicher DNA-Schädigung zu untersuchen. Es zeigte sich, dass eine gleichzeitige Inkubation mit 5 µM CHDI die DNA-schädigende Wirkung von 40 nM und 80 nM BTZ nach 24 Stunden signifikant steigern konnte. In einem weiteren Teil dieser Studie konnte gezeigt werden, dass CHDI in der Lage ist die Zytotoxizität von BTZ über 48 Stunden signifikant zu erhöhen.

So vermochten es 5 µM CHDI den 48 Stunden IC_{50}-Wert von BTZ von 10,1 nM auf 1,67 nM (Faktor 6,05) signifikant in A2780 Zellen zu senken. In TOV21GcisR Zellen konnten 7,50 µM CHDI den 48 Stunden IC_{50}-Wert von BTZ von 7,78 nM auf 0,63 nM (Faktor 12,3) signifikant senken. Aus den Ergebnissen dieser Studie ist ableitbar, dass die Kombination aus dem, vor allem zur Anwendung an hämatologischen Tumoren untersuchten, Proteasom-Inhibitor Bortezomib und dem Klasse IIa selektiven CHDI, der bisher nicht an Ovarialkarzinomzellen untersucht wurde, Vorteile in der Behandlung von weniger aggressiven Formen von Ovarialkrebs zeigen könnte.

Effekte dualer Wirkstoffe mit alkylierender und HDAC-inhibitorischer Wirkkomponente

Die letzte Studie dieser Arbeit *Hydroxamic Acids Immobilized on Resins (HAIRs): A Toolbox for the Synthesis of Dual-Targeting HDAC Inhibitors and HDAC Degraders (PROTACs)* (Sinatra et al.) beschäftigte sich mit der Evaluierung von neuartigen dualen Inhibitoren, welche sowohl alkylierende als auch HDAC-inhibitorische Wirkung zeigen (112). Die Substanzen wurden im Arbeitskreis von Prof. Finn Hansen von Laura Sinatra synthetisiert und im Rahmen dieser Arbeit hinsichtlich ihres Einflusses auf die Auslösung von Apoptose hin untersucht. Die dazugehörigen Experimente wurden an Kopf-Hals-Tumor- und Glioblastom-Zelllinien durchgeführt. Es konnte gezeigt werden, dass die dualen Verbindungen in Abhängigkeit der Aktivierung Caspase 3/7 zur Auslösung von Apoptose führten. Außerdem konnte eine DNA-Schädigung im γH2AX-Assay nachgewiesen werden, welche vorwiegend auf die alkylierenden Eigenschaften der Verbindungen zurückzuführen sein wird. Als wichtigstes Ergebnis der Studie konnte gezeigt werden, dass die Hit-Verbindung dieser Synthesereihe bessere Effekte hinsichtlich Zytotoxizität, Caspase 3/7 Aktivierung und Bildung von γH2AX zeigte als die äquimolare Kombinationsbehandlung bestehend aus den beiden Ausgangssubstanzen.

Finale Schlussfolgerungen

Zur tieferen Untersuchung der Rolle von HDACi mit verschiedenen Selektivitäten in der Therapie von Ovarialkarzinomen wurden im Rahmen dieser Arbeit diverse Experimente bzw. Studien durchgeführt. Die folgenden Ansätze für Kombinationstherapien haben sich aufgrund ihres synergistischen Verhaltens zwischen den Kombinationspartnern als besonders vielversprechend herauskristallisiert und könnten wertvolle Impulse für die klinische Behandlung dieser Tumore liefern:

- Kombination von Cisplatin mit Panobinostat an EC-Ovarialkarzinomen,
- Kombination von CHDI-00390576 und Bortezomib an EC- und Cisplatin-resistenten CC-Ovarialkarzinomen,
- Kombination von Cisplatin mit Klasse I HDACi (wie Entinostat) an HGS-Ovarialkarzinomen,
- Kombination von Cisplatin mit Entinostat und EGFRi oder PI3K(/mTOR)i an EC- und HGS-Ovarialkarzinomen.

5 Literaturverzeichnis

1. Welch DR, Hurst DR. Defining the Hallmarks of Metastasis. Cancer Res. 15. Juni 2019;79(12):3011–27.

2. Suhail Y, Cain MP, Vanaja K, Kurywchak PA, Levchenko A, Kalluri R, u. a. Systems Biology of Cancer Metastasis. Cell Syst. 28. August 2019;9(2):109–27.

3. Cooper GM. The Cell. 2nd Aufl. Sinauer Associates; 2000.

4. Wagner U, Reuß A. S3-Leitlinie „Diagnostik, Therapie und Nachsorge maligner Ovarialtumoren“: Leitlinienprogramm Onkologie, Deutsche Krebsgesellschaft, Deutsche Krebshilfe, AWMF: Langversion 3.0, 2019, AWMF-Registernummer: 032/035OL. Forum (Genova). Oktober 2019;34(5):413–5.

5. Köbel M, Rahimi K, Rambau PF, Naugler C, Le Page C, Meunier L, u. a. An Immunohistochemical Algorithm for Ovarian Carcinoma Typing. Int J Gynecol Pathol Off J Int Soc Gynecol Pathol. September 2016;35(5):430–41.

6. Sobin LH, Gospodarowicz MK, Wittekind C, International Union against Cancer, Herausgeber. TNM classification of malignant tumours. 8th ed. Chichester, West Sussex, UK ; Hoboken, NJ: Wiley-Blackwell; 2017. 309 S.

7. Berek JS, Kehoe ST, Kumar L, Friedlander M. Cancer of the ovary, fallopian tube, and peritoneum. Int J Gynecol Obstet. Oktober 2018;143:59–78.

8. Buttmann-Schweiger N, Kraywinkel K. Epidemiologie von Eierstockkrebs in Deutschland. Onkol. 1. Februar 2019;25(2):92–8.

9. Burger RA, Brady MF, Rhee J, Sovak MA, Kong G, Nguyen HP, u. a. Independent radiologic review of the Gynecologic Oncology Group Study 0218, a phase III trial of bevacizumab in the primary treatment of advanced epithelial ovarian, primary peritoneal, or fallopian tube cancer. Gynecol Oncol. Oktober 2013;131(1):21–6.

10. Oza AM, Cook AD, Pfisterer J, Embleton A, Ledermann JA, Pujade-Lauraine E, u. a. Standard chemotherapy with or without bevacizumab for women with newly diagnosed ovarian cancer (ICON7): overall survival results of a phase 3 randomised trial. Lancet Oncol. August 2015;16(8):928–36.

11. Stark D, Nankivell M, Pujade-Lauraine E, Kristensen G, Elit L, Stockler M, u. a. Standard chemotherapy with or without bevacizumab in advanced ovarian cancer: quality-of-life outcomes from the International Collaboration on Ovarian Neoplasms (ICON7) phase 3 randomised trial. Lancet Oncol. März 2013;14(3):236–43.

12. Farmer H, McCabe N, Lord CJ, Tutt ANJ, Johnson DA, Richardson TB, u. a. Targeting the DNA repair defect in BRCA mutant cells as a therapeutic strategy. Nature. 14. April 2005;434(7035):917–21.

13. Sakai W, Swisher EM, Karlan BY, Agarwal MK, Higgins J, Friedman C, u. a. Secondary mutations as a mechanism of cisplatin resistance in BRCA2-mutated cancers. Nature. 28. Februar 2008;451(7182):1116–20.

14. Pfisterer J, Ledermann JA. Management of platinum-sensitive recurrent ovarian cancer. Semin Oncol. April 2006;33(2 Suppl 6):S12-16.

15. Rottenberg S, Disler C, Perego P. The rediscovery of platinum-based cancer therapy. Nat Rev Cancer. Januar 2021;21(1):37–50.

16. Gore ME, Fryatt I, Wiltshaw E, Dawson T, Robinson BA, Calvert AH. Cisplatin/carboplatin cross-resistance in ovarian cancer. Br J Cancer. November 1989;60(5):767–9.

17. Zhou J, Kang Y, Chen L, Wang H, Liu J, Zeng S, u. a. The Drug-Resistance Mechanisms of Five Platinum-Based Antitumor Agents. Front Pharmacol. 2020;11:343.

18. Ghosh S. Cisplatin: The first metal based anticancer drug. Bioorganic Chem. 11. April 2019;88:102925.

19. Binks SP, Dobrota M. Kinetics and mechanism of uptake of platinum-based pharmaceuticals by the rat small intestine. Biochem Pharmacol. 15. September 1990;40(6):1329–36.

20. Holzer AK, Samimi G, Katano K, Naerdemann W, Lin X, Safaei R, u. a. The copper influx transporter human copper transport protein 1 regulates the uptake of cisplatin in human ovarian carcinoma cells. Mol Pharmacol. Oktober 2004;66(4):817–23.

21. Komatsu M, Sumizawa T, Mutoh M, Chen ZS, Terada K, Furukawa T, u. a. Copper-transporting P-type adenosine triphosphatase (ATP7B) is associated with cisplatin resistance. Cancer Res. 1. März 2000;60(5):1312–6.

22. Cui Y, König J, Buchholz JK, Spring H, Leier I, Keppler D. Drug resistance and ATP-dependent conjugate transport mediated by the apical multidrug resistance protein, MRP2, permanently expressed in human and canine cells. Mol Pharmacol. Mai 1999;55(5):929–37.

23. Wang D, Lippard SJ. Cellular processing of platinum anticancer drugs. Nat Rev Drug Discov. April 2005;4(4):307–20.

24. Ishida S, Lee J, Thiele DJ, Herskowitz I. Uptake of the anticancer drug cisplatin mediated by the copper transporter Ctr1 in yeast and mammals. Proc Natl Acad Sci U S A. 29. Oktober 2002;99(22):14298–302.

25. Katano K, Kondo A, Safaei R, Holzer A, Samimi G, Mishima M, u. a. Acquisition of resistance to cisplatin is accompanied by changes in the cellular pharmacology of copper. Cancer Res. 15. November 2002;62(22):6559–65.

26. Rocha CRR, Silva MM, Quinet A, Cabral-Neto JB, Menck CFM, Rocha CRR, u. a. DNA repair pathways and cisplatin resistance: an intimate relationship. Clinics [Internet]. 2018 [zitiert 14. Mai 2020];73. Verfügbar unter: http://www.scielo.br/scielo.php?script=sci_abstract&pid=S1807-59322018000200317&lng=en&nrm=iso&tlng=en

27. Fachinformation Cisplatin Teva 1 mg / ml Konzentrat zur Herstellung einer Infusionslösung. 2017.

28. Oronsky B, Ray CM, Spira AI, Trepel JB, Carter CA, Cottrill HM. A brief review of the management of platinum-resistant-platinum-refractory ovarian cancer. Med Oncol Northwood Lond Engl. Juni 2017;34(6):103.

29. Ushijima K. Treatment for recurrent ovarian cancer-at first relapse. J Oncol. 2010;2010:497429.

30. Galluzzi L, Vitale I, Michels J, Brenner C, Szabadkai G, Harel-Bellan A, u. a. Systems biology of cisplatin resistance: past, present and future. Cell Death Dis. Mai 2014;5(5):e1257–e1257.

31. Galluzzi L, Senovilla L, Vitale I, Michels J, Martins I, Kepp O, u. a. Molecular mechanisms of cisplatin resistance. Oncogene. April 2012;31(15):1869–83.

32. Chen HHW, Kuo MT. Role of glutathione in the regulation of Cisplatin resistance in cancer chemotherapy. Met-Based Drugs. 2010;2010.

33. Chen G, Waxman DJ. Role of cellular glutathione and glutathione S-transferase in the expression of alkylating agent cytotoxicity in human breast cancer cells. Biochem Pharmacol. 15. März 1994;47(6):1079–87.

34. Aida T, Takebayashi Y, Shimizu T, Okamura C, Higasimoto M, Kanzaki A, u. a. Expression of copper-transporting P-type adenosine triphosphatase (ATP7B) as a prognostic factor in human endometrial carcinoma. Gynecol Oncol. April 2005;97(1):41–5.

35. Chen HHW, Yan J-J, Chen W-C, Kuo MT, Lai Y-H, Lai W-W, u. a. Predictive and prognostic value of human copper transporter 1 (hCtr1) in patients with stage III non-small-cell lung cancer receiving first-line platinum-based doublet chemotherapy. Lung Cancer Amst Neth. Februar 2012;75(2):228–34.

36. Chaney SG, Sancar A. DNA repair: enzymatic mechanisms and relevance to drug response. J Natl Cancer Inst. 2. Oktober 1996;88(19):1346–60.

37. Kunkel TA, Erie DA. DNA mismatch repair. Annu Rev Biochem. 2005;74:681–710.

38. Jun HJ, Ahn MJ, Kim HS, Yi SY, Han J, Lee SK, u. a. ERCC1 expression as a predictive marker of squamous cell carcinoma of the head and neck treated with cisplatin-based concurrent chemoradiation. Br J Cancer. 8. Juli 2008;99(1):167–72.

39. Dabholkar M, Bostick-Bruton F, Weber C, Bohr VA, Egwuagu C, Reed E. ERCC1 and ERCC2 expression in malignant tissues from ovarian cancer patients. J Natl Cancer Inst. 7. Oktober 1992;84(19):1512–7.

40. Vaisman A, Varchenko M, Umar A, Kunkel TA, Risinger JI, Barrett JC, u. a. The role of hMLH1, hMSH3, and hMSH6 defects in cisplatin and oxaliplatin resistance: correlation with replicative bypass of platinum-DNA adducts. Cancer Res. 15. August 1998;58(16):3579–85.

41. Smith J, Tho LM, Xu N, Gillespie DA. The ATM-Chk2 and ATR-Chk1 pathways in DNA damage signaling and cancer. Adv Cancer Res. 2010;108:73–112.

42. Hanahan D, Weinberg RA. Hallmarks of Cancer: The Next Generation. Cell. März 2011;144(5):646–74.

43. Vicencio JM, Galluzzi L, Tajeddine N, Ortiz C, Criollo A, Tasdemir E, u. a. Senescence, apoptosis or autophagy? When a damaged cell must decide its path--a mini-review. Gerontology. 2008;54(2):92–9.

44. Kroemer G, Mariño G, Levine B. Autophagy and the integrated stress response. Mol Cell. 22. Oktober 2010;40(2):280–93.

45. Nakamura M, Tsuji N, Asanuma K, Kobayashi D, Yagihashi A, Hirata K, u. a. Survivin as a predictor of cis-diamminedichloroplatinum sensitivity in gastric cancer patients. Cancer Sci. Januar 2004;95(1):44–51.

46. Karczmarek-Borowska B, Filip A, Wojcierowski J, Smoleń A, Pilecka I, Jabłonka A. Survivin antiapoptotic gene expression as a prognostic factor in non-small cell lung cancer: in situ hybridization study. Folia Histochem Cytobiol. 2005;43(4):237–42.

47. Kato J, Kuwabara Y, Mitani M, Shinoda N, Sato A, Toyama T, u. a. Expression of survivin in esophageal cancer: correlation with the prognosis and response to chemotherapy. Int J Cancer. 20. März 2001;95(2):92–5.

48. Slamon DJ, Godolphin W, Jones LA, Holt JA, Wong SG, Keith DE, u. a. Studies of the HER-2/neu proto-oncogene in human breast and ovarian cancer. Science. 12. Mai 1989;244(4905):707–12.

49. Allis CD, Jenuwein T. The molecular hallmarks of epigenetic control. Nat Rev Genet. August 2016;17(8):487–500.

50. Bates SE. Epigenetic Therapies for Cancer. Longo DL, Herausgeber. N Engl J Med. 13. August 2020;383(7):650–63.

51. Dupont C, Armant DR, Brenner CA. Epigenetics: definition, mechanisms and clinical perspective. Semin Reprod Med. September 2009;27(5):351–7.

52. Drexler HG. Review of alterations of the cyclin-dependent kinase inhibitor INK4 family genes p15, p16, p18 and p19 in human leukemia-lymphoma cells. Leukemia. Juni 1998;12(6):845–59.

53. Kulis M, Esteller M. DNA methylation and cancer. Adv Genet. 2010;70:27–56.

54. Wan J, Gao Y, Zeng K, Yin Y, Zhao M, Wei J, u. a. The levels of the sex hormones are not different between type 1 and type 2 endometrial cancer. Sci Rep. Dezember 2016;6(1):39744.

55. Srijaipracharoen S, Tangjitgamol S, Tanvanich S, Manusirivithaya S, Khunnarong J, Thavaramara T, u. a. Expression of ER, PR, and Her-2/neu in endometrial cancer: a clinicopathological study. Asian Pac J Cancer Prev APJCP. 2010;11(1):215–20.

56. van der Horst PH, Wang Y, Vandenput I, Kühne LC, Ewing PC, van Ijcken WFJ, u. a. Progesterone inhibits epithelial-to-mesenchymal transition in endometrial cancer. PloS One. 2012;7(1):e30840.

57. Wik E, Ræder MB, Krakstad C, Trovik J, Birkeland E, Hoivik EA, u. a. Lack of estrogen receptor-α is associated with epithelial-mesenchymal transition and PI3K alterations in endometrial carcinoma. Clin Cancer Res Off J Am Assoc Cancer Res. 1. März 2013;19(5):1094–105.

58. Guan J, Xie L, Luo X, Yang B, Zhang H, Zhu Q, u. a. The prognostic significance of estrogen and progesterone receptors in grade I and II endometrioid endometrial adenocarcinoma: hormone receptors in risk stratification. J Gynecol Oncol. Januar 2019;30(1):e13.

59. Darwiche N. Epigenetic mechanisms and the hallmarks of cancer: an intimate affair. Am J Cancer Res. 2020;10(7):1954–78.

60. EMA. Vorinostat MSD: Withdrawn application [Internet]. European Medicines Agency. 2009 [zitiert 16. Dezember 2020]. Verfügbar unter: https://www.ema.europa.eu/en/medicines/human/withdrawn-applications/vorinostat-msd

61. EMA. EPAR: Istodax [Internet]. European Medicines Agency. 2012 [zitiert 16. Dezember 2020]. Verfügbar unter: https://www.ema.europa.eu/en/medicines/human/EPAR/istodax

62. Jones PA, Issa J-PJ, Baylin S. Targeting the cancer epigenome for therapy. Nat Rev Genet. Oktober 2016;17(10):630–41.

63. Sanaei M, Kavoosi F. Histone Deacetylases and Histone Deacetylase Inhibitors: Molecular Mechanisms of Action in Various Cancers. Adv Biomed Res. 2019;8:63.

64. Hassell KN. Histone Deacetylases and their Inhibitors in Cancer Epigenetics. Dis Basel Switz. 1. November 2019;7(4).

65. Ropero S, Esteller M. The role of histone deacetylases (HDACs) in human cancer. Mol Oncol. Juni 2007;1(1):19–25.

66. Johnstone RW. Histone-deacetylase inhibitors: novel drugs for the treatment of cancer. Nat Rev Drug Discov. April 2002;1(4):287–99.

67. New M, Olzscha H, La Thangue NB. HDAC inhibitor-based therapies: can we interpret the code? Mol Oncol. Dezember 2012;6(6):637–56.

68. Dokmanovic M, Clarke C, Marks PA. Histone deacetylase inhibitors: overview and perspectives. Mol Cancer Res MCR. Oktober 2007;5(10):981–9.

69. Bendris N, Lemmers B, Blanchard J-M, Arsic N. Cyclin A2 mutagenesis analysis: a new insight into CDK activation and cellular localization requirements. PloS One. 2011;6(7):e22879.

70. Asfaha Y, Schrenk C, Alves Avelar LA, Hamacher A, Pflieger M, Kassack MU, u. a. Recent advances in class IIa histone deacetylases research. Bioorg Med Chem. November 2019;27(22):115087.

71. Shen Y-F, Wei A-M, Kou Q, Zhu Q-Y, Zhang L. Histone deacetylase 4 increases progressive epithelial ovarian cancer cells via repression of p21 on fibrillar collagen matrices. Oncol Rep. Februar 2016;35(2):948–54.

72. Ahn MY, Kang DO, Na YJ, Yoon S, Choi WS, Kang KW, u. a. Histone deacetylase inhibitor, apicidin, inhibits human ovarian cancer cell migration via class II histone deacetylase 4 silencing. Cancer Lett. 28. Dezember 2012;325(2):189–99.

73. Zhang L, Zhang J, Jiang Q, Zhang L, Song W. Zinc binding groups for histone deacetylase inhibitors. J Enzyme Inhib Med Chem. Dezember 2018;33(1):714–21.

74. He X, Li Z, Zhuo X-T, Hui Z, Xie T, Ye X-Y. Novel Selective Histone Deacetylase 6 (HDAC6) Inhibitors: A Patent Review (2016-2019). Recent Patents Anticancer Drug Discov. 2020;15(1):32–48.

75. Pulya S, Amin SA, Adhikari N, Biswas S, Jha T, Ghosh B. HDAC6 as privileged target in drug discovery: A perspective. Pharmacol Res. 7. November 2020;105274.

76. Linciano P, Benedetti R, Pinzi L, Russo F, Chianese U, Sorbi C, u. a. Investigation of the effect of different linker chemotypes on the inhibition of histone deacetylases (HDACs). Bioorganic Chem. Januar 2021;106:104462.

77. EddingPharm Oncology Co., LTD. A Randomized Phase III Clinical Study of Entinostat/Placebo in Combination With Exemestane in Chinese Patients With Hormone Receptor-positive Advanced Breast Cancer [Internet]. clinicaltrials.gov; 2019 Sep [zitiert 16. Dezember 2020]. Report No.: NCT03538171. Verfügbar unter: https://clinicaltrials.gov/ct2/show/NCT03538171

78. National Cancer Institute (NCI). A Randomized Phase III Trial of Endocrine Therapy Plus Entinostat/Placebo in Patients With Hormone Receptor-Positive Advanced Breast Cancer [Internet]. clinicaltrials.gov; 2020 Nov [zitiert 16. Dezember 2020]. Report No.: NCT02115282. Verfügbar unter: https://clinicaltrials.gov/ct2/show/NCT02115282

79. Marek L, Hamacher A, Hansen FK, Kuna K, Gohlke H, Kassack MU, u. a. Histone deacetylase (HDAC) inhibitors with a novel connecting unit linker region reveal a selectivity profile for HDAC4 and HDAC5 with improved activity against chemoresistant cancer cells. J Med Chem. 24. Januar 2013;56(2):427–36.

80. Nandi D, Tahiliani P, Kumar A, Chandu D. The ubiquitin-proteasome system. J Biosci. März 2006;31(1):137–55.

81. Adams J, Palombella VJ, Sausville EA, Johnson J, Destree A, Lazarus DD, u. a. Proteasome inhibitors: a novel class of potent and effective antitumor agents. Cancer Res. 1. Juni 1999;59(11):2615–22.

82. Collins GA, Goldberg AL. The Logic of the 26S Proteasome. Cell. 18. Mai 2017;169(5):792–806.

83. Bard JAM, Goodall EA, Greene ER, Jonsson E, Dong KC, Martin A. Structure and Function of the 26S Proteasome. Annu Rev Biochem. 20 2018;87:697–724.

84. Budenholzer L, Cheng CL, Li Y, Hochstrasser M. Proteasome Structure and Assembly. J Mol Biol. 10 2017;429(22):3500–24.

85. Catalgol B. Proteasome and cancer. Prog Mol Biol Transl Sci. 2012;109:277–93.

86. Medina-Martinez I, Barrón V, Roman-Bassaure E, Juárez-Torres E, Guardado-Estrada M, Espinosa AM, u. a. Impact of Gene Dosage on Gene Expression, Biological Processes and Survival in Cervical Cancer: A Genome-Wide Follow-Up Study. PLoS ONE [Internet]. 30. Mai 2014 [zitiert 16. November 2020];9(5). Verfügbar unter: https://www.ncbi.nlm.nih.gov/pmc/articles/PMC4039463/

87. Dressman MA, Baras A, Malinowski R, Alvis LB, Kwon I, Walz TM, u. a. Gene Expression Profiling Detects Gene Amplification and Differentiates Tumor Types in Breast Cancer. Cancer Res. 1. Mai 2003;63(9):2194–9.

88. Bortezomib Monograph for Professionals [Internet]. Drugs.com. [zitiert 22. November 2020]. Verfügbar unter: https://www.drugs.com/monograph/bortezomib.html

89. Anonymous. Velcade [Internet]. European Medicines Agency. 2018 [zitiert 22. November 2020]. Verfügbar unter: https://www.ema.europa.eu/en/medicines/human/EPAR/velcade

90. WHO model list of essential medicines [Internet]. [zitiert 22. November 2020]. Verfügbar unter: https://www.who.int/publications-detail-redirect/WHOMVPEMPIAU2019.06

91. Bonvini P, Zorzi E, Basso G, Rosolen A. Bortezomib-mediated 26S proteasome inhibition causes cell-cycle arrest and induces apoptosis in CD-30+ anaplastic large cell lymphoma. Leukemia. April 2007;21(4):838–42.

92. Manasanch EE, Orlowski RZ. Proteasome inhibitors in cancer therapy. Nat Rev Clin Oncol. Juli 2017;14(7):417–33.

93. Seoul National University Hospital. A Phase II Trial to Evaluate the Efficacy of Bortezomib and Pegylated Liposomal Doxorubicin in Patients With BRCA Wild-type Platinum-resistant Recurrent Ovarian Cancer [Internet]. clinicaltrials.gov; 2020 Jan [zitiert 24. November 2020]. Report No.: NCT03509246. Verfügbar unter: https://clinicaltrials.gov/ct2/show/NCT03509246

94. Usami M, Kikuchi S, Takada K, Ono M, Sugama Y, Arihara Y, u. a. FOXO3a Activation by HDAC Class IIa Inhibition Induces Cell Cycle Arrest in Pancreatic Cancer Cells: Pancreas. Januar 2020;49(1):135–42.

95. Chen B, Zhong D, Monteiro A. Comparative genomics and evolution of the HSP90 family of genes across all kingdoms of organisms. BMC Genomics. 17. Juni 2006;7:156.

96. Chen B, Piel WH, Gui L, Bruford E, Monteiro A. The HSP90 family of genes in the human genome: insights into their divergence and evolution. Genomics. Dezember 2005;86(6):627–37.

97. Gupta RS. Phylogenetic analysis of the 90 kD heat shock family of protein sequences and an examination of the relationship among animals, plants, and fungi species. Mol Biol Evol. November 1995;12(6):1063–73.

98. Hoter A, El-Sabban ME, Naim HY. The HSP90 Family: Structure, Regulation, Function, and Implications in Health and Disease. Int J Mol Sci. 29. August 2018;19(9).

99. Scheibel T, Siegmund HI, Jaenicke R, Ganz P, Lilie H, Buchner J. The charged region of Hsp90 modulates the function of the N-terminal domain. Proc Natl Acad Sci U S A. 16. Februar 1999;96(4):1297–302.

100. Louvion JF, Warth R, Picard D. Two eukaryote-specific regions of Hsp82 are dispensable for its viability and signal transduction functions in yeast. Proc Natl Acad Sci U S A. 26. November 1996;93(24):13937–42.

101. Meng X, Devin J, Sullivan WP, Toft D, Baulieu EE, Catelli MG. Mutational analysis of Hsp90 alpha dimerization and subcellular localization: dimer disruption does not impede "in vivo' interaction with estrogen receptor. J Cell Sci. Juli 1996;109 (Pt 7):1677–87.

102. Soti C, Vermes A, Haystead TAJ, Csermely P. Comparative analysis of the ATP-binding sites of Hsp90 by nucleotide affinity cleavage: a distinct nucleotide specificity of the C-terminal ATP-binding site. Eur J Biochem. Juni 2003;270(11):2421–8.

103. Armstrong HK, Koay YC, Irani S, Das R, Nassar ZD, Australian Prostate Cancer BioResource, u. a. A Novel Class of Hsp90 C-Terminal Modulators Have Pre-Clinical Efficacy in Prostate Tumor Cells Without Induction of a Heat Shock Response. The Prostate. 2016;76(16):1546–59.

104. Oude Munnink TH, Korte MA de, Nagengast WB, Timmer-Bosscha H, Schröder CP, Jong JR de, u. a. (89)Zr-trastuzumab PET visualises HER2 downregulation by the HSP90 inhibitor NVP-AUY922 in a human tumour xenograft. Eur J Cancer Oxf Engl 1990. Februar 2010;46(3):678–84.

105. Eccles SA, Massey A, Raynaud FI, Sharp SY, Box G, Valenti M, u. a. NVP-AUY922: a novel heat shock protein 90 inhibitor active against xenograft tumor growth, angiogenesis, and metastasis. Cancer Res. 15. April 2008;68(8):2850–60.

106. Nagengast WB, de Korte MA, Oude Munnink TH, Timmer-Bosscha H, den Dunnen WF, Hollema H, u. a. 89Zr-bevacizumab PET of early antiangiogenic tumor response to treatment with HSP90 inhibitor NVP-AUY922. J Nucl Med Off Publ Soc Nucl Med. Mai 2010;51(5):761–7.

107. Zhang Z, Xie Z, Sun G, Yang P, Li J, Yang H, u. a. Reversing drug resistance of cisplatin by hsp90 inhibitors in human ovarian cancer cells. Int J Clin Exp Med. 2015;8(5):6687–701.

108. Ui T, Morishima K, Saito S, Sakuma Y, Fujii H, Hosoya Y, u. a. The HSP90 inhibitor 17-N-allylamino-17-demethoxy geldanamycin (17-AAG) synergizes with cisplatin and induces apoptosis in cisplatin-resistant esophageal squamous cell carcinoma cell lines via the Akt/XIAP pathway. Oncol Rep. Februar 2014;31(2):619–24.

109. Tatokoro M, Koga F, Yoshida S, Kawakami S, Fujii Y, Neckers L, u. a. Potential role of Hsp90 inhibitors in overcoming cisplatin resistance of bladder cancer-initiating cells. Int J Cancer. 15. August 2012;131(4):987–96.

110. Bandolik JJ, Hamacher A, Schrenk C, Weishaupt R, Kassack MU. Class I-Histone Deacetylase (HDAC) Inhibition is Superior to pan-HDAC Inhibition in Modulating Cisplatin Potency in High Grade Serous Ovarian Cancer Cell Lines. Int J Mol Sci. 22. Juni 2019;20(12):3052.

111. Rodrigues Moita AJ, Bandolik JJ, Hansen FK, Kurz T, Hamacher A, Kassack MU. Priming with HDAC Inhibitors Sensitizes Ovarian Cancer Cells to Treatment with Cisplatin and HSP90 Inhibitors. Int J Mol Sci. Januar 2020;21(21):8300.

112. Sinatra L, Bandolik JJ, Roatsch M, Sönnichsen M, Schoeder CT, Hamacher A, u. a. Hydroxamic Acids Immobilized on Resins (HAIRs): Synthesis of Dual-Targeting HDAC Inhibitors and HDAC Degraders (PROTACs). Angew Chem Int Ed Engl. 7. Dezember 2020;59(50):22494–9.

113. Sinatra L, Bandolik JJ, Roatsch M, Sönnichsen M, Schoeder CT, Hamacher A, u. a. Hydroxamic Acids Immobilized on Resins (HAIRs): Synthese von Dual-Target-HDAC-Inhibitoren und HDAC-PROTACs. Angew Chem. 7. Dezember 2020;132(50):22681–7.

114. Yarden Y, Schlessinger J. Epidermal growth factor induces rapid, reversible aggregation of the purified epidermal growth factor receptor. Biochemistry. 10. März 1987;26(5):1443–51.

115. Yarden Y. The EGFR family and its ligands in human cancer. signalling mechanisms and therapeutic opportunities. Eur J Cancer Oxf Engl 1990. September 2001;37 Suppl 4:S3-8.

116. Linggi B, Carpenter G. ErbB receptors: new insights on mechanisms and biology. Trends Cell Biol. Dezember 2006;16(12):649–56.

117. Oda K, Matsuoka Y, Funahashi A, Kitano H. A comprehensive pathway map of epidermal growth factor receptor signaling. Mol Syst Biol. 2005;1:2005.0010.

118. Normanno N, De Luca A, Bianco C, Strizzi L, Mancino M, Maiello MR, u. a. Epidermal growth factor receptor (EGFR) signaling in cancer. Gene. 17. Januar 2006;366(1):2–16.

119. Chung YW, Kim S, Hong JH, Lee JK, Lee NW, Lee YS, u. a. Overexpression of HER2/HER3 and clinical feature of ovarian cancer. J Gynecol Oncol. September 2019;30(5):e75.

120. Bull Phelps SL, Schorge JO, Peyton MJ, Shigematsu H, Xiang L-L, Miller DS, u. a. Implications of EGFR inhibition in ovarian cancer cell proliferation. Gynecol Oncol. Juni 2008;109(3):411–7.

121. Glaysher S, Bolton LM, Johnson P, Atkey N, Dyson M, Torrance C, u. a. Targeting EGFR and PI3K pathways in ovarian cancer. Br J Cancer. 1. Oktober 2013;109(7):1786–94.

122. Tan C-S, Gilligan D, Pacey S. Treatment approaches for EGFR-inhibitor-resistant patients with non-small-cell lung cancer. Lancet Oncol. September 2015;16(9):e447–59.

123. Nelson MH, Dolder CR. Lapatinib: a novel dual tyrosine kinase inhibitor with activity in solid tumors. Ann Pharmacother. Februar 2006;40(2):261–9.

124. Solca F, Dahl G, Zoephel A, Bader G, Sanderson M, Klein C, u. a. Target binding properties and cellular activity of afatinib (BIBW 2992), an irreversible ErbB family blocker. J Pharmacol Exp Ther. November 2012;343(2):342–50.

125. Li D, Ambrogio L, Shimamura T, Kubo S, Takahashi M, Chirieac LR, u. a. BIBW2992, an irreversible EGFR/HER2 inhibitor highly effective in preclinical lung cancer models. Oncogene. 7. August 2008;27(34):4702–11.

126. Wind S, Schnell D, Ebner T, Freiwald M, Stopfer P. Clinical Pharmacokinetics and Pharmacodynamics of Afatinib. Clin Pharmacokinet. 2017;56(3):235–50.

127. Zeng Q, Wang J, Cheng Z, Chen K, Johnström P, Varnäs K, u. a. Discovery and Evaluation of Clinical Candidate AZD3759, a Potent, Oral Active, Central Nervous System-Penetrant, Epidermal Growth Factor Receptor Tyrosine Kinase Inhibitor. J Med Chem. 22. Oktober 2015;58(20):8200–15.

128. Alpha Biopharma (Jiangsu) Co., Ltd. A Randomized, Open-label, Controlled, Multi-Center Phase II/III Study to Assess the Efficacy and Safety of AZD3759 vs. a Standard of Care EGFR TKI, as First Line Treatment to EGFR Mutation Positive Advanced NSCLC With CNS Metastases [Internet]. clinicaltrials.gov; 2020 Juli [zitiert 5. November 2020]. Report No.: NCT03653546. Verfügbar unter: https://clinicaltrials.gov/ct2/show/NCT03653546

129. AstraZeneca. A Phase I, Open-label, Multicentre Study to Assess the Safety, Tolerability, Pharmacokinetics and Preliminary Anti-Tumour Activity of AZD3759 or AZD9291 in Patients With EGFR Mutation Positive Advanced Stage Non Small Cell Lung Cancer (NSCLC) [Internet]. clinicaltrials.gov; 2020 Okt [zitiert 5. November 2020]. Report No.: NCT02228369. Verfügbar unter: https://clinicaltrials.gov/ct2/show/NCT02228369

130. Rusnak DW, Lackey K, Affleck K, Wood ER, Alligood KJ, Rhodes N, u. a. The effects of the novel, reversible epidermal growth factor receptor/ErbB-2 tyrosine kinase inhibitor, GW2016, on the growth of human normal and tumor-derived cell lines in vitro and in vivo. Mol Cancer Ther. Dezember 2001;1(2):85–94.

131. Ferrarotto R, Gold KA. Afatinib in the treatment of head and neck squamous cell carcinoma. Expert Opin Investig Drugs. Januar 2014;23(1):135–43.

132. Rosanò L, Di Castro V, Spinella F, Tortora G, Nicotra MR, Natali PG, u. a. Combined targeting of endothelin A receptor and epidermal growth factor receptor in ovarian cancer shows enhanced antitumor activity. Cancer Res. 1. Juli 2007;67(13):6351–9.

133. Ohta T, Ohmichi M, Shibuya T, Takahashi T, Tsutsumi S, Takahashi K, u. a. Gefitinib (ZD1839) increases the efficacy of cisplatin in ovarian cancer cells. Cancer Biol Ther. April 2012;13(6):408–16.

134. LoRusso PM. Inhibition of the PI3K/AKT/mTOR Pathway in Solid Tumors. J Clin Oncol Off J Am Soc Clin Oncol. 01 2016;34(31):3803–15.

135. Yang J, Nie J, Ma X, Wei Y, Peng Y, Wei X. Targeting PI3K in cancer: mechanisms and advances in clinical trials. Mol Cancer. 19. Februar 2019;18(1):26.

136. Ediriweera MK, Tennekoon KH, Samarakoon SR. Role of the PI3K/AKT/mTOR signaling pathway in ovarian cancer: Biological and therapeutic significance. Semin Cancer Biol. 2019;59:147–60.

137. Mabuchi S, Kuroda H, Takahashi R, Sasano T. The PI3K/AKT/mTOR pathway as a therapeutic target in ovarian cancer. Gynecol Oncol. April 2015;137(1):173–9.

138. Raphael J, Desautels D, Pritchard KI, Petkova E, Shah PS. Phosphoinositide 3-kinase inhibitors in advanced breast cancer: A systematic review and meta-analysis. Eur J Cancer Oxf Engl 1990. 2018;91:38–46.

139. Park S, Kim YS, Kim DY, So I, Jeon J-H. PI3K pathway in prostate cancer: All resistant roads lead to PI3K. Biochim Biophys Acta Rev Cancer. 2018;1870(2):198–206.

140. Wullschleger S, Loewith R, Hall MN. TOR signaling in growth and metabolism. Cell. 10. Februar 2006;124(3):471–84.

141. Saxton RA, Sabatini DM. mTOR Signaling in Growth, Metabolism, and Disease. Cell. 09 2017;168(6):960–76.

142. Zinzalla V, Stracka D, Oppliger W, Hall MN. Activation of mTORC2 by Association with the Ribosome. Cell. März 2011;144(5):757–68.

143. Gewinner C, Wang ZC, Richardson A, Teruya-Feldstein J, Etemadmoghadam D, Bowtell D, u. a. Evidence that Inositol Polyphosphate 4-Phosphatase Type II Is a Tumor Suppressor that Inhibits PI3K Signaling. Cancer Cell. August 2009;16(2):115–25.

144. Patch A-M, Christie EL, Etemadmoghadam D, Garsed DW, George J, Fereday S, u. a. Whole-genome characterization of chemoresistant ovarian cancer. Nature. 28. Mai 2015;521(7553):489–94.

145. Burger MT, Pecchi S, Wagman A, Ni Z-J, Knapp M, Hendrickson T, u. a. Identification of NVP-BKM120 as a Potent, Selective, Orally Bioavailable Class I

PI3 Kinase Inhibitor for Treating Cancer. ACS Med Chem Lett. 13. Oktober 2011;2(10):774–9.

146. Domcke S, Sinha R, Levine DA, Sander C, Schultz N. Evaluating cell lines as tumour models by comparison of genomic profiles. Nat Commun. 9. Juli 2013;4:2126.

147. Beaufort CM, Helmijr JCA, Piskorz AM, Hoogstraat M, Ruigrok-Ritstier K, Besselink N, u. a. Ovarian Cancer Cell Line Panel (OCCP): Clinical Importance of In Vitro Morphological Subtypes. PLoS ONE [Internet]. 17. September 2014 [zitiert 6. Mai 2019];9(9). Verfügbar unter: https://www.ncbi.nlm.nih.gov/pmc/articles/PMC4167545/

148. Array Biopharma, now a wholly owned subsidiary of Pfizer. A Phase Ib, Open-label, Multi-center, Dose-escalation and Expansion Study of an Orally Administered Combination of BKM120 Plus MEK162 in Adult Patients With Selected Advanced Solid Tumors [Internet]. clinicaltrials.gov; 2020 Sep [zitiert 12. November 2020]. Report No.: NCT01363232. Verfügbar unter: https://clinicaltrials.gov/ct2/show/NCT01363232

149. Novartis Pharmaceuticals. A Phase IA, Multicenter, Open-label Dose Escalation Study of BKM120, Administered Orally in Adult Patients With Advanced Solid Malignancies [Internet]. clinicaltrials.gov; 2013 Apr [zitiert 12. November 2020]. Report No.: NCT01068483. Verfügbar unter: https://clinicaltrials.gov/ct2/show/NCT01068483

150. Novartis Pharmaceuticals. A Phase III Randomized, Double Blind, Placebo Controlled Study of BKM120 With Fulvestrant, in Postmenopausal Women With Hormone Receptor-positive HER2-negative AI Treated, Locally Advanced or Metastatic Breast Cancer Who Progressed on or After mTOR Inhibitor Based Treatment [Internet]. clinicaltrials.gov; 2019 Jan [zitiert 12. November 2020]. Report No.: NCT01633060. Verfügbar unter: https://clinicaltrials.gov/ct2/show/NCT01633060

151. Novartis Pharmaceuticals. A Randomized, Double-blind, Placebo Controlled, Phase II/III Study of BKM120 Plus Paclitaxel in Patients With HER2 Negative Inoperable Locally Advanced or Metastatic Breast Cancer, With or Without PI3K Pathway Activation. [Internet]. clinicaltrials.gov; 2017 Jan [zitiert 12. November 2020]. Report No.: NCT01572727. Verfügbar unter: https://clinicaltrials.gov/ct2/show/NCT01572727

152. Adlai Nortye Biopharma Co., Ltd. The BURAN Study of Buparlisib (AN2025) In Combination With Paclitaxel Compared to Paclitaxel Alone, in Patients With Recurrent or Metastatic Head and Neck Squamous Cell Carcinoma [Internet]. clinicaltrials.gov; 2020 Apr [zitiert 12. November 2020]. Report No.: NCT04338399. Verfügbar unter: https://clinicaltrials.gov/ct2/show/NCT04338399

153. Markman B, Tabernero J, Krop I, Shapiro GI, Siu L, Chen LC, u. a. Phase I safety, pharmacokinetic, and pharmacodynamic study of the oral phosphatidylinositol-3-kinase and mTOR inhibitor BGT226 in patients with advanced solid tumors. Ann Oncol Off J Eur Soc Med Oncol. September 2012;23(9):2399–408.

154. Novartis Pharmaceuticals. A Phase I/II, Multi-center, Open-label Study of BGT226, Administered Orally in Adult Patients With Advanced Solid Malignancies Including Patients With Advanced Breast Cancer [Internet]. clinicaltrials.gov; 2012 Nov [zitiert 12. November 2020]. Report No.: NCT00600275. Verfügbar unter: https://clinicaltrials.gov/ct2/show/NCT00600275

155. Novartis Pharmaceuticals. A Phase I Study of BGT226, Administered Orally in Adult Patients With Advanced Solid Tumor in Japan [Internet]. clinicaltrials.gov; 2018 Sep [zitiert 12. November 2020]. Report No.: NCT00742105. Verfügbar unter: https://clinicaltrials.gov/ct2/show/NCT00742105

156. Maira S-M, Stauffer F, Brueggen J, Furet P, Schnell C, Fritsch C, u. a. Identification and characterization of NVP-BEZ235, a new orally available dual phosphatidylinositol 3-kinase/mammalian target of rapamycin inhibitor with potent in vivo antitumor activity. Mol Cancer Ther. Juli 2008;7(7):1851–63.

157. Novartis Pharmaceuticals. A Dose-finding Phase Ib Study Followed by an Open-label, Randomized Phase II Study of BEZ235 Plus Paclitaxel in Patients With HER2 Negative, Inoperable Locally Advanced or Metastatic Breast Cancer [Internet]. clinicaltrials.gov; 2020 Sep [zitiert 12. November 2020]. Report No.: NCT01495247. Verfügbar unter: https://clinicaltrials.gov/ct2/show/NCT01495247

158. Fazio N, Buzzoni R, Baudin E, Antonuzzo L, Hubner RA, Lahner H, u. a. A Phase II Study of BEZ235 in Patients with Everolimus-resistant, Advanced Pancreatic Neuroendocrine Tumours. Anticancer Res. Februar 2016;36(2):713–9.

159. Pongas G, Fojo T. BEZ235: When Promising Science Meets Clinical Reality. The Oncologist. September 2016;21(9):1033–4.

160. Cellosaurus cell line A2780 (CVCL_0134) [Internet]. [zitiert 20. Dezember 2020]. Verfügbar unter: https://web.expasy.org/cellosaurus/CVCL_0134

161. Hallas-Potts A, Dawson JC, Herrington CS. Ovarian cancer cell lines derived from non-serous carcinomas migrate and invade more aggressively than those derived from high-grade serous carcinomas. Sci Rep. Dezember 2019;9(1):5515.

162. Eva A, Robbins KC, Andersen PR, Srinivasan A, Tronick SR, Reddy EP, u. a. Cellular genes analogous to retroviral onc genes are transcribed in human tumour cells. Nature. Januar 1982;295(5845):116–9.

163. Hernandez L, Kim MK, Lyle LT, Bunch KP, House CD, Ning F, u. a. Characterization of ovarian cancer cell lines as in vivo models for preclinical studies. Gynecol Oncol. August 2016;142(2):332–40.

164. Buick RN, Pullano R, Trent JM. Comparative properties of five human ovarian adenocarcinoma cell lines. Cancer Res. August 1985;45(8):3668–76.

165. Cellosaurus cell line Caov-3 (CVCL_0201) [Internet]. [zitiert 20. Dezember 2020]. Verfügbar unter: https://web.expasy.org/cellosaurus/CVCL_0201

166. Cellosaurus cell line OVCAR-3 (CVCL_0465) [Internet]. [zitiert 20. Dezember 2020]. Verfügbar unter: https://web.expasy.org/cellosaurus/CVCL_0465

167. Cellosaurus cell line Kuramochi (CVCL_1345) [Internet]. [zitiert 17. Mai 2019]. Verfügbar unter: https://web.expasy.org/cellosaurus/CVCL_1345

168. Cellosaurus cell line OVSAHO (CVCL_3114) [Internet]. [zitiert 17. Mai 2019]. Verfügbar unter: https://web.expasy.org/cellosaurus/CVCL_3114

169. Cellosaurus cell line HEY (CVCL_0297) [Internet]. [zitiert 20. Dezember 2020]. Verfügbar unter: https://web.expasy.org/cellosaurus/CVCL_0297

170. Sanders YY, Hagood JS, Liu H, Zhang W, Ambalavanan N, Thannickal VJ. Histone deacetylase inhibition promotes fibroblast apoptosis and ameliorates pulmonary fibrosis in mice. Eur Respir J. Mai 2014;43(5):1448–58.

171. Glozak MA, Seto E. Histone deacetylases and cancer. Oncogene. August 2007;26(37):5420–32.

172. Shah RR. Safety and Tolerability of Histone Deacetylase (HDAC) Inhibitors in Oncology. Drug Saf. 1. Februar 2019;42(2):235–45.

173. Van Veggel M, Westerman E, Hamberg P. Clinical Pharmacokinetics and Pharmacodynamics of Panobinostat. Clin Pharmacokinet. 1. Januar 2018;57(1):21–9.

174. Tzogani K, van Hennik P, Walsh I, De Graeff P, Folin A, Sjöberg J, u. a. EMA Review of Panobinostat (Farydak) for the Treatment of Adult Patients with Relapsed and/or Refractory Multiple Myeloma. The Oncologist. Mai 2018;23(5):631–6.

Liste von Publikationen

Jan J. Bandolik, Alexandra Hamacher, Christian Schrenk, Robin Weishaupt, Matthias U. Kassack, Class I-Histone Deacetylase (HDAC) Inhibition is Superior to pan-HDAC Inhibition in Modulating Cisplatin Potency in High Grade Serous Ovarian Cancer Cell Lines, *International Journal of Molecular Science*s, **2019**, 20(12), 3052

Yodita Asfaha, Christian Schrenk, Leandro A. Alves Avelar, Friedrich Lange, Chenyin Wang, **Jan J. Bandolik**, Alexandra Hamacher, Matthias U. Kassack, Thomas Kurz, Novel alkoxyamide-based histone deacetylase inhibitors reverse cisplatin resistance in chemoresistant cancer cells, *Bioorganic & Medicinal Chemistry,* **2020**, 28(1), 115108

Laura Sinatra, **Jan J. Bandolik**, Martin Roatsch, Melf Sönnichsen, Clara T. Schoeder, Alexandra Hamacher, Andrea Schöler, Arndt Borkhardt, Jens Meiler, Sanil Bhatia, Matthias U. Kassack, Finn K. Hansen, Hydroxamic Acids Immobilized on Resins (HAIRs): A Toolbox for the Synthesis of Dual-Targeting HDAC Inhibitors and HDAC Degraders (PROTACs), *Angewandte Chemie International Edition,* **2020**, 59, 22494-22499

Ana J. Rodrigues Moita*, **Jan J. Bandolik***, Finn K. Hansen, Thomas Kurz, Alexandra Hamacher, Matthias U. Kassack, Priming with HDAC inhibitors Sensitizes Ovarian Cancer Cells to Treatment with Cisplatin and HSP90 Inhibitors, *International Journal of Molecular Sciences,* **2020**, 21(21), 8300 [* geteilte Erstautorschaft]

Kim Thao Le, **Jan J. Bandolik**, Matthias U. Kassack, Claudia Pätzold, Marc Appelhans, Claus M. Paßreiter, New acetophenones and chromenes from the leaves of Melicopa barbigera A. Gray, *Molecules*, **2021**, 26(3), 688

Jan J. Bandolik, Alexander J. Skerhut, Alexandra Hamacher, Matthias U. Kassack, *Synergism of the Class IIa Selective Histone Deacetylase Inhibitor CHDI-00390576 and the Proteasome Inhibitor Bortezomib in Ovarian Cancer Cell Lines* (eingereicht bei *Cancers* am 05.03.2021)

Posterpräsentationen

Jan J. Bandolik, Alexandra Hamacher, Matthias U. Kassack, Inhibitors of histone deacetylase can increase the potency of classical cytostatic agents in ovarian cancer by induction of apoptosis. *Conference Systems Epigenetics*, 27.-30. November **2018**, Amsterdam, Niederlande

Jan J. Bandolik, Alexandra Hamacher, Matthias U. Kassack, Inhibitors of histone deacetylase can increase the potency of classical cytostatic agents in ovarian cancer by induction of apoptosis. *9th Mildred Scheel Cancer Conference*, 15.-16. Mai **2019**, Bonn, Deutschland

Danksagung

Ich danke meinem Doktorvater, Prof. Dr. Matthias U. Kassack, für die Überlassung des interessanten Themas und für die Anregungen, sowie die konstruktive Kritik während meiner Promotionsphase.

Frau Prof. Dr. Tanja Fehm danke ich herzlich für die Übernahme des Koreferats.

Ein besonderer Dank gilt Dr. Alexandra Hamacher: Auf der einen Seite hast Du meine Doktorarbeit offiziell als Co-Betreuerin unterstützt, auf der anderen Seite warst Du unabhängig davon, ob es um berufliche oder persönliche Belange ging, immer für mich da. Durch Deine besonders positive, offene und ehrliche Art sowie professionelle Lehre hast Du (nicht nur) mich bereits im Studium für die Wissenschaft begeistern können. Ich bedanke mich für die unzähligen Einführungen in unsere Labormethoden (die wahre Großmeisterin des Western Blots und FACS-Flüsterin bist und bleibst eindeutig Du), die Kunst der Zellkultur und die immer wieder lustigen Diskussionen und Gespräche über Digitalisierungspotentiale, die Dich zu einer waschechten *digital native* gemacht haben. Auch unsere Ausflüge mit Chenyin und Alexander werden mir positiv in Erinnerung bleiben. Unsere Konferenzteilnahme 2018 in Amsterdam wird allerdings ein Highlight außer Konkurrenz bleiben. Danke für Alles!

Sehr herzlich bedanke ich mich bei Prof. Dr. Georg Kojda für die Weiterbildung zum Fachapotheker für Arzneimittelinformation parallel zur Promotionsarbeit.

Ich bedanke mich besonders bei Dr. Ana Moita für die allgemeine, wenn auch leider zu kurze, Einführung in unser Labor und die Zellkultur in meinen ersten Wochen und Dr. Chenyin Wang für die Einführung am „Imager“ und die daraus resultierenden interessanten Gespräche. Weiterhin bedanke ich mich bei Alexander „AJ“ Skerhut, Dr. Fritz „Opa“ Lange, Christian Schrenk, Lukas Bollmann, Dr. Parichat Sureechatchaiyan, Dr. Stefanie Hagenow, Jens Hagenow, Dr. Aleksandra Zivkovic, Nadine Horstick-Muche und Kathrin Christoph.

Vielen Dank an meine Kolleginnen und Kollegen in der Betreuung des Arzneimittelanalytik-Praktikums. Weiterhin vielen Dank an Dr. Yodita Asfaha für die gemeinsame zeitweise Leitung des Chemie-Vorkurses.

Ich bedanke mich bei allen (ehemaligen) Mitgliedern des Teams der Sanavita-Apotheke für Ihren wertvollen Beitrag zu meiner praktischen Ausbildung zum Apotheker. Insbesondere danke ich Jürgen Erlemann, Silke & Marc Baumert, Claudia Becker, Melanie Blum, Alexander Cadeddu, Helma Engel, Ina Gerdes, Ilka Grünwald, Katharina Hartmann, Ines Haser, Cemile Kindac, Pia Kossack, Daniela Marquardt, Patricia Meier-Schöße, Dr. Elisabeth Rüller, Tamim Sawas, Birgit Schmitz und Petra Weber.

Ein ganz besonders herzlicher Dank gebührt meinen langjährigen Freunden und Vertrauten Lucas Rachner & Florian Jansen, Julia Andresen, Simon Weber, Katharina Wehr, Lena Wertenbruch, Dominique Komander, Alexander Skerhut, Tatjana Solscheid, Christina Coesfeld, Alexander Cadeddu, Daniel Dragomir, Matthias & Stefanie Kölsch, Sebastian Zeller, Daniel & Lisa Hildebrandt und zu guter Letzt ganz besonders Timmy Walther für Eure Zeit, Eure Unterstützung, unsere Erlebnisse, Gespräche, Diskussionen und einfach Alles! Ich hoffe und freue mich auf noch viele weitere Jahre mit jeder/m Einzelnen von Euch!

Der letzte Dank gilt meinen Eltern, Sigrid und Detlef, meiner Schwester Lisa und meiner Großmutter Margarete. Ihr habt mich an jeder Station meines Lebens bedingungslos unterstützt, an mich geglaubt und alle wichtigen Entscheidungen konstruktiv begleitet. Vielen Dank, dass Ihr mir jegliche Art von Ausbildung ermöglicht habt. Ohne Euch wäre ich wohl nicht zu dem Menschen geworden, der ich bin.

Eidesstattliche Erklärung

Ich versichere an Eides Statt, dass die Dissertation von mir selbstständig und ohne unzulässige fremde Hilfe unter Beachtung der „Grundsätze zur Sicherung guter wissenschaftlicher Praxis an der Heinrich-Heine-Universität Düsseldorf“ erstellt worden ist.

Die Dissertation wurde in der vorgelegten oder einer ähnlichen Form bei keiner anderen Institution eingereicht. Ich habe bisher keine erfolglosen Promotionsversuche unternommen.

Düsseldorf, den 18.03.2021

(Jan Bandolik)